N77-23488

NASA
CR
135186
c.1

TECH LIBRARY KAFB, NM
0062724

NASA CR-135186
R76-115

NASA

FINAL REPORT

SMALL, HIGH-PRESSURE LIQUID HYDROGEN TURBOPUMP

LOAN COPY: RETURN TO AFWL
TECHNICAL LIBRARY, KIRTLAND AFB, NM

by

A. Csomor and R. Sutton

Rockwell International
Rocketdyne Division

prepared for
NATIONAL AERONAUTICS AND SPACE ADMINISTRATION

NASA-Lewis Research Center
Contract NAS3-17794
R. E. Connelly, Project Manager

11 MAY 1978

NOTICE

This report was prepared as an account of Government sponsored work. Neither the United States, nor the National Aeronautics and Space Administration (NASA), nor any person acting on behalf of NASA:

A.) Makes any warranty or representation, expressed or implied, with respect to the accuracy of the information contained in this report, or that the use of any information, apparatus, method, or process disclosed in this report may not infringe privately-owned rights; or

B.) Assumes any liabilities with respect to the use of, or for damages resulting from the use of, any information, apparatus, method or process disclosed in this report.

As used above, "person acting on behalf of NASA" includes any employee or contractor of NASA, or employee or such contractor, to the extent that such employee or contractor of NASA or employee of such contractor prepares, disseminates, or provides access to any information pursuant to his employment or contract with NASA, or his employment with such contractor.

Requests for copies of this report should be referred to

National Aeronautics and Space Administration
Scientific and Technical Information Facility
P.O. Box 33
College Park, Md. 20740

Attention: SAF/DL, ACQ Division

TECH LIBRARY KAFB, NM
0062724

1. Report No.	2. Government Accession No.	3. Recipient's Catalog No.
NASA CR-135186		

4. Title and Subtitle	5. Report Date
SMALL, HIGH-PRESSURE HYDROGEN TURBOPUMP	18 May 1977
	6. Performing Organization Code

7. Author(s)	8. Performing Organization Report No.
A. Csomor and R. Sutton	R76-115
	10. Work Unit No.

9. Performing Organization Name and Address	11. Contract or Grant No.
Rocketdyne Division of Rockwell International 6633 Canoga Avenue Canoga Park, California 91304	NAS3-17794
	13. Type of Report and Period Covered Final Report (August 1973-April 1976)

12. Sponsoring Agency Name and Address	14. Sponsoring Agency Code
National Aeronautics and Space Administration Washington, D.C. 20546	

15. Supplementary Notes

Project Manager, Robert Connelly, NASA-Lewis Research Center, Cleveland, Ohio

16. Abstract

A high-pressure, liquid hydrogen turbopump was designed, fabricated, and tested to a maximum speed of 9739 rad/s (93,000 rpm) and a maximum pump discharge pressure of 2861 N/cm^2 (4150 psia). The approaches used in the detail analysis and design of the turbopump are described, and fabrication methods are discussed. Data obtained from gas generator tests, turbine performance calibration, and turbopump testing are presented.

17. Key Words (Suggested by Author(s))	18. Distribution Statement
Hydrogen Turbopump Centrifugal Pump Axial Flow Turbine Balance Piston	

19. Security Classif. (of this report)	20. Security Classif. (of this page)	21. No. of Pages	22. Price*
Unclassified	Unclassified	290	

* For sale by the National Technical Information Service, Springfield, Virginia 22151

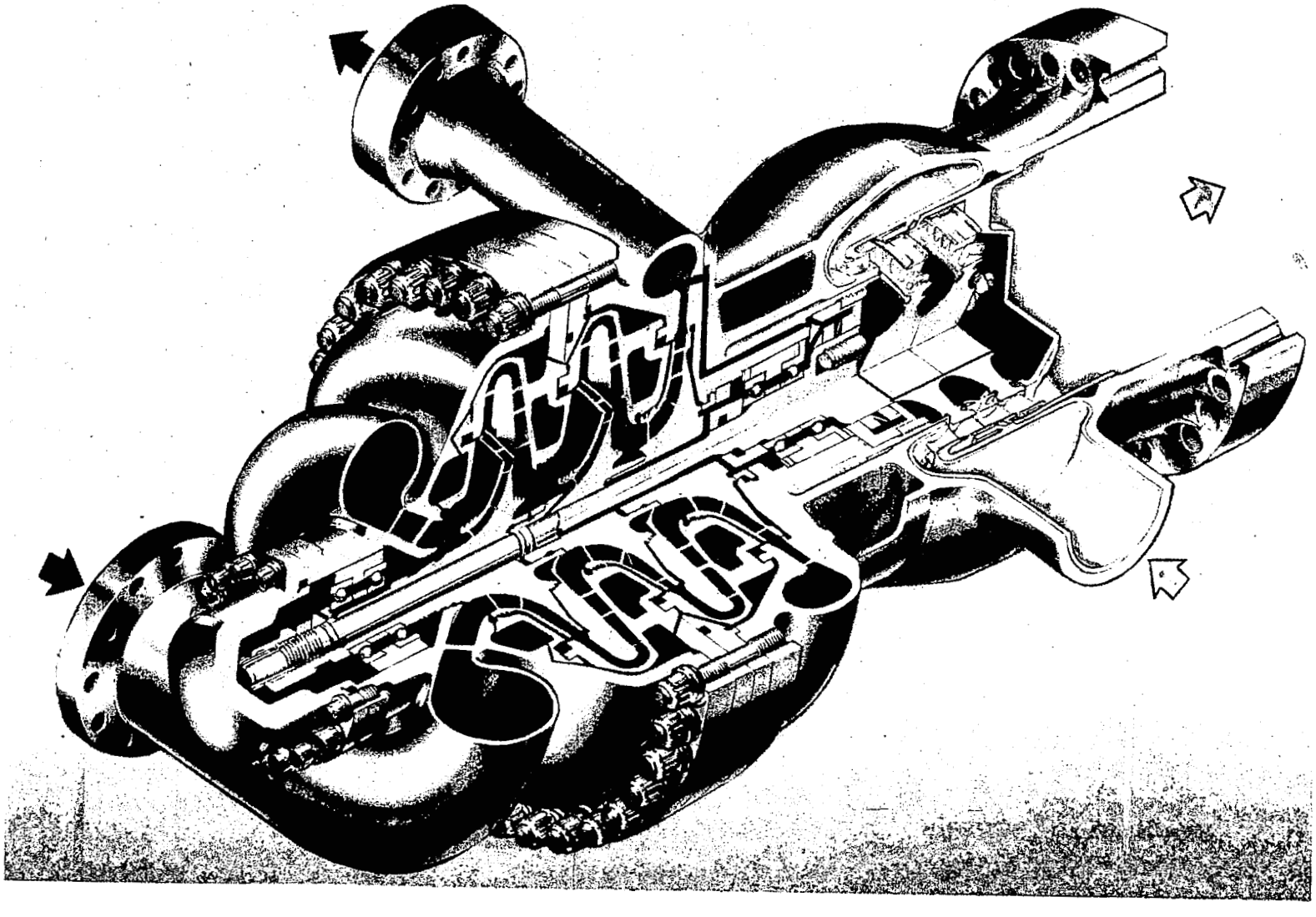

Mark 48-F LH_2 Turbopump

FOREWORD

The work herein was conducted from August 1973 to April 1976 by personnel from the Advanced and Propulsion Engineering and Engineering Test units at Rocketdyne, a division of Rockwell International, under Contract NAS3-17794. Mr. Robert Connelly, Lewis Research Center, was NASA project manager. At Rocketdyne Mr. Harold Diem, Program Manager, Mr. A. T. Zachary, Project Manager, and Mr. A. Csomor, Project Engineer, were responsible for the direction of the program.

Important contributions to the conduct of the program and to the preparation of the report material were made by the following Rocketdyne personnel:

Combustion Devices	Mr. R. F. Sutton
Turbomachinery	Mr. S. B. Macaluso
Turbomachinery	Dr. E. D. Jackson
Consultant	Dr. K. Rothe

CONTENTS

ILLUSTRATIONS

TABLES

SUMMARY

The objective of this program was to establish the technology for small, high-pressure, liquid hydrogen (LH_2) pumping capability. Turbopumps in this category are needed for applications in small, high-performance, reusable, versatile, staged-combustion rocket engines.

To accomplish the above objective, analysis and design effort was expended to produce specifications and shop drawings in sufficient detail to permit fabrication of test hardware. The design includes a three-stage centrifugal pump with radial diffusers and internal crossovers. Power to the pump is developed by an axial-flow, two-stage, reaction-type turbine, using the combustion products of LH_2 and liquid oxygen (LO_2). Rotor axial thrust control is provided by incorporating a self-compensating, double-acting balance piston as an integral part of the third-stage impeller rear shroud. The rotor is supported on a pair of ball bearings on each end. All bearings are cooled by recirculating LH_2 internally through them. A controlled-gap, shaft-riding seal is used to prevent turbine hot gases from entering the pump region. The nominal design speed of the rotor was established at 9947 rad/s (95,000 rpm).

Hardware for two turbopump assemblies was fabricated. Two types of impellers were included: (1) an integral impeller whose flow passages were formed by electrical-discharge machining (EDM), and (2) a split impeller which was fabricated by machining in two pieces, then welding to form the assembly. Only the integral impellers were utilized during the testing covered by this report.

A hot-gas generator was designed with a film-cooled body and an injector similar to the engine preburner to make maximum use of existing combustion technology. The gas generator was tested on LIMA stand in the Propulsion Research Area at Rocketdyne's Santa Susana Field Laboratory (SSFL) for a total of 15 tests resulting in acceptable hot-gas thermal gradients and satisfactory hardware condition.

The turbine was calibrated at Wiley Laboratories utilizing gaseous nitrogen (GN_2) as the driving medium. The output was measured with a torquemeter. The turbine efficiency was measured at 79% compared with a predicted design value of 75%.

The LH_2 turbopump assembly also was tested at LIMA stand of Rocketdyne's Propulsion Research Area. Ten tests were conducted on one turbopump assembly, accumulating a total time of 884 seconds. Liquid hydrogen was used as the pump fluid, and the turbine was propelled by ambient-temperature gaseous hydrogen (GH_2). The test speed ranged up to 9739 rad/s (93,000 rpm). Pump discharge pressures ranging up to 2883 N/cm^2 (4182 psia), and flowrates up to 0.032 m^3/s (509 gpm) were generated.

Analysis of the fluid dynamic data revealed that, at speeds below 8376 rad/s (80,000 rpm), the generated pump head was as predicted and the pump isentropic efficiency was slightly higher than predicted. At speeds approaching the design level, the performance of the pump first stage deteriorated somewhat, causing the overall head to fall below the predicted value. The data also disclosed higher-than-predicted temperatures for the coolant of both bearing sets.

The mechanical operation of the turbopump gave evidence of a basically sound design. The entire initial test series was performed on a single build, and the speed limitation of 9739 rad/s (93,000 rpm) was imposed only the by drive gas supply. No evidence of structural failure or detrimental rotor vibrations was present. Disassembly of the turbopump revealed only minor hardware discrepanices.

INTRODUCTION

System studies have been conducted to determine the feasibility of developing a reusable vehicle for performing future Air Force and NASA space maneuvering missions. These studies have shown that, over the thrust range of interest, high-pressure, staged-combustion-cycle engines offer the highest specific impulse and payload capability. A review of the vehicle and engine system study results indicates that a single-bell-nozzle, staged-combustion-cycle engine at 88,964 (20,000 pounds) thrust level is near optimum for the DOD and NASA mission requirements.

This program was initiated to provide the required hydrogen turbopump technology base for subsequent development of a high-performance, staged-combustion rocket engine.

Technology items of particular interest during the course of the current development program include fabrication of impeller passages by EDM; split impeller design and fabrication techniques; balancing of small, high-speed, multipart shafts; hydrogen-embrittlement protection; balance piston design and operation; high DN bearings; and assembly and measurement procedures for small turbopump assemblies. In addition, work was performed on concentric-element LO_2/LH_2 injectors.

The objectives of this program were to design, fabricate, and test a high-pressure LH_2 turbopump capable of meeting the performance requirements of the 88,964 N (20,000 pounds) thrust, staged-combustion-cycle engine; demonstrate its basic capability; and identify any areas where additional effort due to technology limitations is required to place a future engine program on a solid basis.

Rocketdyne has assigned the designation "Mark 48-F Turbopump" to the small, high-pressure, LH_2 turbopump design generated under this contract. The two terms will be used interchangeably through this report.

DISCUSSION

ANALYSIS AND DESIGN

ASE Engine Configuration

The objective of this program was to establish the technology base for small, high-pressure LH_2 pumping capability for application on the Advanced Space Engine (ASE). The basic performance parameters for the ASE have been established in a preliminary design task, the results of which are reported in Ref. 1.

A schematic of the ASE is presented in Fig. 1. It is a staged-combustion-cycle engine using LH_2 and LO_2 as propellants. The major components comprising the engine are two, low-pressure gas-driven boost pumps; two, high-pressure pumps; a preburner; a regeneratively cooled combustion chamber and nozzle; dump cooled nozzle extension; and valves.

The small, high-pressure LH_2 turbopump effort performed under this contract was directed toward establishing the technology for the main hydrogen turbopump.

Turbopump Requirements

The performance requirements for the Mark 48-F turbopump are listed in Table 1. The pump is required to deliver 2.74 kg/s (6.04 lb/sec) of LH_2 starting with an inlet pressure of 49 N/cm^2 (71 psia) provided by the low-pressure pump, to a discharge pressure of 3140 N/cm^2 (4560 psia). The propellant gas for the turbine is a mixture of free hydrogen and steam, resulting from the combustion of LH_2 and LO_2. The gas is provided at a temperature of 1033 K (1860 R) and an inlet pressure of 2360 N/cm^2 (3420 psia). The total gas flowrate available is 3.02 kg/s (6.66 lb/sec). The horsepower requirement of the pump is matched by adjusting the pressure ratio across the turbine. Since turbine pressure ratio has a strong influence on the attainable engine combustion pressure in a staged combustion cycle, it is to be maintained at the lowest possible level. As noted in Table 1, the mechanical operating requirements included multiple starts with long operating durations and potentially long coast times between operations.

The values noted in Table 1 deviate slightly from the requirements expressed in the original contract work statement. Refined computer runs of the engine balance indicated minor shifts in the required pump discharge pressure, turbine inlet temperature and pressure, as well as turbine hot-gas flowrate. The revised values were incorporated in the requirements with the NASA project manager's approval.

In addition to the performance criteria noted in Table 1, the contract work statement included certain ground rules relating primarily to the structural analysis and mechanical design of the turbopump. These ground rules are enclosed in Appendix A.

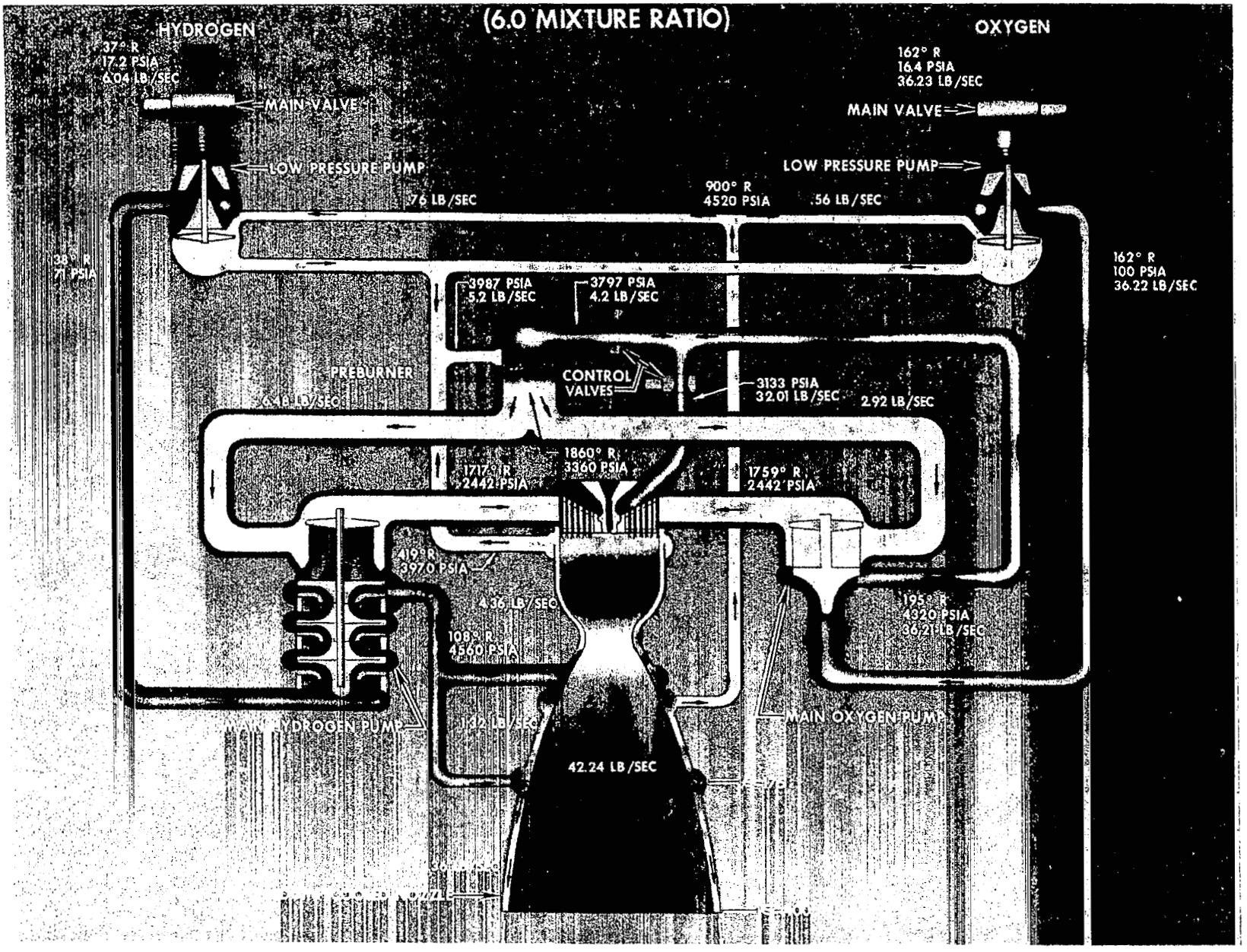

Figure 1. ASE System Schematic

TABLE 1. MARK 48-F TURBOPUMP NOMINAL DESIGN CONDITIONS

	SI Units	English Units
Pump		
Type	Centrifugal	
Propellant	LH_2	
Inlet pressure	49 N/cm^2	71 psia
Inlet temperature	21-23 K	38-41 R
Discharge pressure	3140 N/cm	4560 psia
Mass flow	2.74 kg/s	6.04 lb/sec
Number of stages	3	
Turbine		
Working fluid	O_2/H_2 combustion products	(H_2 x H_2O)
Inlet temperature	1033 K	1860 R
Inlet pressure	2360 N/cm^2	3420 psia
Pressure ratio	Minimum necessary to develop pump horsepower requirements	
Flowrate	3.02 kg/s	6.66 lb/sec
Number of stages	2	
Type	Full admission	

Turbopump

Capable of operation at pumped-idle conditions, i.e., approximately 5 to 10% full thrust

Off-design operation:	+20% Q/N at full thrust down to 30% Q/N at 20% N
Service life between overhauls:	*300 thermal cycles or 10 hours accumulated run time
Service-free life:	*60 thermal cycles or 2 hours accumulated run time
Maximum single run duration:	2000 seconds
Maximum time between firings during mission:	14 days
Minimum time between firings during mission:	1 minute
Maximum storage time in orbit (dry):	52 weeks

*Thermal cycle defined as engine start (to any thrust level) and shutdown.

Certain elements of the requirements noted above had a particularly significant impact on the technology requirements of the turbopump and the ensuing design configuration. In the area of the pump, the combination of low flowrate and high discharge pressure imposed a difficult impeller fabrication task because of the relatively narrow passages required compared with the outer diameter. The desire for high efficiency, compact packaging, and light weight placed the rotor speed into the 9423 to 10,470 rad/s (90,000 to 100,000 rpm) range, pushing bearing DN value to the 2.0×10^6 mm rpm limit noted in the Design Ground Rules (Appendix A). The bearing operation at high DN values in a turbopump installation as well as the dynamic behavior of the rotor at high speeds needed to be demonstrated.

Because of the high operating speed involved, the bearings would not be able to take an appreciable axial thrust load. This condition dictated that an axial thrust balance device be employed. The operating characteristics of such a device also required evaluation. In the turbine, the performance of a small turbine with a high-power density and low-pressure ratio (approximately 1.4) needed to be demonstrated.

From a structural consideration, the requirement for 300 thermal cycles was significant in that it established low-cycle fatigue criteria and eventually necessitated incorporating a liner in the turbine manifold to limit the maximum thermal gradients in structural walls.

Turbopump Description

The configuration of the Mark 48-F turbopump is shown in Fig. 2. The turbopump assembly requirements are established on Rocketdyne drawing RS009601E, a copy of which is included in Appendix B.

The pumping elements consist of three centrifugal impellers containing six full and six partial vanes, a radial diffuser after each impeller, and an internal crossover passage following the first- and second-stage diffusers. Liquid hydrogen is introduced to the pump and delivered from the pump through a scroll-shaped inlet and discharge, respectively. The pump end of the rotor assembly is formed by the impeller hubs, which are piloted relative to each other and maintained axially tight by a central tie bolt. The two pump crossovers are mounted on the pump through the externally accessible flanges. Although this feature results in additional external seal joints and weight, it facilitates measuring all significant interstage pressure levels. The cavities between the crossovers and the external housings are sealed from the main flow passages by axial flange seals, and they are vented to the pump inlet. Thus, the external flange seals are subjected to pump inlet pressure only, and should not pose a leakage problem. Internal recirculation around the impellers is minimized by step labyrinth seals in the front and rear shrouds. The seal lands are plated with silver to prevent hard metal-to-metal rubbing, and still facilitate maintaining close radial clearances.

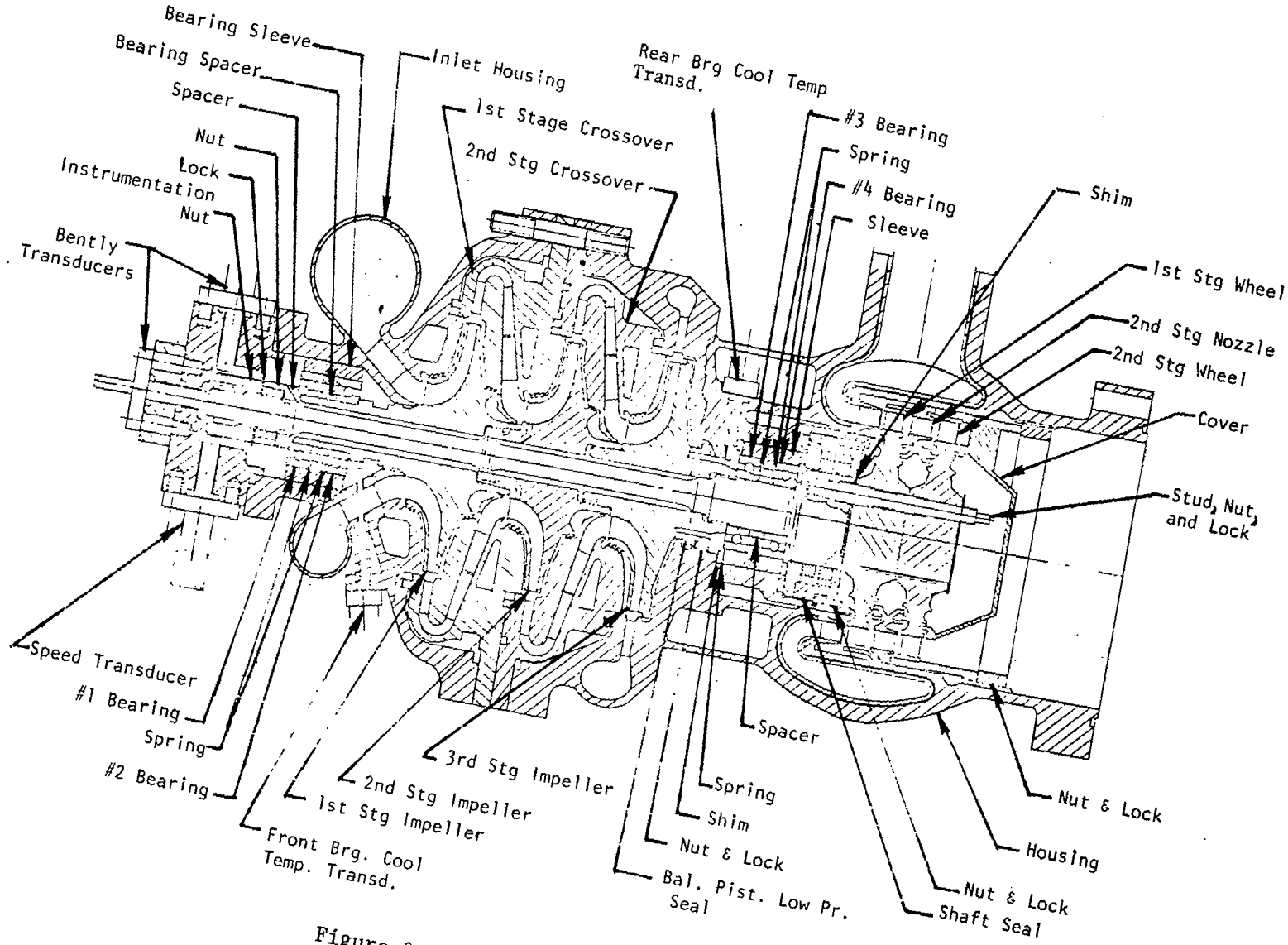

Figure 2. Mark 48-F Turbopump Assembly

The turbine is a two-stage reaction type with an overall pressure ratio of 1.443. Approximately 52% of power is developed in the first stage and 48% in the second stage. The wheels are attached to the shaft by three body-bound studs which also transmit the torque. Axial holes are incorporated in the disks to provide a path for the shaft seal leakage, which is used as a coolant. The downstream side of the second-stage wheel is covered with a shield to reduce heating effect of the exhaust gas on the disk. Low-cycle fatigue necessitates incorporating a sheet metal liner into the inlet manifold to reduce thermal gradients during start and cutoff. The liner is approximately 1.57 mm (0.062 inch) thick, and includes bleed holes to equalize the pressure on either side.

Axial thrust control is maintained by using a self-compensating balance piston incorporated in the back shroud of the third-stage impeller. To operate the balance piston, fluid from the discharge of the third-stage impeller is passed through a high-pressure orifice at the tip of the impeller, then through a low-pressure orifice located near the hub into the rear bearing cavity. From the bearing cavity, the fluid is returned to the inlet of the second-stage impeller through an annular passage between the shaft and the impeller hubs.

The rotor is supported radially by two pairs of duplex, angular-contact, 20 mm ball bearings, axially preloaded to prevent the balls from skidding. The rear bearings are retained axially through a spring-loaded cartridge so that they will also absorb transient axial rotor loads. Cooling of the pump end bearings is accomplished by bleeding LH_2 from the hub area between the first- and second-stage impellers, passing the fluid through an annular passage at the center of the first-stage impeller to the pump end, then in reverse direction through the bearings and back to the eye of the first-stage impeller. Cooling of the turbine end bearings is effected by bleeding coolant fluid from the pump discharge, introducing it to an area on the turbine side of the bearings, and allowing it to flow through the bearings where it joins the balance piston fluid and returns to the eye of the second-stage impeller. Additional coolant is provided for the rear bearings by the fluid which leaks through the pump side of the shaft seal.

To separate the pump and turbine regions, a controlled-gap, shaft-riding seal is employed. Since the pressure on the pump side of the seal is lower than on the turbine side, the middle of the seal is pressurized with LH_2 supplied from the pump discharge. In this manner, a positive flow of liquid hydrogen toward the turbine is ensured, and entry of hot gas into the pump is prevented. As noted above, the LH_2 which leaks through the shaft seal toward the pump is used to lubricate the bearings. The fluid which leaks to the turbine is used to cool the turbine disks.

Configuration Selection

The baseline configuration of the turbopump was defined by the Statement of Work as a three-stage, centrifugal pump powered by a two-stage, full-admission turbine. To select the design within that concept definition which best meets the objectives of the program, several alternatives were evaluated. The principal options and their effect on the turbopump are discussed in the following.

Number of Pump Stages. In accordance with the Statement of Work as noted above, the analysis and design effort was restricted to a three-stage pump. Prior to the actual contract effort, a two-stage version of the pump was evaluated by Rocketdyne, and the results of that study are included here for reference.

Table 2 presents a summary of the principal design parameters generated in the preliminary analysis of the two-stage pump. For comparison, the values obtained for the three-stage configuration are included.

The two-stage concept was attractive from the standpoint that it offered the possibility of a simpler design, fewer number of parts, and lower cost. On the other hand, it was encumbered with three major disadvantages. Producibility of the shrouded impellers presented difficulties in view of the small discharge width, 2.0 mm (0.079 inch), and relatively large tip diameter, 12.19 cm (4.8 inches). Furthermore, the tip speed of the impeller was very high, 640 m/s (2100 ft/sec), pushing the limits of the available material strength levels. Finally, because of the lower-stage specific speed at which a two-stage unit operates, the attainable efficiency was lower (53.4%). With the three-stage configuration, several potentially difficult aspects of the design were alleviated and better performance was obtained; therefore, it represents a more advantageous approach.

Speed Selection. The primary hydrodynamic coefficients, impeller tip speed, and rotational speed were approximately the same for the configurations under practical consideration. Values for these parameters could be selected for the initial iteration before detail design features were fixed. The head coefficient value ($\psi = 0.576$) for the impeller was selected to obtain high efficiency and to ensure system stability. Once the stage head coefficient was selected, the required impeller tip speed was fixed by the following relationship:

$$u_2 = \left(\frac{Hg}{\psi}\right)^{1/2}$$

where

u_2 = impeller tip speed

g = gravitational acceleration

ψ = stage head coefficient

H = head required per stage to deliver the specified discharge pressure

The desired impeller tip speed value can be attained at several rotor speed levels by selecting an appropriate tip diameter. The speed range investigated for this application extended from 7853 to 13,088 rad/s (75,000 to 125,000 rpm). Within the speed range studied, the stage specific speed varied from

$$0.20 \text{ to } 0.33 \ \frac{\text{rad/s } (\text{m}^3/\text{s})^{1/2}}{(\text{J/kg})^{3/4}} \quad (550 \text{ to } 900 \text{ rpm gpm}^{1/2}/\text{ft}^{3/4}).$$

TABLE 2. COMPARISON OF TWO- AND THREE-STAGE PUMP CHARACTERISTICS

	Two Stage	Three Stage
Rotor Speed	10,470 rad/s (100,000 rpm)	9950 rad/s (95,000 rpm)
Impeller Tip Width	2.00 mm (0.079 inch)	3.81 mm (0.150 inch)
Impeller Tip Diameter	12.19 cm (4.8 inches)	10.31 cm 4.058 inch)
Impeller Tip Speed	640 m/s (2100 ft/sec)	513 m/s (1683 ft/sec)
Stage Specific Speed	$\left(500 \frac{\text{rpm}\sqrt{\text{gpm}}}{\text{ft}^{3/4}}\right)$	$\left(694 \frac{\text{rpm}\sqrt{\text{gpm}}}{\text{ft}^{3/4}}\right)$
Pump Horsepower	2072 kW (2780 hp)	1896 kW 2543 hp)
Pump Overall Efficiency	53.4%	58%

These values were substantially below the specific speed value that results in the maximum attainable efficiency for centrifugal pumps; consequently, the pump efficiency increased with higher values of speed. Thus, from the standpoint of efficiency, the highest possible speed was desirable. With higher speeds, the impeller diameter decreased and the tip width increased, which was desirable from a weight/envelope and producibility consideration as well. The upper speed limit was defined by the DN (diameter, mm x speed, rpm) value of the turbine end bearing, which reached the maximum specified in the Statement of Work ($DN_{max} = 2 \times 10^6$) at 10,470 rad/s (100,000 rpm). Subsequently, the speed was reduced to a nominal design value of 9946 rad/s (95,000 rpm) to satisfy the h0-hour life requirement with the turbine rotor blades which could not be met at the higher speed level.

Pump Inlet Type. The radial-entry, volute-type inlet configuration of the pump was selected to optimize engine packaging. It was anticipated that the low-pressure pump will have a scroll-shaped volute with a radial discharge, and that the high-pressure fuel turbopump will be mounted on the engine with pump inlet side down. Under these conditions, the fluid is transferred from the low-pressure pump to the high-pressure pump most efficiently, both from the standpoint of fluid friction and engine weight, with a radial inlet on the high-pressure pump.

A volute-type inlet was used to provide prewhirl at the first-stage impeller inlet. The impeller inlet prewhirl permitted a larger impeller discharge blade angle for reduced stress as well as a reduced inlet relative velocity for increased impeller efficiency. The volute-type inlet provided low losses, permitted the bearings to be located outboard of the impeller inlet, and resulted in engine installation flexibility.

Impeller Type. The use of shrouded versus open-face impellers was evaluated. Open-face impellers are easier to fabricate and are capable of higher tip speeds; however, the low flowrates bring about a very low impeller blade height in this turbopump. As a result, the clearance between the impeller vanes and housing would have to be held impractically close to maintain high performance. Furthermore, small changes in the axial position of the rotor would bring about large shifts in pump performance. In constrast, with a shrouded impeller, there is no need to hold the axial clearance close, and performance is independent of rotor position. Despite the fact that the impeller hub had to be longer to carry the shroud centrifugal loads and fabrication was more difficult, performance considerations dictated that shrouds be used. An important side benefit of adding the shrouds was that the stiffness of the impeller was increased which, in turn, reduced the relative deflection in the balance piston. This was of particular significance because of the high-pressure loads involved.

Diffuser Type. The use of radial-vaned diffusers as opposed to an open volute with one or two tongues was evaluated. The radial-vane configuration was selected for three reasons: (1) by reducing the velocity of the fluid in the volute to approximately one-half of the impeller discharge velocity, fluid friction losses, which are proportional to velocity squared, were reduced; (2) the pressure around the periphery of the impeller was more uniform with

a vaned diffuser, therefore the radial loads were smaller; and (3) the diffuser vanes provided an efficient tie for the pressure vessel formed by the volute walls, thereby reducing the housing wall thickness requirement.

Turbine Orientation. The comparative effect of orienting the turbine flow toward the pump or away from the pump was analyzed from axial thrust, performance, and structural considerations. The pump or turbine performance was not affected by turbine flow direction, but there was a significant effect on net total thrust. The axial thrust of the selected design could be balanced satisfactorily only if the turbine flow was directed away from the pump. From a mechanical and structural standpoint, it was found that the least complicated and most economical design, from cost and weight standpoint, could be obtained by supporting the first-stage nozzle on the pump housing and orienting the flow away from the pump. This design had the advantage that inlet and exhaust manifolding was not an integral part of the critical working components of the turbine. As a result, the manifolding could be modified to accommodate any future engine packaging needs without affecting either the fluid-dynamic or structural behavior of the turbine. The turbine-to-pump housing connection was made identical to the visualized flightweight design. This way, all thermal conditions that may influence flight design operations are duplicated in this technology task.

Pump Hydrodynamic Analysis

Pump Inlet Design. As noted above, the pump inlet configuration was strongly influenced by the Advanced Space Engine (ASE) design layout, which resulted in optimum packaging with a scroll-shaped inlet. A scroll-shaped inlet can be accommodated either with an open-volute-type approach, or one in which vanes are included to provide structural support and guidence to the flow. The latter concept was selected because it presents a means for imparting prewhirl to the fluid entering the first-stage impeller. Prewhirl, in turn, facilitates a larger impeller discharge blade angle, which is desirable from the standpoint of producibility.

Figure 3 shows the dimensions of the leading and trailing edges of the inlet cascade. As already mentioned, these vanes are also needed for structural reasons. Twenty percent of the volume containing the vanes is needed to satisfy stress requirements. This sets the vane thickness. Figure 4 shows the vane system resulting in an actual metal volume of 20.7%. Figure 5 shows the vane angle variation, and Fig. 6 shows the area variation along the flow path from A to B (Fig. 1).

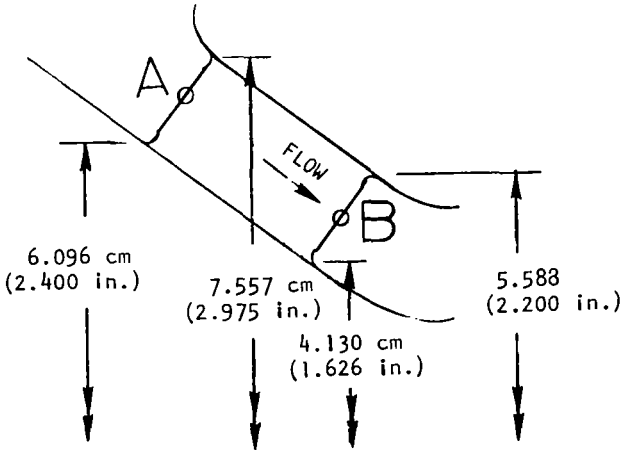

Figure 3. Pump Inlet Vane

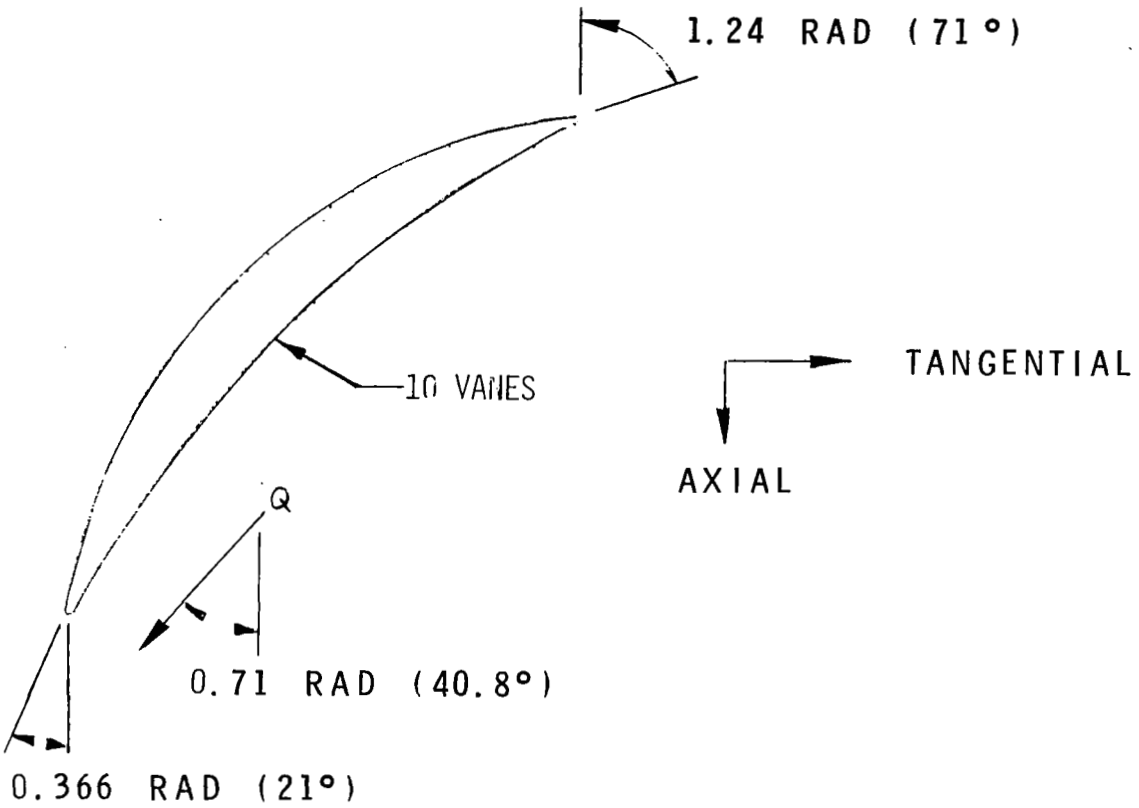

Figure 4. Mark 48-F Pump Inlet Vane Configuration

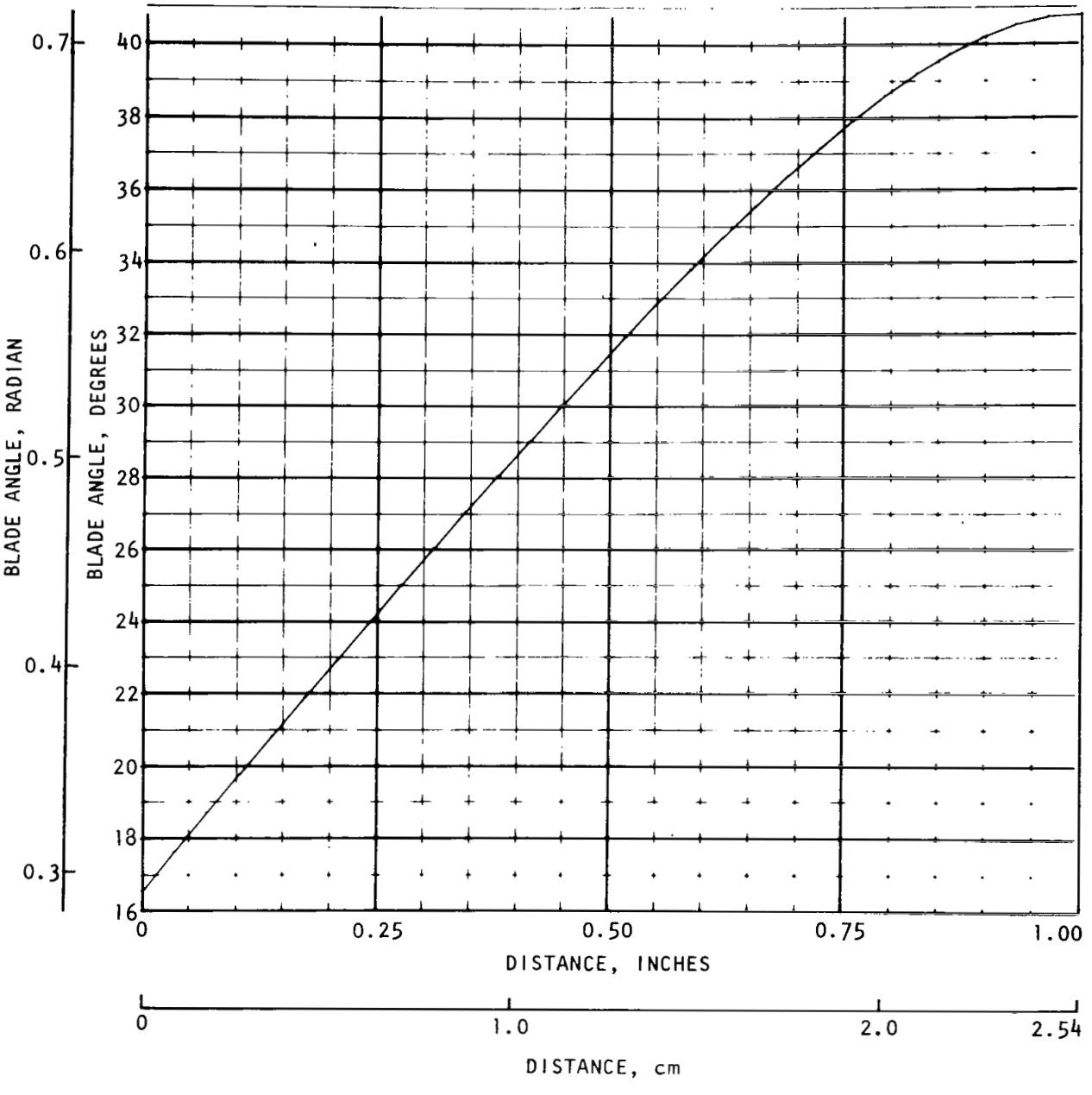

Figure 5. Mark 48-F Pump Inlet Vane Angle Variation

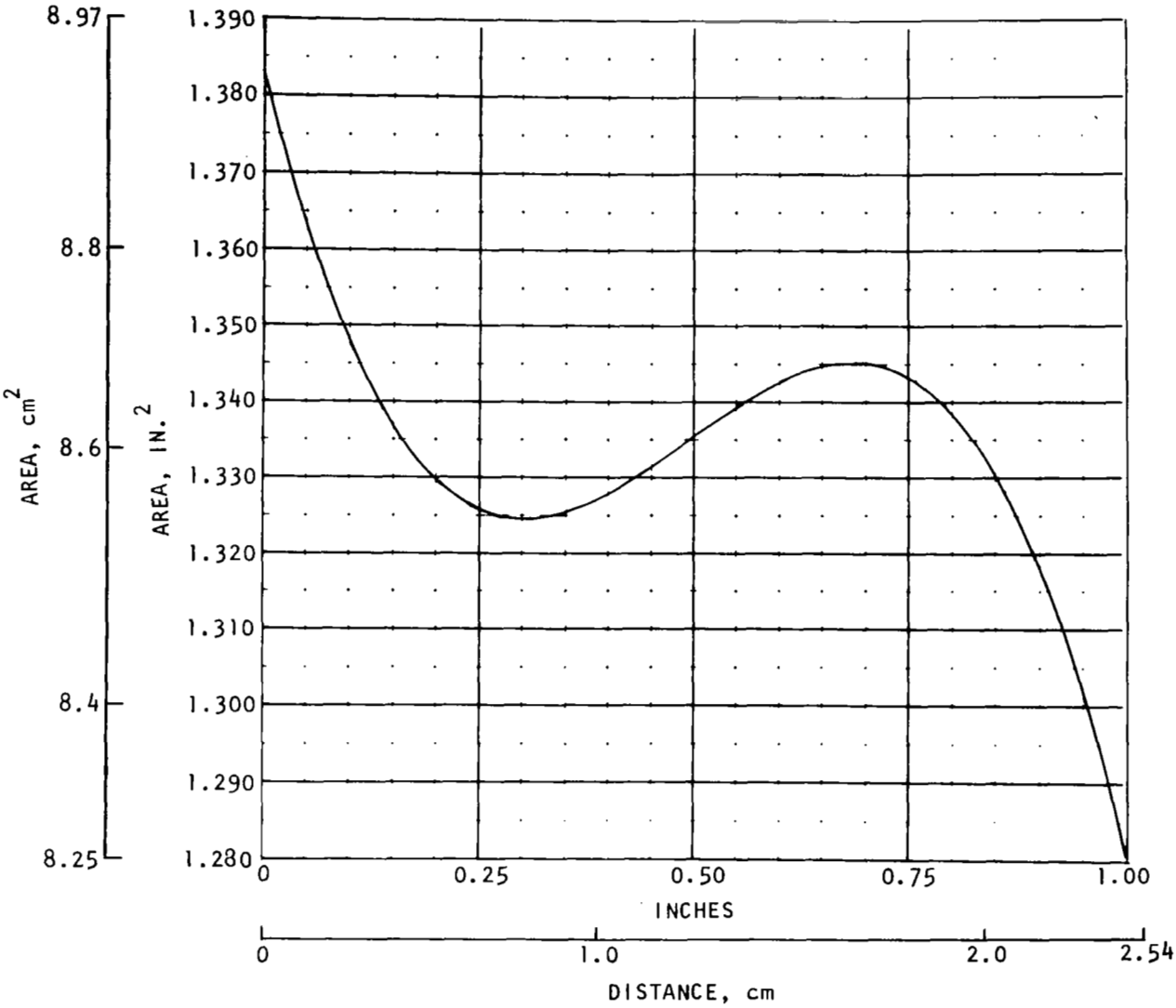

Figure 6. Mark 48-F Pump Inlet Variation at Guide Vanes

Impeller Design. The required isentropic stage headrise to satisfy the discharge pressure of 3144 N/cm^2 (4560 psia) is 153,000 J/kg (51,334 feet). With an operating speed of 9947 rad/s (95,000 rpm) and a delivered flowrate of 0.0396 m^3/s (627.5 gpm) the stage specific speed is 695. Since the speed cannot be increased due to bearing and turbine limitations, the only way to optimize efficiency is to use a high head coefficient. However, producibility has in this case an overriding influence.

To obtain a high strength/weight ratio, titanium was selected as the impeller material. The technology exists to produce complex shrouded titanium impellers by casting; however, the fracture toughness of such a casting at LH_2 temperatures is highly suspect. Other approaches to producing a complex shrouded impeller, such as diffusion bonding and powder metallurgy, would require an extensive and expensive development effort that was not within the scope of this program. As a result, the decision was made to fabricate the impellers by either pantographing or electrical discharge machining (EDM). Both of these means impose a limitation on the number of blades to be used as well as the discharge angle and wrap angle.

For a high head coefficient, a large number of blades is desirable. Strictly from a hydrodynamic point of view, the optimum impeller would have contained six full blades, six partial blades, and a second set of 12 partial blades at the discharge (6 + 6 + 12), with a discharge angle of 0.52 radians of (30 degrees). This would have yielded a head coefficient of approximately 0.65 (Fig. 16 of NASA Report SP 8109). Such an impeller, however, cannot be manufactured by the methods selected above. Producibility required the number of blades to be reduced to 6 + 6 with a discharge blade of 0.65 radian (37.5 degrees). The flow range is slightly reduced (Fig. 7) and, due to the lower number of blades, a head coefficient of approximately 0.58 can be expected. This reduces the obtainable efficiency because the impeller diameter increases.

Impeller Inlet. The impeller inlet diameter must be selected so that the required suction specific speed lies within the range of available experience. Due to the size, however, the producibility of the impeller has a major influence. To obtain sufficient NPSH margin to ensure that the pump meets the suction requirements, the inlet diameter should be as large as possible. Producibility, however, sets a limit since, by increasing the inlet eye diameter, the blade angle becomes flatter. As a result, machining becomes more difficult. The hub diameter at the impeller inlet was established as 3.1 cm (1.22 inches), the minimum value allowed by mechanical design considerations. The eye diameter was determined as 4.83 cm (1.90 inches) after a study in which hydrodynamic goals and producibility limitations were reconciled. To assess the required impeller suction specific speed, the following approach was taken: It was assumed that the required impeller NPSH is equal to 4 x $cm^2/2$ g. The factor 4 is selected to account for the relatively thick impeller blade leading edge, which is not shaped in accordance with the rules of inducer leading-edge design. Taking the calculated leakage flow into account, the axial inlet velocity is 44.7 m/s (146.5 ft/sec) which results in a required NPSH of

$$NPSH_{req} = 3981 \text{ J/kg}$$
$$= 406 \text{ m (1332 feet)}$$

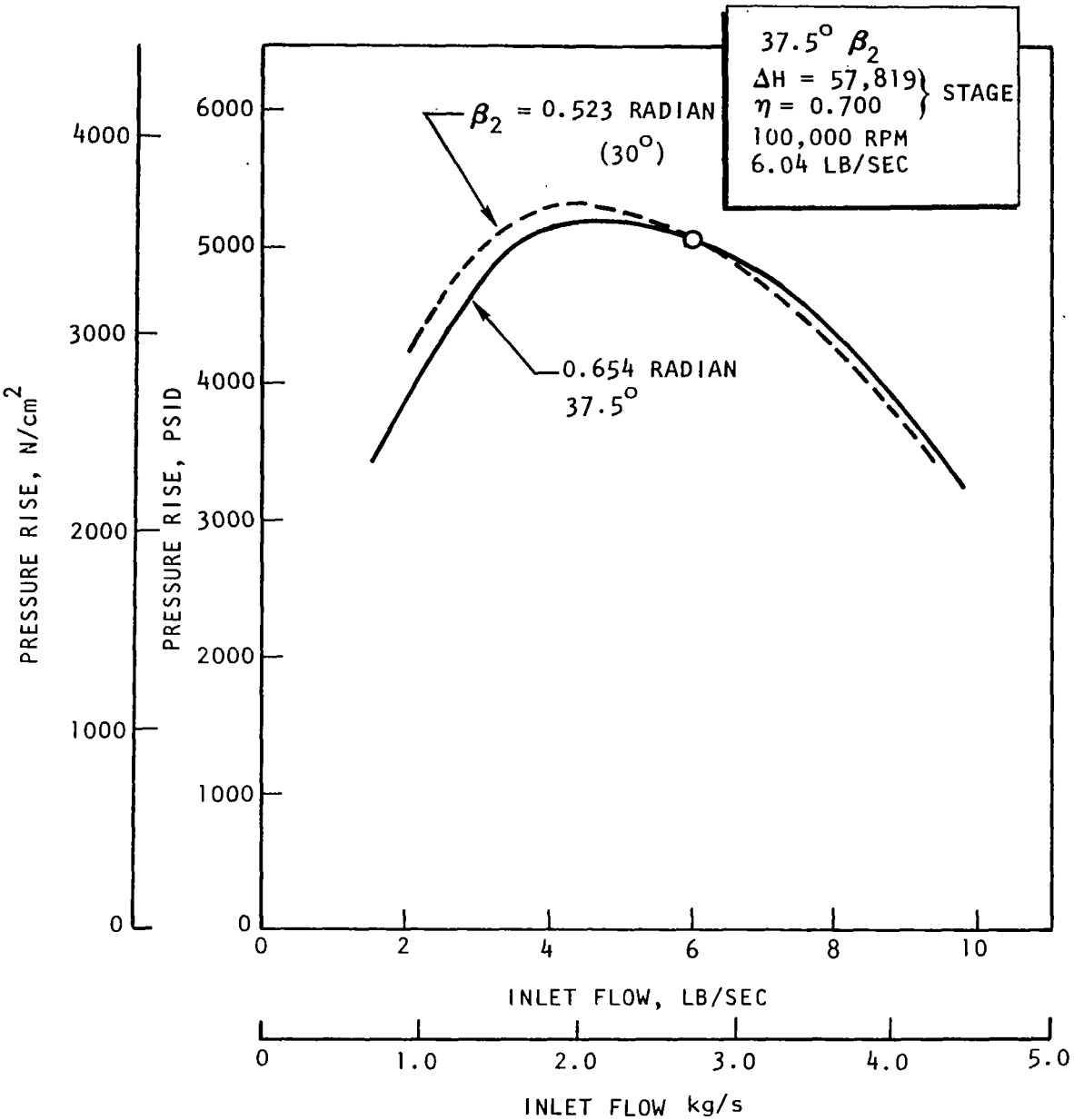

Figure 7. Mark 48-F Head-Flow Characteristics With 0.523 and 0.654 Radian (30 and 37.5 degrees) Impeller Discharge Angles

Impeller Blading. With inlet and discharge blade angles established, the major concern was to obtain a blade shape which would result in an acceptable velocity distribution and which could be manufactured. As stated above, the 0.65 radian (37.5 degrees) discharge angle and the tip width of 3.81 mm (0.15 inch), is acceptable. The question, however, still remains how much wrap angle (θ) can be incorporated. From the manufacturing point of view a small wrap angle is desired, from the hydrodynamic point of view a larger one. The lower limit of θ is dictated by the blade loading. Therefore, several blade designs were evaluated with the result that a wrap angle of 2.4 radian (135 degrees) was selected for the full blades and 0.9 radian (52 degrees) for the partial. This satisfies both manufacturing and hydrodynamic considerations.

Figure 9 shows the blade thickness distribution. Fluid velocity relative to the impeller blades at the inner and outer stream tubes are given in Fig. 10 and 11, and pressure loading profile is indicated in Fig. 12. Cross sections of the impeller flow passage, with wrap angle distributions for the full and partial vanes, are included in Fig. 13 and 14.

Crossover Design. The crossover design is based on the results of an experimental program that was conducted for the SSME high-pressure turbopump. The crossover design which yielded the highest efficiency used a radial diffuser followed by a 3.14-radian (180 degrees) vaneless turn. After the turn, the flow entered a tandem diffuser (two blade rows guiding the flow to the entrance of the following stage). Figure 8 shows the concept schematically.

The first step, therefore , was to define the diffuser which follows the impeller and which is identical for all three stages. The diffuser inlet diameter was set at 11 cm (4.36 inches), which results in a gap of 3.8 mm (0.15 inch) between impeller discharge and diffuser inlet. This value represented an acceptable compromise between the tendency to minimize the gap to maintain low hydrodynamic losses and the desire to maintain a sufficiently large clearance to avoid large pressure fluctuations on the impeller vanes.

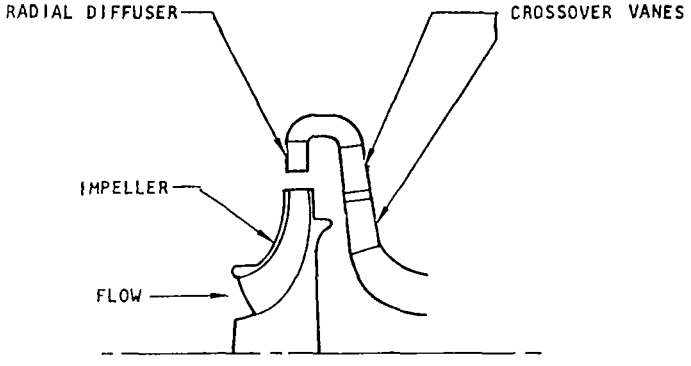

Figure 8. Radial Diffuser and Crossover

The diffuser is also a structural member requiring approximately 40% metal volume. After several iterations, this condition was satisfied by using 11 vanes with a discharge diameter of 13.9 cm (5.48 inches).

The inlet and exit width of the diffuser is set at 3.8 mm (1.5 inch). The flow leaves the impeller at an angle of 0.14 radian (8.2 degrees) from tangential, resulting in a c_u component of 367 m/s (1204 ft/sec) and a c_u component of 53 m/s (174 ft/sec). Based on these flow conditions, the diffuser passage is calculated using Rocketdyne's diffuser program. The results are shown in

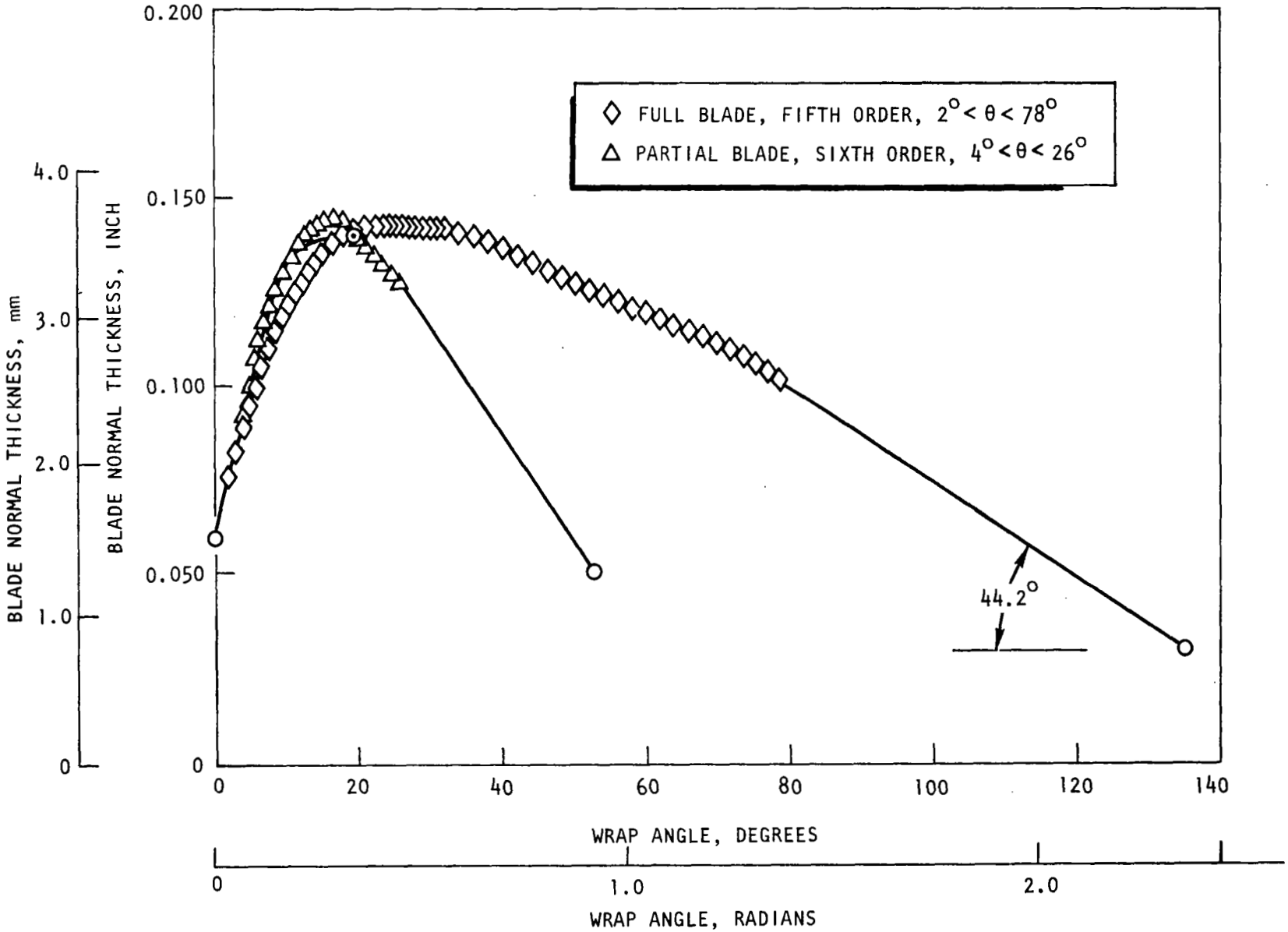

Figure 9. Mark 48-F Fuel Impeller Vane Thickenss Distribution

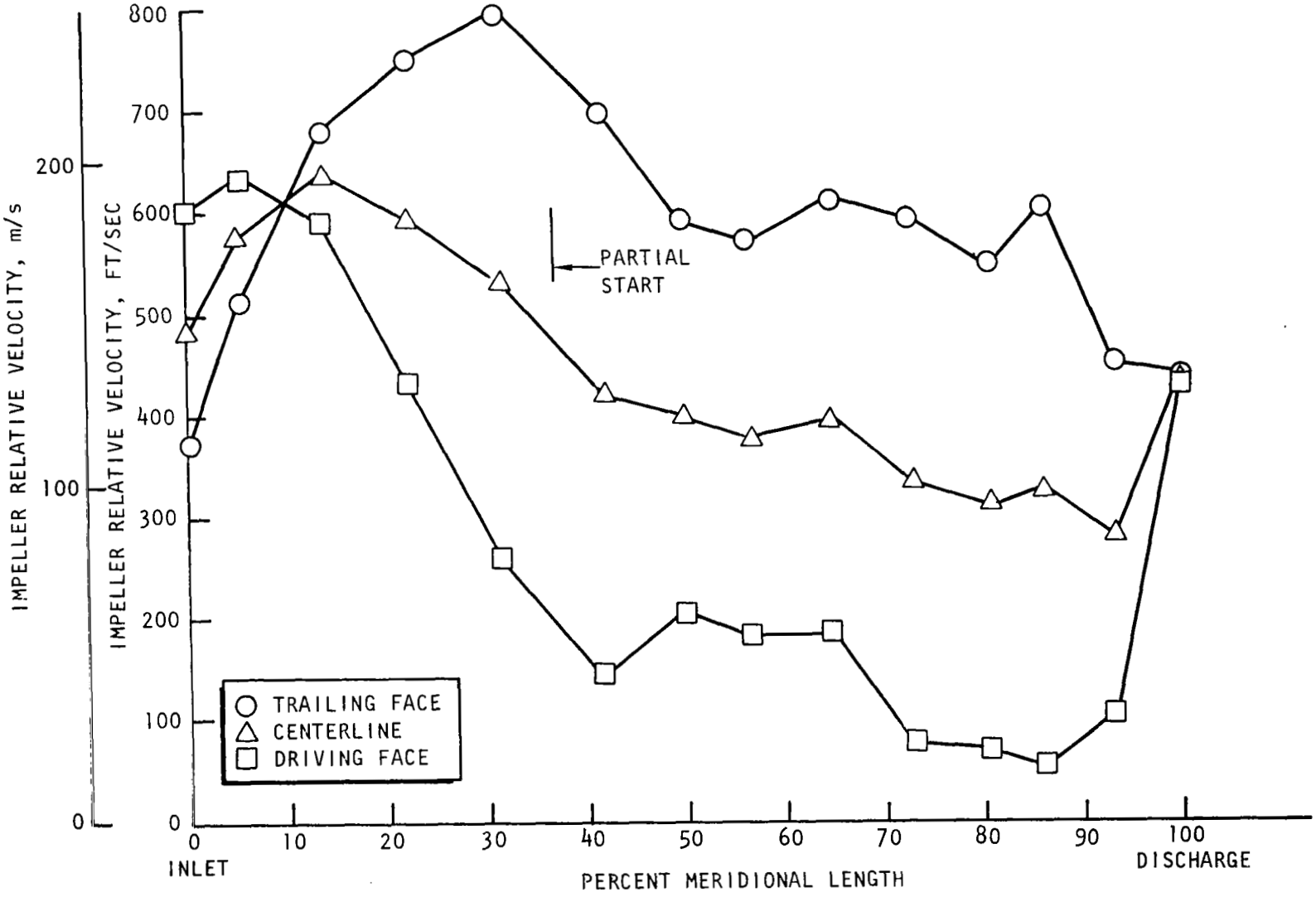

Figure 10. Fuel Impeller Relative Velocities, Inner Streamtube

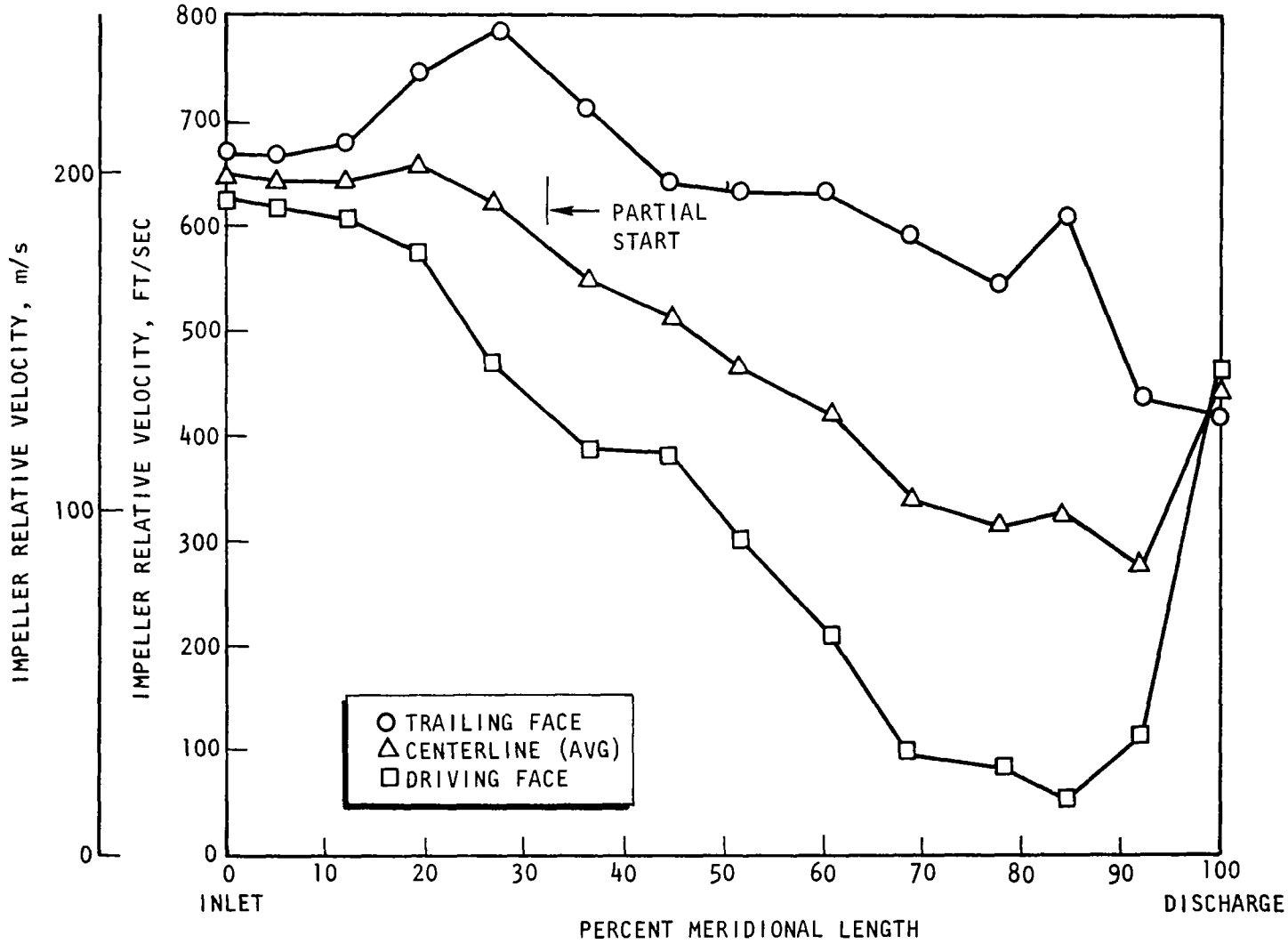

Figure 11. Fuel Impeller Relative Velocities, Outer Streamtube

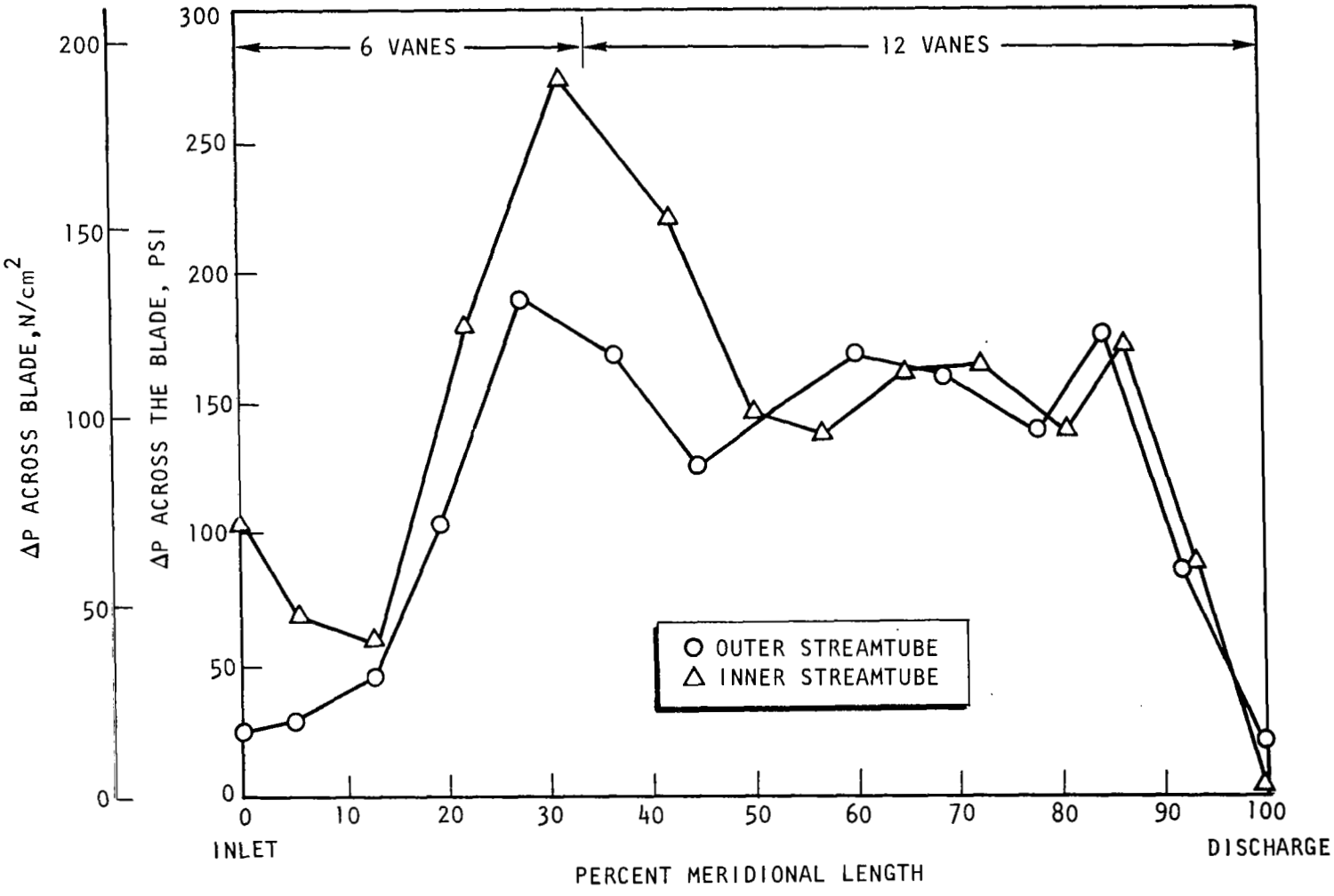

Figure 12. Fuel Impeller Pressure Loading

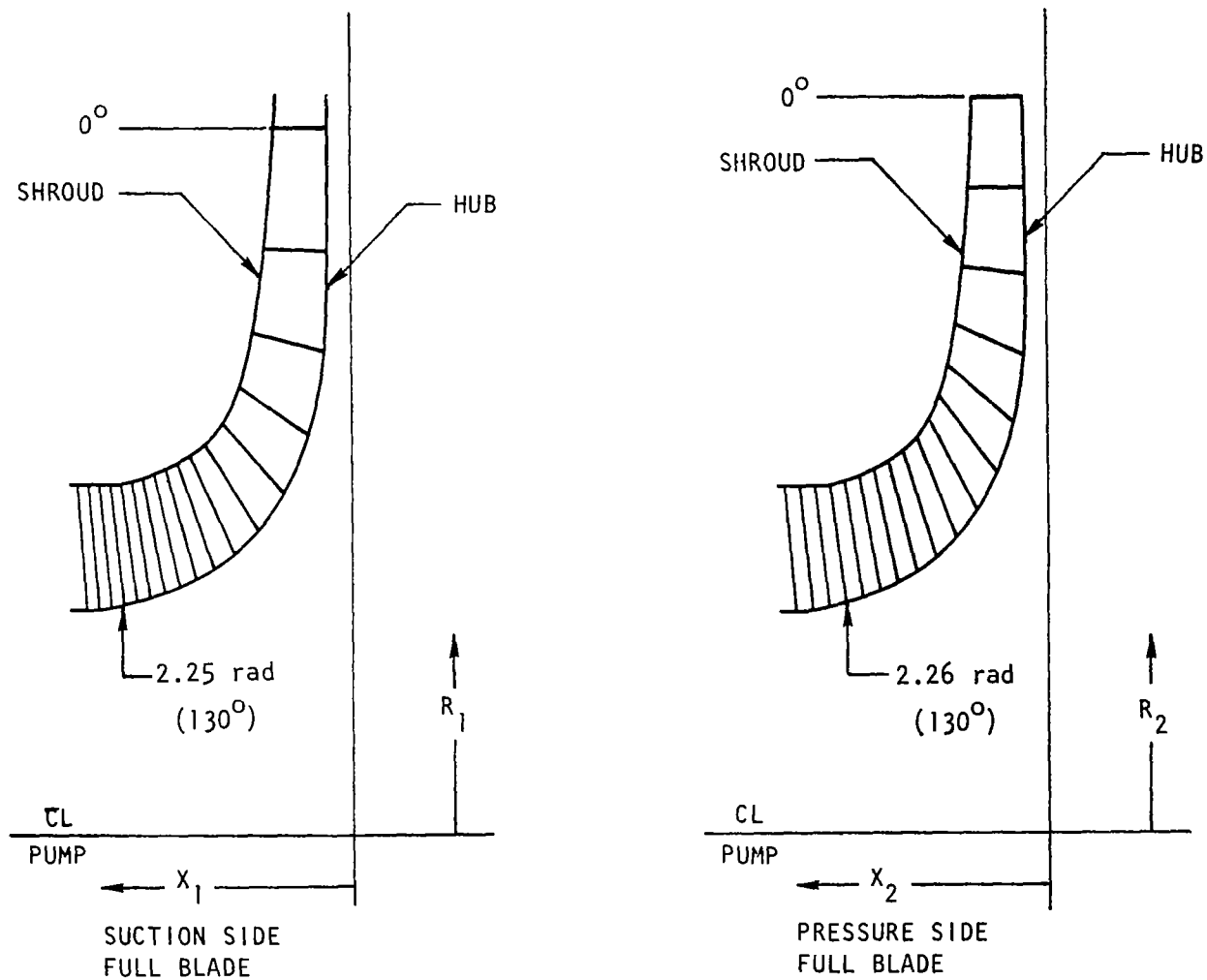

Figure 13. Impeller Cross-Section Layout With Full Blade Wrap Angles

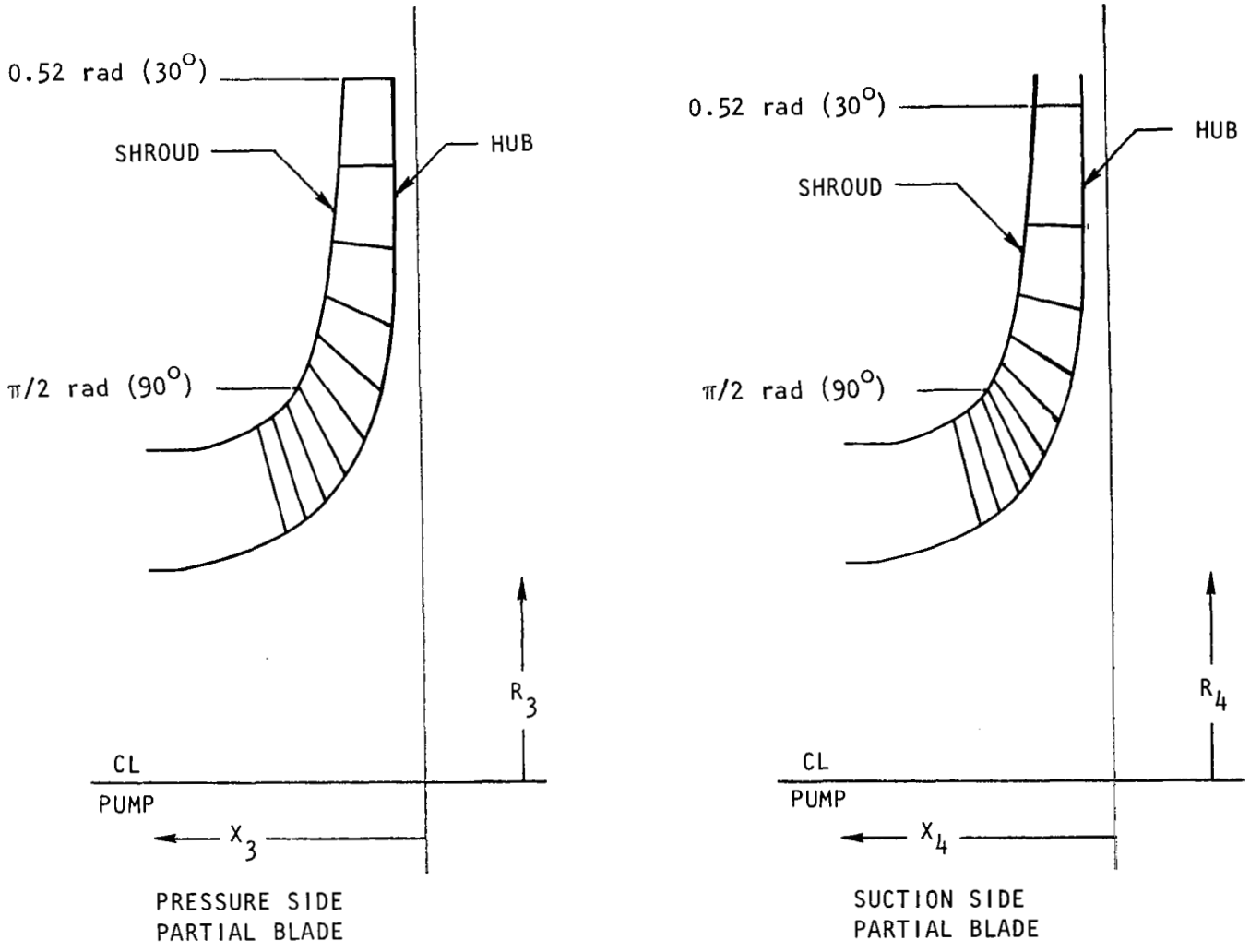

Figure 14. Impeller Cross-Section Layout With Partial Blade Wrap Angles

Fig. 15 through 18. Figure 15 shows the vane angle variation along the diffuser passage, and Fig. 16 presents the area. Figure 17 shows the pressure distribution on the vane suction and pressure side, and Fig. 18 illustrates the diffuser cascade.

The radial vaned diffuser is followed by a vaneless turning passage in which the radial direction of the flow is turned 2.8 radions (162 degrees) to guide the fluid inward toward the eye of the next impeller. The turning passage is followed by two rows of vanes, where the fluid is further diffused. At the exit from the final row of blades, the fluid is directed at an angle such that the impeller blade angles established for the first stage can be used for all stages. The number of vanes in each of the two blade rows is set at 17. The turning in the first row is 0.339 radions (19.4 degrees) which, with a solidity of 2.08 results in a diffusion factor of 0.589. The turning in the second row is set to 0.72 radian (41.3 degrees) which, with a solidity of 1.53 results in a diffusion factor of 0.603.

Volute. The volute which follows the diffuser of the third stage is folded over away from the turbine. This type is selected because it results in a stable secondary volute flow pattern and, consequently, an optimum efficiency.

The calculated velocities at the third-stage diffuser exit are:

Circumferential velocity	C_u	= 183 m/s (600 ft/sec)
Radial velocity	C_m	= 41 m/s (134 ft/sec
Absolute velocity	C	= 187 m/s (615 ft/sec)
Velocity direction		= 0.219 radian (12.6 degrees)

The volute area distribution was calculated in 0.35 radian (20 degrees) wrap angle intervals, using a recovery factor of 0.70 and a blockage factor of 0.70. The resulting area distribution is shown in Fig. 19.

Pump Performance Prediction. The overall pump headrise and efficiency was calculated based on the isentropic enthalpy rise obtained from actual properties.

The isentropic headrise is defined as:

$$H_{is} = J \times \Delta h_{is}$$

where

Δh_{is} = Isentropic headrise from actual fluid properties, J/kg (Btu/lb)

J = Mechanical equivalent of heat (1.0 in SI units, 778 in English units)

H_{is} = Headrise, J/kg (ft-lb/lb)

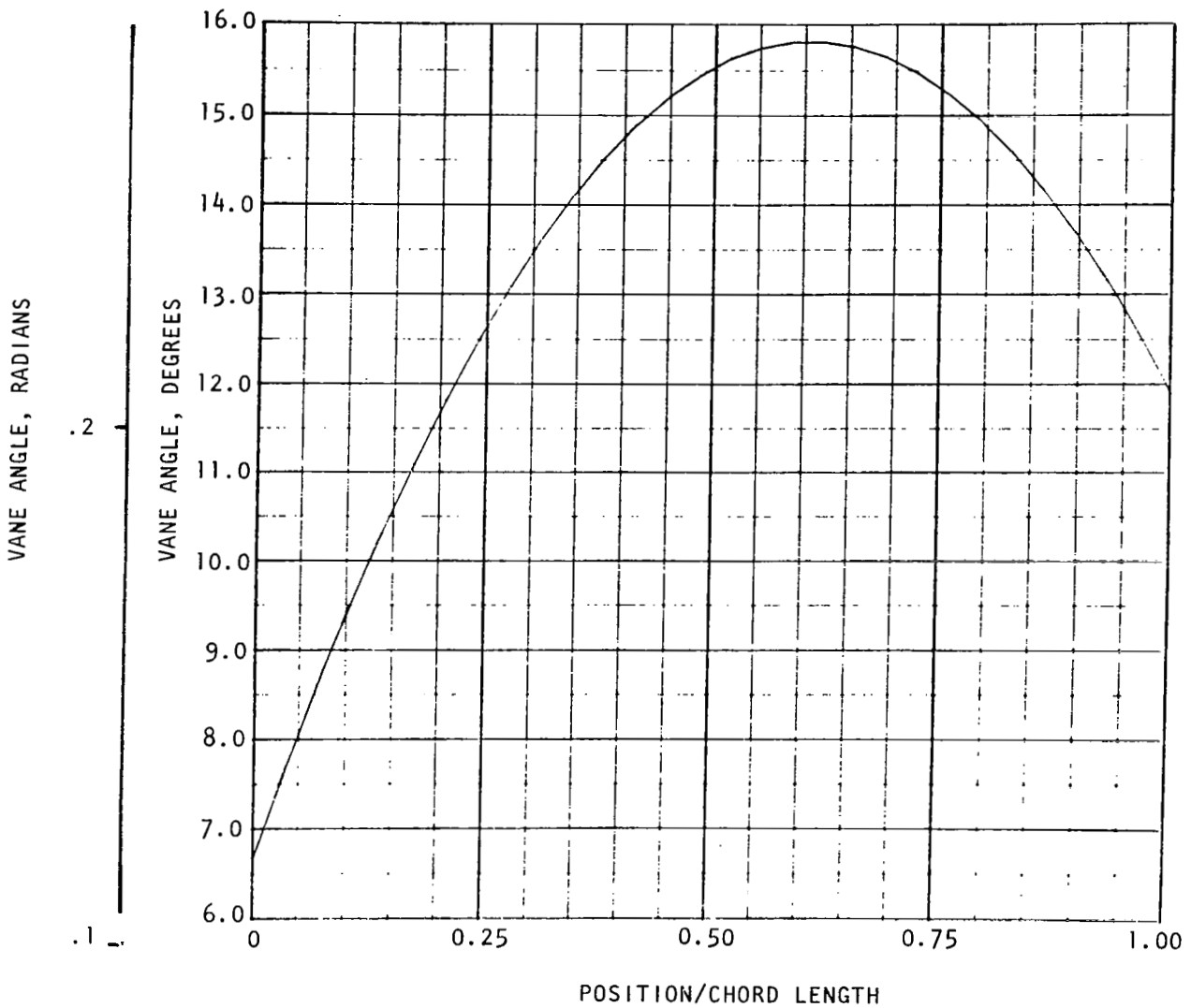

Figure 15. Mark 48-F Pump Diffuser Vane Angle

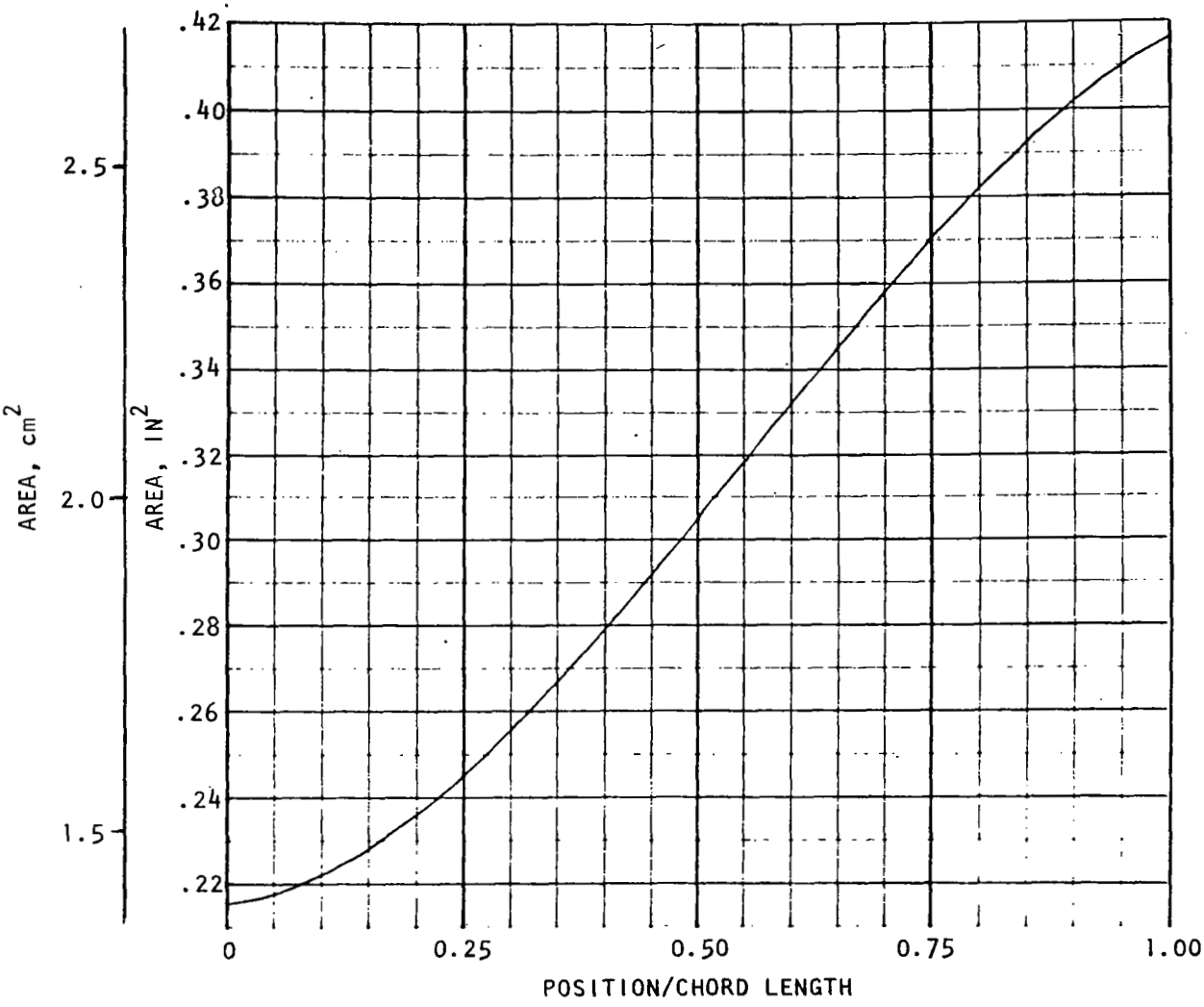

Figure 16. Mark 48-F Pump Diffuser Area

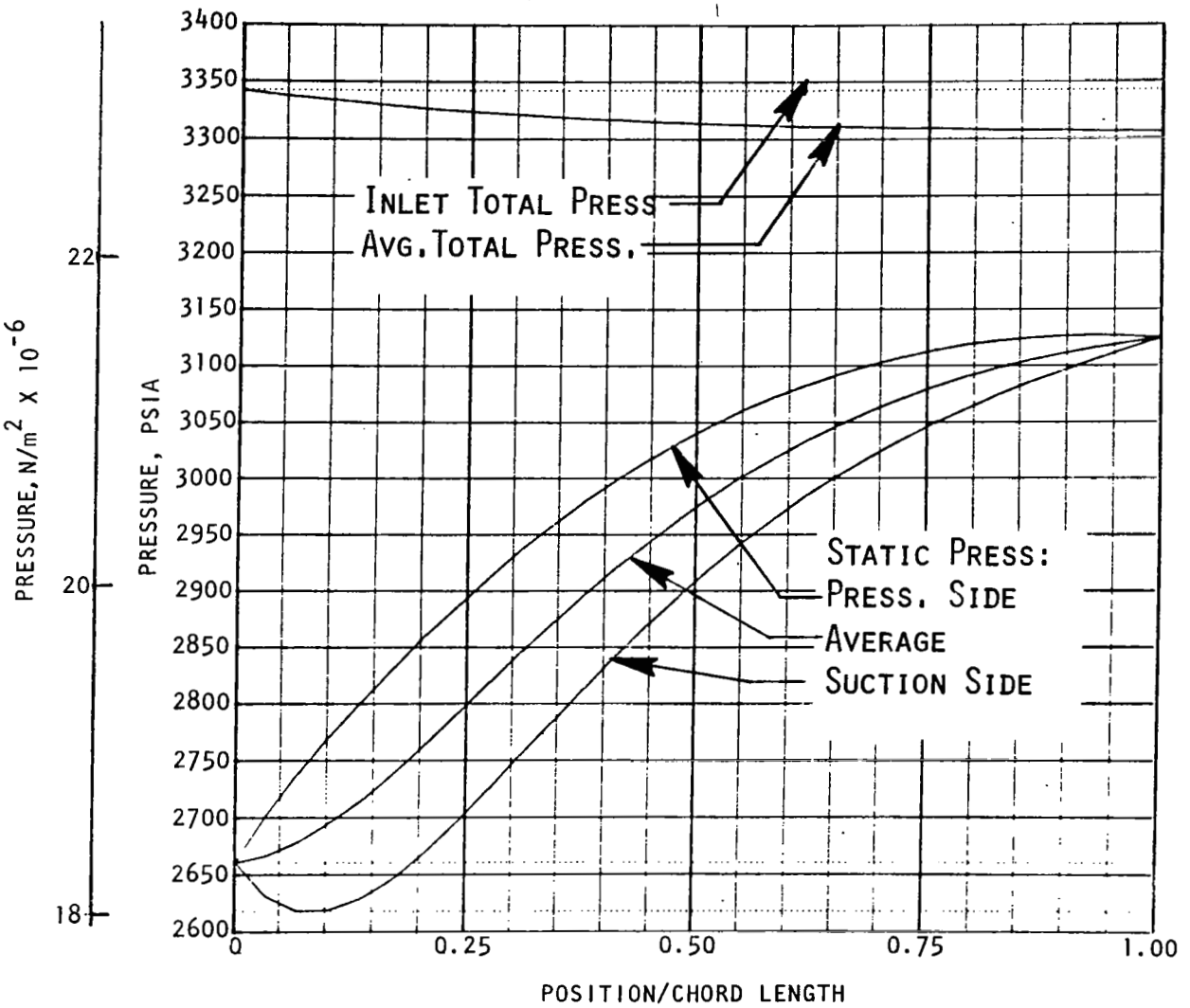

Figure 17. Mark 48-F Pump Diffuser Pressure Diagram

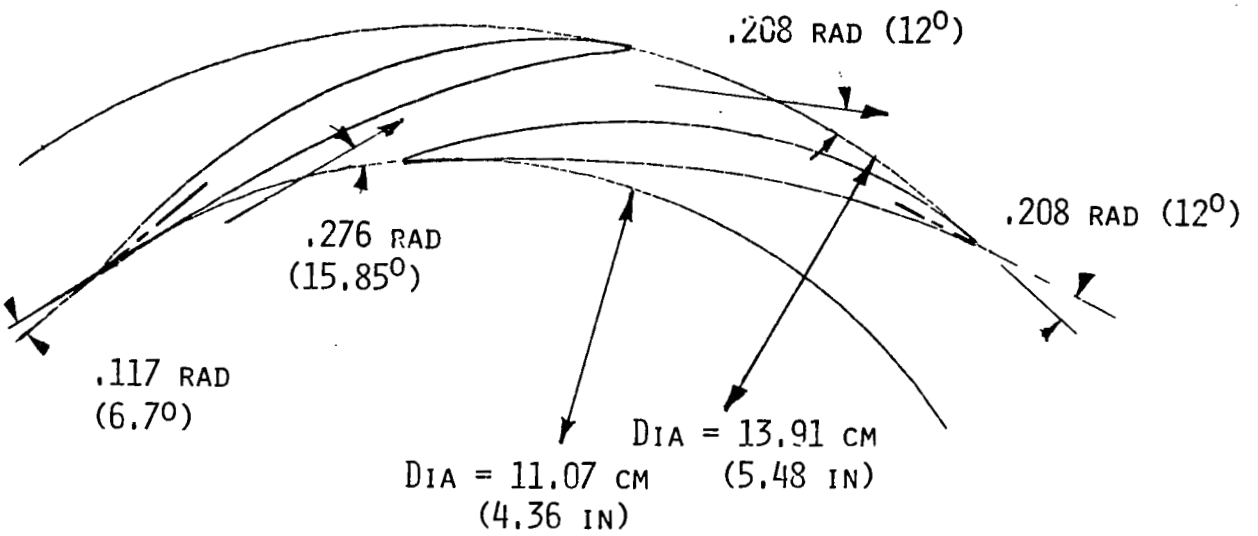

- NUMBER OF VANES = 11
- DIFFUSION FACTOR = .583
- PRESS. RECOVERY = 3.2×10^6 N/M^2 (464 PSI)

Figure 18. Mark 48-F Pump Diffuser Design

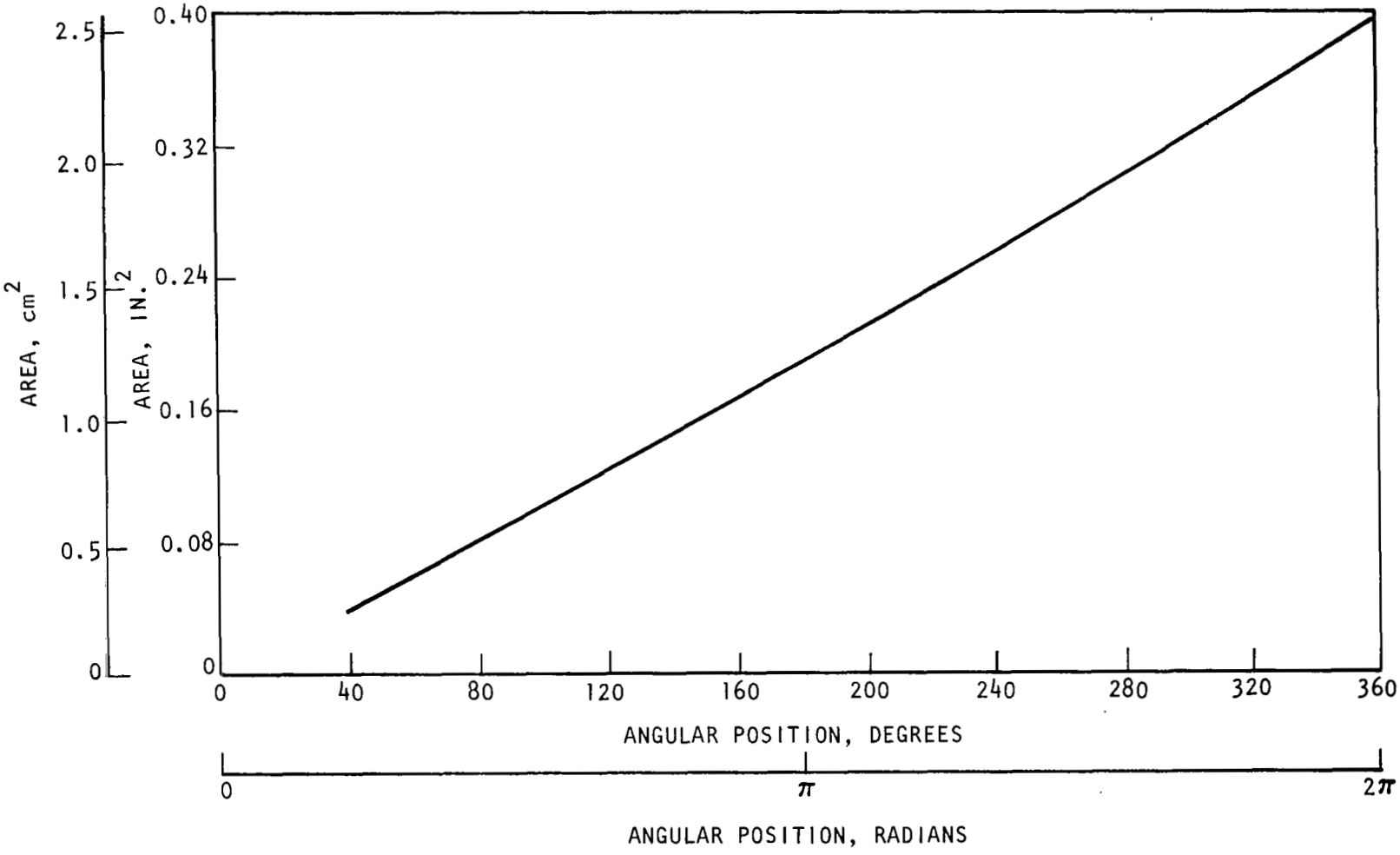

Figure 19. Mark 48-F Pump Volute Area Distribution

With that, the efficiency is calculated

$$is = \frac{\Delta h_{is}}{\Delta h_{act}} = \text{(see Fig. 20)}$$

The process is assumed to be adiabatic. The isentropic enthalpy rise represents the ideal pump (without losses). The losses are assumed to go into heating, resulting in an actual temperature $T2_{act}$.

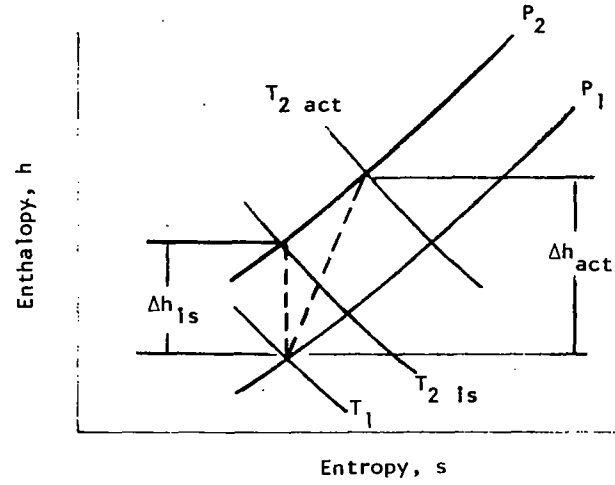

Figure 20. Mollier Diagram

To establish the theoretical performance of the pump, the energy added to the fluid is calculated successively at each pump element as well as the losses incurred as a result of friction, internal leakage, etc. The predicted state points in the adiabatic compression process are shown on an h-s diagram in Fig. 21. Based on this analysis, the isentropic efficiency of the pump was calculated as 58% by the realtionship:

$$s = \frac{h_2 - h_1}{h_3 - h_1}$$

$$= \frac{176{,}600 - (-227{,}800)}{464{,}800 - (-227{,}800)} = 58\% \text{ (SI units)}$$

$$= \frac{76 - (-98)}{200 - (-98)} = 58\% \text{ (English units)}$$

This approach yields lower values than using the ploytropic process and, at the same time, is more representative of the real process, which is closer to constant volume. The losses used in computing the pump characteristic are summarized in Table 3, and the pump map is shown in Fig. 22. A summary of the principal pump design parameters is included in Table 4. Figures 23 through 26 present the pressure, temperature, internal flow, and fluid density levels calculated at significant stations of the turbopump.

Turbine Aerothermodynamic Analysis

The Mark 48 turbine design represents an advancement in the state-of-the-art with regard to turbine horsepower developed relative to turbine size and weight. This turbine design was influenced principally by the operational constraints of the staged-combustion-cycle type engine for which this component is being investigated. The design pressure ratio and mass flow requirements had the greatest effect on the configuration. Pressure ratio was minimized to a value

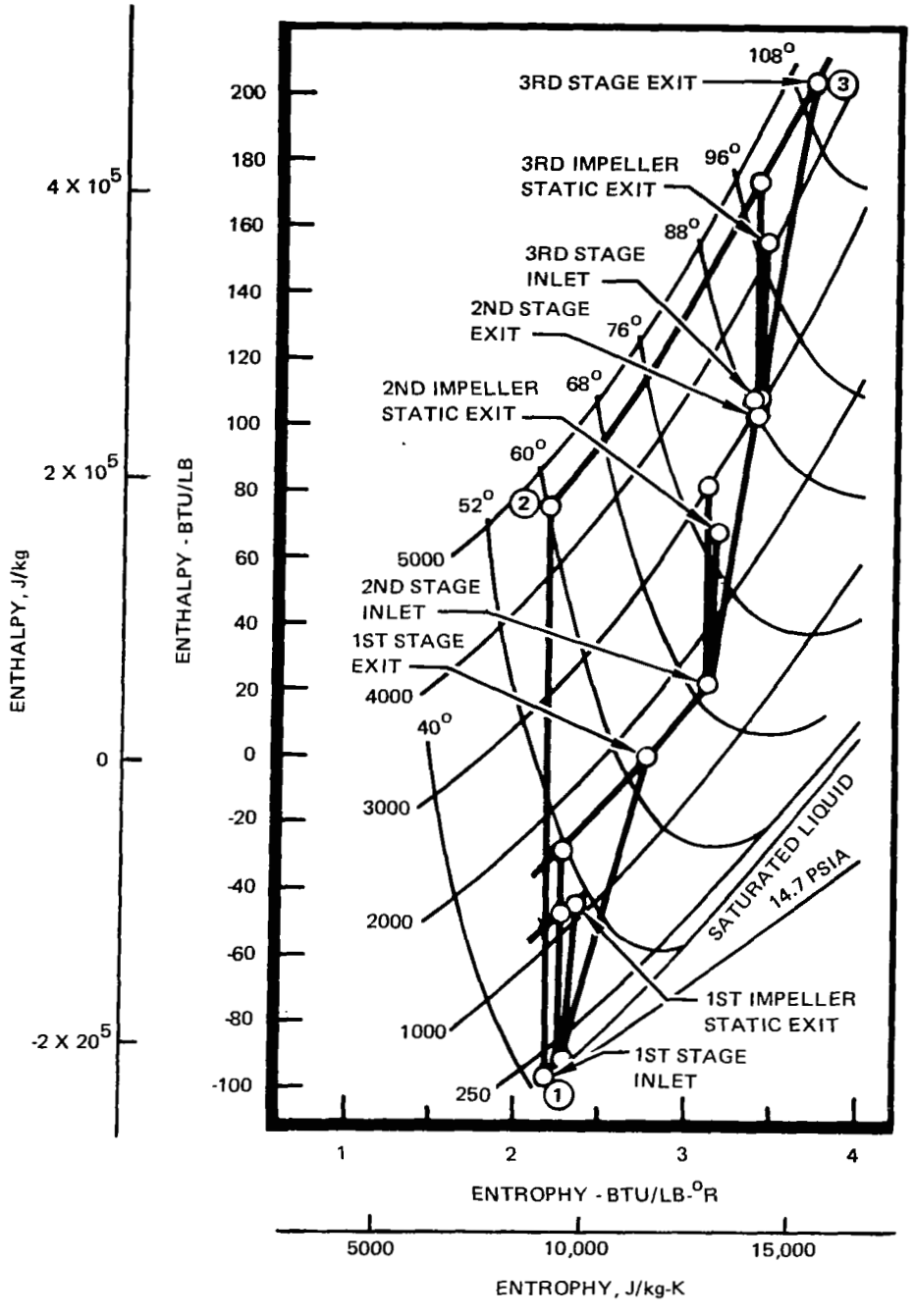

Figure 21. Liquid Hydrogen Pump Mollier Diagram

TABLE 3. MARK 48-F PUMP LOSS PARAMETERS

	Impeller		Vaneless Space	Diffuser		Volute
	In	Out		In	Out	
Blockage	1.0	0.8		0.9	0.85	
Roughness	0.000063		0.000063	0.000063		0.000063
Momentum Loss Coefficient	-		-	-		0.00198
Incidence Loss Coefficient	0.00239		-	0.0007		-
Skin Friction Loss Coefficient	0.00826		0.01139	0.02313		0.01221
Diffusion Loss Coefficient	0.00023		-	0.01386		-
Exit Diffuser Loss Coefficient	-		-	-		0.00119

*Q = 653 gpm; N = 95,000 rpm

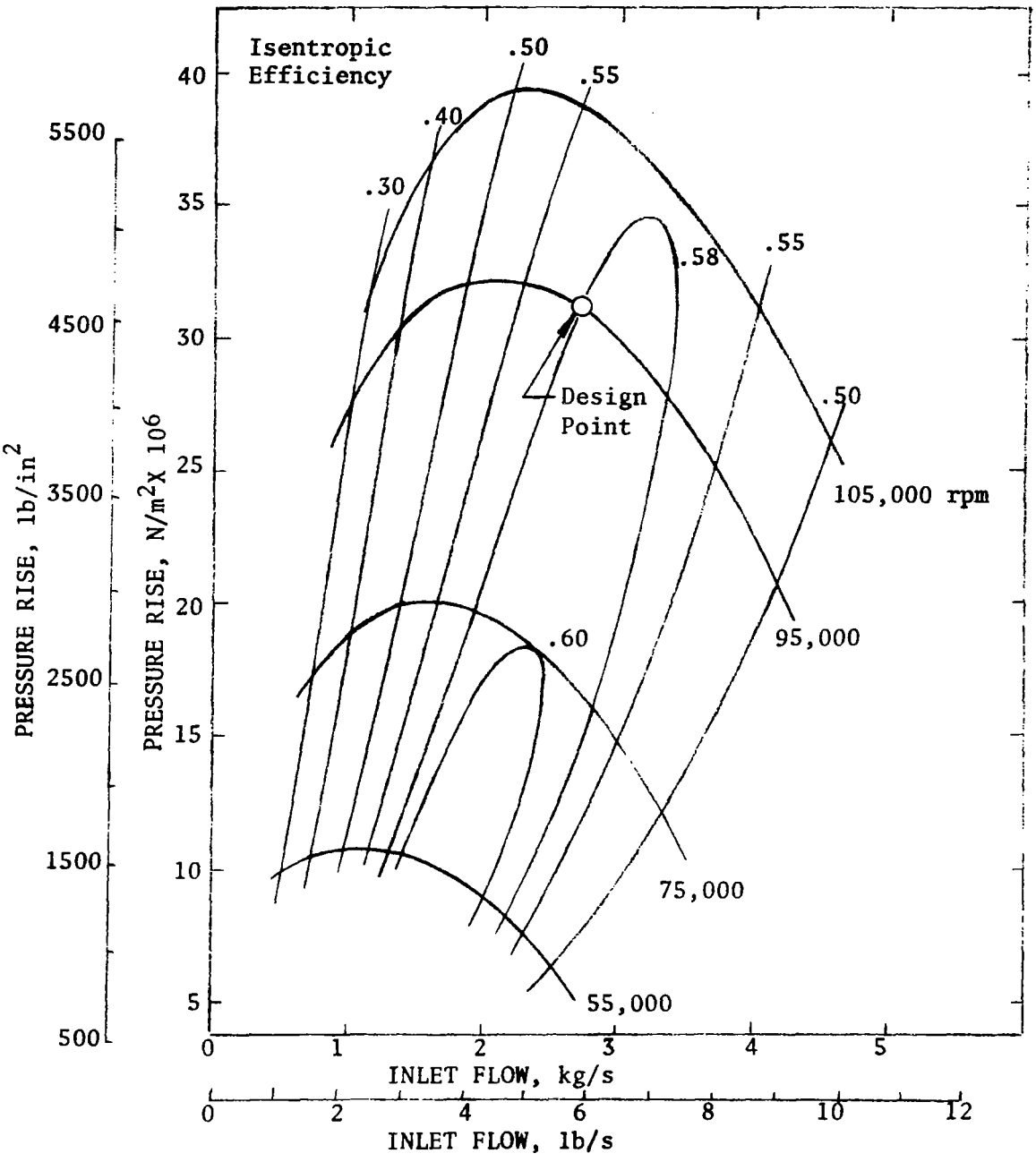

Figure 22. Mark 48F Pump Performance

TABLE 4. SMALL, HIGH-PRESSURE LH_2 TURBOPUMP NOMINAL DESIGN PARAMETERS

	SI Units	English Units
Number of Stages	3	3
Impeller Inlet Tip Diameter	4.826 cm	1.90 inches
Impeller Inlet Hub Diameter	3.099 cm	1.22 inches
Impeller Inlet Angle at Tip	0.28 radian	16 degrees
Impeller Inlet Angle at Hub	0.45 radian	26 degrees
Number of Impeller Vanes at Inlet	6	6
Number of Impeller Vanes at Discharge	12	12
Impeller Discharge Diameter	10.31 cm	4.058 inches
Impeller Discharge Angle	0.655 radian	37.5 degrees
Impeller Discharge Width	3.81 mm	0.150 inch
Impeller Tip Speed	512.97 m/s	1683 ft/sec
Vaned Diffuser Inlet Diameter	11.07 cm	4.36 inches
Vaned Diffuser Discharge Diameter	13.91 cm	5.48 inches
Number of Diffuser Vanes	11	11
Diffuser Passage Width	3.81 mm	0.150 inch
Crossover Inlet Diameter	13.72 cm	5.4 inches
Crossover First-Row Discharge Diameter	9.779 cm	3.9 inches
Crossover Second-Row Discharge Diameter	6.35 cm	2.5 inches
Crossover Inlet Angle	0.206 radian	11.8 degrees
Crossover First-Row Discharge Angle	0.471 radian	27 degrees
Crossover Second-Row Inlet Angle	0.394 radian	26.6 degrees
Crossover Second-Row Discharge Angle	1.047 radians	60 degrees
Isentropic Head/Stage	15,647 m	51,334 feet
Overall Isentropic Head	41,415 m	135,876 feet
Stage Head Coefficient	0.576	0.576
Impeller Inlet Flow Coefficient (First Stage)*	0.159	0.159
Impeller Inlet Flow Coefficient (Second and Third Stage)*	0.194/0.1875	0.194/0.1875
Impeller Discharge Flow Coefficient (First Stage)*	0.071	0.071
Impeller Discharge Flow Coefficient (Second and Third Stage)	0.086	0.086
Stage Isentropic Efficiency	70.0%	70.0%
Overall Isentropic Efficiency	58%	58%
Shaft Speed	9946 rad/s	95,000 rpm
Pump Power	1896 kW	2543 hp
Required NPSP	406 m	1332 feet

*Value based on zero blockage

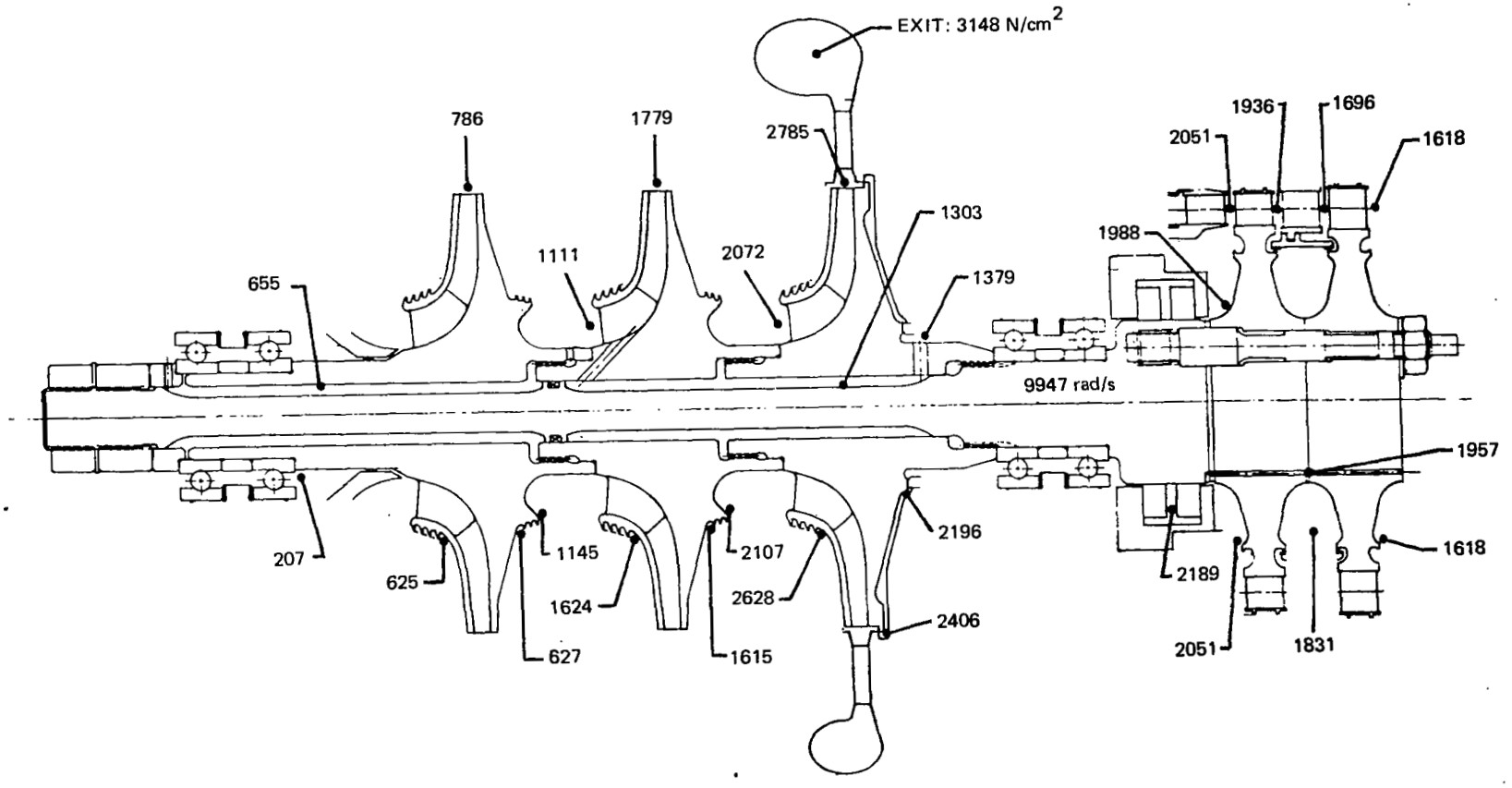

Figure 23. Mark 48 Fuel Turbopump Static Pressures (SI Units)

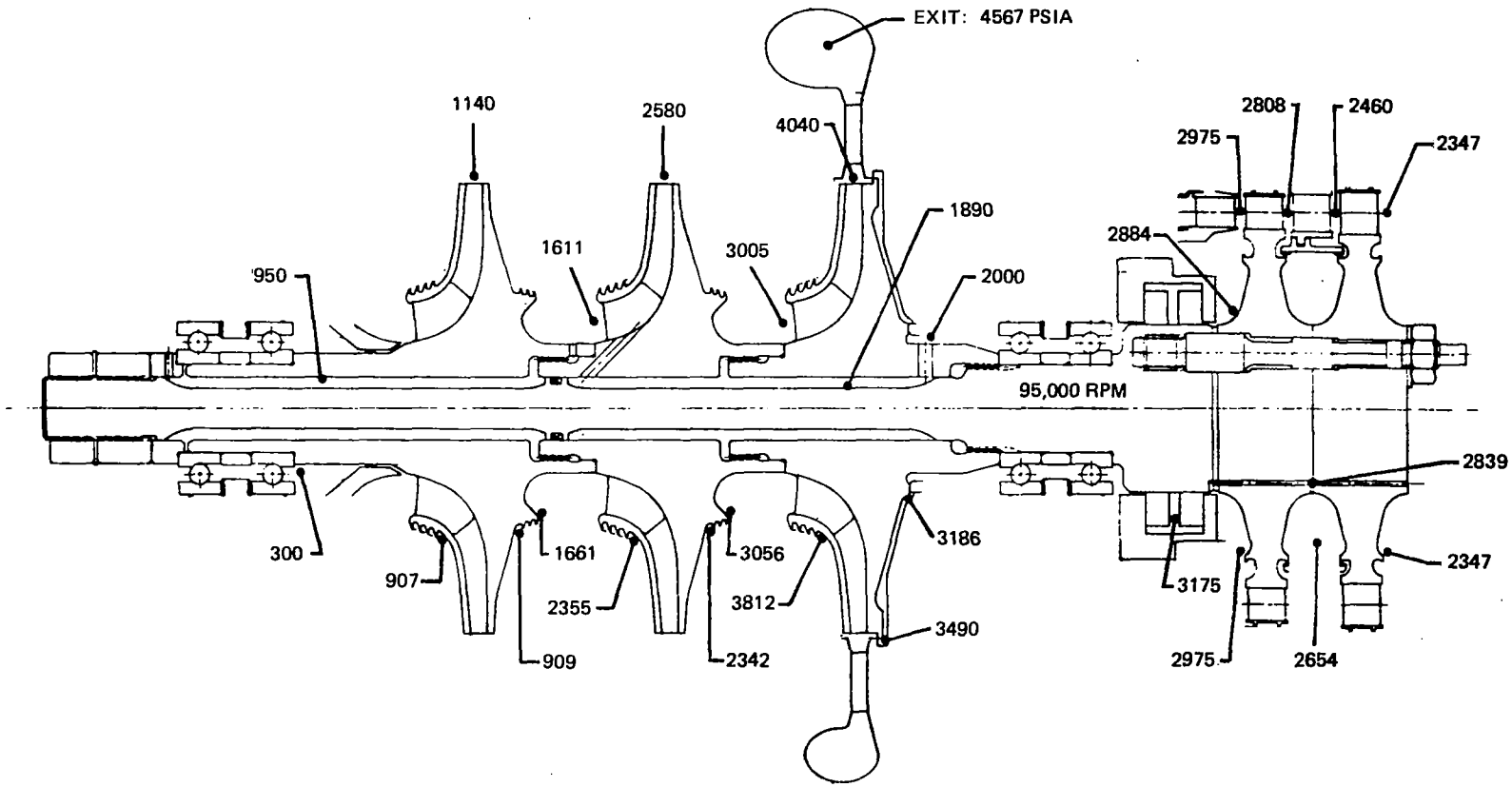

Figure 23. Mark 48 Turbopump Static Pressure (English Units)

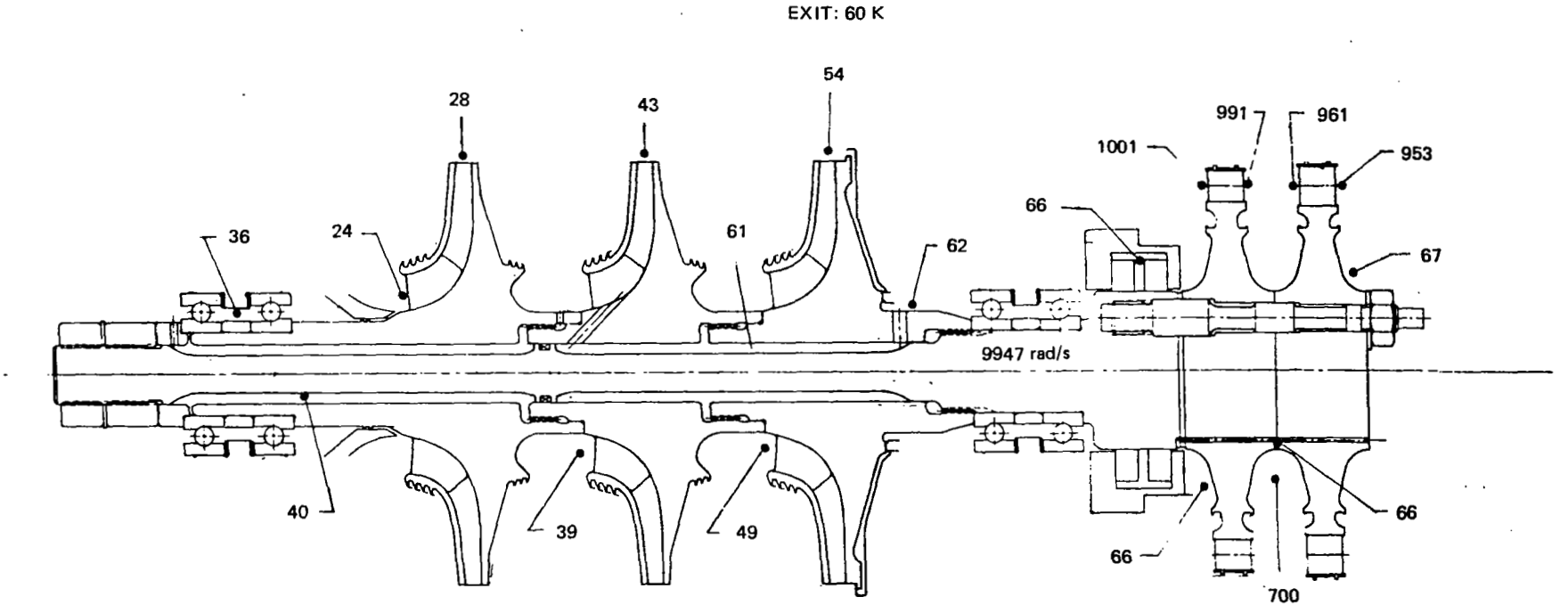

Figure 24. Mark 48-F Turbopump Fluid Static Temperature (SI Units)

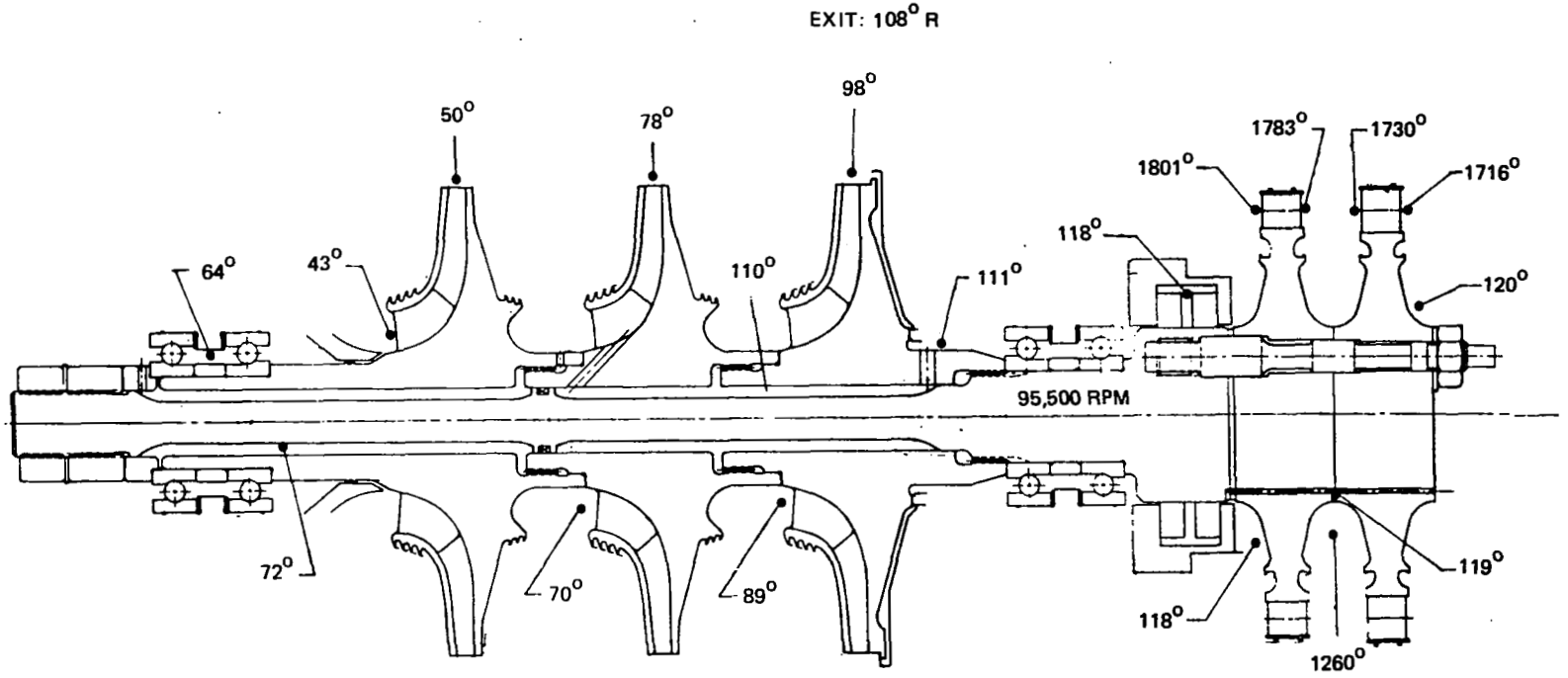

Figure 24. Mark 48-F Turbopump Fluid Static Temperature (English Units)

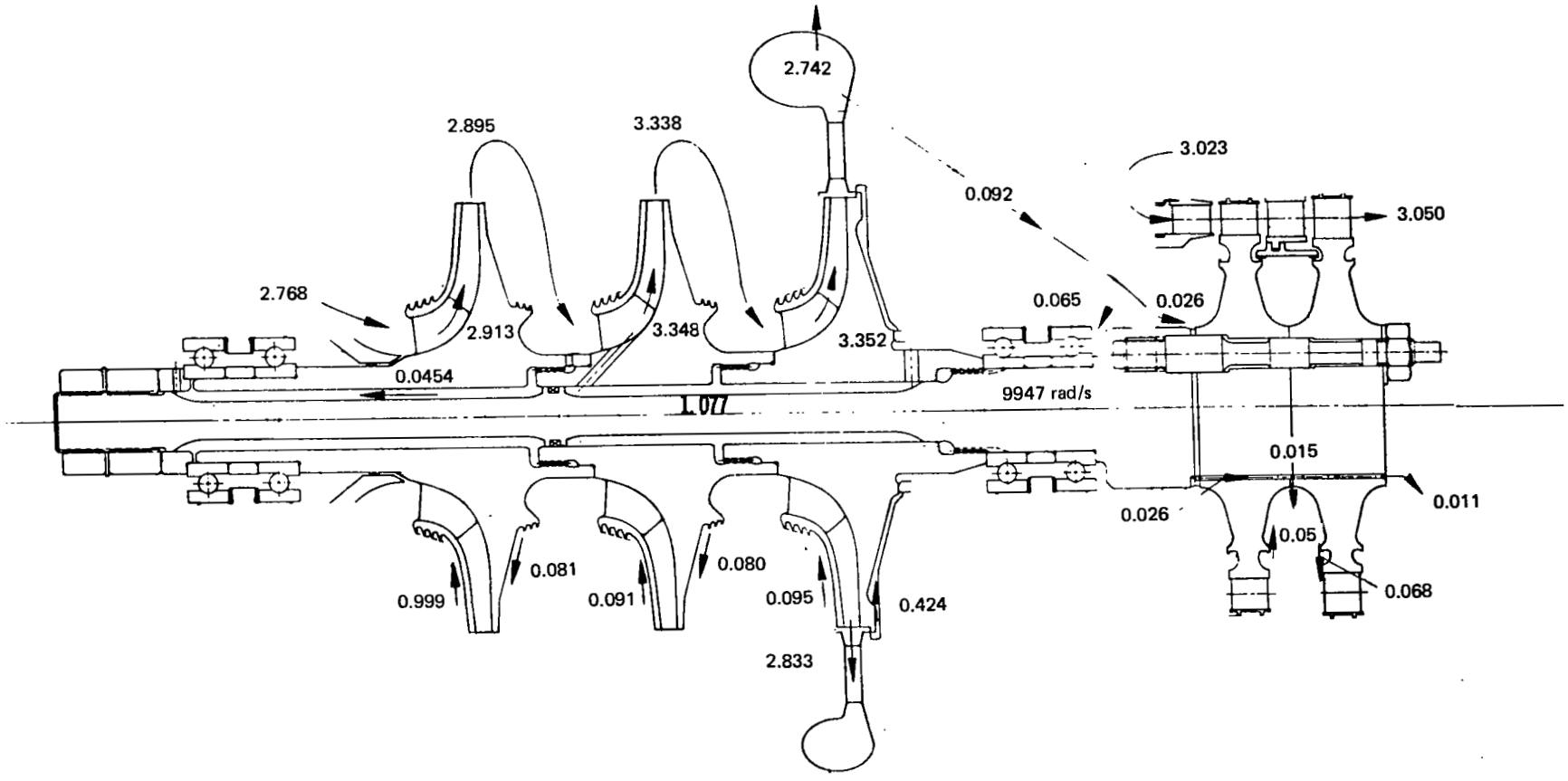

Figure 25. Mark 48-F Turbopump Flows (SI Units)

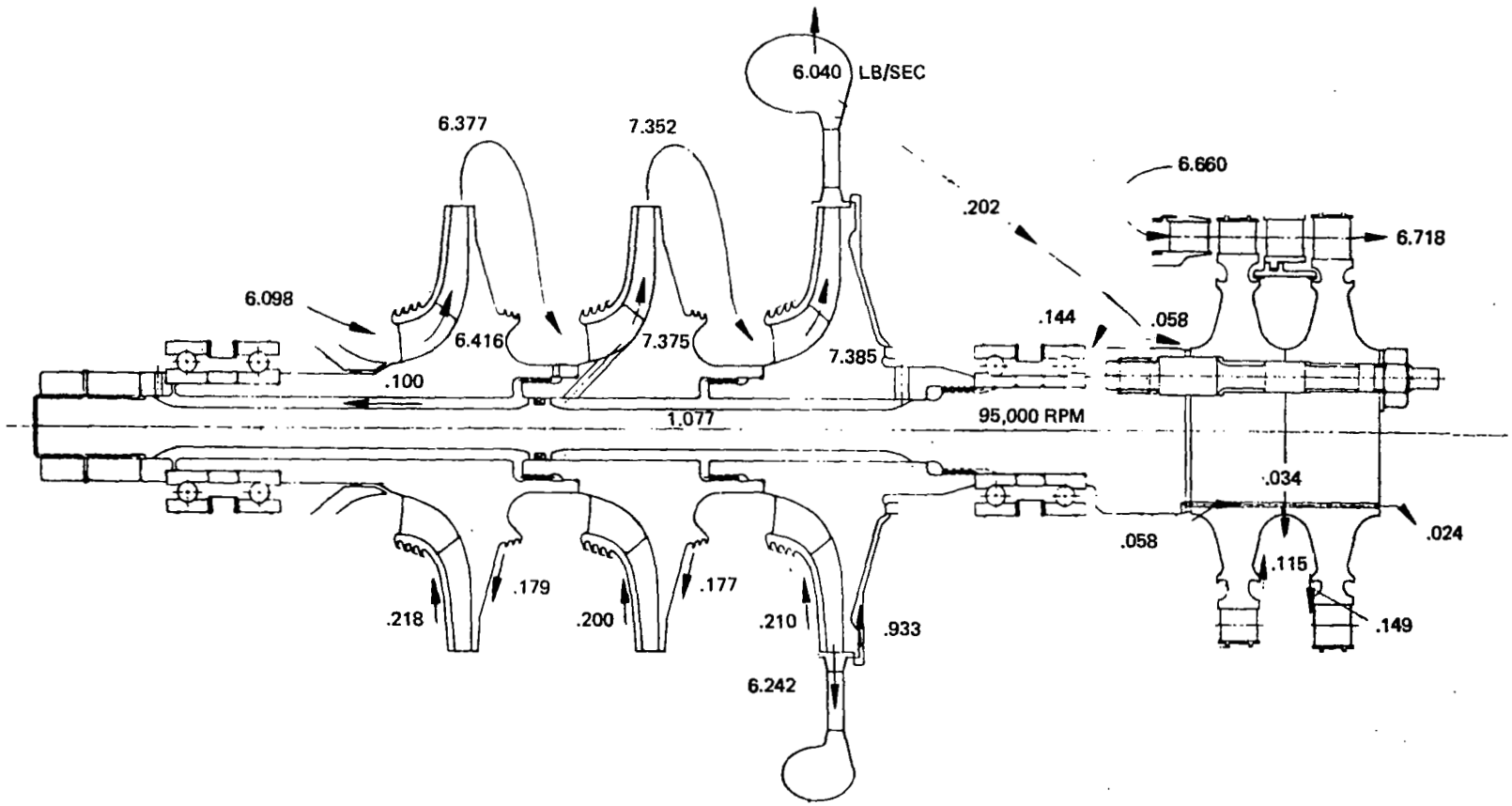

Figure 25. Mark 48-F Turbopump Flows (English Units)

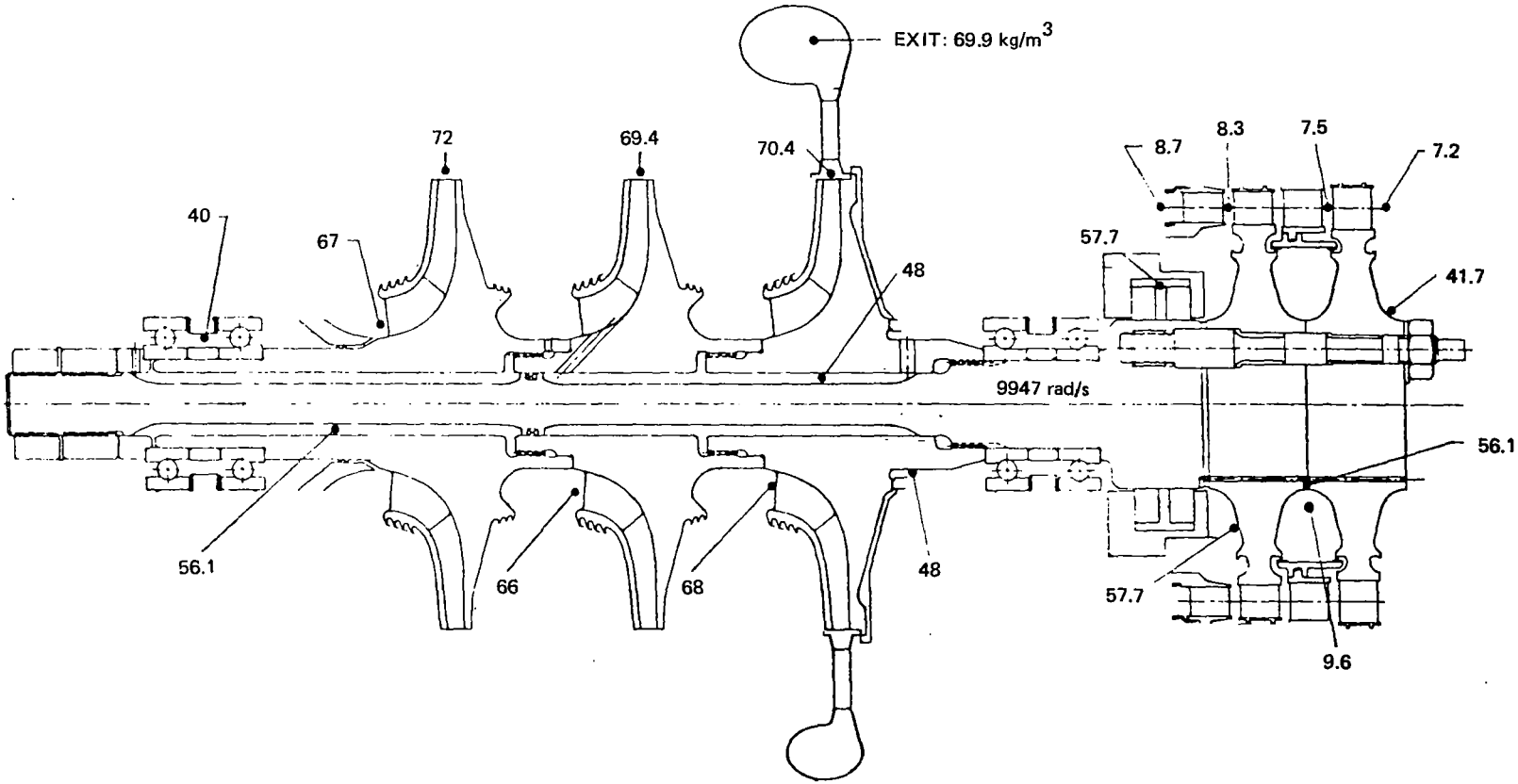

Figure 26. Mark 48 Fuel Turbopump Fluid Densities (SI Units)

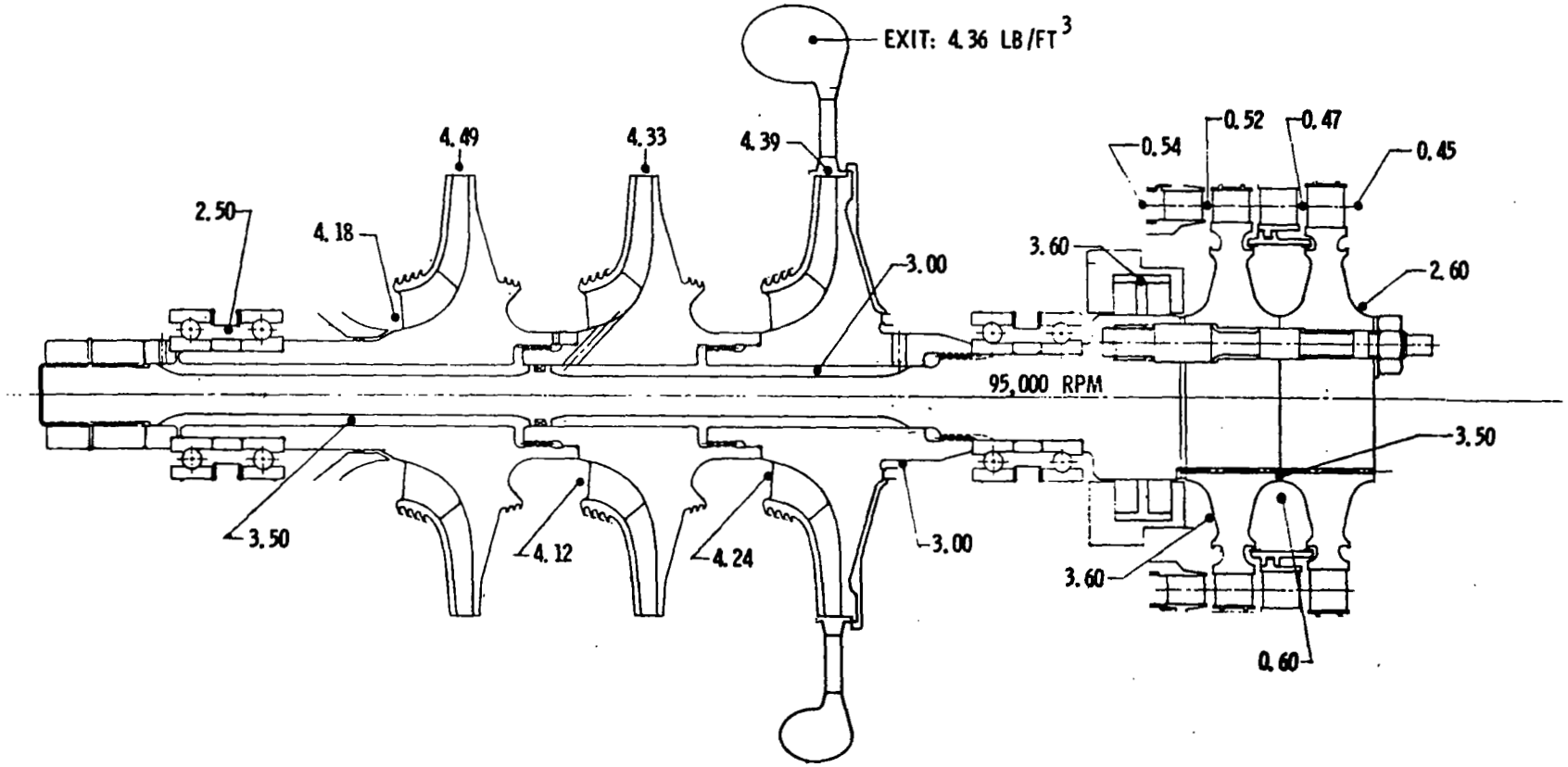

Figure 26. Mark 48 Fuel Turbopump Fluid Densities (English Units)

of 1.443 (T-T)* to maximize thrust chamber design pressure, and overall engine performance. The turbine design speed and power, which were fixed by the hydrogen pump requirements in this turbopump, are respectively 9947 rad/s (95,000 rpm) and 2543 horsepower. The preburner provides turbine LO_2/LH_2 working fluid at a total inlet pressure of 2358 N/cm^2 (3420 psi), a total inlet temperature of 1033 K (1860 R), and a mass flowrate of 3.02 kg/s (6.66 lb/sec). A tabulation of principal turbine parameters appears in Table 5.

The gas path design was evolved with LO_2/LH_2 combustion gas properties established by the Joint Army-Navy-Navy-NASA-Air Force committee. At the 1.443 (T-T) design pressure ratio, the turbine isentropic available energy [Δh_s, T-S**] is 858 kJ/kg (369 Btu/lb). The required turbine power cannot be developed by a single-row configuration; for the subsonic gas path conditions in this application, a two-stage reaction design was selected.

The distribution of the 1.443 pressure ratios across the four gas-path elements is critical in this type, small-size turbine configuration. In the final design, the power split between the first and second stages is 52% and 48%, respectively. The design velocity ratio [u/c_o, T-T] was fixed at 0.483. At the 9947 rad/s (95,000 rpm) design speed, the pitch line velocity is 442 m/s (1451 ft/sec); the turbine pitch diameter is constant at 8.89 cm (3.50 inches). Figure 27 depicts the turbine velocity diagram at design conditions; the first- and second-stage velocity distribution was attained with 29.7% and 26.0% reaction, respectively.

The working fluid total effective energy [Δh_e], at each gas-path station, consists of the sum of the effective gas expansion energy [Δh_{es}], and the effect kinetic energy [Δh_{ev}] of the fluid. The effective expansion energy in the nozzles and reaction blading was calculated by adjusting the isentropic available energy [Δh_s] for the pressure ratio(s) existing across each gas-path element, and for turbulence and friction losses with applicable expansion energy coefficients [ϕ^2]. The energy and loss coefficients used for this design were evolved during previous rocket turbine development programs, and were selected as a function of nozzle and rotor deflection angles and widths, and flow conditions.

The working fluid kinetic energy [Δh_v] at the entrance of a nozzle or rotor is equivalent to the fluid velocity at that station. The h_v is normally corrected for friction losses with a kinetic energy loss coefficient [ψ^2], and for incidence and inlet relative Mach number losses.

The total effective energy [Δh_e] available to the nozzle and rotor gas paths is made up of the sum of the effective expansion energy [Δh_{ev}]. The nozzle and blading inlet relative velocities are all subsonic, and no Mach number corrections were necessary. The expansion energy and kinetic energy coefficients, which were applied to the Mark 48-F turbine design, appear in Table 6. A station-to-station tabulation of the turbine gas-path design pressure

*Total to total
**Total to static

TABLE 5. TURBINE DESIGN OPERATING CONDITIONS

	SI Units	English Units
1. Configuration	Two-Reaction Stages	
2. Working Fluid	LO_2/LH_2	
3. Turbine Total Inlet Pressure (P_t)	2358 N/cm^2	3420 psia
4. Turbine Total Inlet Temperature (T_{t1})	1033 K	1860 R
5. Turbine Pressure Ratio (PR_t) (T-T)	1.443	
6. Turbine Mass Flowrate (W_t)	3.02 Kg/s	6.66 lb/sec
7. Turbine Speed, (N)	9947 rad/s	95,000 rpm
8. Pitch Diameter (D_m)	8.89 cm	3.50 inches
9. Pitch Line Velocity (U_m)	442 m/s	1451 ft/sec
10. Velocity Ratio, Two Stage (U/C_o) (T-T)	0.483	
11. Turbine Efficiency (η_t), % (T-T)	75.4	
12. Turbine Horsepower (hp_t)	1829 kW	2543 hp

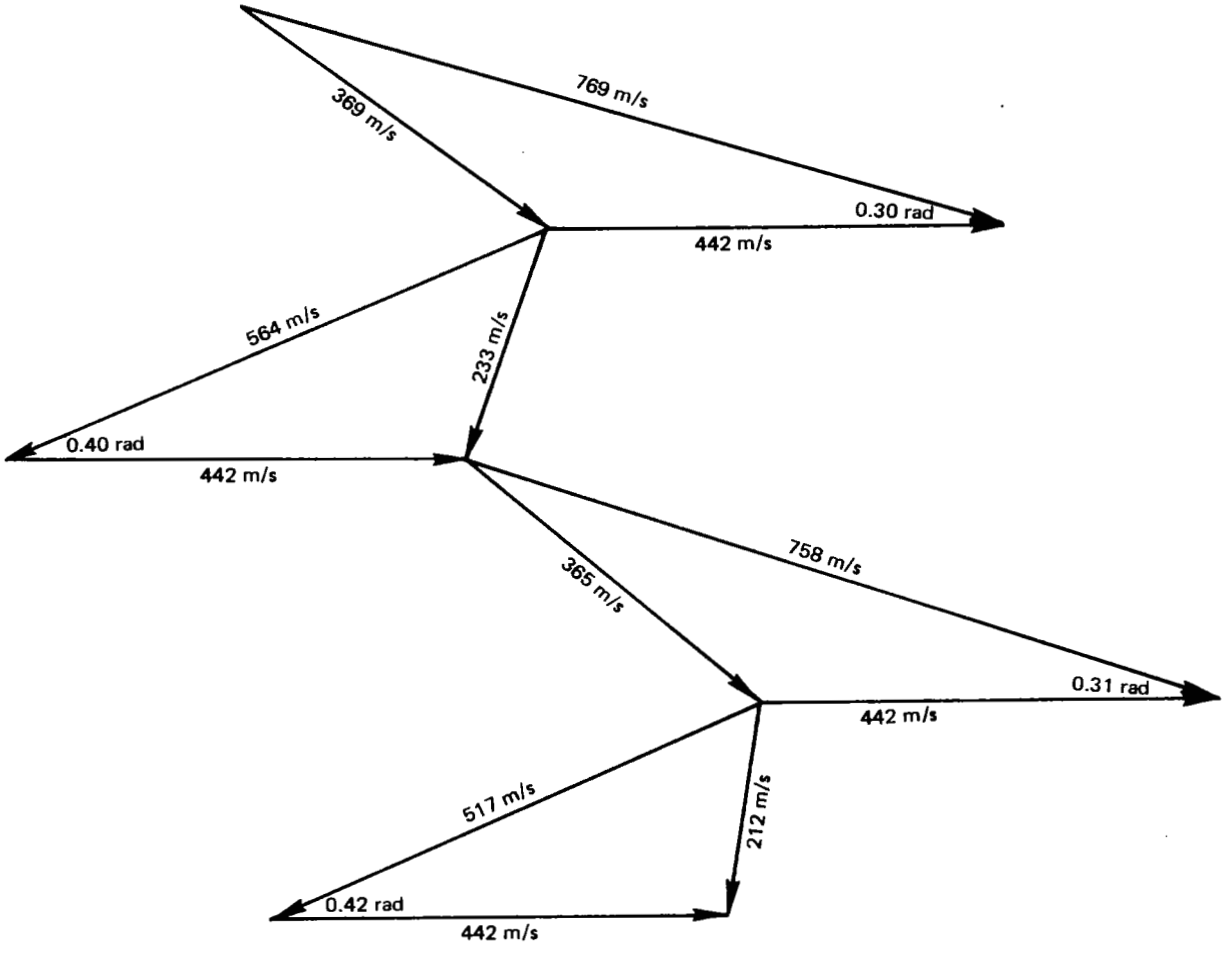

Figure 27. Mark 48-F Turbine Velocity Diagram (SI Units)

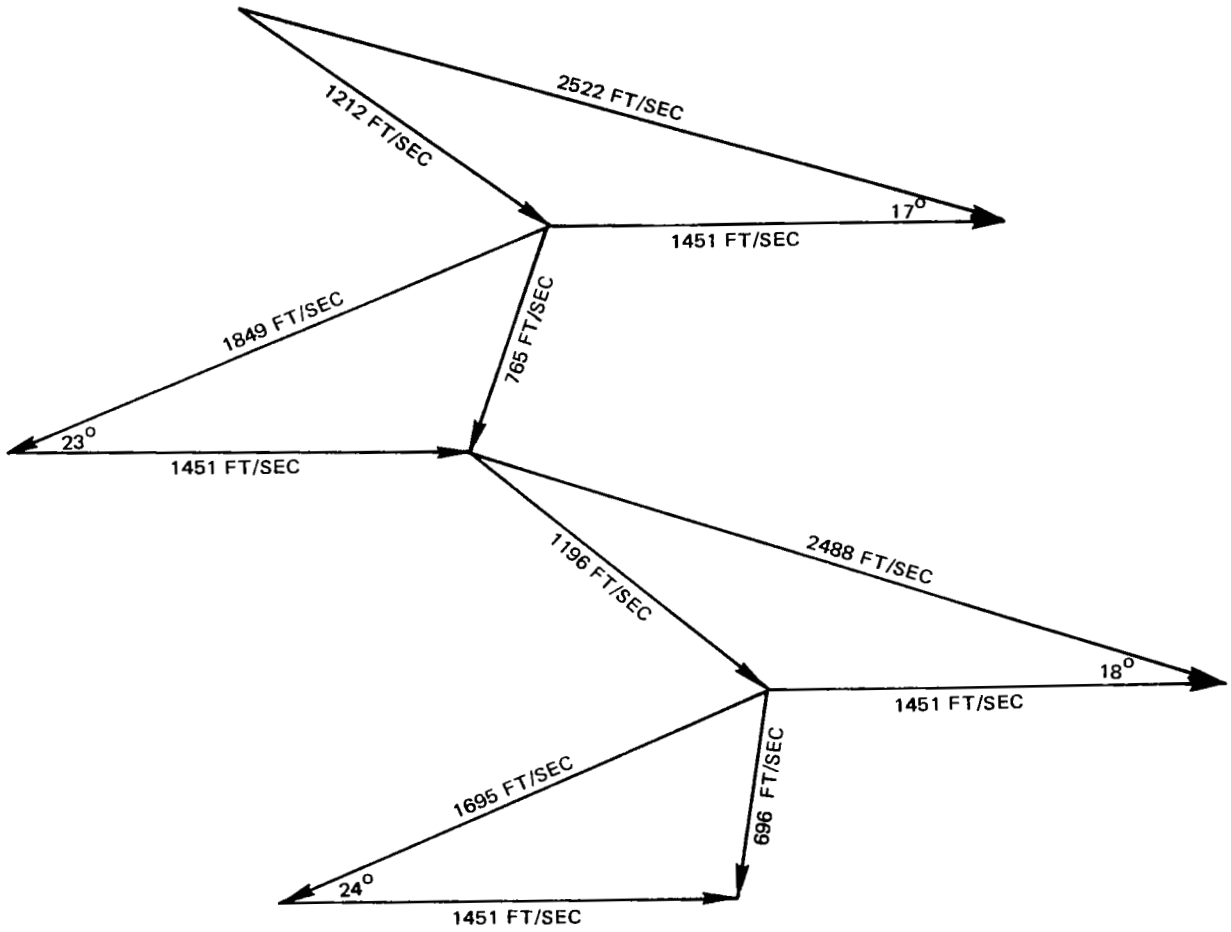

Figure 27. Mark 48-F Turbine Velocity Diagram (English Units)

TABLE 6 . GAS PATH ENERGY COEFFICIENTS

	Expansion Energy Coefficient (ϕ^2)	Kinetic Energy Coefficient (ψ^2)
First Stage		
Nozzle Vanes	0.916	0.000
Rotor Blades	0.832	0.665
Second Stage		
Nozzle Vanes	0.890	0.780
Rotor Blades	0.841	0.681

and temperature distribution data established for this design appears in Fig. 28. The resultant plot of predicted turbine efficiency, for velocity ratios ranging from 0 to 0.60, is depicted in Fig. 29. At design conditions, the predicted turbine efficiency is 75.35% (T-T).

A tabulation of the turbine gas path energy and loss distribution appears in Table 7 . It contains the isentropic enthalpy drop for each gas-path element, the adjustments for expansion energy and kinetic energy losses, and an accounting of available energy and the resulting energy equivalent of turbine work. For the total 832 kJ/kg (359.4 Btu/lb (T-T) [858 kJ/kg, 369 Btu/lb (T-S)] isentropic available energy to the turbine, at design pressure ratio and speed, the energy equivalent of the turbine exit energy loss is 22.3 kJ/kg (9.6 Btu/lb). The turbine exit energy is not charged to the turbine because the engine system subsequently utilizes it in the second phase of combustion in the thrust chamber. Gas-path losses account for 150 kJ/kg (64.4 Btu/lb), and the diagram efficiency adjustments is equivalent to 60.4 kJ/kg (26 Btu/lb). Therefore, for a total 832 kJ/kg (359.4 Btu/lb) (T-T) available in the turbine gas path, 629 kJ/kg (270.81 Btu/lb) are utilized to develop the design shaft horsepower, for a 75.35% (T-T) predicted turbine efficiency. A reheat of 4180 J/kg (1.8 Btu/lb) is experienced in the gas path.

In addition to the aerothermodynamic requirements, the turbine design was influenced by stress and manufacturing constraints associated with the small highly loaded turbine detail parts. A data summary describing the nozzle and blade final design configurations appears in Table 8 . The nozzle vane and blade profiles were laid out for pitch-line state conditions and velocities; the resultant short blading did not require any adjustments for radial-flow variations in the respective flow channels, and are therefore straight sections from root to tip. Analytical predictions of the pressure and suction profile velocity distributions, from the leading- to trailing-edge plains, were established and no unacceptable accelerations were found to exist. Profiles of the nozzle vanes and rotor blades are depicted in Fig. 30 through 33; the corresponding plots of the velocity distribution for these gas-path elements appear in Fig. 34 through 37.

MK48-F TURBINE GAS PATH

WORKING FLUID-LO_2LH_2

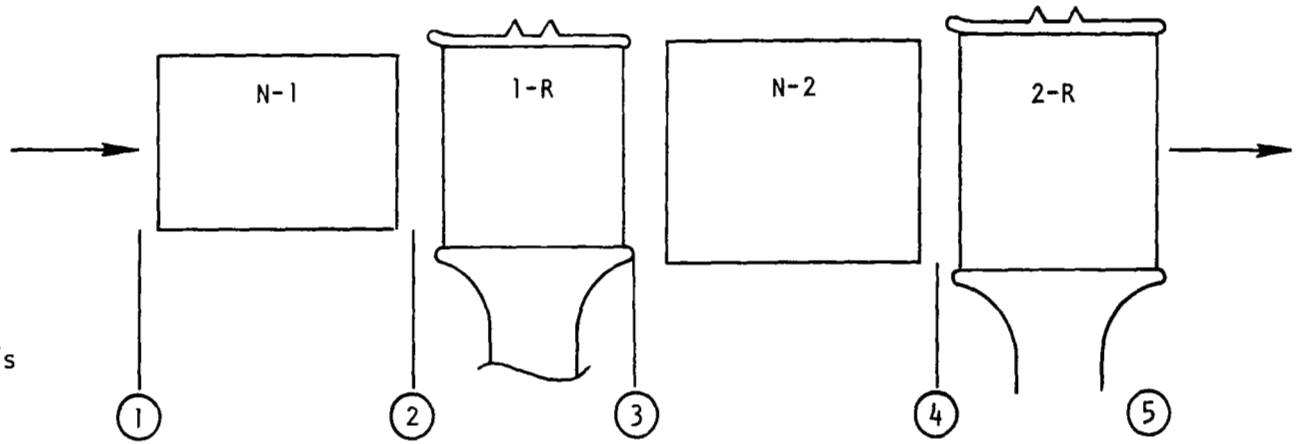

SPEED: 9947 rad/s

STATION	1	2	3	4	5
PRESSURE, N/cm^2					
TOTAL	2358	2115	1959	1747	1635
STATIC		2054	1936	1696	1618
TEMPERATURE, K					
TOTAL	1033	1008	994	969	957
STATIC		1001	991	962	954

STAGE	1	2
PRESSURE RATIO (T-T)	1.204	1.199
REACTION, %	29.7	26.0
U/C_o, (T-S)	0.462	0.476
POWER, %	51.9	48.1

Figure 28. Mark 48-F Turbine Pressure and Temperature Distribution (SI Units)

MK 48-F TURBINE GAS PATH

WORKING FLUID – LO_2 / LH_2

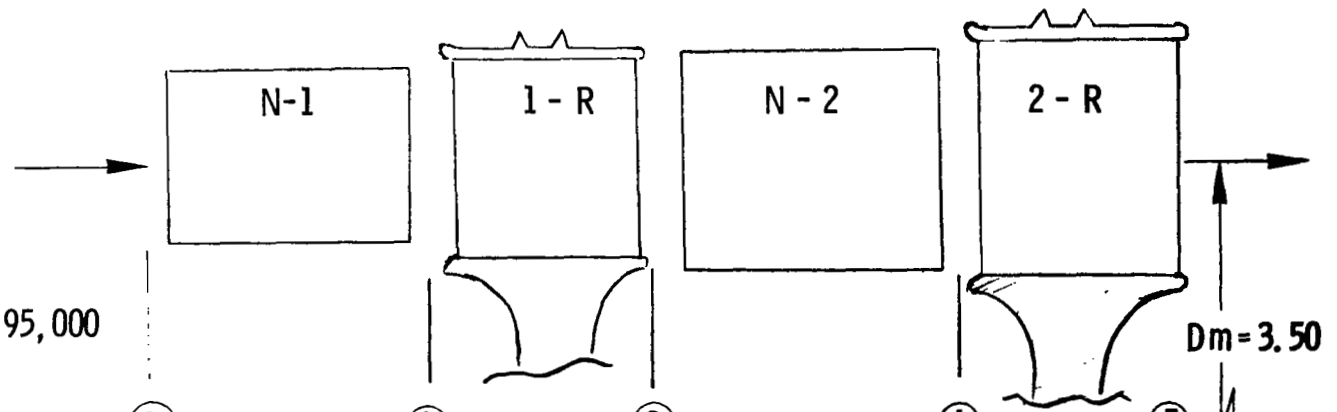

SPEED N, rpm – 95,000

STATION	①	②	③	④	⑤
PRESSURE, PSIA					
TOTAL	3420	3068	2841	2534	2371
STATIC		2979	2808	2460	2347
TEMPERATURE, R					
TOTAL	1860	1815	1789	1744	1722
STATIC		1801	1783	1731	1717

STAGE	1	2
PRESSURE RATIO (T-T)	1.204	1.199
REACTION, %	29.7	26.0
U/C_o , (T-S)	0.462	0.476
HORSEPOWER, (%)	1320 (51.9)	1223 (48.1)

Figure 28. Mark 48-F Turbine Pressure and Temperature Distribution (English Units)

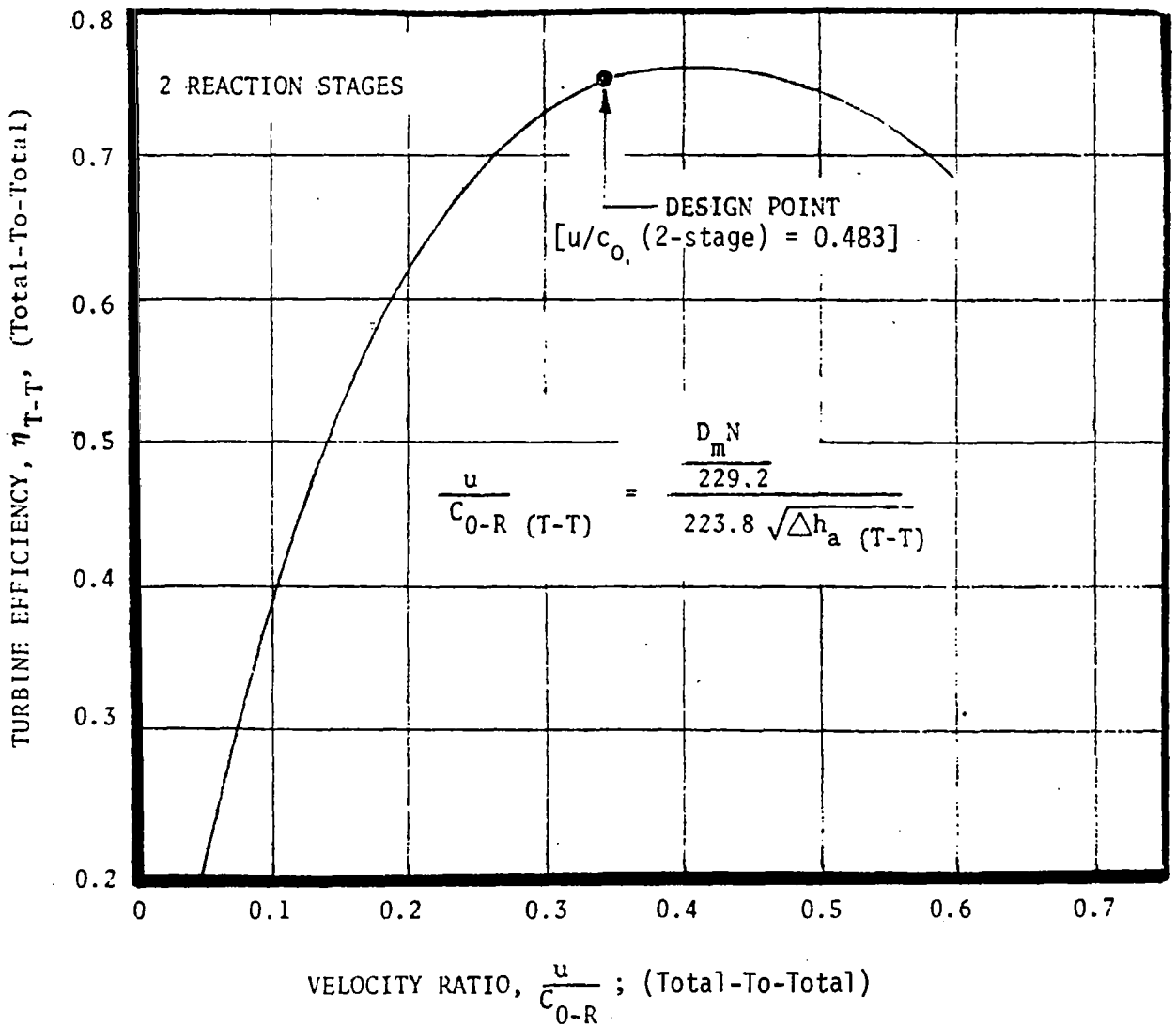

Figure 29. Mark 48-F Turbine Efficiency

TABLE 7. TURBINE ENERGY AND LOSS DISTRIBUTION
(SI UNITS)

(1) Gas Path Losses

	Isentropic Enthalpy (Δh_s), kJ/kg	Effective Expansion Energy (Δh_{es}), kJ/kg	Entering Kinetic Energy (Δh_{ev}), kJ/kg	Effective Kinetic Energy (Δh_{ev}), kJ/kg	Energy Loss (ΔhL), kJ/kg
First-Stage Nozzle Vanes	323.8	296.6			27.2
			68.9	45.8	23.1
First-Stage Rotor Blades	136.1	113.3			22.8
			27.3	21.3	6.0
Second-Stage Nozzle Vanes	297.9	264.9			33.0
			66.0	44.9	21.1
Second-Stage Rotor Blades	104.0	87.4			16.6

(2) Exit Energy Loss, J/kg — 22.3

(3) Turbine Diagram Efficiency Adjustment, J/kg

$(\Delta h_s)\ (\eta_t \text{ Diagram}) = (857.6)\ (0.804) = 689.5$

$(\Delta h_s)\ (\eta_t \text{ Adjustment}) = (857.6)\ (0.734) = \frac{629.5}{60.0}$ — 60.06

(4) Equivalent Leakage Energy Loss kJ/hg — 0

(5) Losses (1)+(2)+(3)+(4) = Δh_L, kJ/kg — 232.1

(6) Turbine Efficiency

$\Delta h_{work} = 629.5$ kJ/kg

$\Delta h_{isentropic} - \Delta h_{work} = 857.6 - 629.5 = 228.1$

$\Delta h_{work} + \Delta h_L = 629.5 + 232.1 = 861.6$

Gas Path Reheat $= 232.1 - 228.1 = 4.0$

$\eta_t = \frac{629.5}{857.6 - 22.3} = 0.7535\ (T\text{-}T)$

$\eta_t = \frac{629.5}{857.6} = 0.734$

TABLE 7. TURBINE ENERGY AND LOSS DISTRIBUTION
(ENGLISH UNITS

(1) Gas Path Losses

	Isentropic Enthalpy (Δh_s), Btu/lb	Effective Expansion Energy (Δh_{es}), Btu/lb	Entering Kinetic Energy (Δh_{ev}), Btu/lb	Effective Kinetic Energy (Δh_{ev}), Btu/lb	Energy Loss (Δh_L), Btu/lb
First-Stage Nozzle Vanes	139.31	127.64			11.67
			29.64	19.69	9.96
First-Stage Rotor Blades	58.57	48.74			9.83
			11.74	9.15	2.60
Second-Stage Nozzle Vanes	128.17	114.00			14.17
			28.39	19.34	9.05
Second-Stage Rotor Blades	44.75	37.62			7.13

(2) Exit Energy Loss, Btu/lb — 9.60

(3) Turbine Diagram Efficiency Adjustment, Btu/lb

$(\Delta h_s)\ (\eta_t \text{ Diagram}) = (369)(0.804) = 296.81$

$(\Delta h_s)\ (\eta_t \text{ Adjustment}) = (369)(0.734) = \frac{270.81}{26.00}$ — 26.00

(4) Equivalent Leakage Energy Loss, Btu/lb — 0.00

(5) Losses (1)+(2)+(3)+(4) = Δh_L, Btu/lb — 99.99

(6) Turbine Efficiency

$\Delta h_{work} = 270.81$ Btu/lb

$\Delta h_{isentropic} - \Delta h_{work} = 369.0 - 270.81 = 98.19$ Btu/lb

$\Delta h_{work} + \Delta h_L = 270.81 + 99.99 = 370.8$ Btu/lb

Gas Path Reheat = 99.99 - 98.19 = 1.8 Btu/lb

$\eta_t = \frac{270.81}{(369.0-9.6)} = 0.7535$ (T-T)

$\eta_t = \frac{270.81}{369.0} = 0.7339$ (T-S)

TABLE 8. TURBINE NOZZLE AND ROTOR BLADE DESIGN

(9947 rad/s; 95,000 rpm)

Stage	1		2	
	N-1	1-R	N-2	2-R
Pitch Diameter (DM), cm	8.89	8.89	8.89	8.89
Number of Elements (Z)	41	52	41	52
Height, cm	0.711	0.737	0.762	0.838
Throat Area, cm^2	4.55	6.50	5.34	8.14
Inlet Angle, radian	1.57	0.65	1.24	0.70
Exit Angle, radian	0.30	0.40	0.31	0.42
Pitch Line Velocity (U), m/s	-	442	-	442
Leading Edge, mm	2.39	1.12	0.69	1.12
Trailing Edge (R), mm	0.18	0.18	0.18	0.18
N = 9947 rad/s				(SI Units)

Stage	1		2	
	N-1	1-R	N-2	2-R
Pitch Diameter (DM), inches	3.500	3.500	3.500	3.500
Number of Elements (Z)	41	52	41	52
Height, inch	0.280	0.290	0.300	0.330
Throat Area, $in.^2$	0.705	1.008	0.827	1.261
Inlet Angle, degrees	90	37.5	70.8	40
Exit Angle, degrees	17	23	18	24
Pitch Line Velocity (U), ft/sec	-	1451	-	1451
Leading Edge, inch	0.094 (Ellipse)	0.044 (Ellipse)	R = 0.027	0.044 (Ellipse)
Trailing Edge (R), inch	0.007	0.007	0.007	0.007
N = 95,000 rpm				(English Units)

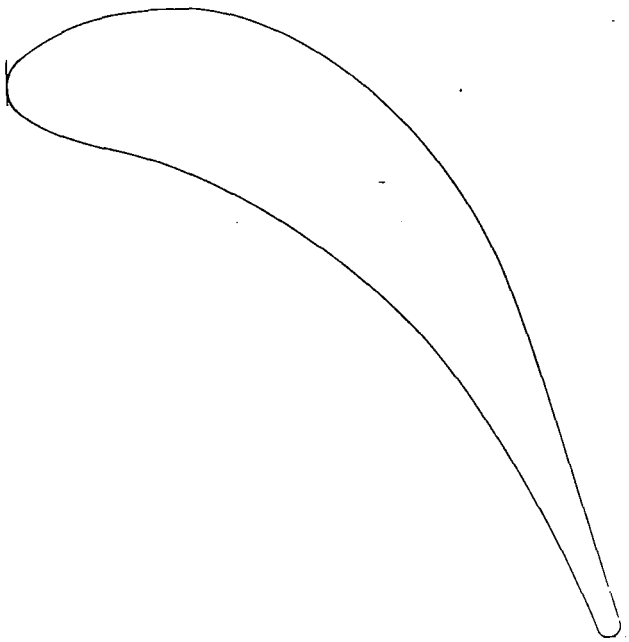

Figure 30. Mark 48-F Turbine First-Stage Nozzle Vane Shape

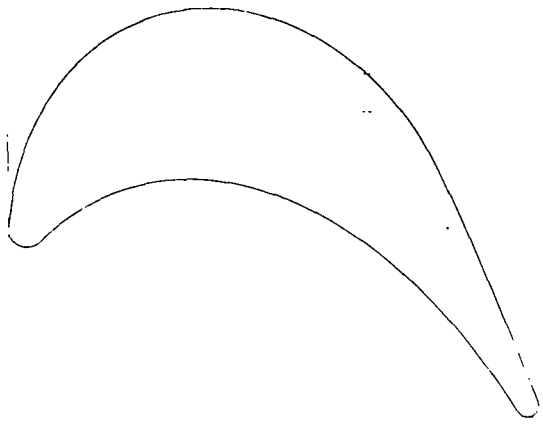

Figure 31. Mark 48-F Turbine First-Stage Rotor Blade Shape

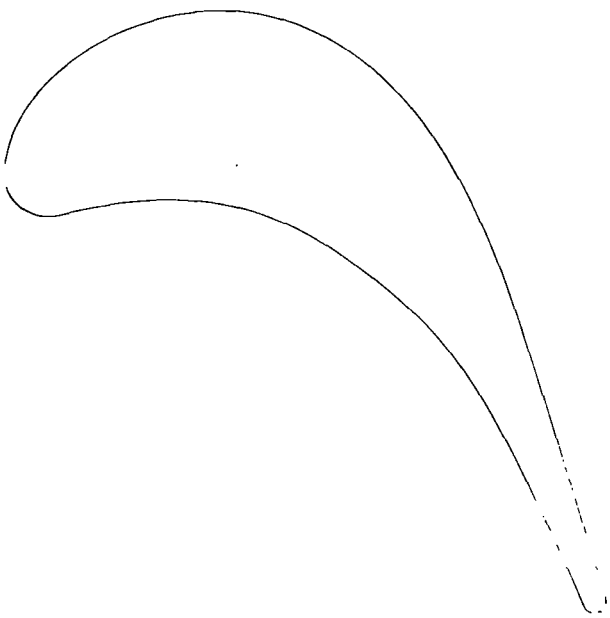

Figure 32. Mark 48-F Turbine Second-Stage Nozzle Vane Shape

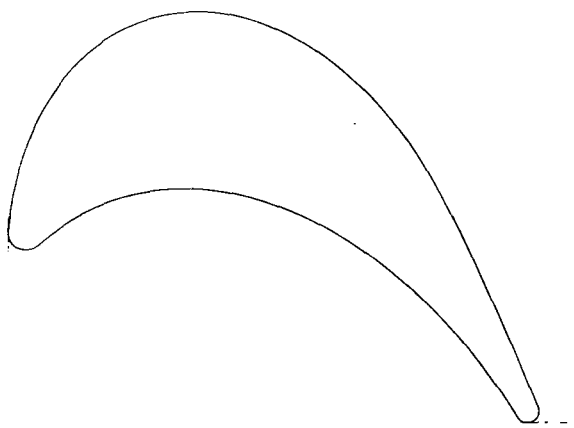

Figure 33. Mark 48-F Turbine Second-Stage Rotor Blade Shape

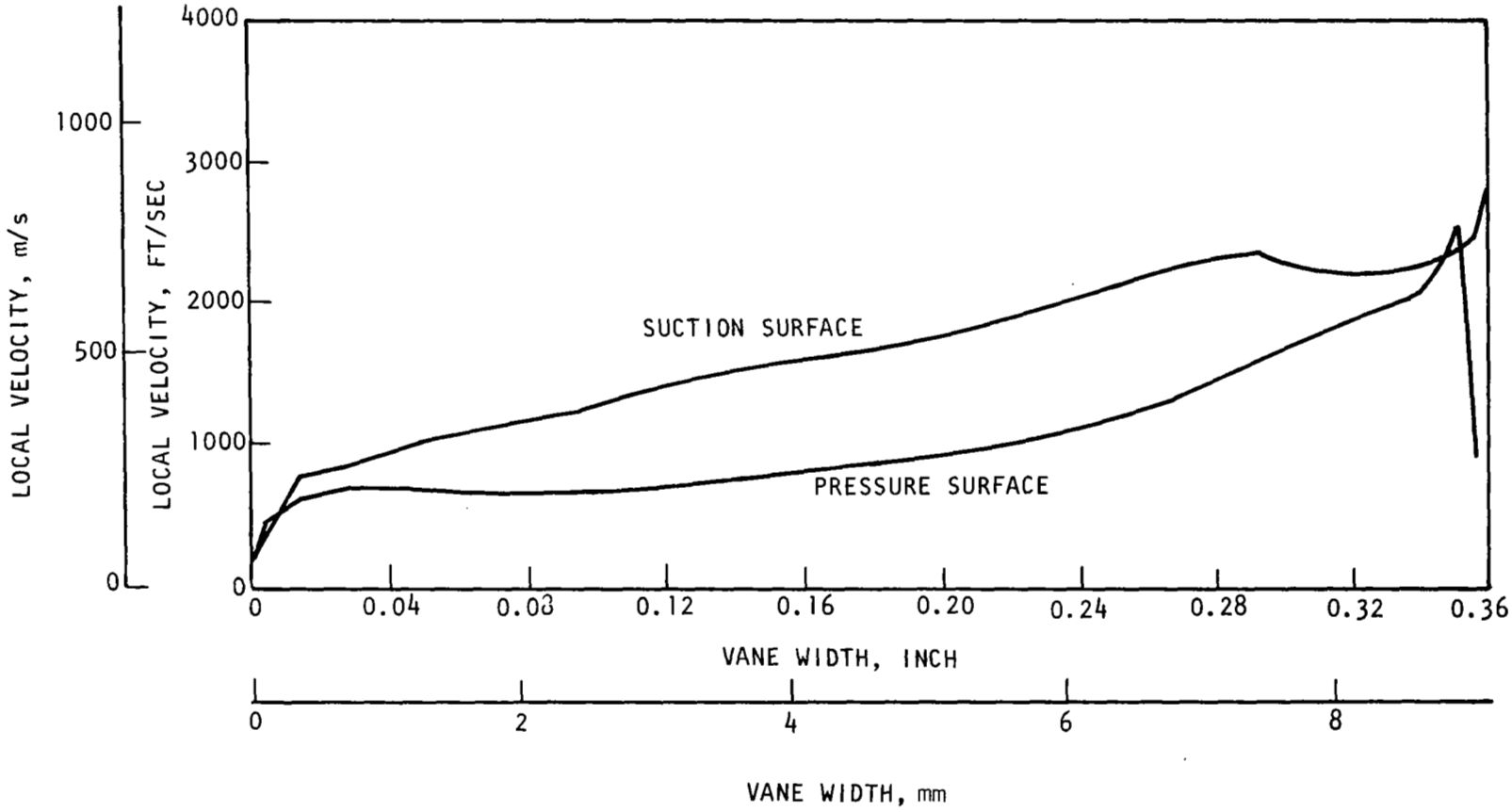

Figure 34. Mark 48-F Turbine First-Stage Nozzle

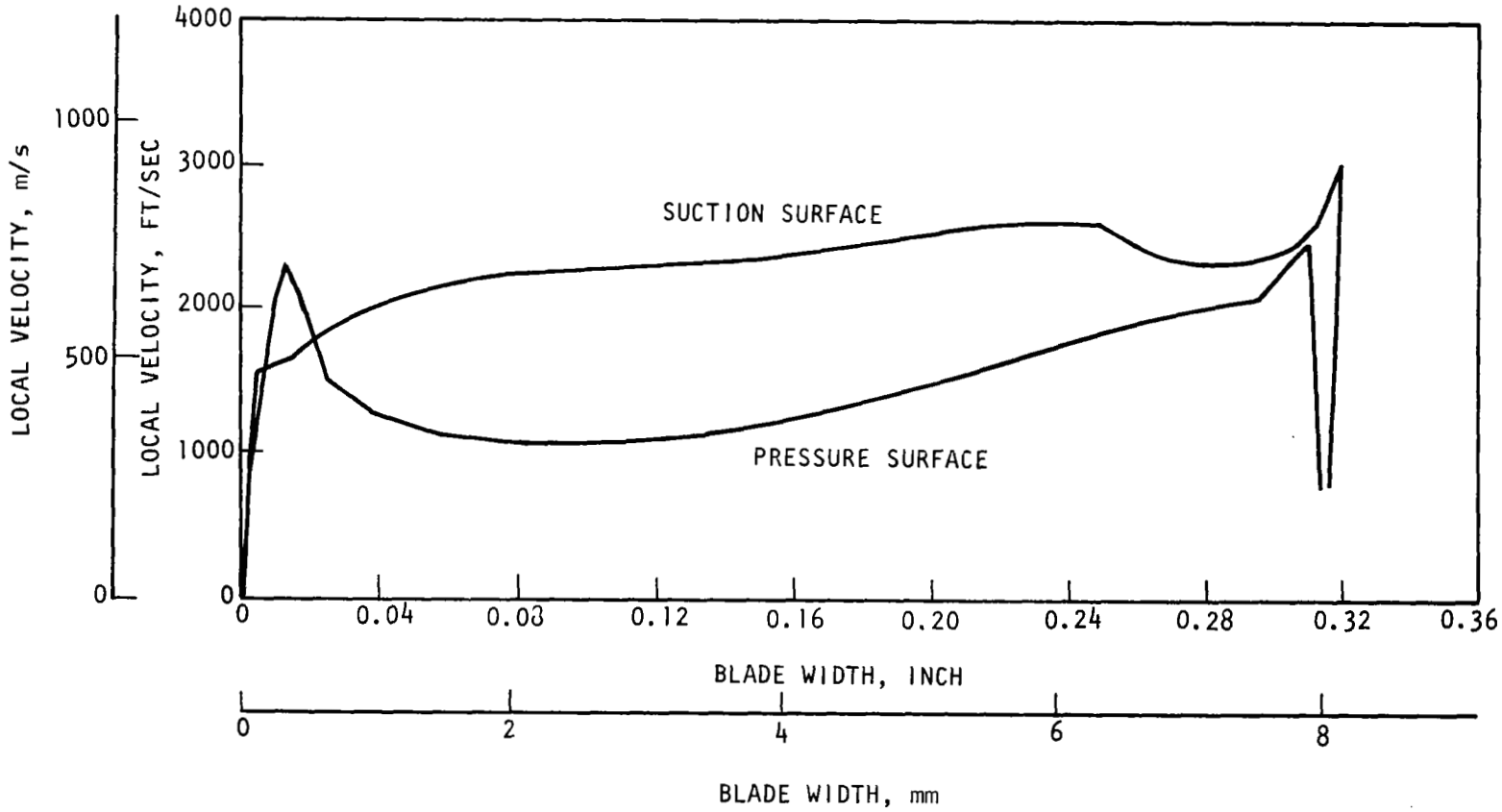

Figure 35. Mark 48-F Turbine First-Stage Rotor

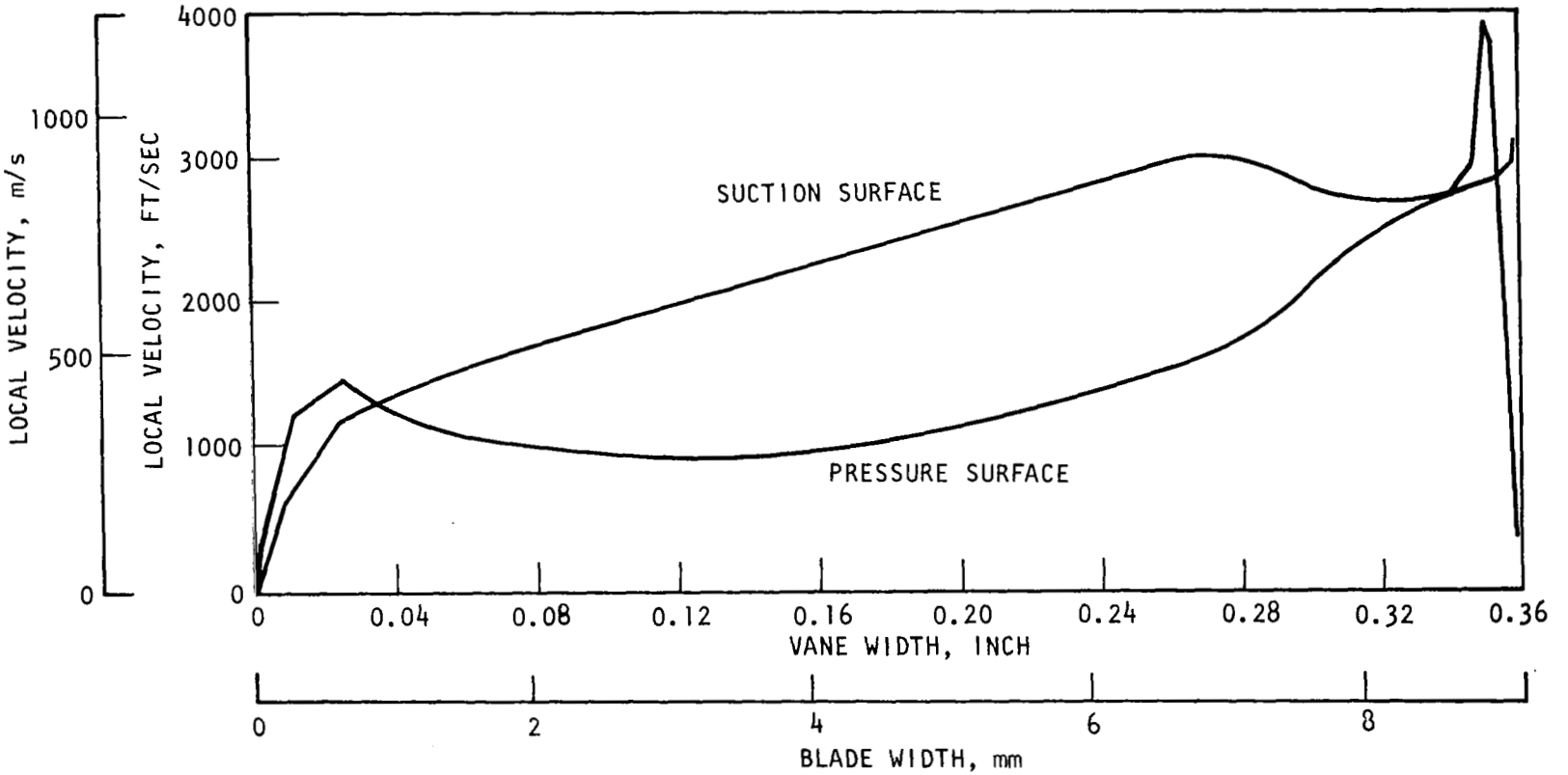

Figure 36. Mark 48-F Turbine Second-Stage Nozzle

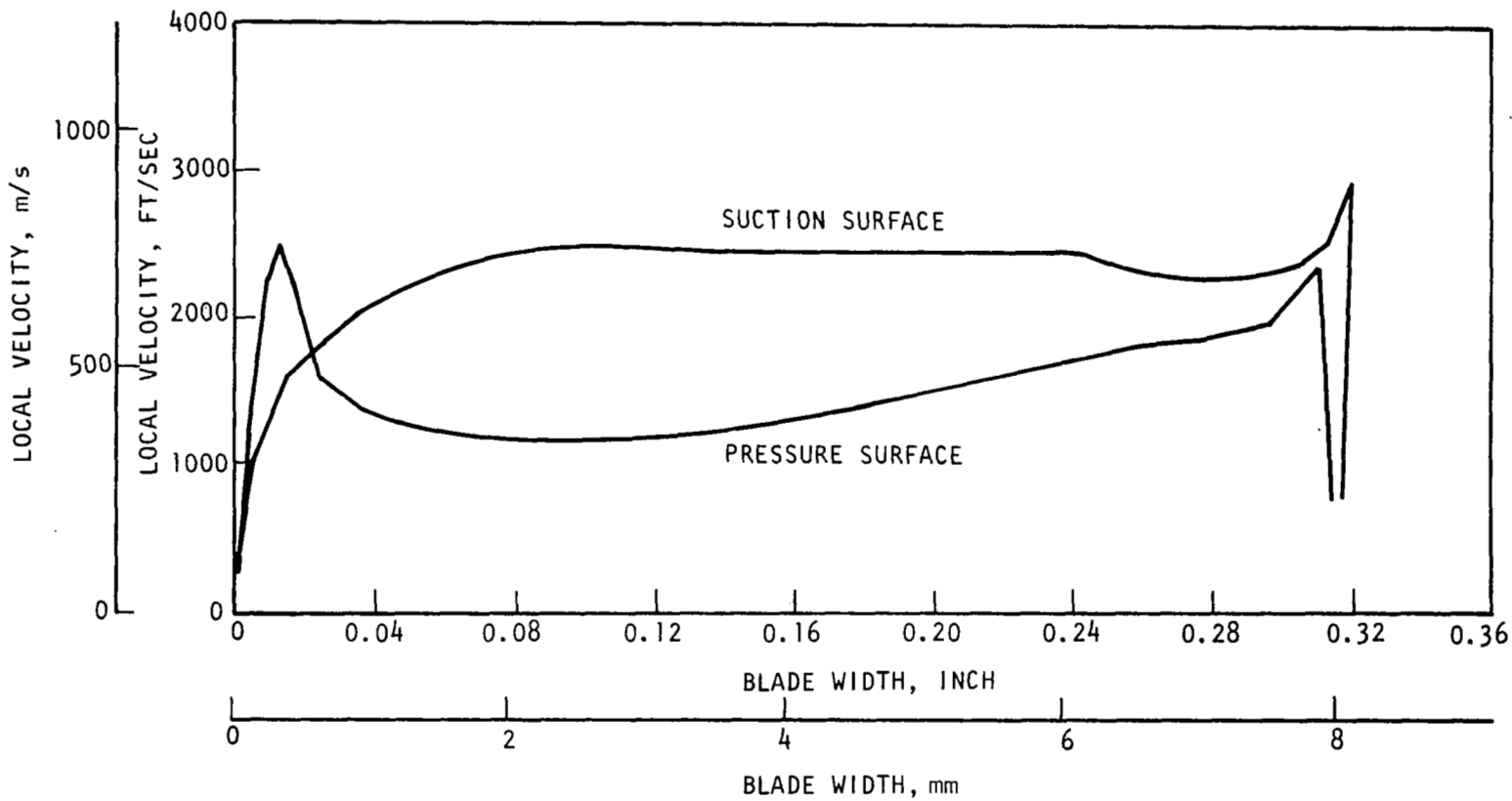

Figure 37. Mark 48-F Turbine Second-Stage Rotor

Axial Thrust Control

For a high-speed turbopump with hydrogen-cooled bearings, it is mandatory to balance the axial forces without asking the bearings to carry part of this axial load. During the design study, a large number of different turbopump design concepts were studied. The result was that the axial thrust could be balanced only by using a balance piston and flowing the turbine gases away from the pump.

The axial forces of the three pump stages are balanced as close as possible against the turbine axial forces by setting the impeller wear ring diameters so that the remaining forces are minimized. This remaining axial force is then balanced by a balance piston which is integral with the third-stage impeller. Axial thrust balancing devices always reduce pump efficiency due to the unavoidable leakage losses as well as to the disk friction losses. Therefore, the integral design concept is used since it avoids the additional disk friction losses inherent with a separate balance piston, and maintains the number of internal recirculation paths at a minimum. Figure 38 shows the balance piston flow loop. Because of constraints on the available radial space, the high-pressure orifice, as assembled, does not include a radial overlap feature between the rotating and stationary members. The positive diametral clearance of 0.076 mm (0.003 inch) which exists at assembly between those two components is reduced to zero by differential contraction during chilldown. Subsequently, as a result of centrifugal growth of the impeller, an overlap of 0.127 mm (0.005 inch) is realized at the nominal operating speed of 9947 rad/s (95,000 rpm).

The total balance piston axial travel at operating temperature and nominal speed is 0.254 mm (0.010 inch). Figure 39 shows the nominal forces acting on the impellers and the turbine. Figure 40 shows the net balance piston restoring force and flow as a function of the balance piston position.

Bearing Design

The Mark 48-F bearings are 20 mm bore, angular-contact ball bearings arranged in two spring-preload pairs. The forward pair is located immediately in front of the first-stage impeller; the aft pair is located between the third-stage impeller and the shaft seal. Both pairs are cooled by recirculating liquid hydrogen.

The Mark 48-F and Mark 48-0 bearings are identical. Dual use of the same bearing is technically feasible the bearing loading and speeds are compatible with both the design speed of the fuel pump 9947 rad/s (95,000 rpm) and that of the liquid oxygen pump, 7329 rad/s (70,000 rpm). Economy in procurement was also effected by purchasing only one type of specially designed bearing.

The internal geometry of the bearing was optimized for 9947 rad/s (95,000 rpm) and formalized into the Rocketdyne Source Control Drawing, RES1174 (Fig. 41). There was no existing bearing with satisfactory details, so a special bearing was designed and fabricated with the following features.

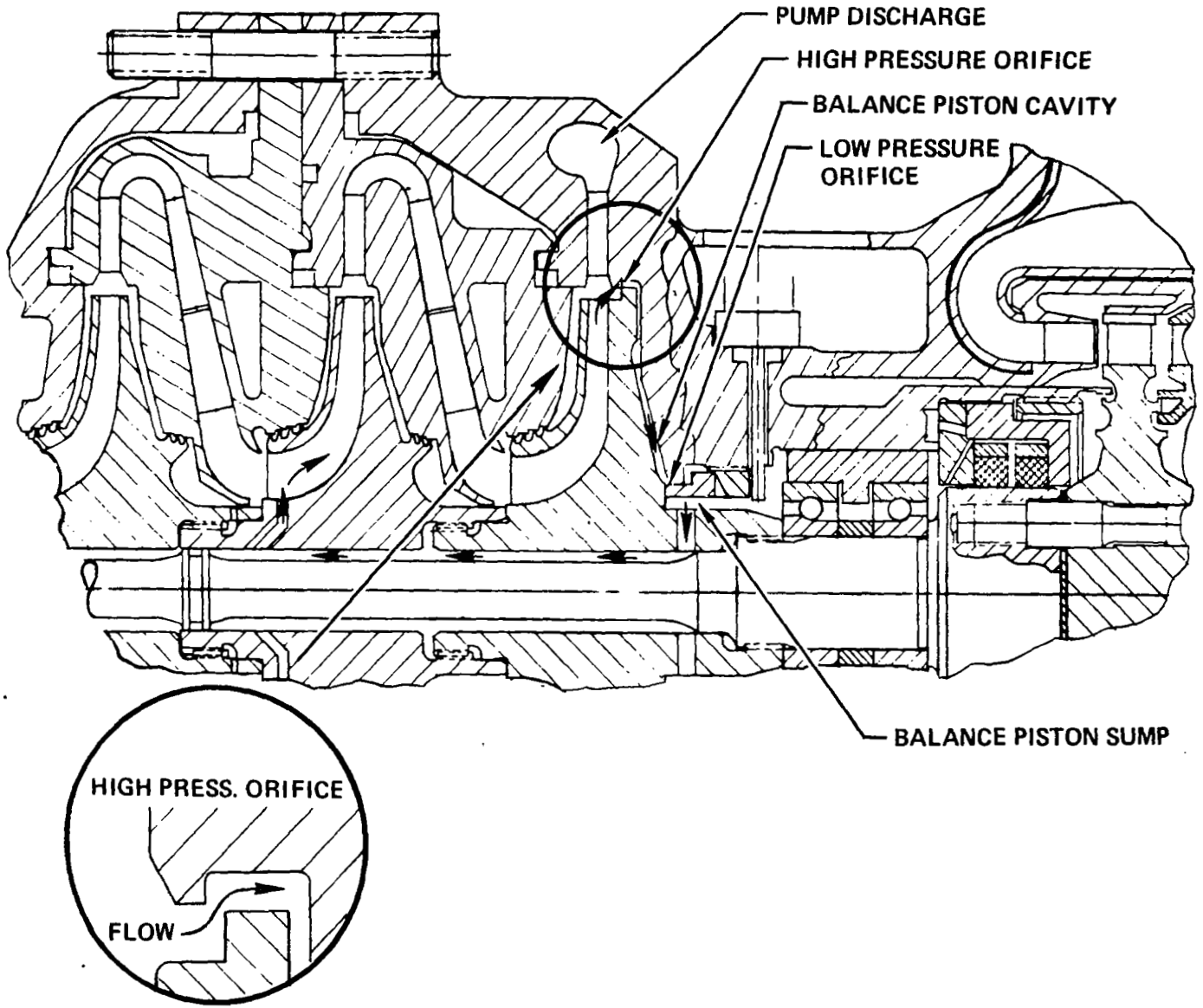

Figure 38. Mark 48-F Balance Piston Fluid Flow Path

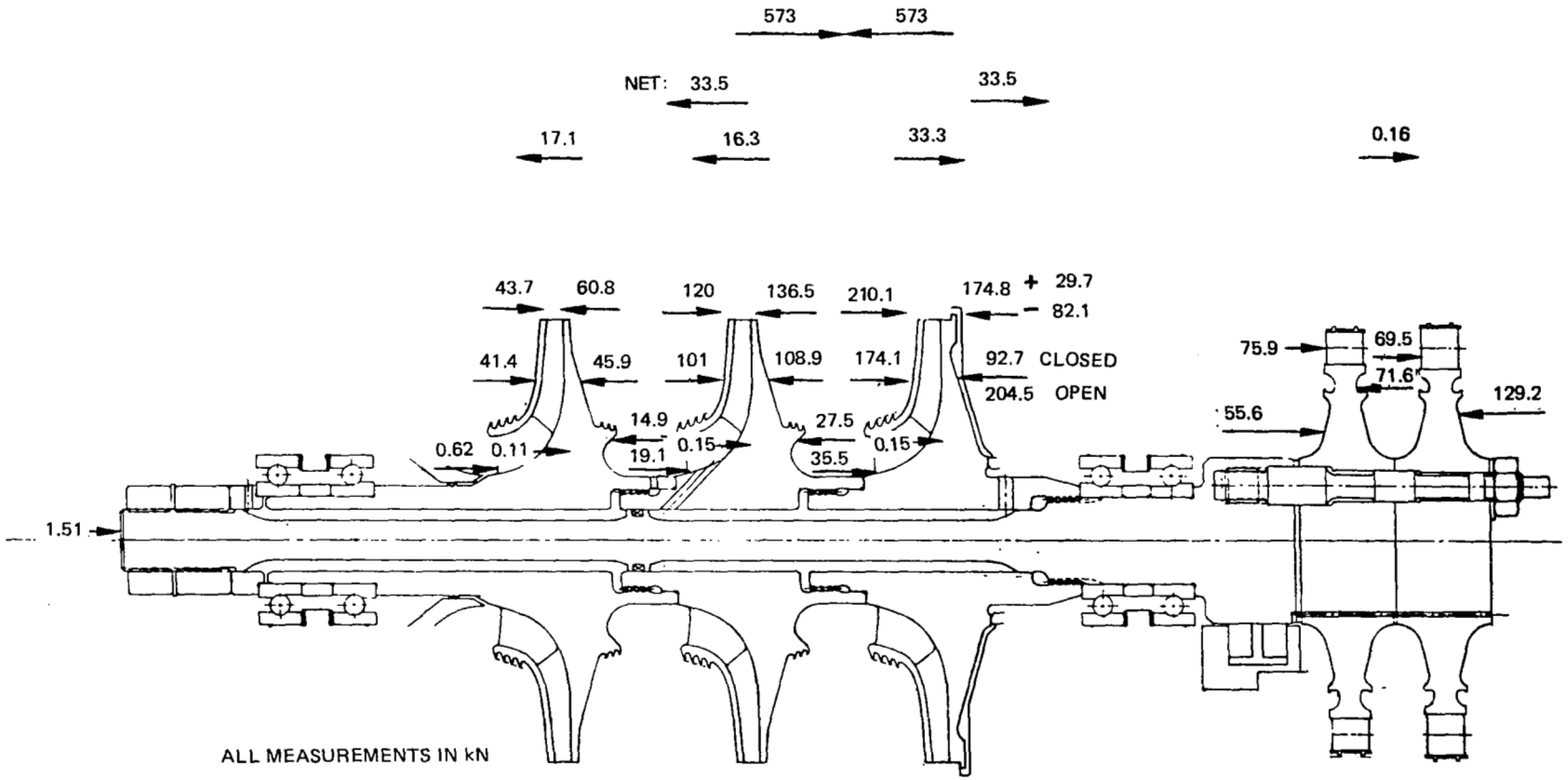

Figure 39. Mark 48-F Turbopump Axial Forces
(SI Units)

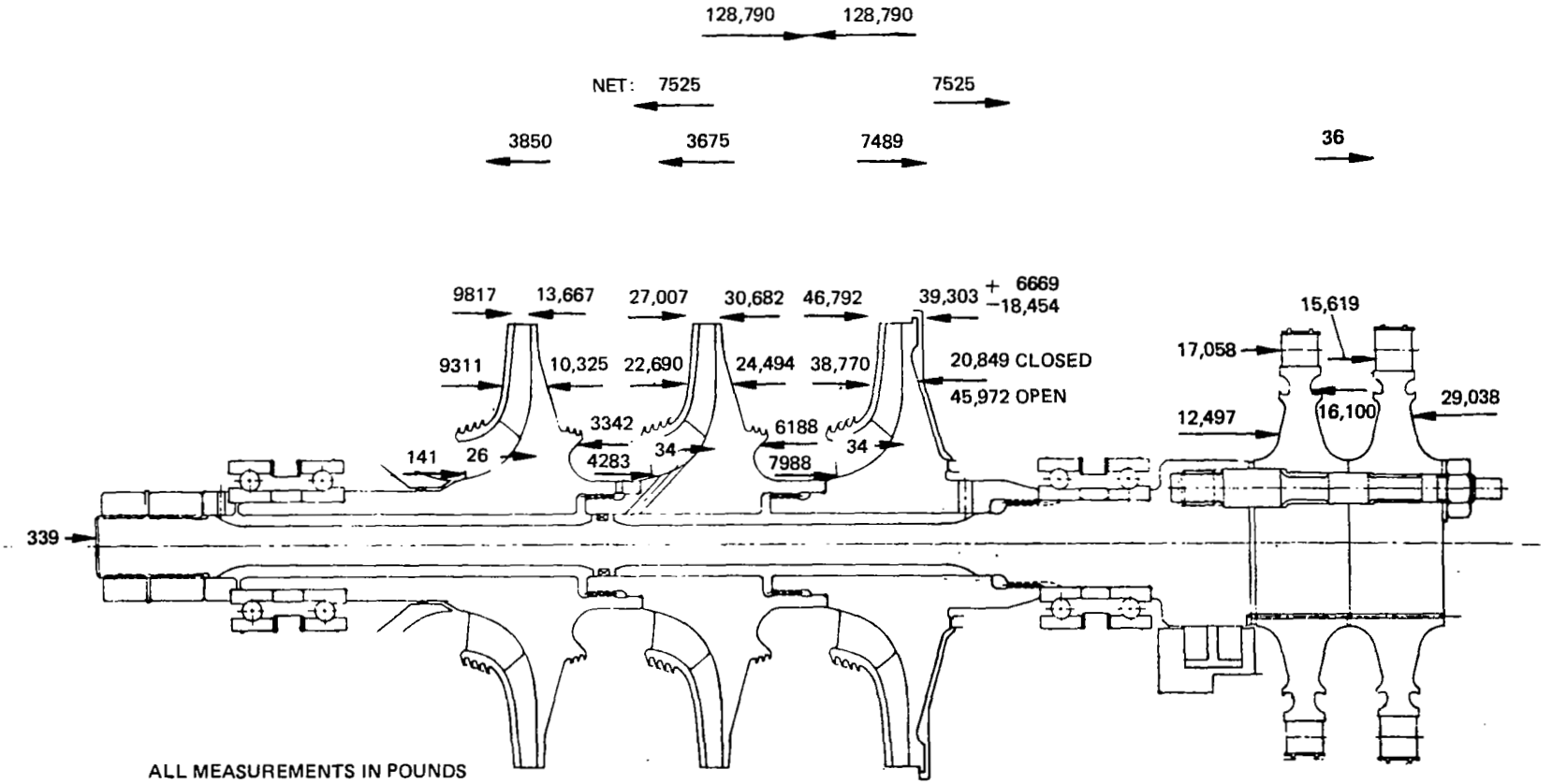

Figure 39. Mark 48-F Turbopump Axial Forces (English Units)

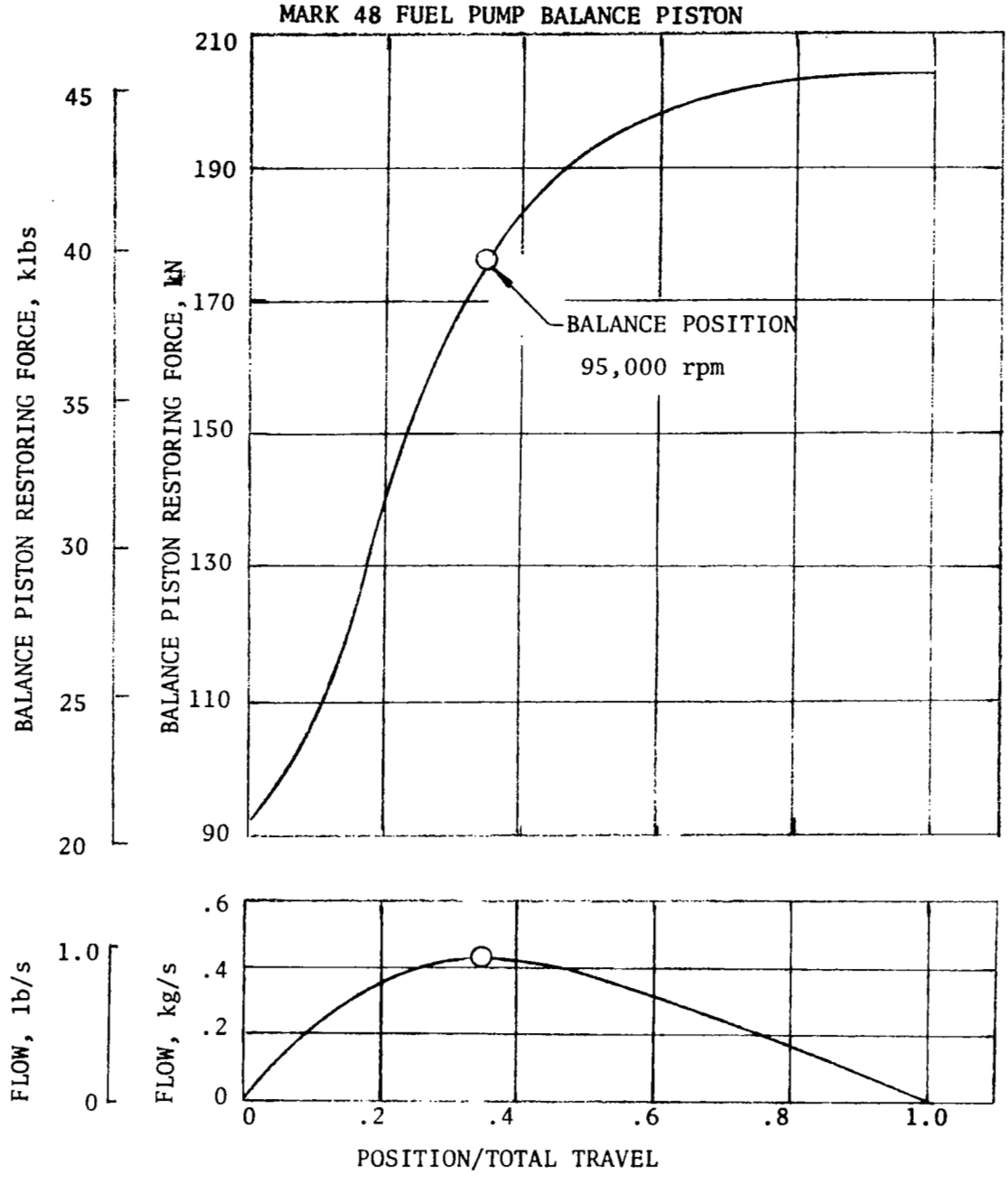

Figure 40. Mark 48 Fuel Pump Balance Piston

CHARACTERISTIC	ENGLISH UNITS	SI UNITS
ENVELOPE DIMS. -		
BORE	.78725 $^{+.00015}_{-.00000}$ DIA.	20 mm
OUTER DIA.	1.5354 $^{+.0000}_{-.0002}$ DIA.	39 mm
WIDTH (INDIVIDUAL RINGS)	.3937 $^{+.0000}_{-.0100}$	10 mm
(ACROSS BEARING)	.393 $\pm$.002 10 m	
INTERNAL GEOMETRY -		
PITCH DIA.	1.175 DIA. (REF.)	29.8 mm
RACE RADII (OUTER RACE)	52% OF BALL DIA. (REF.)	
(INNER RACE)	53% OF BALL DIA. (REF.)	
DIAMETRAL CLEARANCE (UNFITTED)	.0020 TO .0023 IN.	0.051 TO 0.058
(OPERATING)	.0011 TO .0014 IN. (REF.)	0.028 TO 0.036
BALL COMPLEMENT (NUMBER)	TEN	
(DIAMETER)	.1875 DIA. (NOMINAL)	4.76 mm
SHOULDER HEIGHTS (OUTER RACE)	20% OF BALL DIA. (REF.)	
(INNER RACE)	23% OF BALL DIA. (REF.)	
CAGE CLEARANCES (BALL POCKET)	.020 TO .025 IN.	0.51 TO 0.64 m
(GUIDING LAND)	.003 TO .009 IN.	0.08 TO 0.22 m
MATERIALS -		
RACES	CEVM 440-C R_C 58-62	
BALLS	CEVM 440-C R_C 60-64	
CAGE	GLASS FABRIC SUPPORTED TEFLON (ARMALON)	
CAGE WEB THICKNESS (AT PITCH DIA.)	.156 IN. (REF.)	3.96 mm

8. IDENTIFY FACES "A" & "B"
7. BALLS SHALL BE AFBMA GRADE 5
6. BEARING TOLERANCES NOT SHOWN SHALL BE PER
5. CLEAN & PACKAGE FOR LIQUID HYDROGEN SER
4. THE ARMALON CAGE SHALL MEET REQUIRMENTS
3. ONLY THE ITEM DESCRIBED ON THIS DWG WHEN SUPPLIER LISTED, IS APPROVED BY ROCKETDYNE, IN THE APPLICATION SPECIFIED HEREON. A SUBS USED WITHOUT PRIOR TESTING & APPROVAL BY
2. THE ITEM SHALL BE DURABLY & LEGIBLY MARKED ADDITION THE ROCKETDYNE CONTROL DWG NO. SH
1. MFG. SHALL PREPARE ANY NEW DWGS REQD & ASS & SHALL OBTAIN ROCKETDYNE ENGRNG. REVIEW C

NOTE UNLESS OTHERWISE SPECIFIED

SI UNITS
20 mm
39 mm
10 mm
29.8 mm
051 TO 0.058 mm
028 TO 0.036 mm
4.76 mm
51 TO 0.64 mm
08 TO 0.22 mm
3.96 mm

REVISIONS			
LTR	DESCRIPTION	DATE	APPROVED
	1. MAY BE REWORKED 2. CANNOT BE REWORKED 3. RECORD CHANGE 4. NOW SHOP PRACTICE 5. PARTS MADE OK		

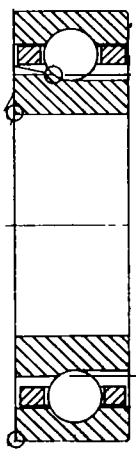

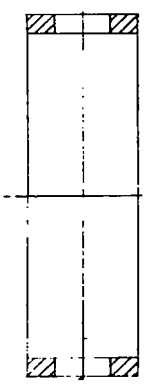

ROCKETDYNE CONTROL NO. & SUFFIX NO.	APPROVED SOURCE OF SUPPLY MFR. NAME AND ADDRESS	CODE IDENT.	MFR. PART NO.
-01 ( )			

Figure 41. Bearing Design

HALL BE PER ABEC 7.
DROGEN SERVICE. (CLEAN & DRY)
QUIRMENTS OF RB0130-013
S DWG WHEN PROCURED FROM THE
ROCKETDYNE, CANOGA PARK, CALIF. FOR USE
EON. A SUBSTITUTE ITEM SHALL NOT BE
PROVAL BY ROCKETDYNE.
BLY MARKED PER MIL-STD-130. IN
DWG NO. SHALL BE MARKED ON THE ITEM.
REQD & ASSIGN PART NO. PER MIL-D-1000
IG. REVIEW OF PROPOSED CHANGES.

SOURCE CONTROL DRAWING

HEAT TREAT | FINISH | MATL

UNLESS OTHERWISE SPECIFIED: DIMENSIONS ARE IN INCHES AND APPLY PRIOR TO FINISH.
125/ MACH. SURF. ROUGHNESS
TOLERANCES ON: ANGLES ± 0° 30' DECIMALS .XX ± .03 .XXX ± .010
HOLES NOTED "DRILL"

OVER	THRU	TOLERANCE
.0600	.0400	+ .0015 — .0010
.0400	.1300	+ .0020 — .0010
.1300	.2250	+ .0025 — .0010
.2500	.5000	+ .0030 — .0010
.5000	.7500	+ .0040 — .0010
.7500	1.2500	+ .0050 — .0010
1.2500	2.5000	+ .0060 — .0010

DO NOT SCALE PRINT

DWN	F. BERNARD	DATE 11-73
CHK		DATE 11-73
DRGN		
MATL		
STRUCT		
DESIGN ACTIVITY APVD		DATE

Rocketdyne North American Rockwell — Canoga Park, California — McGregor, Texas

BEARING, BALL - ANGULAR CONTACT

SIZE	CODE IDENT NO.	DRAWING NO.
D	02602	RES1174

SCALE 4/1 | SHEET

RES1174

54-5

1. Bearing Size. The dimensions of the dynamic components were minimized to reduce the inertial forces due to speed as far as possible, even though the liquid hydrogen pump bearings DN value of 1.9×10^6 is within the state of technology for liquid hydrogen-cooled bearings.

   The pitch diameter and outer race outer diameter were made different than those existing for a standard metric envelope to accommodate, at minimum size, the thicker inner race cross section required to withstand the bolt tension load in the Mark 48-F turbopump. The thicker inner race is also less prone to brittle fracture from tensile and thermal stresses.

2. Ball Complement. A ball diameter of 4.7625 mm (0.1875 inch) was selected in preference to the off-the-shelf bearing size of 5.556 mm (0.21875 inch) to reduce the centrifugal force and extend the fatigue life of the outer race. The number of balls was set at 10 to maintain a web thickness in the cage of over 3.81 mm (0.150 inch) to provide adequate wear life and cage strength.

3. Race Radii. The race radii, which are expressed as curvature (% of ball diameter), were selected to obtain maximum fatigue life consistent with practical manufacturing limitations. The outer race conforms closely to the ball surface with a 52% curvature. Lower curvatures (closer conformity) is avoided because excessive nonrolling action will occur in the ball-race contact. In addition, contact angle will vary rapidly for small changes in bearing internal clearance due to manufacturing tolerances, press fits, and thermal expansion.

   The bearing's fatigue life is maximized if the lives of the inner and outer races are equal. Therefore, the inner race curvature of 53% was selected to balance the race lives. Use of a higher (less conforming) curvature on the inner race is a reversal of commercial practice for low-speed bearings. It was done here to maintain reasonable life, contact angle, and clearance for the overall bearing while maximizing the fatigue life of the outer race, which is adversely affected by ball centrifugal forces at high speeds.

4. Race Shoulder Heights. The race shoulders were made deep enough to contain the ball contact "prints" at the contact stress limited axial load. This configuration takes full advantage of the bearing's potential capacity and, at the same time, does not excessively restrict the coolant flow area.

5. Cage Dimensions. The cage is outer land guided, so its outer diameter is dictated by the outer race inner diameter (dependent on bearing pitch diameter, ball diameter, and shoulder height) and adequate minimum clearance. Cage diametral clearance of 0.076 mm, (0.003 inch) minimum at ambient temperature is based on experience with larger cryogenic bearings and scaled to bearing size. The cage inner diameter

was selected to maximize coolant flow area and to ensure that the ball equators would meet the cylindrical section of the ball pockets with a minimum of 0.254 mm (0.010 inch) margin. The ball is then prevented from "plowing under" the cage. The resulting diametral clearance between the cage inner diameter and the inner race outer diameter is 1.778 mm (0.070 inch) to 1.930 mm (0.076 inch), resulting in a minimum coolant flow area of 86.6 mm^2 (0.134 $in.^2$). The cage axial cross-sectional area is 170 mm^2 (0.263 $inch.^2$). To provide adequate cage wear-life and strength, the cage web thickness between the ball pockets was held to 3.81 mm (0.150 inch) minimum in selecting the number of balls (10). The resulting nominal cage web thickness at the pitch diameter is 3.96 mm (0.156 inch).

The cage ball pocket clearance was made large at 0.51 to 0.64 mm (0.020 to 0.025 inch) to permit ball position adjustments during operation without excessive cage forces. Adequate pocket clearance has been found to greatly reduce the amount of heat generated at the cage where radial loads or misalignments occur.

6. Diametral Clearance. The specified diametral clearance as measured on an unmounted bearing was based on the value required for dynamic operation, with additional amounts to compensate for the expansion of the inner race due to press fit on the shaft and centrifugal expansion of the inner race at speed.

Analysis. The selected bearing design was analyzed using a digital computer program which calculates forces, deflections, and stresses for each ball, and overall forces, deflections, and fatigue life of the individual races and the entire bearing. The spring preloads required for satisfactory operation of the bearing were calculated using an emprically developed relationship of ball size, speed, contact angle, and pitch diameter. The preload required is 431 N (97 pounds) for the LH_2 pump bearing.

In selecting the bearing design, a comparison was made of the effect on life of using the minimum bore diameter with the resulting bearing pitch diameter and required preload. Figure 42 presents the B_1 (99% survival) life for a 19 mm bore and a 20 mm bore bearing. To obtain a standard bore size as well as provide some margin on the shaft size, 20 mm was selected. As can be seen in Fig. 42, no substantial benefit in life would have been achieved by using a 19 mm bore bearing. The 10,476 rad/s (100,000 rpm) speed used in the Mark 48-F bearing analysis was later reduced to 9947 rad/s (95,000 rpm), but this change would not alter the results significantly. Figure 43 presents the selected design's fatigue life (shown here as B_{10} or 90% survival life) as a function of axial load at the Mark 48-F speed of 9947 rad/s (95,000 rpm). The preload criterion resulted in a required axial load of 431 N (97 pounds) at this condition.

Figure 44 presents the analytical values of radial stiffness (used in shaft dynamic analysis) as a function of axial load and speed. Radial stiffness affects shaft dynamic response and is affected by axial load; therefore, proper design and deflection control of the preload springs are important.

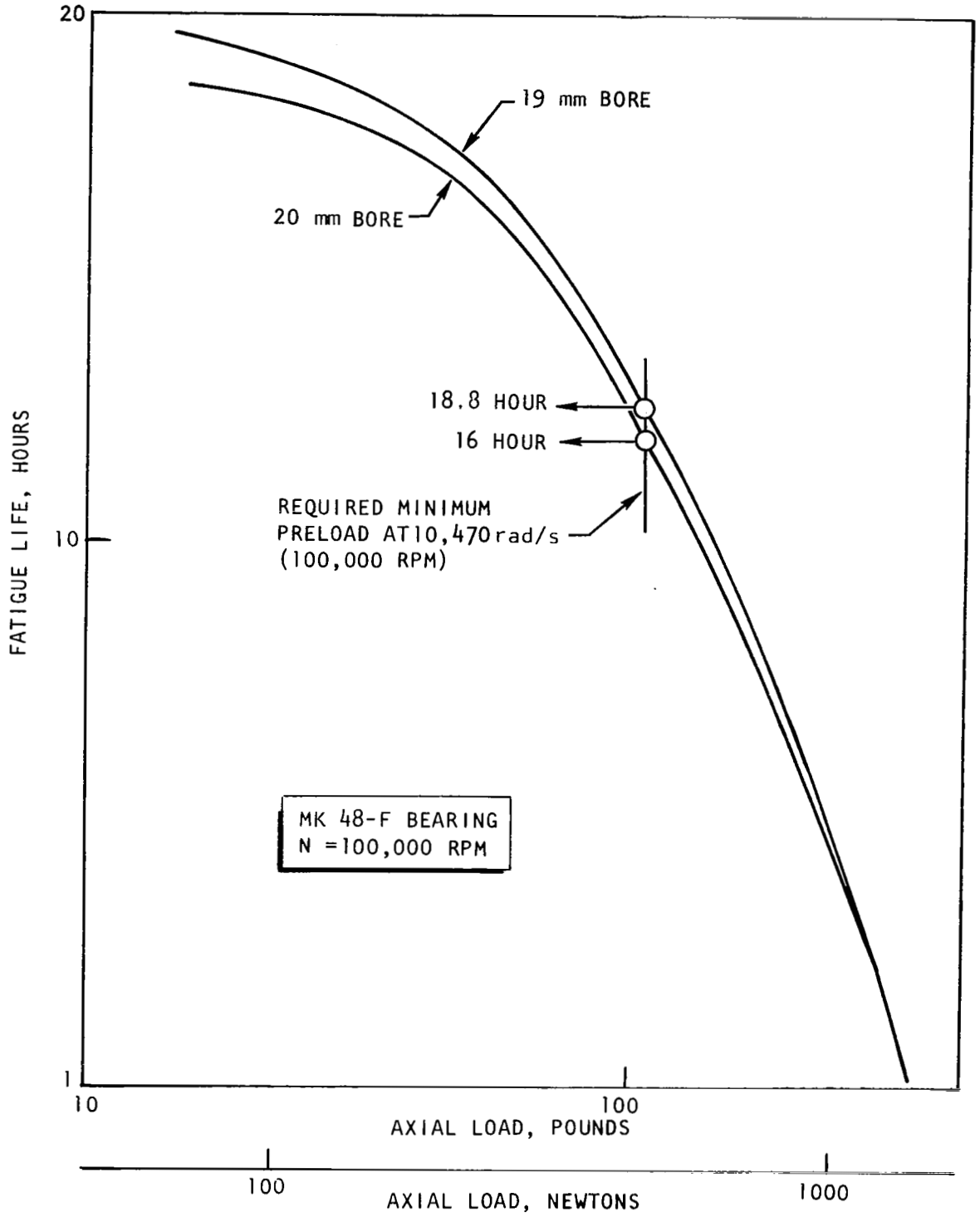

Figure 42. Mark 48-F Bearing B_1 Life

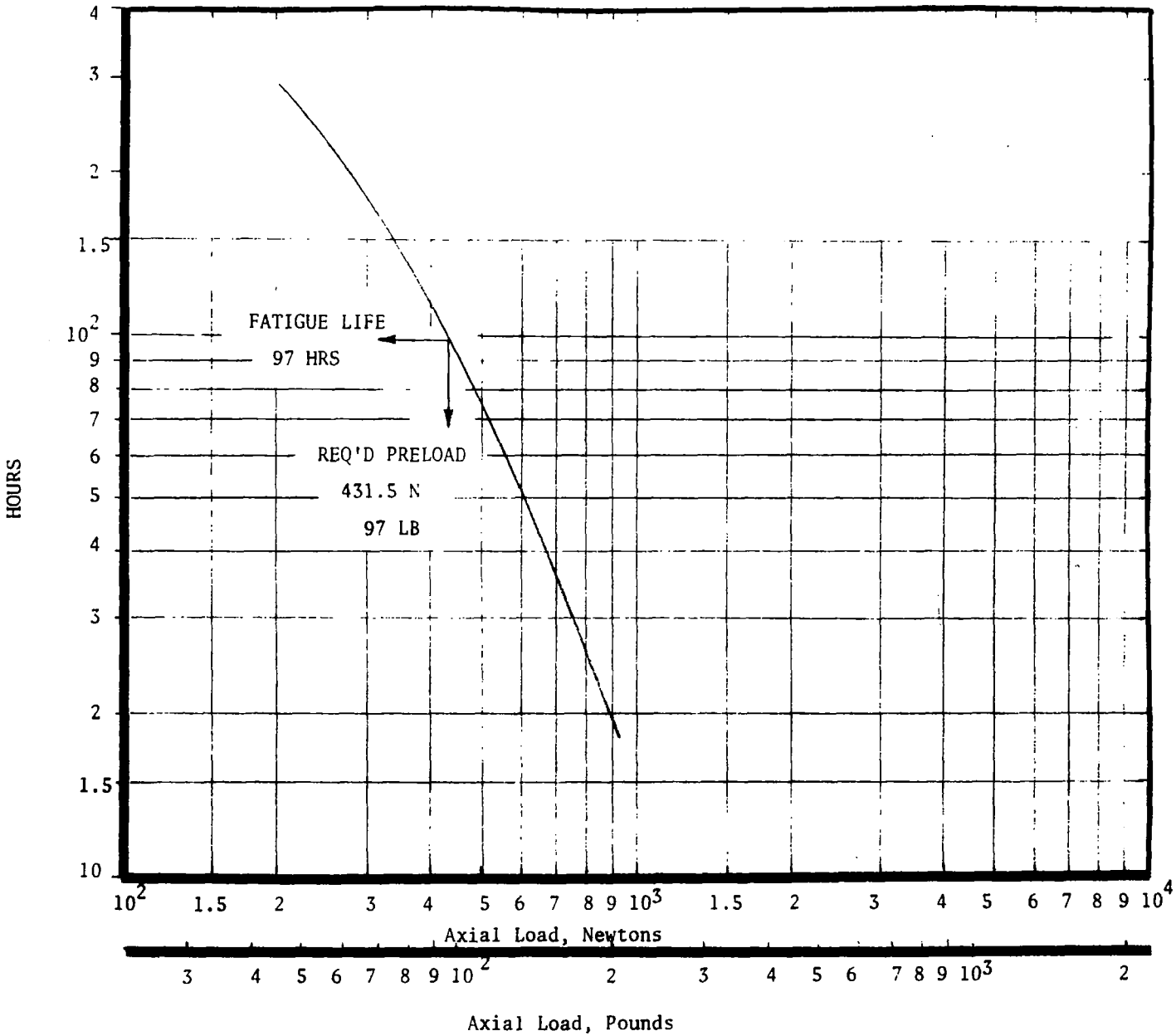

Figure 43. Mark 48-F Bearing Life vs Axial Load

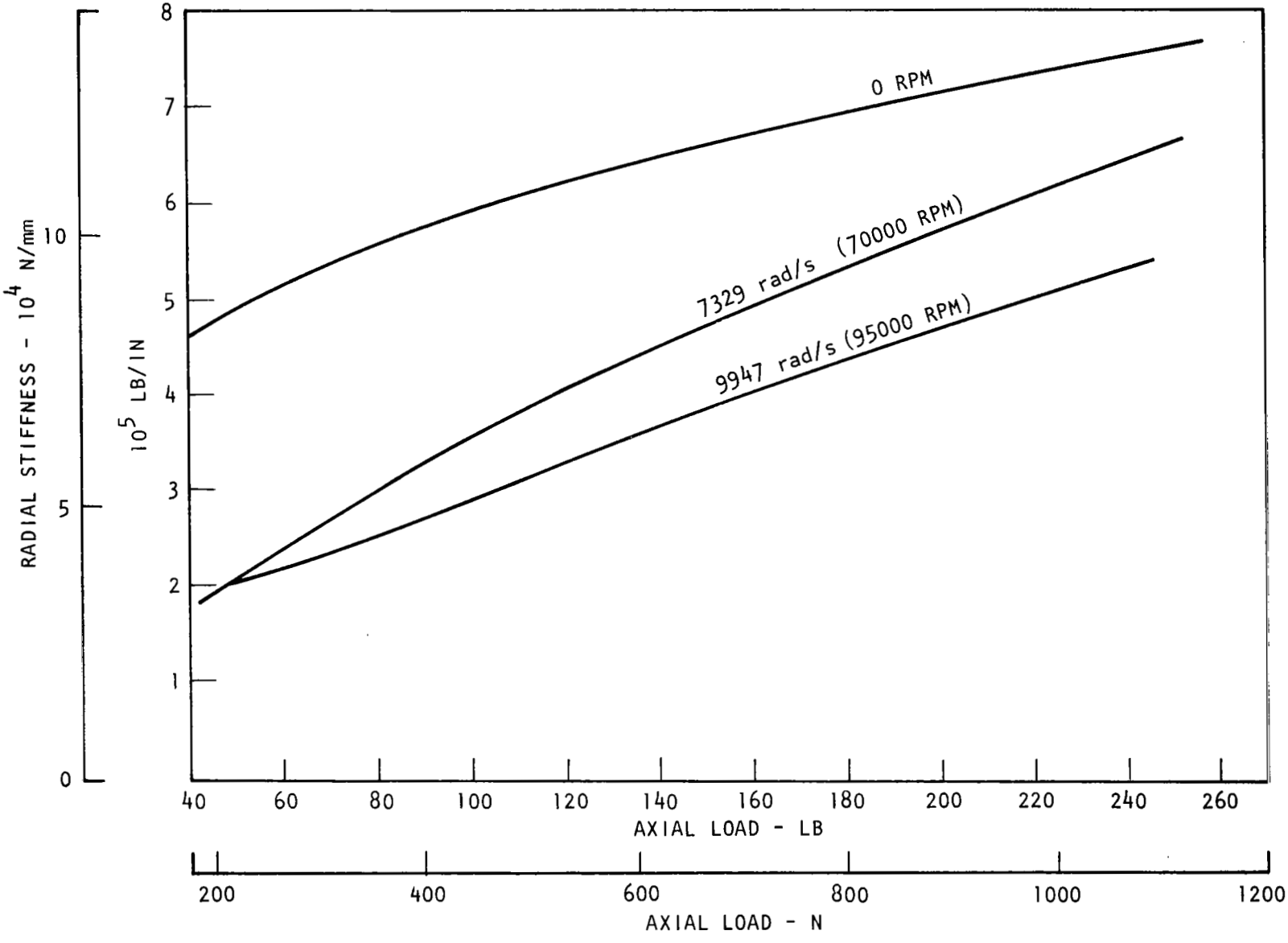

Figure 44. Mark 48-F Bearing Stiffness Versus Axial Load

Figure 45 presents the effect of speed on the relative axial deflections for given axial loads. This relationship was used in specifying the thickness of the inner race spacers so that both the following will be achieved:

1. Adequate preload at speed

2. Compensation for the increased loading by speed effects, therefore avoiding unnecessary increase in axial load with attendant reduction in life.

The turbopump configuration is such that it will accommodate not only the extra-light 20 mm bearings selected by Rocketdyne, but also the heavier ball bearings and the hybrid bearing selected by Mechanical Technology, Inc., in a parallel bearing technology program sponsored by Lewis Research Center. The installation of the three bearing configurations is illustrated in Fig. 46 through 48.

Seal Design

Ingress of turbine propellant gas into the pump region is prevented by a controlled-gap, shaft-riding seal. Although the pump and turbine fluids are chemically compatible, the turbine fluid contains steam, which would freeze when in contact with LH_2; therefore, it must be kept out of the pump where it could have a detrimental effect, particularly on the bearings.

Since the pressure on the pump side of the seal is lower than on the turbine side, the middle of the seal is pressurized with LH_2 supplied from the pump discharge as shown in Fig. 49. In this manner, a positive flow of LH_2 toward the turbine is ensured, and entry of hot gas into the pump is prevented. The LH_2 that leaks through the shaft seal toward the pump is used to lubricate the bearings, and the fluid that leaks to the turbine is used to cool the turbine disks.

The feed passages to the seal are orificed to maintain a pressure level of 2189 N/cm^2 (3175 psia) compared with 1380 N/cm^2 (2000 psia) in the bearing area and 1988 N/cm^2 (2884 psia) on the turbine side. The sum of the leakage and coolant bypass flowrate toward the pump was calculated at 0.065 kg/s (0.144 lb/sec). The leakage toward the turbine was projected to be 0.026 kg/s (0.058 lb/sec).

Shaft Seal Detail Design. The detail features of the shaft seal are illustrated in Fig. 50. Both sealing elements utilize a floating-ring, controlled-gap seal ring. The floating-ring element consists of an inner Am-Cer-Met ring for strength and thermal expansion/contraction control. The outer ring material is selected to provide the same thermal expansion and contraction rate as the shaft material, so that a constant clearance gap is maintained as the temperature changes. The outer ring is sufficiently strong, relative to the inner ring, to control the diameter of the composite ring. The inner ring is maintained in compressive hoop stress with an interference fit.

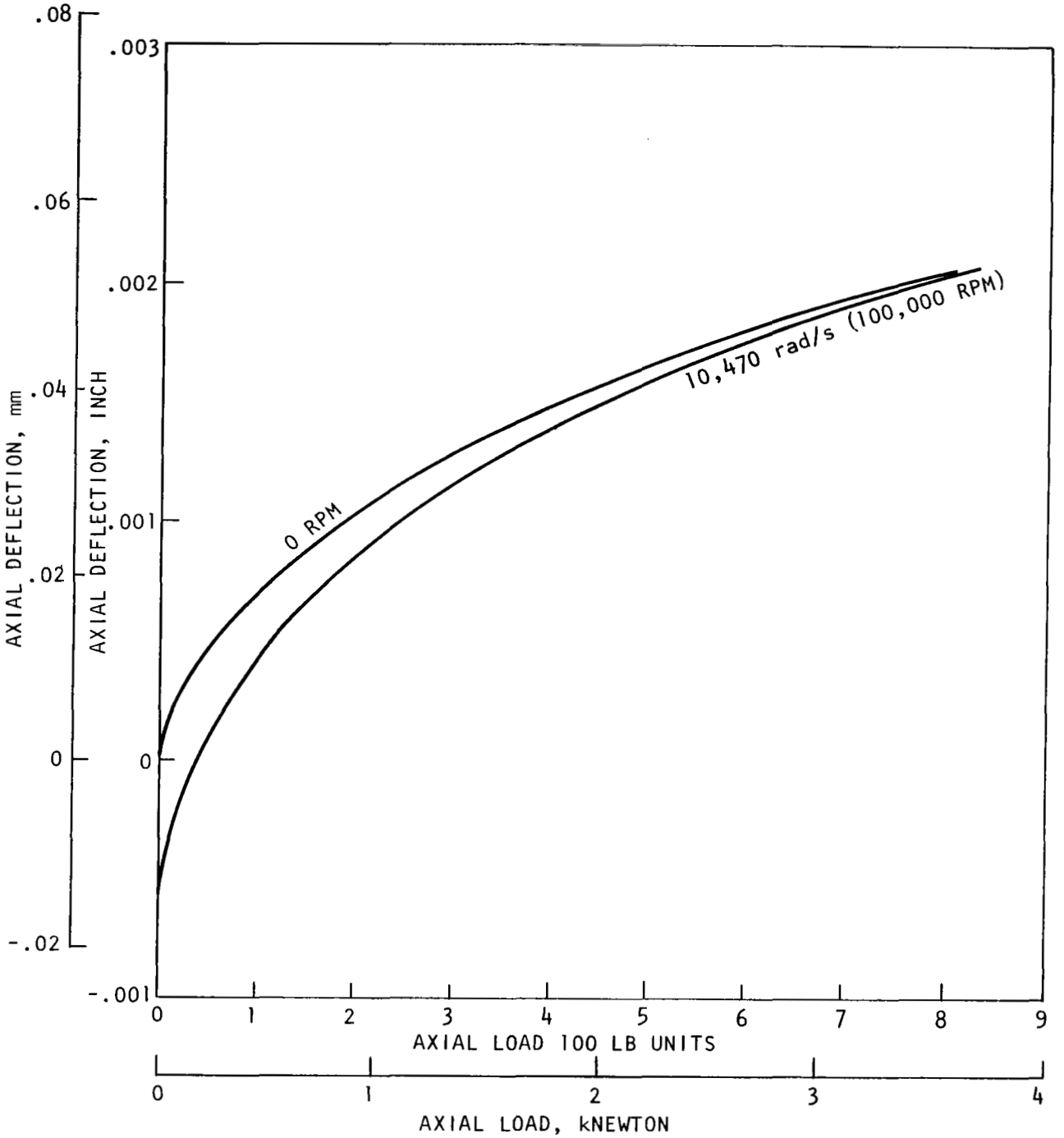

Figure 45. Mark 48-F Bearing Axial Deflection vs Axial Load

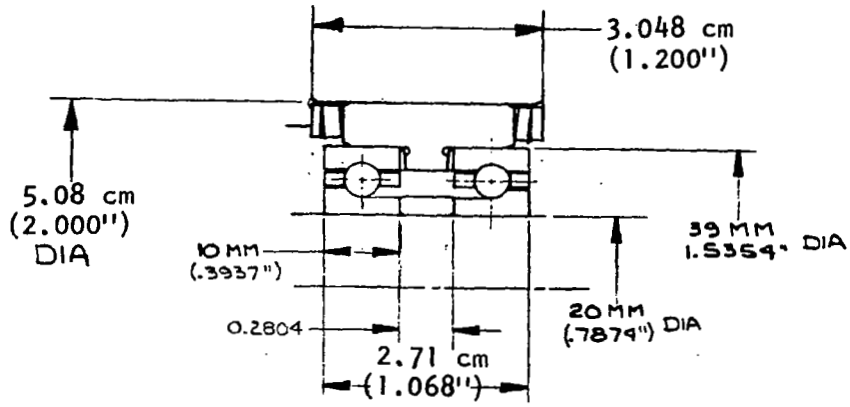

Figure 46. Mark 48-F Turbopump Rocketdyne Bearing Installation

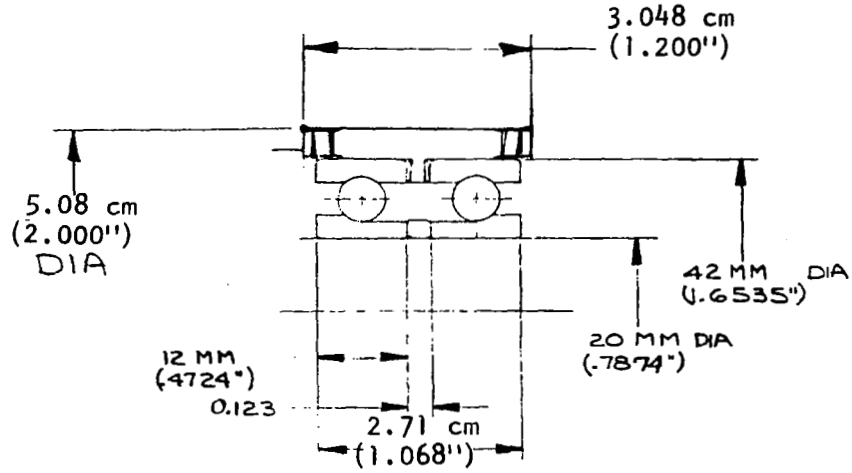

Figure 47. Mark 48-F Turbopump MTI Ball Bearing Installation

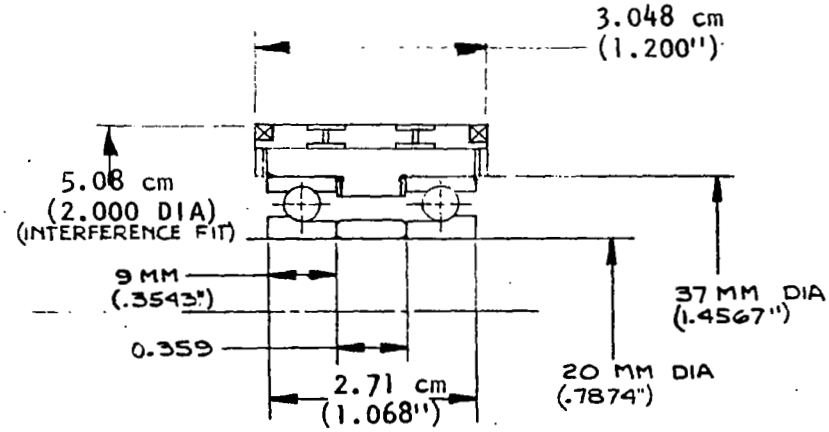

Figure 48. Mark 48-F Turbopump Hybrid Bearing Installation

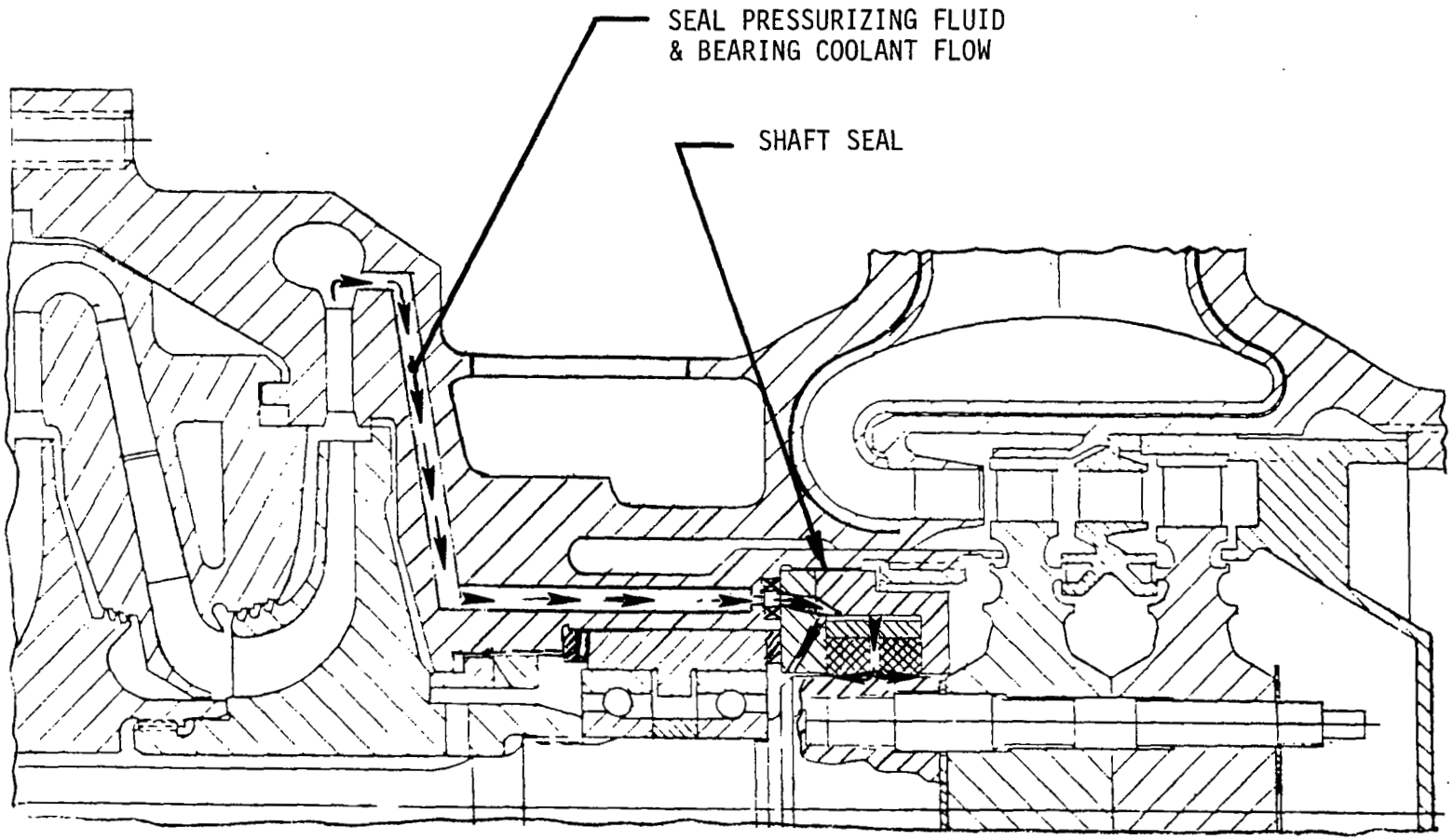

Figure 49. Mark 48-F Turbopump Shaft Seal Configuration

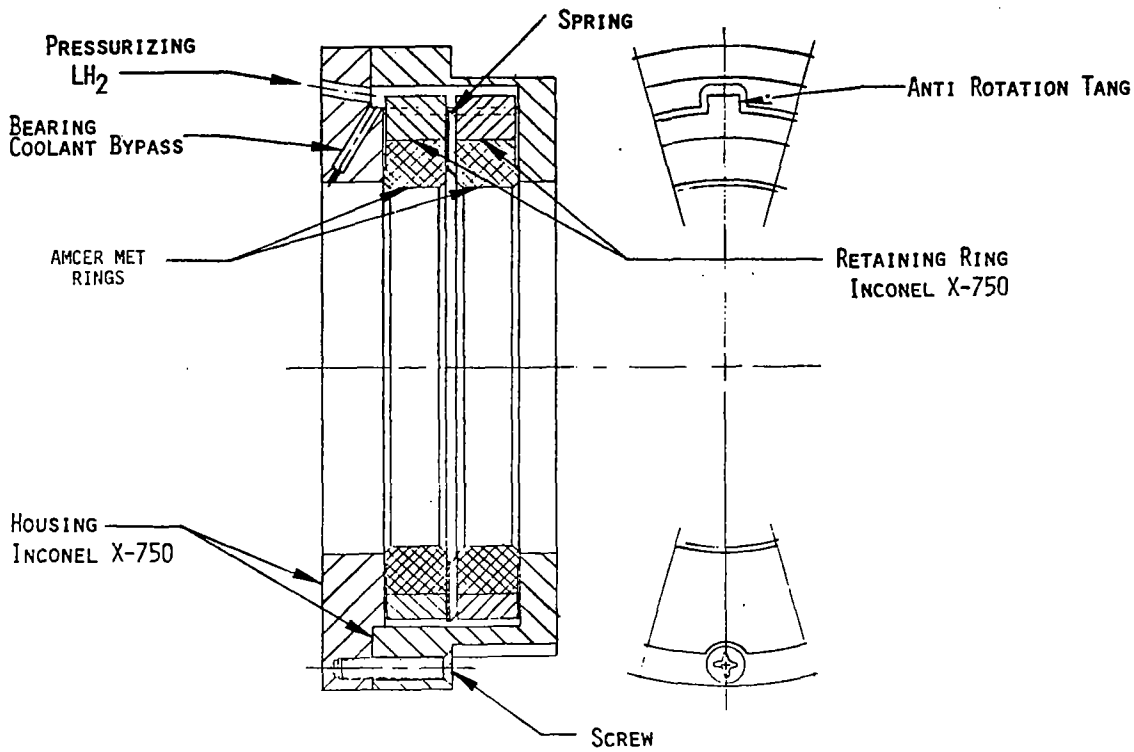

Figure 50. Mark 48-F Shaft Seal

The load induced by unbalanced radial pressure (Fig. 51) is supported by the composite ring in compressive hoop stress. The radial deflection caused by the compressive stress is proportional to ring rigidity. The radial section and modulus of elasticity are selected to minimize the deflection. The initial clearance is adjusted to allow for the deflection and provide the desired operating clearance.

The axial force induced by differential pressure (Fig. 51) loads the floating ring against the stationary housing to provide a static seal. A wave spring is provided to ensure sufficient contact load to maintain a static seal. The seal ring is partially pressure balanced by relieving the axial contact surface and minimizing the housing-to-shaft clearance to reduce the unbalanced axial-pressure-induced load. The floating-ring element is restrained from rotation with two antirotation tangs that engage slots in the housing.

The seal ring clearance gap was established by first performing a thermal analysis to determine the temperature gradient in the turbopump shaft seal area.

A finite-element stress analysis was performed using the temperature distribution and centrifugal loading to establish the shaft operating diameters. The seal ring design was established to maintain the required operating clearance gap. The Inconel X-750 retaining band material has approximately the same thermal contraction and expansion rate as the Inconel 718 shaft material to minimize the gap change due to temperature.

The seal ring design was optimized by utilizing a computer program in which the temperature, pressure, materials, and overall dimensional data are input. The computer calculates the seal ring stresses and deflections for varying radial sections of the retaining band and insert. The seal ring dimensions were then selected, consistent with the proper stress levels, to provide the minimum change in clearance gap. The static ambient seal ring clearance gaps were established, consistent wit the clearance differentials, to provide the required operating clearance gaps. The resulting ambient and operational clearances are listed in Table 9.

TABLE 9. MARK 48-F SHAFT SEAL CLEARANCES

	Pump–Side Ring		Turbine–Side Ring	
	SI Units, mm	English Units, inch	SI Units, mm	English Units, inch
Nominal Ambient Diametral Clearance	0.079	0.0031	0.074	0.0029
Nominal Operational Diametral Clearance	0.046	0.0018	0.046	0.0018

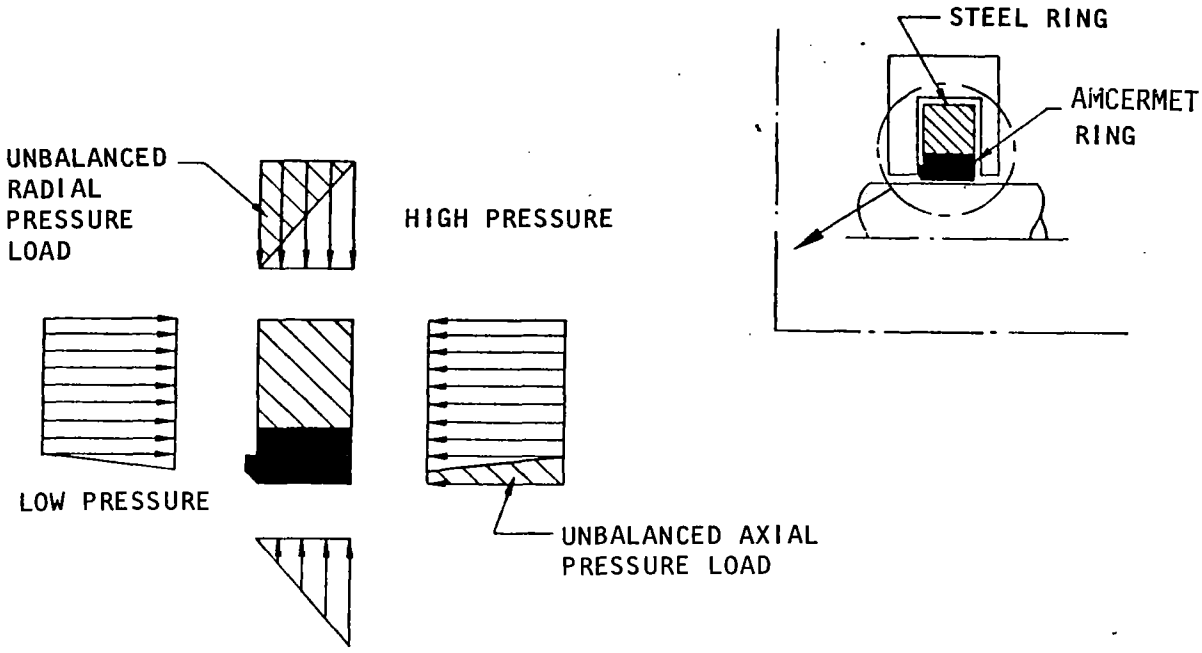

Figure 51. Pressure Forces on a Floating-Ring Seal

Static Flange Seals. All static flange seals are of the pressure-sensitive, metal-spring type illustrated in Fig. 52. The seals are designed and fabricated for each specific application by the Hydrodyne Division of Donaldson Co., Inc. The base material was Inconel X-750, with a 0.0076 mm (0.003 inch) silver plating applied to improve sealing effectiveness.

Impeller Wear Rings. Internal recirculation of LH_2 around the impeller front and rear shrouds is controlled by step-labyrinth wear rings as indicated in Fig. 53. The nominal diametral clearance between the rotating number and stationary platform is set at 0.20 mm (0.008 inch). With this clearance, some rubbing contact is expected because of excentricities and deflections. To moderate the effect of rubbing, a 0.25 mm (0.010 inch) thick layer of silver plating is applied to the stationary platforms.

Rotordynamics

Critical speeds of the rotor were calculated by the lumped parameter method in which the rotor is transformed into a series of mass points whose spacing approximates the mass distribution of the actual rotor. The resulting critical speeds are presented as a function of turbine end bearing spring rates in Fig. 54. The effect of the pump end bearing spring rate is indicated in a parametric form. The predicted radial spring rate of the bearings is 49,000 N/mm (280,000 lb/in.). At this spring rate, the first critical is located at

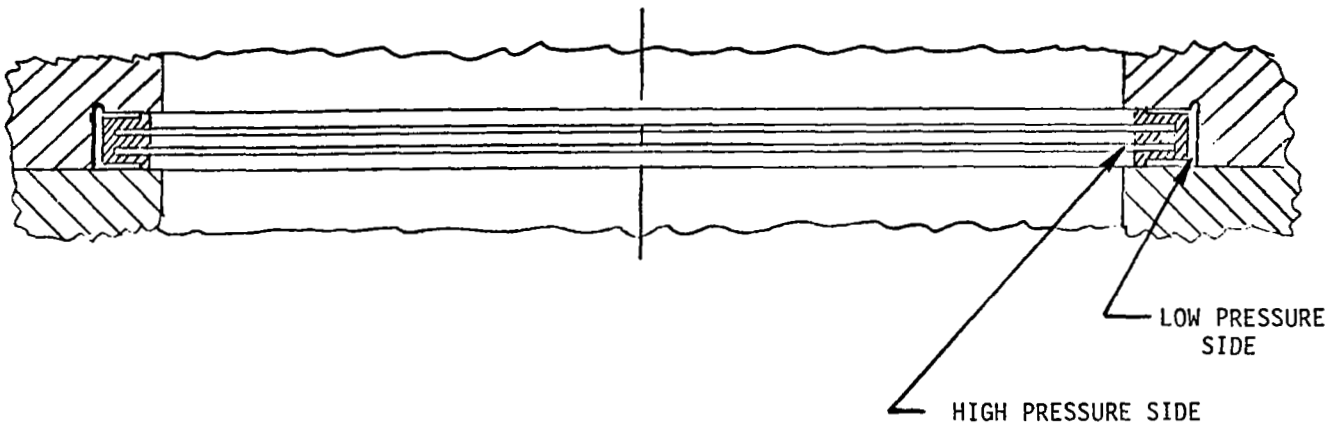

Figure 52. Typical Static Flange Seal Configuration

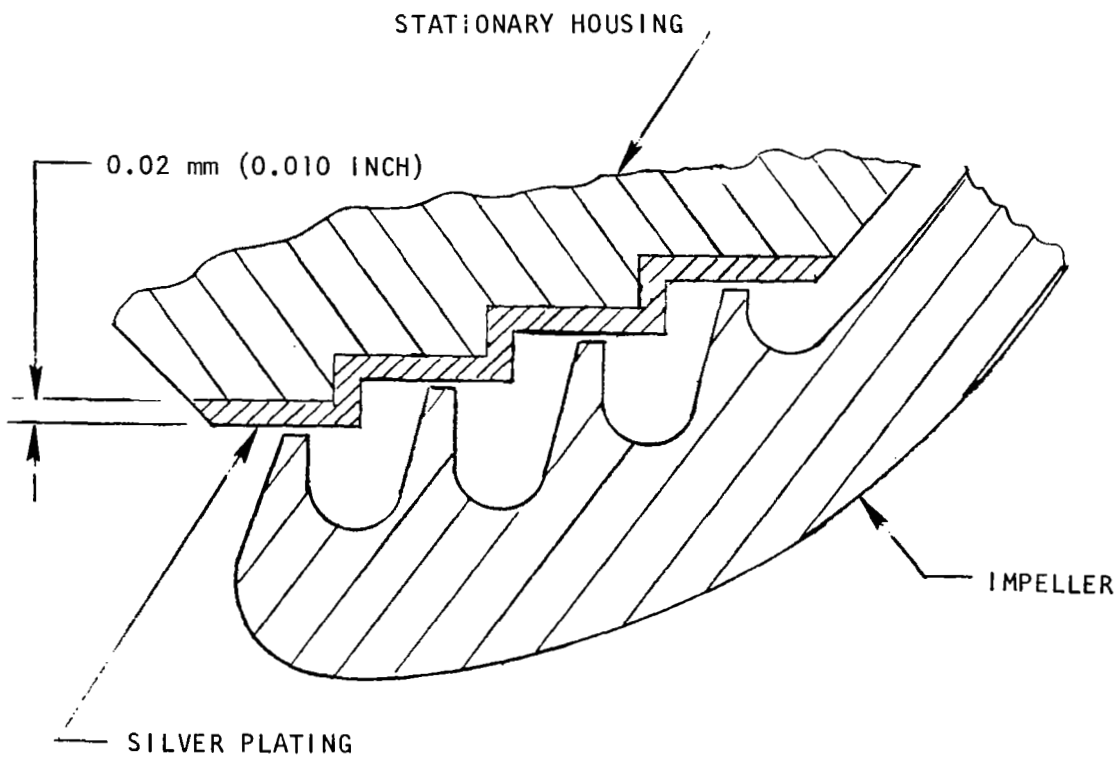

Figure 53. Mark 48-F Impeller Wear Ring

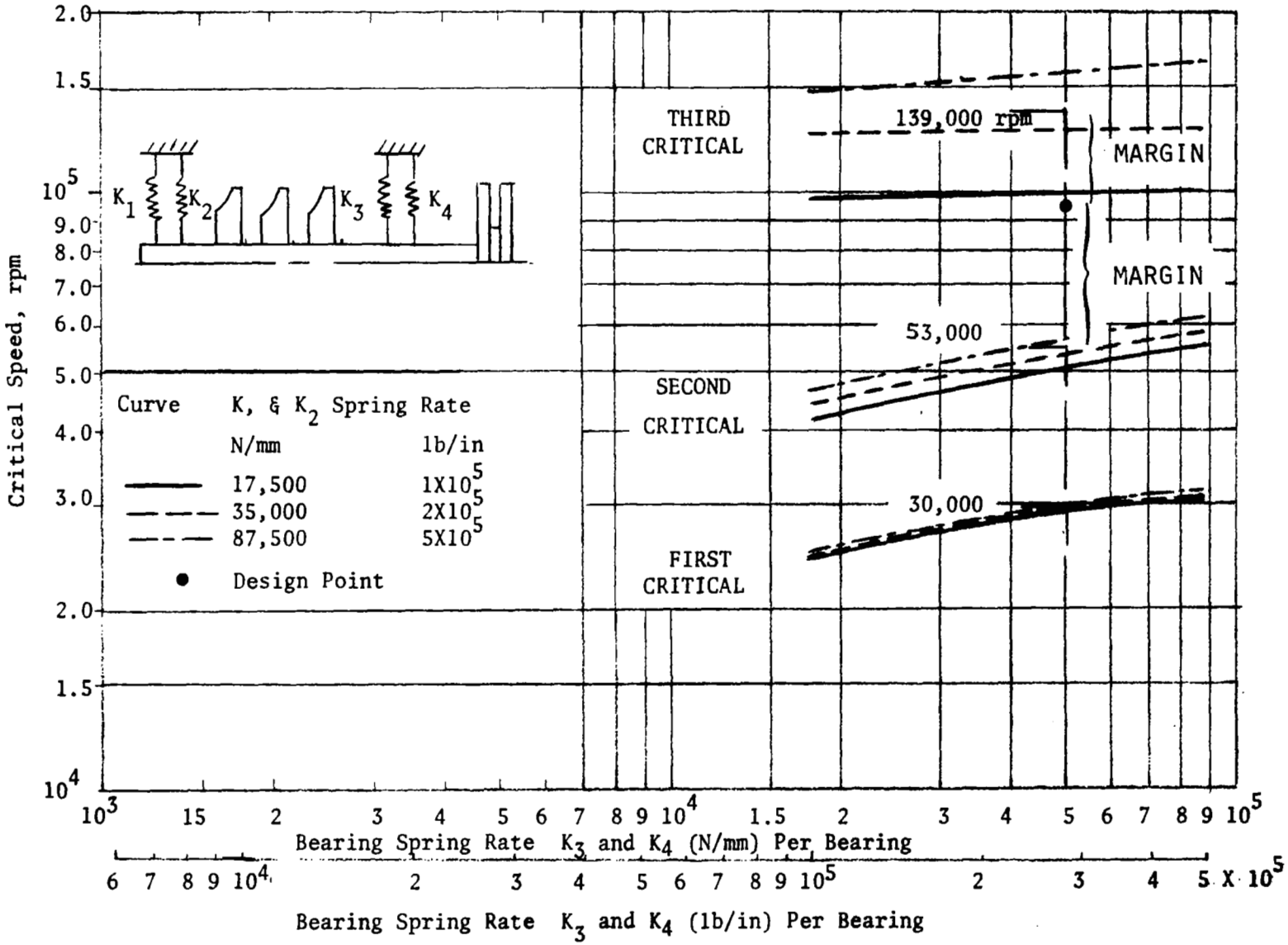

Figure 54. Mark 48-F Turbopump Rotor Critical Speeds

3141 rad/s (30,000 rpm), the second at 5549 rad/s (53,000 rpm), and the third critical at 14,550 rad/s (139,000 rpm). The nominal speed of the pump at 95,000 rpm will be located between the second and third critical with ample margin on each side. The rotor mode shapes at the three critical speeds are shown in Fig. 55.

The pump end of the rotor is formed by the impeller hubs which are piloted relative to each other by interference fits. The critical speed calculations are based on being able to maintain tight axial interfaces at the impeller hubs. To accomplish this, the impellers are preloaded axially with a center tie bolt. The minimum tension in the tie bolt was established at 50,000 N (11,230 pounds), which includes a 50% margin over the anticipated separating load of 33,310 N (7489 pounds) (Fig. 39) between the impellers. The minimum preload on the impellers exists after accounting for differential contraction rates as well as axial shrinkage due to Poisson's effect.

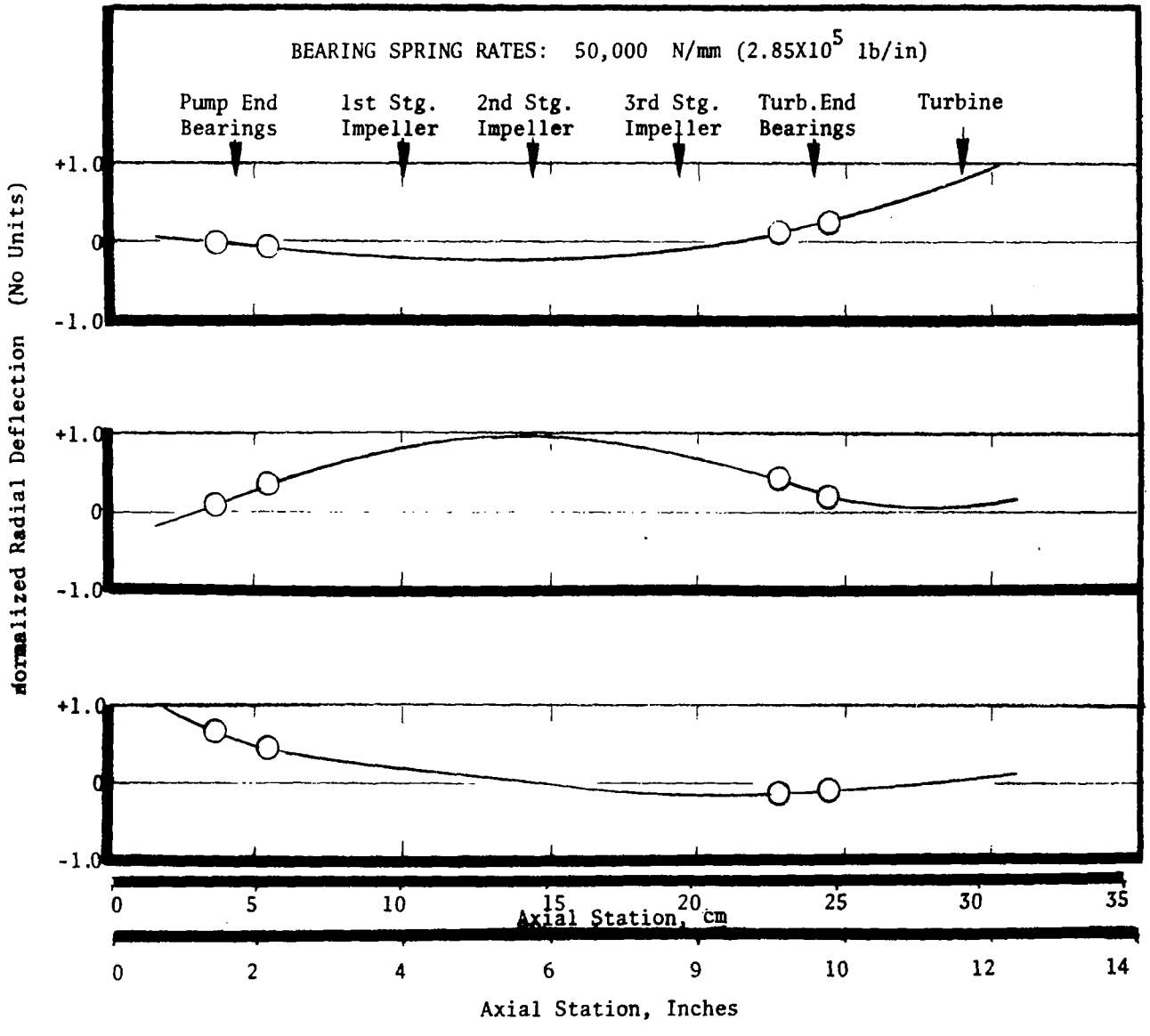

Figure 55. Mark 48-F Turbopump Rotor Mode Shapes

MATERIAL SELECTION

The materials selected for the more significant components of the Mark 48-F turbopump are indicated in Fig. 56. In Table 10, specifications and properties for these materials are summarized.

The principal criteria for choosing the materials in the pump were: strength and ductility at LH_2 temperature, resistance to corrosion, thermal contraction coefficient, and ease of fabrication.

The inlet housing, the first- and second-stage crossovers, and the pump section of the housing were made of Inoncel 718. Inconel 718 is a nickel-base precipitation hardenable alloy which has both excellent strength and ductility at LH_2 temperatures. All of these parts needed a high-strength material to carry the loads with the required safety margin; also, it was desirable to maintain common thermal coefficients to control critical radial and axial clearances. Silver plating was applied to the inlet housing and crossover labyrinth platforms to permit light contact with the rotating parts in these areas with a minimum of local heating and damage to the mating parts. For the same reason, the stationary land of the balance piston high-pressure orifice was also silver plated.

High stresses induced in the impeller hubs as a result of centrifugal forces dictated that a material with high strength-to-density ratio be used. A titanium alloy containing 5% aluminum and 2.5% tin with extra low interstitial elements was selected. This high-purity alloy was developed for temperatures ranging from 200 K (-100 F) to 20 K (-423 F). To achieve acceptable ductility and toughness at 20 K (-423 F), the content of the impurity interstitial elements (O_2, N_2, H_2) and the substitutional element Fe are held to lower than normal levels by the producing mill. Hence, the designation "Extra Low Interstitial" (ELI) is applied to this alloy.

The high operating pressure and temperatures dictated the use of Rene' 41 for the main structural walls of the turbine manifold. Rene' 41 is a double-vacuum-melted, precipitation-hardenable, nickel-base alloy. Although difficult to fabricate because of strain-age cracking in weld heat-affected zones, it has superior strength in the operating temperature zone of the Mark 48-F turbine manifold.

High thermally induced stresses, particularly during engine cutoff, necessitated the use of a liner inside the turbine manifold walls to reduce temperature gradients. The liner does not carry structural loads (it is perforated). Inconel 903, a iron-nickel-cobalt base alloy with low coefficient of expansion, was chosen for the liner material. It has an expansion rate of 0.0087 mm/mm to 1033 K (1400 F) compared with 0.012 mm/mm with most other high-temperature metals for the same temperature range. It is anticipated that thermally oriented problems with the liner will be minimized by virtue of the lower expansion properties.

The processing of the housing (described in detail under "Fabrication") calls for heat treating the Inconel 718 pump volute section and the principally Rene' 41 turbine manifold to their respective material specifications, and subsequently joining these two subcomponents by welding. To accomplish this without

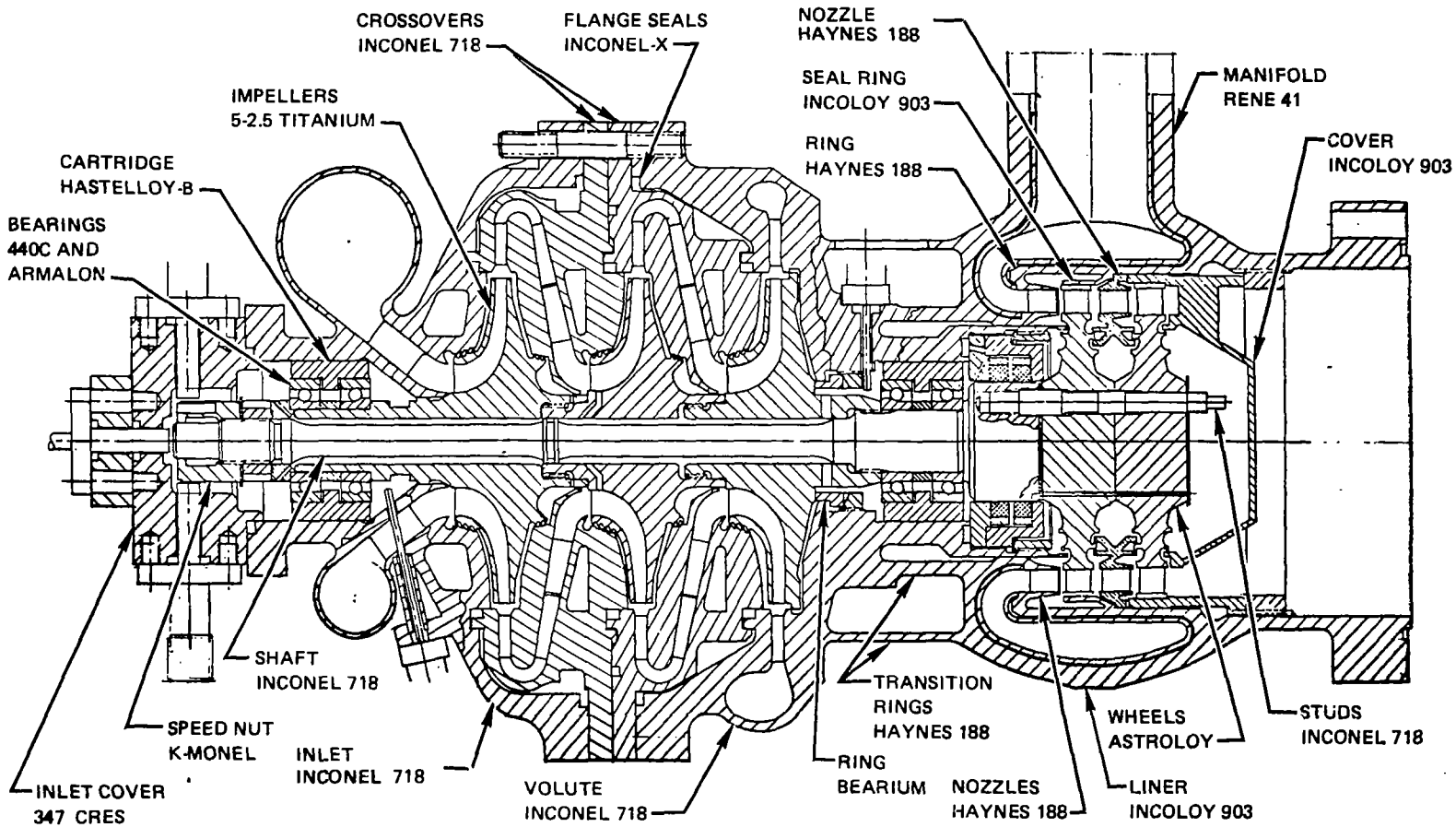

LOCK TABS	302 CRES	SPACERS	410
BOLTS	A286	FLANGE SEALS	INCONEL-X SILVER PLATE
NUTS	A286	WASHERS	302 CRES
SPRINGS	INCONEL 718	LABY LANDS	SILVER PLATE

Figure 56. Mark 48-F Materials Selection

TABLE 10. MARK 48-F TURBOPUMP MATERIAL PROPERTIES (SI UNITS)

Part	Material	Specification	Room Temperature			Operating Temperature				
			F_{TY}, N/cm^2	F_{TU}, N/cm^2	e, %	T, K	F_{TY}, N/cm^2	F_{TU}, N/cm^2	e, %	10-Hour Stress Rupture, N/cm^2
Pump Inlet Cover, Pump Inlet, First Crossover, Second Crossover, Pump Volute, Shaft	Inconel 718	RB0170-153	103,400	124,000	12	78	119,000	143,000	12	-
Impellers	Titanium	RB0170-152	62,000	68,900	12	39	124,000	131,000	10	-
First-Stage Nozzle, Second-Stage Nozzle, HSG Transition	Haynes 188	AMS 5772	38,000	86,000	45	1033	21,000	55,000	26	29,600
Turbine Manifold	Rene' 41	AMS 5712	90,000	117,000	8	1033	75,000	87,000	4	52,000
Turbine Wheel	Astroloy	UDIMET 700	97,000	131,000	16	1033	86,000	100,000	20	
Manifold Liner	Inconel 903	RB170-196	103,000	124,000	12	1033	45,000	50,000	16	≈20,700
Wheel Cover	Inconel 903	RB170-196	103,000	180,000	12	922	82,000	96,000	12	69,000

(ENGLISH UNITS)

Part	Material	Specification	Room Temperature			Operating Temperature				
			F_{TY}, ksi	F_{TU}, ksi	e, %	T, F	F_{TY}, ksi	F_{TU}, ksi	e, %	10-Hour Stress Rupture, ksi
Pump Inlet Cover, Pump Inlet, First Crossover, Second Crossover, Pump Volute, Shaft	Inconel 718	RB0170-153	150	180	12	-320	173	207	12	-
Impellers	Titanium	RB0170-152	90	100	12	-390	180	190	10	-
First-Stage Nozzle, Second-Stage Nozzle, HSG Transition	Haynes 188	AMS5772	55	125	45	1400	30	80	26	43
Turbine Manifold	Rene' 41	AMS 5712	130	170	8	1400	109	126	4	75
Turbine Wheel	Astroloy	UDIMET 700	140	190	16	1400	125	145	20	
Manifold Liner	Inconel 903	RB170-196	150	180	12	1400	65	73	16	≈30
Wheel Cover	Inconel 903	RB170-196	150	180	12	1200	119	139	12	100

annealing the material on either side of the final weld, a transition piece made of Haynes 188 was welded to both sections prior to heat treating. The final weld was then effected by joining Haynes 188-to-Hanyes 188, with is not affected by either the heat treating or welding operations.

Portions of the turbine manifold that are subjected to high-pressure H_2 and which experience a high strain level were protected against hydrogen embrittlement by applying 0.076- to 0.25-mm (0.003- to 0.010-inch) thick dense copper plating to the interior surfaces. Threaded areas were gold plated. A thicker (0.25 to 0.38 mm; 0.010 to 0.015 inch) copper plating layer was applied to the housing, turbine wheel cover, and second-stage nozzle to serve as a turbine tip seal rubbing surface.

The turbine wheel is subject to very high effective stresses from centrifugal, power-bending, and thermal components. To accommodate these stress levels at the elevated temperatures, Astroloy was selected as the wheel material. Astroloy is an age-hardenable, nickel-base alloy which, in addition to providing excellent high-temperature properties, retains adequate ductility in the cryogenic temperature range.

The turbine wheel cover was made from Incoloy 903 to take advantage of its low thermal expansion coefficient and thereby minimize the change in second-stage seal clearance.

Thermal Analysis

Heat transfer analysis was conducted to determine the thermal profile of critical pump and turbine components during transient and steady-state conditions. The chilldown rate of the impeller, starting with an ambient engine, was established. This was of concern not only from hydrodynamic but from a structural consideration, because titanium strength is greatly affected by temperature (Fig. 57). The analysis indicated (Fig. 58) that, with the predicted powered idle-mode flowrate of 22% of full-thrust flow, the impeller reached 39 K (-390 F) in 20 seconds. This was an acceptable time interval for chilldown for the engine; therefore, the stress analysis results, which are based on 39 K (-390 F) properties, were considered proper.

Thermal analysis of the turbine included start and cutoff transients as well as steady-state conditions. One-dimensional analysis was used for transients, and two-dimensional analysis for steady-state conditions. The results indicated that, because of the idle-mode operation which precedes engine starts, the start transients did not have an appreciable effect on turbine life.

In contrast, the shutoff transients introduced a significant thermal shock due to a hydrogen lag, which produced a high thermal gradient and correspondingly high strain in the pressure walls. To increase the low-cycle fatigue life, a thin liner was incorporated inside the manifold to shield the pressure walls. Its effect was to increase thermal resistance. With the liner, the wall differential temperature was reduced to 518 K (600 F), as shown in Fig. 59. Furthermore, the maximum thermal strain was delayed until 2 seconds after cutoff when the strains from pressure loads are low.

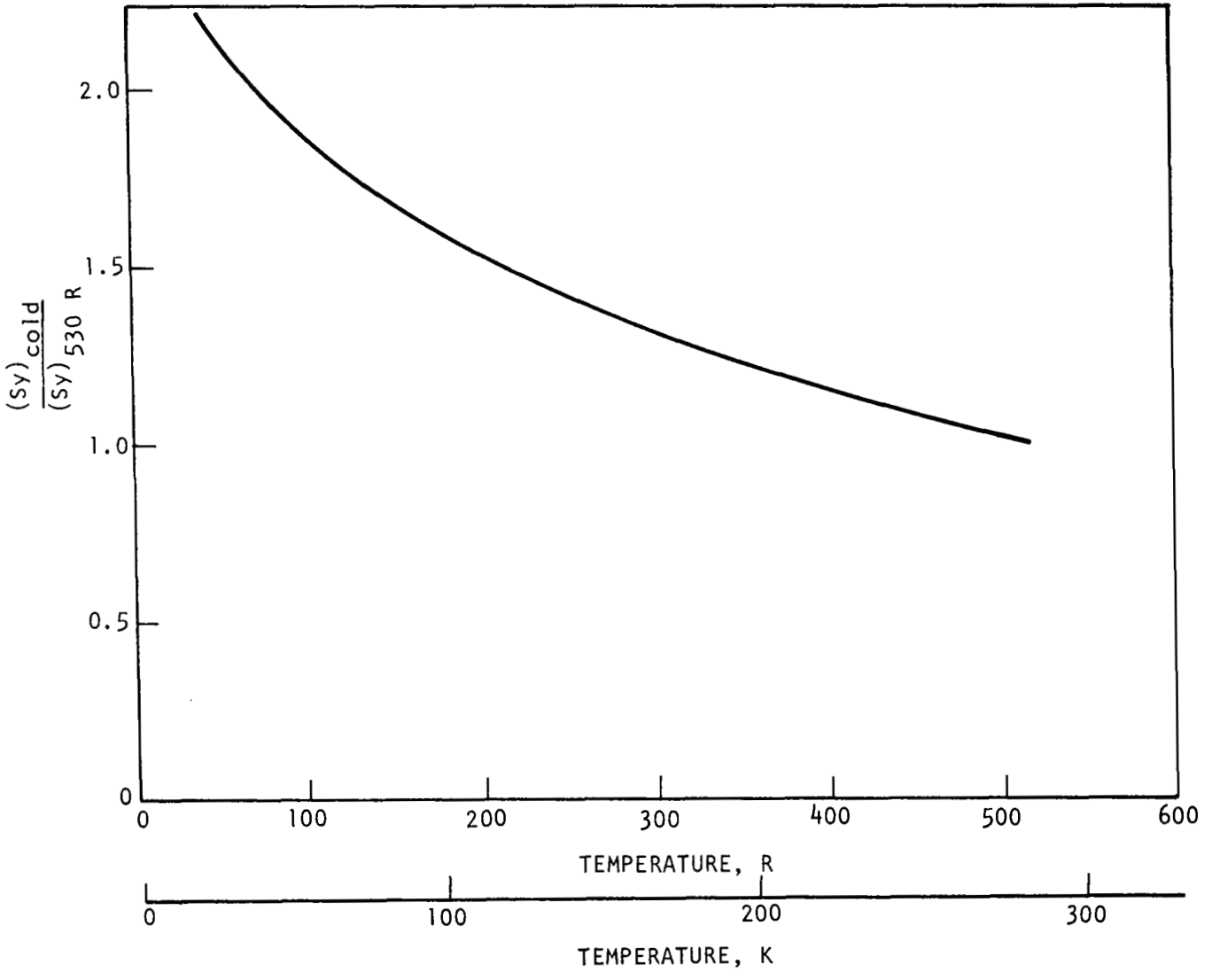

Figure 57. Titanium (5.0 Al-2.5 Sn) Strength Ratio vs Temperature

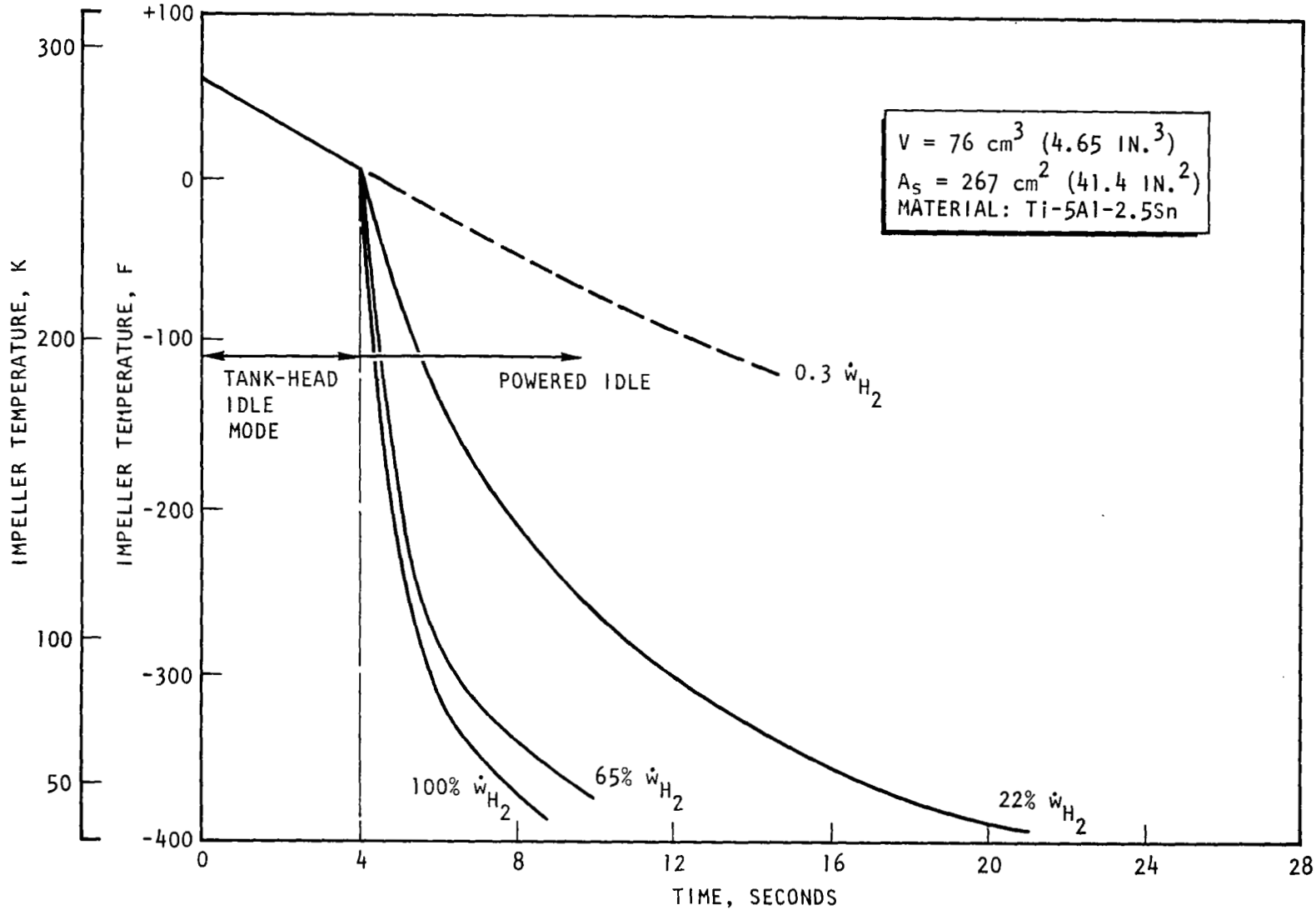

Figure 58. Mark 48-F LH_2 Turbopump Impeller Average Temperature or Time

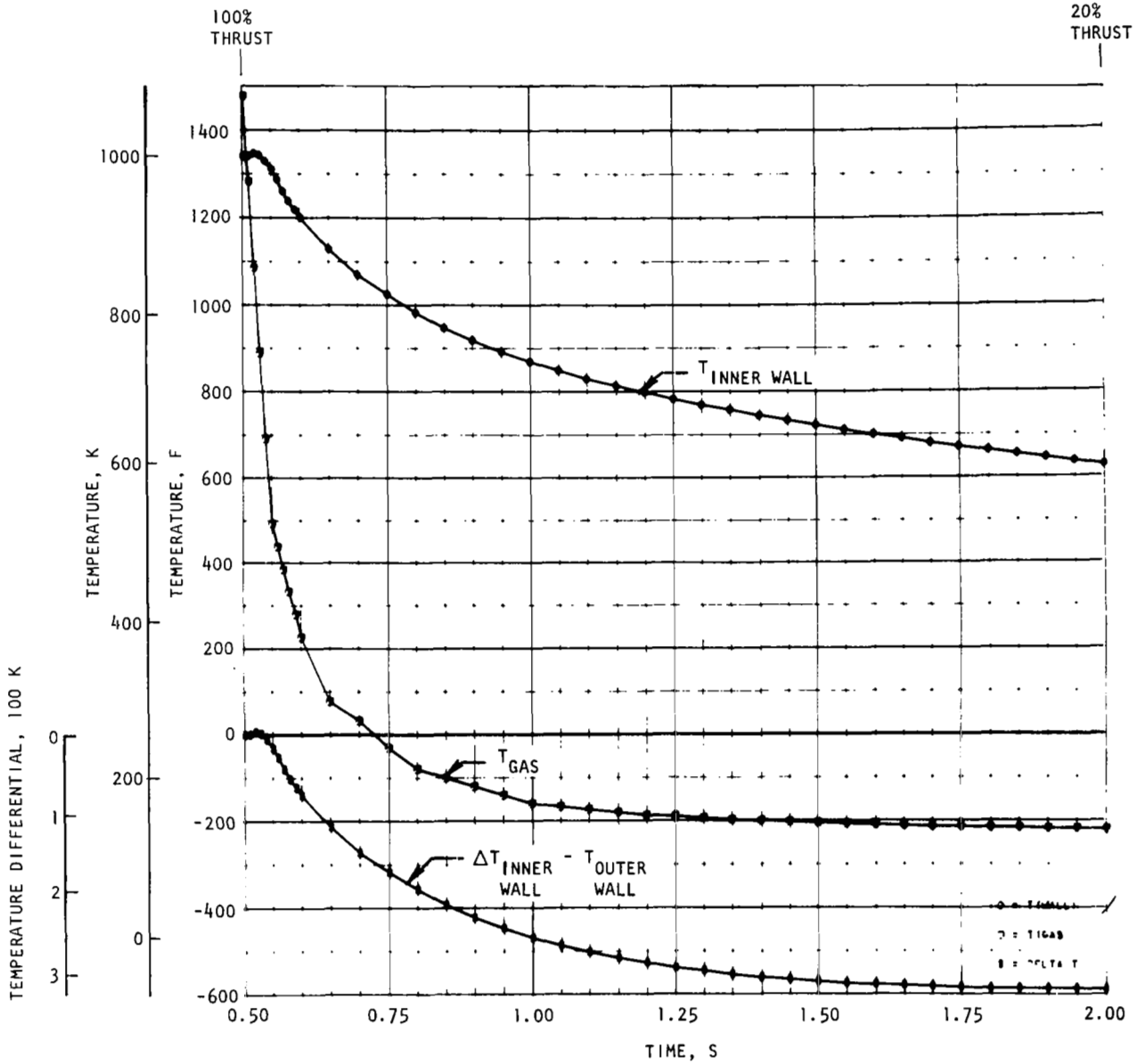

Figure . ASE Turbine Manifold Transient (Engine Shutdown)

The steady-state isotherm map calculated for the turbine first-stage disk is presented in Fig. 60. The disk thermal profile is based on using the shaft seal flow for disk cooling. The coolant is routed through the first- and second-stage disk hubs through small bleeder holes. A cover is incorporated downstream of the second-stage wheel to provide a thermal blanket.

The temperature of the turbine blades during steady-state conditions is equal to the gas temperature. Idle-mode operation minimizes the severity of start transients. In contrast, the hydrogen lag during cutoff produces a substantial thermal gradient (Fig. 61), which must be considered in the stress analysis and projected life of the blade.

Stress Analysis

Inlet Housing. A plate analysis of the inlet housing was performed accounting for pressure loads and full axial loads from the crossovers (222,000 N, 50,000 pounds). The maximum calculated stress was 515 x 10^6 N/m^2 (74,600 psi). This stress level, in conjunction with the minimum ultimate strength of Inconel 718 of 125 N/m^2 (180 ksi), resulted in a conservative factor of safety of 2.4. The stress levels in the torus due to pressure were negligible; therefore, the torus wall thickness was established by fabrication criteria.

Pump Housing. A summary of the structural analysis performed on the pump housing is presented in Table 11. A finite-element analysis was performed of the critical zones. The initial sizing of the hardware was done using cast Inconel 718 material properties. Subsequently, the design was finalized using a wrought, welded structure, but the wall thicknesses were retained at their original values. As a consequence, the safety factors with the higher-strength material increased to the conservative values noted in Table 11. The finite-element model of the pump housing, and constant-strain and constant-stress map are illustrated in Fig. 62 through 64.

TABLE 11. MARK 48-F PUMP HOUSING STRESS ANALYSIS

Stress Identification	Calculated Stress		Factor of Safety
	N/cm^2	ksi	
Maximum Combined Stress	36,500	53	3.4
In Discharge, from Pressure	19,300	28	6.4
In Weld	17,200	25	4.3

Comments: (1) Material: Inconel 718
(2) Axial deflection of balance piston high-pressure orifice relative to rear bearing shoulder = 0.0043 cm (0.0017 inch)

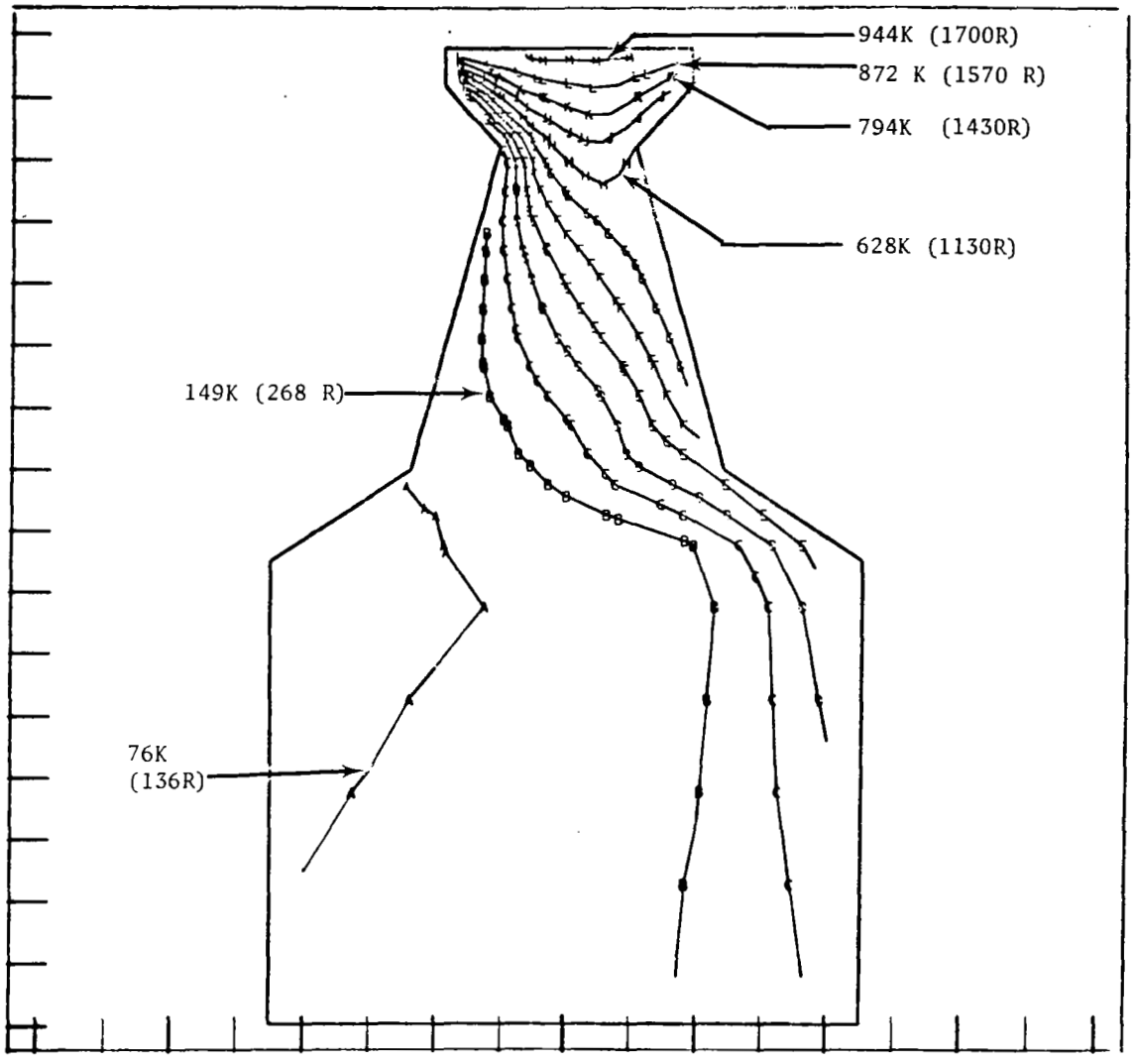

Figure 60. Steady-State Isotherm for Mark 48-F First Turbine Disk

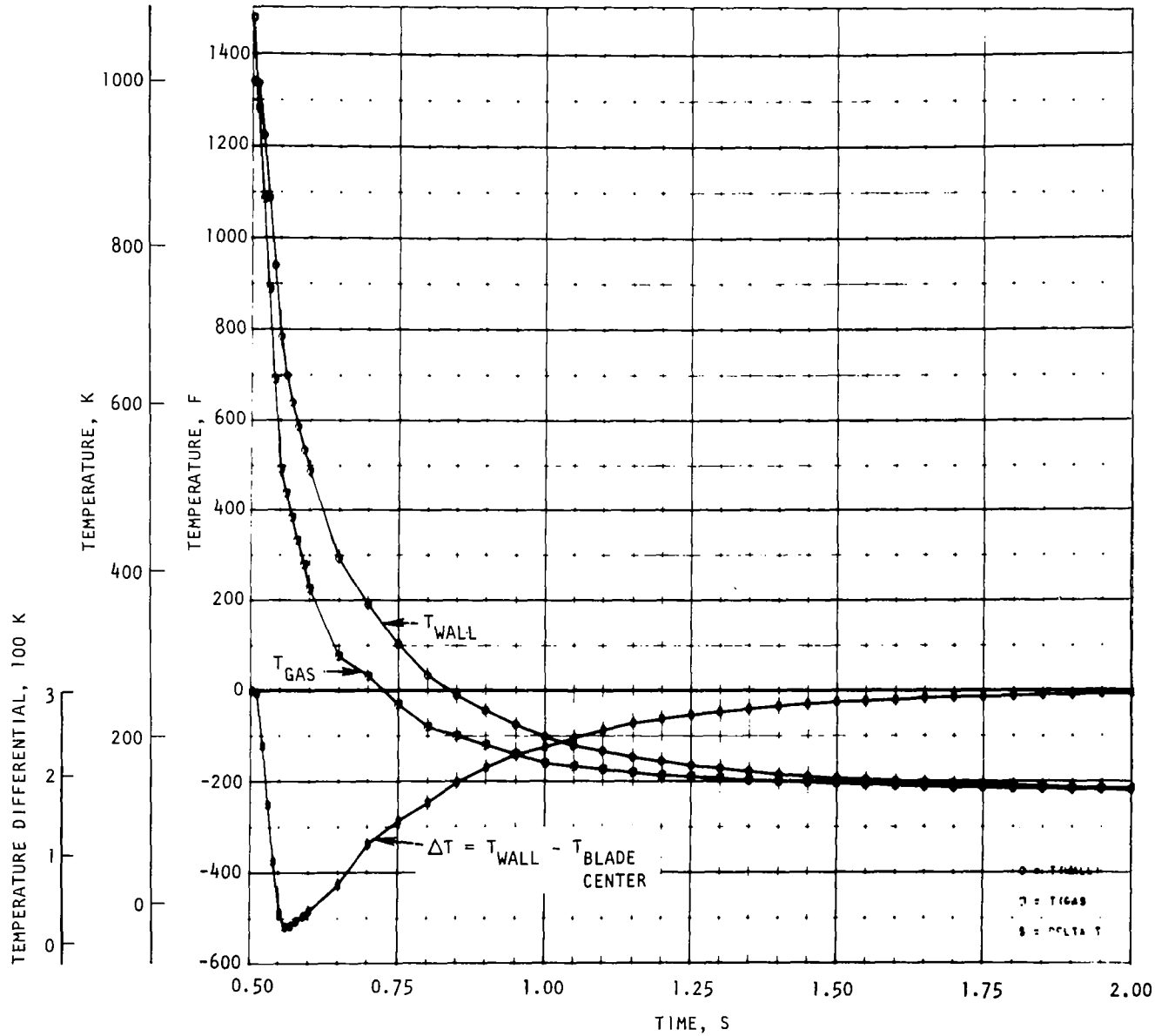

Figure 61. ASE Turbine Blade Transient (Engine Shutdown)

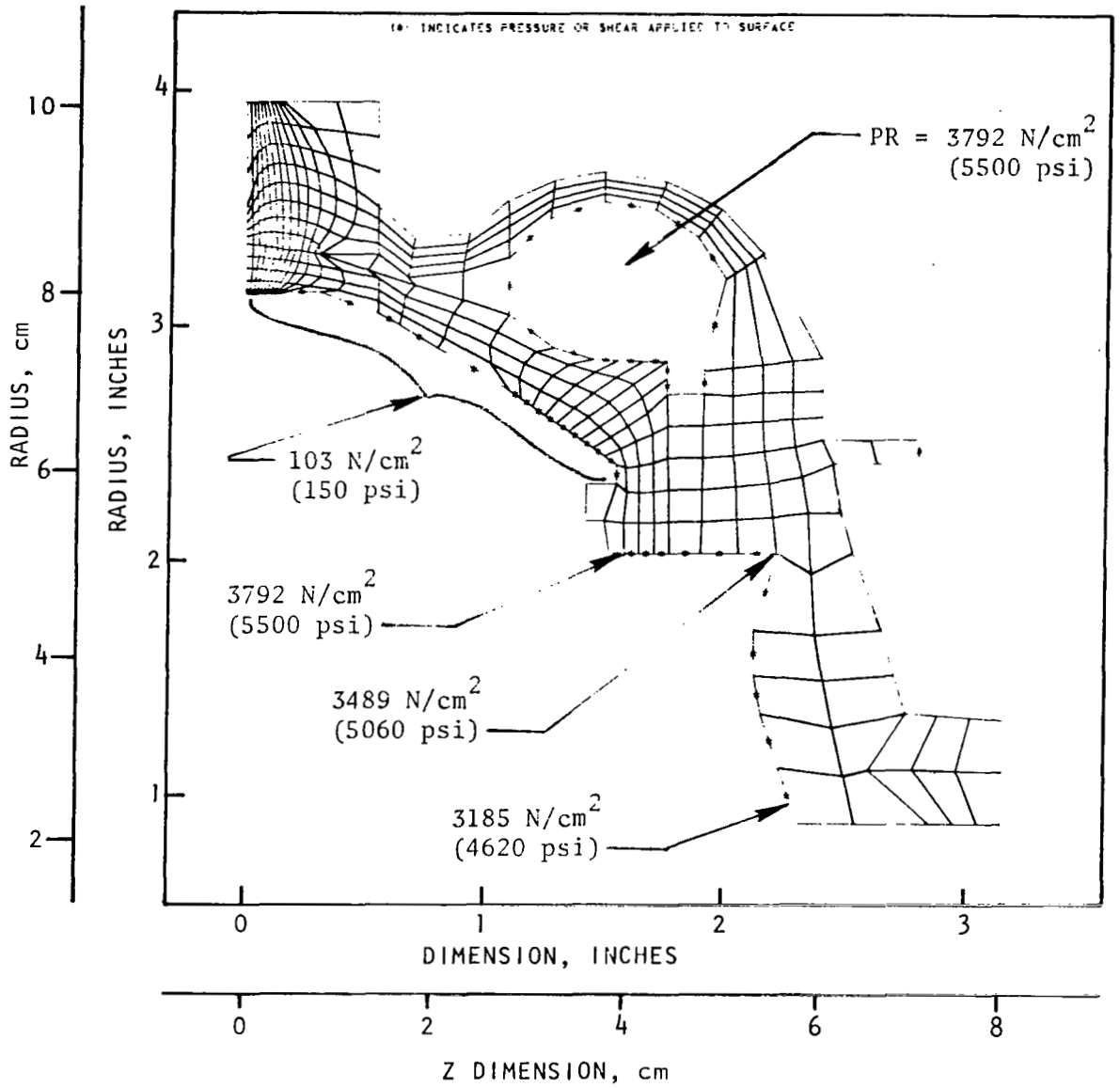

Figure 62. Mark 48-F Pump Housing Finite-Element Model

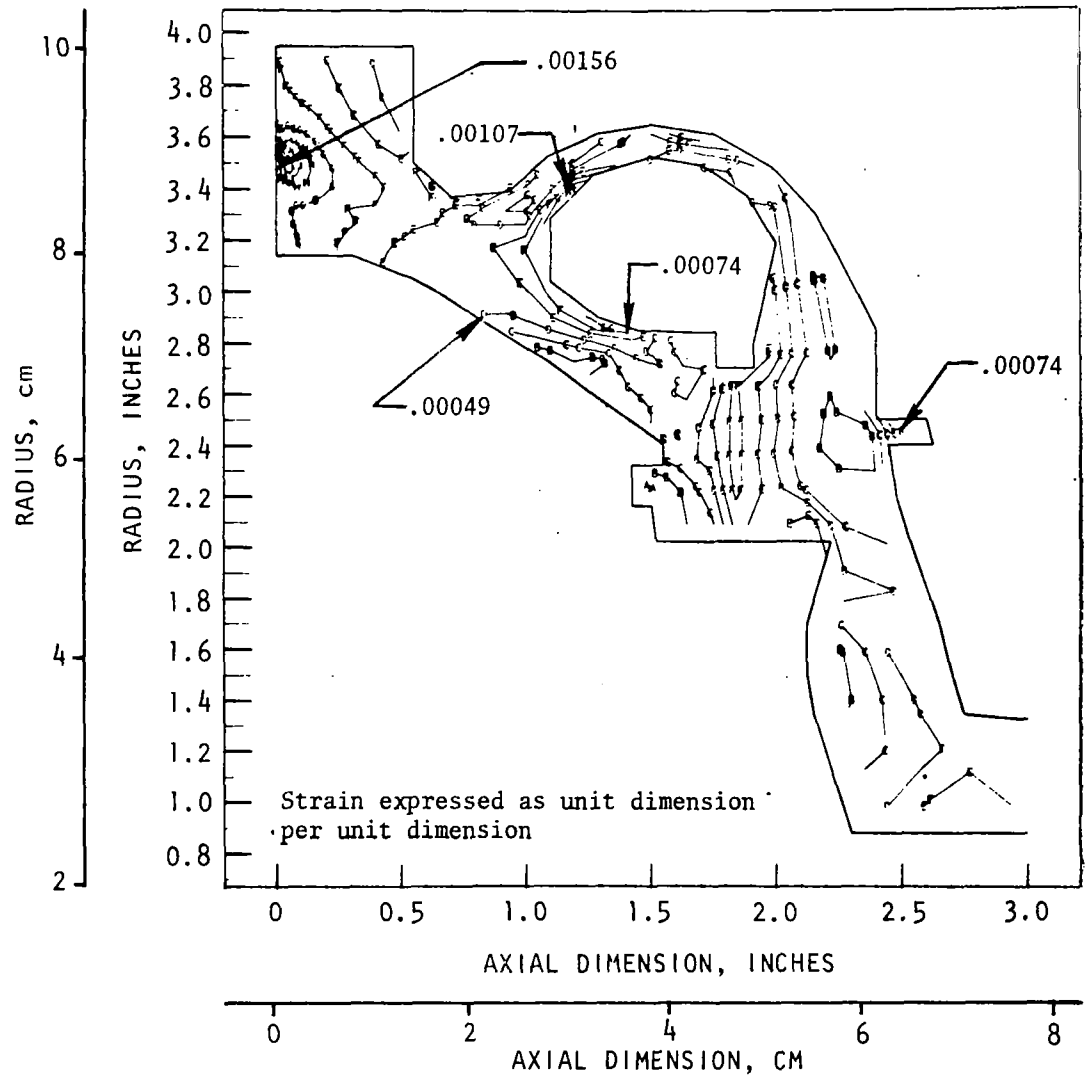

Figure 63. Mark 48-F Pump Housing Constant-Strain Map

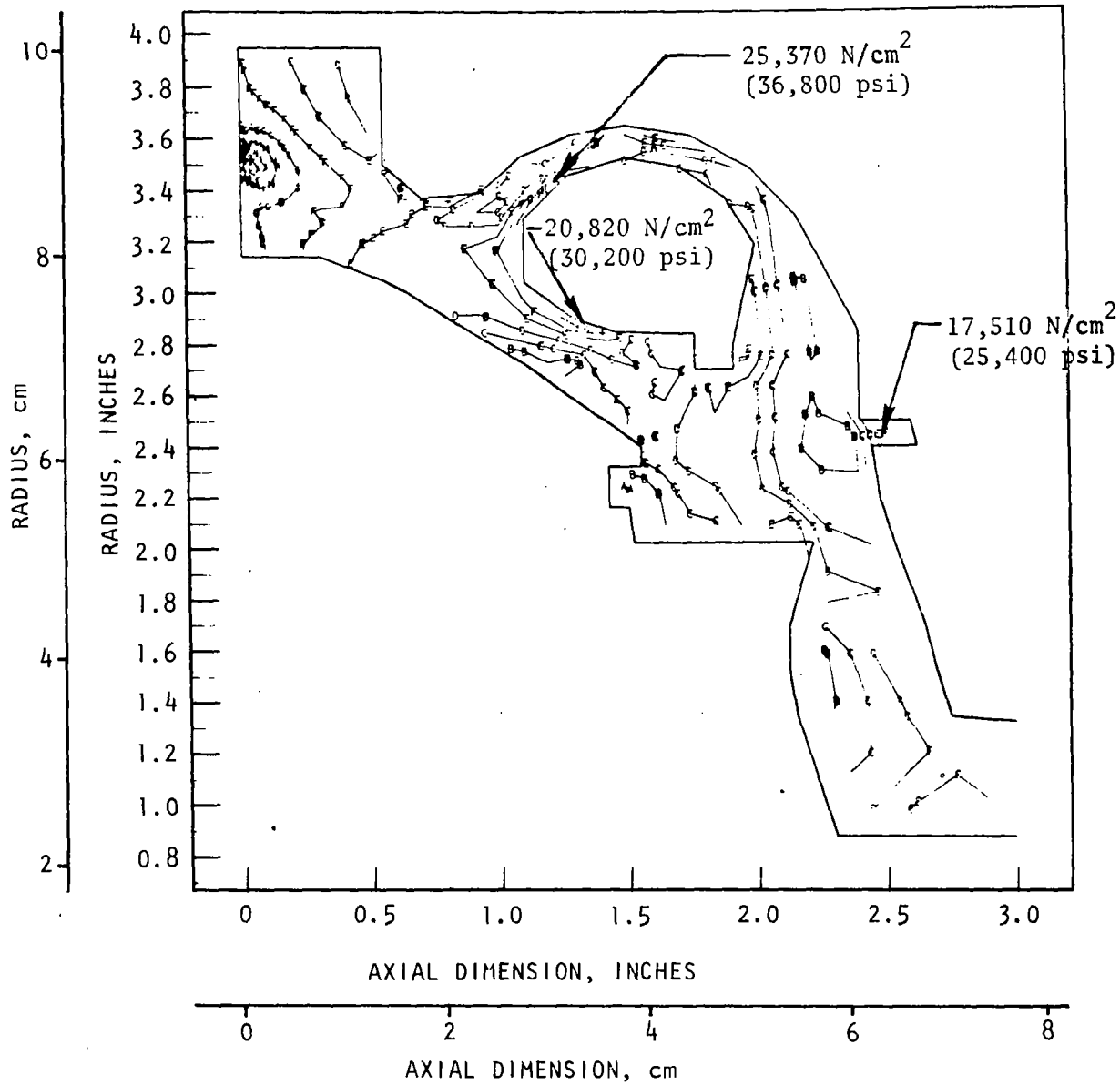

Figure 64. Mark 48-F Pump Housing Constant-Stress Map

The deflection of the balance piston high-pressure orifice relative to the rear bearing shoulder is of interest inasmuch as this affects the total balance piston gap and the bearing axial preloads during operation. As noted in Table 11, this deflection was calculated at 0.0043 cm (0.0017 inch). The magnitude of the deflection is acceptable since appropriate compensation can be included in the turbopump assembly to obtain the desired operating gap and preload.

Crossovers. Stress analysis of the pump crossovers was performed using forged Inconel 718 properties. The results of the analysis were as follows:

1. Crossovers analyzed for rotation
   - θ = 0.000343 radian (0.197 degrees)
   - Ring bending stresses = 38.6 N/m^2 (5600 psi)
2. Maximum bending stress on enclosed chamber = 400 N/m^2 (58,000 psi)
   - Safety factor = 3.1
3. Axial translation analyzed
   - Assuming all load in cantilever bending
     - Axial translation = 0.028 cm (0.011 inch)
     - Bending stress = 533.6 x 10^6 N/m^2 (77,400 psi)
     - Safety factor = 2.3
   - Part of this load actually carried by inlet housing, sized to carry total load
4. Crossover vanes analyzed for separating load
   - Maximum stress <70 x 10^6 N/m^2 (10,000 psi)

Thus, the minimum factor of safety is more than adequate at 2.3 on ultimate strength. Neither the extent of angular rotation or axial displacement are expected to present any difficulty in the functioning of the pump.

Impellers. A finite-element analysis was performed of the impellers using 5.0Al-2.5Sn forged titanium properties. An operating temperature of 39 K (-390 F) was assumed. The finite-element models and constant-stress maps of each impeller are presented in Fig. 65 through 68. The salient conclusions from the analysis were:

1. Second-stage impeller backplate most critical due to backplate return holes
2. Predicted burst speed at operating temperature = 13,650 rad/s (130,400 rpm)
3. Allowable operating speed = 11,370 rad/s (108,600 rpm)
4. Maximum stress including stress concentration = 823 x 10^6 N/m^2 (111,000 psi)

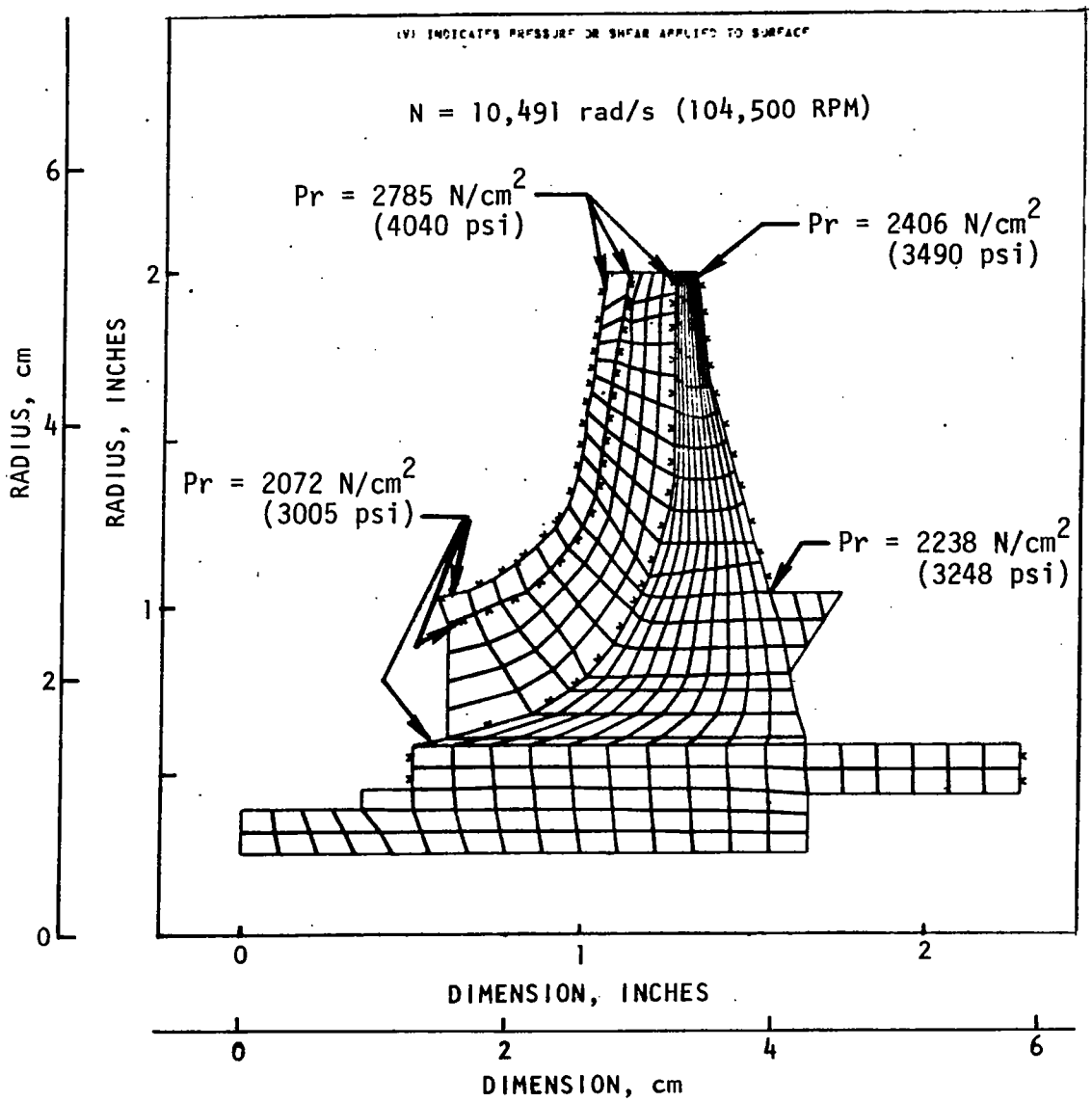

Figure 65. Mark 48-F First- and Second-Stage Impellers Finite-Element Model

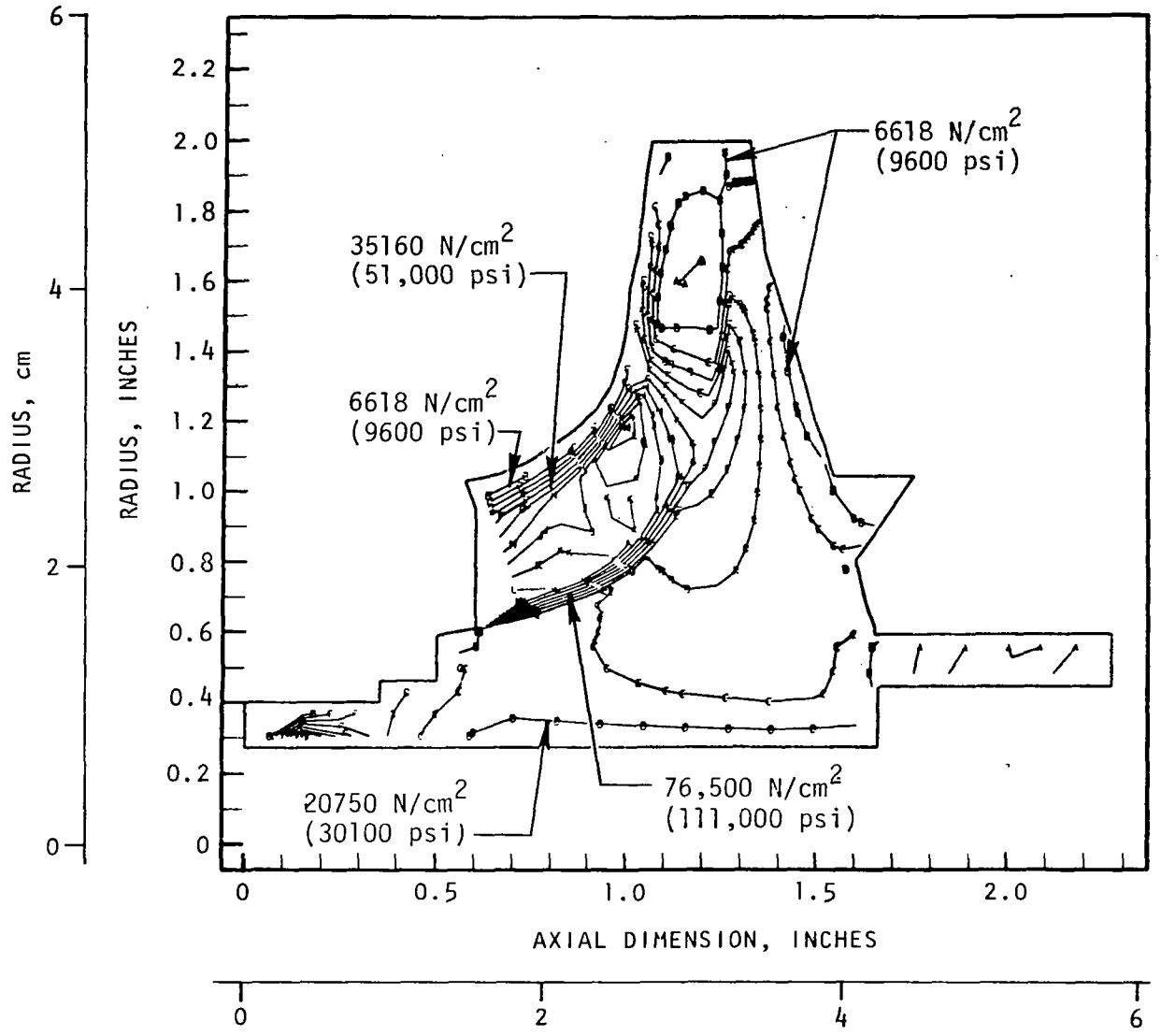

Figure 66. Mark 48-F First- and Second-Stage Impellers Constant-Stress Map

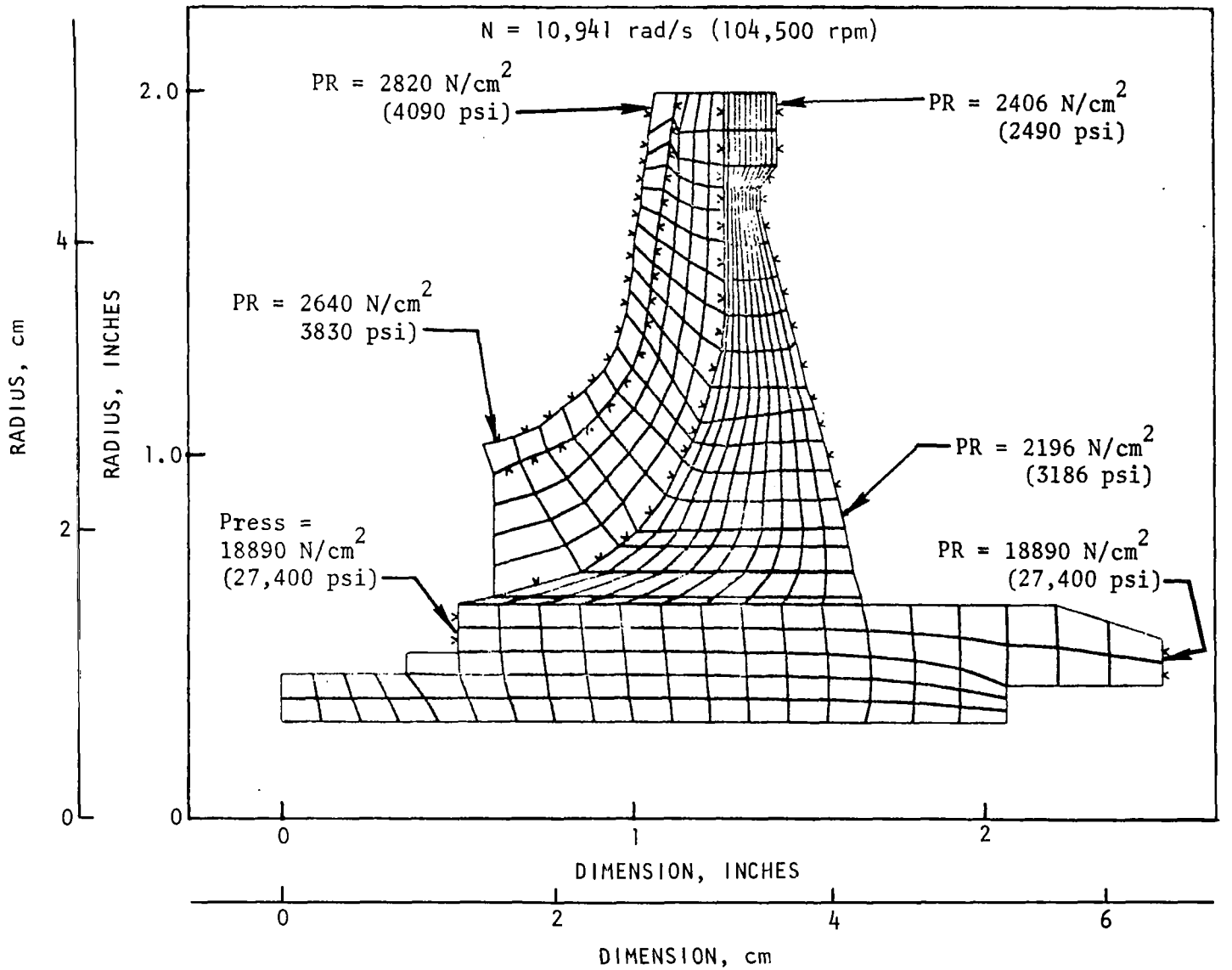

Figure 67. Mark 48-F Third-Stage Impeller Finite-Element Model

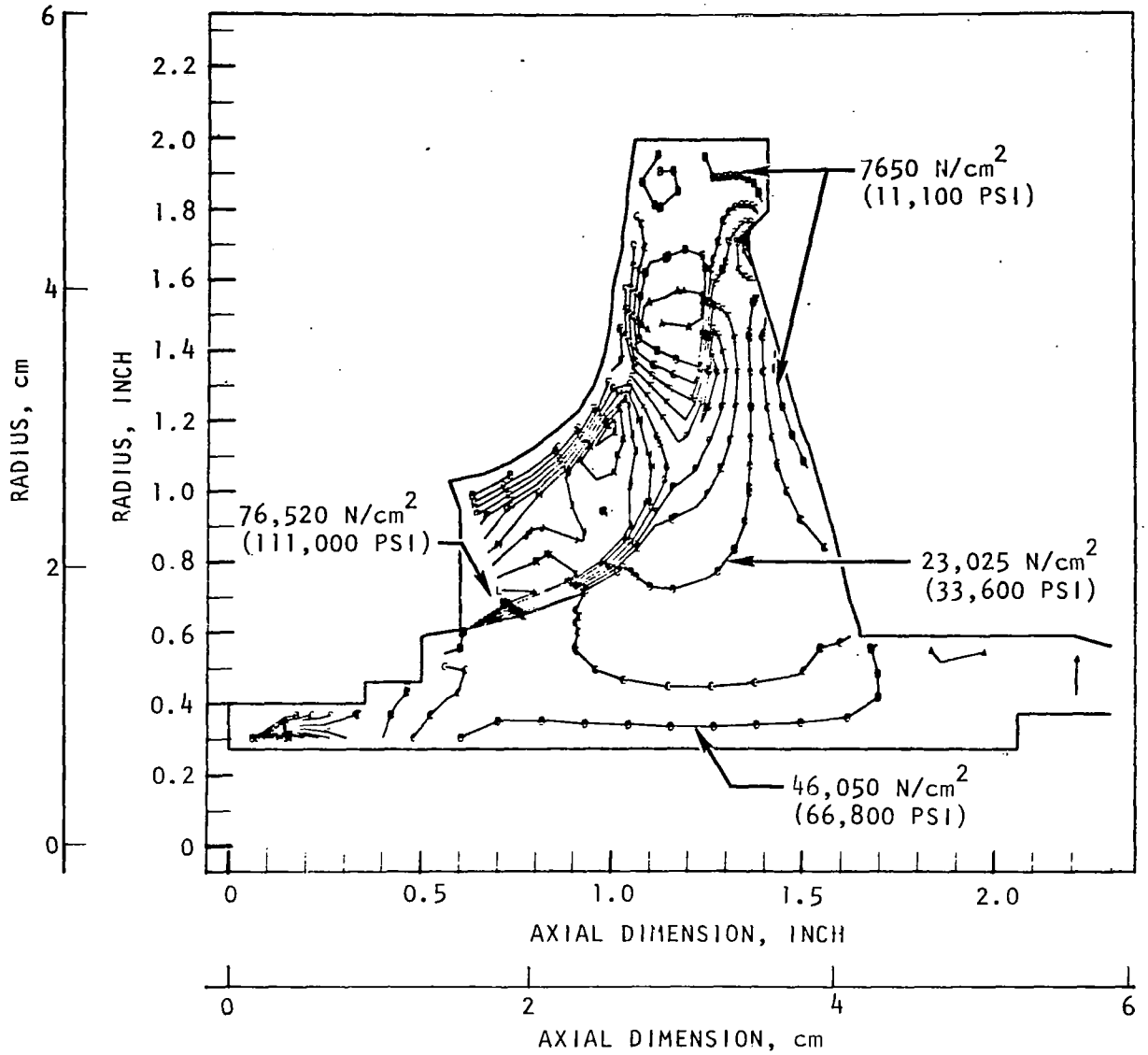

Figure 68. Mark 48-F Third-Stage Impeller Constant-Stress Map

5. Average tangential stress = 474 x 10^6 N/m^2 (68,800 psi)

6. Safety factor at maximum N of 10,941 rad/s (104,500 rpm) on burst = 1.55 (on stress)

Turbine Disk. Similarly, a finite-element analysis was accomplished on the turbine disks, accounting for power, thermal, and centrifugal effects. The finite-element model is shown in Fig. 69. The critical factor in designing the turbine disks was low-cycle fatigue due to thermal effects. For this consideration, the maximum strain rather than stress is the controlling criterion. Constant strain lines calculated for the first-stage disk are presented in Fig. 70. The maximum strain shown permits a cyclic life of over 800 cycles, with a safety factor of 4, which exceeds by a substantial margin the 300-cycle minimum requirement. The results of the analysis are summarized in the following:

1. First disk is the more critically stressed of the two.

2. Maximum strain in the first-stage disk = 0.0085 cm/cm

3. Predicted first-stage burst speed at maximum operating temperature = 13,580 rad/s (129,700 rpm).

4. Allowable first-stage speed at maximum operating temperature = 11,300 rad/s (108,000 rpm).

5. First-stage, low-cycle-fatigue limit = 800 cycles with safety factor of 4.

Turbine Blades. Stress analysis of the turbine blades disclosed that because of the high temperatures and centrifugal stresses, the 10-hour life requirement was difficult to meet without blade cooling. An effective cooling system would have increased the complexity and cost of the hardware, and would have introduced a severe performance penalty, particularly considering the low pump flowrates involved.

The alternatives considered in the design are presented in Table 12. The values apply to the first-stage blades which are the most critical because of the higher temperatures imposed. The first six alternatives listed in Table 12 were not viable from the standpoint of producibility or capability to meet the speed, life, or performance requirements. As a result, the nominal operating speed of the rotor was reduced from 10,470 rad/s (100,000 rpm) to 9946 rad/s (95,000 rpm), and the integral blade configuration with hollow, shrouded blades was accepted for final design. In cases 7 through 10, the capabilities with the accepted design as a function of temperature, speed, and life are denoted. Case 10 describes the results of operating the turbine at maximum speed and maximum temperature simultaneously. Under this condition, the life of the turbine blade is limited to slightly over 1 hour.

If the turbine is to be operated at maximum speed for 10 hours, the inlet temperature must be limited to 1070 K (1925 R) maximum (case 8). The predicted life of the first-stage turbine blade when operating at nominal inlet temperature (1111 K; 2000 R) and nominal speed (9948 rad/s, 95,000 rpm) is 400 hours.

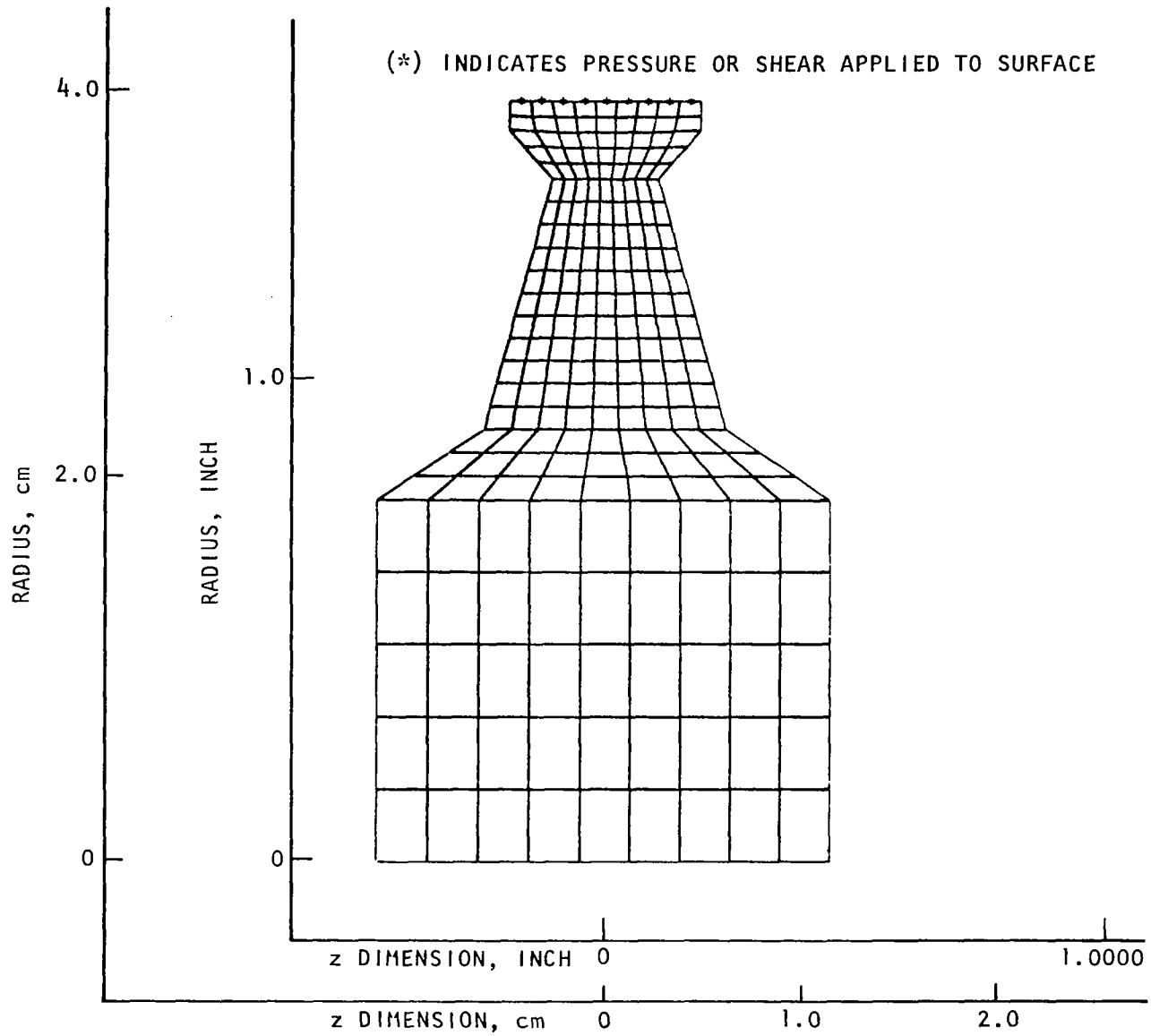

Figure 69. Mark 48-F First- and Second-Stage Turbine Disk Finite-Element Model

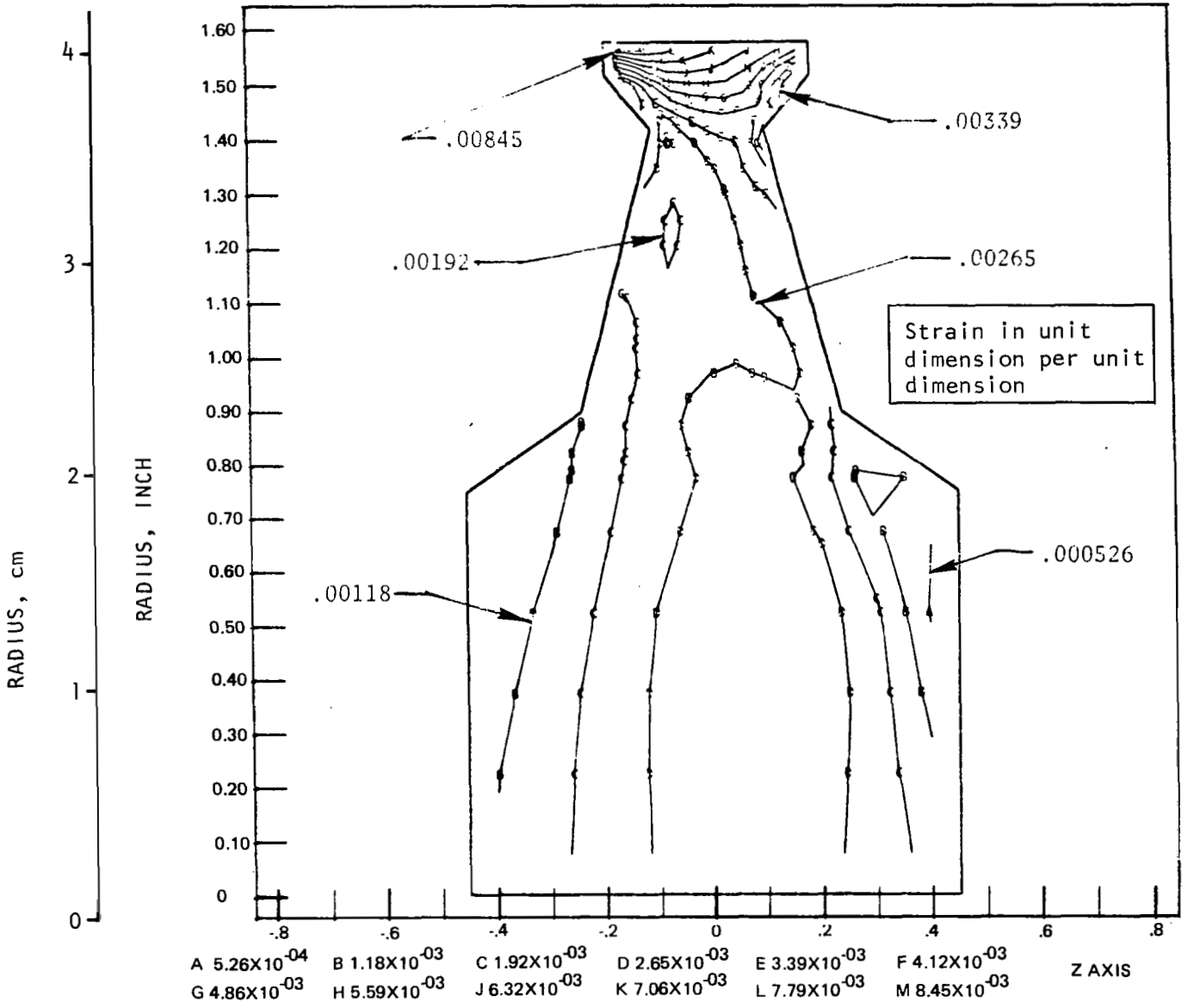

Figure 70. Mark 48-F Turbine First-Stage Disk, Constant-Strain Map

TABLE 12. MARK 48-F TURBINE BLADE CONFIGURATION SUMMARY

(SI UNITS)

Case	Pitch Diameter, cm	First-Stage Rotor Blade Height, cm	Blade Attachment	Blade Configuration	Material	Life, hours	Temperature, K		Maximum Allowable Speed, rad/s	Turbine Performance at 1033 K	
							Inlet	Blade		Nominal Speed, rad/s	Efficiency %
1	--	--	Weld	--	--	--	--	--	--	--	--
2	8.89	0.864	Fir Tree	Shrouded Solid	Astroloy	10	1111	1078	7,277*	10,470	76.5
3	8.89	0.864	Integral	Shrouded Solid			1111	1078	8,376	10,470	76.5
4	8.89	0.864		Shrouded Hollow			1111	1078	9,109	10,470	76.5
5	8.89	0.864		Unshrouded Hollow			1111	1078	10,260	10,470	70.1
6	9.35	0.737		Shrouded Hollow			1111	1078	9,528	9,947	76.2
7	8.89	0.737		Shrouded Hollow			1111	1078	9,789	9,947	75.5
8	8.89	0.737		Shrouded Hollow			1069	1036	10,941	9,947	75.5
9	8.89	0.737		Shrouded Hollow		30	1033	1011	10,941	9,947	75.5
10	8.89	0.737		Shrouded Hollow		1	1111	1078	10,941	9,947	75.5

*Limited by disk stress

(ENGLISH UNITS)

Case	Pitch Diameter, inches	First-Stage Rotor Blade Height, inch	Blade Attachment	Blade Configuration	Material	Life hours	Temperature		Maximum Allowable Speed, rpm	Turbine Performance at 1860 F	
							Inlet	Blade		Nominal Speed, rpm	Efficiency, %
1	--	--	Weld	--	--	--	--	--	--	--	--
2	3.5	0.340	Fir Tree	Shrouded Solid	Astroloy	10	2000 R 1540 F	1480 F	69,500	100,000*	76.5
3	3.5	0.340	Integral	Shrouded Solid			2000 R 1540 F	1480 F	80,000		76.5
4	3.5	0.340		Shrouded Hollow			2000 R 1540 F	1480 F	87,000		76.5
5	3.5	0.340		Unshrouded Hollow			2000 R 1540 F	1480 F	98,000		70.1
6	3.68	0.290		Shrouded Hollow			2000 R 1540 F	1480 F	91,000	95,000	76.2
7	3.5	0.290		Shrouded Hollow			2000 R 1540 F	1480 F	93,500		75.5
8	3.5	0.290		Shrouded Hollow			1925 R 1465 F	1405 F	104,500		75.5
9	3.5	0.290		Shrouded Hollow		30	1860 R 1400 F	1360 F	104,500		75.5
10	3.5	0.290		Shrouded Hollow		1	2000 R 1540 F	1480 F	104,500		75.5

*Limited by disk stress

TABLE 12. MARK 48-F TURBINE BLADE CONFIGURATION SUMMARY

(SI UNITS)

r,	First-Stage Rotor Blade Height, cm	Blade Attachment	Blade Configuration	Material	Life, hours	Temperature, K		Maximum Allowable Speed, rad/s	Turbine Performance at 1033 K		Remarks
						Inlet	Blade		Nominal Speed, rad/s	Efficiency, %	
	--	Weld	--	--	--	--	--	--	--	--	Astroloy is not weldable
	0.864	Fir Tree	Shrouded Solid	Astroloy	10	1111	1078	7,277*	10,470	76.5	
	0.864	Integral	Shrouded Solid			1111	1078	8,376	10,470	76.5	Maximum N too low
	0.864		Shrouded Hollow			1111	1078	9,109	10,470	76.5	Maximum N too low
	0.864		Unshrouded Hollow			1111	1078	10,260	10,470	70.1	Efficiency low
	0.737		Shrouded Hollow			1111	1078	9,528	9,947	76.2	Maximum N too low
	0.737		Shrouded Hollow			1111	1078	9,789	9,947	75.5	Accepted configuration
	0.737		Shrouded Hollow			1069	1036	10,941	9,947	75.5	
	0.737		Shrouded Hollow		30	1033	1011	10,941	9,947	75.5	
	0.737		Shrouded Hollow		1	1111	1078	10,941	9,947	75.5	

isk stress

(ENGLISH UNITS)

r,	First-Stage Rotor Blade Height, inch	Blade Attachment	Blade Configuration	Material	Life hours	Temperature		Maximum Allowable Speed, rpm	Turbine Performance at 1860 F		Remarks
						Inlet	Blade		Nominal Speed, rpm	Efficiency, %	
	--	Weld	--	--	--	--	--	--	--	--	Astroloy is not Weldable
	0.340	Fir Tree	Shrouded Solid	Astroloy	10	2000 R 1540 F	1480 F	69,500	100,000*	76.5	
	0.340	Integral	Shrouded Solid			2000 R 1540 F	1480 F	80,000		76.5	Maximum N too low
	0.340		Shrouded Hollow			2000 R 1540 F	1480 F	87,000		76.5	Maximum N too low
	0.340		Unshrouded Hollow			2000 R 1540 F	1480 F	98,000		70.1	Efficiency low
	0.290		Shrouded Hollow			2000 R 1540 F	1480 F	91,000	95,000	76.2	Maximum N too low
	0.290		Shrouded Hollow			2000 R 1540 F	1480 F	93,500		75.5	Accepted configuration
	0.290		Shrouded Hollow			1925 R 1465 F	1405 F	104,500		75.5	
	0.290		Shrouded Hollow		30	1860 R 1400 F	1360 F	104,500		75.5	
	0.290		Shrouded Hollow		1	2000 R 1540 F	1480 F	104,500		75.5	

isk stress

The calculated stress levels used in the above analysis are:

Centrifugal stress	= 37,200 N/cm^2	(54,000 psi)
Gas bending stress	= 4800 N/cm^2	(6900 psi)
Maximum stresses at blade root	= 42,000 N/cm^2	(60,900 psi)

The calculated stress levels of the second-stage turbine blades were similar:

Centrifugal stress	= 38,000 N/cm^2	(55,100 psi)
Gas bending stress	= 3500 N/cm^2	(5900 psi)
Maximum stresses at blade root	= 41,500 N/cm^2	(61,000 psi)

The temperature levels present at the second-stage blade are lower and, as a result, the predicted life is slightly higher.

Turbine Manifold. The turbine manifold was analyzed, using a finite-element approach, accounting for pressure and thermally induced loads. Because of thermal gradients at engine cutoff, an Incoloy 903 liner was incorporated to attenuate the strain levels in the structural walls. With the liner, a low-cycle fatigue life of 200 cycles was achieved with a factor of safety of 4.0. The finite-element model for the turbine manifold is shown in Fig. 71, and the constant-strain map is included in Fig. 72. Table 13 presents a summary of the strain levels and predicted life for the various parts of the manifold

TABLE 13. MARK 48-F TURBINE MANIFOLD PREDICTED LOW-CYCLE FATIGUE LIFE

Location	Strain (nondimensional)	Low-Cycle Fatigue Life With 4.0 Safety Factor
Torus*	0.0068	850 cycles
Exhaust Cylinder	0.0076	600 cycles
Inlet Transition*	0.0093	200 cycles
*With 0.16 mm (0.062 inch) liner		

Split Impeller Design

Experience in fabricating the impeller from an integral forging revealed that, because of lack of accessibility, it was difficult to produce parts which consistently met print requirements. As a result, an effort was initiated to modify the impeller design to improve producibility. The approach adopted was to fabricate the impellers in two pieces and, after the internal hydrodynamic passages are generated, join the two halves.

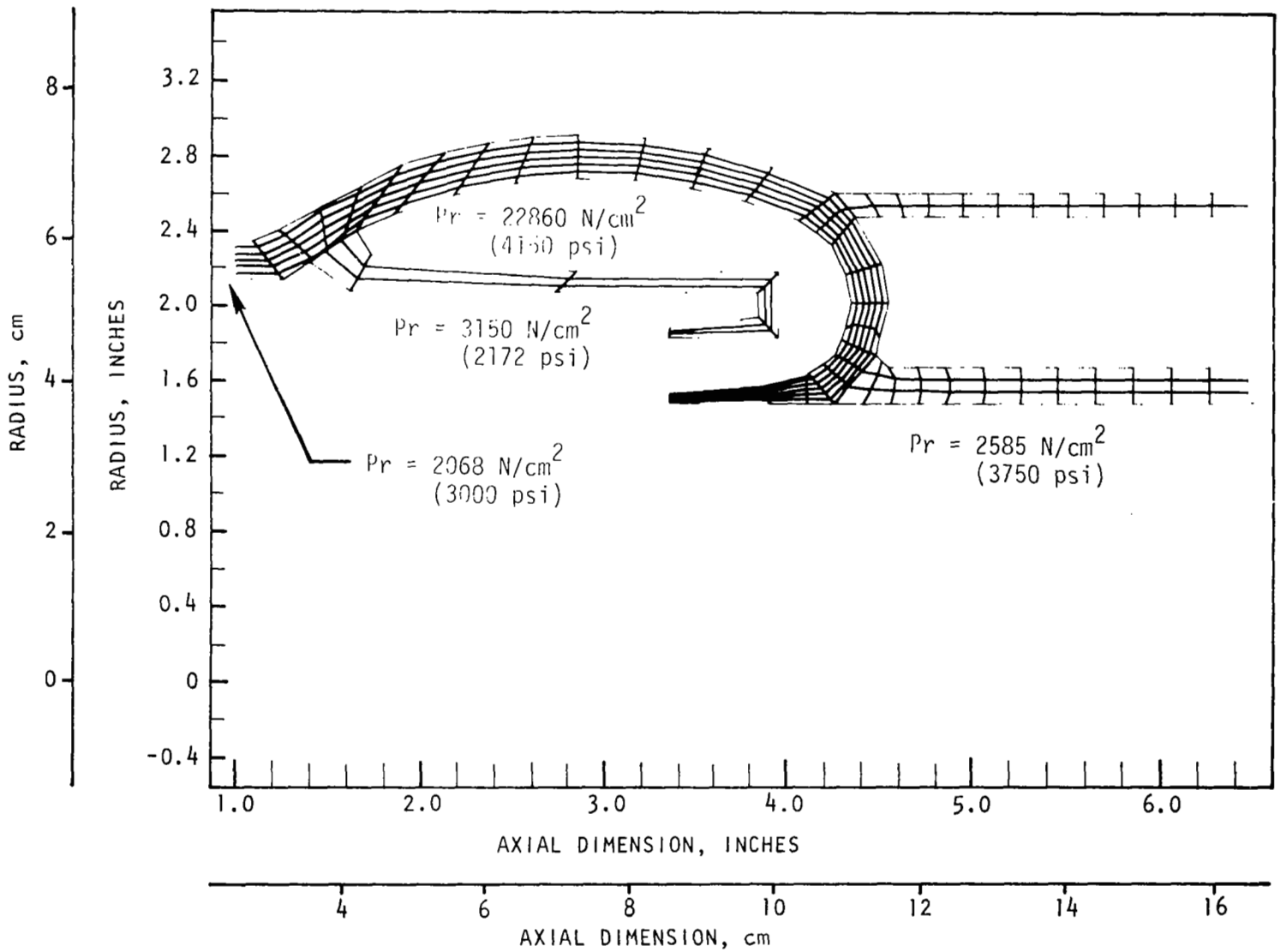

Figure 71. Mark 48-F Turbine Manifold Finite-Element Model

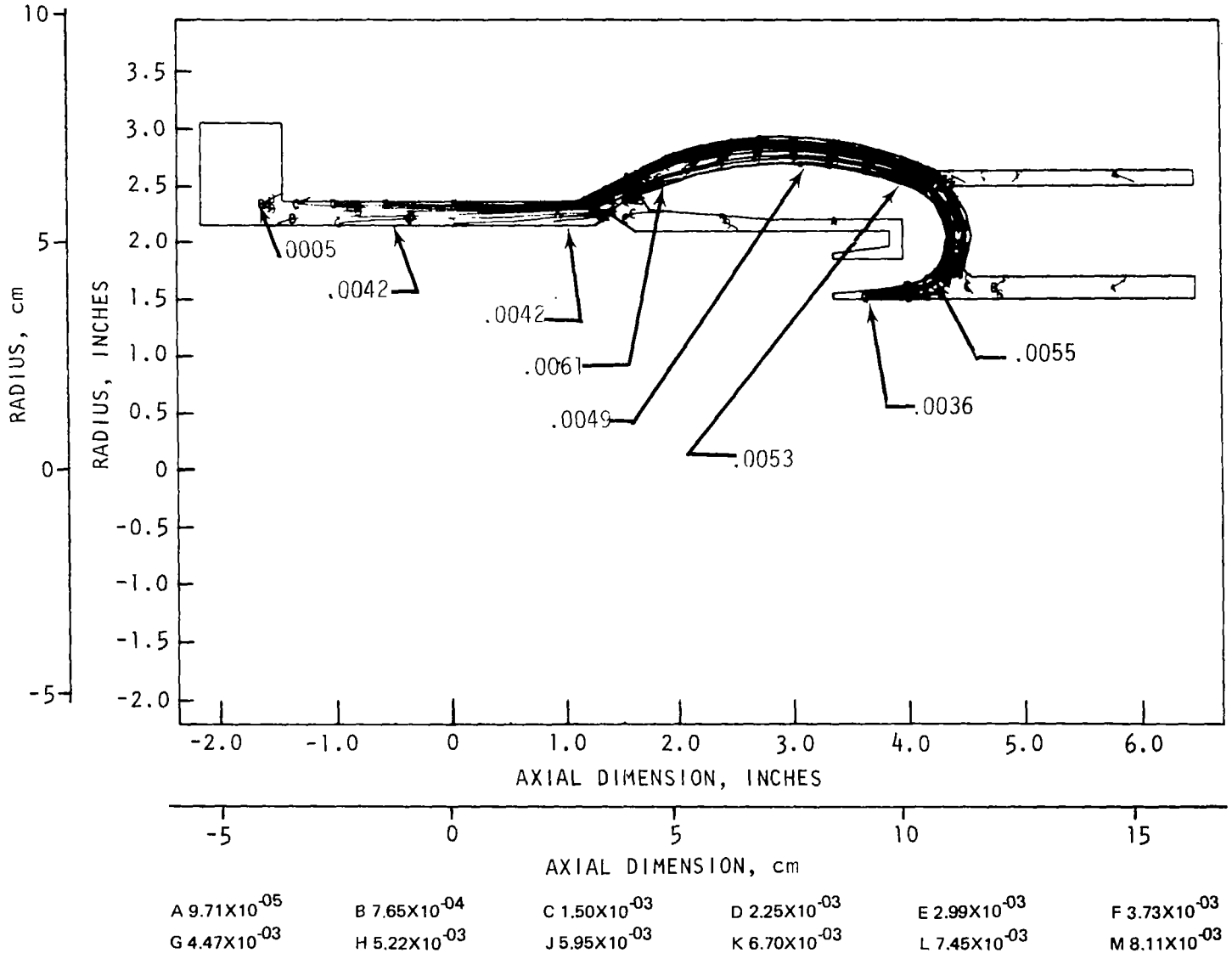

Figure 72. Mark 48-F Turbine Manifold Constant-Strain Map

The design layout which defined the interface between the preimpeller and main impeller is shown in Fig. 73. In formulating the configuration of the interface, there were several important considerations; the most significant of these are discussed in the following:

The location of interface was established by the requirement of accessibility to both subcomponents and to maintain an adequate stress distribution. The interface is located at approximately 1.58 rad (90 degrees) wrap angle of the full 2.36 rad (135 degree) wrap. This provides excellent accessibility to machine the hydrodynamic passages of both details, and leaves sufficient hub material to support the main impeller. The location of the interface is immediately upstream of the leading edge of the partial vanes; therefore, only the full vanes are involved in the split. The front shroud labyrinths are all located on the preimpeller, and the weld joint is located adjacent to the labyrinths, at a small diameter where the added mass required for the joint does not present a stress problem.

Initially, the interface was planned as a mechanical gap, but the weld joint was added to maintain the axial deflection at an acceptable level and to eliminate a potential recirculation leak path around the front shroud. To ensure a Class I weld, the joint is ultrasonically inspected. Provisions are included to facilitate ultrasonic inspection by including excess material outside the weld, which is removed after the inspection is accomplished.

The preimpeller is installed with a combination of heating and pressing. An interference fit of 0.104 to 0.114 mm (0.0041 to 0.0045 inch) is maintained at the piloting diameter to ensure positive piloting at all operating conditions. Axially, the preimpeller will bottom at the hub. To ensure the best possible contact, the mating surfaces at the hub are being held to an 0.0025 mm (0.0001 inch) normality. The preimpeller is preloaded axially during the welding operation as a precaution; although, with the heavy diametral interference fit, a loss in axial contact is not probable.

Tooling is used to position the two parts relative to each other during the assembly procedure to ensure proper matching of the vane surfaces at the interface.

The effective stress at the weld, composed of tangential, radial, and axial stresses, was calculated at 42,000 N/cm^2 (60,600 psi). The tangential stress at the weld joint is 49,000 N/cm^2 (71,000 psi), and is the major contributor of the total effective stress. Treating the effective stress as steady-state stress and using the mechanical properties of a Class I, 5Al-2.5Sn ELI titanium GTA weldment (as welded) at 61 K (-350 F) temperature, the ultimate and yield factors of safety are 2.47 and 2.37, respectively.

The finite-element grid and isostress plots of the effective stresses for the entire impeller are shown in Fig. 74 and 75. Figure 76 and 77 include an enlarged grid and isostress plots of the preimpeller section.

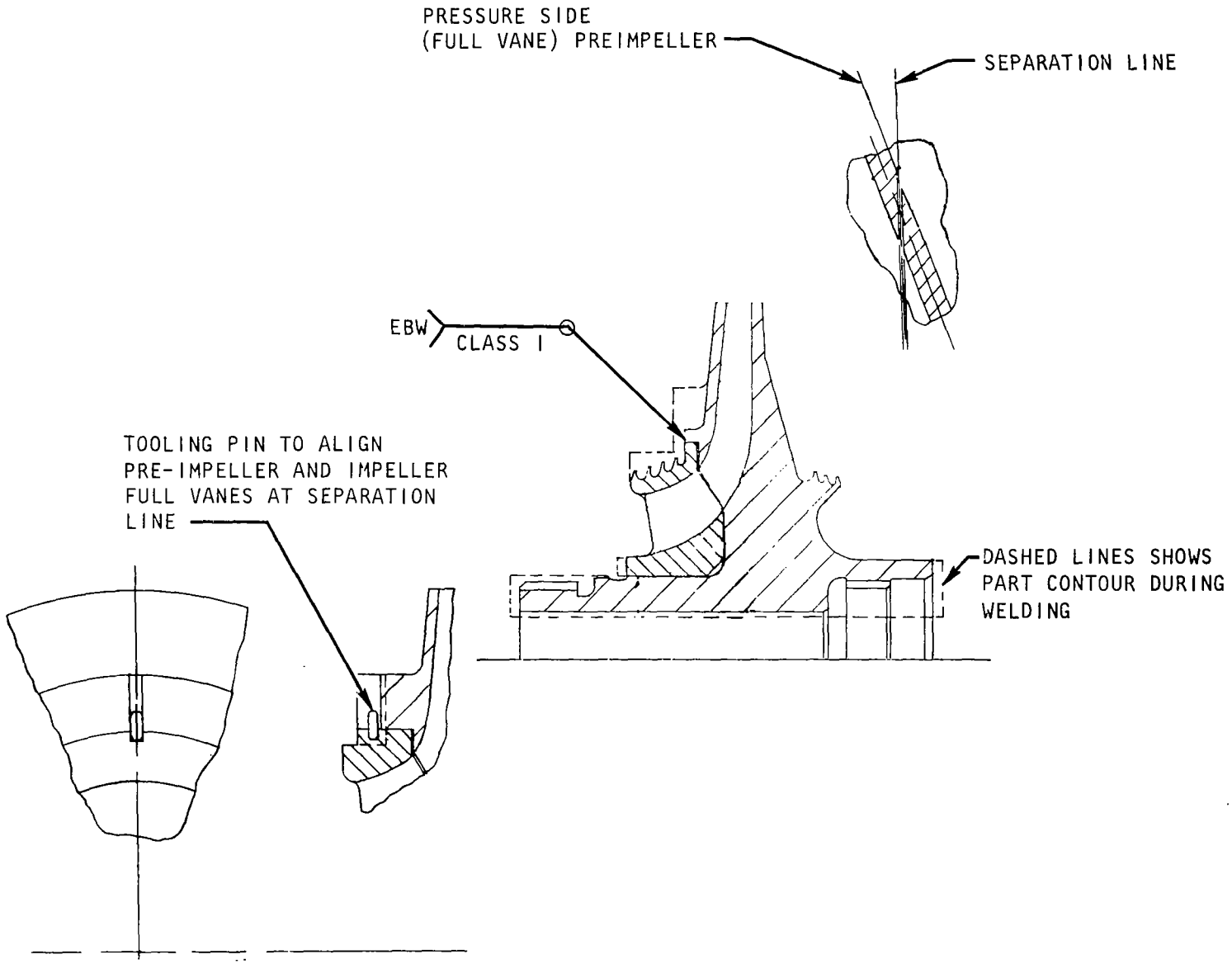

Figure 73. Mark 48-F Split Impeller

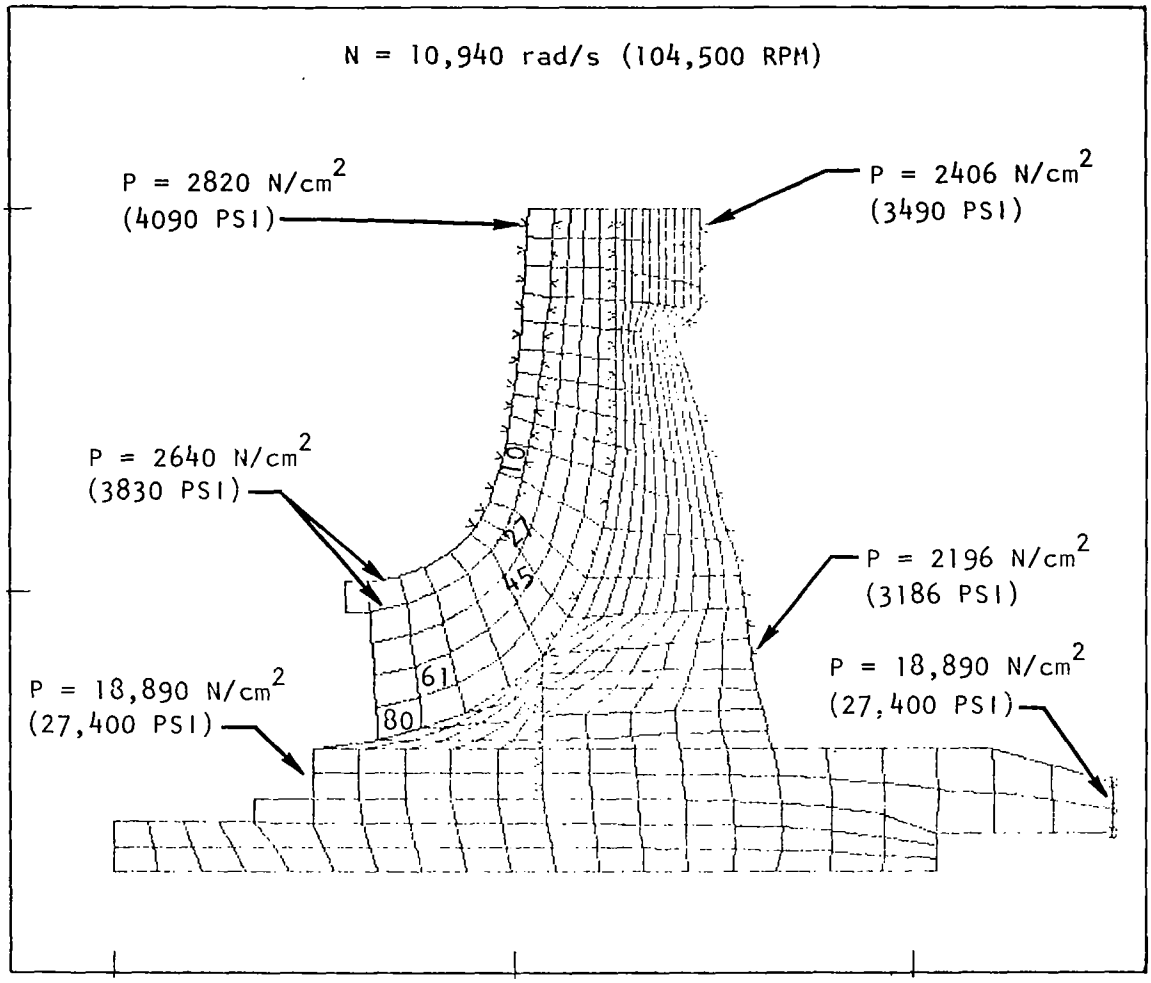

Figure 74. Mark 48-F Third-Stage Impeller Underformed Structure

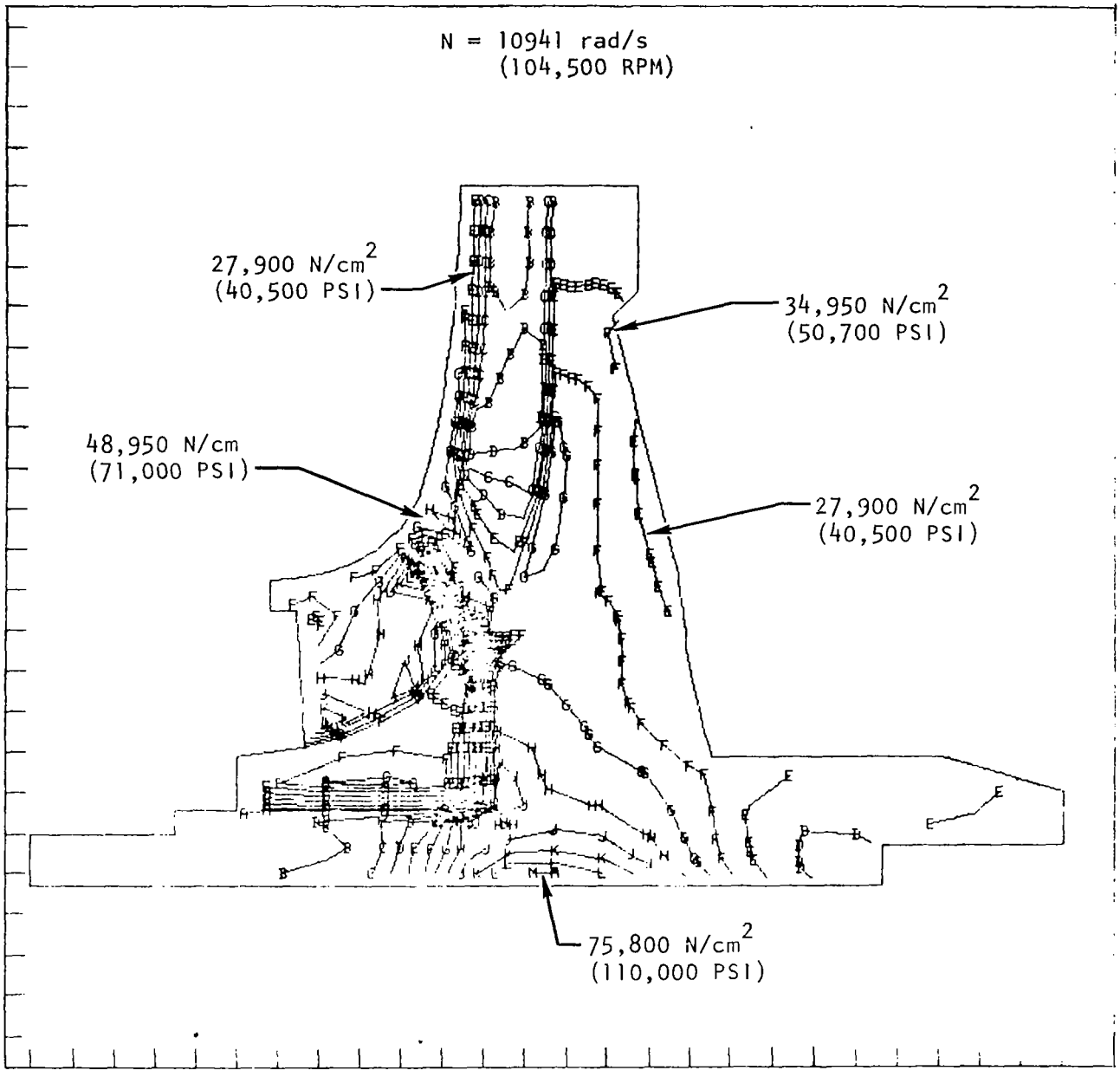

Figure 75. Mark 48-F First-Stage Impeller

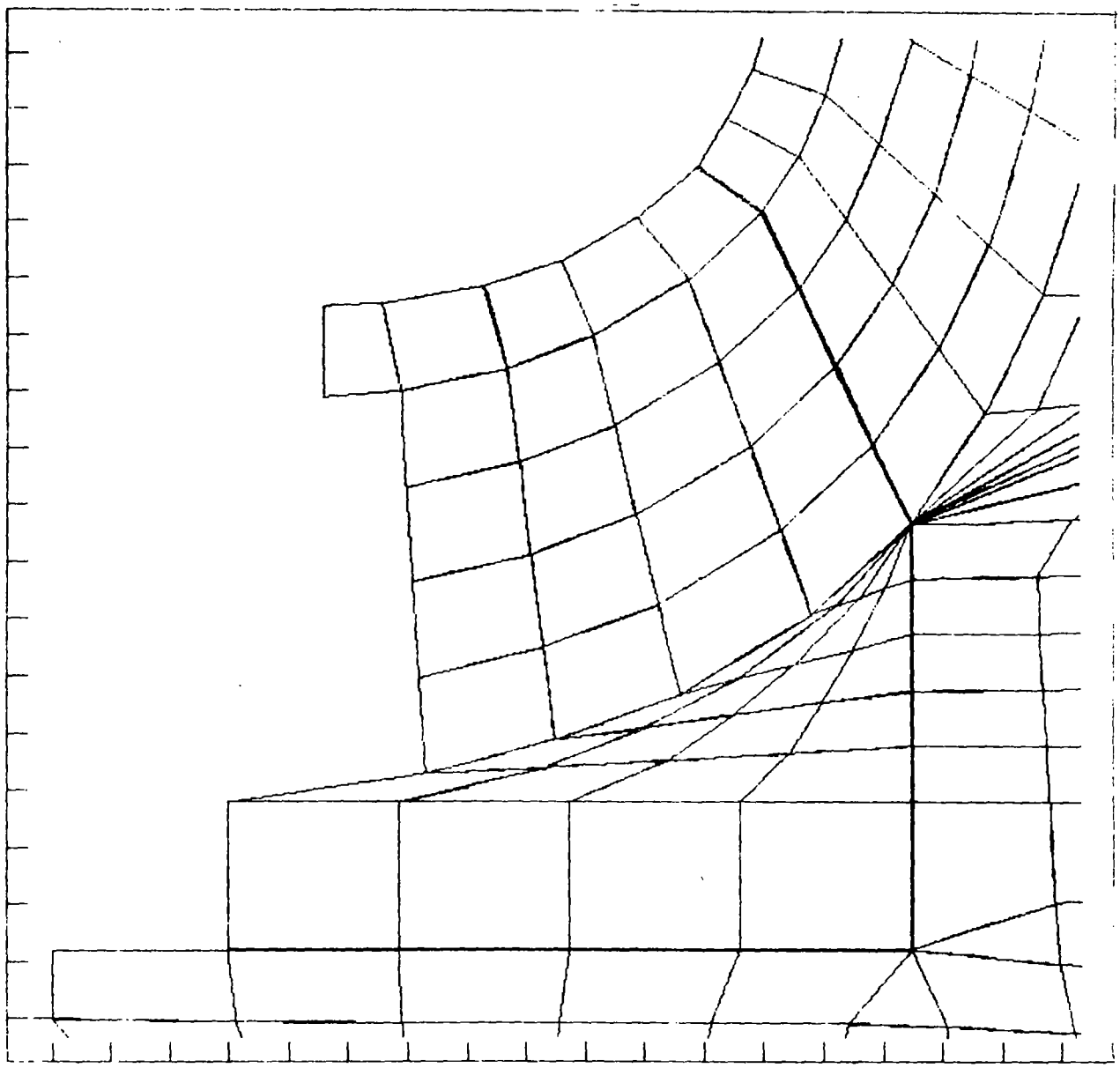

Figure 76. Enlarged End of Preimpeller

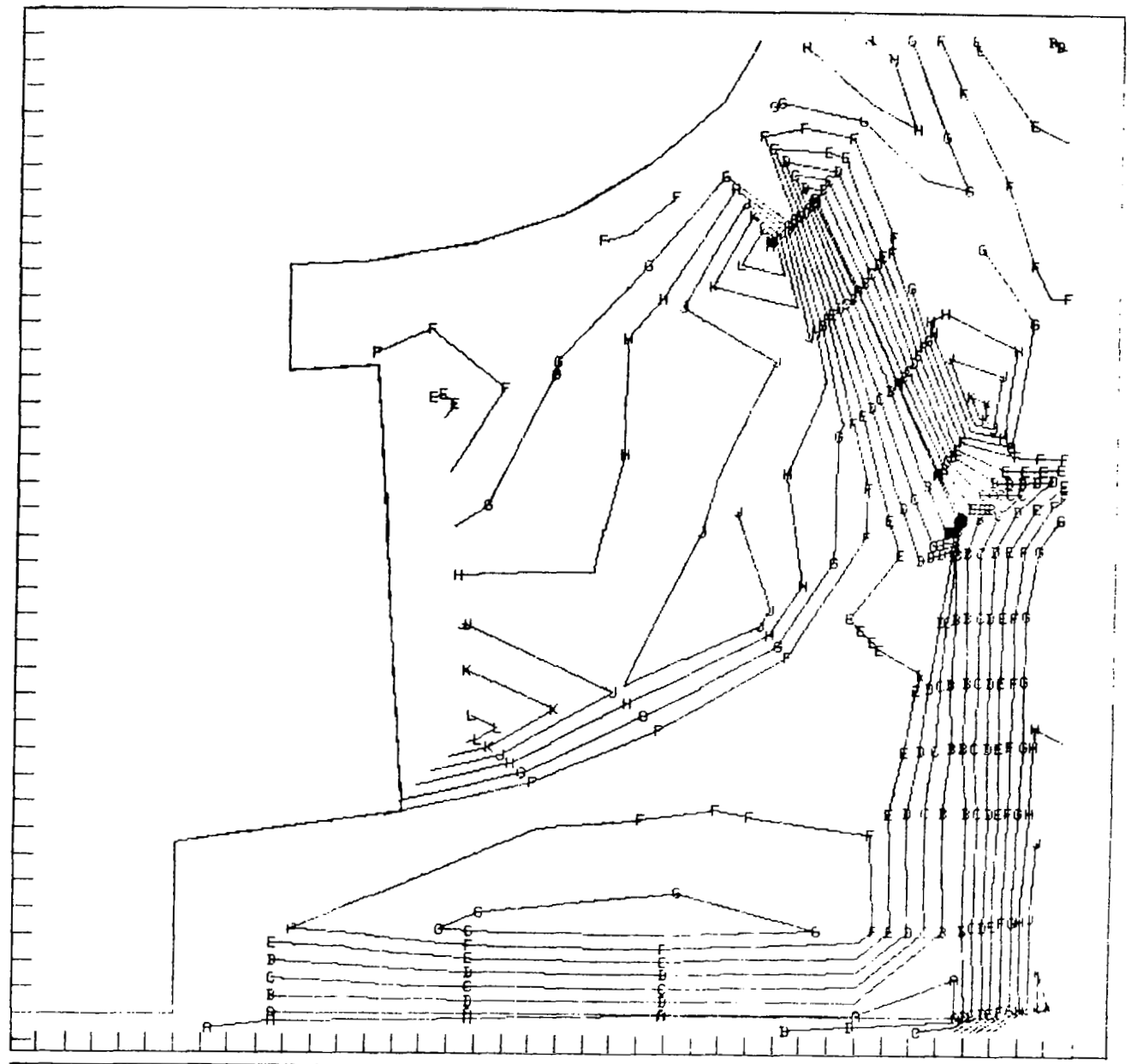

Figure 77. Mark 48-F Split Impeller Preimpeller Effective Stress

The total axial deflection of the balance piston high-pressure seal relative to the low-pressure seal is less than 0.076 mm (0.003 inch) at 9946 rad/s (95,000 rpm) with the welded impeller. Therefore, a total balance piston gap can be maintained at 0.254 mm (0.010 inch), which was used in the pump performance prediction. The deflected shape of the impeller is shown in Fig. 78.

A fatigue analysis of the impeller weld joint was made. Because of the orientation of the weld joint, there is an axial gap between the preimpeller and the main impeller. This results in a mechanical notch for weld joint strains in the axial direction. The maximum axial strain range at the notch adjacent to the weld is 0.0048, using the structural finite-element model calculated axial strain and a notch factor of 3. Based on the above strain range and the low-cycle fatigue life capability of a Class 1 GTA weld joint of 5-2.5 titanium at 61 K (-350 F), the joint cycle life is in excess of 10,000 cycles, which satisfies the minimum requirement of 1200 cycles (300 duty cycles times a safety factor of 4).

GTAW joints have been evaluated, and the predicted minimum strength values have been developed in accordance with Fig. 79. These values are being used as design properties for both GTAW and EB weldments. The values are considered conservative since, in all cases, properties of EB welds have been demonstrated to be superior to properties resulting from GTAW.

Gas Generator

The gas generator was designed as a piece of special test equipment to provide the drive gas for turbopump testing. The requirements imposed to meet the basic intent of such a facility item were: (1) stable operation at all operating points, (2) repeatable high performance, (3) uniform exhaust gas temperature profile, (4) reliable ignition, and (5) durability and long life.

The gas generator design uses separate injector and combustor assemblies which are attached with a bolted flange (Fig. 80). The injector has 15 coaxial injection elements, which are designed for stable operation, high performance, and complete mixing. The nominal operating parameters for the injection elements are given in Table 14. Analysis of the element design, using the Rocketdyne Steady-State Combustion Model, indicated complete combustion within a distance of 8.89 cm (3.5 inches) from the injector face (Fig. 81). The output from this model was also used to conduct a Priem analysis to evaluate the sensitivity of the combustion process to transverse acoustic modes in the combustor. The results of this analysis indicated the gas generator will have stability superior to the J-2 and J-2S engines (higher A), which exhibited dynamic stability to all but intermediate size bombs (Fig. 82). The injector element was also designed with adequate injection pressure drop ($P/P_c = 0.13$) to isolate the gas generator from feed-system-coupled modes of instability.

The injection elements are a self-contained design in which each element is built as a brazed assembly for individual calibration (Fig. 83). The elements have a recessed oxidizer post with four centering devices for positive alignment within the fuel sleeve. Narrow slits are used at the entrance of the fuel sleeve

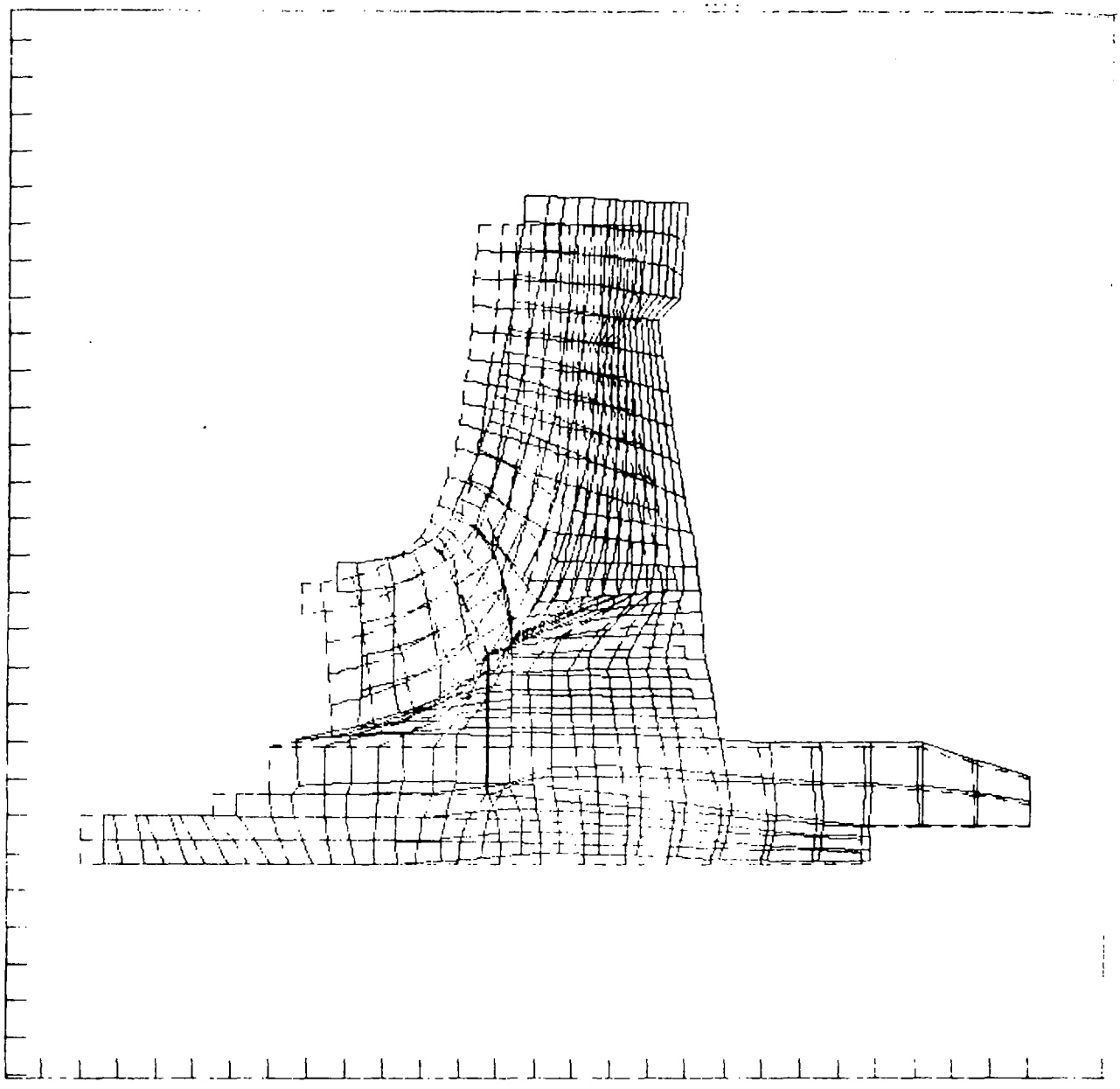

Figure 78. Deflected Shape of Split Impeller

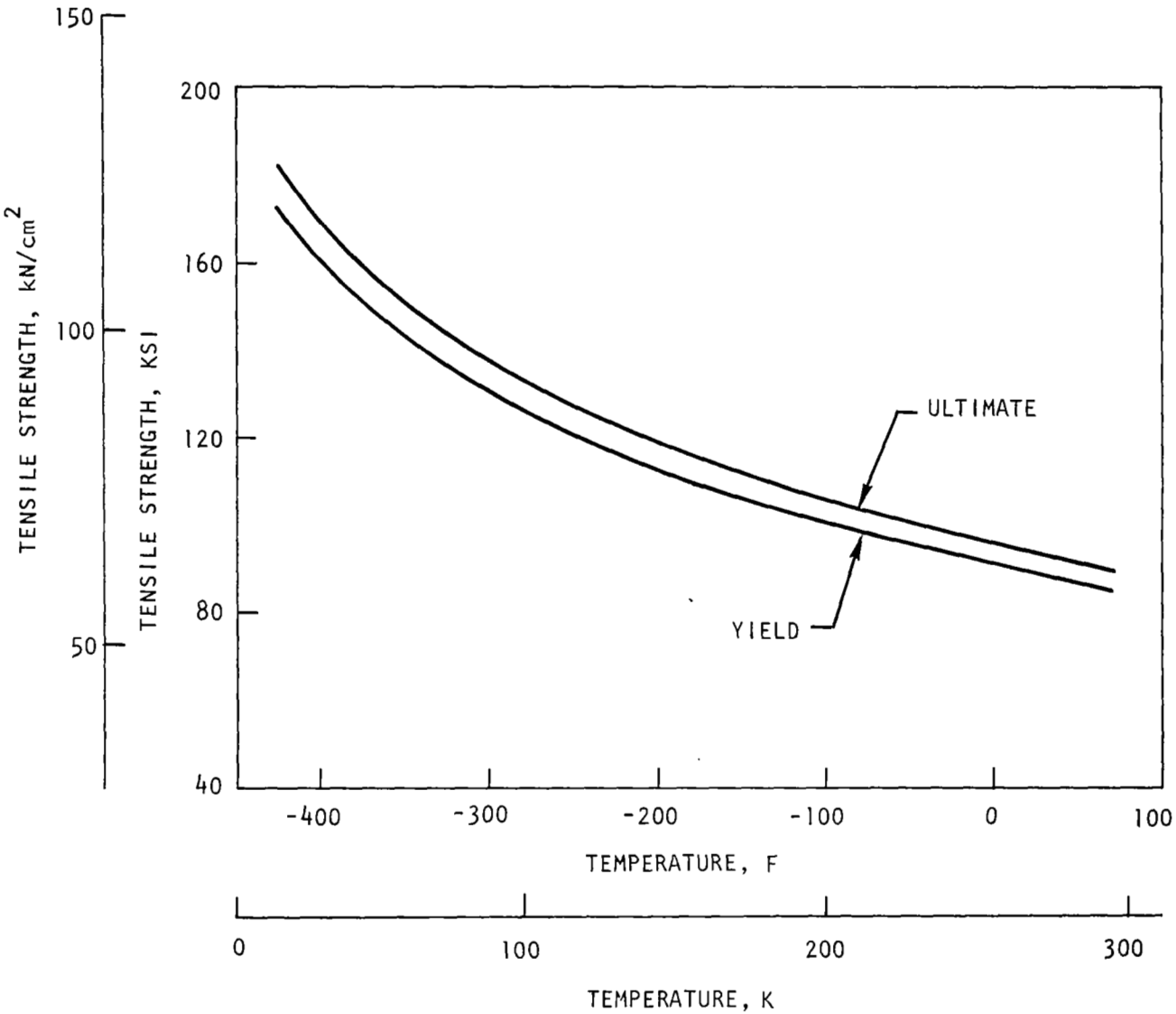

Figure 79. Titanium (5.0 Al-2.5 Sn) Predicted Minimum Tensile Strength

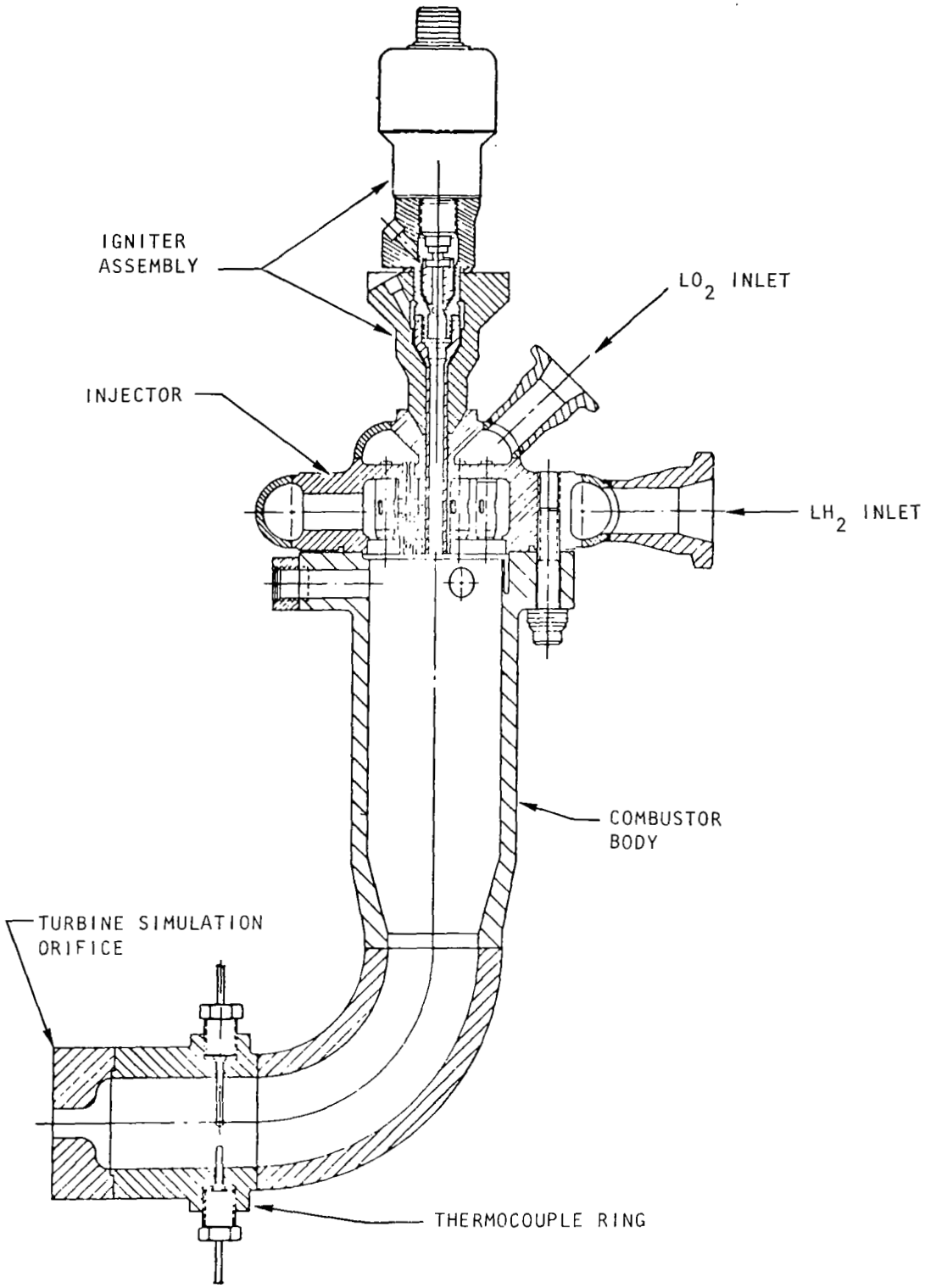

Figure 80. LH_2 Turbopump Gas Generator

TABLE 14. GAS GENERATOR INJECTOR ELEMENTS

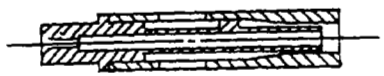

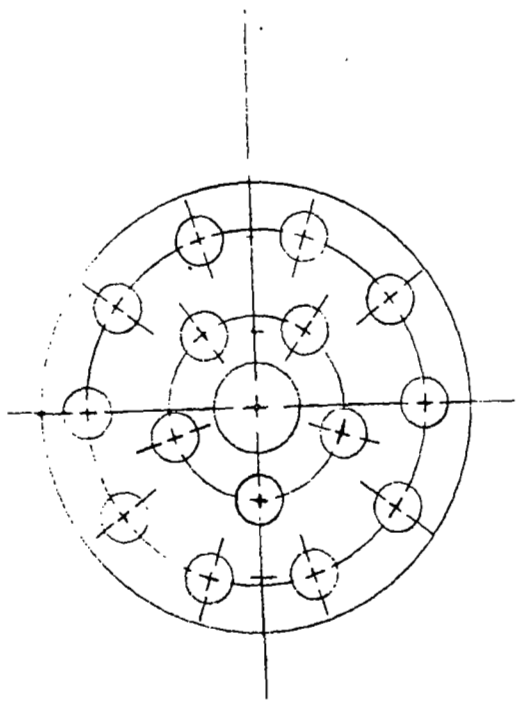

Nominal Operating Parameters	SI Units	English Units
Number of Elements	15	
Flowrate/Element	0.20 kg/s	0.44 lb/sec
Oxidizer Injection Velocity	24.4 m/s	80 ft/sec
Fuel Injection Velocity	190.5 m/s	625 ft/sec
Minimum Fuel Sleeve Gap	3.8×10^{-4} m	0.015 inch
Number of Center Devices		4

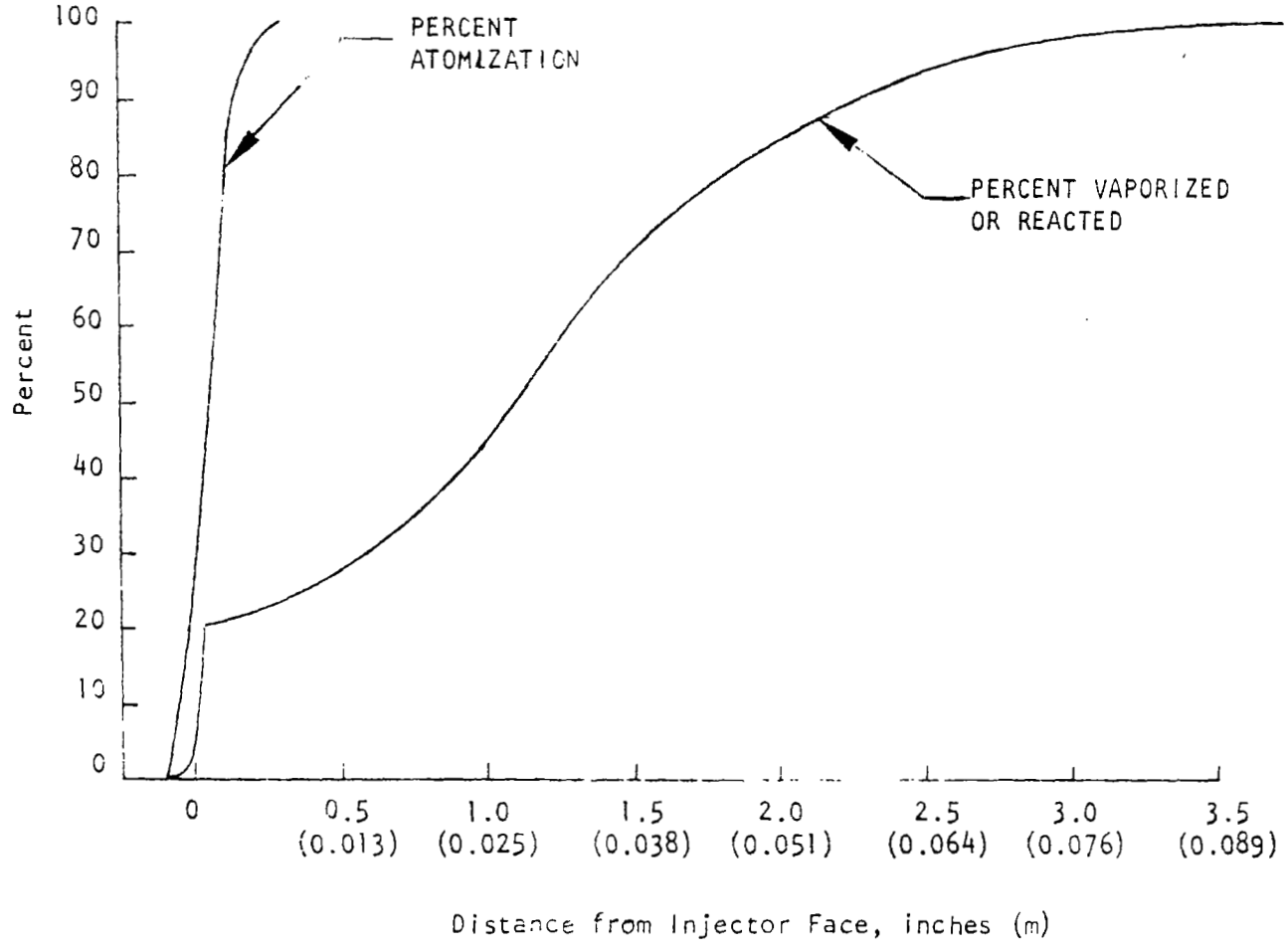

Figure 81. Gas Generator Coaxial Element

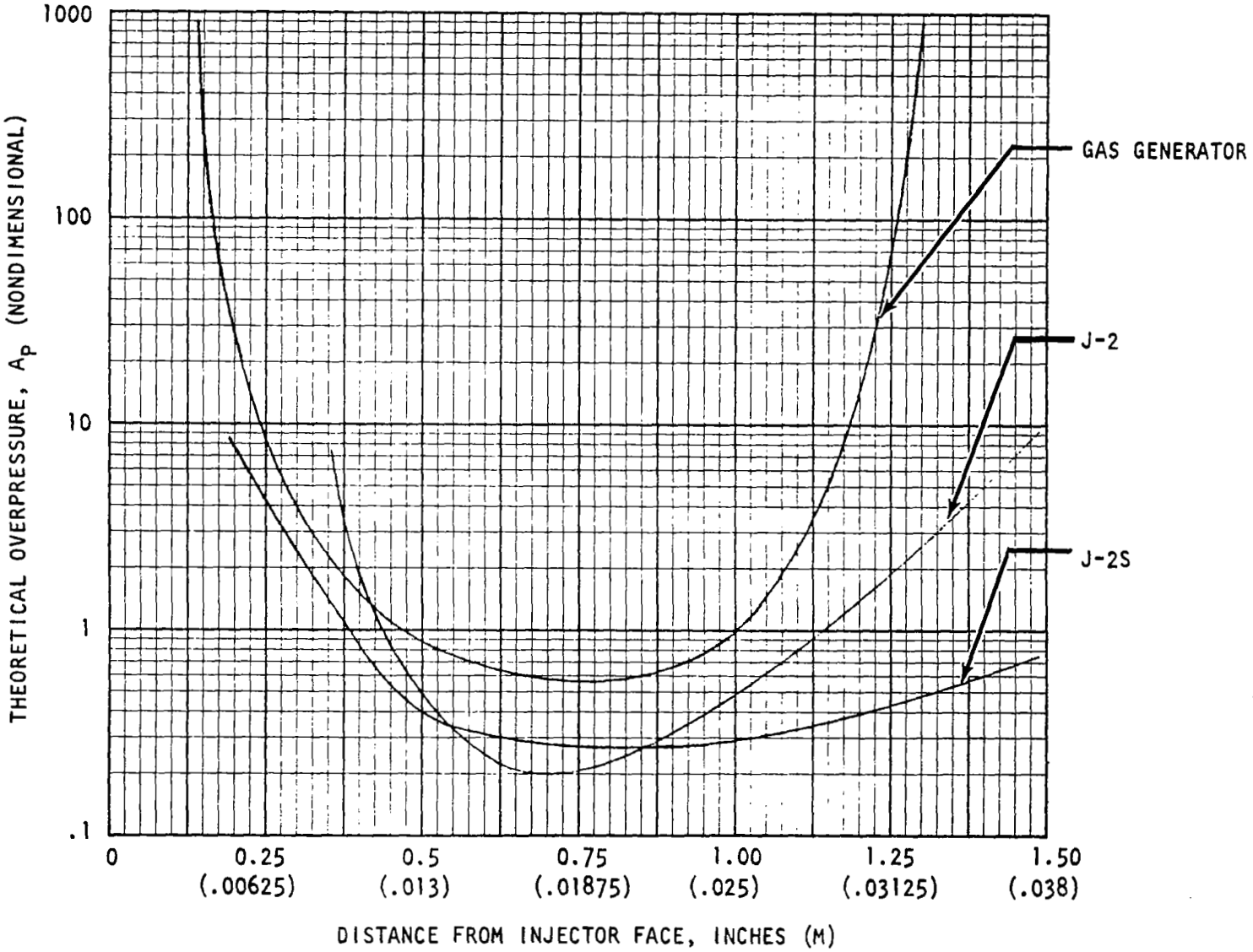

Figure 82. Gas Generator Priem Analysis

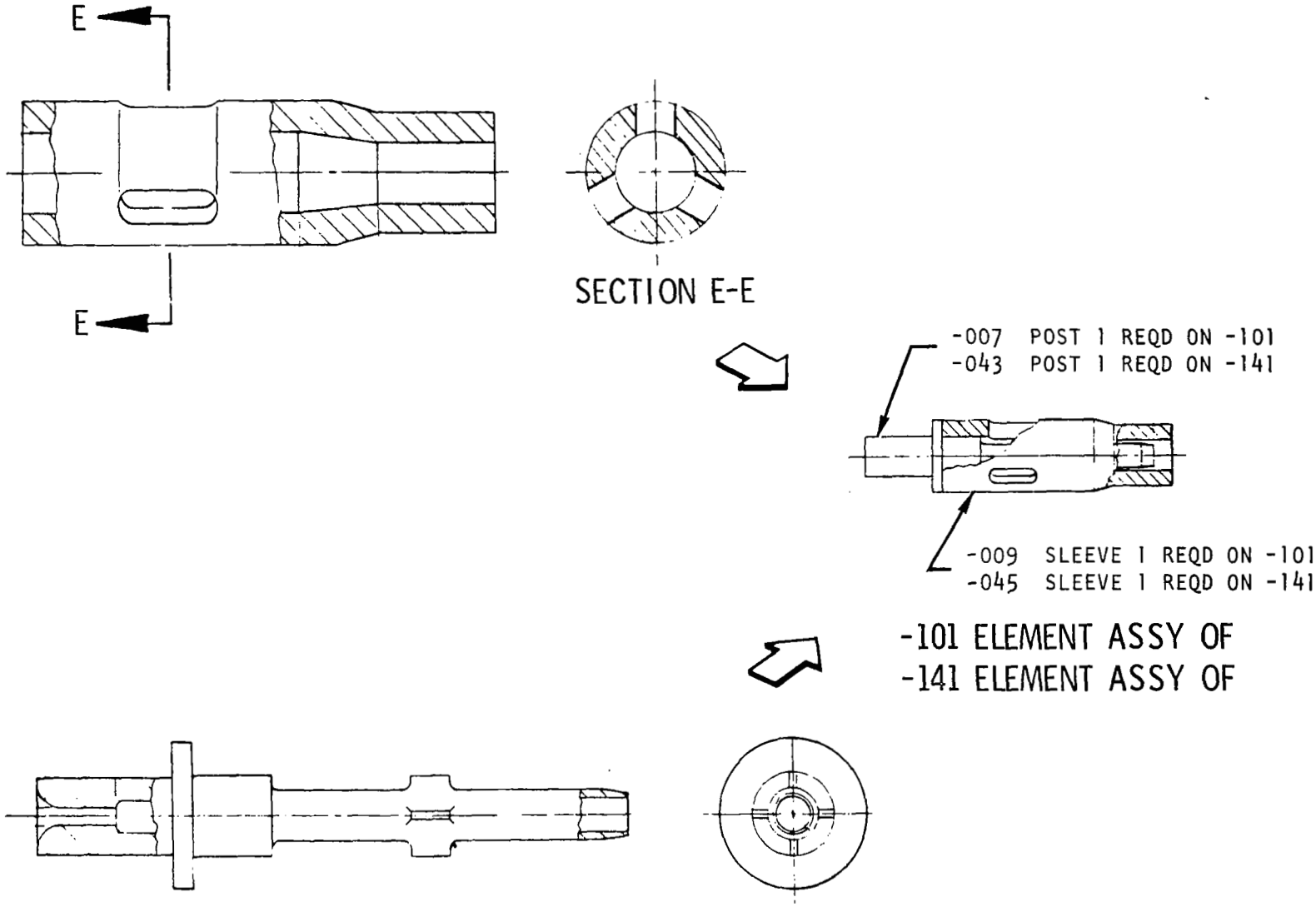

Figure 83. Injector Element

to act as filters to protect the minimum internal fuel flow area from being restricted by contamination. The element material is CRES 304L.

The injector body is an all-welded assembly fabricated from CRES 347. The injector elements and NARloy faceplate are brazed into the injector body. GRAYLOC fittings are used as propellant inlets to interface with the test facility. An envelope has been retained in the center of the injector for potential use of a spark igniter.

The combustor is an all-welded assembly of the combustor body, elbow, and transition section. Added margin for complete mixing and a uniform exit temperature has been provided by using the elbow to induce circulation. The combustor is cooled by film coolant injected from orifices at the periphery of the injector. The film coolant temperature is shown in Fig. 84 as a function of the distance from the injector face.

Acoustic absorbers were placed in the combustor wall, directly below the injector face, to provide added stability margin by damping acoustic modes in the combustor. A summary of acoustic absorber experience (Fig. 85) shows that the design open area of the gas generator acoustic absorber lies in a favorable position relative to previous experience.

A welded transition section was used between the gas generator and turbine manifold because analysis showed that the high temperature in this area would prohibit effecting a positive seal with a flanged joint. The joint is fabricated by welding the Inconel 625 transition piece to the Rene' 41 turbine manifold (Fig. 86). This weld is then heat treated. After the Inconel 625 gas generator transition piece is welded to the combustor elbow, the two transition pieces are joined with an EB weld. The gas generator transition piece has a liner section which extends over the transition piece welded to the turbine manifold. This forms a thermal barrier which ensures that the life of the protected transition piece is consistent with that of the turbine manifold. The design of the transition section allows the gas generator to be removed and rewelded to the turbine manifold without harming the heat treat or weld between Rene' 41 and Inconel 625 since the rework can be made in the protected Inconel 625 transition pieces.

Ignition of the gas generator was to be accomplished using pyrotechnic igniters similar to the Rocketdyne P/N 651876 igniter extensively used for J-2 gas generator and turbopump development testing. Two pyrotechnic igniter ports were provided in the combustor. The subsequent development of a spark torch igniter under company funding based on prior work conducted under NASA-LeRC direction precluded the necessity of utilizing the pyrotechnic igniters.

FABRICATION

Component Fabrication

The methods employed in fabricating the major components of the LH_2 turbopump are discussed in the following paragraphs.

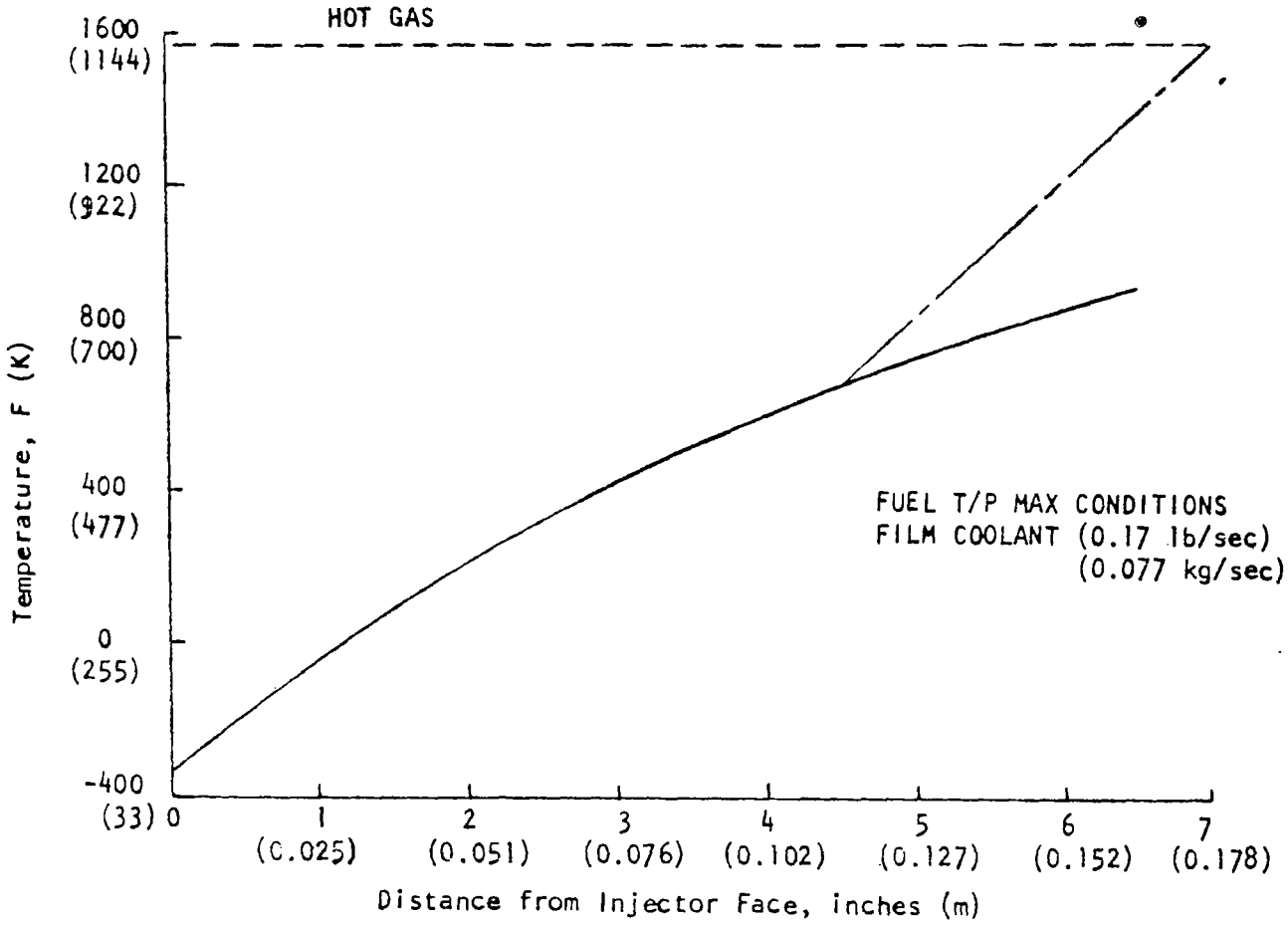

Figure 84. Gas Generator Film Coolant Temperature

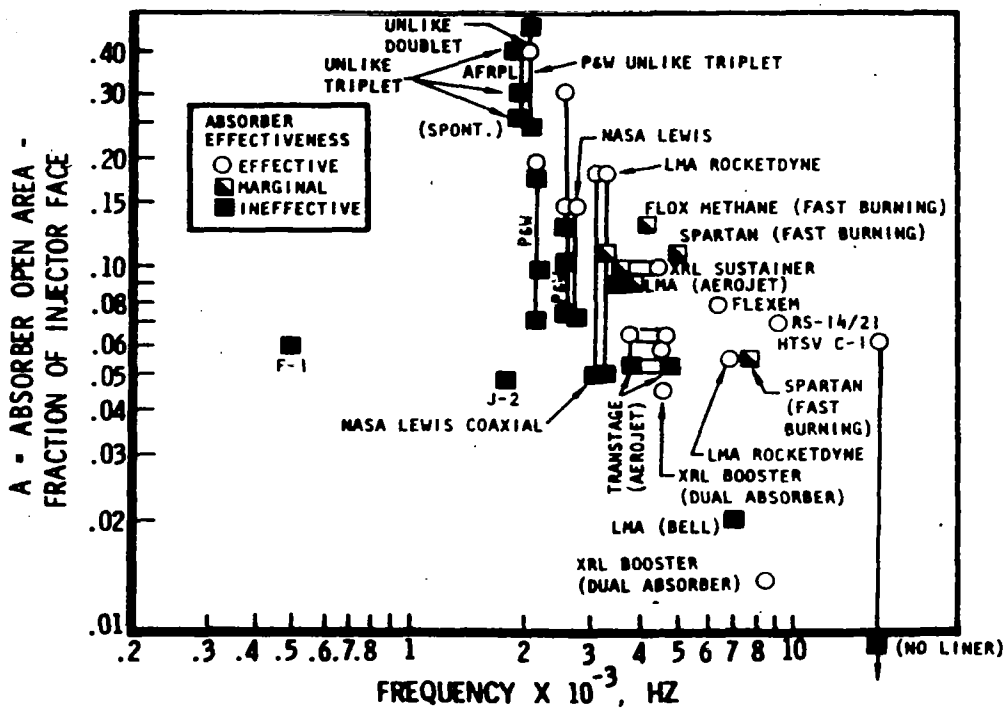

Figure 85. Absorber Experience

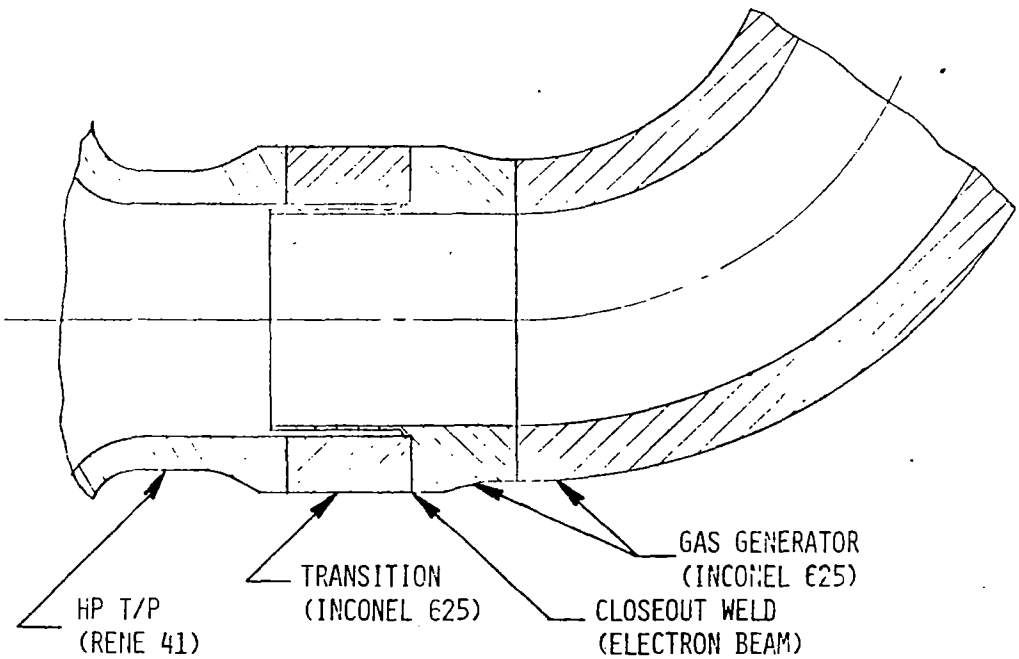

Figure 86. Turbopump to Gas Generator Transition Joint

Pump Inlet. The pump inlet housing, shown in Fig. 87, was a welded assembly of components machined or formed from Inconel 718 wrought material. The inlet guide vanes were generated by pantographing, as illustrated in Fig. 88. Figure 89 shows the housing in a stage of partial completion, with the component containing the guide vanes welded to the dome, but before the inlet torus was attached. The completed inlet housing are shown in Fig. 90.

An alternate design approach for the pump inlet was investigated for potential cost reduction. In this approach, the radial scroll-shaped inlet (Fig. 90) was replaced by an axial entry, as illustrated in Fig. 91. Bids received from three vendors based on the conceptual sketch shown in Fig. 91 revealed that the axial inlet would be slightly more expensive. As a result, the original design concept was retained.

Pump Crossovers. The crossovers were fabricated in three sections from Inconel 718, as illustrated in Fig. 92. The internal hydrodynamic passages, including the radial diffuser and the rows of crossover guide vanes, were generated by EDM. One of the setups for forming the diffuser vanes is shown in Fig. 93. The three components prior to assembly are shown in Fig. 94.

After all the internal passages were established, the components were joined by EB welding, and the assembly was heat treated and finish machined. A 0.254 mm (0.010 inch) thick silver plating was applied to the impeller labyrinth lands.

Impellers. The impellers were fabricated from single pieces of 5.0Al-2.5Sn titanium forgings. External features, hubs, and splines were machined by conventional methods. The internal flow passages were generated by EDM from the inlet and discharge side. A typical EDM setup in which the vane leading edges were formed is illustrated in Fig. 95.

Considerable difficulty was experienced in obtaining a satisfactory passage shape in the transition zone between the inlet and discharge because of the lack of accessibility with an integral front shroud. Several reworks were made in that area to eliminate discontinuities and protrusions in the flow channel. The delivered impellers deviated somewhat from the drawing in that the vanes did not have a continuous twist from inlet to discharge, and in certain areas the vanes were undersize. As a result of the difficulties encountered in producing the impellers to print, a design modification was made in which the impeller is fabricated in two pieces and joined by EB welding. The details of this approach are described elsewhere in this report.

Each of the completed integral impellers was submitted to proof spinning, in which they were spun up to a speed of 8376 rad/s (80,000 rpm) at ambient temperature. No failures or permanent deformations were encountered.

A finished second-stage impeller is shown in Fig. 96. The three impellers stacked on the rotor are illustrated in Fig. 97.

Turbine Wheels. The turbine wheels were machined from integral Astroloy forgings. Because of the integral shroud at the outer diameter of the wheel, the blade surfaces were generated by the EDM from the upstream and downstream side,

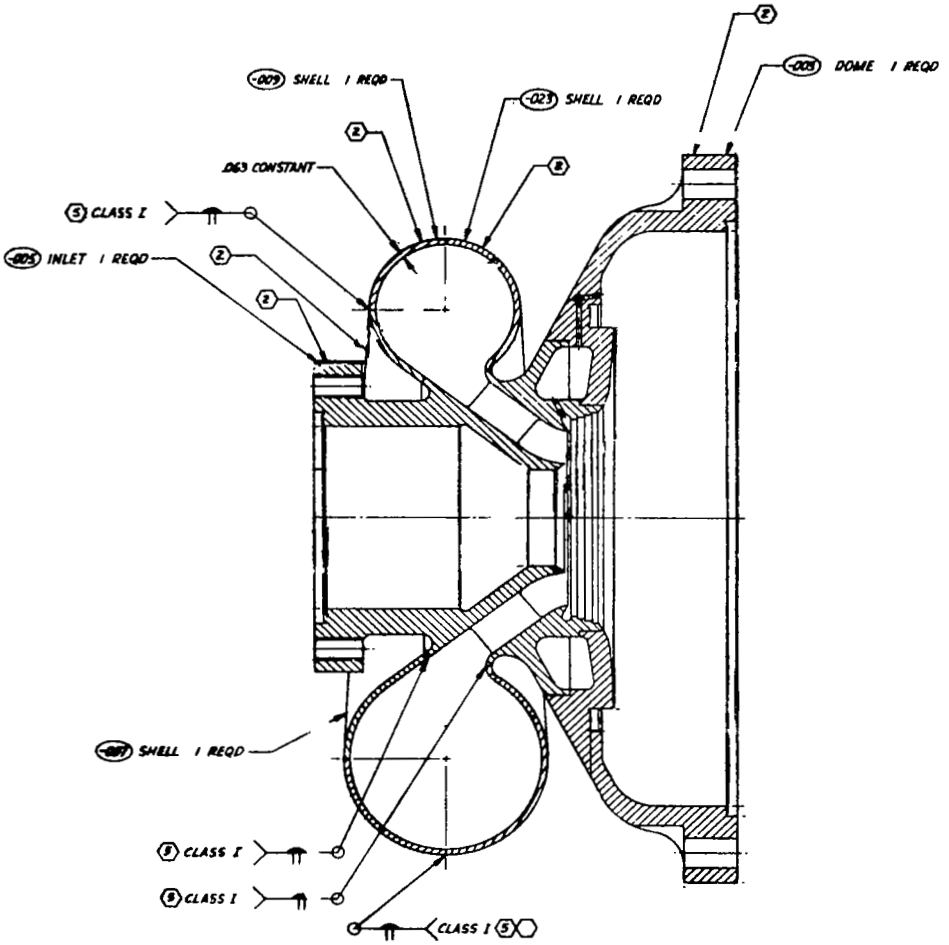

Figure 87. Pump Inlet Housing

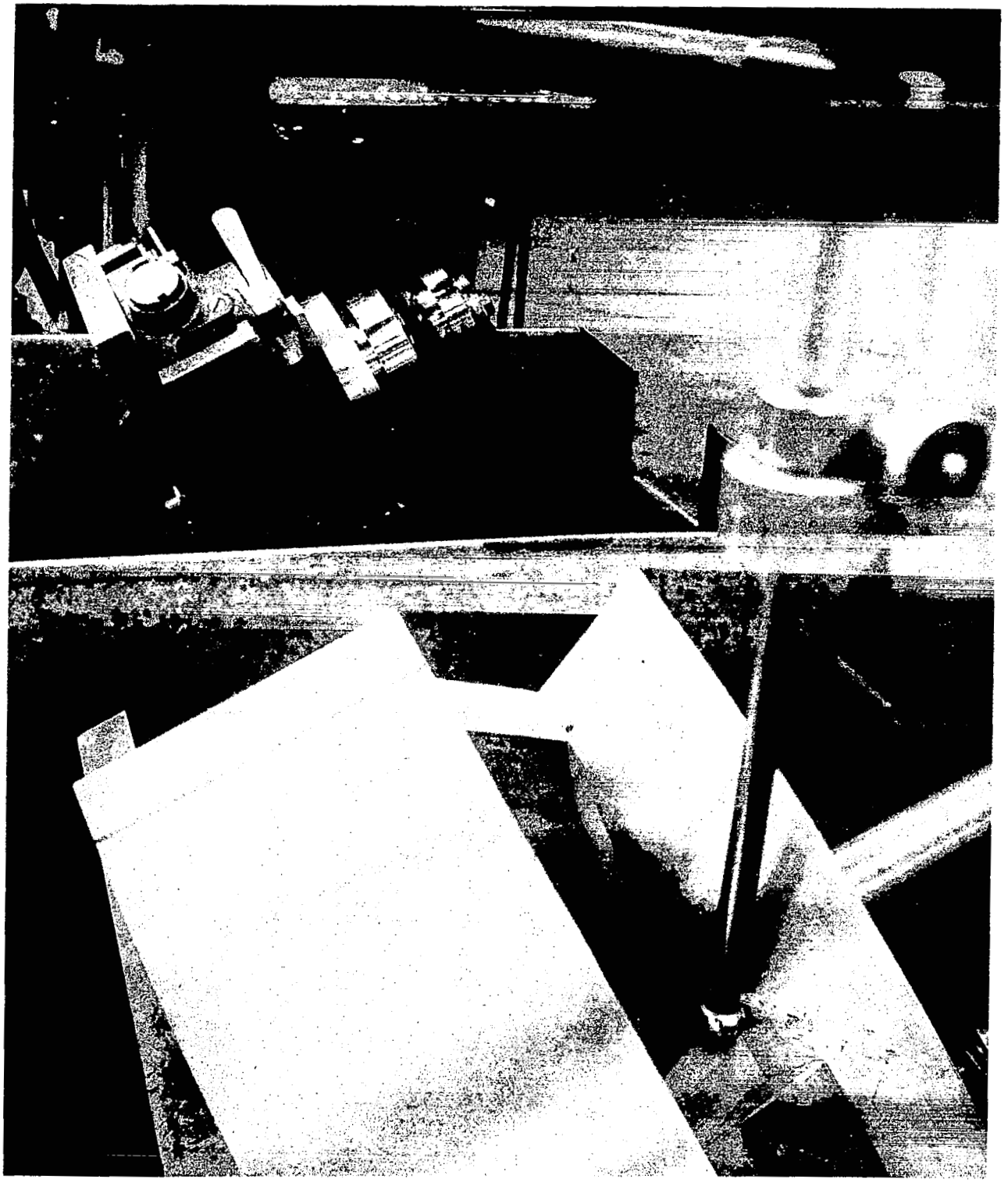

1XY52-10/2/74-C1L*

Figure 88. Mark 48-F Inlet Housing Guide Vane Pantographing

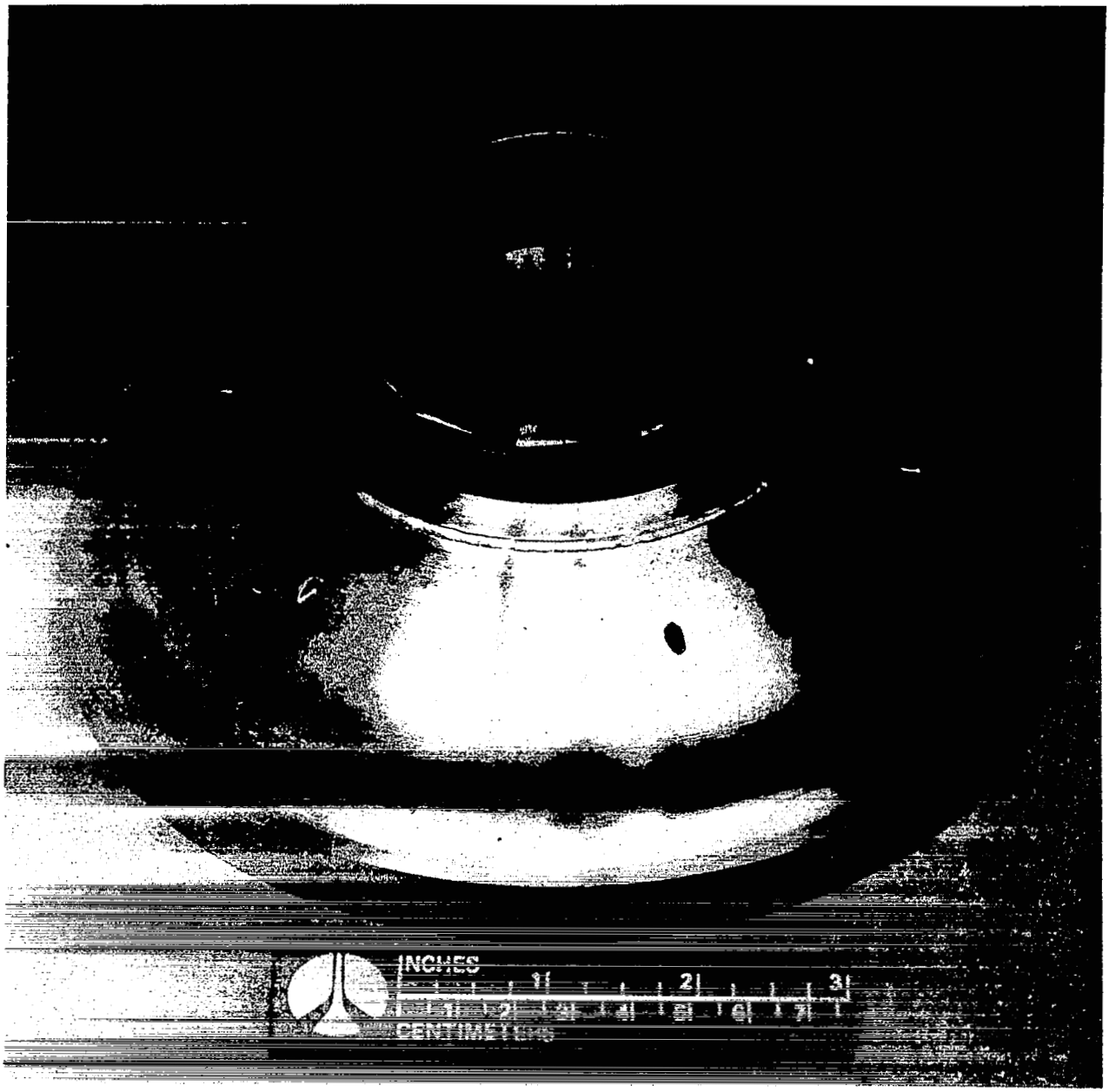

1XY52-12/17/74-C1A*

Figure 89. Partially Completed Mark 48-F Inlet Housing

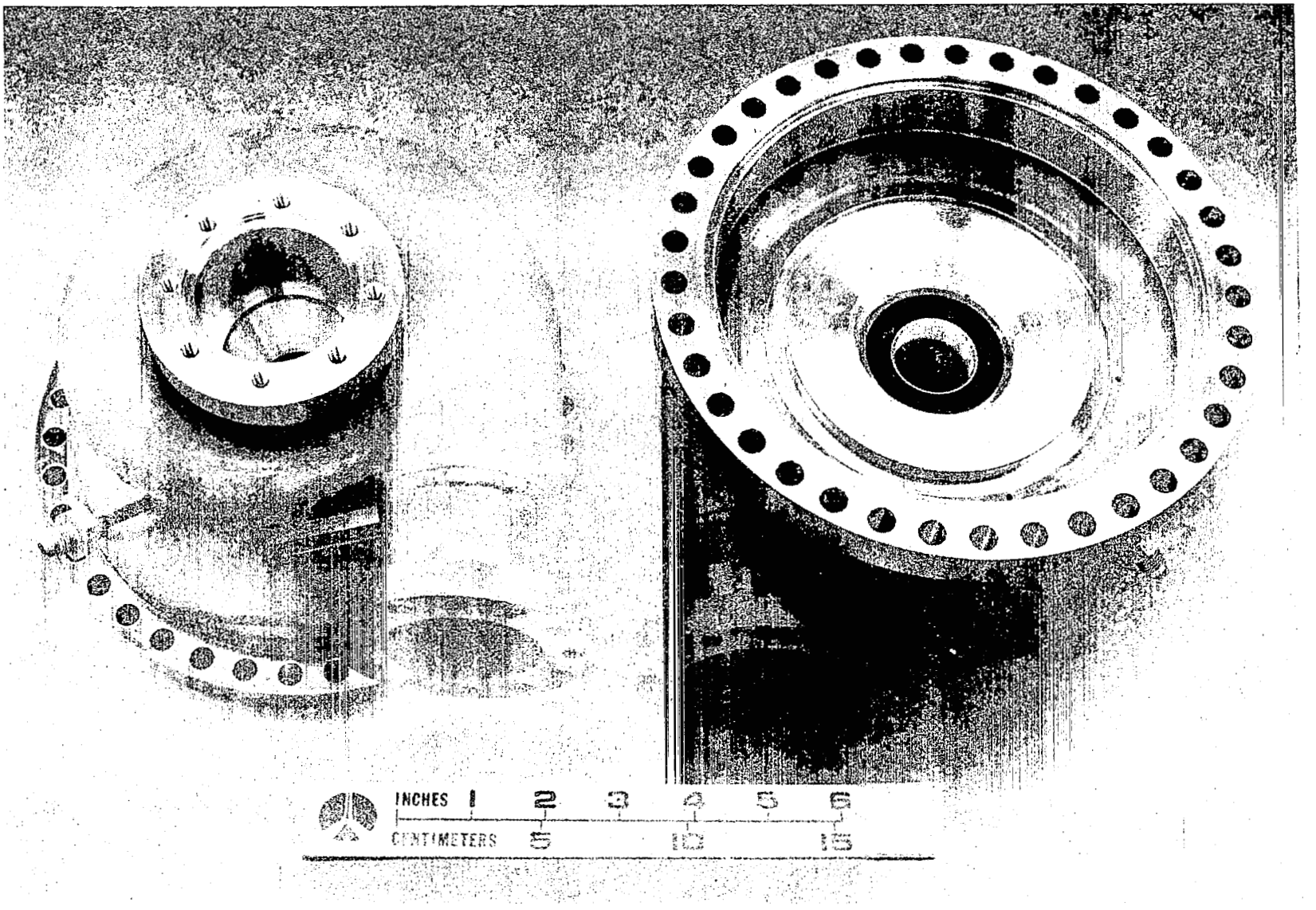

1XY52-3/19/75-C1*

Figure 90. Mark 48-F Inlet Housings

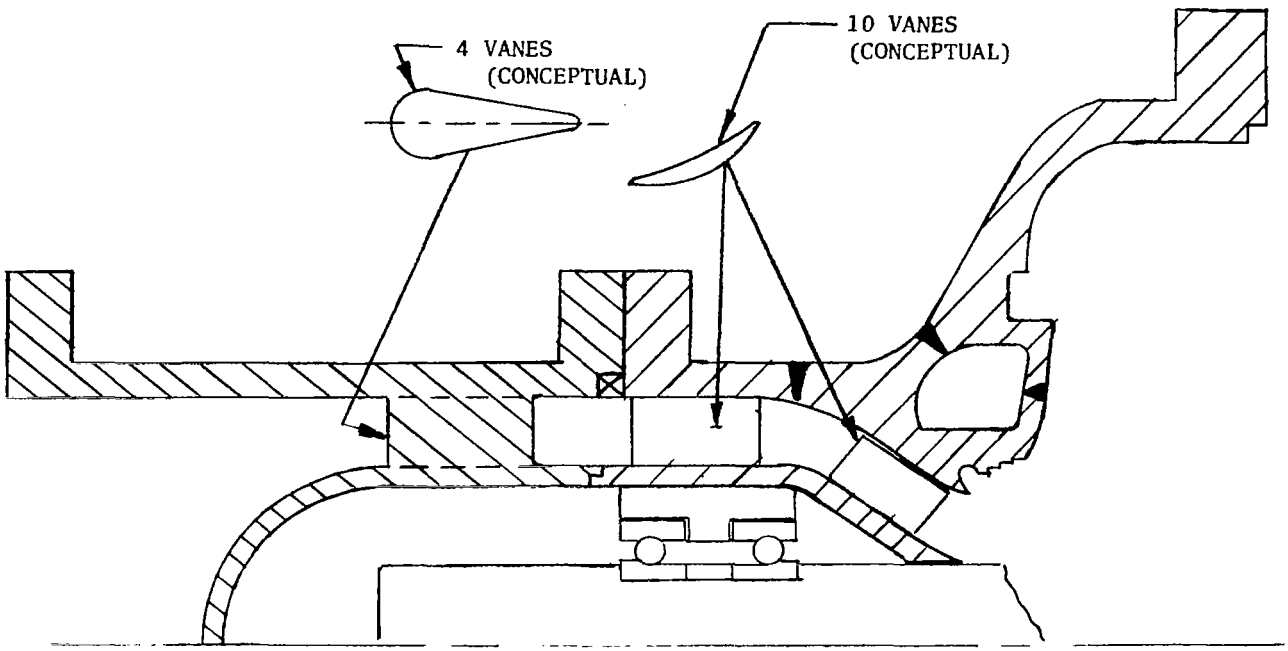

Figure 91. Mark 48-F Turbopump Axial Entry Pump Inlet

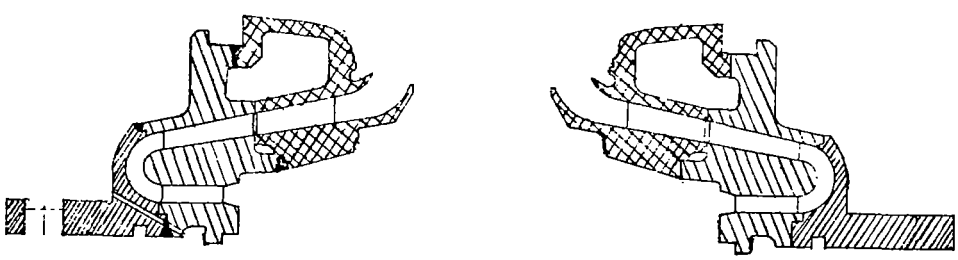

Figure 92. Crossover Fabrication

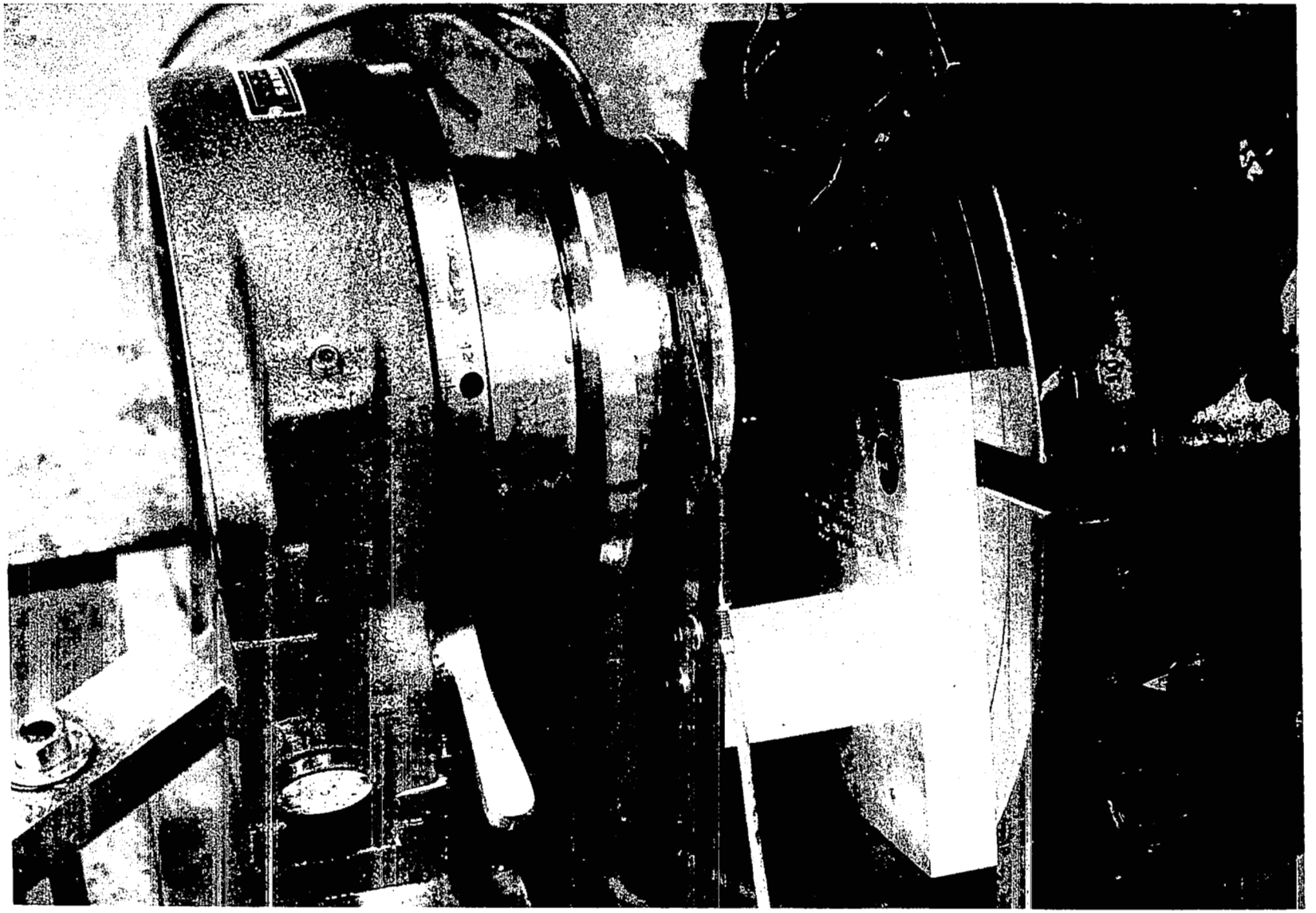

1XY52-8/19/74-C1 1*

Figure 93. Mark 48-F Diffuser EDM Setup

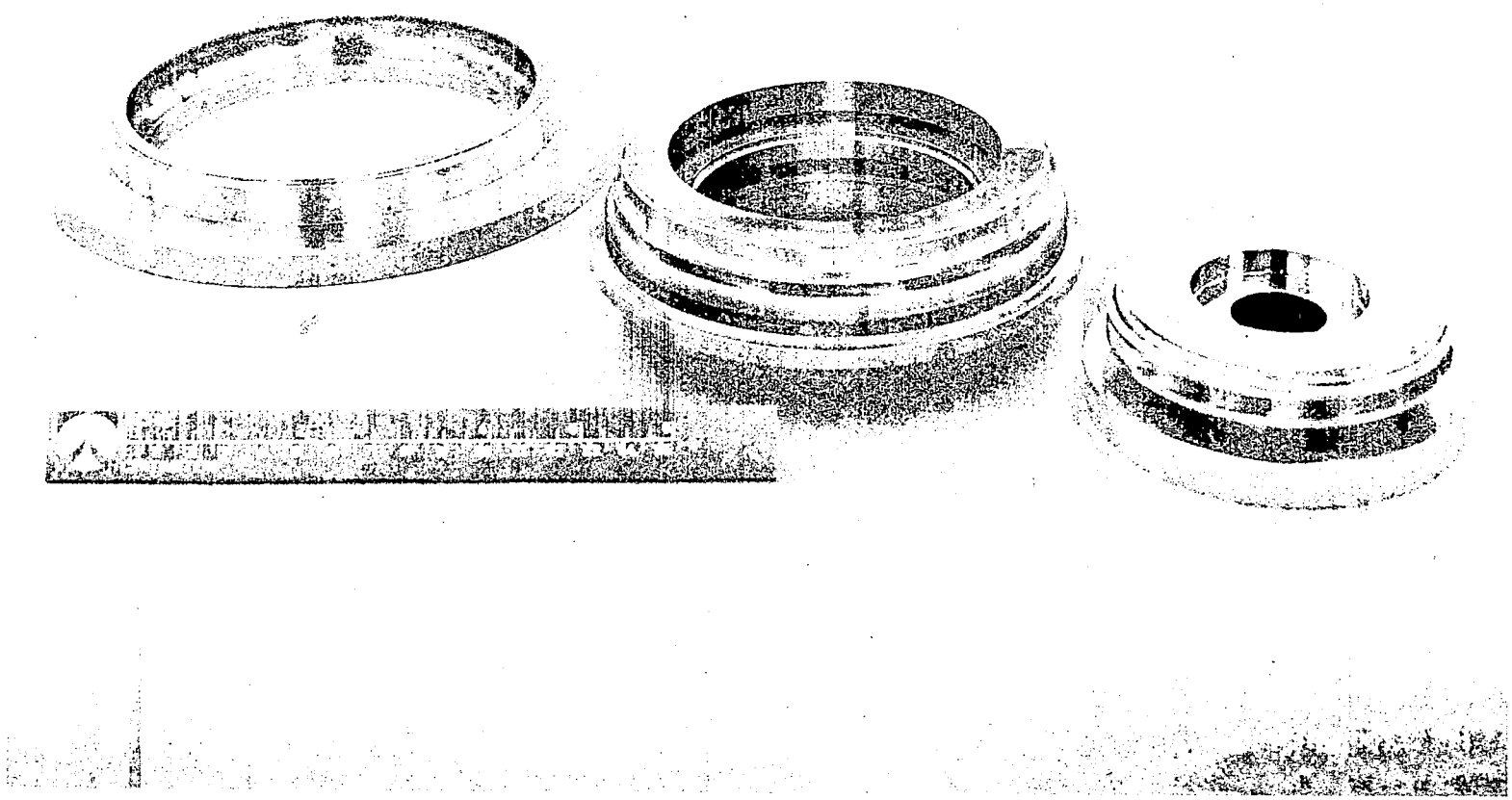

1XY52-11/21/74-C1C*

Figure 94. LH_2 Pump Crossover Details Before Welding

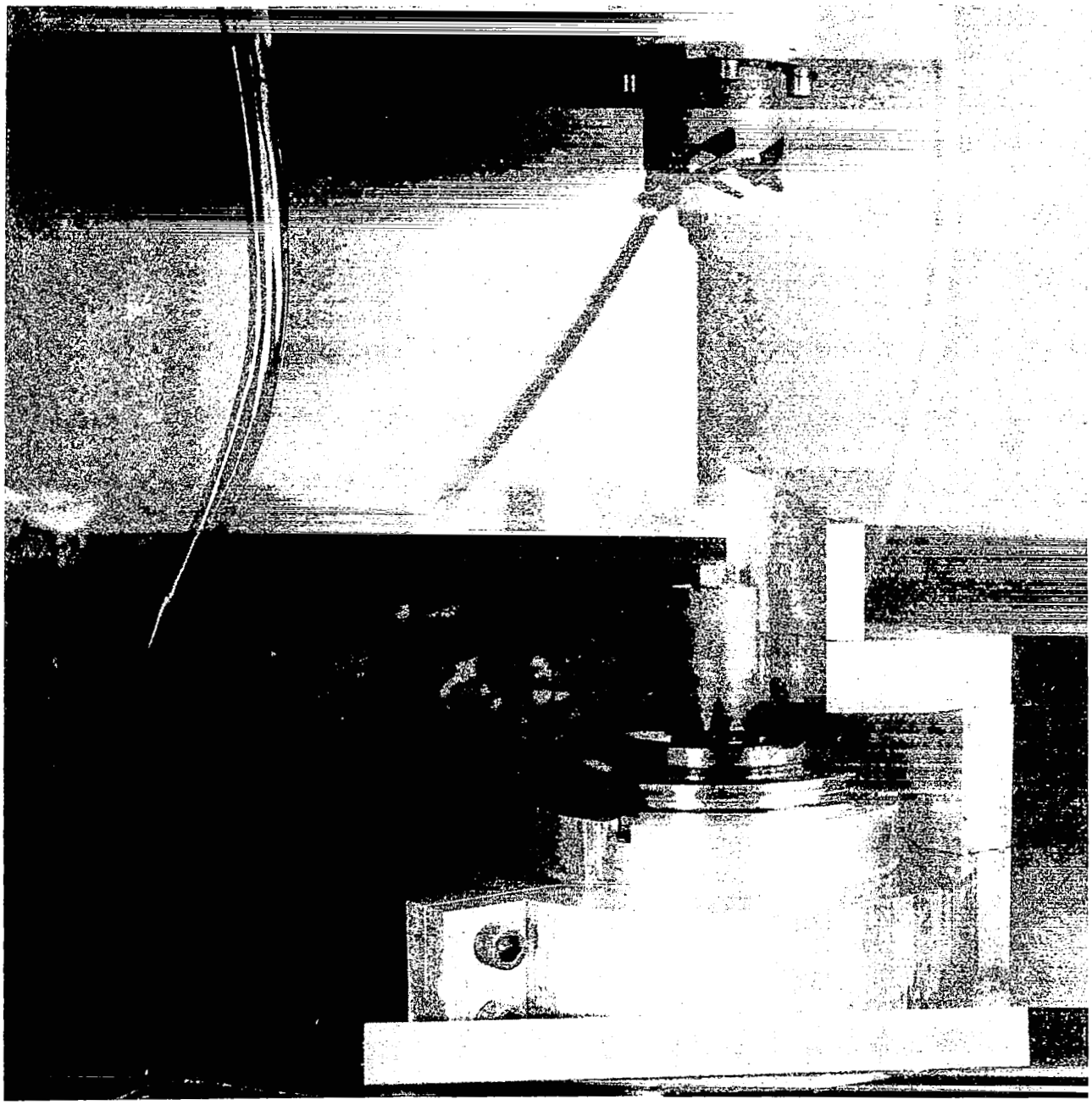

1XY52-10/2/74-C1H*

Figure 95. Impeller EDM-ing Set-Up

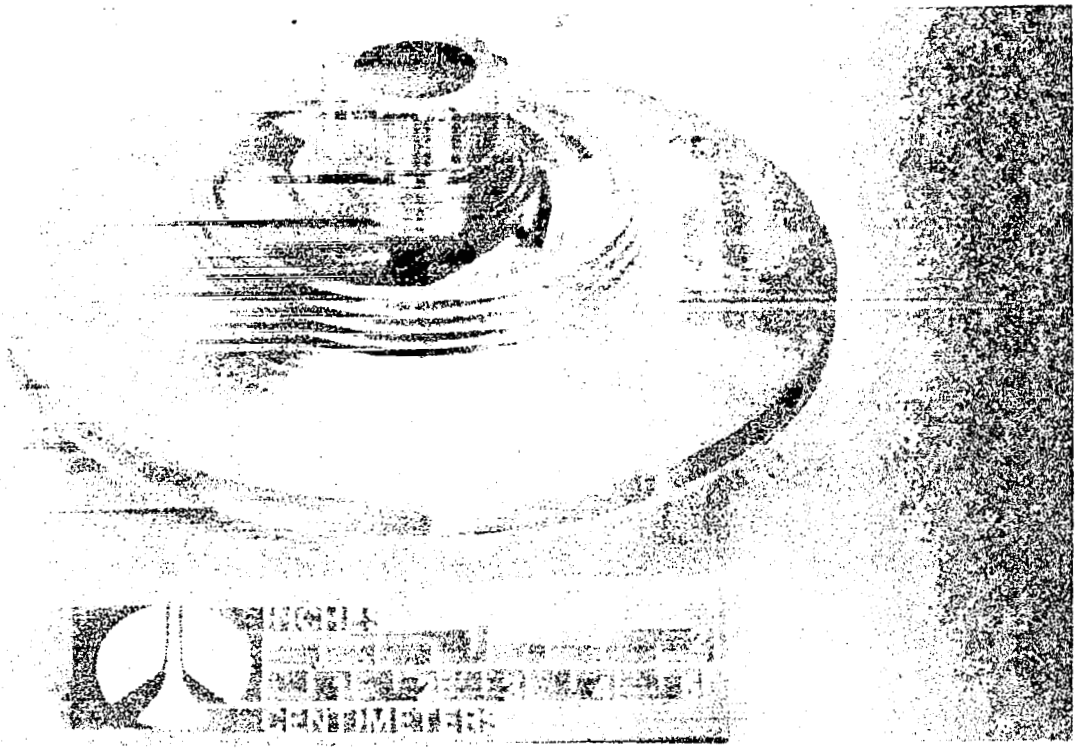

1XY25-5/15/75-C1D*

Figure 96. Second Stage Impeller

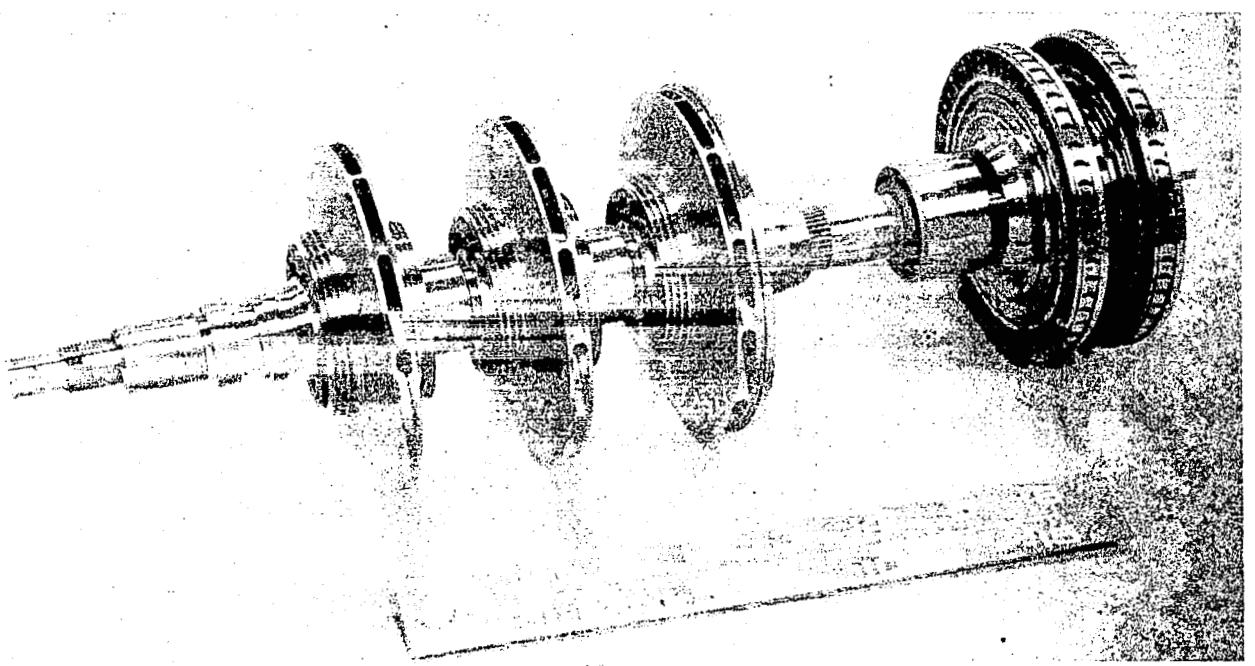

1XY52-6/12/75-C1C*

Figure 97. LH_2 Turbopump Rotor

respectively. All blade surfaces were formed concurrently with a one-piece electrode, shown in Fig. 98. The lightening holes at the center of the blades were also formed by EDM. The completed first- and second-stage wheels are shown in Fig. 99 with the center tie bolt.

Housing. The most complex component of the turbopump to fabricate was the housing. It incorporated, in a single welded structure, the pump third-stage diffuser and discharge volute and, on the turbine end, the inlet manifold and first-stage nozzle (Fig. 100). In its initial stages of manufacture, the housing was fabricated in two separate groups. The construction of the housing is illustrated in Fig. 100. The chronology of processing is depicted in Fig. 101.

The pump end of the housing was machined from two major forgings. The -003 component, which contained the third-stage diffuser, was machined from an Inconel 718 forging, with the diffuser vanes formed by EDM (Fig. 101, step 1). The contours of the -005 volute cap (Fig. 101, step 2) were machined by pantographing (Fig. 101, step 3) from Inconel 718, and the two pieces were joined by EB welding (Fig. 101, step 4). Transition rings (-027 and -029) of Haynes 188 material were attached, by EB welding, in the area where the turbine manifold was to be joined to the pump housing. At this stage, the pump end of the housing was heat treated to Inconel 718 specifications (Fig. 101, step 5).

The fabrication of the turbine manifold progressed in a parallel effort with the above, as shown in Fig. 101. The turbine first-stage nozzle was made from Haynes 188 alloy by EDM of the flow passages (Fig. 101, step 1). A 1.52 mm (0.060 inch) thick line was constructed from Incoloy 903 sheet metal to reduce thermal gradients across the main pressure walls. The contacting side of the liner was etched to produce local high spots and thereby reduce the surface area in contact. The liner was installed "loose" between the two manifold halves, i.e., without weld attachment to allow it to expand and contract without constraints (Fig. 101, step II).

The two manifold halves were machined from Rene' 41 and assembled by tungsten inert gas (TIG) welding (Fig. 101, step III). Parts of the manifold, which were analytically predicted to be subject to high strain, were plated (Fig. 101, step IV) 0.076 to 0.25 mm (0.003 to 0.010 inch) thick with copper to provide hydrogen-environment-embrittlement protection. Haynes 188 transition rings were welded to the turbine manifold in two areas where it was to be attached to the pump volute housing.

At this stage (Fig. 101, step V), the welded manifold assembly was heat treated to Rene' 41 specification.

The welded and heat-treated pump housing and turbine manifold were joined (Fig. 101, step 6) by EB welding at the Haynes 188 transition rings. The rings were of sufficient length to leave the heat-treated Inconel 718 and Rene' 41 on the pump and turbine end unaffected by the weld heating. After the final welding was accomplished, the housing internal features and flanges were finish machined to print requirements (Fig. 101, step 7).

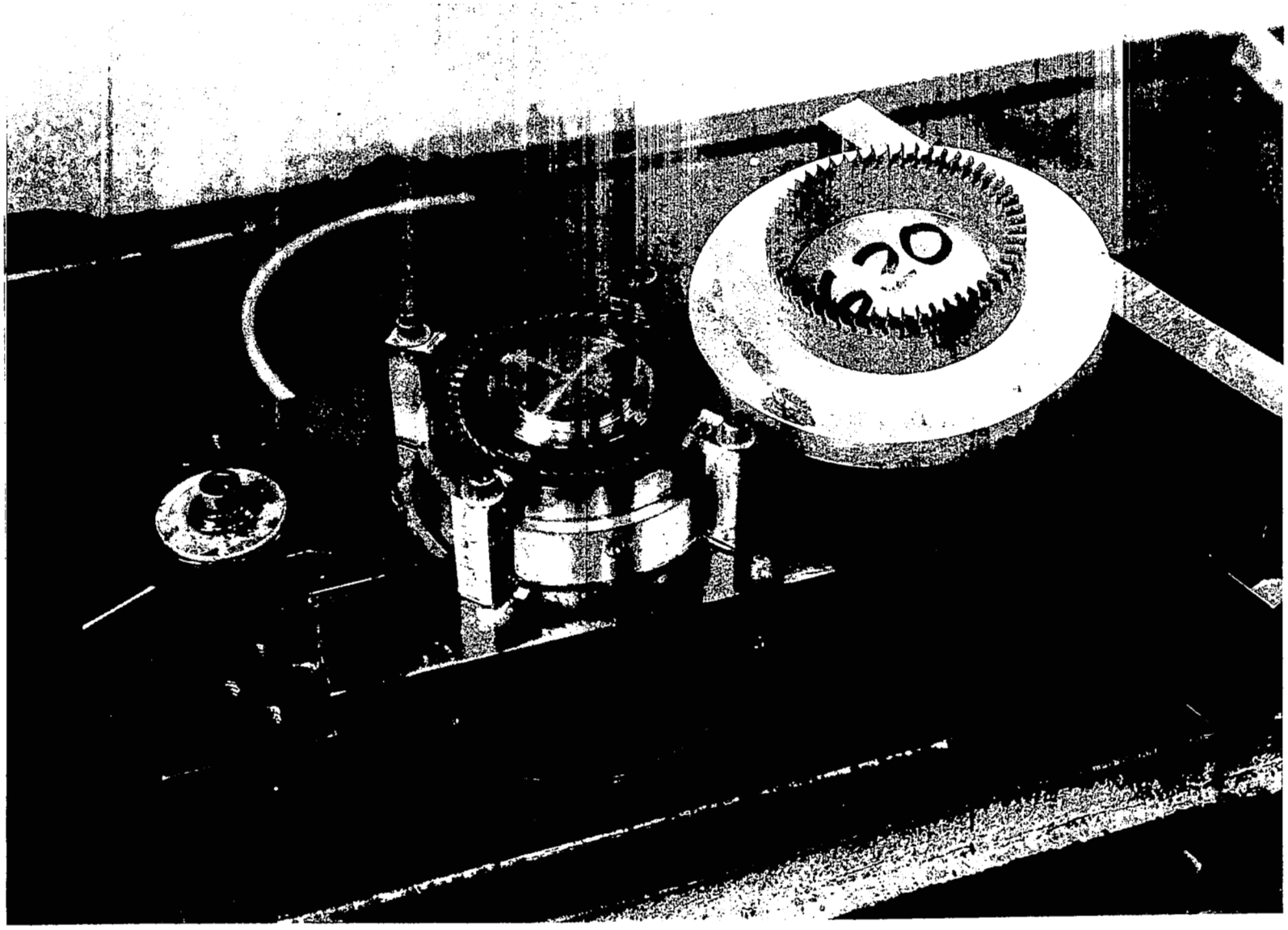

1XY52-8/19/74-C1L*

Figure 98. Turbine Wheel Machining Set-up & Electrode

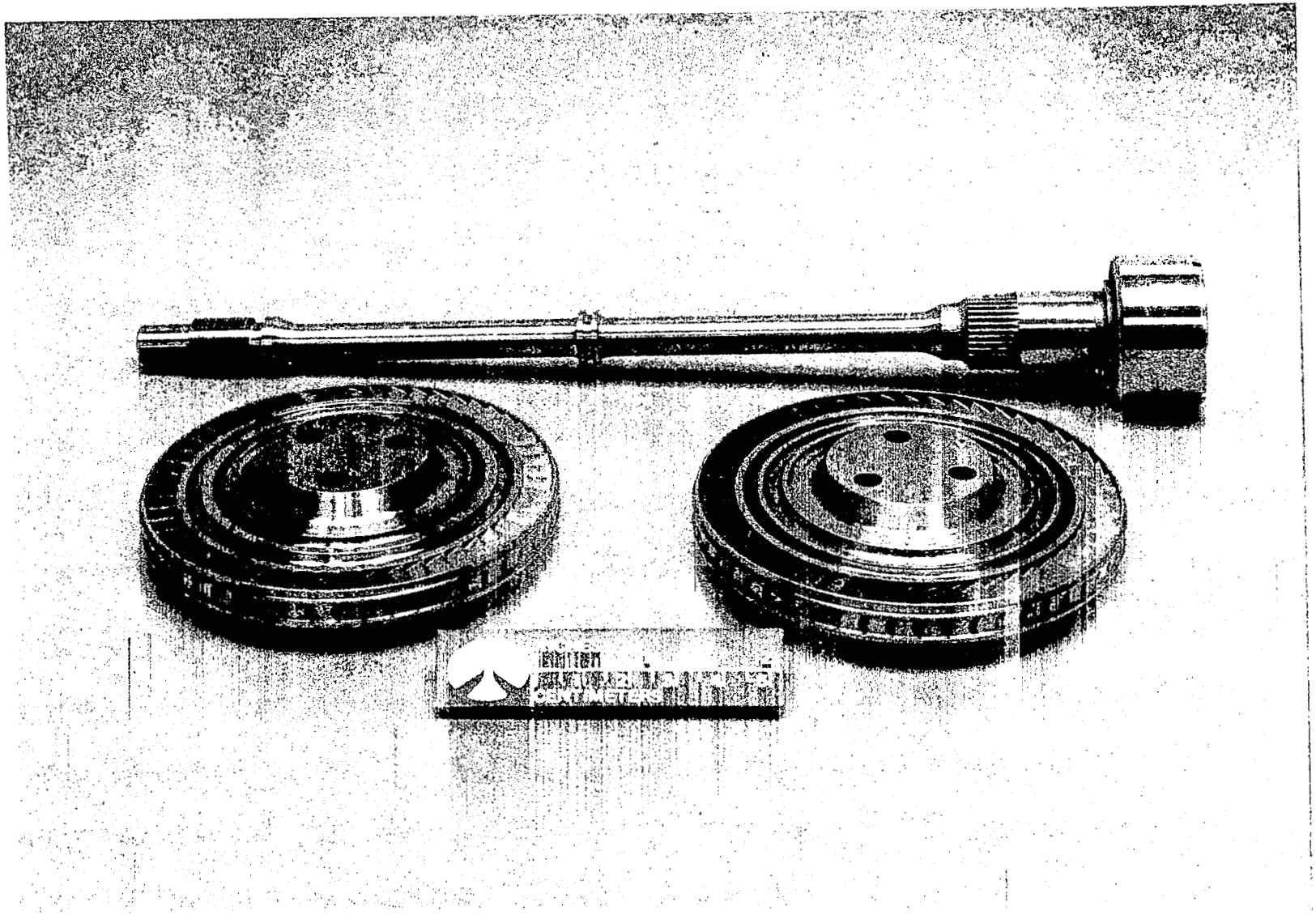

1XY25-5/15/75-C1C*

Figure 99. Turbine Wheels & Center Tie Bolt

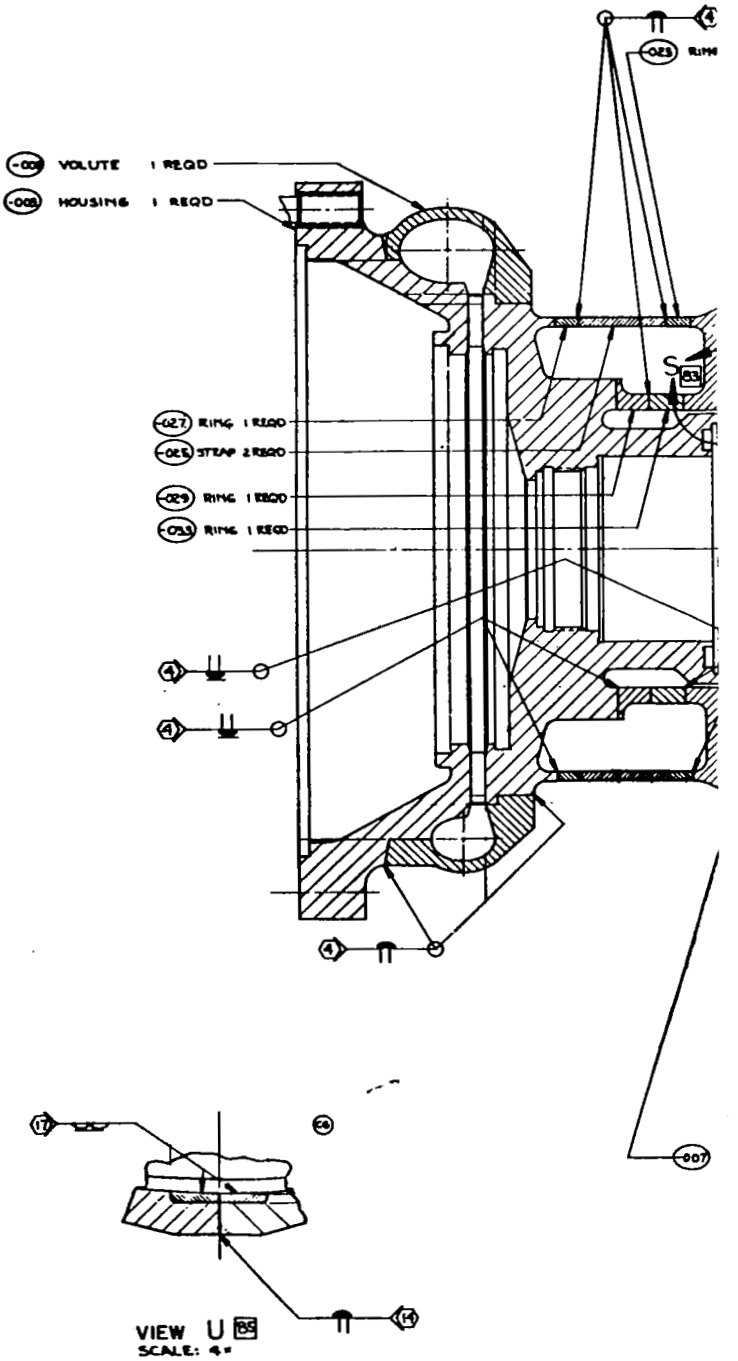

VIEW U
SCALE: 4"

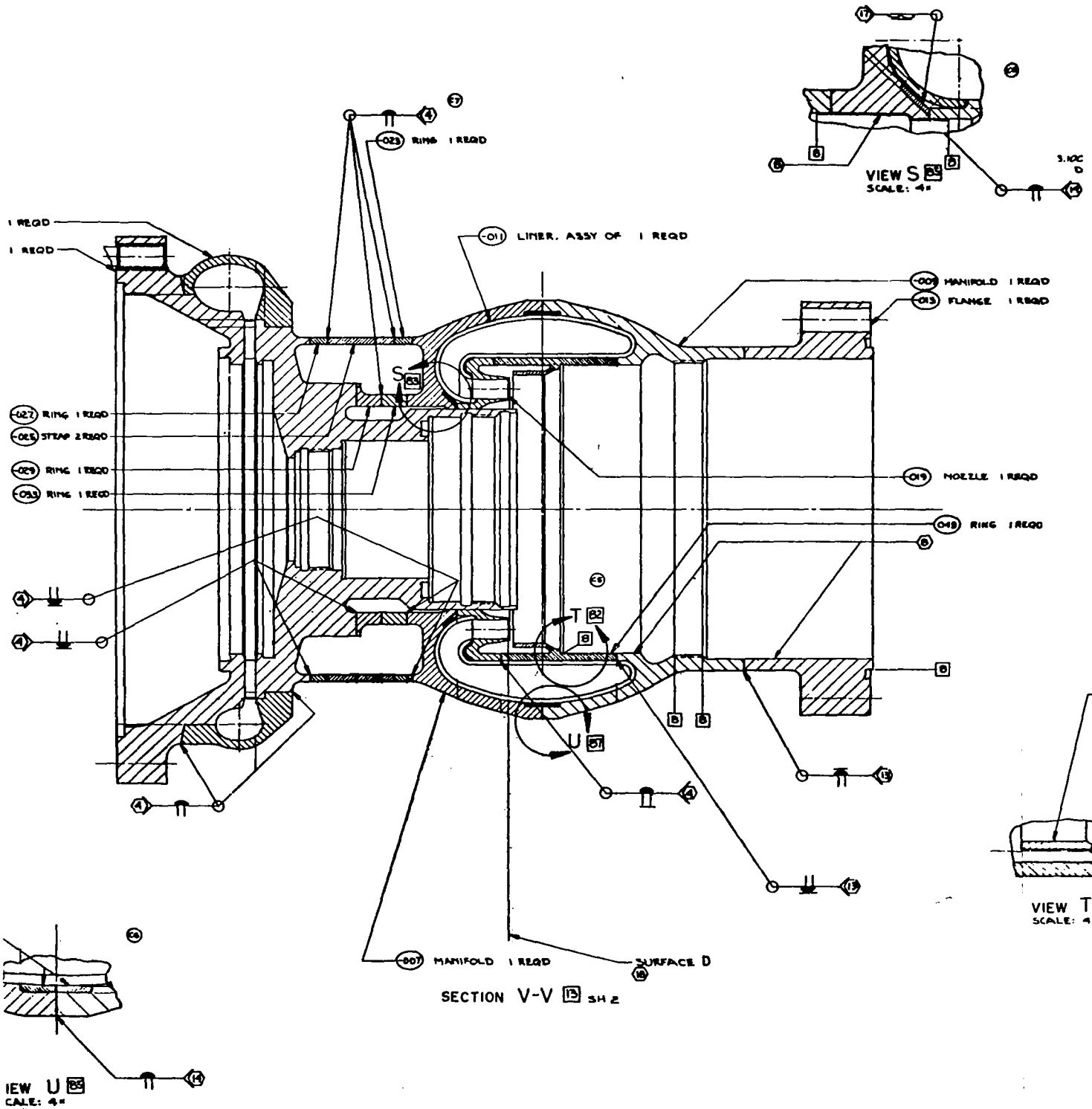
-023 RING 1 REQD
-011 LINER, ASSY OF 1 REQD
-007 MANIFOLD 1 REQD
-013 FLANGE 1 REQD
-027 RING 1 REQD
-025 STRAP 2 REQD
-029 RING 1 REQD
-033 RING 1 REQD
-019 NOZZLE 1 REQD
-048 RING 1 REQD
-007 MANIFOLD 1 REQD
SURFACE D
VIEW S
SCALE: 4"
-017 SEAL
VIEW T
SCALE: 4"
SECTION V-V SH 2
IEW U
CALE: 4"

Figu

Turbopump Assembly

Rotor Balance. Because of the high operating speeds involved and the stacked rotor configuration, the balancing procedure had to eliminate internal moments resulting from component imbalance, as well as moment and force vector imbalance of the rotor as a unit. To accomplish this, balancing was performed as follows:

1. The first- and third-stage impellers were assembled on the shaft with a short spacer between them. Two turbopump bearings, axially preloaded in the bearing sleeves as in the turbopump installation, were used to support the rotor on either end. Temporary wax corrections were made in the planes of the two impeller shrouds. To ensure that the spacer between the impellers was not affecting the measured imbalance, its angular position was rotated 1.57 rad (180 degrees) relative to the other parts, and dimensional measurements were repeated and the amount of imbalance compared. No significant difference was noted.

2. The second-stage impeller was installed in place of the balance spacer and its imbalance was determined, maintaining constant the wax corrections on the first- and third-stage impellers. Wax correction was applied to the shroud of the second-stage impeller.

3. The turbine wheels were added to the rotor assembly, and their imbalance was temporarily corrected with wax. The balance assembly is shown in the Gisholt cradle in Fig. 102.

4. Repeatability checks were performed to ensure that the imbalance remained within an acceptable tolerance band on repeated disassemblies and reassemblies.

5. Final balance corrections were made by grinding material from each impeller shroud, the turbine disks, and the instrumentation nut.

The final runout measurements of the critical surfaces are noted in Fig. 103. The Gisholt balancing machine used is capable of detecting a displacement of 0.0006 mm (25 μ inches). With the weight of 3.746 kg (8.25 pounds) of the Mark 48-F rotor, this translates into a radial load of 227 N (51 pounds) at 9946 rad/s (95,000 rpm) shared by the four turbopump bearings. The foregoing corresponds to an inbalance of 0.22 g cm (0.09 g inch); the repeatability check indicated a variation in the measured inbalance of 0.127 g cm (0.05 g inch), which would result in a radial load of 125 N (28 pounds). Either inbalance level is compatible with the capability of the bearings.

Turbopump Assembly Procedure. The buildup of the turbopump was accomplished in the following sequence:

1. Parts were cleaned for LH_2 service.

2. Front and rear bearing inner-race spacer thicknesses were established to provide the proper bearing preloads.

3. The thickness of the turbine wheel spacer was established to provide the proper nozzle-to-rotor axial clearance.

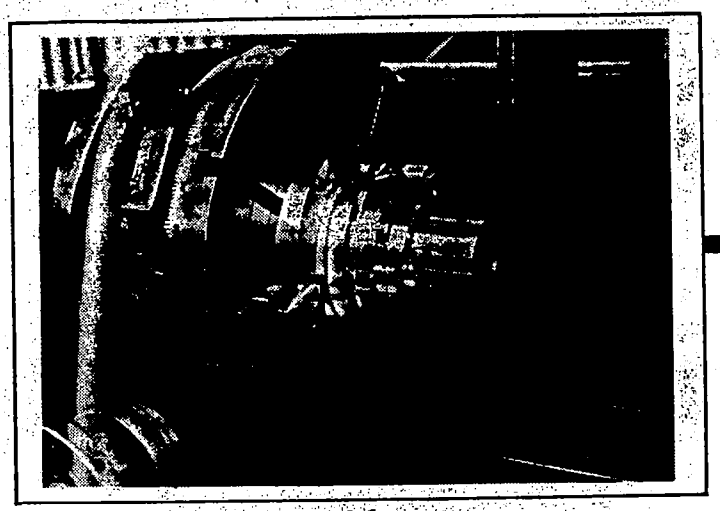

1

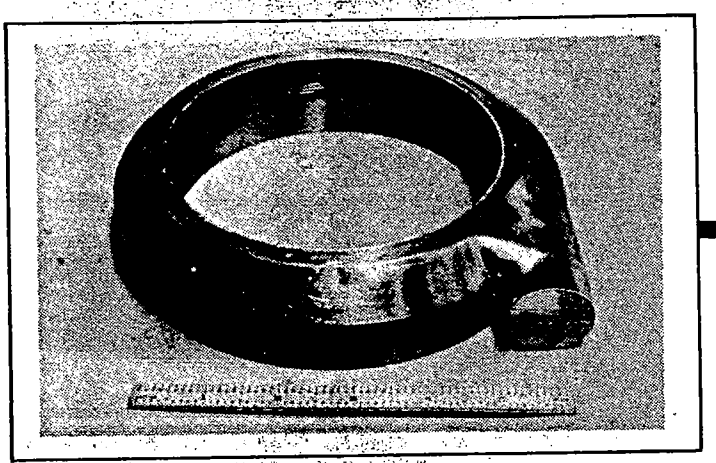

2

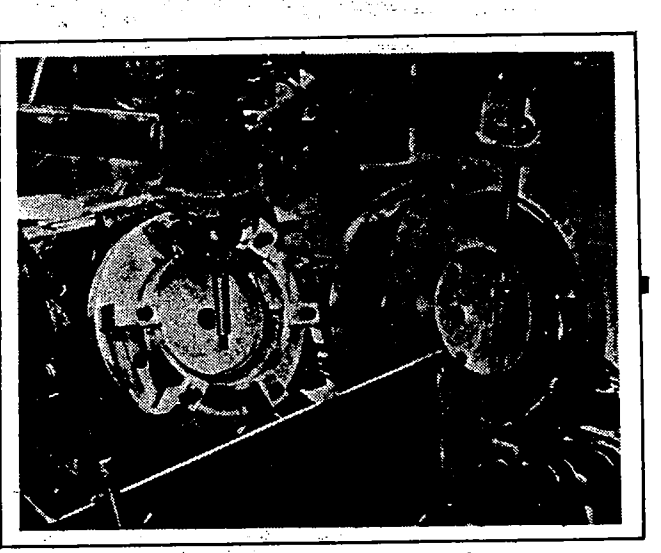

3

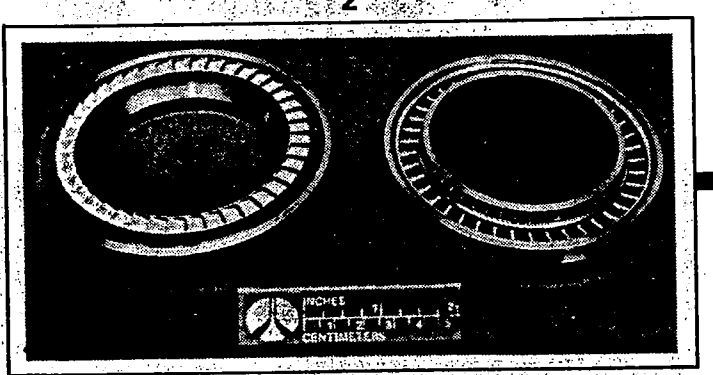

I

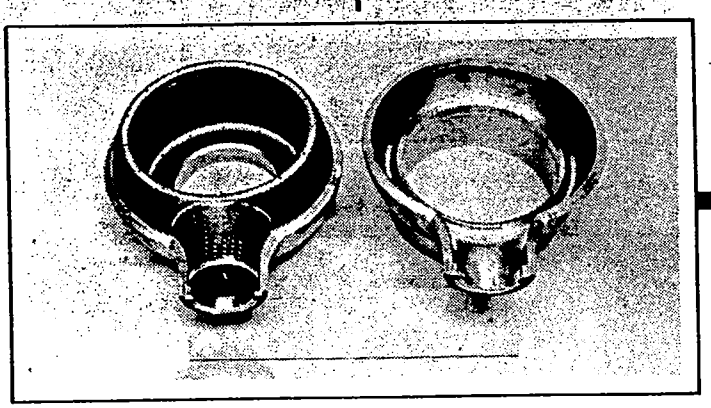

II

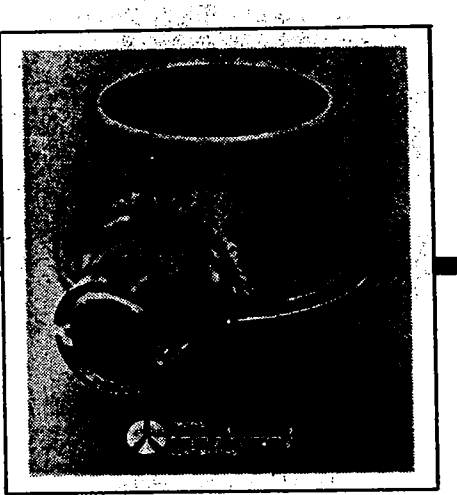

III

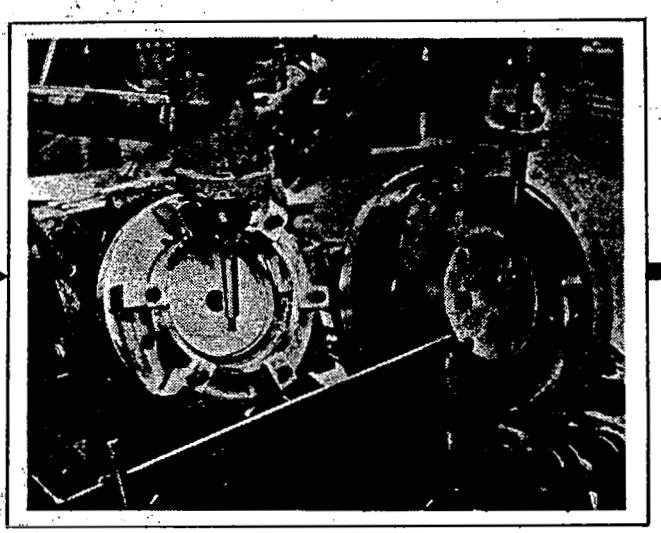

3

4

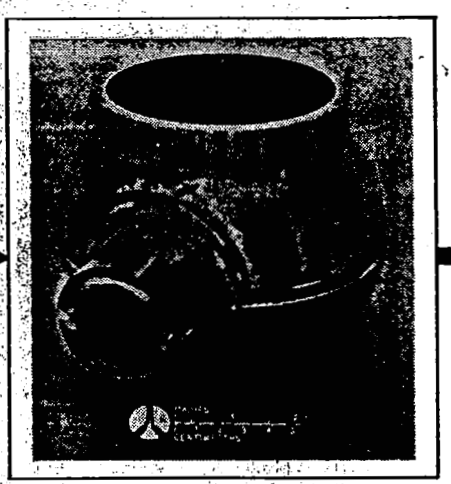

III

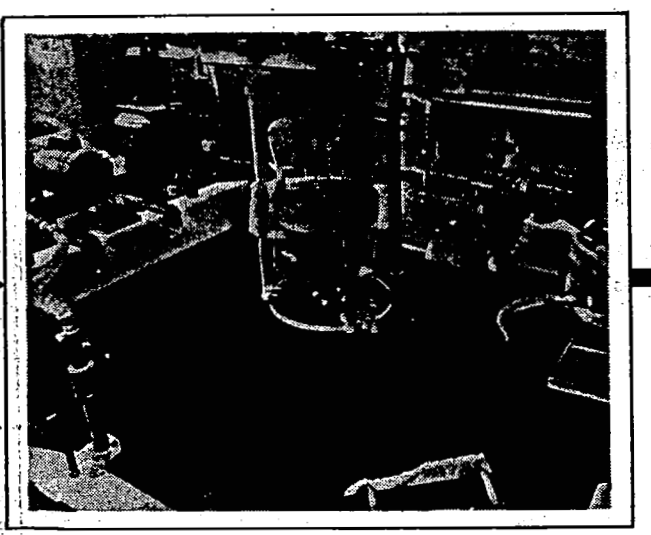

IV

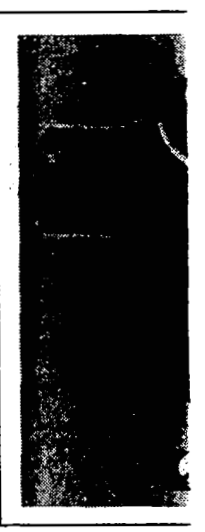

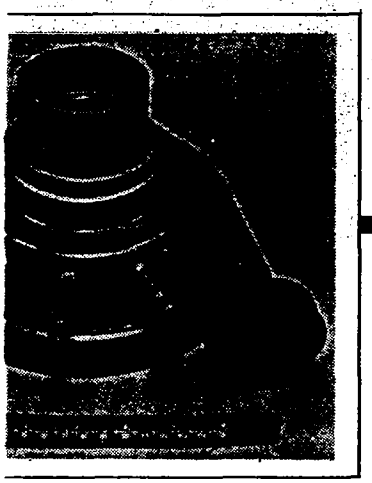

5

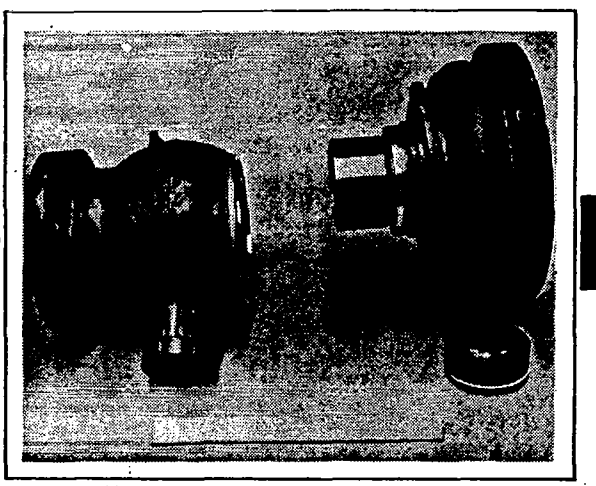

6

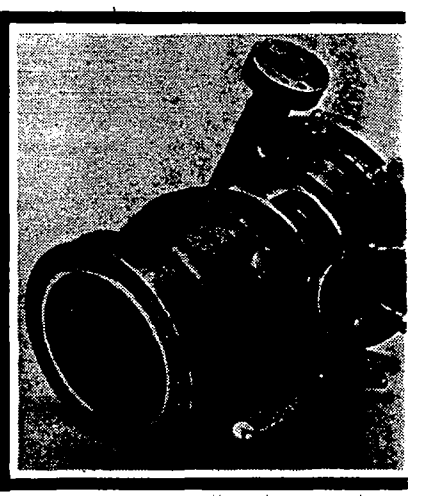

7

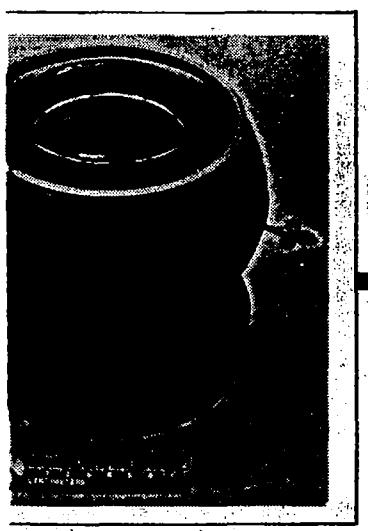

V

Figure 101. Mark 48-F Housing Fabrication Process

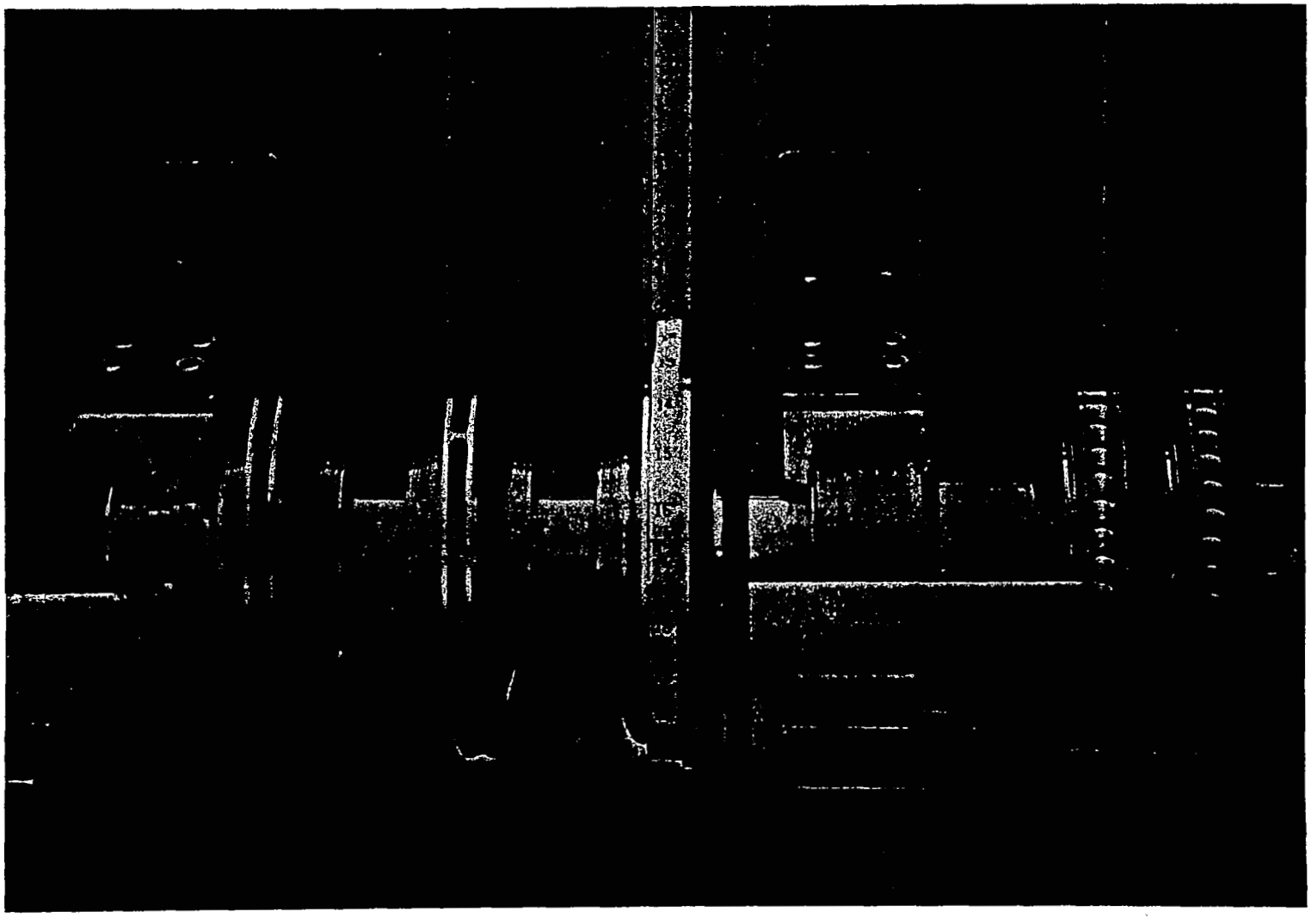

1HS52-12/8/75-C1B

Figure 102. Mark 48-F Balancing Setup

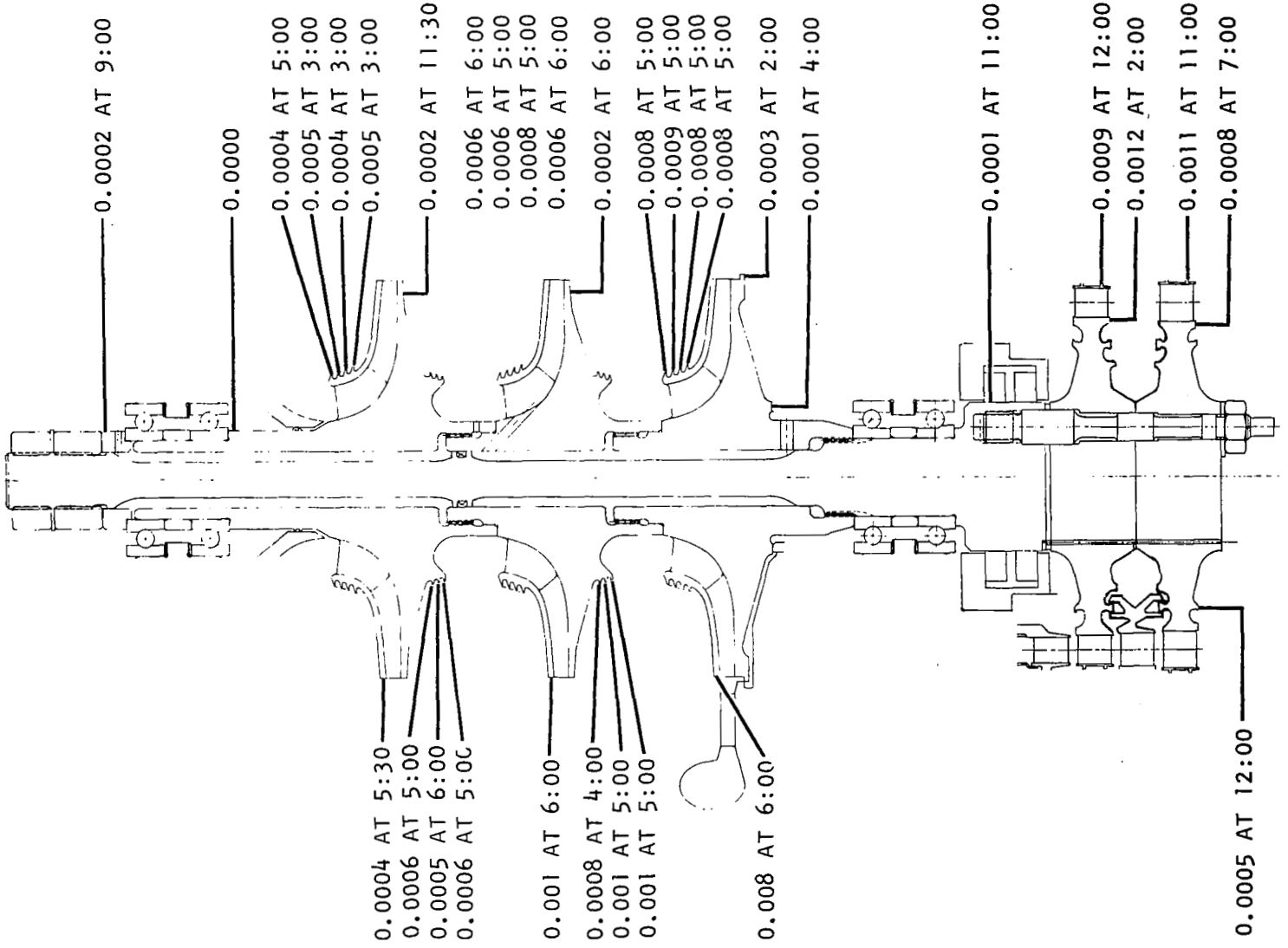

Figure 103. Mark 48-F Balance Assembly Radial Runouts (TIR, inch)

4. The thickness of the balance piston low-pressure orifice ring was established to obtain the desired balance piston travel.
5. Dimensions were taken to establish the axial position of the impellers when bottomed on the adjacent parts to permit calculation of minimum clearances later in the build.
6. Bearing, shaft seal, and impeller radial clearances were measured.
7. The rotor assembly was balanced.
8. The balance piston low-pressure orifice ring was installed.
9. The rear bearing cartridge front and rear shim thicknesses were established by performing a rotor push-pull test with a partially assembled turbopump at ambient temperature.
10. A "cold" check was performed at LN_2 temperature to determine and adjust the bearing load at zero piston low-pressure orifice clearance.
11. The partial assembly used for rotor push-pull tests was disassembled, leaving in the housing the balance piston low-pressure seal, shaft, rear bearing package, shaft seal, and the third-stage impeller.
12. Successively, the second-stage crossover, second-stage impeller, first-stage crossover, first-stage impeller, and the inlet housing were assembled, measuring for each stage the minimum axial clearances.
13. The front bearing package was added and the shaft was preloaded by stretching on an Instron tensile tester to 54,700 N (12,300 pound) load, torquing the retaining nut while the shaft was under tensile load. A total stretch of 0.686 mm (0.027 inch) was obtained on the shaft in this manner.
14. The bearing preloads were verified at ambient and LN_2 temperatures.
15. The turbine was assembled by installing the wheel spacer, retaining studs, first-stage wheel, second-stage nozzle, second-stage wheel, retaining nuts, and wheel cover. Axial minimum and blade-to-blade clearances were established at each step.
16. On the pump inlet end, the instrumentation nut and front cover were installed and the speed pickup, temperature transducers, and Bently proximity transducers were added.
17. Electrical checks were performed, and the pump was leak-checked with gaseous helium (GHe) at 21 N/cm^2 (30 psig).

The clearances measured relative to the front bearing and instrumentation probes are shown in Fig. 104. Figure 105 shows the impeller labyrinth radial clearances. In Fig. 106, the clearances relating to the rear bearings and shaft seal are presented. The axial clearances between turbine components are noted in Fig. 107. The radial clearances in the turbine, as established during the calibration build, are included in Fig. 108.

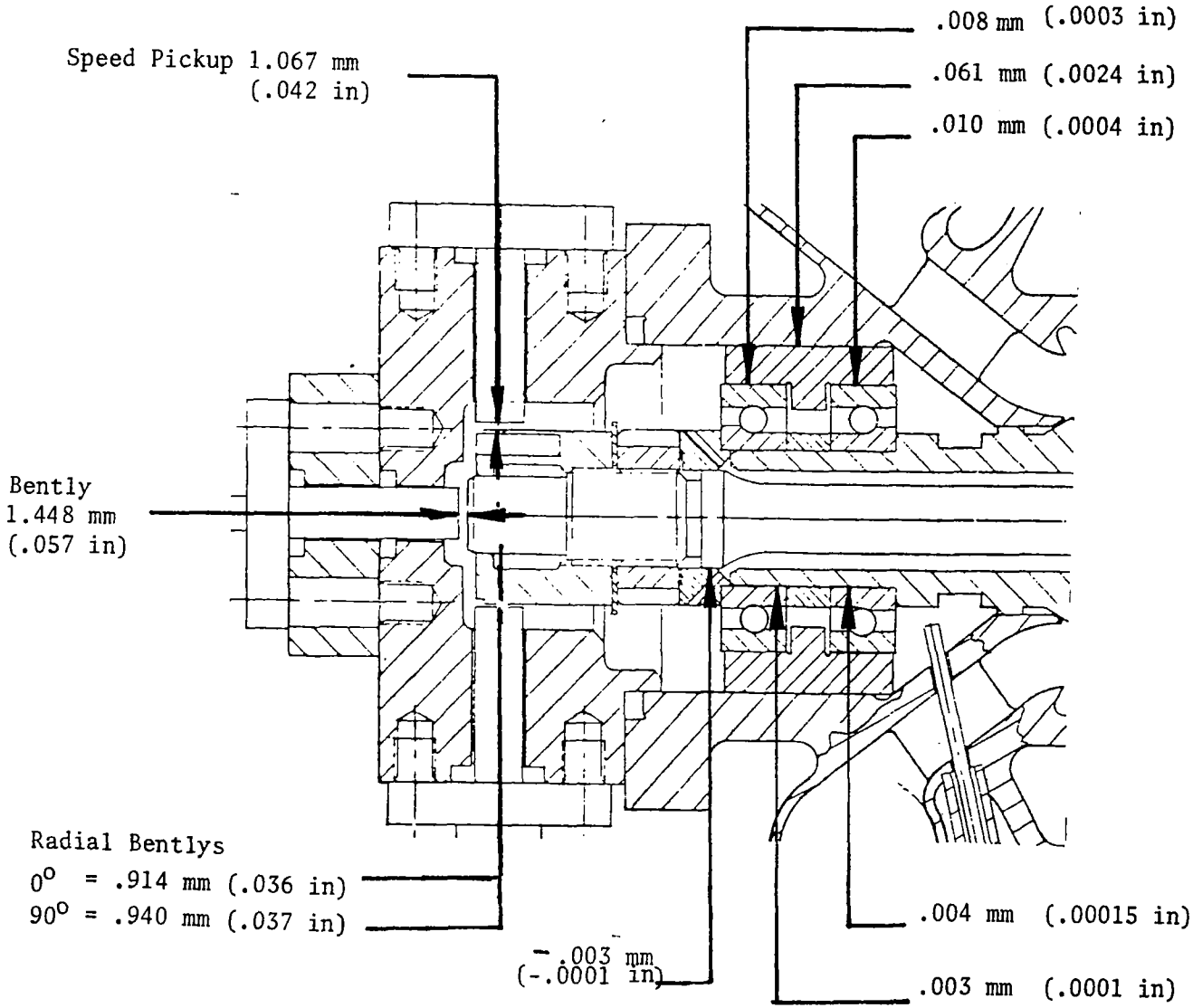

Figure 104. Mark 48-F S/N 01-0 Assembly Instrumentation and Front Bearing Clearances

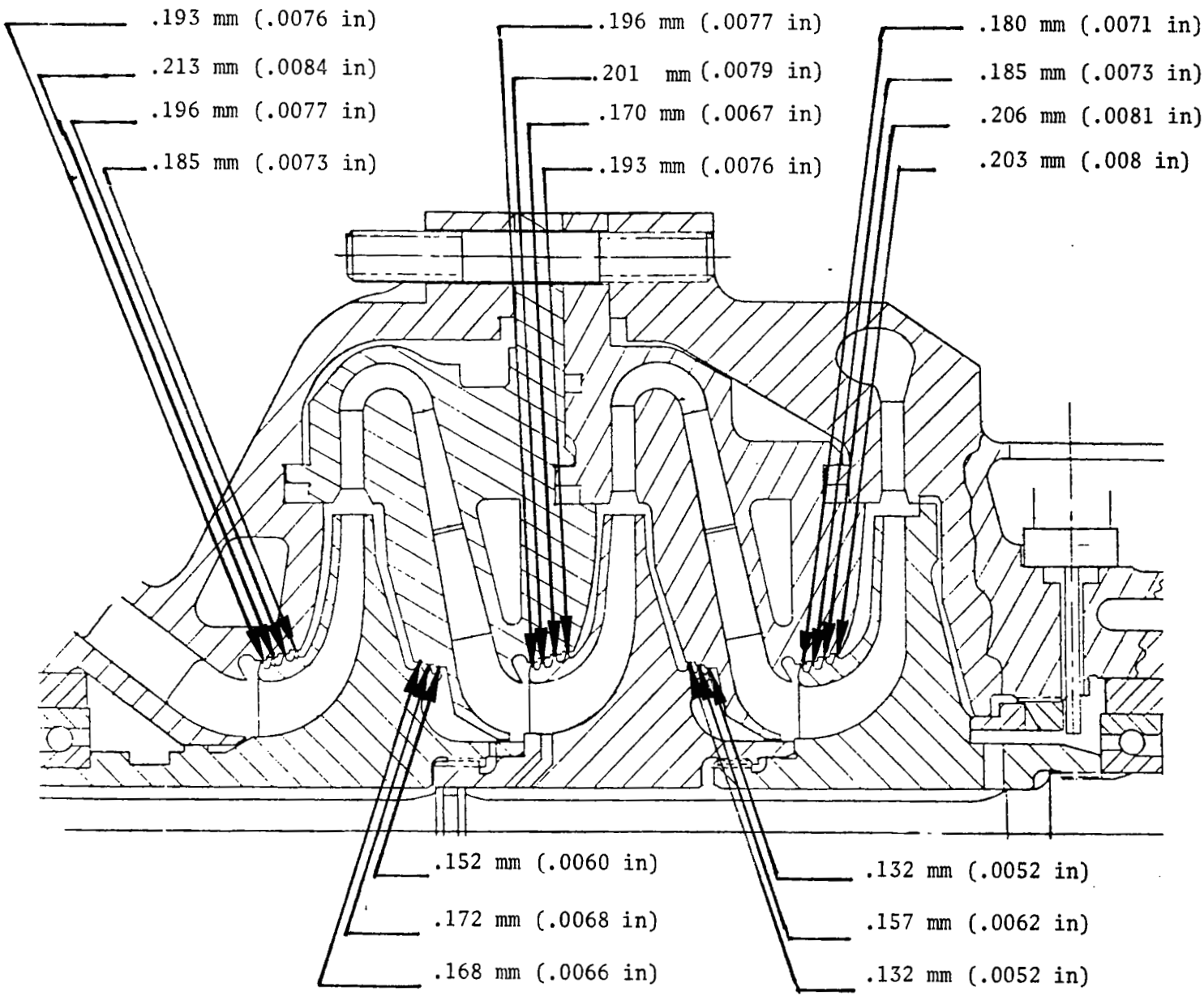

Figure 105. Mark 48-F S/N 01-0 Assembly Impeller Labyrinth Clearances

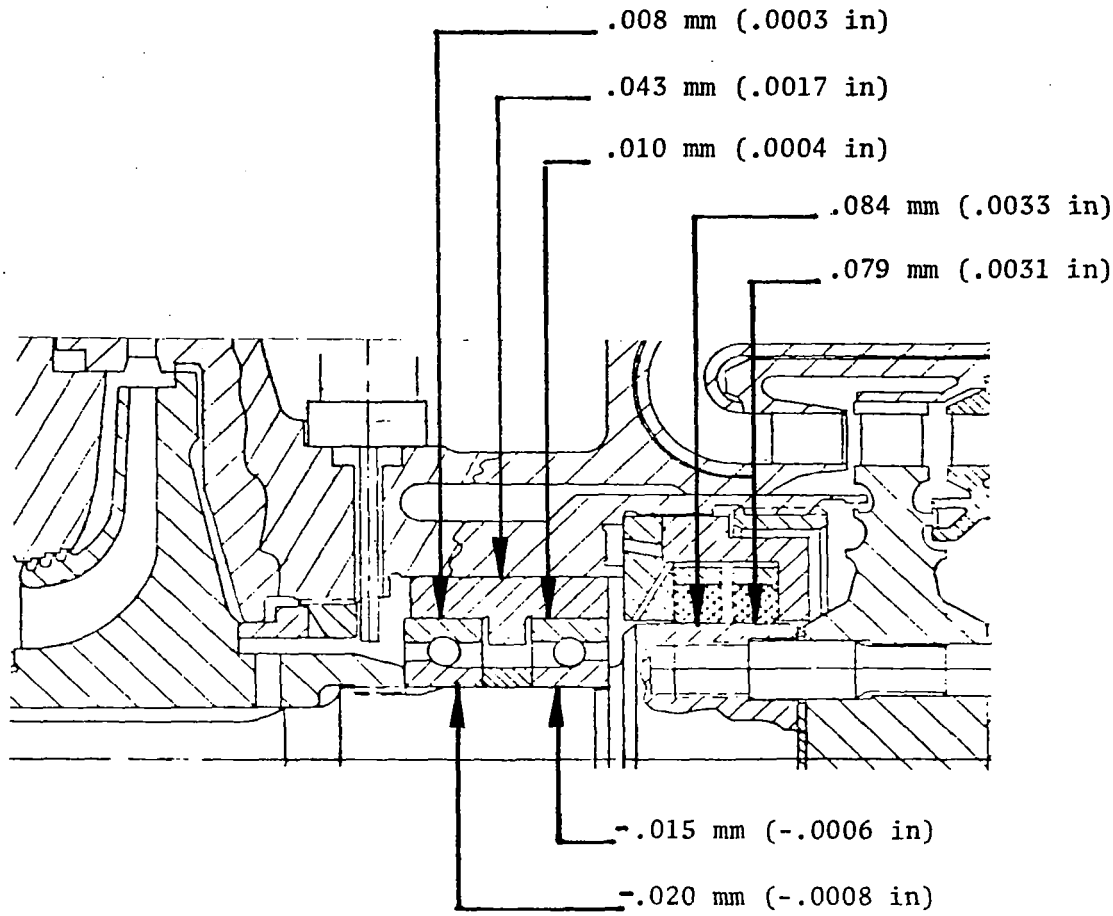

Figure 106. Mark 48-F Turbine S/N 01-0 Axial Clearances

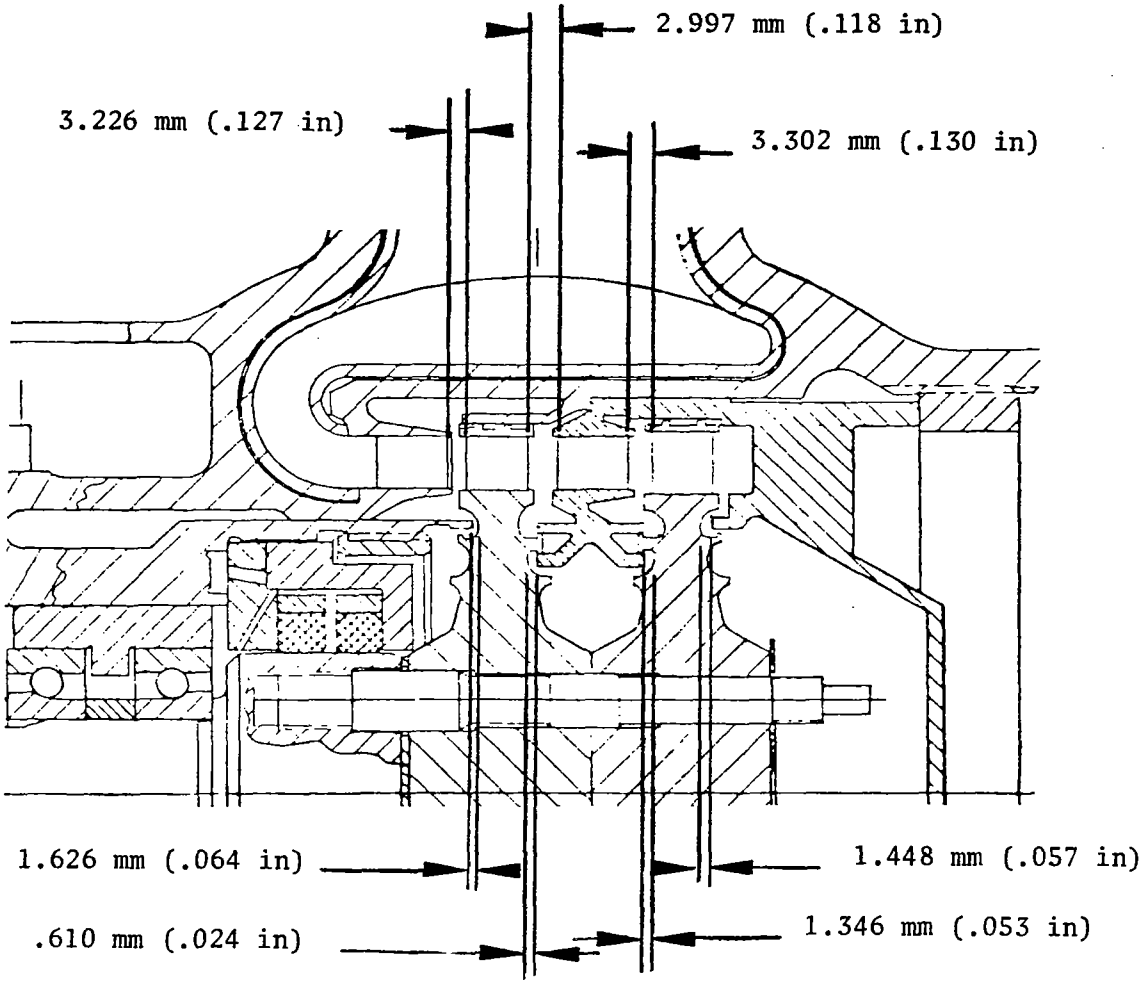

Figure 107. Mark 48-F Turbine S/N 01-0 Axial Clearances

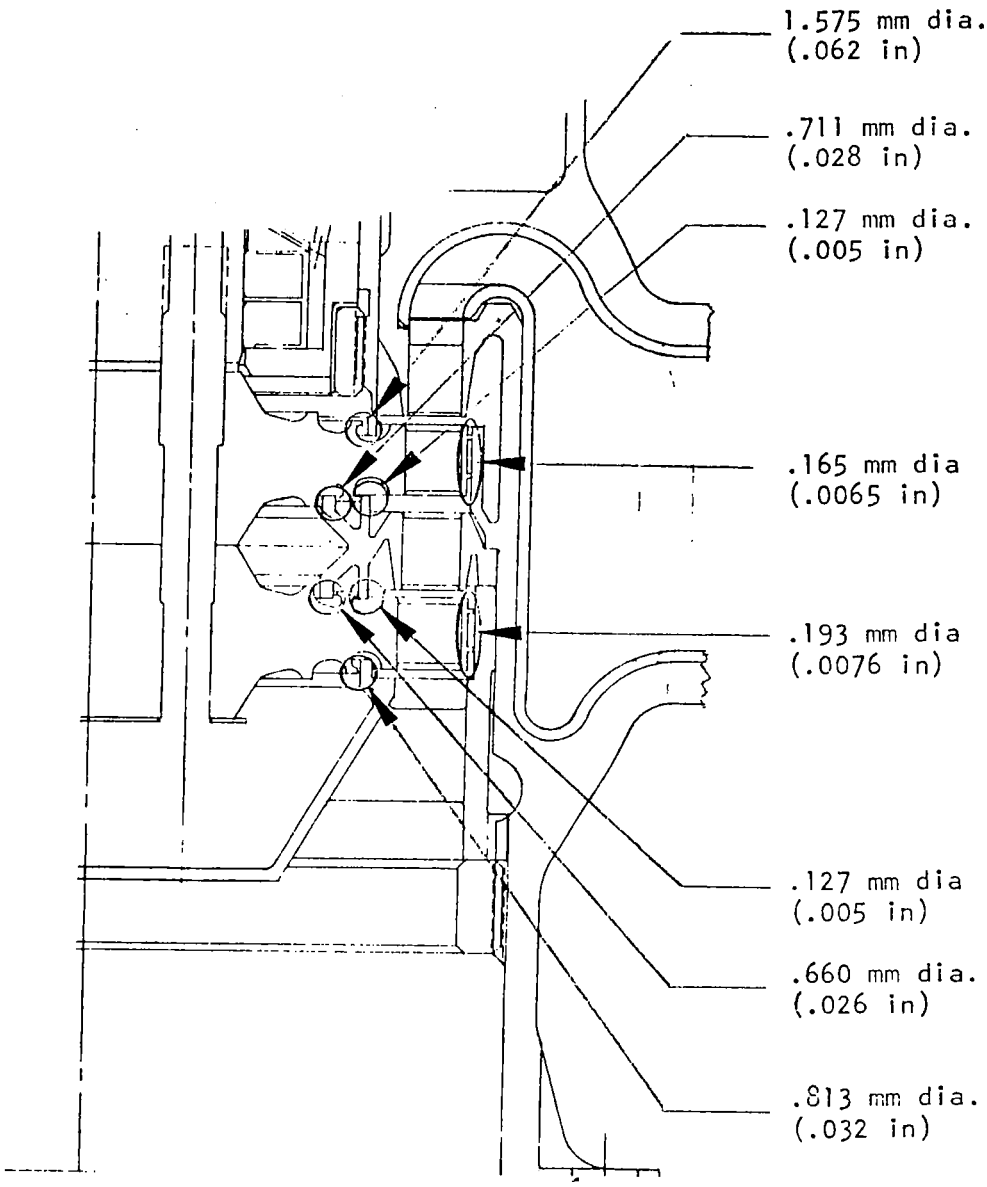

Figure 108. Mark 48-F Turbine S/N 01-0 Radial Clearances

Each of the two pairs of bearings is preloaded internally by two Belville springs located at the outer races. A minimum axial load of 431 N (97 pounds) is required to prevent the balls from skidding on the races at the design speed of 9946 rad/s (95,000 rpm). The actual preload on the bearings is measured by building a preliminary assembly consisting of the two bearings, the bearing cartridge, two Belville springs and the inner race spacer. With the inner race stack clamped axially tight with a tool, the axial motion of the outer races as a function of applied load is measured. The inner race spacer thickness is adjusted until the required preload is obtained. The actual load curve, obtained for the pump and turbine end bearings is shown in Fig. 109 and 110, respectively.

The pump end bearing cartridge is free to move inside the inlet housing bore; therefore, the spring preloads are the only axial loads experienced by those bearings. In contrast, the turbine end bearing cartridge is restrained axially so that those bearings will restrain the rotor position within certain limits. The planned rotor position/axial load relationship is illustrated in Fig.111. The objective is to have the bearings absorb 1793 N (403 pounds) of rotor axial load toward the turbine side at the point where the balance piston low-pressure orifices faces come in contact, and similarly absorb 1779 N (400 pounds) of load toward the direction of the pump when the balance piston high-pressure orifices are axially aligned. This will hold the rotor in the desired position statically and during the low-speed transient phase.

To obtain the actual bearing loads versus rotor axial position characteristics, a push-pull test is made, in which axial load is applied to the rotor through a force gage, and rotor motion is monitored with dial gages. The setup is illustrated in Fig. 112. Adjustments are made in the thickness of the shims located on either end of the bearing cartridge until the desired load-travel relationship is obtained. The results of the push-pull tests obtained at ambient temperature are shown in Fig. 113. The test is repeated with the pump chilled with LN_2 to simulate cryogenic conditions. The results obtained on the cold push-pull test are presented in Fig. 114.

The LN_2 load check was performed only toward the low-pressure side because, at zero speed and pressure, a forward load of 1780 N (400 pounds) is achieved at a negative high-pressure orifice axial clearance. This, combined with the fact that at cryogenic temperatures there is a radial overlap of the orifices, could damage the orifices if a significant load toward the pump side were imposed.

Turbopump Weights

During assembly, the principal components of the turbopump as well as the completed unit was weighed. A breakdown of the measured weights is included in Table 15.

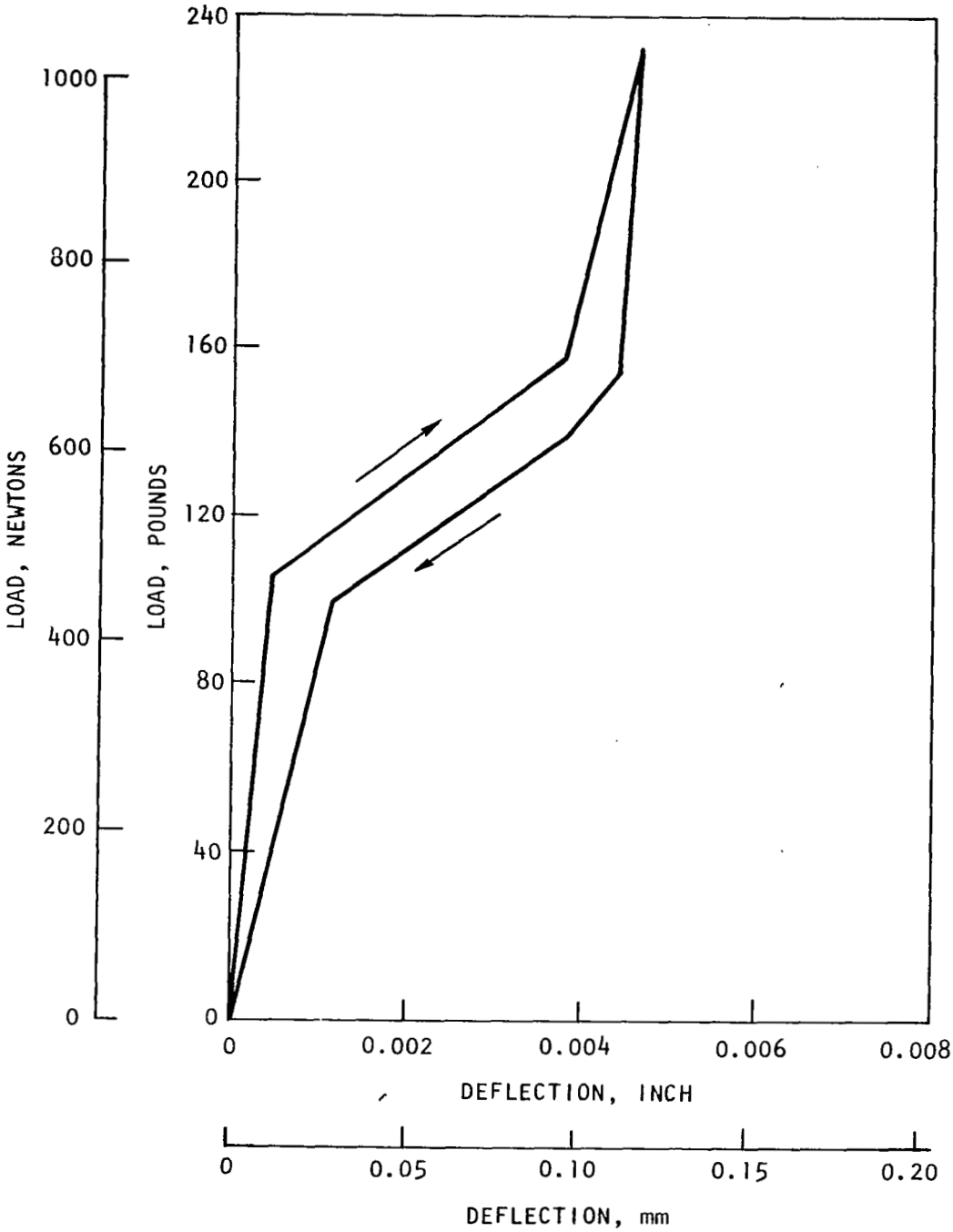

Figure 109. Mark 48-F Front Bearing Preload

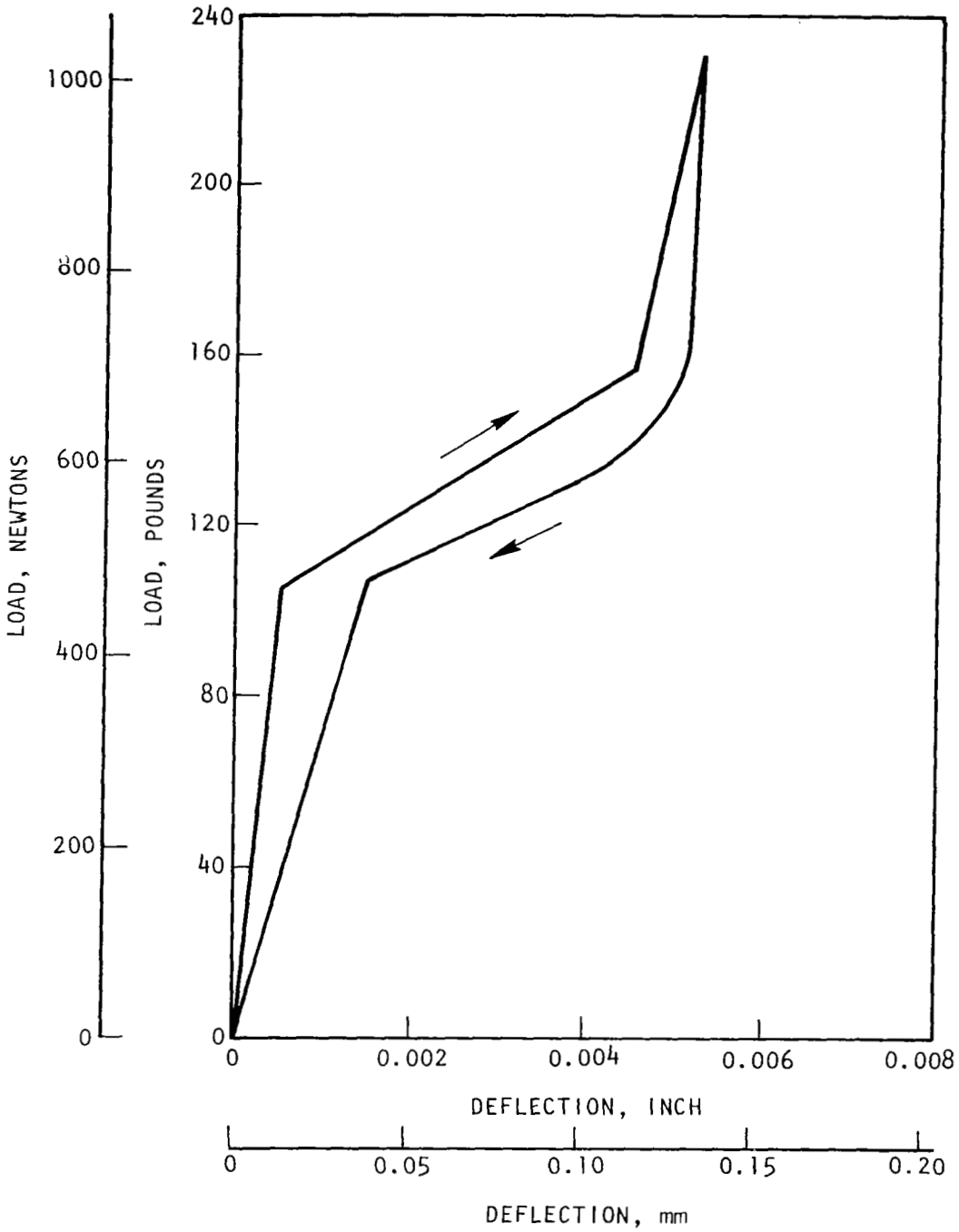

Figure 110. Mark 48-F Rear Bearing Preload

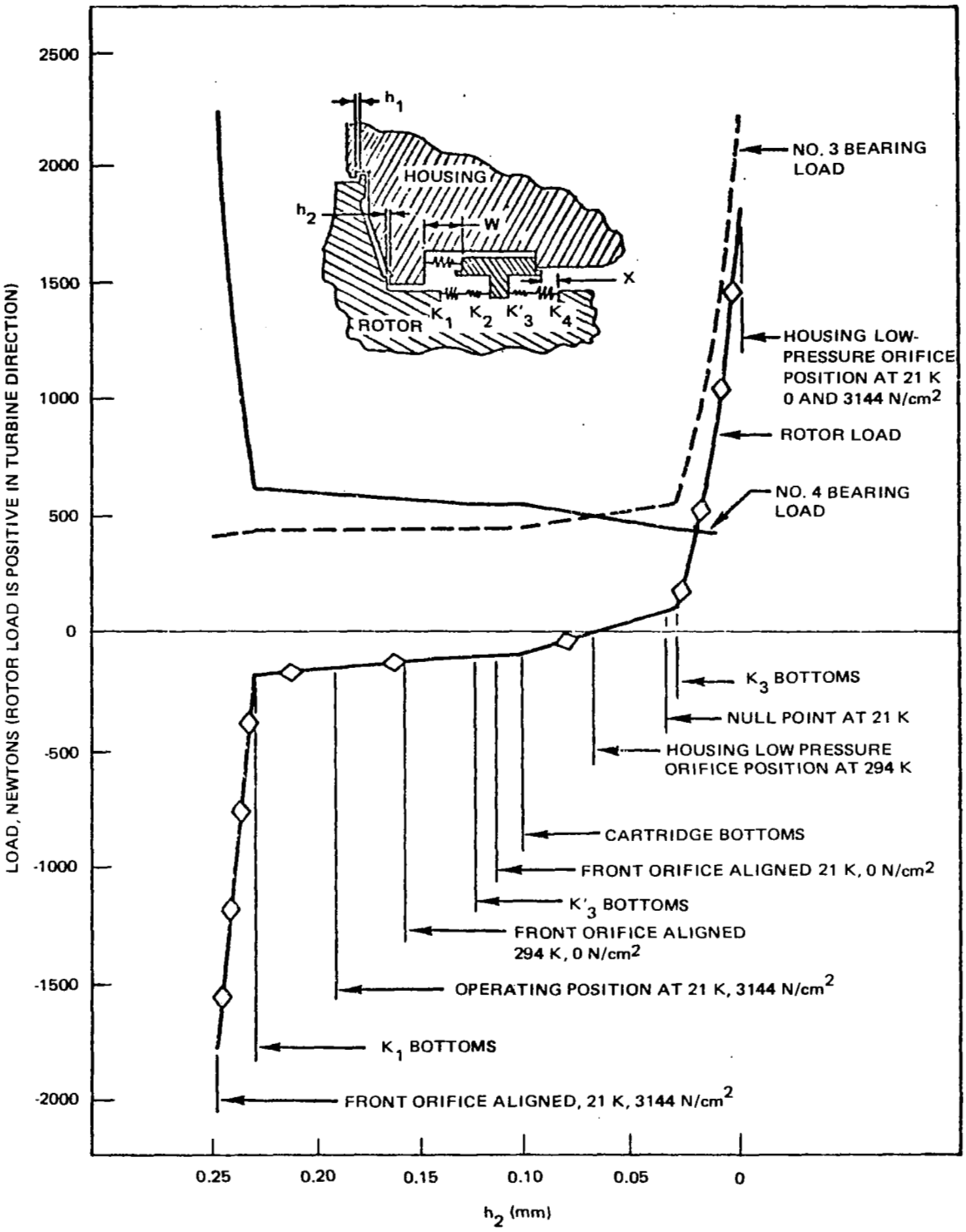

Figure 111. Mark 48-F Turbopump Bearing Loads vs Piston Position (SI Units)

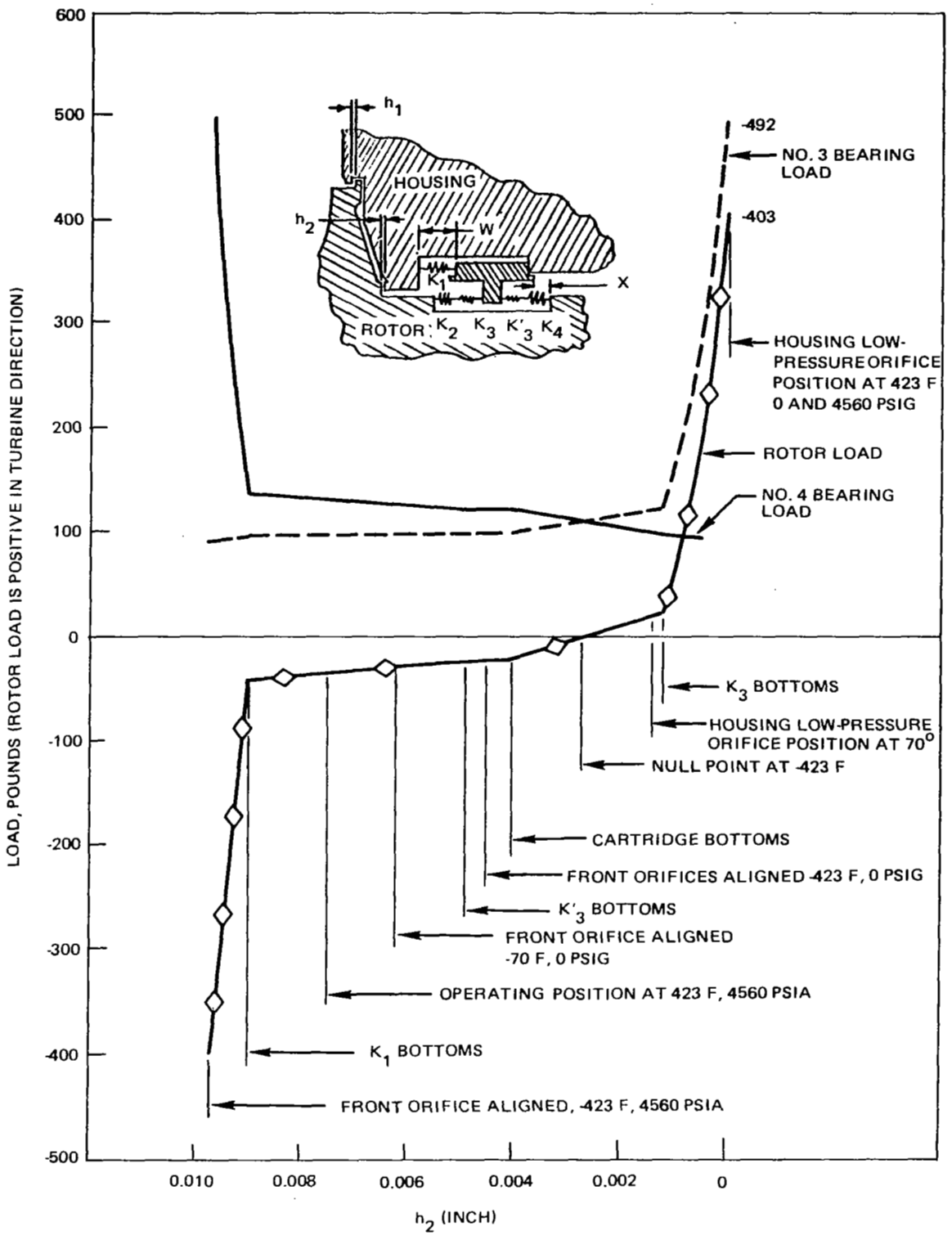

Figure 111. Mark 48-F Turbopump Bearing Loads vs Piston Position (English Units

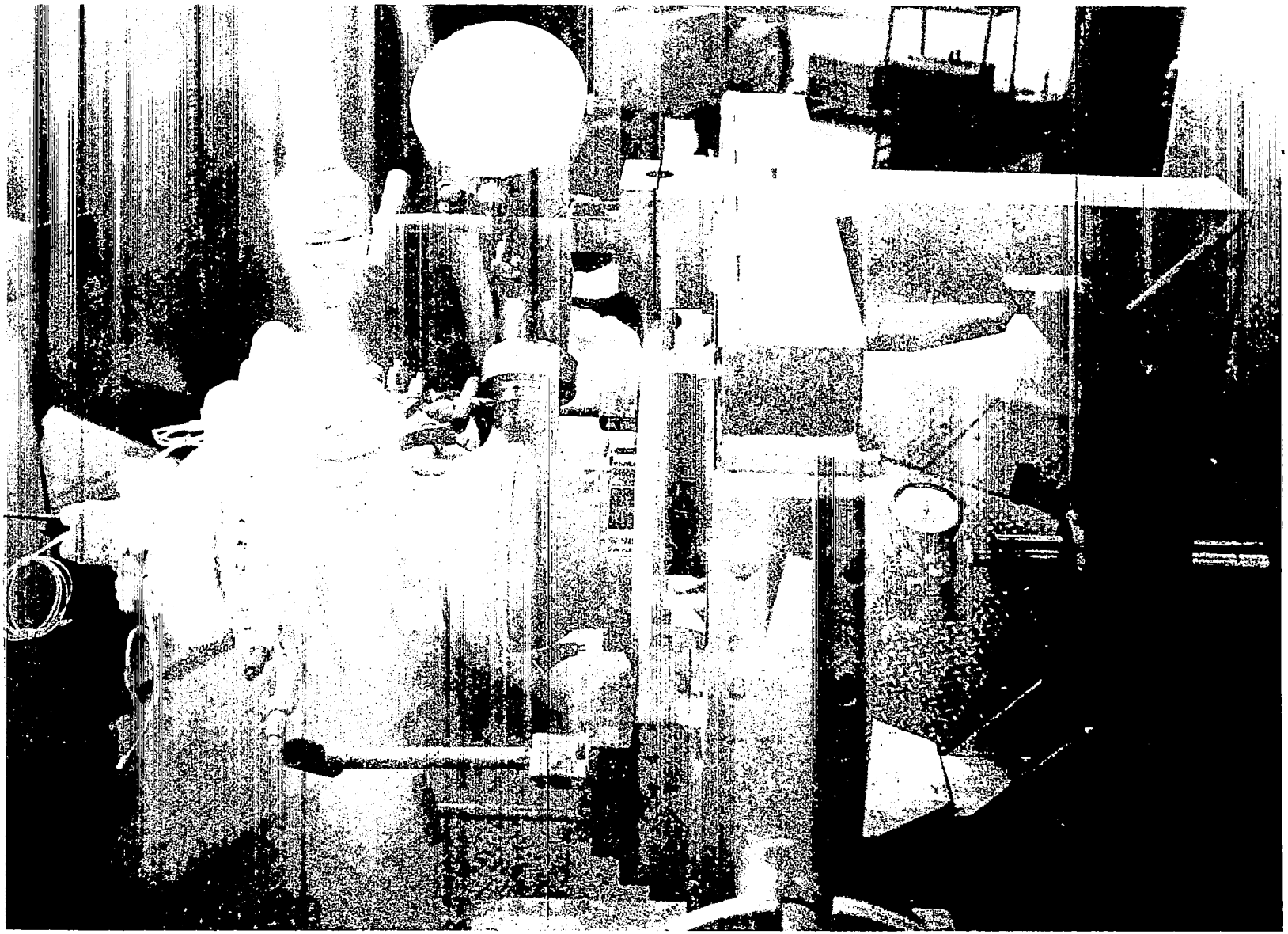

1HS54-2/19/76-C2*

Figure 112. Mark 48-F Turbopump Assembly Push/Pull Setup

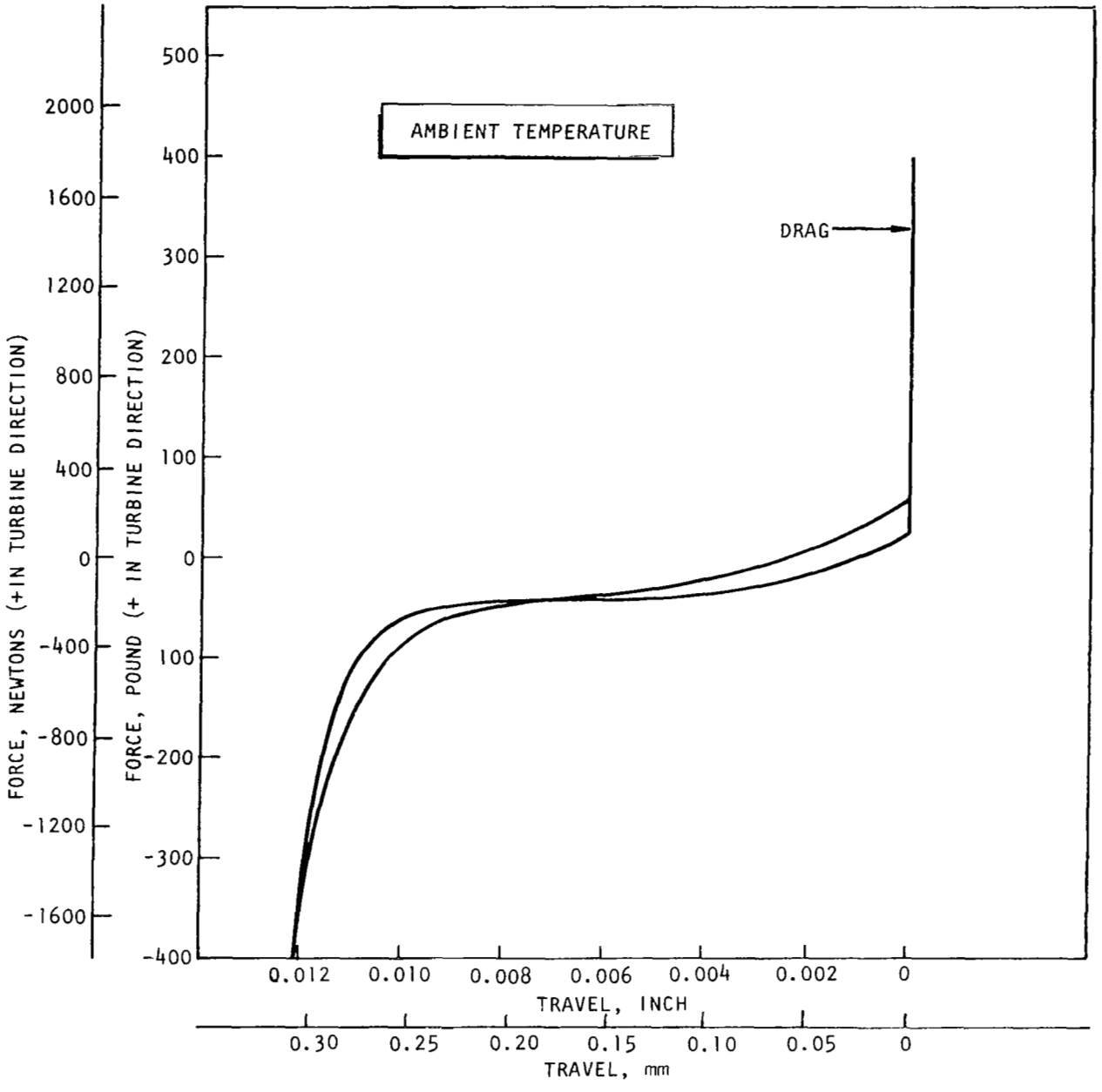

Figure 113. Mark 48-F Bearing Preload, Ambient Temperature

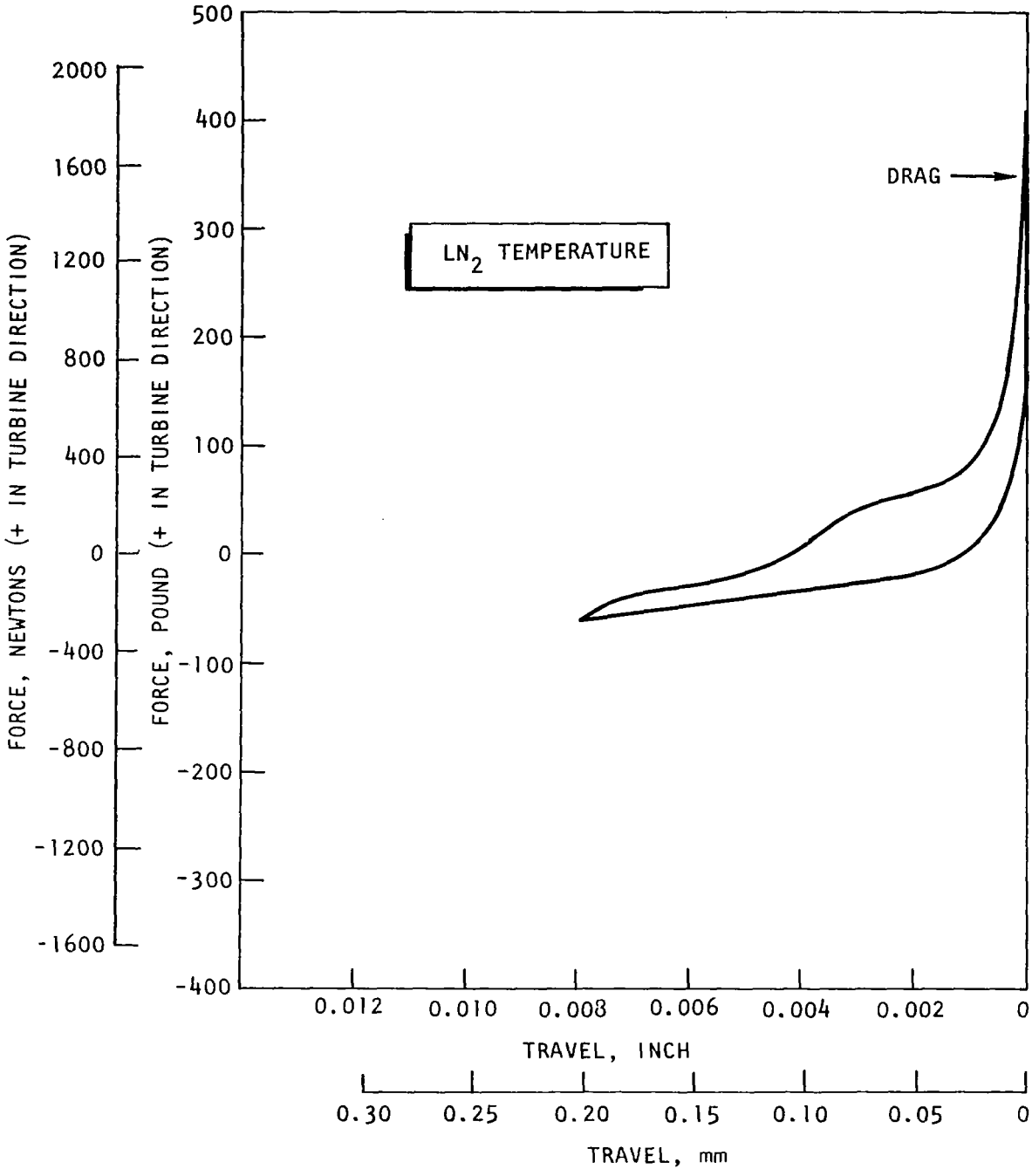

Figure 114. Mark 48-F Bearing Preload, LN_2 Temperature

TABLE 15. MARK 48-F TURBOPUMP WEIGHTS

	Weight	
	kg	pounds
Pump Inlet	5.0	11.0
Housing (including GG)	22.7	50.0
First-Stage Crossover	4.5	10.0
Second-Stage Crossover	4.0	9.0
Turbine Second-Stage Nozzle	0.2	0.5
Turbine First-Stage Wheel	0.54	1.2
Turbine Second-Stage Wheel	0.54	1.2
Shaft	0.45	1.0
First-Stage Impeller	0.45	1.0
Second-Stage Impeller	0.4	0.9
Third-Stage Impeller	0.4	0.9
Miscellaneous	4.42	9.3
Total Weight	43.6	96.0
Rotor Weight	3.7	8.25

TESTING

Gas Generator Testing

To operationally characterize the LH_2 Mark 48-F turbopump assembly prior to actual engine testing, a gas generator assembly (P/N RS005024) was developed and hot-fire tested. The gas generator assembly was tested in the Propulsion Research Area (PRA) at Rocketdyne's Santa Susana Field Laboratory (SSFL). The 3447 N/cm^2 (5000-psi) propellant tank ratings provided sufficient operating margin for the required gas generator rated chamber pressure of 2344 N/cm^2 (3400 psia). Figures 115 and 116 show the gas generator installation in the Lima stand of PRA.

The LH_2 turbopump gas generator test program was concluded successfully after a total of 15 hot-fire tests. Nine of these tests were conducted on injector unit No. 2, while the remaining tests were conducted on injector unit No. 3. Tables 16A and 16B are performance summaries of those tests conducted during the development hot-fire program.

Three anomalies were uncovered during the testing effort: (1) igniter ceramic cracking, (2) failure to achieve ignition on several tests and, (3) hot streaks and a moderate amount of erosion at the combustor body internal wall. The igniter ceramic cracking problem was resolved by reducing the chamber pressure buildup rate by slowing down the opening rate of the main LO_2 valve.

In the case of the failure of the igniter to achieve ignition, the cause has been attributed to the lack of a spark at designed air gap location (electrode/ igniter adapter manifold). Actual spark current flow was recorded for these tests (016-022, -023, and -024), but the preferential current path was determined to be across the spark plug ceramic to spark plug outer shell, an area shielded by the boron nitride cap. Any oxygen gas ionized by the spark in this location would have little chance to reach the igniter injection area due to the torturous path length. The boron nitride cap was removed prior to test 016-025, but the forward end piece of boron nitride was retained in the assembly. Each subsequent test achieved ignition without incident.

Five hot streaks were observed in the combustor during the testing of the two LH_2 turbopump gas generator injectors. In the case of injector unit No. 2, the hot streaks appeared only as surface discolorations after the 7.3-second mainstage test, and no erosion was noted. In the case of injector unit No. 3, one hot streak (downstream of injector element 1-5) progressed to a moderate amount of combustor wall erosion during a 24-second mainstage test (016-029). The erosion is shown in photographs of Fig. 117 through 119.

Also during the testing effort, an associated problem was identified in that a large temperature gradient was observed at the exit of the combustor. The gradient 244 K (440 R) from the wall to the center of the exit elbow was recorded on an eight-thermocouple temperature rake as shown in Fig. 120. The gradient versus distance from the wall is shown in Fig. 121. Also, as shown, the hot core is well centered within the flowstream, indicating that the smooth

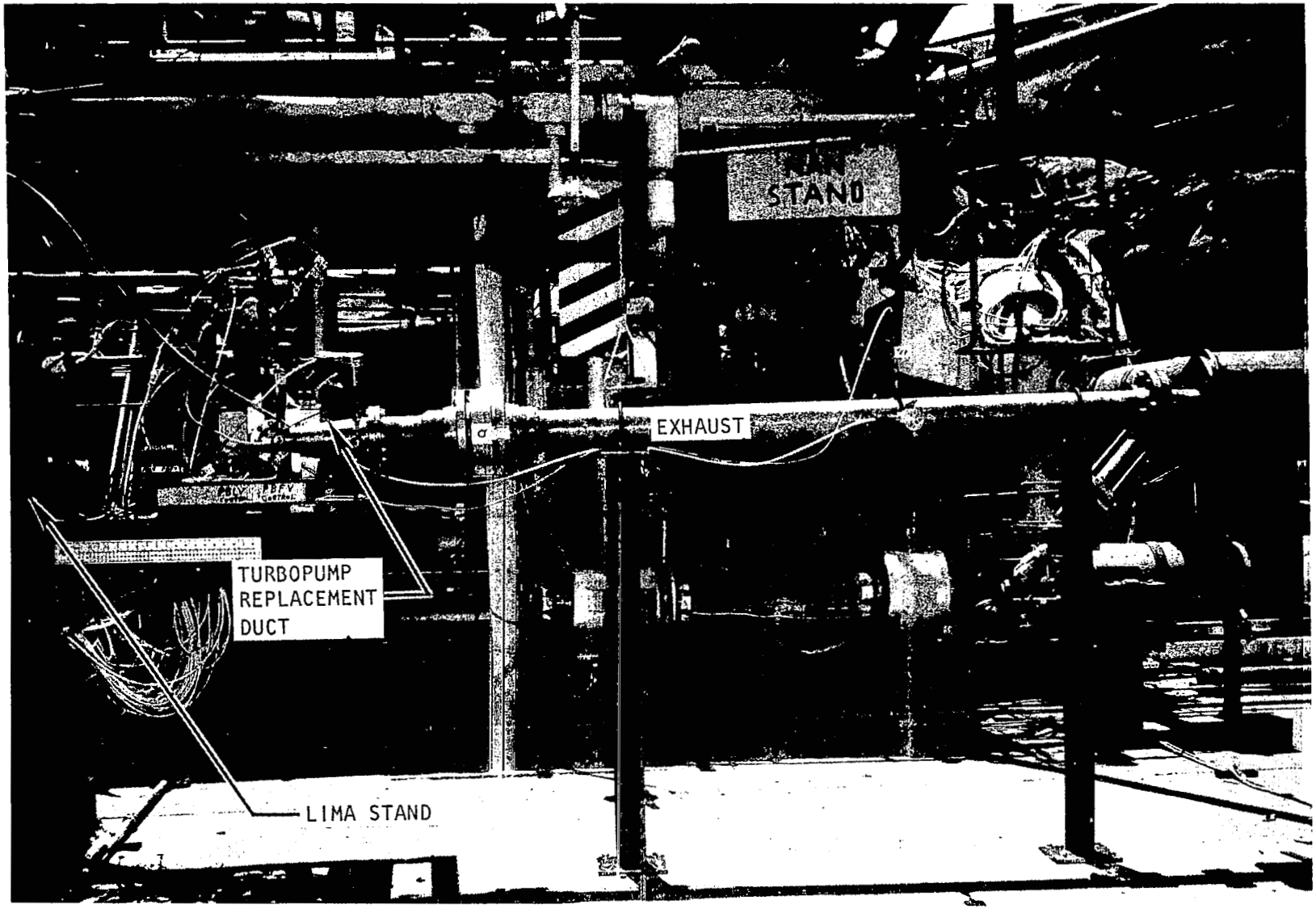

1SM63-7/24/75-S1A

Figure 115. Gas Generator Installation

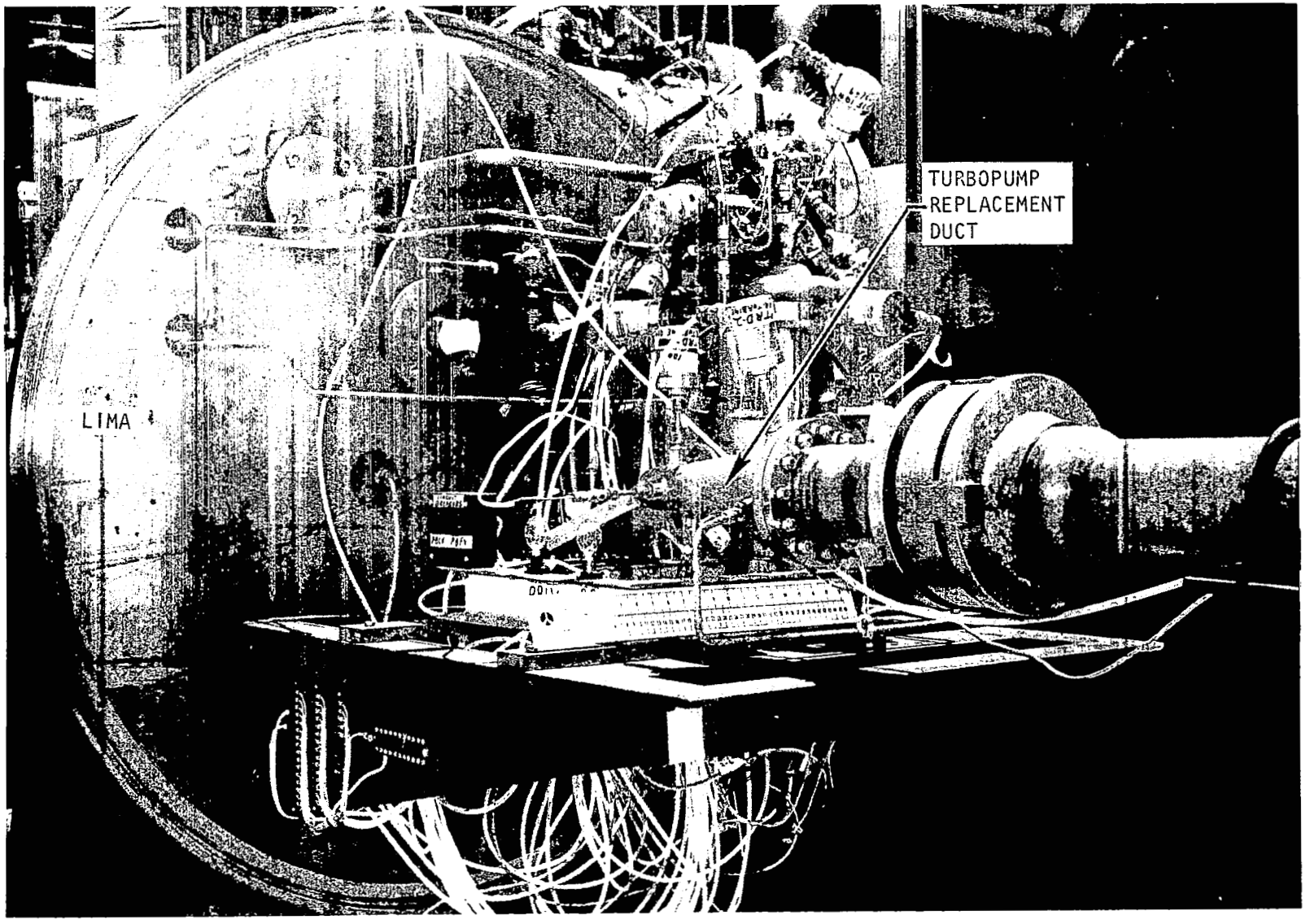

1SM63-7/24/75-S1B

Figure 116. Gas Generator Installation

TABLE 16A. LH_2 TURBOPUMP GAS GENERATOR TEST SUMMARY (SI UNITS)

Test No.	Test Date 1975	Test Type	Duration sec*	P_c N/cm^2	Combustion Temperature, K	Oxidizer Flowrate, kg/s	Fuel Flowrate, kg/s	MR	Oxidizer Ignition Flow, kg/s	Fuel Ignition Flow, kg/s	Ignition MR
016-018	8/5	Ignition	2.0	96.5	708	-	-	-	0.0224	0.0252	0.89
016-019	8/15	Ignition	2.0	100	766	-	-	-	0.0229	0.0245	0.93
016-020	8/20	Mainstage	1.5	2176	634				0.0184	0.0215	0.86
016-021	8/20	Mainstage	5.0	2196	729				0.0179	0.0213	0.84
016-022	8/25	No Ignition									
016-023	8/25	No Ignition									
016-024	8/26	No Ignition									
016-025	8/26	Mainstage	1.2	2125	498				0.0181	0.0236	0.77
016-026	8/26	Mainstage	7.3	2267	939				0.0131	0.0210	0.62
**016-027	8/26	Mainstage	2.2	2267	746				0.0175	0.0234	0.75
**016-028	8/26	Mainstage	3.5	2218	701				0.0176	0.0225	0.78
**016-029	8/26	Mainstage	24.0	2191	898				0.0191	0.0225	0.85
**016-045	11/18	Mainstage	10.0	2375	821				0.0167	0.0195	0.85
**016-046	11/18	Mainstage	22.0	2370	883				0.0173	0.0200	0.87
**016-047	11/26	Mainstage	20.0	2374	988				0.0172	0.0212	0.81

*Mainstage duration determined from main propellant ignition to cutoff

**LH_2 turbopump injector unit No. 3

NOTE: Tests 016-045, 046, and 047 were conducted with the 90-degree miter bend combustor configuration.

TABLE 16B. LH_2 TURBOPUMP GAS GENERATOR TEST SUMMARY (ENGLISH UNITS)

Test No.	Test Date 1975	Test Type	Duration sec*	P_c, psia	Combustion Temperature, R	Oxidizer Flowrate, lb/sec	Fuel Flowrate, lb/sec	MR	Oxidizer Ignition Flow lb/sec	Fuel Ignition Flow lb/sec	Ignition MR
016-018	8/5	Ignition	2.0	140	1274	-	-	-	0.0494	0.0556	0.89
016-019	8/15	Ignition	2.0	145	1379	-	-	-	0.0505	0.541	0.93
016-020	8/20	Mainstage	1.5	3157	1141	2.543	4.199	0.61	0.0405	0.0473	0.86
016-021	8/20	Mainstage	5.0	3185	1312	2.747	3.814	0.72	0.0394	0.0469	0.84
016-022	8/25	No Ignition									
016-023	8/25	No Ignition									
016-024	8/26	No Ignition									
016-025	8/26	Mainstage	1.2	3083	897	1.726	4.445	0.61	0.0399	0.0521	0.77
016-026	8/26	Mainstage	7.3	3289	1691	2.071	3.267	0.94	0.0289	0.0464	0.62
**016-027	8/26	Mainstage	2.2	3289	1343	3.121	4.094	0.76	0.0385	0.0516	0.75
**016-028	8/26	Mainstage	3.5	3218	1262	3.023	4.176	0.72	0.0388	0.0496	0.78
**016-029	8/26	Mainstage	24.0	3178	1617	3.052	3.286	0.93	0.0422	0.0497	0.85
**016-045	11/18	Mainstage	10.0	3445	1477	3.051	3.791	0.806	0.0368	0.0430	0.85
**016-046	11/18	Mainstage	22.0	3438	1590	3.123	3.553	0.879	0.0382	0.0441	0.87
**016-047	11/26	Mainstage	20.0	3444	1778	3.187	3.273	0.972	0.0380	0.0468	0.81

*Mainstage duration determined from main propellant ignition to cutoff
**LH_2 turbopump injector unit No. 3
NOTE: Tests 016-045, 046, and 047 were conducted with the 90-degree miter bend combustor configuration

1HS35-9/9/75-C1B*

Figure 117. Combustor Internal Erosion

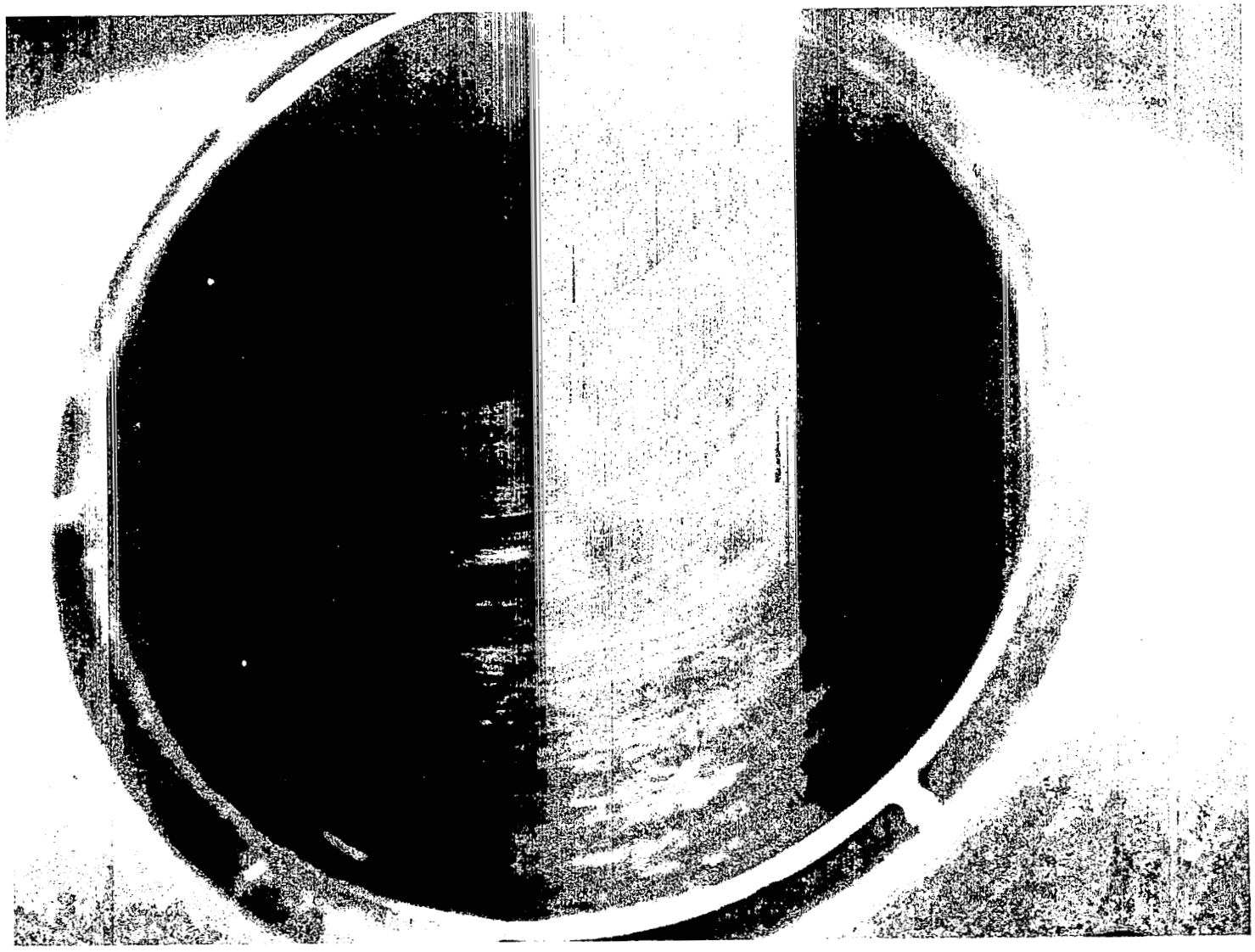

1HS35-9/9/75-C1C*

Figure 118. Combustor Internal Heat Marks

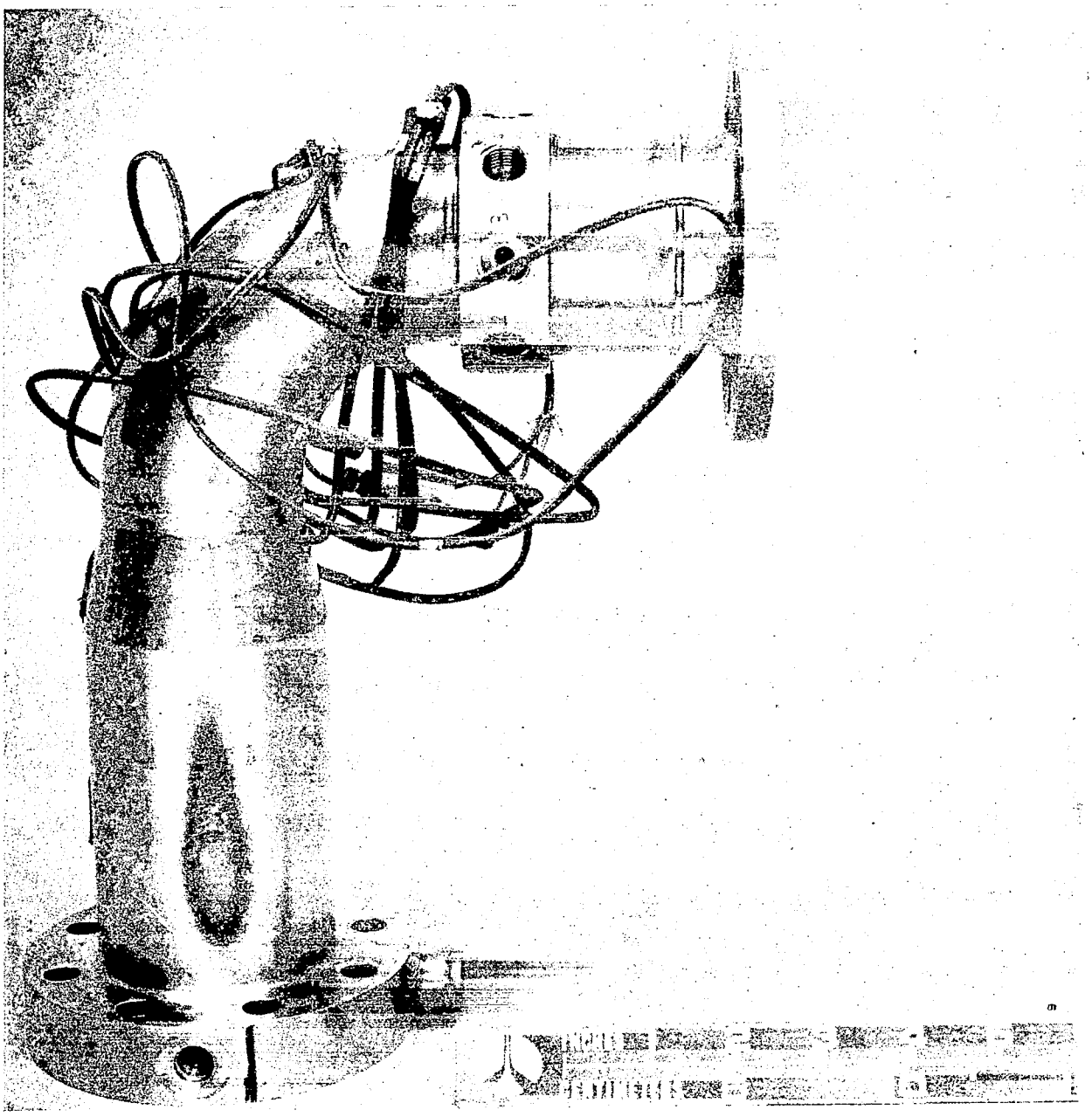

1HS35-9/9/75-C1A*

Figure 119. Combustor Heat Penetration

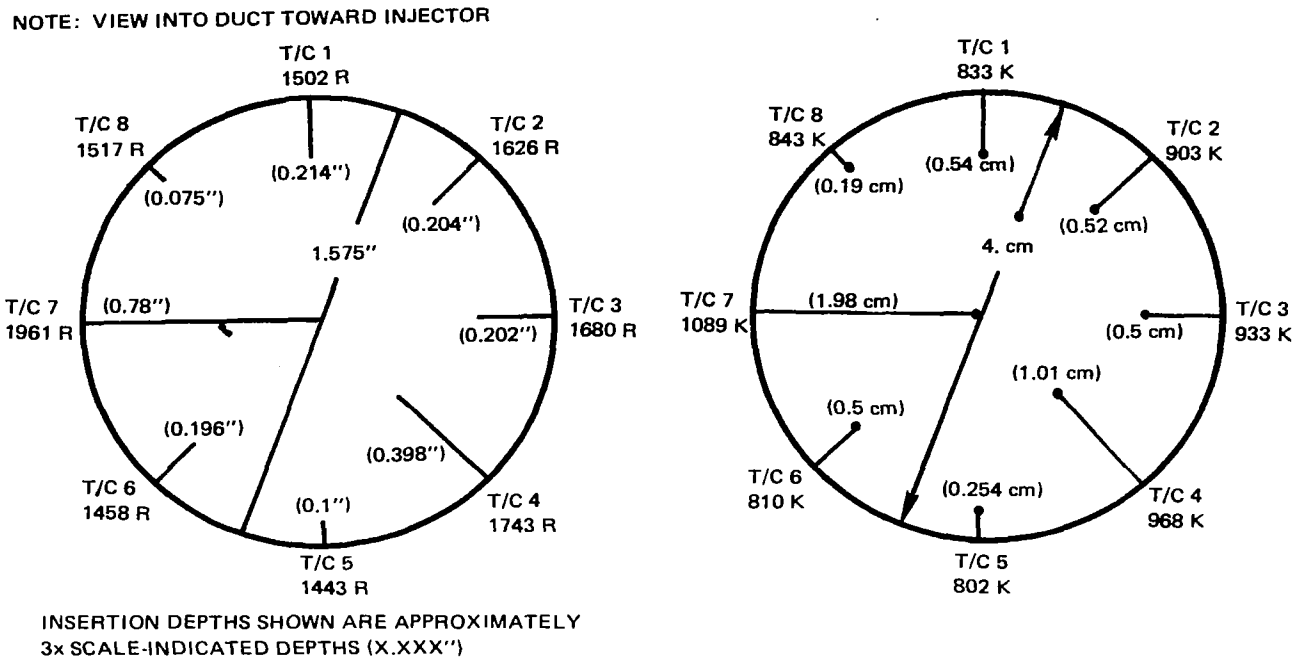

Figure 120. Thermocouple Rake Installation and Typical Temperature Measurements

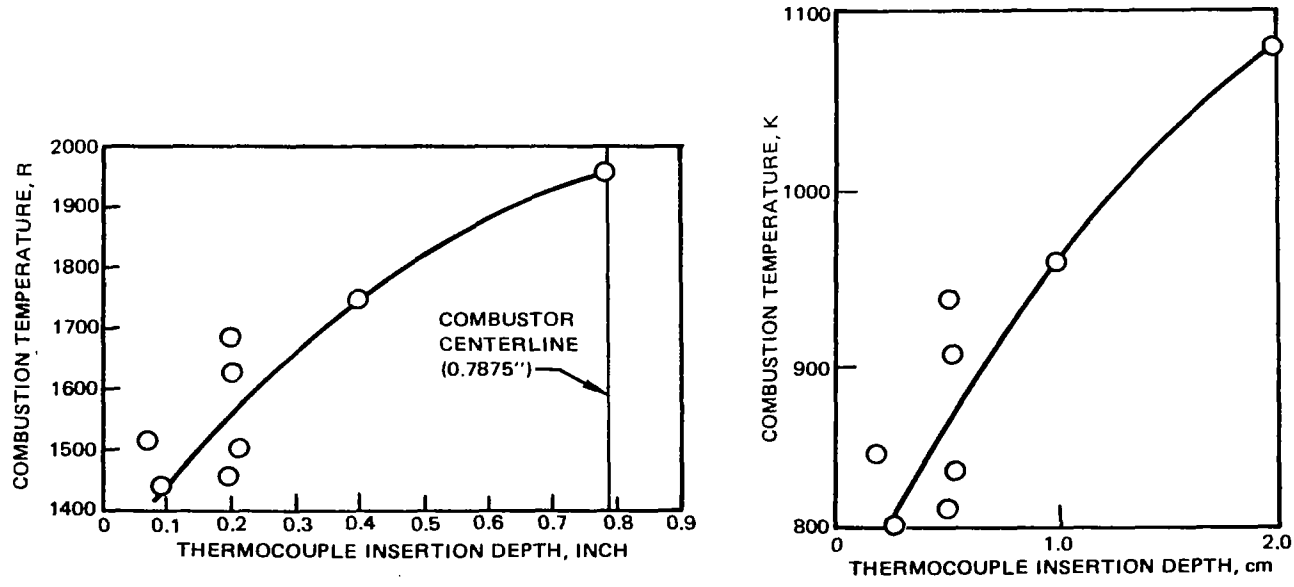

Figure 121. Combustion Temperature vs Thermocouple Insertion Depth

elbow could be a contributing factor by imposing some type of centrifuge effect on the exit gases. However, it is more likely that injector element flowstream deflection is more likely and, therefore, poses a more significant problem.

The combustor and injector were shipped to Canoga Park, California for detailed analysis. Injector units 2 and 3 were water flowed in the laboratory in the as-tested condition to evaluate any possible flow maldistribution. Figure 122 shows the results of the oxidizer-side flow distribution tests on injector unit No. 3 (produced combustor erosion). Note that the two streams directed toward the outside (toward the combustor wall) are the exact elements which produced the hot streaks in the combustor. The element on the left (1-5) eroded the combustor wall. These water-flow tests were run at low flowrates and pressures with no back pressure; the fuel side of the injector was similarly water flow tested with no gross abnormality noted. Injector unit No. 2 was also flow tested, and revealed that two LO_2 stream elements, which were known to produce hot streaks, were diverted outward toward the combustion wall. The flow stream impingement pattern noted for these injectors was repeated over several flow tests. Tables 17A and 17B show the data collected during the water flow testing of injector unit No. 3.

Following the water-flow tests, the injectors were inspected dimensionally. Figure 123 is a schematic of the LH_2 injector unit 3 face, showing the relative locations and the identifications of the elements. The arrows next to the element show the post offset direction as well as the amount of offset in radians (degrees, minutes). Figure 123 also tabulates the actual angular misalignments. A similar inspection was made on injector unit No. 2; all posts were within 0.009 radian (32 minutes) of normality. Tables 18A and 18B show the results of injector unit 3 dimensional inspections. Since injector unit 3 had produced the erosion of the combustor, a more thorough analysis of the suspected elements (1-5 and 1-8) plus one which appeared to be within acceptable tolerances (2-3) was accomplished. Figure 124 through 126 presents the results of the cup dimensions of those elements. Generally, elements 1-8 and 2-3 appeared to have the least amount of annular (sleeve to LO_2 post) dimensional discrepancies, while element 1-5 (eroded area of combustor) has the most pronounced difference. Evaluation of dimension LO_2 d_1 (Fig. 126), with respect to the geometry of the combustor, shows the LO_2 posts to be pointing toward the wall of the combustor. This alignment would produce a high-mixture-ratio, high-temperature region, and probably caused the observed erosion.

As a result of the analysis of the combustor hot streak and high exit gas temperature gradient, the following design changes were made to the next hot-fire test series (016-045-047):

1. The film coolant flow was increased from about 4.5 to 9.5% by machining film coolant orifices adjacent to each outer coaxial element from 0.051 to 0.086 mm (0.020 to 0.034 inch) to provide better protection for the wall.
2. The film coolant impingement pattern was moved further into combustor section by removing 0.076 mm (0.030 inch) material from injector to combustor mating flange to prevent possible impingement on acoustic cavity opening.

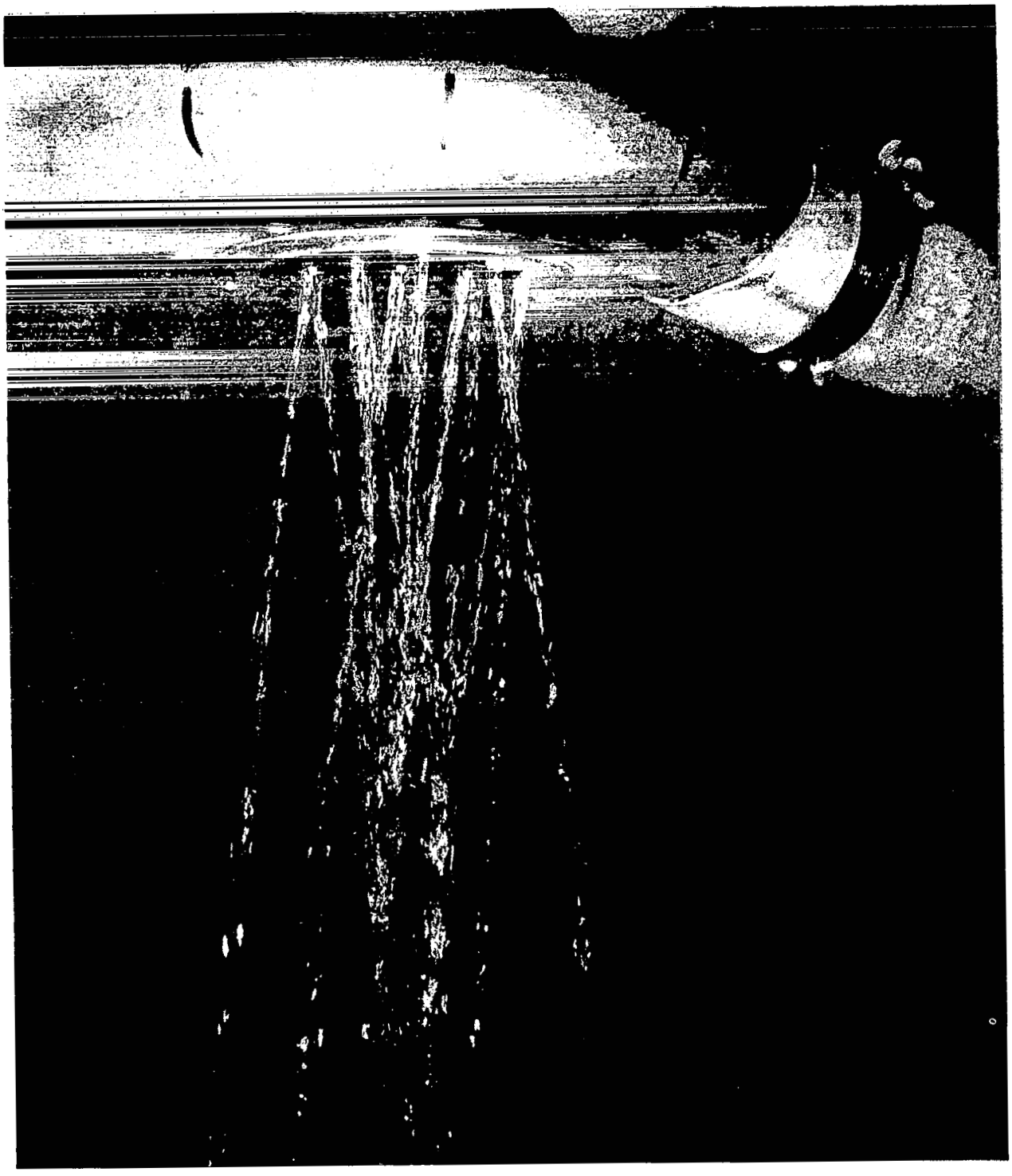

1HS49-9/5/75-C1B

Figure 122. Injector Water Flow Test

TABLE 17A. LH_2 INJECTOR UNIT NO. 3 WATER FLOW TEST RESULTS (SI UNITS)

Element No.	LO_2 Post Flowrate, kg/s	Fuel Sleeve Flowrate, kg/s	Film Coolant No.	Film Coolant Flowrate, kg/s
1-1	0.0152	0.0317	FC-1	0.00125
1-2	0.0152	0.0316	-2	0.00111
1-3	0.0147	0.0305	-3	0.00111
1-4	0.0147	0.0320	-4	0.00111
1-5	0.0152	0.0310	-5	0.00125
1-6	0.0149	0.0303	-6	0.00125
1-7	0.0118	0.0307	-7	0.00125
1-8	0.0149	0.0321	-8	0.00125
1-9	0.0145	0.0312	-9	0.00125
1-10	0.0149	0.0307	-10	0.00125
2-1	0.0150	0.0316	-11	0.00111
2-2	--	0.0295	-12	0.00097
2-3	0.0149	0.0312	-13	0.00125
2-4	0.0150	0.0317	-14	0.00111
2-5	0.0139	0.0299	-15	0.00111
			-16	0.00139
			-17	0.00139
			-18	0.00111
			-19	0.00153
			FC-20	0.00111
	Q_t = 0.2196	Q_t = 0.4657		Q_t = 0.0242
	$\overline{Q}$ = 0.0146	$\overline{Q}$ = 0.0310		$\overline{Q}$ = 0.0012
	σ = ±0.0008	σ = ± 0.00076		σ ±0.0001

NOTE:
1. Film coolant percent = 5.2
2. These data should be reviewed on individual LO_2 or LH_2 system relations for variations only within that system.
3. Upstream pressures limited to 0.69 to 9.7 N/cm^2 due to laboratory setup conditions.

TABLE 17B. LH_2 INJECTOR UNIT NO. 3 WATER FLOW TEST RESULTS (ENGLISH UNITS)

Element No.	LO_2 Post Flowrate, gpm	Fuel Sleeve Flowrate, gpm	Film Coolant No.	Film Coolant Flowrate, gpm
1-1	0.109	0.228	FC-1	0.009
1-2	0.109	0.227	-2	0.008
1-3	0.106	0.219	-3	0.008
1-4	0.106	0.230	-4	0.008
1-5	0.109	0.223	-5	0.009
1-6	0.107	0.218	-6	0.009
1-7	0.085	0.221	-7	0.009
1-8	0.107	0.231	-8	0.009
1-9	0.104	0.224	-9	0.009
1-10	0.107	0.221	-10	0.009
2-1	0.108	0.227	-11	0.008
2-2	--	0.212	-12	0.007
2-3	0.107	0.224	-13	0.009
2-4	0.108	0.228	-14	0.008
2-5	0.100	0.215	-15	0.008
			-16	0.010
			-17	0.010
			-18	0.008
			-19	0.011
			FC-20	0.008
	Q_t = 1.579	Q_t = 3.348		Q_t = 0.174
	$\overline{Q}$ = 0.1052	$\overline{Q}$ = 0.223		$\overline{Q}$ = 0.0087
	σ = ±0.006	σ = ±0.0055		σ = ±0.0009

NOTE:
1. Film coolant percent = 5.2
2. These data should be reviewed on individual LO_2 or LH_2 system relations for variations only within that system.
3. Upstream pressures limited to 1 to 4 psig due to laboratory setup conditions.

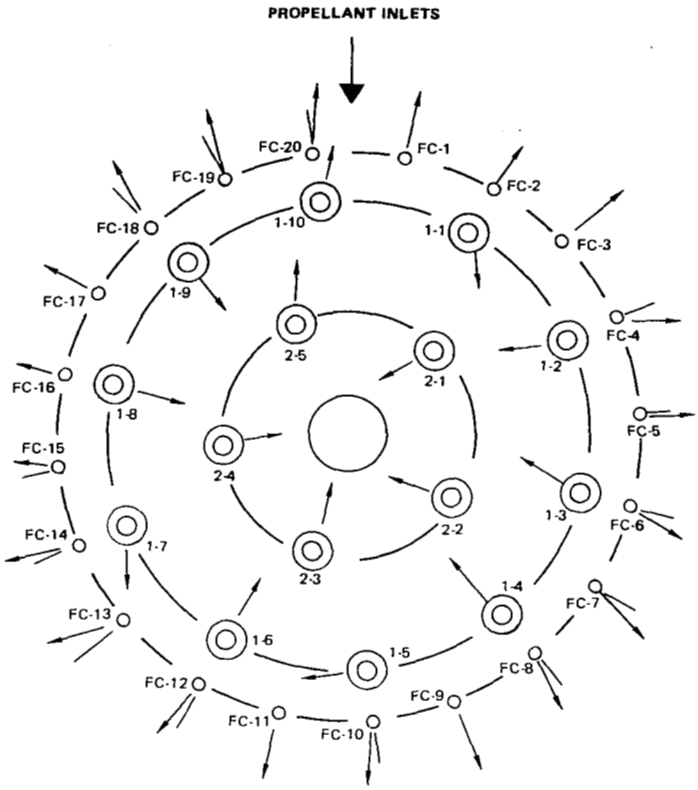

NOTE. 1. LN_2 TURBOPUMP INJECTOR FACE SHOWN
2. LO_2 TURBOPUMP FACE HAS ELEMENT ROW 1 BLANK
3. FC-1 = FUEL COOLANT DESIGNATION

Coaxial Element Identification	LO_2 Post Misalignment		Film Coolant Identification	Radial Misalignments	
	radians	minutes		radians	minutes
1-1	0.0087	30	FC-1	0.0023	8
1-2	0.0032	11	-2	0	0
1-3	0.00189	65	-3	0.0029	10
1-4	0.0087	30	-4	0.0076	26
1-5	0.0137	47	-5	0	0
1-6	0.0044	15	-6	0.0044	15
1-7	0.0125	43	-7	0.0070	24
1-8	0.0102	35	-8	0.0108	37
1-9	0.0087	30	-9	0	0
1-10	0.0189	65	-10	0.0015	5
2-1	0.0102	35	-11	0	0
2-2	0.0244	84	-12	0.0108	37
2-3	0.0058	20	-13	0.0105	36
2-4	0.0224	77	-14	0.0058	20
2-5	0.0087	30	-15	0.0157	54
			-16	0	0
			-17	0	0
			-18	0.0067	23
			-19	0.0049	17
			FC-20	0.0116	40

Figure 123. Unit No. 3 LH_2 Turbopump Injector Face Dimensional Inspection Results

TABLE 18A. INJECTOR INSPECTION RESULTS, LH_2 TURBOPUMP INJECTOR UNIT NO. 3

(SI UNITS)

Element No.	LO_2 Post ID, cm (0.221 $^{+0.0076}_{-0.0000}$)		LO_2 Post Orifice, cm (0.1143 ±0.0013)		Fuel Sleeve ID, cm (0.3886 $^{+0.0254}_{-0.0000}$)		Post Depth, cm (0.254 ±0.0127)		ID No.	Film Coolant Orifice Size, cm (0.0508 ±0.00508)		Film Coolant Angle, radian (0.087 ±0.0087)	
	U/N 2	U/N 3	U/N 2	U/N 3	U/N 2	U/N 3	U/N 2	U/N 3		U/N 2	U/N 2	U/N 2	U/N 3
1-1	0.2184	0.2243	0.0853	0.1156	0.3912	0.3922	0.2616	0.2718	FC-1	0.0508	0.0521	0.1076	0.0960
1-2	0.2184	0.2235	0.1133	0.1130	0.3924	(5)	0.2667	0.2692	-2	0.0508	0.0521	0.1059	0.0998
1-3	0.2210	0.2210	0.0965	0.1133	0.3907	0.3912	0.2692	0.2591	-3	0.0521	0.0516	0.0995	0.1056
1-4	0.2184	0.2184	0.1118	0.1130	0.3932	0.3912	0.2667	0.2642	-4	0.0508	0.0526	0.1018	0.0989
1-5	0.2184	0.2235	0.1138	0.1135	0.3919	(6)	0.2642	0.2616	-5	0.0521	0.0526	0.1070	0.0989
1-6	0.2159	0.2210	0.1118	0.1156	(1)	(7)	0.2718	0.2667	-6	0.0508	0.0526	0.0995	0.1091
1-7	0.2527	0.2210	0.1166	0.0960	0.4181	0.3912	0.2718	0.2667	-7	0.0508	0.0521	0.1033	0.0989
1-8	0.2184	0.2235	0.1138	0.1130	(2)	0.3927	0.2718	0.2642	-8	0.0508	0.0513	0.1062	0.1111
1-9	0.2184	0.2210	0.1156	0.1143	0.3932	0.3942	0.2616	0.2642	-9	0.0508	0.0521	0.0989	0.1076
1-10	0.2210	0.2210	0.1072	0.1158	0.3899	0.3917	0.2667	0.2718	-10	0.0483	0.0521	0.1036	0.1018
2-1	0.2159	0.2240	0.1148	0.1130	(3)	0.3929	0.2591	0.2642	-11	0.0483	0.0521	0.1047	0.0890
2-2	0.2123	0.2235	0.1158	0.1130	(4)	(8)	0.2591	0.2616	-12	0.0483	0.0523	0.1004	0.0995
2-3	0.2123	0.2210	0.1161	0.1148	0.3937	0.3955	0.2565	0.2591	-13	0.0508	0.0521	0.0989	0.0989
2-4	0.2123	0.2210	0.1168	0.1151	0.3891	0.3937	0.2591	0.2642	-14	0.0508	0.0518	0.0989	0.1076
2-5	0.2121	0.2210	0.1156	0.1123	0.3929	0.3912	0.2642	0.2642	-15	0.0508	0.0518	0.1021	0.0998
									-16	0.0483	0.0526	0.0992	0.1091
									-17	0.0508	0.0518	0.1006	0.0960
									-18	0.0483	0.0526	0.1047	0.1085
									-19	0.0508	0.0521	0.1091	0.0983
									FC-20	0.0508	0.0516	0.0966	0.1062

(1) Varied 0.3927 to 0.3962
(2) Varied 0.3912 to 0.3945
(3) Varied 0.3929 to 0.3942
(4) Vareid 0.3894 to 0.3929
(5) Varied 0.3912 to 0.3927
(6) Varied 0.3917 to 0.3950
(7) Varied 0.3917 to 0.3955
(8) Varied 0.3891 to 0.3932

TABLE 18B. INJECTOR INSPECTION RESULTS, LH_2 TURBOPUMP INJECTOR UNIT NO. 3
(ENGLISH UNITS)

Element No.	LO_2 Post ID, inch (0.087 $^{+0.003}_{-0.000}$)		LO_2 Post Orifice, inch (0.045 ±0.005)		Full Sleeve ID, inch (0.153 $^{+0.001}_{-0.000}$)		Post Depth, inch (0.100 ±0.005)		ID No.	Film Coolant Orifice Size, inch (0.020 ±0.002)		Film Coolant Angle, (5° ±0.5)	
	U/N 2	U/N 3	U/N 2	U/N 3	U/N 2	U/N 3	U/N 2	U/N 3		U/N 2	U/N 3	U/N 2	U/N 3
1-1	0.086	0.0883	0.0336	0.0455	0.154	0.1544	0.103	0.107	FC-1	0.020	0.0205	6° 10'	5° 30'
1-2	0.086	0.0880	0.0446	0.0445	0.1545	(5)	0.105	0.106	-2	0.020	0.0205	6° 04'	5° 43'
1-3	0.087	0.0870	0.0380	0.0446	0.1538	0.154	0.106	0.102	-3	0.0205	0.0203	5° 42'	6° 03'
1-4	0.086	0.0860	0.0440	0.0445	0.1548	0.154	0.105	0.104	-4	0.020	0.0207	5° 50'	5° 40'
1-5	0.086	0.0880	0.0448	0.0447	0.1543	(6)	0.104	0.103	-5	0.0205	0.0207	6° 08'	5° 40'
1-6	0.085	0.0870	0.0440	0.0455	(1)	(7)	0.107	0.105	-6	0.020	0.0207	5° 42'	6° 15'
1-7	0.0995	0.0870	0.0459	0.0378	0.1646	0.154	0.107	0.105	-7	0.020	0.0205	5° 55'	5° 40'
1-8	0.086	0.0880	0.0448	0.0445	(2)	0.1546	0.107	0.104	-8	0.020	0.0202	6° 05'	6° 20'
1-9	0.086	0.0870	0.0455	0.0450	0.1548	0.1552	0.103	0.104	-9	0.020	0.0205	5° 40'	6° 10'
1-10	0.087	0.0870	0.0422	0.0456	0.1535	0.1542	0.105	0.107	-10	0.019	0.0205	5° 56'	5° 50'
2-1	0.085	0.0882	0.0452	0.0445	(3)	0.1547	0.102	0.104	-11	0.019	0.0205	6° 00'	5° 06'
2-2	0.0836	0.0880	0.0456	0.0445	(4)	(8)	0.102	0.103	-12	0.019	0.0206	5° 45'	5° 42'
2-3	0.0836	0.0870	0.0457	0.0452	0.155	0.1557	0.101	0.102	-13	0.020	0.0205	5° 40'	5° 40'
2-4	0.0836	0.0870	0.0460	0.0453	0.1532	0.1550	0.102	0.104	-14	0.020	0.0204	5° 40'	6° 10'
2-5	0.0835	0.0870	0.0455	0.0442	0.1547	0.1540	0.104	0.104	-15	0.020	0.0204	5° 51'	5° 43'
									-16	0.019	0.0207	5° 41'	5° 15'
									-17	0.020	0.0204	5° 46'	5° 30'
									-18	0.019	0.0207	6° 00'	6° 13'
									-19	0.020	0.0205	6° 15'	5° 38'
									FC-20	0.020	0.0203	5° 32'	6° 05'

(1) Varied 0.1542 to 0.156
(2) Varied 0.154 to 0.1553
(3) Varied 0.1547 to 0.1552
(4) Varied 0.1533 to 0.1547
(5) Varied 0.154 to 0.155
(6) Varied 0.1542 to 0.1555
(7) Varied 0.1542 to 0.1557
(8) Varied 0.1532 to 0.1548

TYPE INJECTOR LH_2

UNIT NO. 3

ELEMENT NO. 1-5

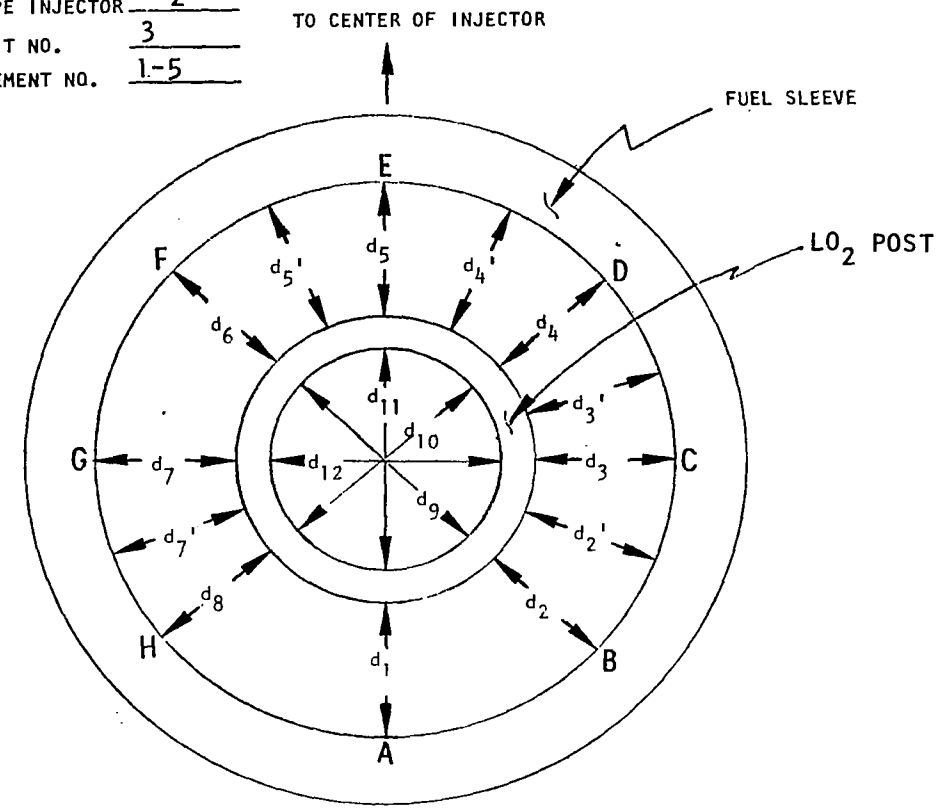

All dimensions in millimeters

d_1 = 0.320	d_5 = 0.511	d_9 = 2.332	$\overline{AE}$ = 3.924
d_2 = 0.333	d_6 = 0.432	d_{10} = 2.289	$\overline{BF}$ = 3.940
d_3 = 0.432	d_7 = N/M*	d_{11} = 2.301	$\overline{CG}$ = 3.955
d_4 = N/M*	d_8 = 0.305	d_{12} = 2.306	$\overline{DH}$ = 3.952
d_2' = 0.353	d_3' = 0.457	d_4' = 0.508	d_5' = 0.508
d_7' = 0.353			

*N/M = NOT MEASURED

Figure 124. Coaxial Element Evaluation ASE Preburner Injector, Unit 3, Element 1-5 (SI Units)

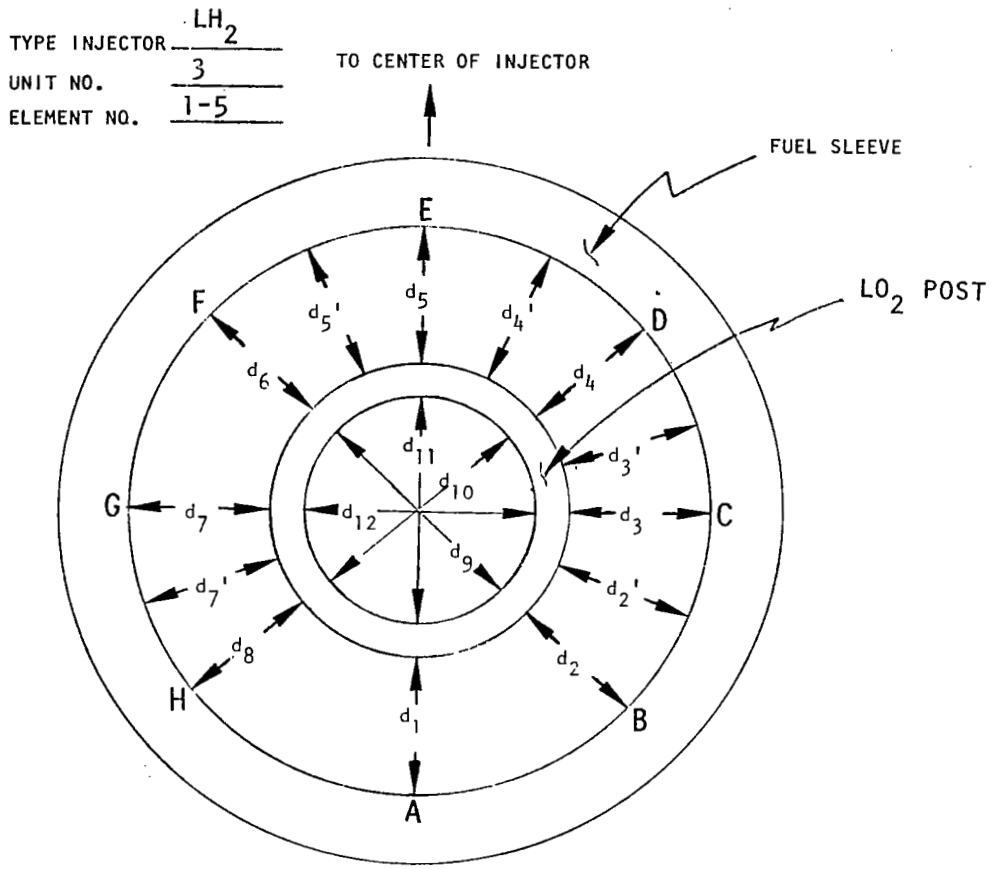

All dimensions in inches

d_1 = 0.0126	d_5 = 0.0201	d_9 = 0.0918	$\overline{AE}$ = 0.1545
d_2 = 0.0131	d_6 = 0.017	d_{10} = 0.0901	$\overline{BF}$ = 0.1551
d_3 = 0.017	d_7 = N/M*	d_{11} = 0.0906	$\overline{CG}$ = 0.1557
d_4 = N/M*	d_8 = 0.012	d_{12} = 0.0908	$\overline{DH}$ = 0.1556
d_2' = 0.0139	d_3' = 0.018	d_4' = 0.020	d_5' = 0.020
d_7' = 0.0139			

*N/M = NOT MEASURED

Figure 124. Coaxial Element Evaluation ASE Preburner Injector, Unit 3, Element 1-5 (English Units)

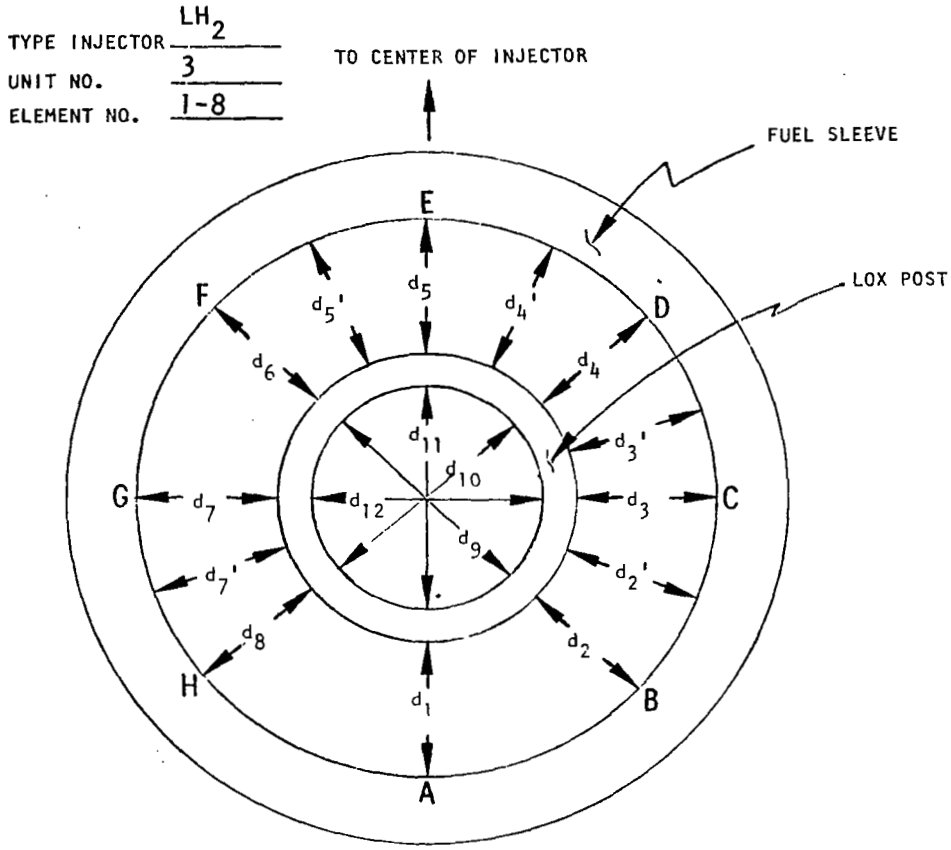

All dimensions in millimeters

d_1 =	0.427	d_5 =	0.417	d_9 =	2.296	$\overline{AE}$ =	3.932
d_2 =	0.411	d_6 =	0.422	d_{10} =	2.344	$\overline{BF}$ =	3.950
d_3 =	0.417	d_7 =	0.427	d_{11} =	2.299	$\overline{CG}$ =	3.952
d_4 =	0.409	d_8 =	0.409	d_{12} =	2.347	$\overline{DH}$ =	3.967

Figure 125. Coaxial Element Evaluation ASE Preburner Injector, Unit 3. Element 1-8 (SI Units)

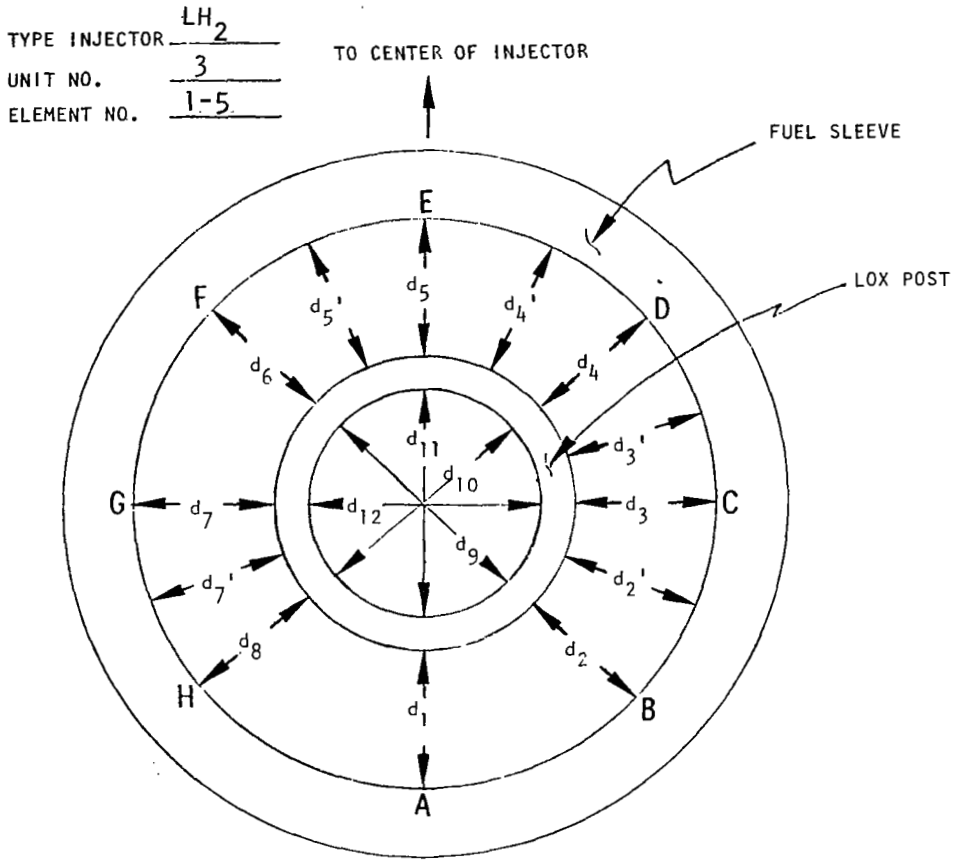

All dimensions in inches

d_1 = 0.0168	d_5 = 0.0164	d_9 = 0.0904	$\overline{AE}$ = 0.1548
d_2 = 0.0162	d_6 = 0.0174	d_{10} = 0.0923	$\overline{BF}$ = 0.1555
d_3 = 0.0164	d_7 = 0.0168	d_{11} = 0.0905	$\overline{CG}$ = 0.1556
d_4 = 0.0161	d_8 = 0.0161	d_{12} = 0.0924	$\overline{DH}$ = 0.1562

Figure 125. Coaxial Element Evaluation ASE Preburner Injector, Unit 3, Element 1-8 (English Units)

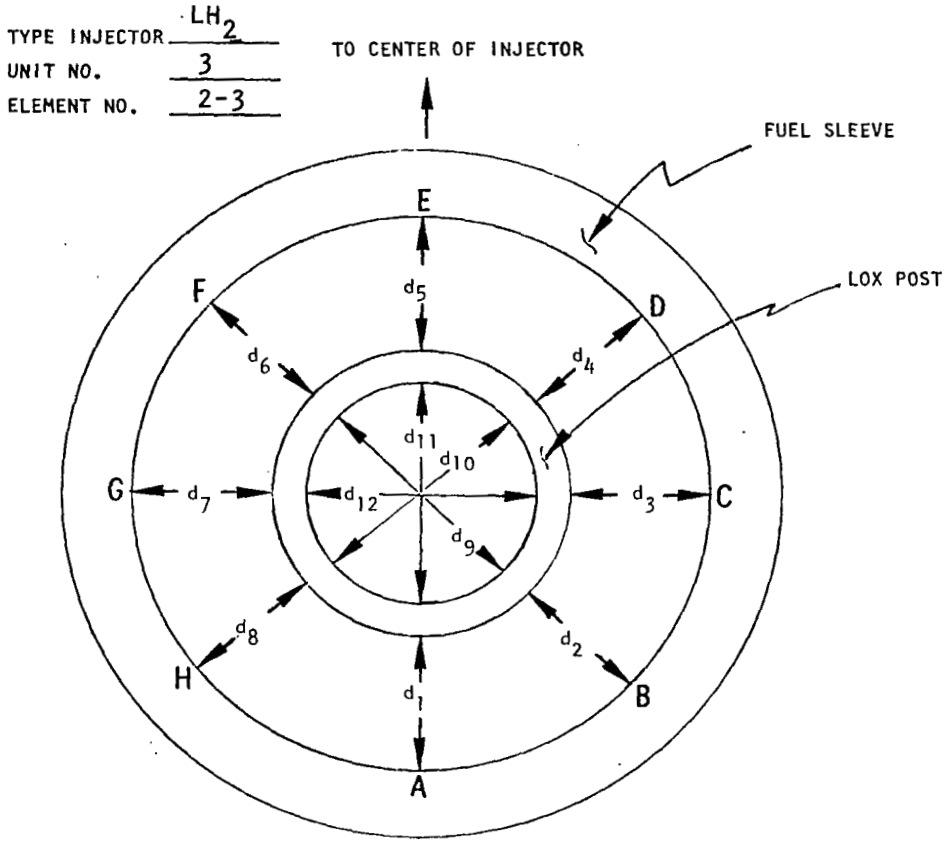

All dimensions in millimeters

d_1 = 0.399	d_5 = 0.450	d_9 = 2.271	$\overline{AE}$ = 3.970
d_2 = 0.363	d_6 = 0.495	d_{10} = 2.306	$\overline{BF}$ = 3.988
d_3 = 0.371	d_7 = 0.508	d_{11} = 2.271	$\overline{CG}$ = 3.975
d_4 = 0.399	d_8 = 0.465	d_{12} = 2.240	$\overline{DH}$ = 4.011

Figure 126. Coaxial Element Evaluation ASE Preburner Injector, Unit 3, Element 2-3 (SI Units)

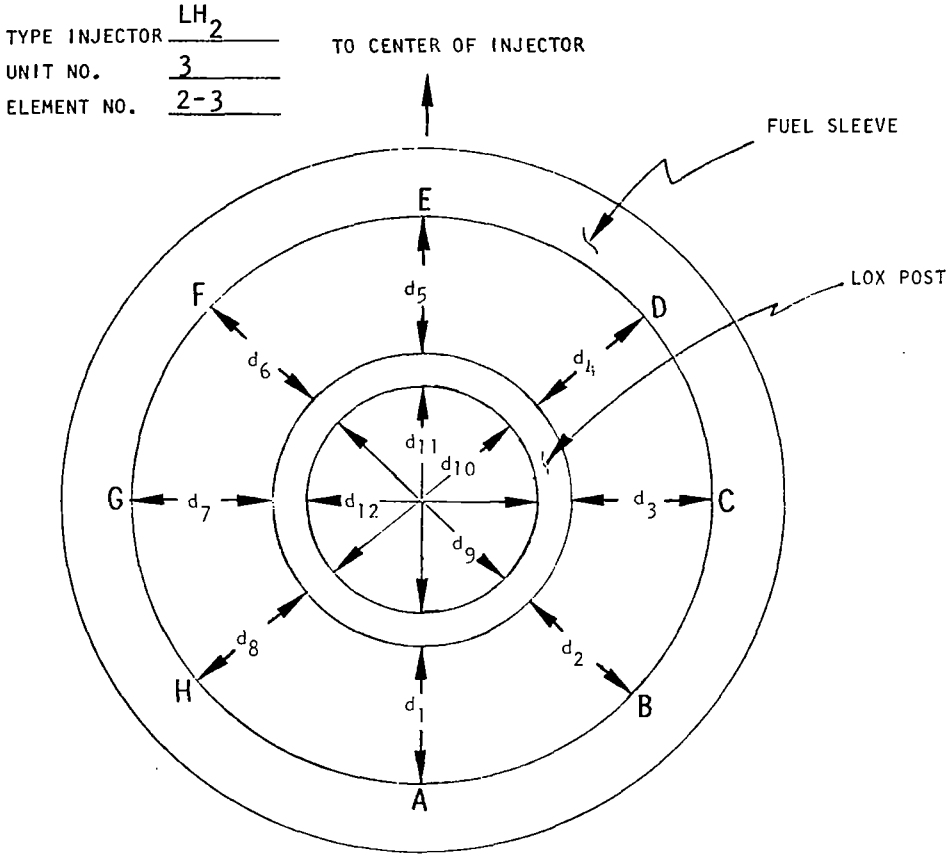

Figure 126. Coaxial Element Evaluation ASE Preburner Injector, Unit 3, Element 2-3 (English Units)

3. Since the acoustic cavities have been observed to collect moisture following a test, drain holes 0.762 mm (0.030 inch) in diameter were machined into acoustic cavity. This design change will not negate the effectiveness of the acoustic cavities.

4. Three bosses were provided to determine the temperature profile in the large section of the combustor upstream of the converging section. The three temperature measurements monitor (a) wall temperature below the previous eroded area in-line with the larger film coolant orifice 0.864 mm (0.034 inch), (b) the center core temperature, and (c) wall temperature below the smaller film coolant orifice 0.508 mm (0.020 inch) about 2.09 radians (120 degrees) from measurement (b) above.

5. The LO_2 posts of injector unit No. 3 were straightened mechanically prior to next test. Records of any post movements will be maintained.

6. The quarter torus section was changed to a 1.57 radian (90 degree) miter bend. This design change was made to ensure adequate mixing of the exhaust gases to maintain a more uniform temperature from the core to the outer wall. Figure 127 is a sketch of the changes to the combustor body.

Three tests comprised the final gas generator calibration test series for mainstage durations of 10, 22, and 20 seconds, respectively. Results of the test effort demonstrated that the current facility LH_2 tank volume would safely permit LH_2 turbopump gas generator nominal mainstage tests of 20 seconds duration, including allowances for fuel lead and cutoff lag flow volumes.

The overall objective of these final tests was to evaluate the effects of changing the quarter-torus section of the combustor to a 1.57 radian (90 degree) miter bend (Fig. 127). The miter bend was installed to enhance propellant mixing and thereby reduce the previously observed thermal gradient between the core and wall gas temperatures.

Figure 128 shows the Lima test facility installation of the LH_2 turbopump gas generator with the 1.57 radian (90 degree) miter bend. The results of the testing show that the 1.57 radian (90 degree) miter bend achieved the desired effect, in that, the thermal gradient was reduced from about 244 K (440 R) before the combustor modification to about 81 K (145 R) after the combustor modification. Figure 129 shows the comparison of the combustor exit plane (i.e., turbine inlet) gas temperature versus thermocouple immersion depth both before and after the combustor modification. In addition to the eight exit plane thermocouples, three additional thermocouples were installed in the upper combustion zone about 15.24 cm (6 inches) below the injector face. These thermocouples were inserted 2.54, 15.24, and 29.21 mm (0.1, 0.6, and 1.15 inches) into the combustor gas flow.

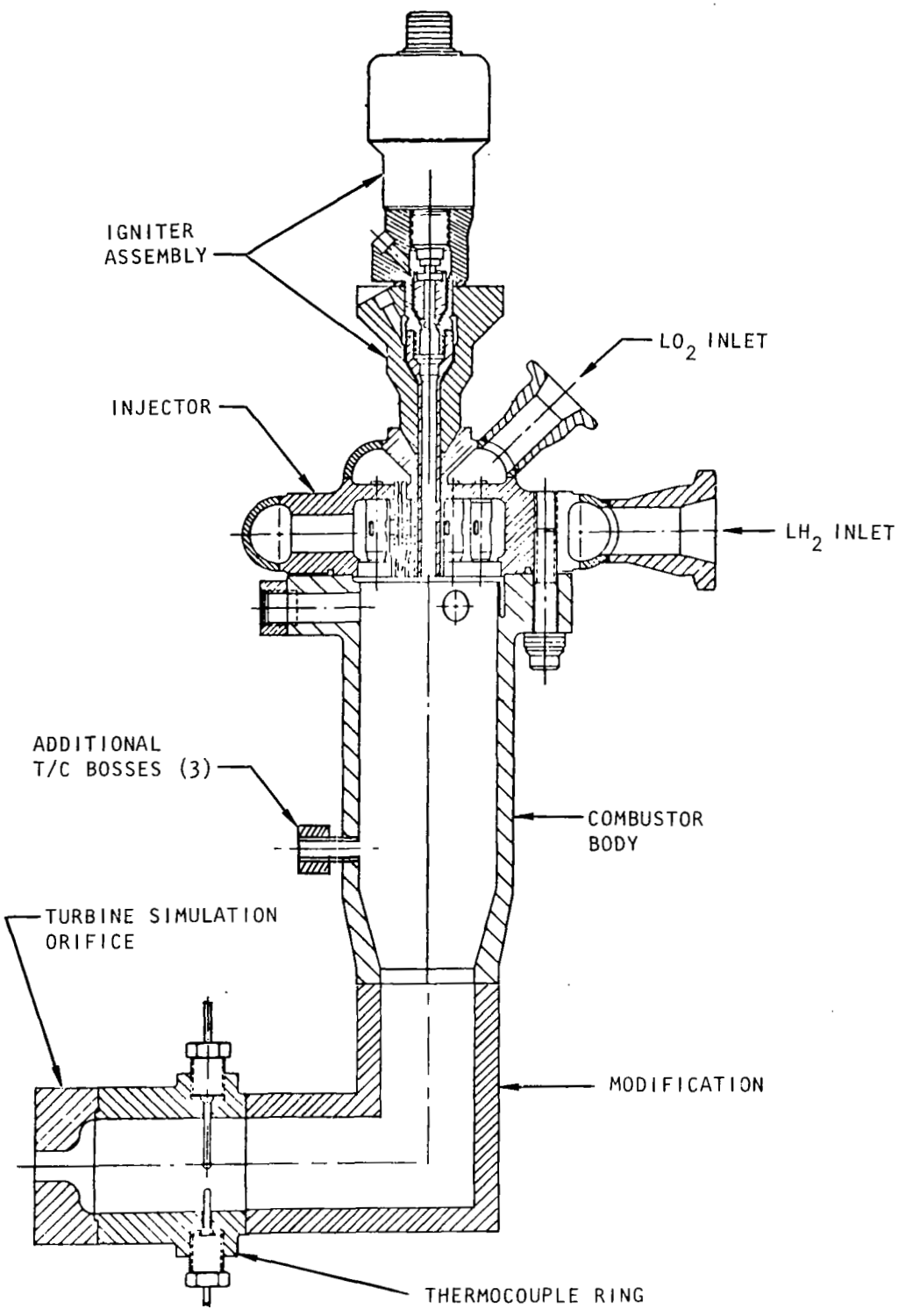

Figure 127. Small, High-Pressure Gas Generator Combustor Modifications

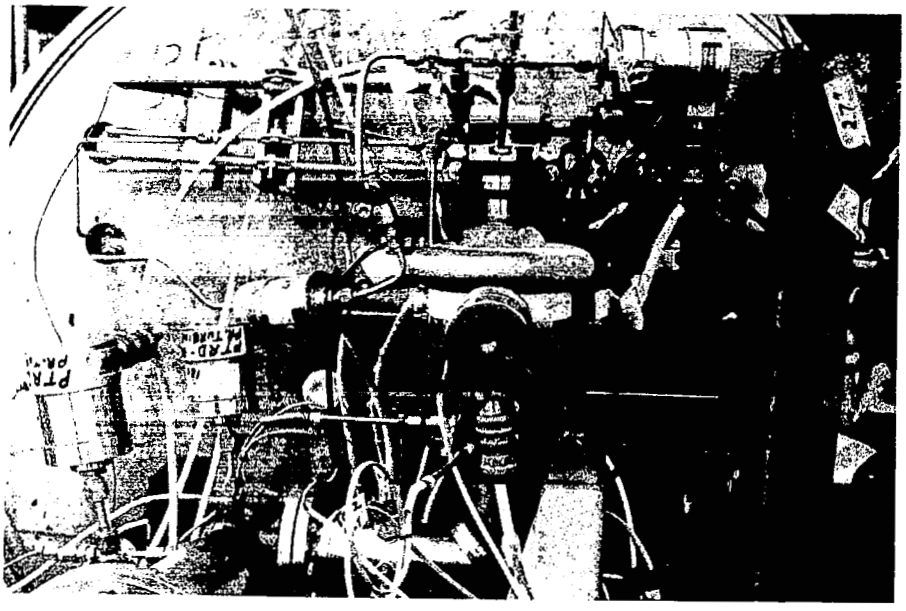

5AJ33-12/1/75-S1B

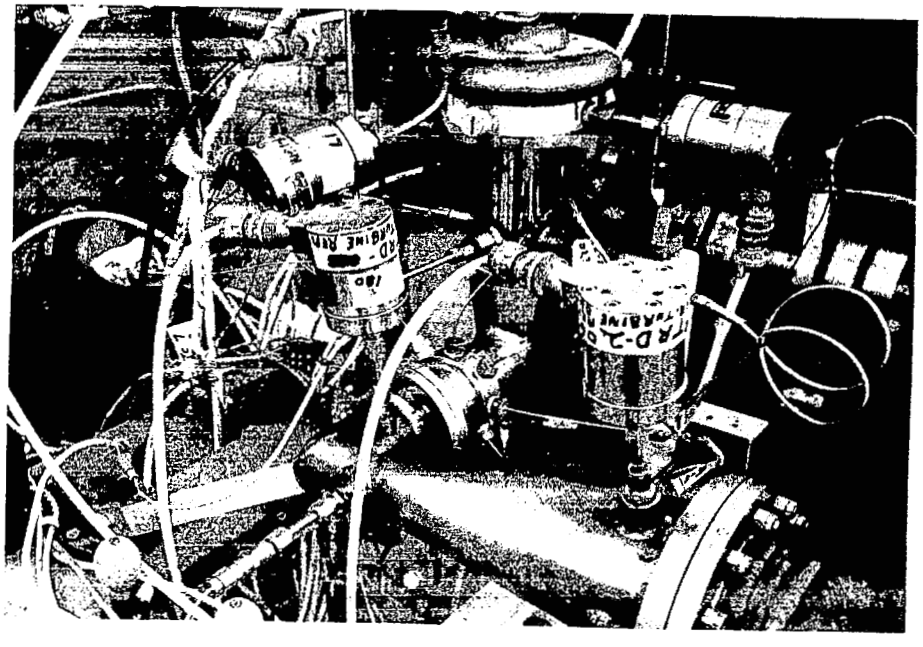

5AJ33-12/1/75-S1A

Figure 128. LH_2 Turbopump Gas Generator Installation (Lima Stand, PRA)

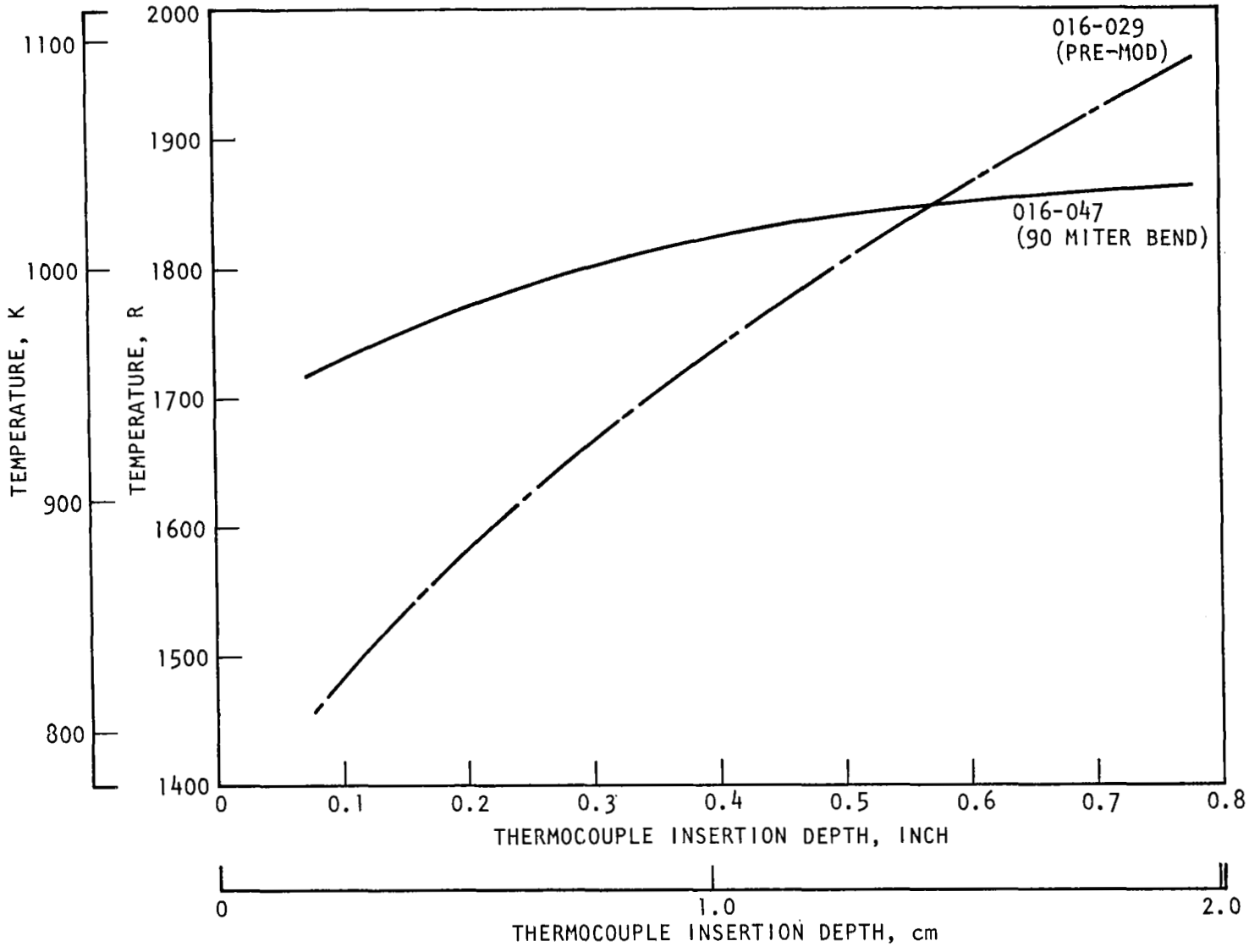

Figure 129. LH_2 Turbopump Gas Generator Exit Plane Temperature Profile

Figure 131 shows the temperature profile in the upper combustion zone for test 016-047. These thermocouples were not installed before the combustor modification; therefore, no direct comparison of the upper combustion zone temperature profile was possible. From the results of these tests, it is recommended that the 1.57 radian (90 degree) miter bend be incorporated into the combustor body for testing with the LH_2 turbopump.

The hardware condition following these series of tests was satisfactory with no damage noted. Figure 132 shows the condition of the injector (unit 3M) face.

Figure 133 is an injector performance predication map for injector unit 3M showing the relationship of LO_2 injection pressure versus fuel injection pressure versus the performance target of P_c, MR, and temperature.

The injector element design is shown in Fig. 130. Measurements of the 0.381 mm (0.015 inch) fuel sleeve annulus indicated some oxidizer post bias and, therefore, the straightening of posts and the imposing of some mechanical method for maintaining them straight, may be sufficient. The results of the test effort indicate that, for concentric-element injectors designed to use LH_2 as the fuel, small annulli can result in flow stream deflection, and a hot core or possible wall streaking can result. Alternatives, such as decreasing the number of elements, have possible performance and weight implications and, therefore, the maintaining of straight elements (without disturbing the fuel flow) in an area to be investigated.

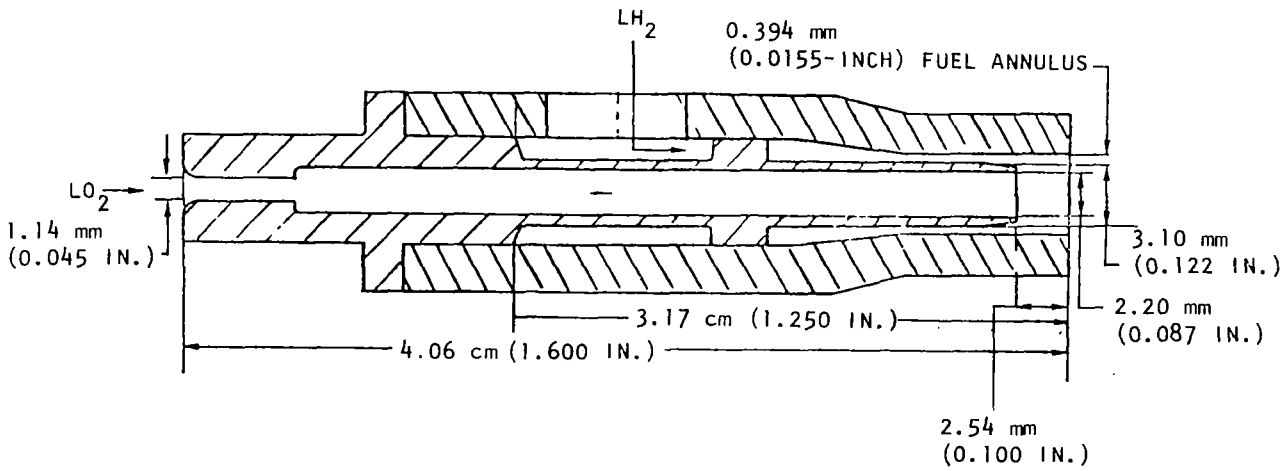

Figure 130. ASE LH_2 Turbopump Gas Generator Injector Element (Cross Section)

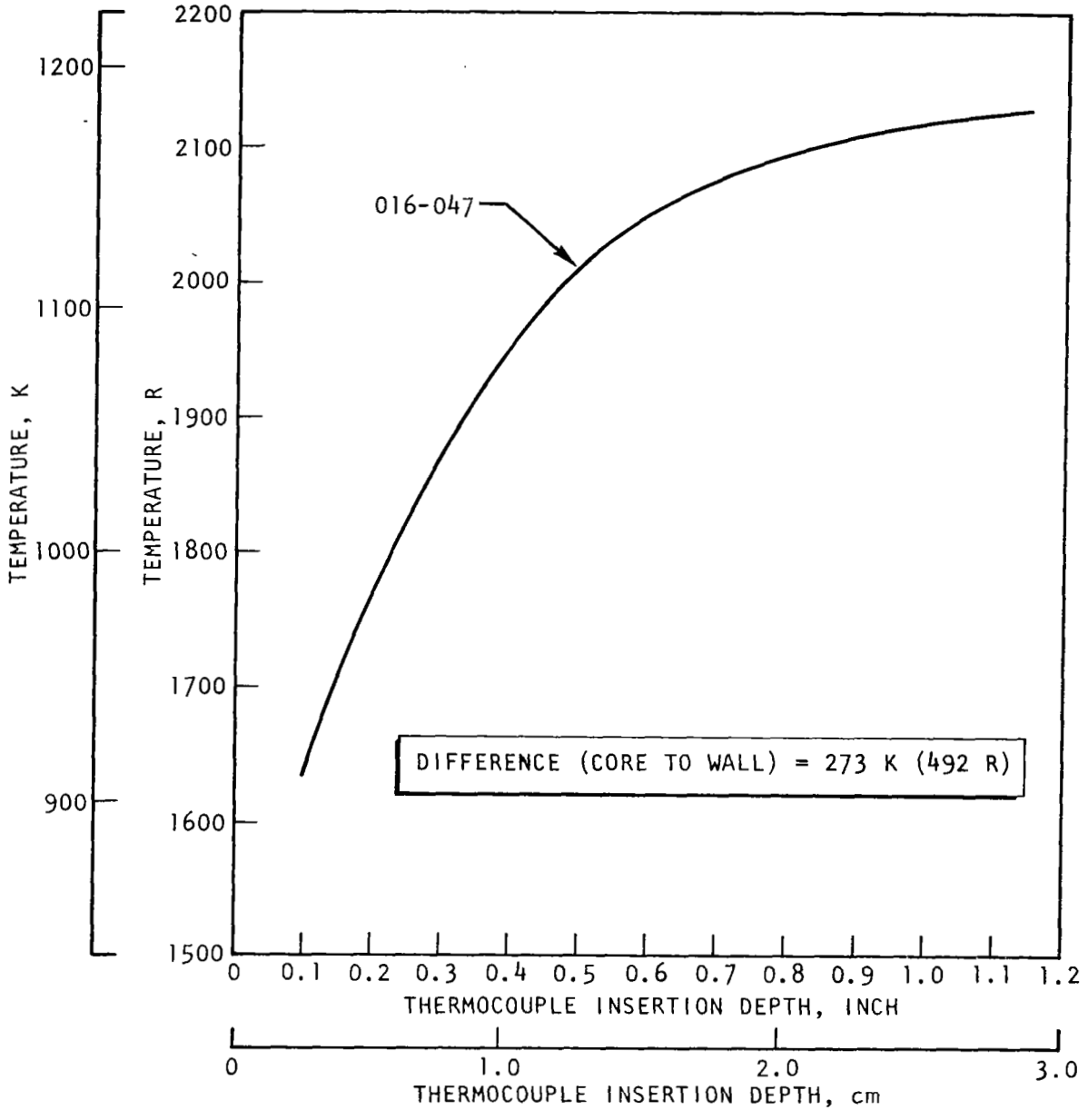

Figure 131. LH_2 Turbopump Gas Generator Combustion Zone Temperature Profile

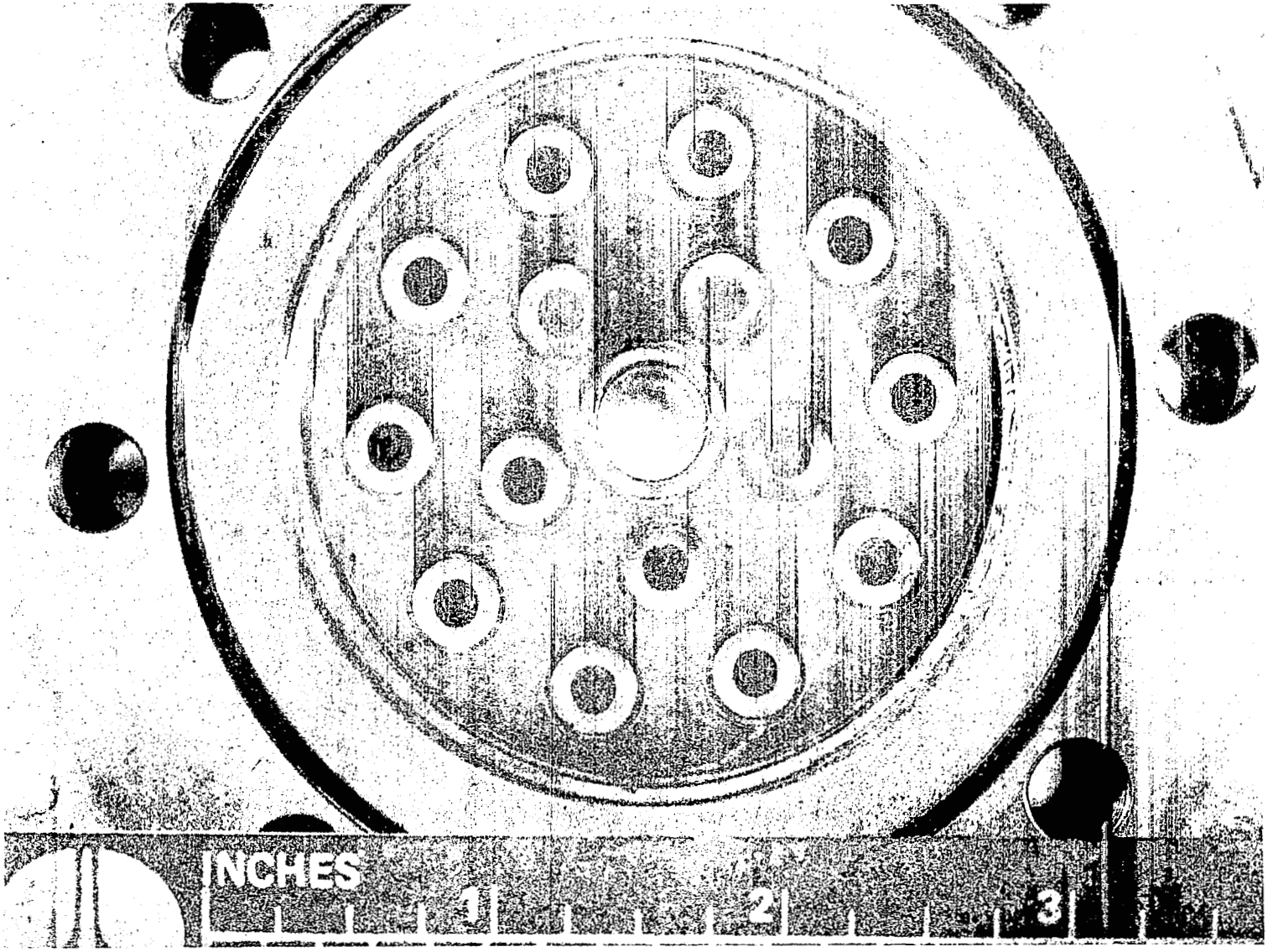

1SM35-11/17/75-S2A

Figure 132. Injector Unit 3M Following Test

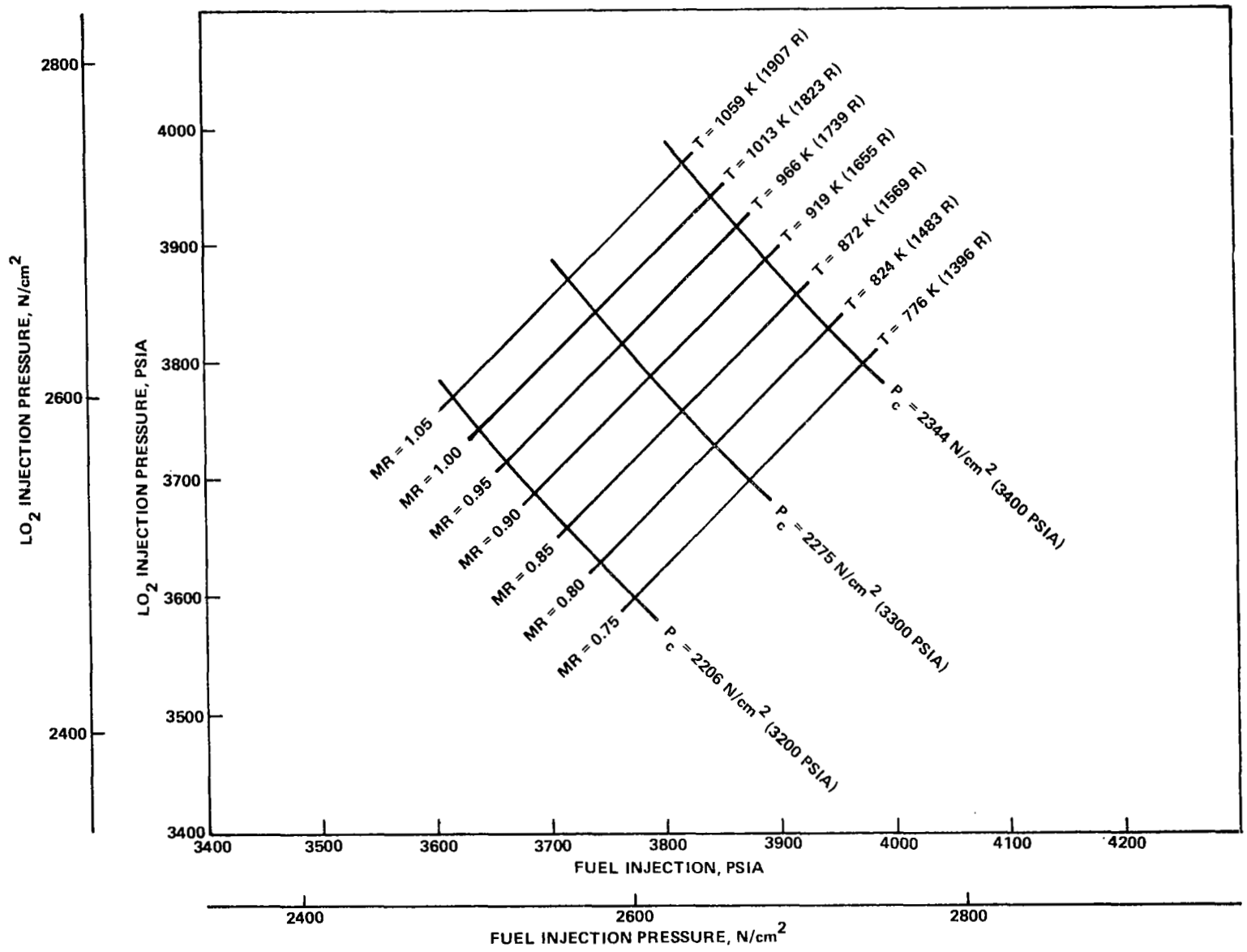

Figure 133. Injector Performance Map

Turbine Calibration Testing

Calibration of the Mark 48-F turbine to establish its aerothermodynamic performance was accomplished with ambient-temperature GN_2 as the propellant. The rotor speeds were maintained in the range of 1050 rad/s (10,000 rpm) to 2600 rad/s (25,000 rpm) to simulate the operational wheel tip speed/gas spouting velocity ratios (U/C_o).

The testing was performed at Wyle Laboratory in El Segundo, California. The basic test setup is illustrated in Fig. 134 and 135. Power developed by the turbine was absorbed by a Mark 4 pump which recirculated water from a reservoir. A Lebow in-line torquemeter was installed between the turbine and the power-absorbing pump to indicate the torque developed by the turbine. The test unit installed in the Wyle facility is shown in Fig.136 and 137.

The tests were started on 12 August 1976, and were conducted in essentially two series. The first series (Table 19) was conducted at turbine speeds up to 2200 rad/s (21,000 rpm) and U/C_o range from 0.16 to 0.39. This test series was interrupted when a sudden change in the rotor torque characteristics was observed. The turbine was removed from the test stand disassembled for inspection. It was found that the slave thrust bearing on the turbine side of the rotor had failed. The failure was diagnosed as originating in the phenolic cage from three potential causes: (1) insufficient lubricity of the Freon 13 coolant used, (2) residual stresses in the cage from flairing the ends of the tubular rivets, (3) corrosion of the races and ball due to water condensation between tests.

The turbine was rebuilt, using a thrust bearing with solid cage rivets, and testing was resumed with oil as the bearing lubricating fluid instead of Freon. No further mechanical problems were encountered.

Testing was concluded by obtaining the required data points at the higher velocity ratios (Table 20). These tests were performed primarily at rotor speeds of 2100 and 2600 rad/s (20,000 and 25,000 rpm). Two data points at low-velocity ratios which were covered during earlier tests were repeated to validate the continuity of the data. The repeated points fell within the band of expected data scatter. Analysis of test data shows predicted turbine performance was achieved through the full range of test velocity ratios. Tests 006 through 014 were conducted during the second test phase for velocity ratios ranging from 0.197 to 0.552, and speeds from 2110 to 2640 rad/s (19,220 to 25,247 rpm). Three tests were made at velocity ratios (U/C_o (T-T) = 0.197, 0.227, 0.311) equivalent to those run during the first-phase turbine tests 001 through 005; turbine performance was repeated as shown by the velocity ratio/turbine efficiency data plot in Fig. 138. Turbine efficiencies were calculated with developed horsepowers calculcated with Lebow torquemeter data, and isentropic available energy and GN_2 working fluid mass-flow calculated at the respective operating points. Turbine efficiencies were also calculated using an alternate method which used measured total temperature drop ($\Delta T_{(T-T)}$ across the turbine; good agreement exists between turbine efficiency data calculated with Lebow torque data and measured turbine temperature drop.

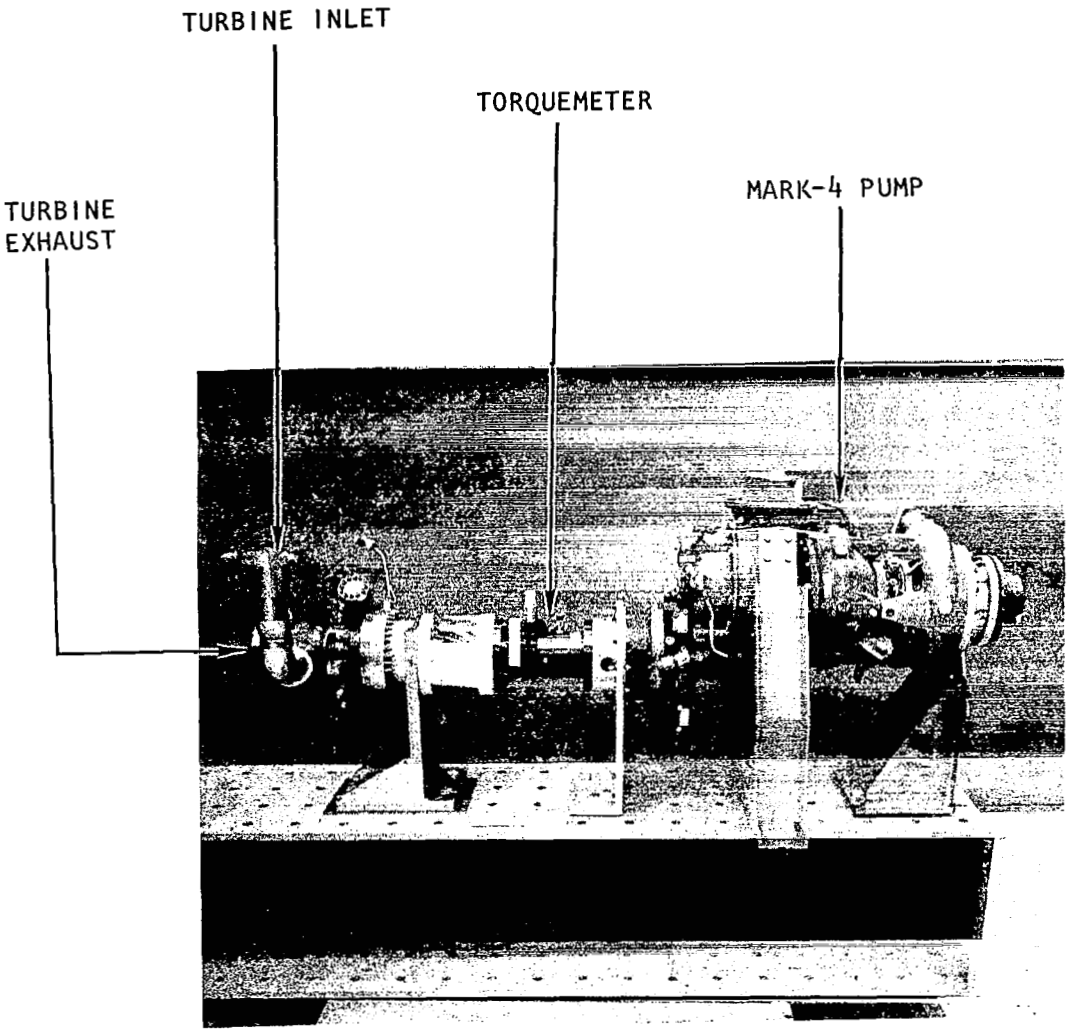

Figure 134. Mark 48-F Turbine Calibration Test Setup

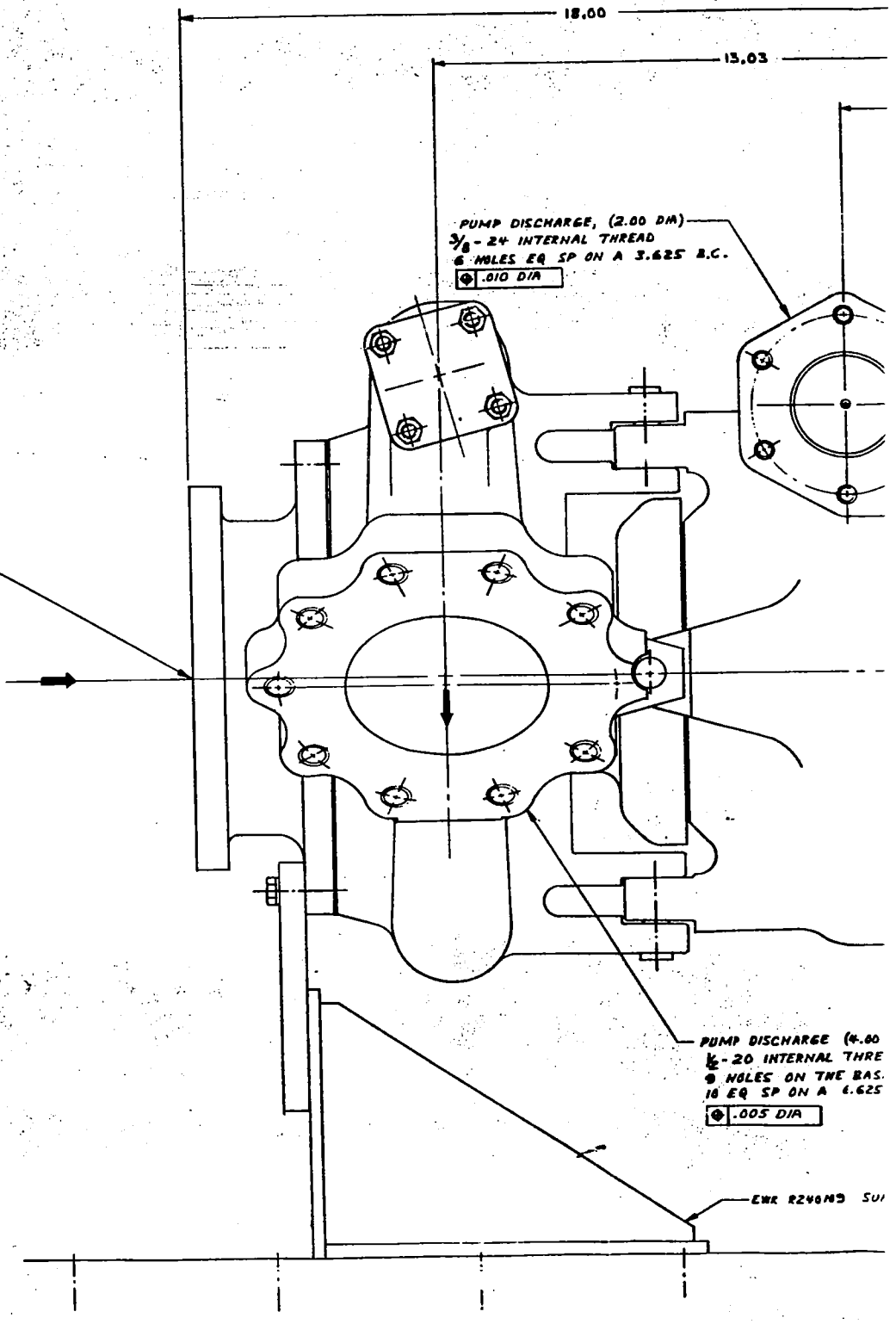
18.00
13.03
PUMP DISCHARGE, (2.00 DIA)
3/8 - 24 INTERNAL THREAD
6 HOLES EQ SP ON A 3.625 B.C.
.010 DIA
PUMP INLET (5.00 DIA)
.343 DIA BOLT HOLES
8 HOLES EQ SP ON A 6.750 B.C.
.010 DIA
PUMP DISCHARGE (4.60
- 20 INTERNAL THRE
9 HOLES ON THE BAS
18 EQ SP ON A 6.625
.005 DIA
EWR R240M3 SU

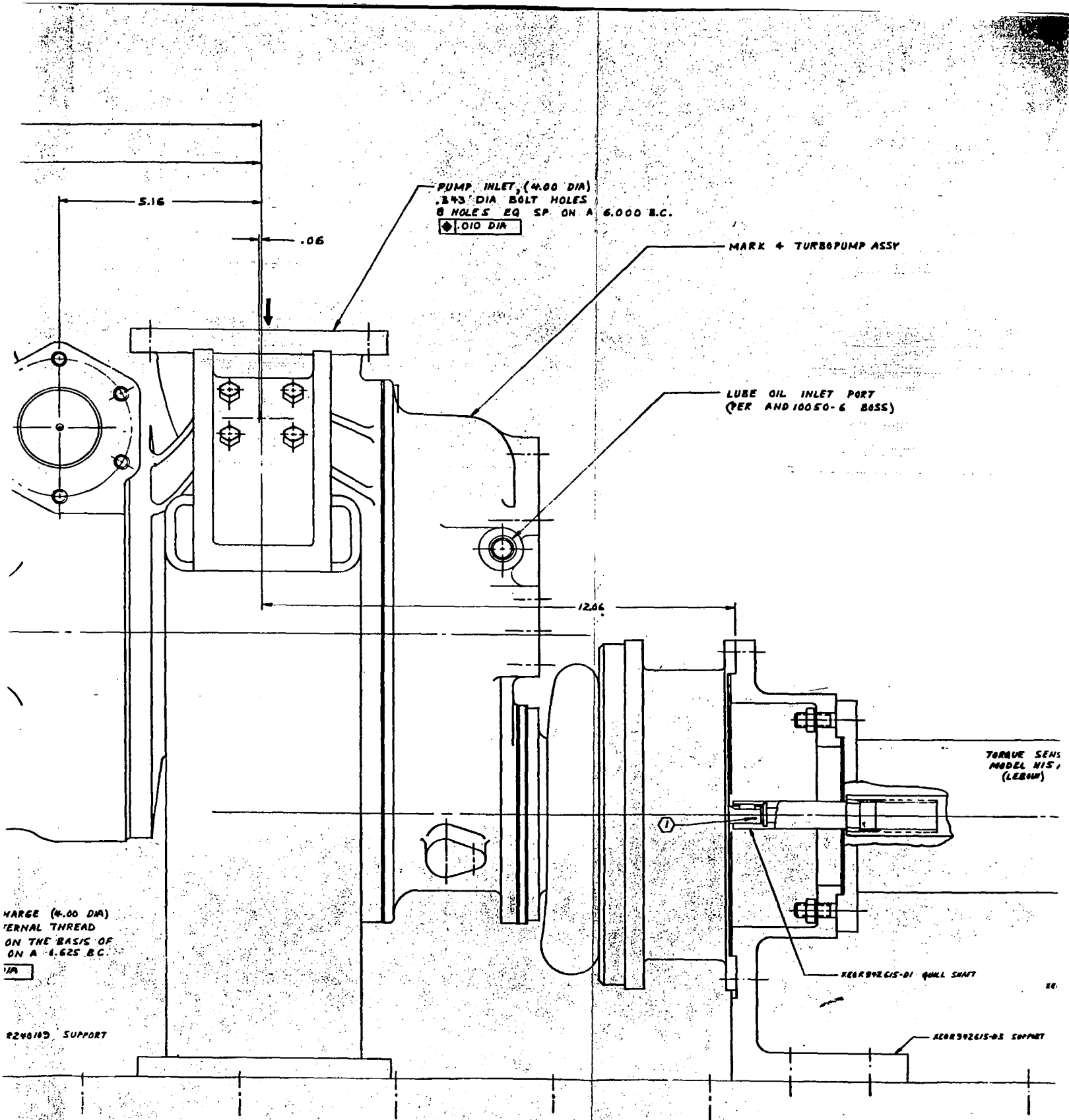

1 DEFLECT END OF SHAFT TO PREVENT

FUEL PUMP

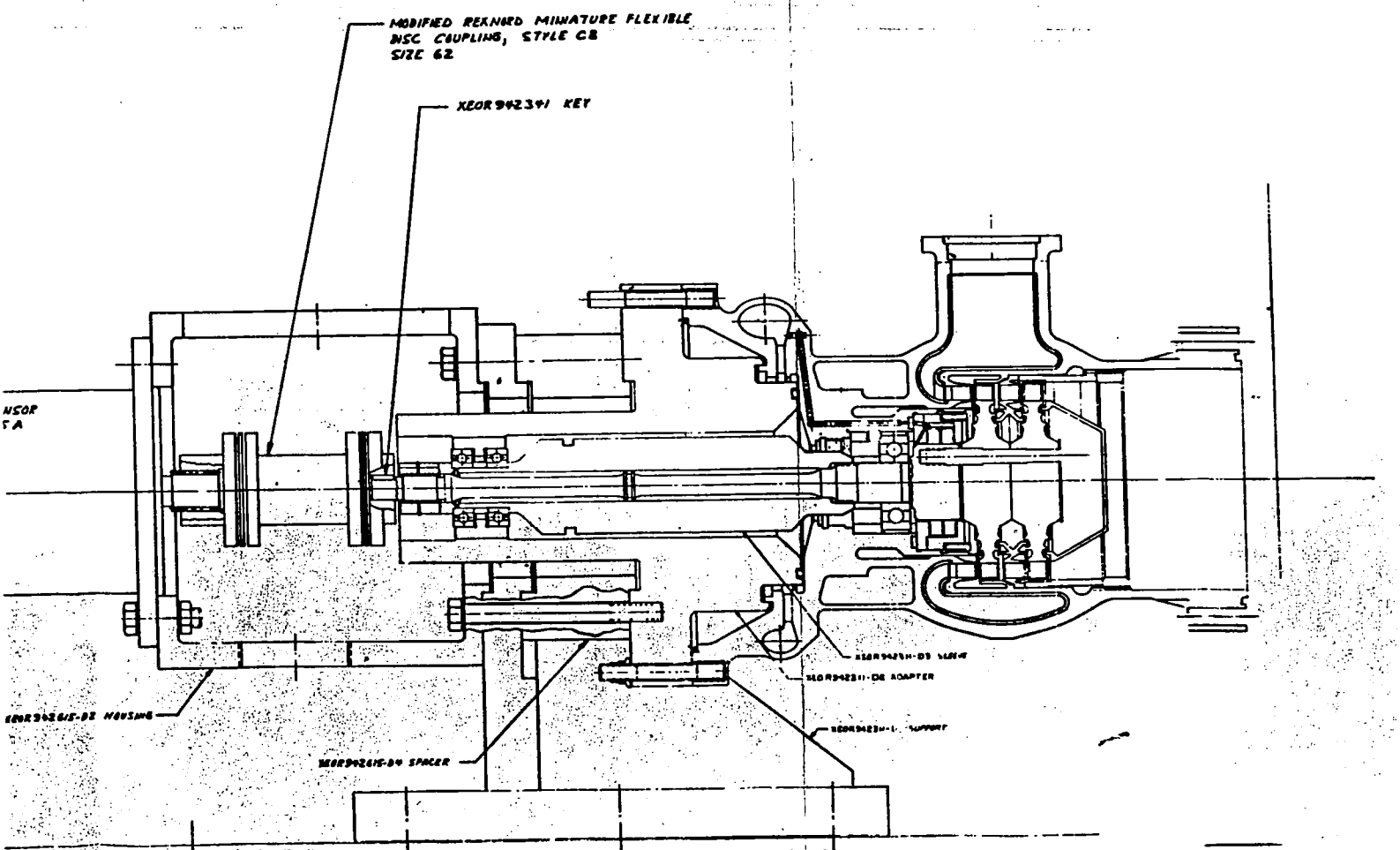

Figure 135. Mark 48-F Turbine Calibration Setup

T KEY MOVEMENT IN THE AXIAL DIRECTION

1P

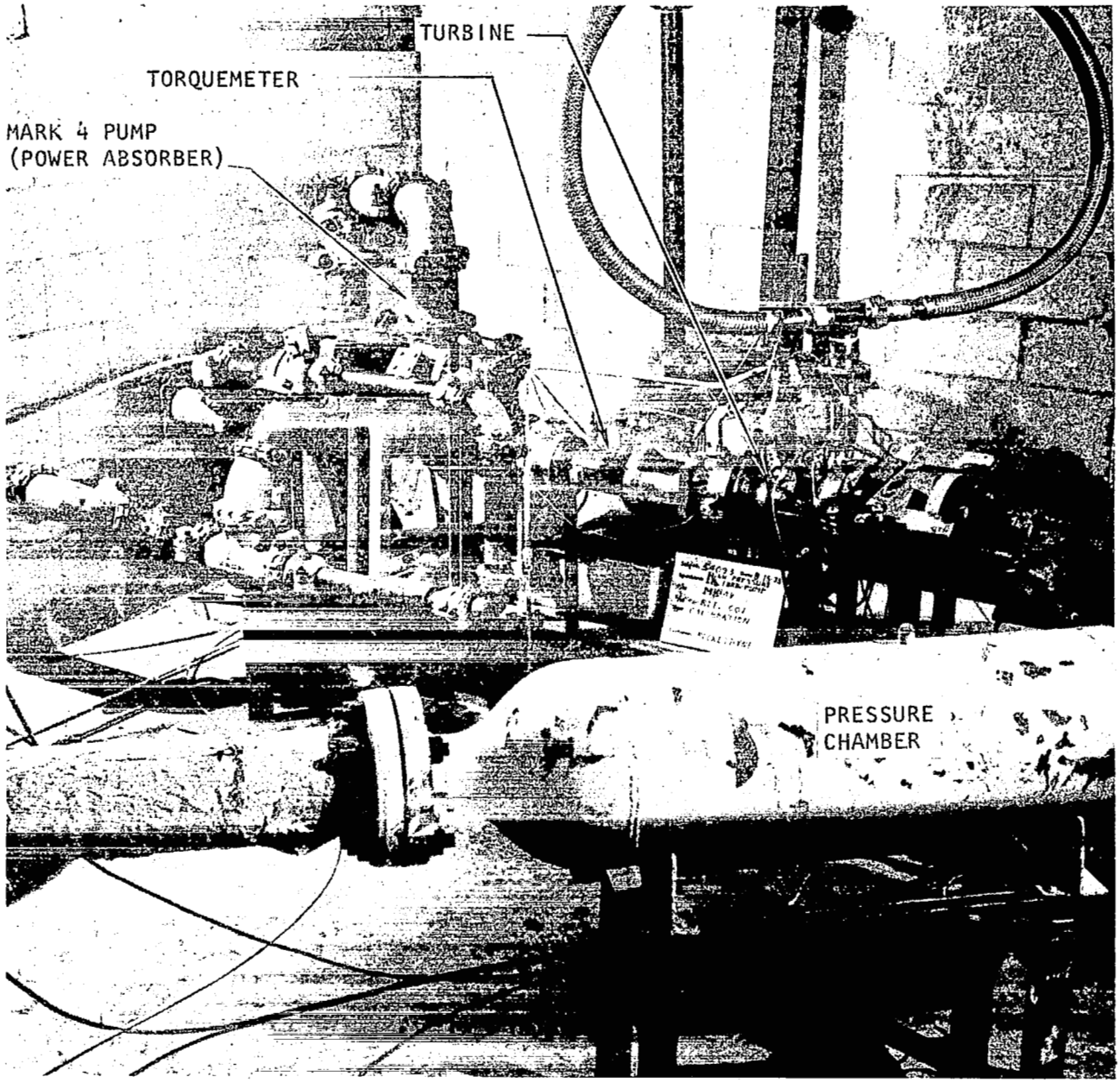

Figure 136. Small, High-Pressure Turbine Calibration Installation (View A)

TABLE 19. MARK 48-F TEST DATA FRO

Run No.	Run Slice	Run Date	Barometric Pressure, mm Hg	Sonic Flow Nozzle Inlet Total Temperature, K	Sonic Flow Nozzle Inlet Static Pressure, N/cm^2	Turbine Inlet Total Temperature, K	Turbine Exit Static Temperature, (T_2), K	Turb Inlet Press N/c
001	1	8-11-75	760.9	256.1	54	267.8	253.4	9
002	1	8-12-75	763.8	255.5	34	265.6	247.2	6
	3		763.3	259.2	45	267.8	255.8	10
	4			259.0	43	268.2	255.0	9
	5			256.7	61	268.1	252.8	13
	6			257.2	68	268.9	257.8	16
003	1	8-13-75	764.8	*	65	253.9	*	12
	2		764.8	*	80	253.9	*	30
	3		763.8	*	94	254.4	*	18
	4		763.8	*	103	254.4	*	24
	5		763.8		136	255.6		33
004	1	8-15-75		253.6	90	266.9	241.7	15
005	1	8-22-75	761.7	249.7	103	261.1	244.4	21
	2		761.7	243.3	110	257.8	235.0	23
	3		761.7	240.6	110	256.1	232.2	22
	4		761.7	238.9	109	255.0		22

*No temperature data recorded.

Run No.	Run Slice	Run Date	Barometric Pressure, in. Hg	Sonic Flow Nozzle Inlet Total Temperature, F	Sonic Flow Nozzle Inlet Static Pressure, psia	Turbine Inlet Total Temperature, F	Turbine Exit Static Temperature (T_2), F	Turb Inlet Press psi
001	1	8-11-75	29.96	1.0	79	22	-3.8	13
002	1	8-12-75	30.06	0	49	18	-15	9
	3		30.05	6.5	65	22	0.5	14
	4			6.2	63	22.8	-1	13
	5			2	88	22.5	-5	19
	6			3	98	24	4	24
003	1	8-13-75	30.11	*	94	-3	*	18
	2		30.11	*	116	-3	*	44
	3		30.07	*	137	-2	*	26
	4		30.07	*	149	-2	*	36
	5		30.07		197	0		48
004	1	8-15-75	30.1	-3.5	130	20.5	-25	23
005	1	8-22-75	29.99	-10.5	150	10	-20	30
	2		29.99	-22	160	4	-37	33
	3		29.99	-27	160	1	-42	33
	4		29.99	-30	158	-1		33

*No temperature data recorded.

)ATA FROM WYLE LABORATORIES, EL SEGUNDO, CALIFORNIA

SI UNITS

ıe atic ure, K	Turbine Inlet Total Pressure, N/cm^2	Turbine Inlet Static Pressure, N/cm^2	Turbine Exit Total Pressure, N/cm^2	Turbine Exit Static Pressure, N/cm^2	Turbine Inlet Manifold Pressure, N/cm^2	Turbine Torque, Nm	Turbine Speed, rad/s	ΔT $(T\text{-}S_R)$, K	Δh J/kg	U/C_{o_R} $(T\text{-}T)$	η_t $(T\text{-}T)$	η_t U/C_{o_R}
	94	86	55	55	9	18.9	947	14.3	0.047	0.165	0.58	3.53
	62	60	34	36	59	11.3	1178	18.3	0.054	0.205	0.64	5.11
	103	100	76	76	98	10.2	1047	11.9	0.030	0.246	0.76	5.07
	93	90	64	63	87	11.1	1035	13.2	0.034	0.225	0.71	3.14
	134	130	92	92	126	12.5	1381	15.3	0.036	0.293	0.76	2.61
	168	163	130	130	162	12.4	1161	11.1	0.026	0.289	0.80	2.77
	126	125	82	81	124	14.1	1698					
	304	165	118	117	163	14.2	1576					
	182	181	126	125	179	13.9	1763					
	248	246	195	195	245	13.6	1586					
	334	330	270	269	332	14.0	1633					
7	159	159	97	97	160		1995	25.3	0.060			
4	212	204	123	120	193	23.2	1773	16.7	0.051	0.316	0.79	2.49
)	231	220	139	142	214	21.1	1978	22.8	0.049	0.362	0.79	2.17
2	228	220	132	137	210	20.3	2153	23.9	0.052	0.382	0.77	2.01
	229	220	132	137	210	19.8	2199		0.051	0.391	0.77	1.98

ENGLISH UNITS

ıe atic ture F	Turbine Inlet Total Pressure, psig	Turbine Inlet Static Pressure, psig	Turbine Exit Total Pressure, psig	Turbine Exit Static Pressure, psig	Turbine Inlet Manifold Pressure, psig	Turbine Torque, in.-lb	Turbine Speed, rpm	ΔT $(T\text{-}S_R)$, F	Δh Btu/lb	U/C_{o_R} $(T\text{-}T)$	η_t $(T\text{-}T)$	η_t U/C_{o_R}
3	137	125	80	79.5	13.1	167	9,050	25.8	12.18	0.1648	0.5815	3.5258
	90	87	50	52	85	100	11,250	33	13.967	0.2052	0.6387	5.1126
5	149	145	110	110	142	91	10,000	21.5	7.677	0.2460	0.7564	5.0748
	135	130	93	91	126	98	9,881	23.8	8.954	0.2251	0.7077	3.1439
	194	188	134	133	183	111	13,193	27.5	9.457	0.2925	0.7627	2.6075
	243	237	189	189	235	110	11,088	20	6.861	0.2886	0.7984	2.7665
	183	182	119	117	180	125	16,215					
	441	239	171	169	237	126	15,044					
	264	263	183	182	260	123	16,841					
	360	357	283	283	356	120	15,148					
	484	479	391	390	482	124	15,597					
	231	230	140	140	232		18,050	45.5	15.711			
	307	296	178	174	280	205	16,938	30	13.329	0.3163	0.7878	2.4906
	335	320	201	206	310	187	18,888	41	12.6638	0.3619	0.7852	2.1697
	330	320	191	198	305	180	20,568	43	13.488	0.3818	0.7687	2.0134
	332	320	191	198	305	175	21,000		13.421	0.3908	0.7734	1.9790

TABLE 20. MARK 48-F TURBINE TEST DATA FROM WYLE LABORATORIES,

(SI UNITS)

Test No.	Test Slice	Test Date 1975	Barometric Pressure, mm Hg	Sonic Flow Nozzle Inlet Total Temperature, K	Sonic Flow Nozzle Inlet Static Pressure, N/cm^2	Turbine Inlet Total Temperature, K	Turbine Exit Total Temperature, K	Turbine Inlet Manifold Pressure (Static), N/cm^2	Turbine Exit Total Pressure, N/cm^2	Turbine Exit Static Pressure, N/cm^2	Tur To
006	2	11/11	761.0	252	65	268	247	159	110	103	
007	1	11/11	761.0	248	83	261	245	138	100	93	
008	1	11/11	761.0	255	48	268	253	83	56	52	
009	2	11/12	762.5	247	112	271	239	203	114	114	
010	1	11/12	761.0	258	172	276	254	345	234	234	
	2	11/12	761.0	253	145	275	249	274	174	165	
011	1	11/13	761.0	253	148	271	248	283	193	190	
	2	11/13	761.0	252	148	271	248	283	193	190	
012	2	11/13	759.5	253	224	269	252	455	338 C	334	
	3	11/13	759.5	251	163	267	250	331	243 C	241	
013	1	11/14	762.0	243	176	262	241	337	214 C	210	
014	1	11/17	756.9	242	228	258	241	427	310 C	303	

- *Lebow Torquemeter data
- Working fluid: GN_2
- C = (Pressure Static, Test) + (Pressure Dynamic, Calculated)

(ENGLISH UNITS)

Test No.	Test Slice	Test Date 1975	Barometric Pressure, in. Hg	Sonic Flow Nozzle Inlet Total Temperature, F	Sonic Flow Nozzle Inlet Static Pressure, psig	Turbine Inlet Total Temperature, F	Turbine Exit Total Temperature, F	Turbine Inlet Manifold Pressure (Static), psig	Turbine Exit Total Pressure, psig	Turbine Exit Static Pressure, psig
006	2	11/11	29.96	- 6.0	94	22.0	-14.5	230	160	150
007	1	11/11	29.96	-13.0	120	9.0	-19.0	200	145	135
008	1	11/11	29.96	0	70	22.0	- 4.0	120	82	75
009	2	11/12	30.02	-16.0	163	27.5	-30.0	295	165	165
010	1	11/12	29.96	5.0	250	37.0	2.0	500	340	340
	2	11/12	29.96	- 4.0	210	34.5	-12.0	398	252	240
011	1	11/13	29.97	- 5.0	215	28.0	-14.0	410	280	275
	2	11/13	29.97	- 6.0	215	27.0	-14.0	410	280	275
012	2	11/13	29.90	- 4.0	325	24.0	- 6.0	660	491 C	485
	3	11/13	29.90	- 9.0	237	21.0	-10.0	480	353.2 C	350
013	1	11/14	30.00	-23.0	255	11.0	-26.5	490	310 C	305
014	1	11/17	29.80	-23.5	331	4.0	-26.0	620	450 C	440

- *Lebow Torquemeter data
- Working fluid: GN_2
- C = (Pressure Static, Test) + (Pressure Dynamic, Calculated)

ATA FROM WYLE LABORATORIES, EL SEGUNDO, CALIFORNIA

(SI UNITS)

Turbine Inlet Manifold Pressure (Static), N/cm^2	Turbine Exit Total Pressure, N/cm^2	Turbine Exit Static Pressure, N/cm^2	Turbine Torque,* N·m	Turbine Speed (N_t), rad/s	Turbine Temperature Drop (ΔT) (Total-to-Total), K	Isentropic Enthalpy Drop (Δh_s), J/kg	Velocity Ratio (U, C_o) (re TU 827) (T-T)	Turbine Efficiency (η_t) (T-T)
159	110	103	14.0	2012	276	0.042		
138	100	93	20.1	1081	271	0.037	0.227	70.8
83	56	52	14.4	1004	270	0.042	0.197	66.3
203	114	114	29.4	1990	287	0.067	0.311	79.1
345	234	234	23.4	2529	277	0.048	0.467	76.8
274	174	165	23.1	2592	281	0.055	0.445	78.7
283	193	190	25.4	2077	279	0.046	0.390	80.9
283	193	190	25.4	2092	278	0.046	0.394	81.6
455	338 C	334	26.0	2264	272	0.036	0.481	77.8
331	243 C	241	23.0	1979	273	0.037	0.414	78.4
337	214 C	210	22.6	2491	276			
427	310 C	303	21.1	2643	272	0.037	0.552	

ENGLISH UNITS)

Turbine Inlet Manifold Pressure (Static), psig	Turbine Exit Total Pressure, psig	Turbine Exit Static Pressure, psig	Turbine Torque,* in.-lb	Turbine Speed (N_t), rpm	Turbine Temperature Drop (ΔT) (Total-to-Total), R	Isentropic Enthalpy Drop (Δh_s), Btu/lb	Velocity Ratio (U, C_o) (re TU 827) (T-T)	Turbine Efficiency (η_t) (T-T)
230	160	150	124	19220	36.5	10.99		
200	145	135	178	10329	28.0	9.59	0.227	70.8
120	82	75	127	9586	26.0	11.00	0.197	66.3
295	165	165	260	19009	57.5	17.40	0.311	79.1
500	340	340	207	24150	39.0	12.42	0.467	76.8
398	252	240	205	24759	46.5	14.38	0.445	78.7
410	280	275	225	19842	42.0	12.01	0.390	80.9
410	280	275	225	19981	41.0	11.99	0.394	81.6
660	491 C	485	230	21620	30.0	9.39	0.481	77.8
480	353.2 C	350	203	18900	31.0	9.67	0.414	78.4
490	310 C	305	200	23796	37.5			
620	450 C	440	187	25247	30.0	9.71	0.552	

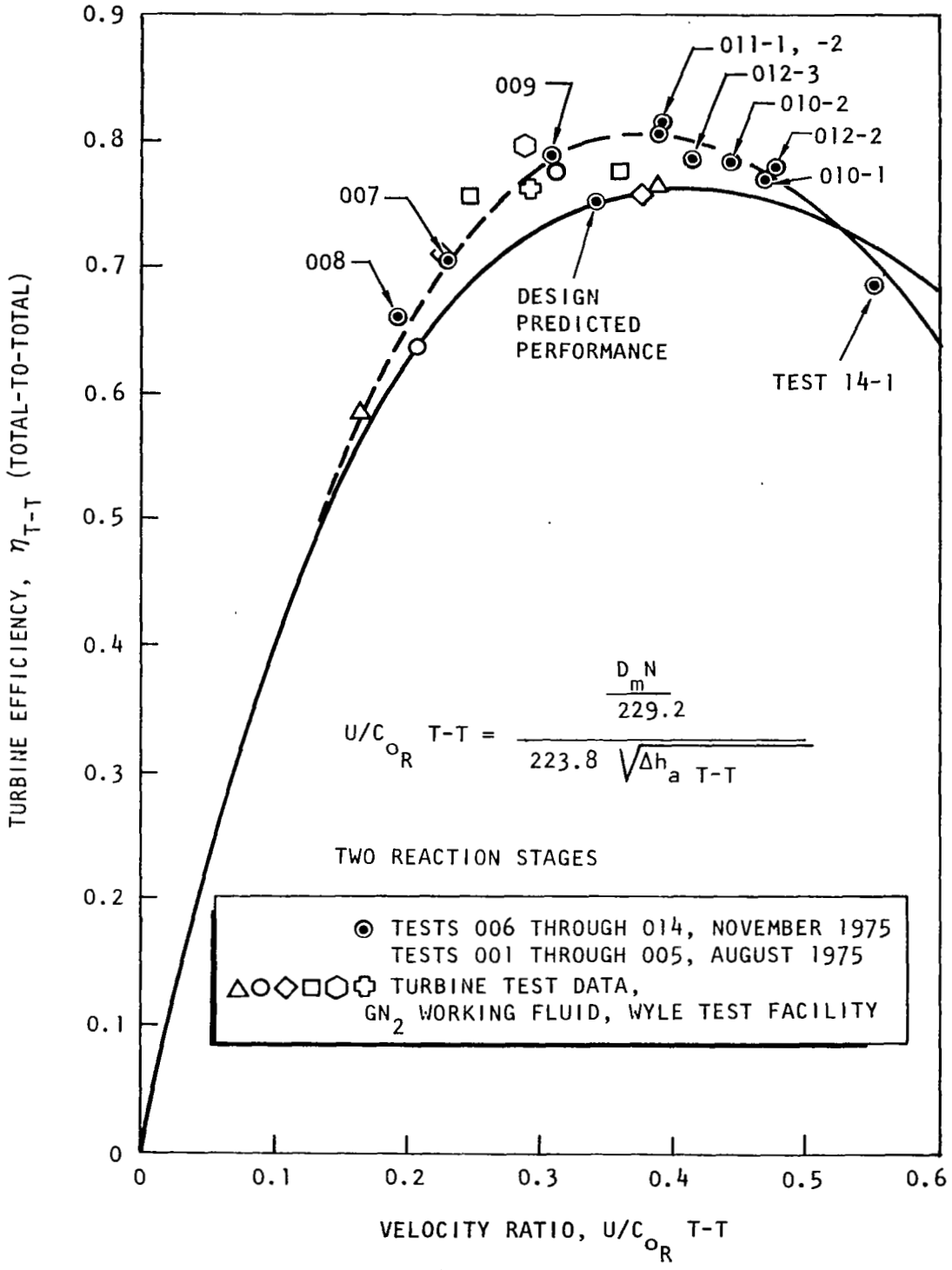

Figure 138. Mark 48-F Turbine Performance

A comparison of the measured performance of the turbine with predicted values shows that, in general, the predicted performance was exceeded. Specifically, at the design velocity ratio of 0.34, the measured efficiency was 79%, 4 percentage points higher than predicted.

Turbopump Testing

Test Discussion. The facility, procedures, and instrumentation used in testing the Mark 48-F turbopump are described in the following.

Facility. Testing of the Mark 48-F turbopump was conducted on Lima Stand in Rocketdyne's Propulsion Research Area at the Santa Susana Field Laboratory. Schematics of the facility for testing with ambient-temperature GH_2 as the turbine propellant, and with a hot-firing gas generator are included in Fig. 139 and 140, respectively.

Countdown Summary. Procedures for conducting specific program tasks for an individual test have been developed for the Lima test facility. The procedures are monitored continuously during the test program, and revised when necessary to achieve a highly reliable test facility operational system. The procedures and countdown are divided between manual and automatic operations. Generally, the pretest procedures are controlled manually, while the actual test is controlled automatically. Table 21 below lists those pretest operational procedures utilized during the testing of the LH_2 turbopump. Appendix C presents the Test Control Logic Block Diagram used during the GH_2 turbine drive testing of the LH_2 turbopump. A review of the logic diagram reveals some instances of manual override operations.

Testing of the LH_2 turbopump was accomplished per the established procedures and control logic system without incident. As the test series progressed, the proficiency of the test countdown increased as a function of the individual systems characterizations.

In the case of the turbopump chilldown and throttle valve setting, precise control of these functions was possible through direct test experience, and proved to be quite repeatable, test to test. In the case of the turbopump chilldown, it was observed that good quality LH_2 propellant inlet conditions (25 K, 45 R) was obtained at (21 N/cm^2) (30-psig) tank pressure and by modulating the turbopump LH_2 flow with the outlet throttle valve. In the case of the test throttle valve position, the pretest GH_2 blowdown tests which characterized the throttle valve and GH_2 spin valve

TABLE 21. LH_2 TURBOPUMP TEST PROCEDURES LIST LIMA STAND - ROCKETDYNE PRA

1.	Pretest Setup
2.	Test Data Sheet
3.	Sequence Test Safety Circuit Checks
4.	LH_2 Turbopump Drying Procedure
5.	Test Conductors Countdown
6.	Critical Parameter Verifications
7.	Comparator Setup Sheet
8.	Sequence Times Setup Sheet

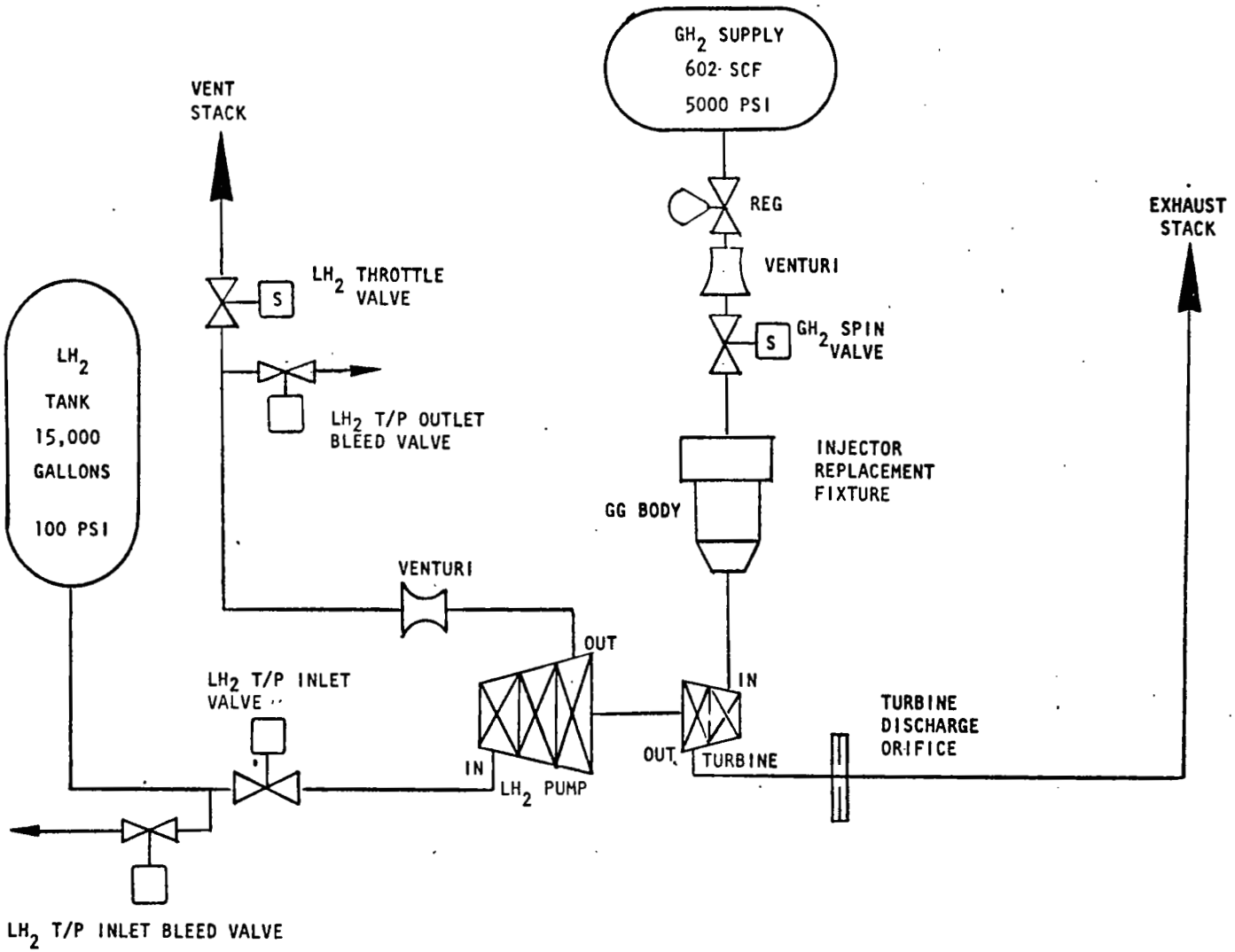

Figure 139. Gaseous Hydrogen Turbine Drive

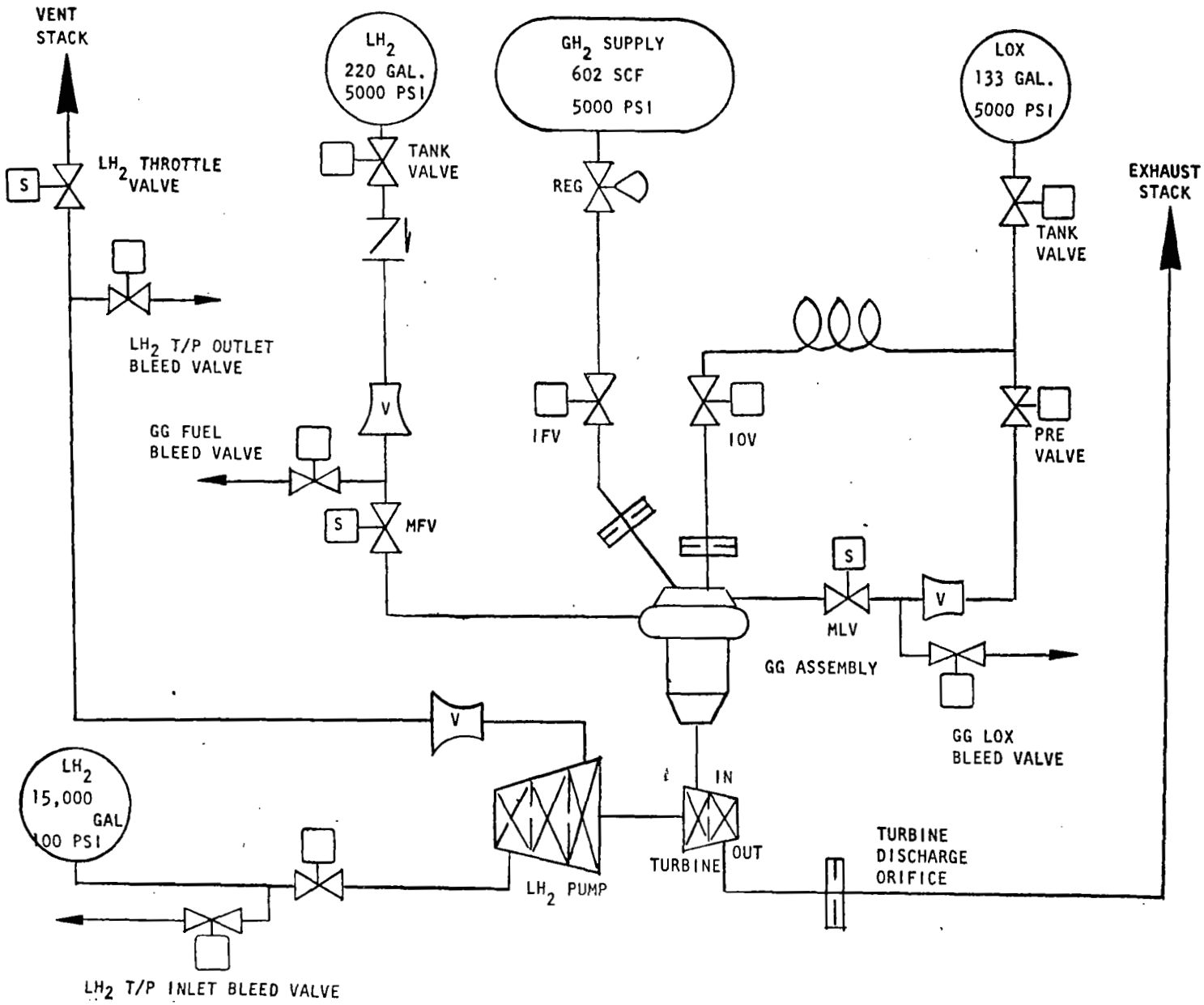

Figure 140. Gas Generator Turbine Drive

operations proved to be an asset in the preliminary settings of the throttle valve to maintain targeted head-flow values.

The countdown, operational, and control functions of the test program were well defined, meeting, in all respects, the requirements set forth in the test plan. Figure 141 is an abbreviated countdown summary applicable for the testing of the Mark 48-F LH_2 turbopump.

- LH_2 Turbopump Chilldown Results. The LH_2 turbopump chilldown procedures followed the normal pretest countdown operations. The chill procedures required a facility line prechill from the LH_2 off-stand storage tank to the turbopump inlet line prevalve prior to introducing LH_2 into the turbopump. The majority of the facility line was vacuum jacketed ($\sim$2/3 total length), while the remaining section was foam and tape insulated. With the LH_2 off-stand tank pressurized to about 21 N/cm^2 (30 psig), a LH_2 run line temperature (bleed flow upstream of the turbopump inlet valve) of about 33 K (-400 F) required about 30 minutes of countdown time. When the facility line was prechilled to 33 K at 21 N/cm^2 (-400 and 300 psig), the turbopump outlet throttle valve was opened to about 10%, then the turbopump inlet valve was opened. LH_2 flow through the turbopump as well as turbopump speed was controlled by the outlet throttle valve until the required LH_2 propellant quality of 25 K at 21 N/cm^2 (45 R at 30 psig) was achieved. The turbopump chill operation required about an additional countdown time of approximately 30 minutes. Total chilldown time for the LH_2 system was about 1 hour of countdown time. As the testing continued, the chilldown techniques were improved until a total chilldown time of only about 20 to 30 minutes was required. Basically, the facility line prechill operation was eliminated, since it was found that adequate chilldown control could be achieved with the turbopump outlet throttle valve and, in addition, a considerable volume of LH_2 was saved in the process. (i.e., For the first test, approximately 26.5 m^3 (7000 gallons) of LH_2 were required, while during the latter tests a total of about 3.8 m^3 (1000 gallons) per test were required.) During the entire test program, acceptable LH_2 inlet quality was achieved for each test to meet the turbopump net positive suction head requirements.

Instrumentation and Redliner. All pressures, temperatures, and flow measurements were recorded on tape by means of the Beckman Model 210 Data Acquisition and Recording System. This system acquires analog data from the transducers, and converts the data to digital form in binary-coded decimal format. The latter is recorded on tapes which are then used for computer processing.

Table 22 presents the instrumentation recorded during the Mark 48-F turbopump testing. Figure 142 is a cross-sectional schematic of the LH_2 turbopump assembly showing the turbopump parameters identification associated with the particular cavity location. Not listed, however, is the high-speed instrumentation which was recorded on FM tape for high-speed analysis of the turbopump rotordynamics. Included in the FM instrumentation were Bently transducers for turbopump shaft movement dynamics and triaxial accelerometers for overall turbopump g-level determination.

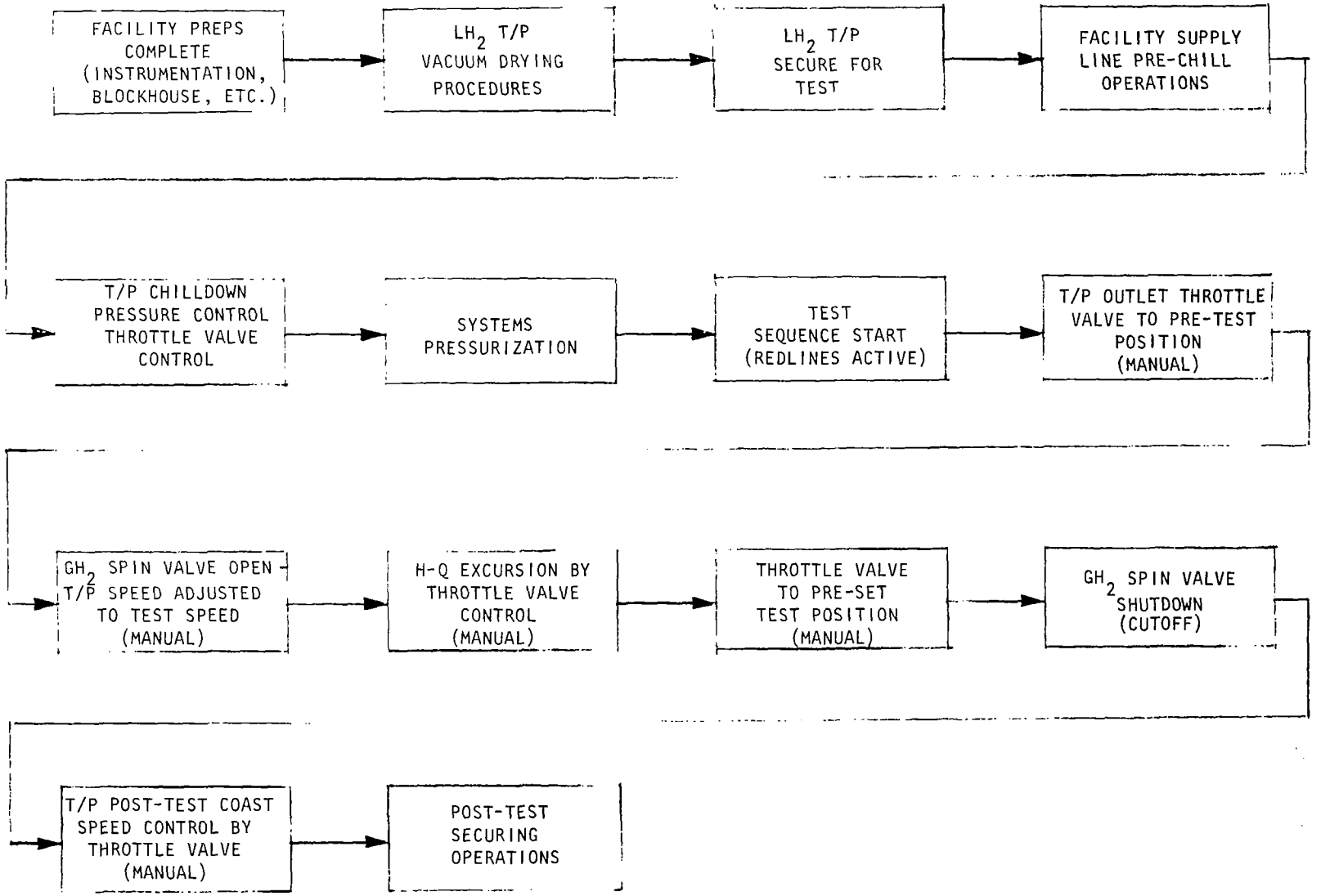

Figure 141. Mark 48-F LH_2 Turbopump Test Countdown Summary

TABLE 22. ADVANCED SPACE ENGINE MARK 48-F HYDROGEN TURBOPUMP TEST INSTRUMENTATION

Parameter	Range (SI Units)	Range (English Units)
Turbine Discharge Temperature	1366 K	2000 F
Turbine Inlet Temperature No. 2	1366 K	2000 F
Turbine Bearing Coolant Temperature	20 K	-425 F
Pump Bearing Coolant Temperature	20 K	-425 F
NAN Power Supply	-	-
LIMA Power Supply	-	-
Temperature Reference Junction	-	-
LH_2 Pump Inlet Temperature No. 1		8.0 MV
LH_2 Pump Inlet Temperature No. 2		8.0 MV
LH_2 Pump Inlet Run Line Temperature		8.0 MV
LH_2 Pump Discharge Temperature No. 1		8.0 MV
LH_2 Pump Discharge Temperature No. 2		8.0 MV
GH_2 Venturi Temperature No. 1		16.0 IC
GH_2 Venturi Temperature No. 2		16.0 IC
GH_2 Venturi Differential Pressure No. 1	241 N/cm^2	350 psi
GH_2 Venturi Differential Pressure No. 2	207 N/cm^2	300 psi
GH_2 Spin Valve Position	-	-
Spin Servo Command	-	-
LH_2 Pump Throttle Valve Position	-	-
GH_2 Venturi Differential Pressure No. 1	348 N/cm^2	500 psi
GH_2 Regulator Upstream Pressure	3480 N/cm^2	5000 psi
Pump Discharge Venturi Throat Pressure	3480 N/cm^2	5000 psi
Low-Pressure LH_2 Tank Pressure	138 N/cm^2	200 psi
Turbine Inlet Static Pressure	3480 N/cm^2	5000 psi
Turbine Manifold Pressure	3480 N/cm^2	5000 psi
Facility Exhaust Duct Pressure	348 N/cm^2	500 psi
Turbine Static Discharge Pressure	3480 N/cm^2	5000 psi

Parameter	Range (SI Units)	Range (English Units)
GH_2 Venturi Upstream Pressure No. 1	3480 N/cm^2	5000 psi
GH_2 Venturi Throat Pressure	3480 N/cm^2	5000 psi
Spin Valve Servo Control Pressure	3480 N/cm^2	5000 psi
Turbine Seal Pressure	3480 N/cm^2	5000 psi
First-Stage Nozzle Pressure	3480 N/cm^2	5000 psi
Turbine Total Discharge Pressure	3480 N/cm^2	5000 psi
Turbine Inlet Total Pressure	3480 N/cm^2	5000 psi
First-Stage Crossover Discharge Pressure	1380 N/cm^2	2000 psi
GH_2 Spin Line Pressure	3480 N/cm^2	5000 psi
Third-Stage Impeller Discharge Pressure	3480 N/cm^2	5000 psi
GH_2 Regulator Outlet Pressure	3480 N/cm^2	5000 psi
Balance Piston Sump Pressure	3480 N/cm^2	5000 psi
LH_2 Pump Venturi Upstream Pressure	3480 N/cm^2	5000 psi
LH_2 Pump Discharge Pressure	3480 N/cm^2	5000 psi
Hydraulic Supply Pressure	2068 N/cm^2	3000 psi
First-Stage Impeller Discharge Pressure	1380 N/cm^2	2000 psi
First-Stage Crossover Inlet Pressure	1380 N/cm^2	2000 psi
First-Stage Crossover Mid-Pressure	1380 N/cm^2	2000 psi
Second-Stage Impeller Front Shroud	3480 N/cm^2	5000 psi
Second-Stage Diffuser Discharge Pressure	3480 N/cm^2	5000 psi
Balance Piston Cavity Pressure	3480 N/cm^2	5000 psi
LH_2 Pump Inlet Pressure No. 1	69	100 psi
LH_2 Pump Inlet Pressure No. 2	241 N/cm^2	350 psi
LH_2 Pump Outlet Throttle Valve Pressure	3480 N/cm^2	5000 psi
Throttle Valve Servo Control Pressure	3480 N/cm^2	5000 psi
Pump Speed	12,560 rad/s	120,000 rpm

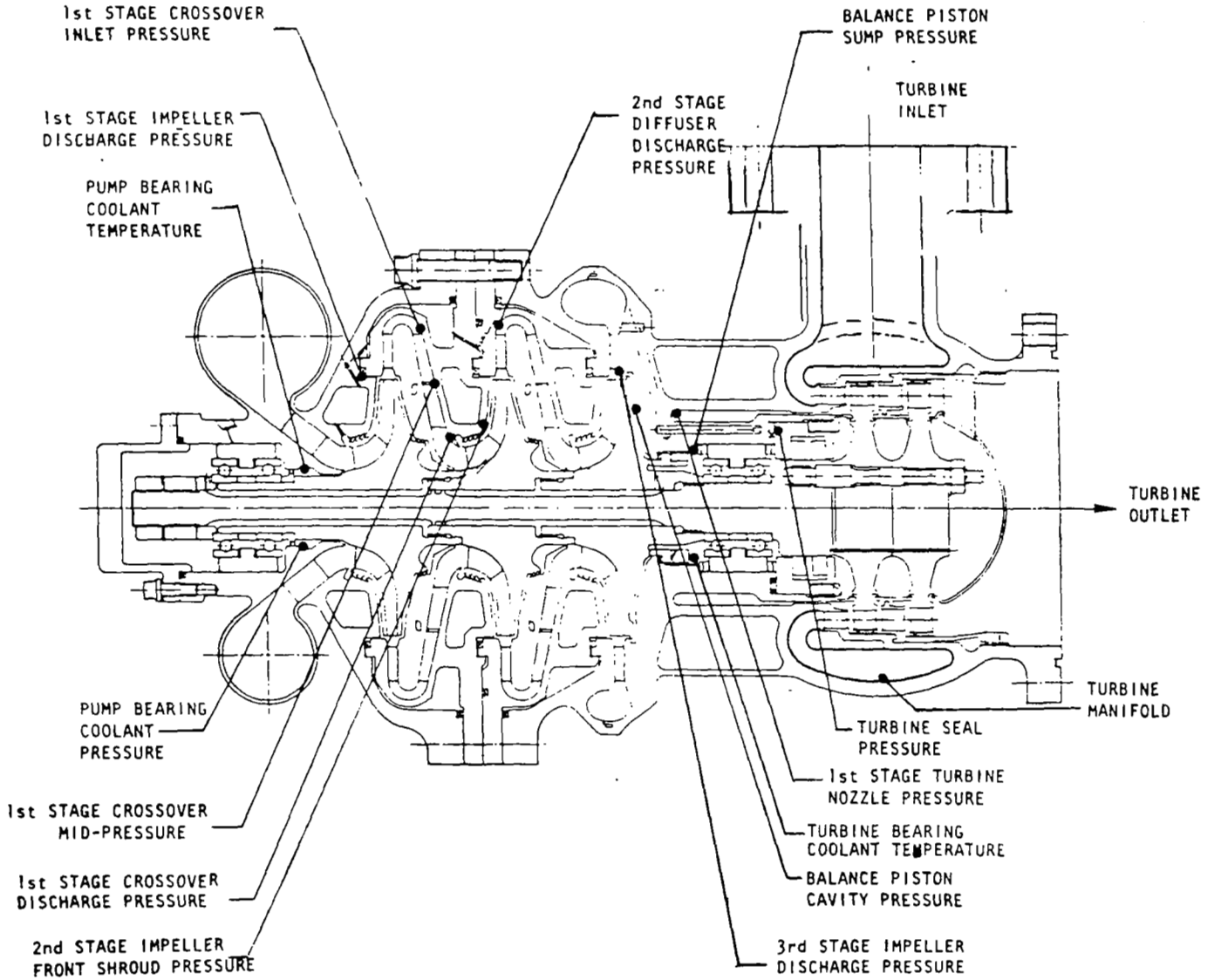

Figure 142. LH_2 Turbopump

During the testing, redlines were assigned to certain key parameters. These redlines in some instances were adjusted for the particular turbopump speed range being evaluated. Tables 23 through 26 present those redlines applicable for turbopump speeds of 1990, 4710, 6280, and 9947 rad/s (19,000, 45,000, 60,000, and 95,000 rpm), respectively.

Test Discussion. Testing of the Mark 48-F turbopump assembly began on 31 March 1976 at the Rocketdyne Propulsion Research Area (PRA). A total of 10 turbopump tests for an accumulated run duration of 884 seconds were satisfactorily conducted on LH_2 turbopump, S/N 01-0. Table 27 presents a summary of those tests conducted, while a more detailed discussion of the tests is presented below.

Test No. 1 (016-001)

Test Date: 3-31-76

Duration: 155 seconds

Objectives:
1. Obtain LH_2 turbopump chilldown characteristics with the turbopump LH_2 inlet pressurized to 21 N/cm^2 (30 psia).
2. Determine the integrity of the turbopump at the idle-mode speed of 1990 rad/s (19,000 rpm). Map the head-flow characteristics by manually adjusting the turbopump speed and flow. Evaluate the turbine discharge back-pressure orificing.

Results: Countdown proceeded without any problems. After sequence start, the turbopump outlet throttle valve was adjusted to 55% to ensure a safe pump outlet back-pressure level for the first test. The GH_2 spin valve was slowly opened manually until a head rise and flow was indicated on the controller operator's X-Y plotter. The turbopump speed was increased manually by further opening of the GH_2 spin valve while adjusting the turbopump outlet throttle valve to obtain the nominal targeted conditions. The test was terminated prematurely due to a low indicated turbopump discharge pressure for the indicated speed and flow valves. Turbopump shutdown was smooth, with no indication of erratic speed behavior.

Analysis: Posttest analysis revealed that the turbopump shaft speed data display was in error by a factor of four. The actual average speed was determined by oscilloscope to be about 523 rad/s (5000 rpm), corresponding to the recorded low turbopump outlet pressure. A maximum speed of 1047 rad/s (10,000 rpm) was achieved (display = 4190 rad/s, (40,000 rpm), but was reduced by control of the GH_2 spin valve due to the erroneous speed display. The cause of the speed display malfunction was traced to the Anadex system. For the next test, the Anadex system was adjusted to give the correct speed indication.

TABLE 23. MARK 48-F TURBOPUMP REDLINES

(1990 rad/s; 19,000 rpm)

Parameter (SI Units)	Automatic	Visual
Pump Inlet Temperature (No. 1), K	25.6 (max)	
Pump Inlet Pressure (No. 2) N/cm^2		Blueline: 52 (min) Redline: 38 (min)
Speed, rad/s	2722	2722 (max)
Pump Bearing Coolant Temperature, K		ΔT = +6 degrees after stabilization
Turbine Bearing Coolant Temperature, K		ΔT = +6 degrees after stabilization
Pump Discharge Pressure, N/cm^2	689	
Balance Piston Cavity Pressure, N/cm^2		$69 < P_{cav} < 207$
Bently Transducer (Radial), mm		0.25
Bently Transudcer (Axial), mm		0.25
Accelerometer, Pump (Radial*), g rms		20
Accelerometer (Axial*), g rms		20
Accelerometer, Turbine (Radial*), g rms	20	
Turbine Inlet Pressure, N/cm^2		103 (max)
*2000 Hz Low-Pass Filter		Target Speed = 1989 rad/s

Parameter (English Units)	Automatic	Visual
Pump Inlet Temperature (No. 1), R	46 (max)	
Pump Inlet Pressure (No. 2), psig		Blueline: 75 (min) Redline: 55 (min)
Speed, rpm	26,000	26,000 (max)
Pump Bearing Coolant Temperature, R		ΔT = +10 degrees after stabilization
Turbine Bearing Coolant Temperature, R		ΔT = +10 degrees after stabilization
Pump Discharge Pressure, psig	1000	
Balance Piston Cavity Pressure, psig		$100 < P_{cav} < 300$
Bently Transducer (Radial), inch		0.010
Bently Transducer (Axial), inch		0.010
Accelerometer, Pump (Radial*), g rms		20
Accelerometer (Axial*), g rms		20
Accelerometer, Turbine (Radial*) g rms	20	
Turbine Inlet Pressure, psig		150
*2000 Hz Low-Pass Filter		Target Speed = 19,000 rpm

TABLE 24. MARK 48-F TURBOPUMP REDLINES

(4710 rad/s; 45,000 rpm)

Parameter (SI Units)	Automatic	Visual
Pump Inlet Temperature (No. 1), K	25.6 (max)	
Pump Inlet Pressure (No. 2), K		Blueline: 52 (min) Redline: 38 (min)
Speed, rad/s	10,160	10,160
Pump Bearing Coolant Temperature, K		ΔT = 6 degrees after stabilization
Turbine Bearing Coolant Temperature, K		ΔT = 6 degrees after stabilization
Pump Discharge Pressure, N/cm^2	2068	
Balance Piston Cavity Pressure N/cm^2		$207 < P_{cav} < 689$
Bently Transducer (radial), mm		0.25
Bently Transducer (Axial), mm		0.25
Accelerometer, Pump (Radial*), g rms		20
Accelerometer (Axial*), g rms		20
Accelerometer, Turbine, Radial*, g rms	20	
Turbine Inlet Pressure, N/cm^2		517 (max)
*2000 Hz Low-Pass Filter		Target Speed = 4712 rad/s

Parameter (English Units)	Automatic	Visual
Pump Inlet Temperature (No. 1), R	46 (max)	
Pump Inlet Pressure (No. 2), psig		Blueline: 75 (min) Redline: 55 (min)
Speed, rpm	97,000	97,000
Pump Bearing Coolant Temperature, R		ΔT = +10 degrees after stabilization
Turbine Bearing Coolant Temperature, R		ΔT = +10 degrees after stabilization
Pump Discharge Pressure, psig	3000	
Balance Piston Cavity Pressure, psig		$300 < P_{cav} < 1000$
Bently Transducer (Radial), inch		0.010
Bently Transducer (Axial), inch		0.010
Accelerometer, Pump (Radial*), g rms		20
Accelerometer, (Axial*), g rms		20
Accelerometer, Turbine (Radial*), g rms	20	
Turbine Inlet Pressure, psig		750 (max)
*2000 Hz Low-Pass Filter		Target Speed = 45,000 rpm

TABLE 25. MARK 48-F TURBOPUMP REDLINES

(6280 rad/s, 60,000 rpm)

Parameter (SI Units)	Automatic	Visual
Pump Inlet Temperature (No. 1), K	25 (max)	
Pump Inlet Pressure (No. 2), N/cm^2		{Blueline: 59 (min) {Redline: 48 (min)
Speed, rad/s	10,160	10,160 (max)
Pump Bearing Coolant Temperature, K		ΔT = +6 degrees after stabilization
Turbine Bearing Coolant Temperature, K		ΔT = +6 degrees after stabilization
Pump Discharge Pressure, N/cm^2	3447	
Balance Piston Cavity Pressure, N/cm^2		$345 < P_{cav} < 1241$
Bently Transducer (Radial), mm		0.25
Bently Transducer (Axial), mm		0.25
Accelerometer, Pump (Radial*), g rms		20
Accelerometer (Axial*), g rms		20
Accelerometer, Turbine (Radial*), g rms	20	
Turbine Inlet Pressure, N/cm^2		1034 (max)
*2000 Hz Low-Pass Filter		Target Speed = 6282 rad/s

Parameter (English Units)	Automatic	Visual
Pump Inlet Temperature (No. 1), R	45 (max)	
Pump Inlet Pressure (No. 2), psig		{ Blueline: 85 (min) { Redline: 70 (min)
Speed, rpm	97,000	97,000 (max)
Pump Bearing Coolant Temperature, R		ΔT = +10 degrees after stabilization
Turbine Bearing Coolant Temperature, R		ΔT = +10 degrees after stabilization
Pump Discharge Pressure, psig	5000	
Balance Piston Cavity Pressure, psig		$500 < P_{cav} < 1800$
Bently Transducer (Radial), inch		0.010
Bently Transducer (Axial), inch		0.010
Accelerometer, Pump (Radial*), g rms		20
Accelerometer, (Axial), g rms		20
Accelerometer, Turbine, (Radial*), g rms	20	
Turbine Inlet Pressure,		1500 (max)
*2000 Hz Low-Pass Filter		Target Speed = 60,000 rpm

TABLE 26. MARK 48-F TURBOPUMP REDLINES

(9947 rad/s; 95,000 rpm)

Parameter (SI Units)	Automatic	Visual
Pump Inlet Temperature (No. 1), K	25 (max)	
Pump Inlet Pressure (No. 2) N/cm^2		Blueline: 59 (min) Redline: 48 (min)
Speed, rad/s	10,160	10,160
Pump Bearing Coolant Temperature, K		ΔT = 6 degrees after stabilization
Turbine Bearing Coolant Temperature, K		ΔT = 6 degrees after stabilization
Pump Discharge Pressure, N/cm^2	3447	
Balance Piston Cavity Pressure, N/cm^2		$965 < P_{cav} < 2895$
Bently Transducer (Radial), mm		0.25 (max)
Bently Transducer (Axial), mm		0.25 (max)
Accelerometer, Pump (Radial*), g rms		20
Accelerometer (Axial*), g rms		20
Accelerometer, Turbine (Radial*), g rms	20	
*2000 Hz Low-Pass Filter	Target Speed = 9947 rad/s	

Parameter (English Units)	Automatic	Visual
Pump Inlet Temperature (No. 1), R	45 (max)	
Pump Inlet Pressure (No. 2), psig		Blueline: 85 (min) Redline: 70 (min)
Speed, rpm	97,000	97,000
Pump Bearing Coolant Temperature, R		ΔT = +10 degrees after stabilization
Turbine Bearing Coolant Temperature, R		ΔT = +10 degrees after stabilization
Pump Discharge Pressure, psig	5000	
Balance Piston Cavity Pressure, psig		$1400 < P_{cav} < 4200$
Bently Transducer (Radial), inch		0.010 (max)
Bently Transducer (Axial), inch		0.010 (max)
Accelerometer, Pump (Radial*), g rms		20
Accelerometer (Axial*), g rms		20
Accelerometer, Turbine (Radial*), g rms	20	
*2000 Hz Low-Pass Filter	Target Speed = 95,000 rpm	

TABLE 27. ADVANCED SPACE ENGINE MARK 48-F HYDROGEN TURBOPUMP TEST HISTORY

(TURBOPUMP S/N 01-0)

Test No.	Date	Duration, Seconds	Accumulated		Remarks
			Starts	Time, Seconds	
016-001	3-31-76	155	1	155	1047 rad/s (10,000 rpm) maximum speed. Average speed of 524 rad/s (5000 rpm). Shaft speed display error by factor of 4. Cutoff due to low indicated discharge pressure.
016-002	3-31-76	33	2	188	Target N = 1989 rad/s (19,000 rpm). Maximum actual N = 1619 rad/s (15,464 rpm). Shaft speed display high by factor of 2. Test cut off erroneously by pump discharge pressure redline.
016-003	4-7-76	90	3	264	Target N = 4712 rad/s (45,000 rpm). Reached 1187 rad/s (11,333 rpm). Shaft speed count in error by factor of 2. Test cutoff due to fire in facility pump inlet line instrumentation fitting.
016-004	4-7-76	133	4	397	Target N = 4712 rad/s (45,000 rpm). Reached 3926 rad/s (37,500 rpm). Test cutoff by erroneous overspeed indication.
016-005	4-7-76	73	5	470	Target N = 4712 rad/s (45,000 rpm). Reached 4712 rad/s (45,000 rpm). Test cutoff by turbine radial accelerometer VSC.
016-006	4-7-76	168	6	638	Target N = 6282 rad/s (60,000 rpm). H-Q excursion at 4712 and 6282 rad/s (45,000 and 60,000 rpm). Test cutoff due to turbine bearing coolant temperature drifting off scale (-355 F).
016-007	4-9-76	31	7	669	Target N = 9423 rad/s (90,000 rpm). Reached 6837 rad/s (65,300 rpm). Cutoff by turbine radial VSC (10 g rms). Shifted turbine radial accel to observer oscilloscope.
016-008	4-9-76	31	8	700	Target N = 9423 rad/s (90,000 rpm). Reached 7853 rad/s (75,000 rpm). Speed limited by available GH_2 pressure (started with 2930 N/cm^2 (4250-psig) tank pressure).
016-009	4-15-76	36	9	736	Target N = 9423 - 9947 rad/s (90,000 - 95,000 rpm). Reached 9737 rad/s (93,000 rpm). Shaft speed display count lost. Pump bearing coolant temperature went off scale (-355 F).
016-010	4-15-76	148	10	884	Target N = 4712 rad/s (45,000 rpm). Actual N = 4712 rad/s 45,000 rpm.

Test No. 2 (016-002)

Test Date: 3-31-76

Duration: 33 seconds

Objectives: 1. Determine the integrity of the turbopump at the idle-mode speed of 1990 rad/s (19,000 rpm). Map the head-flow characteristics by manually adjusting the turbopump speed and flow. Evaluate the turbine discharge back-pressure orificing.

Results: Countdown proceeded without any problems. Based on the first test results, the throttle valve test position was readjusted to about 35% open. The start sequence was smooth with no problems, but the test was terminated prematurely by the turbopump discharge pressure redline 690 N/cm^2 (1000 psig maximum).

Analysis: It was determined that the cutoff was erroneous and, in fact, the pump discharge pressure was about nominal for the actual pump speed. The problem was traced to a pretest pump discharge transducer change. On the first test, 0 to 3445 N/cm^2 (0 to 5000 psig) transducer was used but because of the resolution on the X-Y plotter a 0 to 345 N/cm^2 (0 to 500 psig) transducer was installed to enable a more precise real time evaluation by the controller operator. The full-scale voltage output of the 3445 N/cm^2 (5000 psig) transducer was the same as the full-scale coutput of the 345 N/cm^2 (500 psig) transducer, but the comparator circuit sensitivity was not adjusted. Therefore, the redline circuit erroneously obtained a high discharge pressure electronic signal and automatically initiated cutoff. The speed monitor display system also malfunctioned and was in error by a factor of two. Actual turbopump speed obtained was 1619 rad/s (15,464 rpm). It was determined that the problem was associated with the type of Anadex system being used. Another type of Anadex system was installed to be more compatible with the turbopump speed monitoring system.

Test No. 3 (016-003)

Test Date: 4-7-76

Duration: 90 seconds

Objectives: 1. Map the turbopump performance at 4712 rad/s (45,000 rpm). Mapping to include a flow/speed ratio range of 0.7 to 1.3 of nominal.

2. Evaluate the turbine discharge backpressure orificing.

Results: The test was terminated prematurely by an observer due to a fire in the vicinity of the turbopump.

Analysis: The fire was caused by a loose B-nut on instrumentation in the LH_2 system. Maximum rpm obtained was 1187 rad/s (11,333 rpm); however, the speed data display was again off by a factor of two, but indicated a real time display of nearly 240000 rad/s (23,000 rpm). Since the H-Q-rpm values for these tests were falling on the X-Y plotter precalculated mapping lines, it was decided to use the X-Y plotter exclusively to control the turbopump operation.

Test No. 4 (016-004)

Test Date: 4-7-76

Duration: 133 seconds

Objective:
1. Obtain stabilized turbopump performance at 1989 rad/s (19,000 rpm) for real time manual data acquisition.
2. Map the turbopump performance at 4712 rad/s (45,000 rpm). Mapping to include a flow/speed ratio range of 0.7 to 1.3 of nominal.
3. Evaluate the turbine discharge backpressure orificing.

Results: The turbopump real time manual data acquisition at 1989 rad/s (19,000 rpm) was successfully obtained. The test was terminated prematurely by the turbopump overspeed redline during the speed increase from 1989 to 4712 rad/s (19,000 to 45,000 rpm) level.

Analysis: Maximum turbopump rpm achieved was about 3926 rad/s (37,500 rpm). Actual speed redline was set at 4188 rad/s (40,000 rpm). Turbopump operation appeared normal; therefore, the redline was readjusted to 10,516 rad/s (97,000 rpm) maximum, and another test was attempted.

Test No. 5 (016-005)

Test Date: 4-7-76

Duration: 73 seconds

Objectives:
1. Map the turbopump performance at 4712 rad/s (45,000 rpm). Mapping to include a flow to speed ratio range of 0.7 to 1.3 of nominal.
2. Evaluate the turbine discharge back-pressure orificing.

Results: The targeted 4712 rad/s (45,000 rpm) was achieved, but the test was terminated prematurely by the Vibration Safety Cutoff (VSC) device when the turbine radial accelerometer exceeded 10 g rms).

Analysis: All turbopump performance values appeared normal. The data obtained by the turbine radial accelerometer appeared to be in error. Bently transducers and the remaining two turbopump accelerometer data appeared normal. The turbine radial accelerometer was replaced prior to the next test.

Test No. 6 (016-006)

Test Date: 4-7-76

Duration: 168 seconds

Objectives:
1. Map the turbopump performance at 4712 rad/s (45,000 rpm). Mapping to include a flow to speed ratio range of 0.7 to 1.3 of nominal.
2. Map the turbopump performance at 6282 rad/s (60,000 rpm). Mapping to include a flow/speed ratio range of 0.7 to 1.3 of nominal.
3. Evaluate the turbine back-pressure orificing.

Results: Objectives obtained satisfactorily. The best was terminated near the completion of the H-Q excursion at 6282 rad/s (60,000 rpm) due to the turbine bearing coolant temperature slowly drifting off the chart scale 58 K, (-355 F).

Analysis: An analysis of the turbine pressure ratio revealed a value of 1.44 per the predicted value. Actual turbine back-pressure orifice consisted of nine orifices of approximately equal dimension installed in a facility adapter, P/N 99RS010280. The actual geometrical total area of the turbine discharge orifice(s) is 4.1 cm^2 (0.636 $in.^2$) with well-rounded entrances. For the next test, the turbine bearing coolant temperature chart was rescaled, since no abrupt temperature rise or anomaly was indicated by the data. Following the test, the raw data signal of the turbopump rpm was analyzed from the high-speed FM tape. From the analysis, it was evident that the waveform produced by the circuit was varying as a function of turbopump speed. A detailed explanation of the speed monitoring problem follows.

Figure 143 schematically represents the speed monitoring device used for the Mark 48-F LH_2 turbopump. A permanent magnet (PM) pickup operates by coupling the flux (ϕ) produced (via an internal PM) across the gap (G) being monitored (Fig. 143). As the rotating body (turbopump shaft) moves past the sensing tip of the permanent

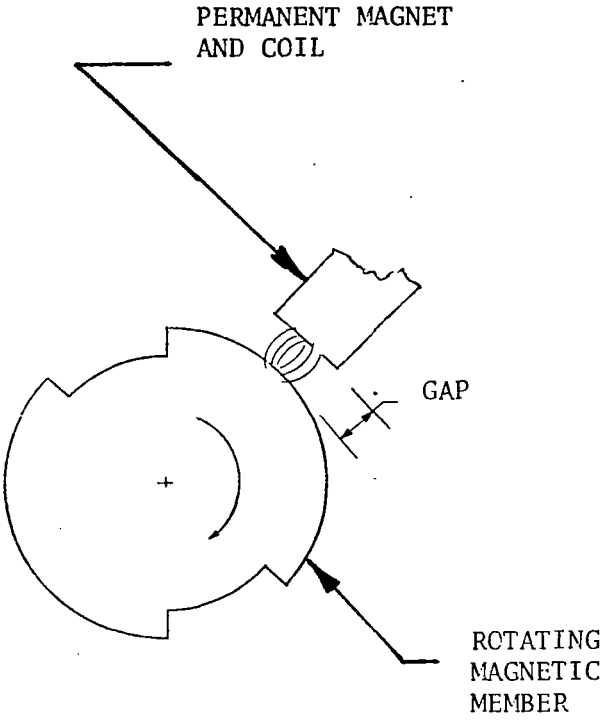

Figure 143. Original Mark 48-F Speed Pickup System

magnet with an angular velocity (ω), the flux across the gap varies as a function of both ω and G [$\phi = f(\omega, G)$]. The voltage induced in the coil of the pickup is expressed by the following equation:

$$e = K\frac{d\phi}{dt} = K\frac{\partial[f(\omega,G)]}{\partial t}$$

(Lenz's law)

If ϕ does not vary sinusoidally (irregular or discontinuous gap variations), $K\, d\phi/dt = \partial$ will not be a pure sinusoid but will contain multiple harmonics corresponding to $\partial(G)/t$. The interaction of the pickup source impedance and the total load impedance (including line effects) causes these harmonics to shift in amplitude and phase as ω varies. Fixed frequency filters become impractical for filtering out these harmonics over wide ranges of ω. Figure 144A shows a low-frequency waveform recorded from the Mark 48-F speed pickup. The distortion resulting from the notched shaft configuration is readily apparent. Figure 144B shows the same pickup waveform distorted at higher frequencies. The effects of harmonics shifting becomes readily apparent. As the waveform becomes more and more distorted, with increasing ω, designing circuitry with sensing thresholds and adequate sensitivity becomes difficult, that is, avoiding the distortion while simultaneously sensing the pulse, becomes impractical.

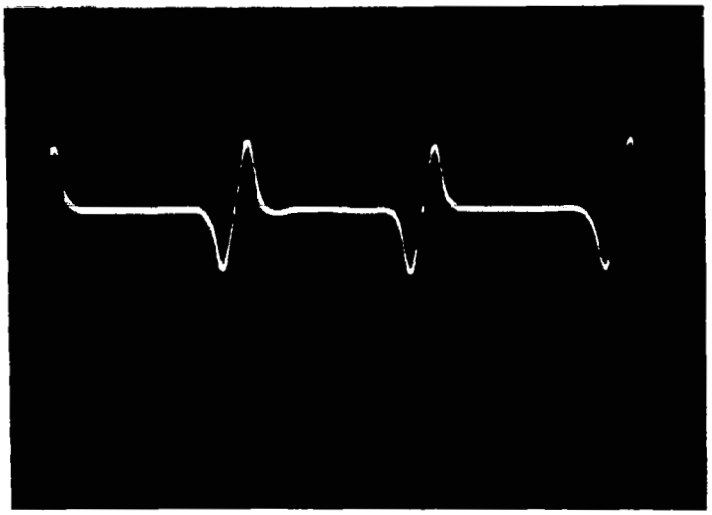

A. LOW-FREQUENCY WAVEFORM

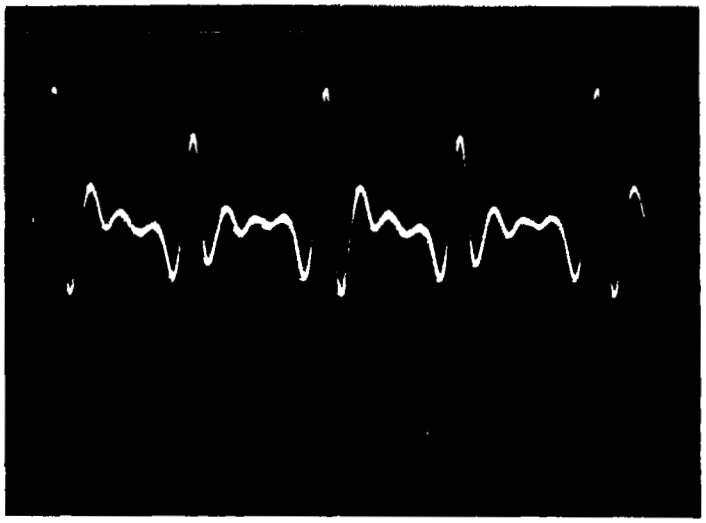

B. HIGH-FREQUENCY WAVEFORM

Figure 144. High-Speed FM Tape Analysis, Mark 48-F LH_2 Turbopump rpm Test 016-006

Figures 145A through 145C represent spectral plots that show the relative harmonic content of the waveform of Fig. 144A and 144B (frequency is the abcissa while amplitude is the ordinate) at different frequencies. Figure 145D (Isoplot) is a similar plot, at reduced amplitude, and shows the harmonic shift at 4-second intervals as ω is increased from zero to 6282 rad/s (60,000 rpm).

The answer to the speed monitoring problem appears to be modifying the contour of the rotating surface so that ϕ varies sinusoidally with the minimum harmonic content. This was an impractical modification to the Mark 48-F turbopump at this time; therefore, a threshold triggering circuit was designed. Figure 146 represents the waveform at about 6282 rad/s (60,000 rpm) taken from the FM tape of test 016-006. Peaks A and B are the pulses produced by the two notched surfaces (evidently a small difference in geometry exists between slot A and slot B resulting in the difference in pulse heights) while peaks C, D, and E are the distortions produced by the harmonics. The threshold monitor circuit was designed to count only those waveform voltage amplitudes greater than the indicated level, H, of Fig. 146. Thus, the distortion produced by the system was ignored for all voltage levels below, H.

Note: During the assembly and checkout of the Mark 48-0 turbopump speed monitoring device, the information and recommendations derived from the LH_2 turbopump testing was used to design the speed-pickup, rotating-shaft geometry shown in Fig. 147A. Figure 147B represents the output of the same pickup (at 2094 rad/s, 20,000 rpm) when installed with the modified shaft design. Consistent outputs were monitored from 1047 to 3141 rad/s (10,000 to 30,000 rpm). It appears that the rotating chord (represented by the flat surface of Fig. 147A) causes the flux to vary more smoothly than the LH_2 turbopump notched configuration, although the waveform is still not a pure sinusoid. However, enough improvement in the waveform has been achieved to produce a usable signal. The distortion is sufficiently low so that effective thresholds and sensitivity values can be set.

Test No. 7: (016-007)

Test Date: 4-9-76

Duration: 31 seconds

Objective:
1. Achieve 9423 rad/s (90,000 rpm) for a stabilized period to evaluate the turbopump integrity and performance.
2. Evaluate turbopump speed and monitor threshold counting circuit.

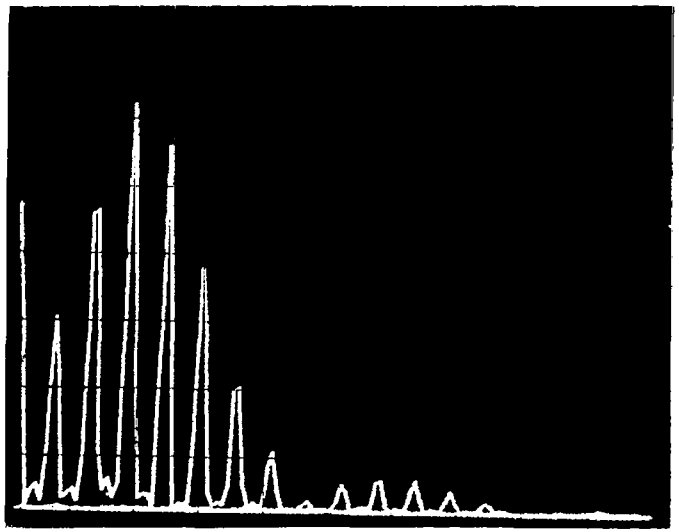

A

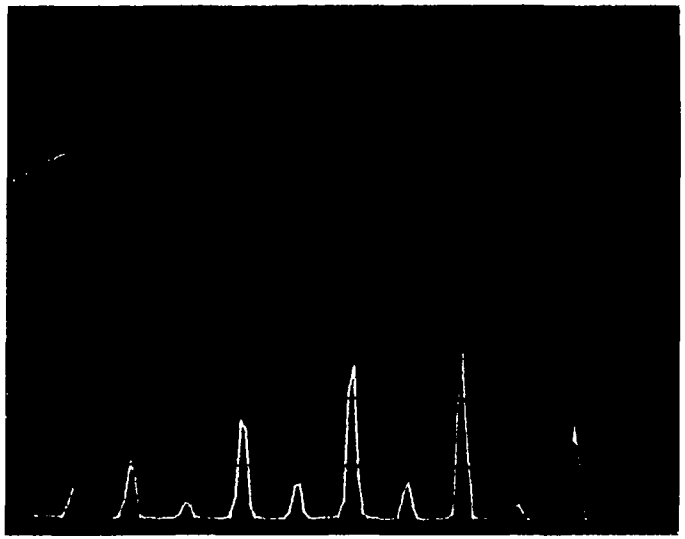

B

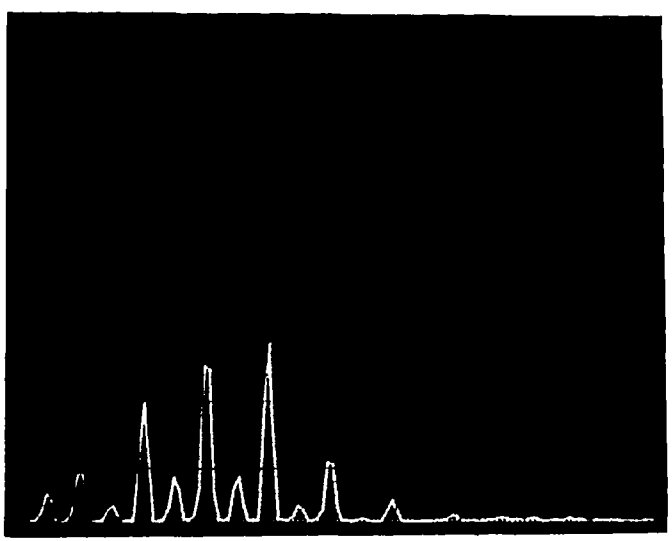

C

D

Figure 145. High-Speed FM Tape Analysis, Mark 48-F Turbopump rpm Spectral Analysis, Test 016-006

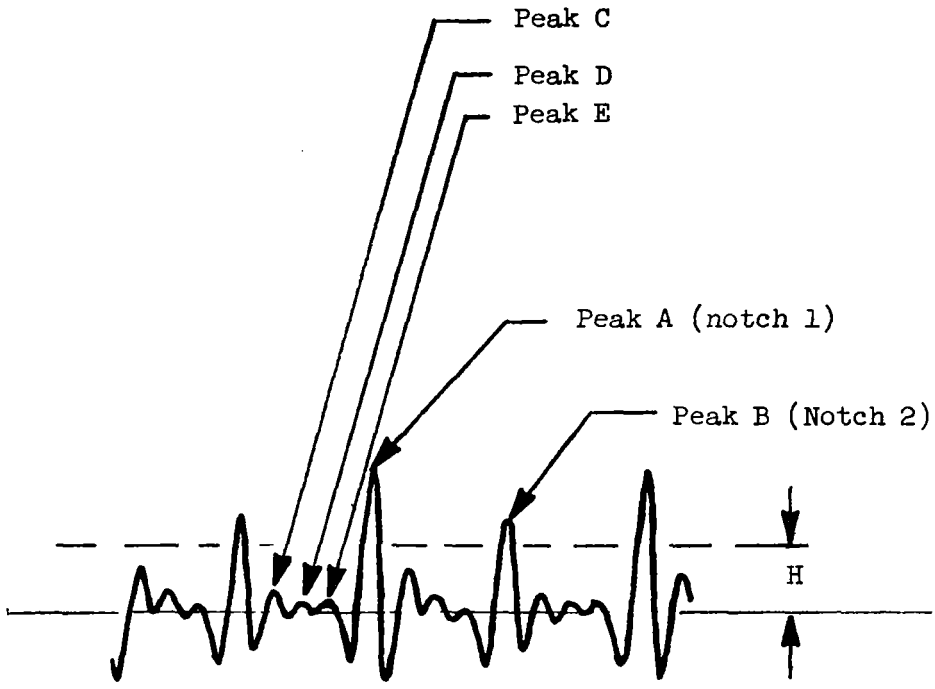

Figure 146. Original Mark 48 Speed Pickup Systems

Results: Maximum rpm achieved was about 6837 rad/s (65,000 rpm) when the Vibration Safety Circuit (VSC) device initiated cutoff due to an indicated greater than 20 g rms value at the turbine radial accelerometer location. Turbopump performance was satisfactory.

Analysis: Test results indicated that the g level ($\geq$10 g rms) assigned was too low, since the remainder of the high-speed rotordynamic instrumentation did not indicate a problem. For the next test, the turbine radial accelerometer output was moved to an oscilloscope, monitored by an observer, and the redline level was increased to 20 g rms. The remainder of the turbopump performance was satisfactory. The speed monitor circuit functioned satisfactorily.

Test No. 8: (016-008)

Test Date: 4-9-76

Duration: 31 seconds

Objective: 1. Achieve 9423 rad/s (90,000 rpm) for a stabilized period to evaluate the turbopump integrity and performance.

2. Evaluate turbopump speed monitor threshold counting circuit.

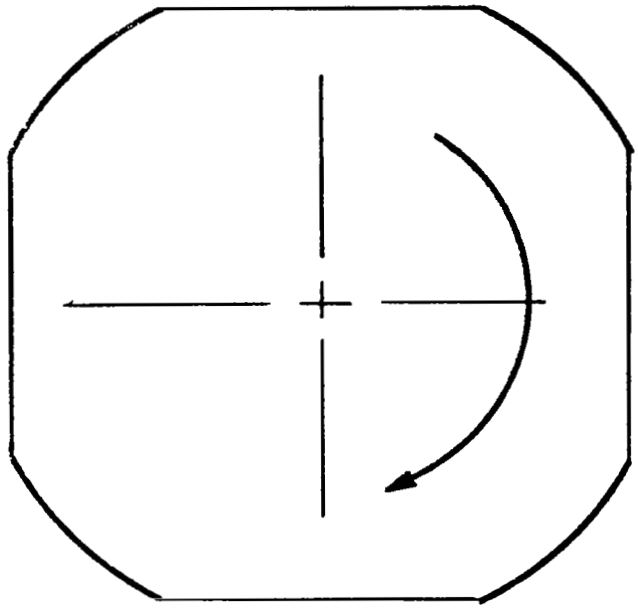

A. MARK 48-0 LO_2 TURBOPUMP SPEED PICKUP SHAFT RELATIVE GEOMETRY (FOUR PULSES PER REVOLUTION)

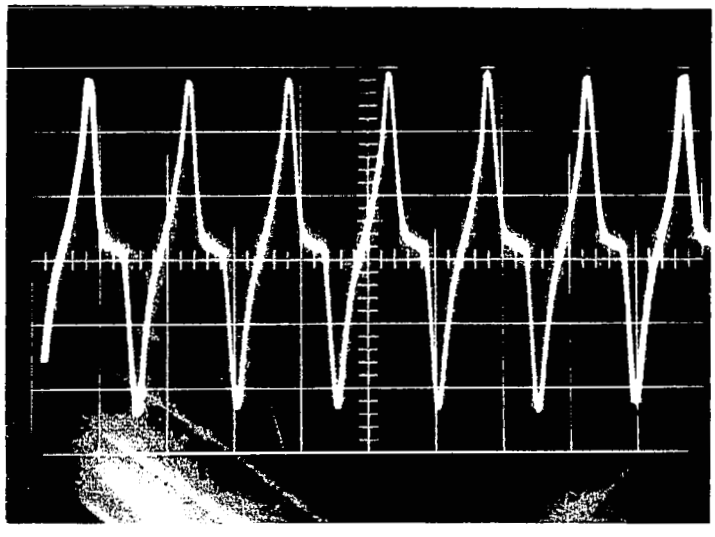

B. LABORATORY TEST RESULTS OF MARK 48-0 LO_2 TURBOPUMP SPEED MONITOR CIRCUIT (3141 RAD/S, 30,000 RPM SHOWN)

Figure 147. Mark 48-0 LO_2 Turbopump Speed Monitor Checkout

Results: The test was terminated due to a lack of sufficient GH_2 turbine drive-gas pressure to achieve the desired 9423 rad/s (90,000 rpm). Actual maximum turbopump speed obtained was about 7853 rad/s (75,000 rpm). Turbopump operation was satisfactory. Prior to the next test, the GH_2 supply line at the gas generator inlet connection was changed from a 2.54 cm to a 5.04 cm (1.0 inch to 2-inch) od line to reduce the line resistance between the GH_2 spin valve and turbine inlet.

Test No. 9: (016-009)

Test Date: 4-15-76

Duration: 36 seconds

Objective:
1. Achieve 9423 to 9947 rad/s (90,000 to 95,000 rpm) for a stabilized period to evaluate the turbopump integrity and performance.
2. Evaluate turbopump speed monitor threshold counting circuit.

Results: Turbopump performance parameters increased smoothly until, at >8376 rad/s (80,000 rpm), the speed monitor display circuit malfunctioned, exhibiting erratic speed counts. A posttest manual count of the raw signal rpm showed that a maximum of 9737 rad/s (93,000 rpm) had been achieved. Actual cutoff was initiated by the turbopump bearing coolant temperature redline observer when the value exceeded the chart scale of 58 K (-355 F).

Analysis: A review of the raw turbopump rpm data on high-speed instrumentation showed that, at increasing values of shaft speed, the absolute magnitude of the waveform decreased. Referring to Fig. 146: Peaks A and B decreased to the point where the threshold monitor value exceeded the actual signal output for peak B, thus halving the speed count. However, the magnitude of peaks A and B fluctuated during the test, accounting for the erratic real time speed display. No problems or hardware damage is suspected due to the higher-than-normal turbopump bearing coolant temperature. Some elevation in bearing temperature is to be expected at higher turbopump shaft speeds.

Test No. 10: (016-010)

Test Date: 4-15-76

Duration: 148 seconds

Objective:
1. Evaluate the integrity of the turbopump at constant 4712 rad/s (45,000 rpm) for 200 seconds or test stand limitation.
2. Evaluate turbopump speed monitor threshold counting circuit at 4712 rad/s (45,000 rpm).

Results: All objectives achieved successfully.

Analysis: Actual turbopump speed was held constant at 4712 rad/s (45,000 rpm) for the duration of the test with manual control of the GH_2 spin valve. Final throttle valve setting was 28% opening to target nominal pump performance. The speed counting display circuit functioned flawlessly at the lower rpm 4712 rad/s (45,000 rpm) and agreed to actual FM and IBM data.

Pump Hydrodynamic Performance. A discussion of the pump hydrodynamic trends observed in the turbopump test data is presented in the following.

Head and Efficiency. The pump pressure rise is shown as a function of the discharge flow in Fig. 148. Representative data points are shown at speeds of 4712, 6282, 7853 and 9947 rad/s (45,000, 60,000, 75,000, and 95,000 rpm). For purposes of comparison, the predicted pressure rise for each of these speeds is also shown over a broad flow range. As can be seen from the figure, the agreement in general is excellent. The head rise at the three lower speeds generally exceeds the prediction slightly, although it also indicates a trend toward a somewhat steeper head-flow relationship so that, at higher flows, the head is below the predicted at some points.

The data obtained at the highest speed levels, near 9423 rad/s (90,000 rpm) fall below the predicted curve. However, the predicted curves were generated as a pressure rise from the first-stage impeller to the pump discharge, and were based on calculated bearing flow and temperature values. To attempt to match the data, a small additional pressure loss must be added to represent the pump inlet configuration, and the measured inlet bearing flow temperature should be used. The former of these corrections has a very small effect, and is a function of the fluid velocity squared. The latter correction is not small because the measured temperature of the bearing coolant flow was much higher than expected. A discussion of this anomaly is presented in a subsection below. It should be noted that the scatter in the data scaled to 9947 rad/s (95,000 rpm) in Fig. 148 should not be interpreted as an indication of a positive H-Q slope. Some of the high-speed data were obtained without sufficient steady-state interval for satisfactory repeatability.

The primary factor postulated as contributing toward the lower performance is incipient cavitation of the first-stage impeller. At the higher speeds, the suction specific speed of the first impeller is increasing with a resulting higher potential for cavitation. This is compounded by the higher temperature of the bearing coolant flow.

Using the pump inlet and discharge pressure and temperatures, the pump isentropic efficiency can be calculated. This isentropic efficiency is very sensitive to the temperature differential across the pump; therefore, at the larger speeds with higher temperature differentials, the accuracy of the temperature measurement is not as critical and a more accurate efficiency can be determined. For example, near 9423 rad/s (90,000 rpm), the temperature differential across the pump is 28 to 33 K (50 to 60 F) but, at 4712 rad/s (45,000 rpm), it is only about 8 K (12 F).

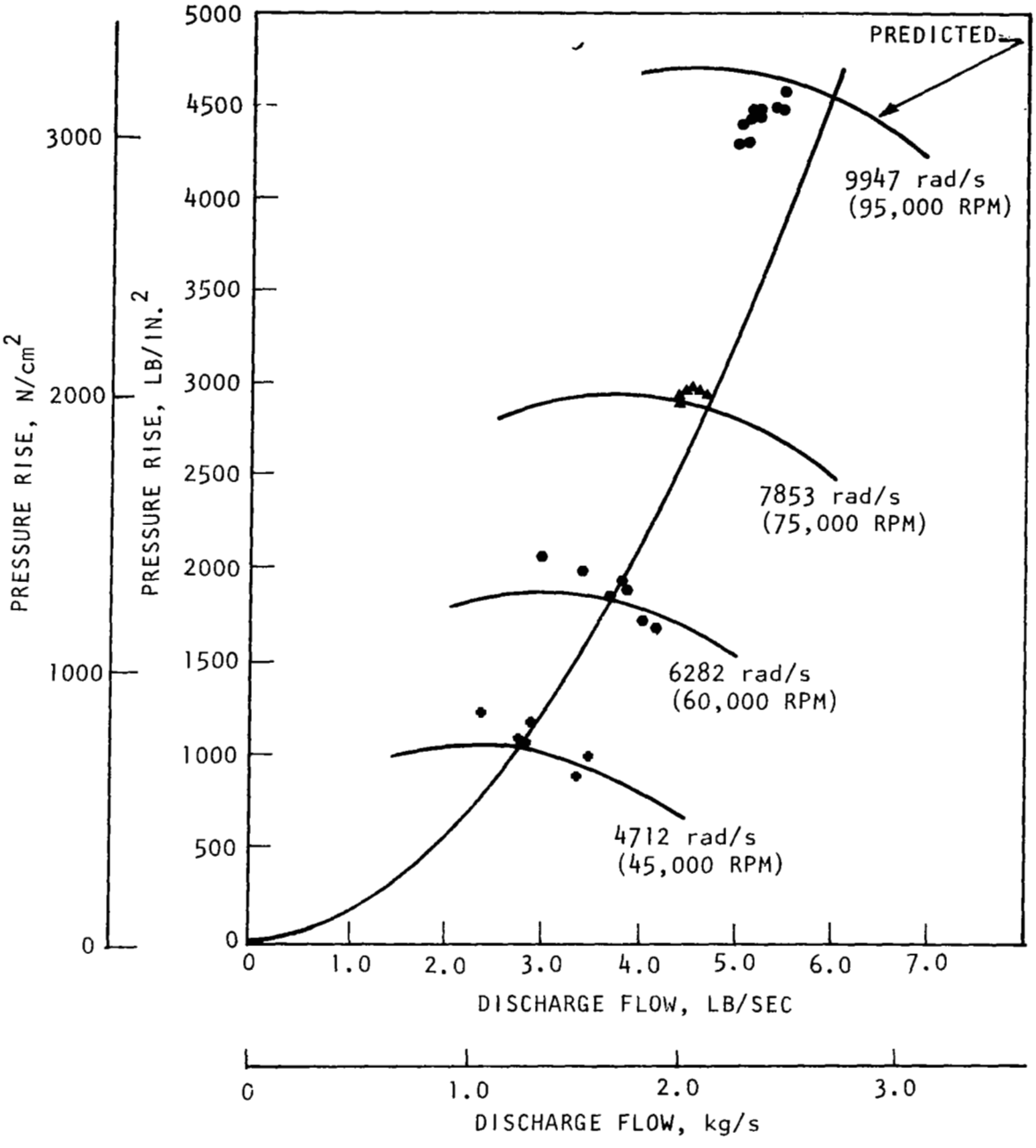

Figure 148. Mark 48-F Pump Performance

The efficiency is expected to vary with Q/N (where Q equals pump flow in gpm, and N is pump speed in rpm) and, due to the thermodynamic characteristics of the hydrogen, will vary with speed. These effects are clearly seen in the data in Fig. 149. The measured efficiencies are higher than predicted and considered to be very good for the size and complexity of this pump. The flow range covered by the data is minimal, so that the shape of the efficiency curves as function of Q/N is somewhat subjective. The data in the speed range of 5235 to 6282 rad/s (50,000 to 65,000 rpm) covers the largest flow range, and was used to establish the general shape of the test data curves. With these curves, the data indicate that the peak efficiency point occurs at a somewhat smaller flow than predicted, but very near the design point Q/N. The curves also indicate that the efficiency is dropping more quickly than predicted at both the high- and low-flow conditions. With small pumps, it generally is more difficult to achieve a broad flow range.

Numerous internal pressure measurements were made at different points through the pump. These internal pressures are, of course, most useful as diagnostic information to uncover the source of performance deficiencies, but no significant performance deficiencies were uncovered in the present test effort. With these internal pressures, a comparison with predicted internal pressures is possible to indicate the consistency of the prediction at intermediate steps. Having met the overall pump performance prediction, it was expected that the intermediate pressures would also be met. This is seen to be the case from Fig. 150 and 151, which compare predicted and test pressures at several stations and at two different speeds. The actual test values are shown by symbols and are arbitrarily corrected by straight lines, not necessarily implying that the pressure varies linearly with distance. For the predicted values, the actual measured inlet and bearing coolant temperatures were used as a starting point.

At the speed of 6125 rad/s (58,500 rpm) (Fig. 150), the predicted and measured values are very close at each point, the measured data showing somewhat better pressure recovery through the second-stage radially outward diffuser than was predicted. At 9423 rad/s (90,000 rpm) (Fig. 151) the first-stage impeller and diffuser appear to be shy in performance. This is compensated somewhat by the good performance of the second diffuser. However, the loss of performance in the first stage could be indicative of a potential cavitation problem, or it may indicate simply that the quality of the first impeller, from a fabrication standpoint, it less than the others, and that this is beginning to show detrimental effects at the higher flows and speeds. It also should be kept in mind that these measured pressures are local static pressures and may not be truly representative of the average static pressure across the station, and that this local value could easily vary from a true average at changing speeds and flows. In general, the overall agreement between measured and predicted values is considered to be very good.

Suction Performance. There was no plan to run a typical cavitation test with pump inlet pressure decreasing until a drop in head occurs due to pump cavitation. In general, the pump inlet pressure was maintained at approximately the constant value of 69 N/cm^2 (100 psia). Therefore, the only changes

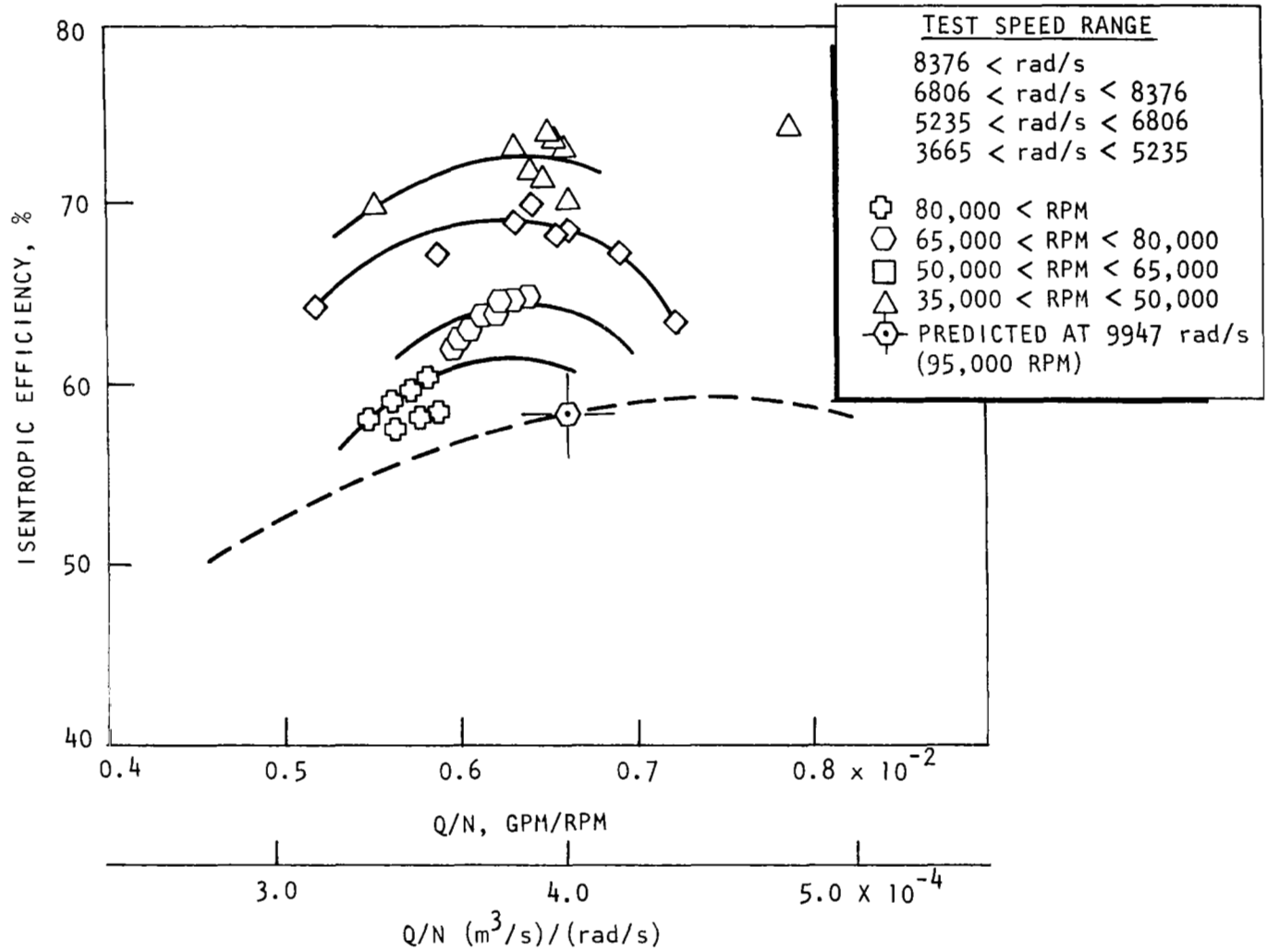

Figure 149. Mark 48-F Pump Efficiency

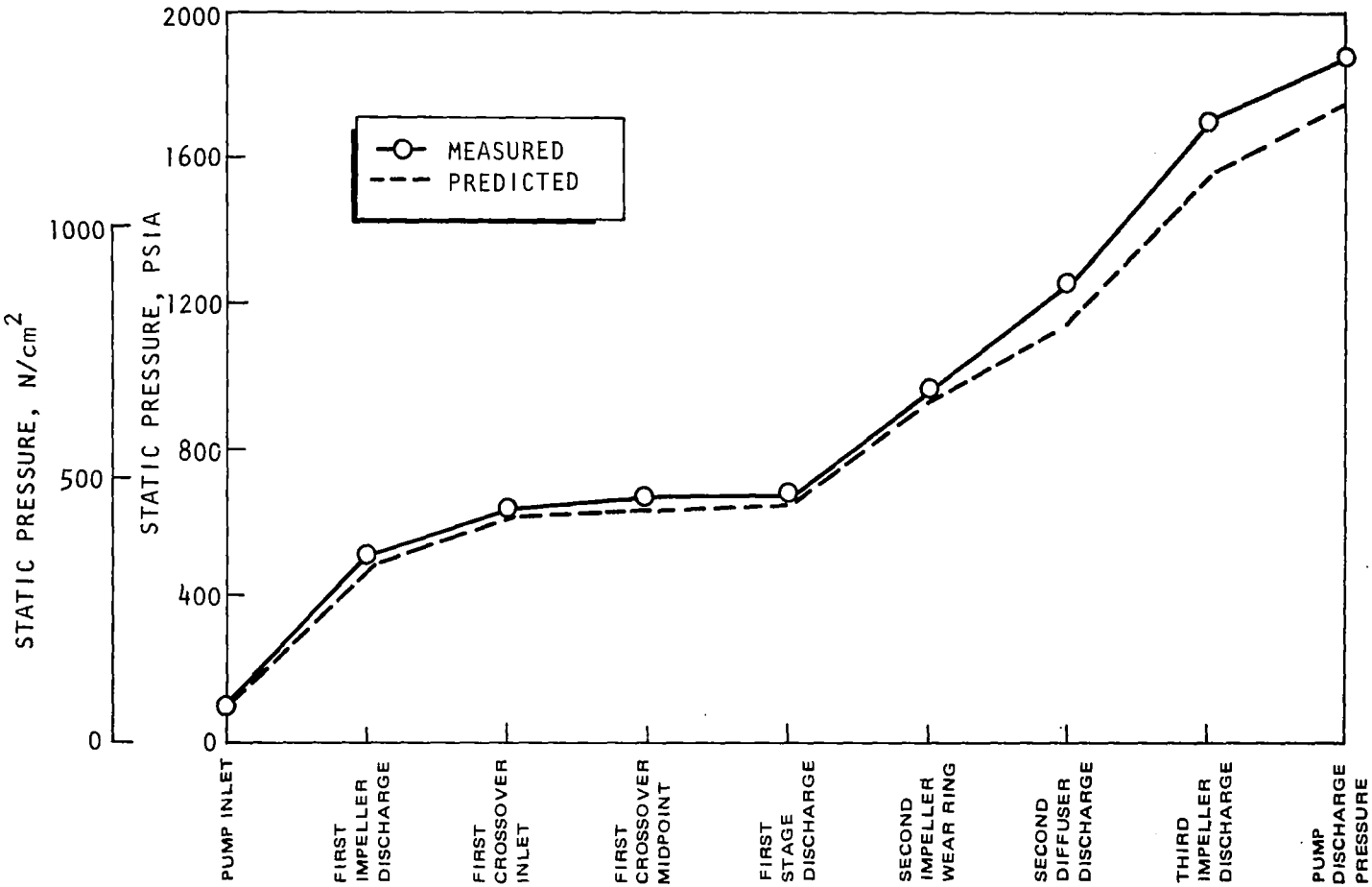

Figure 150. Mark 48-F Pump Test Data: Run 6, Slice 10; N = 6125 rad/s

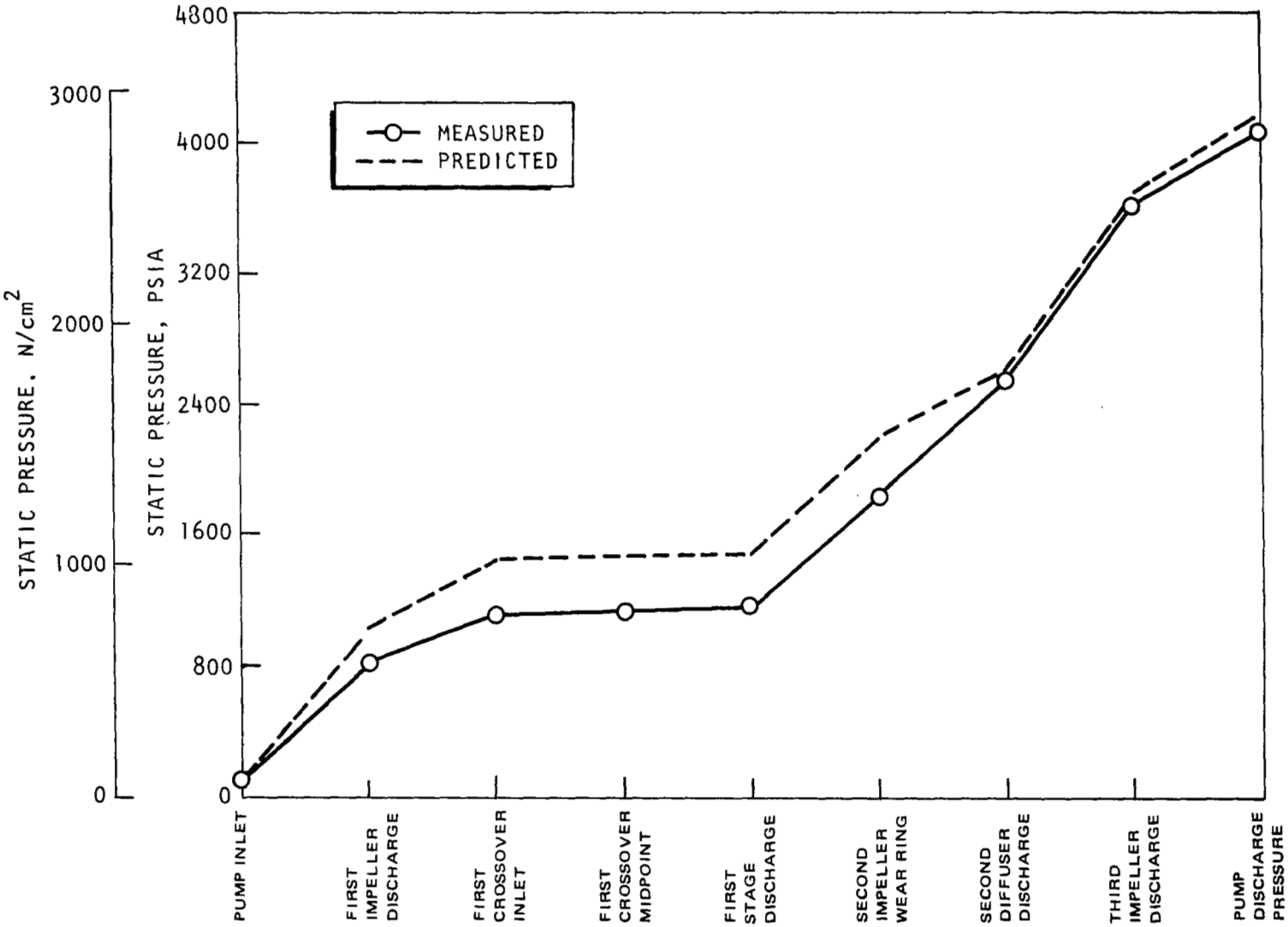

Figure 151. Mark 48-F Pump Test Data; Run 9, Slice 7; N = 9423 rad/s (90,000 rpm)

in the suction specific speed are those resulting from the increase in flow and speed. If the pump inlet pressure and temperature (upstream of the pump inlet manifold) are used to calculate the net positive suction head (NPSH), the resulting suction specific speeds are low throughout the test effort, reaching a maximum of 2.09 $(rad/s)(m^3/s)^{1/2}/(J/kg)^{3/4}$ 5700 rpm $gpm^{1/2}/ft^{3/4}$ at 9737 rad/s (93,000 rpm). However, the critical suction specific speed is that occurring at the first-stage impeller inlet. This requires mixing the estimated front wear-ring leakage and the front bearing coolant flow with the pump inlet flow to establish the average temperature at this point.

Using a 9423 rad/s (90,000 rpm) data point as an example, the suction specific speed, based on pump inlet conditions, was 2.04 $(rad/s)(m^3/s)^{1/2}/(J/kg)^{3/4}$ (5559 rpm $gpm^{1/2}/(ft)^{3/4}$) but, based on calculated impeller inlet conditions, was 2.47 $(rad/s)(m^3/s)^{1/2}/(J/kg)^{3/4}$ (6741 rpm gpm $^{1/2}/ft^{3/4}$), a 21% increase. This increase is large, primarily because of the high temperature of the bearing coolant flow. The necessary flowrate to match the measured bearing discharge temperature is calculated to be approximately 0.00177 kg/s (0.0039 lb/sec).

In an attempt to assess the impact of the bearing coolant flowrate, which is described in detail below, a range of orifice resistance values was studied, the K values used being varied from 1.0 to 1.5. Through this range of K values, the coolant flowrate through the bearing changed by approximately 22%. Even with the higher losses, the flowrate through the bearing was 0.048 kg/s (0.106 lb/sec). With flowrate of this magnitude, it is not possible to explain the high temperature measured at the bearing exit.

The remaining parameters that can affect the coolant flowrate are the areas of the orifices. Orifices 3 and 6 are drilled holes which cannot change. Area A_5 is considerably higher than any other in the system. Therefore, the only critical areas concerning the flowrate through the bearing A_1, A_{7a}, and A_{7b}. A parametric study of these areas was done to establish the areas at these stations that would reduce the flow through the bearing to a rate at which the exit temperature would reach the measured value.

Reducing only area A_1 cannot reduce the flowrate through the bearing below a minimum of approximately 0.027 kg/s (0.06 lb/sec). This is due to the fact that, as the pressure drop through A_1 increases, the flow in segment 2 through the rear wear ring reverses and flows through the bearing. It was found in the analysis that orifice 7a is the controlling orifice past the bearing. The original clearance at orifice 7a is 0.152 mm (0.06 inch). Reducing the gap at orifice 7a to 0.005 mm (0.0002 inch), while holding A constant, the flowrate through the bearing, $\dot{\omega}_3$, is reduced to 0.003 kg/s (0.007 lb/sec). This flowrate would yield the measured exit temperature if the bearing heat output were approximately 1.8 times that analytically predicted, which is quite reasonable. A further reduction in the gap at point 7a to 0.0002 mm (0.0001 inch) reduces $\dot{\omega}_3$ to a rate of 0.0013 kg/s (0.0028 lb/sec) design was expected to achieve a suction specific speed of approximately 4.04 (rad/s) $(m^3/s)^{1/2}/(J/kg)^{3/4}$ (11,000 rpm gpm $^{1/2}/ft^{3/4}$. However, with the small size of the impellers and the corresponding difficulty of maintaining the desired inlet thickness and blade angle distributions, a suction specific speed of

4.04 (rad/s)$(m^3/s)^{1/2}/(J/kg)^{3/4}$ (11,000 rpm $gpm^{1/2}/ft^{3/4}$) could be optimistic, and cavitation effects could be occurring at suction specific speeds of 2.57 (rad/s)$(m^3/s)^{1/2}/(J/kg)^{3/4}$ (7000 rpm $gpm^{1/2}/ft^{3/4}$). (At the design flow and speed, the difference between 2.57 (rad/s)$(m^3/s)^{1/2}/(J/kg)^{3/4}$ (7000 rpm $gpm^{1/2}/ft^{3/4}$) and 4.04 (rad/s)$(m^3/s)^{1/2}/(J/kg)^{3/4}$ (11,000 rpm $gpm^{1/2}/ft^{3/4}$) suction specific speed is approximately 22 N/cm^2 (32 psi) inlet pressure.) In examining all of the data points from test 9 which were near 9423 rad/s (90,000 rpm), there is a rather consistent correlation of higher read rise with lower suction specific speeds based on pump inlet conditions. This too would tend to indicate cavitation effects; although, with data grouped so closely, this observation cannot be interpreted as very conclusive.

In conclusion, although a potentially lower suction performance is indicated than was predicted, the available data do not clearly establish the pump suction performance.

Bearing Coolant Flow. A sketch of the pump-end bearing, including the flow path of coolant, appears in Fig. 152. The path and direction of the coolant flow is from the inlet to the second-stage impeller through the slot resistance No. 1. The flow then splits, part going through the rear wear ring to the first-stage impeller discharge. The remainder of the flow goes through the bearing, eventually discharging at the first-stage impeller inlet.

A temperature probe is located just downstream of the bearing, as shown in Fig. 152. It was found that, during a 9423 rad/s (90,000 rpm) test (run 9, slice 7), the temperature of the coolant exiting the bearing was 87 K (157 R). This temperature is considerably higher than expected. The flowrate of coolant through this bearing was calculated to be approximately 0.045 kg/s (0.1 lb/sec). Analysis of the bearing heat output yields a total of approximately 1118 J/s (1.06 Btu/sec.) for the duplex bearing package. An estimate of the temperature at the second-stage impeller inlet is 37 K (67 R). If design coolant flowrate is achieved, the coolant temperature exiting the bearing should increase by, at most 1 to 1.5 K, (2 to 3 R).

Because of this discrepancy, a parametric study of the bearing coolant flow loop was made. A schematic of the resistances encountered by the coolant flow is shown in Fig. 153. Pressure drops through orifices and line losses are accounted for in the K values at each resistance. The pressure drop through a resistance is defined as:

$$\Delta P = K_i \frac{1}{2g\rho} \frac{\dot{w}_j^2}{A_i^2}$$

Where $\dot{w}_j$ is mass flowrate, ρ is specific weight, A_j is area, and g is gravitational acceleration. The flow system was solved for continuity and pressure balance between stations 1, 2, and 3. The pressure rise between stations 1 and 2 due to whirl on the back side of the impeller was incorporated into the solution. The analysis accounted for density changes due to changes in pressure through the system.

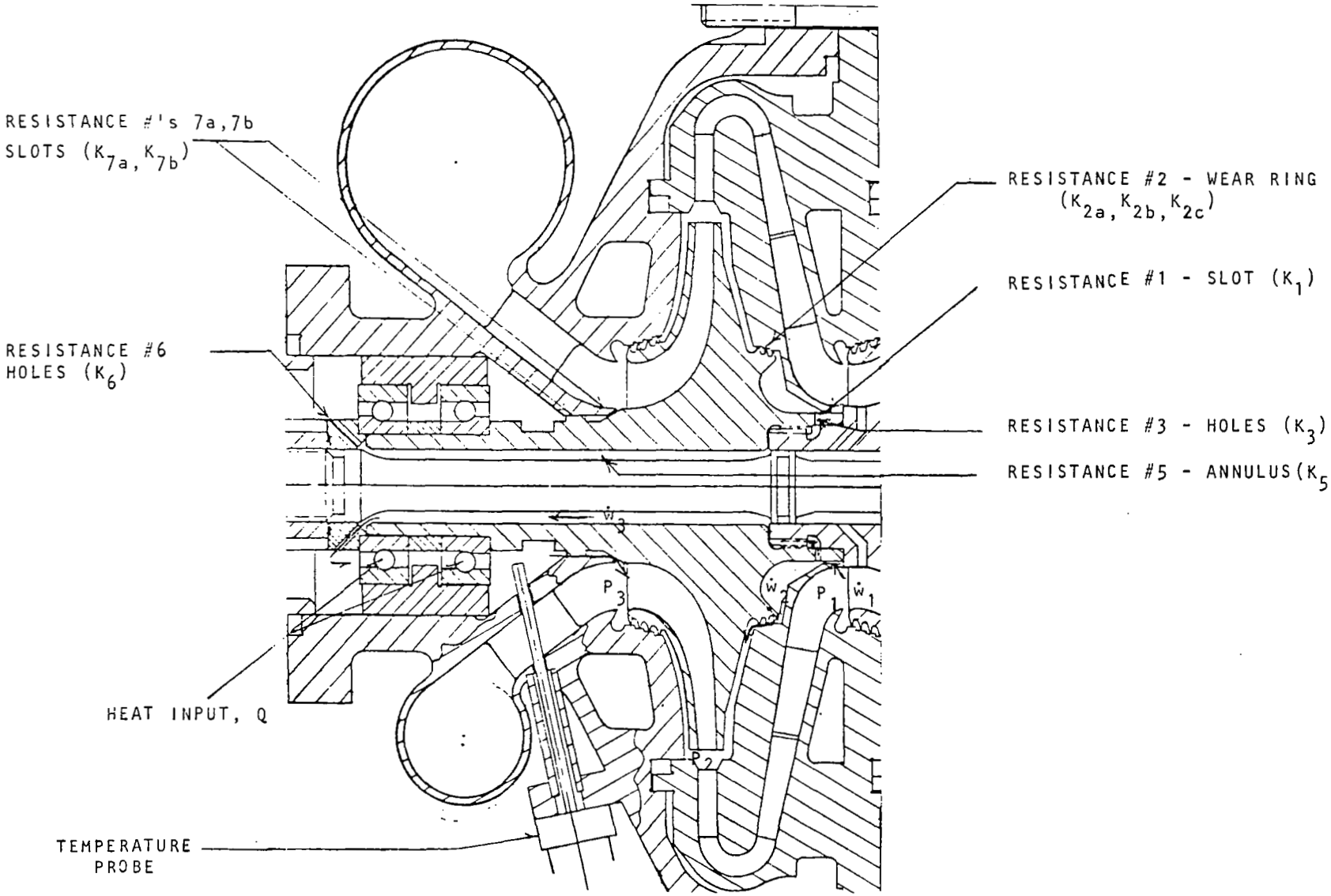

Figure 152. Front Bearing Coolant Flow Path

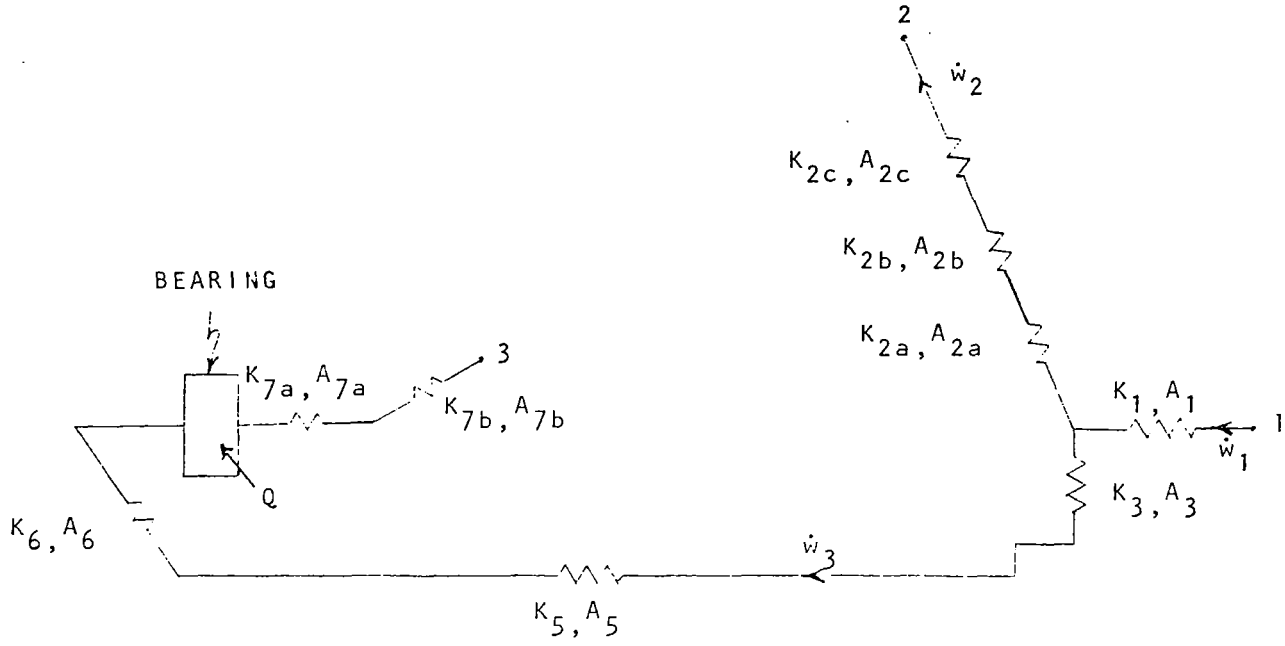

Figure 153. Front Bearing Coolant Resistances

The heat transfer rate (Q) from the bearings to the fluid has the realtionship:

$$Q = C_\rho \, (T_{out} - T_{in}) \, \dot{w}_3$$

Considering T_{out} = 87 K (157 R) and T_{in} = 37 K (67 R), an average specific heat, C_ρ, at the pressure at the bearing is approximately 0.02 J/kg-K (3.0 Btu/lb-R). With the bearing heat input of 118 J/s (1.06 Btu/sec), the necessary flowrate to match the measured bearing discharge temperature is calculated to be approximately 0.0018 kg/s (0.0039 lb/sec). This is approximately 28% lower flowrate than necessary to explain the high temperature at the bearing exit.

Reducing the gap at A_1 to 0.025 mm (0.001 inch) while simultaneously reducing the gap at A_{7a} to 0.005 mm (0.0002 inch) yields a flowrate through the bearing of approximately 0.0015 kg/s (0.0033 lb/sec). This is 15% below the flowrate expected through the bearing due to the high measured bearing exit temperature. The original gap at A_1 is 0.81 mm (0.032 inch).

In effect, to get $\dot{w}_3$ flowrate near the flowrate giving the high temperature measured at the bearing exit, the gap areas of A_1 and A_{7a} must be reduced to approximately 3% of their original values. This appears to be a larger reduction than would be expected but, at the present time, there is no other explanation of the high bearing coolant temperature. Examination of the bearings after testing did not show any heat-banding effects on the bearing balls. Additional testing with more instrumentation is required to further clarify this area.

Balance Piston Performance. In all of the tests, the balance piston appeared to be functioning to achieve a good axial thrust balance. Internal

pressures were available at the third impeller discharge, within the balance cavity, and at the balance piston sump. The pressure within the balance cavity would be expected to have a magnitude between the other two pressures. Observation of the data indicated that the balance cavity pressure also seemed to maintain a relatively constant position between the other two, indicating a very stable operation through all of the tested points of operation. Selected data slices are presented in Fig. 154 to illustrate this. Data from two time slices are shown as solid symbols to distinguish the corresponding pressure because these did not fall in the same relationship with speed as the others.

Two slices were examined in more detail to determine the position of the balance piston both geometrically and within the available thrust range. The results are shown in the following table:

TABLE 28. BALANCE PISTON POSITION

Test	6	9	Design Point
Slice	10	7	-
Speed, rpm	58,500	90,000	95,000
Balance Piston Position, X/S*	0.327	0.356	0.36
Balance Piston Position, F/F_{max}**	0.679	0.722	0.75

*X is the axial gap at the high-pressure orifice, and S is the total balance piston travel.
**F is the thrust on the balance piston face, and F_{max} is the maximum available thrust at that operating condition. F_{max} occurs when the low-pressure orifice is closed.

The predicted value of both X/S and F/F_{max} is almost identical to the values achieved at the 90,000-rpm condition. The internal pressure measurements of the pump also agreed well with predicted values. Therefore, the internal pressures of the turbine must also be very close to the predicted values to achieve the predicted overall thrust.

Turbine Performance. The first-phase performance evaluation tests of the Mark 48-F turbopump assembly were conducted with GH_2 turbine working fluid, and with LH_2 flow through the pump. The results of these tests provide a comparison of the power developed by the turbine with the power required by the pump to deliver the measured pump heads and flows. These data additionally will establish the overall turbopump performance.

The following power calculations were made:

1. Turbine-developed horsepower calculated with turbine isentropic enthalpy $[\Delta S_{(T-T)}]$ available at the test pressure ratio, GH_2 working fluid mass flowrate $[\dot{w}_t]$, turbopump speed $[N_t]$, and turbine component efficiency at the respective test conditions

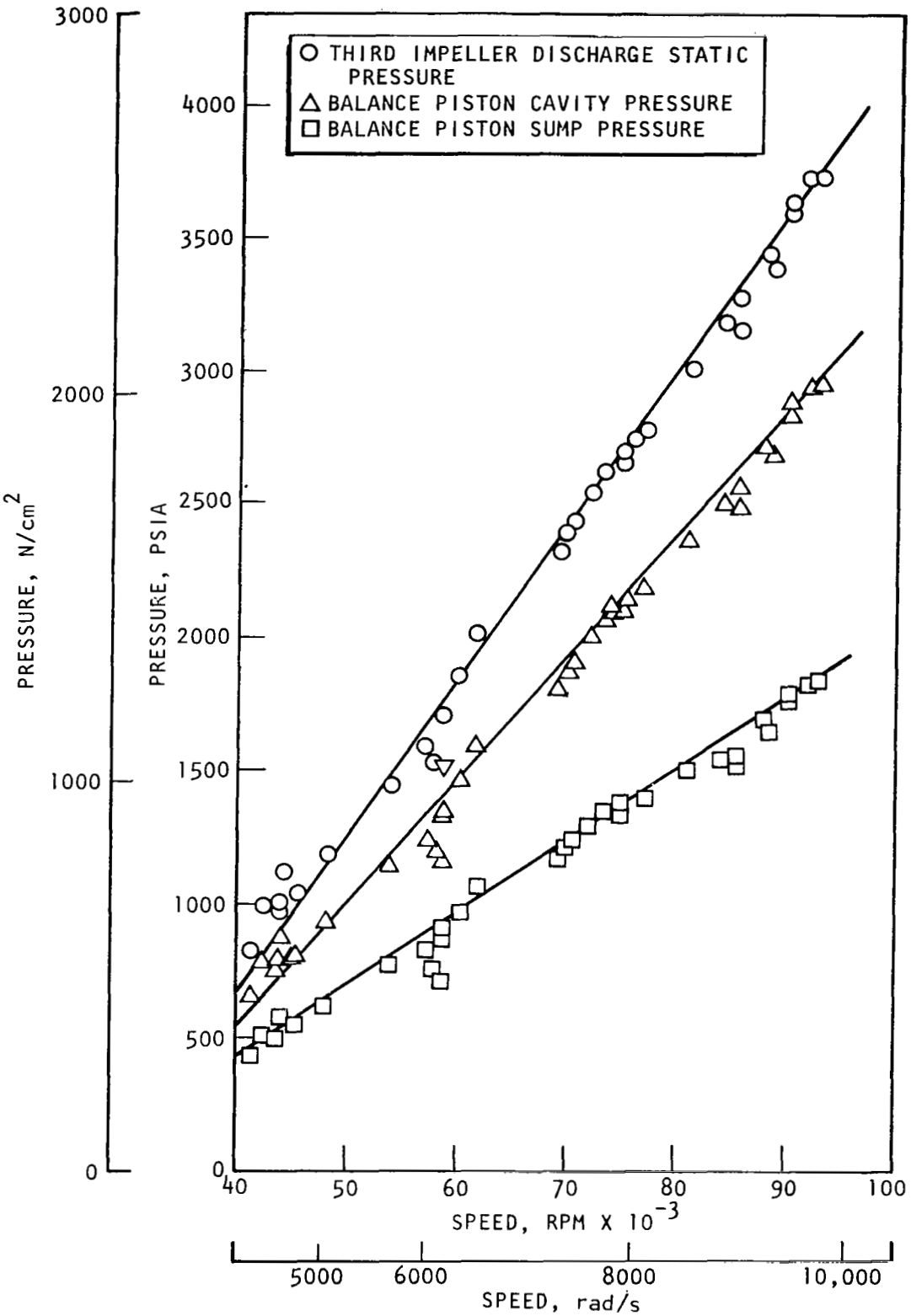

Figure 154. Balance Piston Pressures

2. Turbine horsepower calculated with working fluid total temperature drop [$\Delta T_{(T-T)}$] measured across the turbine, and GH_2 working fluid mass flow [$\dot{w}_t$]
3. Pump horsepower calculated with pump head and flow data at the respective speeds selected for the analysis

Turbine test instrumentation was located as shown on the turbopump assembly drawing (Fig. 155) to obtain the following turbine test parameters for the performance analysis:

1. Turbine total inlet temperature, T_{t_1}, measured at the turbine inlet, downstream of the preburner
2. Turbine inlet static pressure, P_{s_1}, measured at the entrance to the first-stage nozzle
3. Turbine exhaust total pressure, P_{t_2}, measured downstream of the turbine exhaust flange
4. Turbine exhaust total temperature, T_{t_2}, measured downstream of the turbine exhaust flange
5. Turbine speed, N_t

Turbine mass flowrate was calculated with data obtained with a venturi and orifice which were located, respectively, upstream and downstream of the turbine.

The analysis was performed for a range of turbine velocity ratios (U/C_o T-T) from 0.077 to 0.430, and turbine speeds from 1550 to 9737 rad/s (14,800 to 93,000 rpm). A tabulation of pertinent test data appears in Table 29. The performance calculations, which utilized process hydrogen gas properties at the test state conditions, are identical to those used previously to establish turbine aerothermodynamic performance with GN_2 at the Wyle Laboratories, El Segundo, California.

Turbine inlet total pressure was calculated as the sum of the first-stage nozzle inlet static pressure, and dynamic pressure calculated at the entrance plane of the first-stage nozzle. The total-to-total pressure ratio was established with calculated inlet total pressure and turbine test exhaust/total pressure. The turbine-developed horsepower calculation utilized turbine isentropic available energy (T-T) for the respective test pressure ratio, calculated GH_2 mass flowrate corrected for GH_2 compressibility (Z) effects, and turbine efficiency (T-T) corresponding to the test velocity ratio, as plotted in Fig. 138.

$$\text{Turbine-developed horsepower, } hp_{td} = 1.415 \cdot \Delta T_{(T-T)} \cdot C_p \cdot \dot{w}_t$$

where

C_p = process specific heat

Pump horsepower [hp_p] required to drive the liquid-hydrogen pump stages was established with pump fluid horsepower [hp_{pf}] and the pump isentropic efficiency parameter η_{pi} as follows.

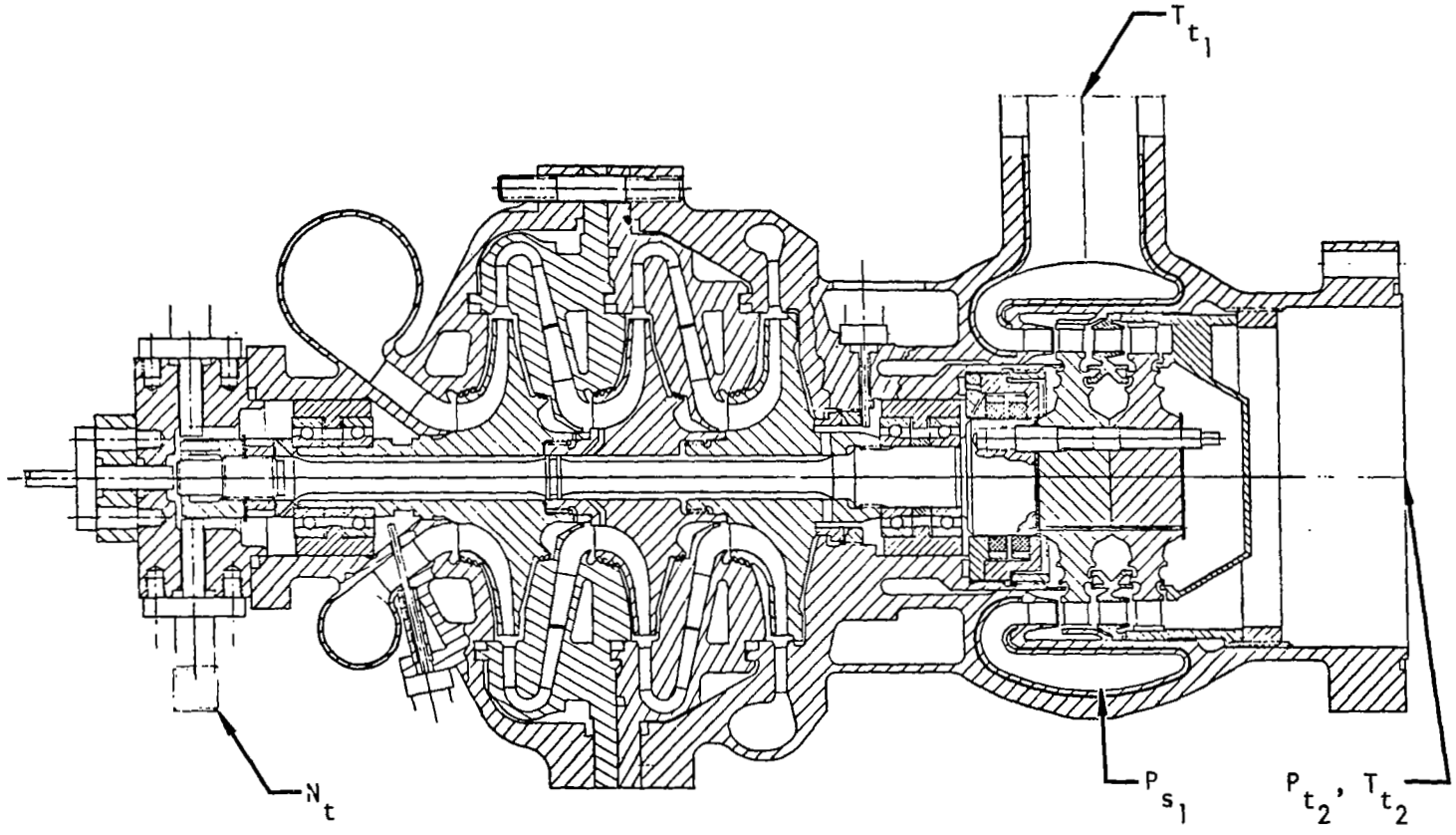

Figure 155. Turbine Instrumentation

TABLE 29. T

(SI

1	2	3	4	4a	5	6	7	8	9	10
Run Number	Time Slice	Speed (N), rad/s	Temperature Total Inlet (T_{t_1}), K	Temperature Total Exit (T_{t_e}), K	Specific Volume at N-1, V_{sp} RTZ/p, m^3/kg	Density, K/m^3	GH_2 Mass Flow (W_t), kg/s	Manifold Inlet Pressure (Static), N/cm^2	Inlet Dynamic Pressure, (P_{dyn}), N/cm^2	P_{t_1} Total Inlet Pressur N/cm^2
2	5	1551	291	233	2.49	0.40	0.11	48.4	0.37	48.7
4	8	3383	296	263	0.47	2.12	0.54	262.0	1.76	263.7
5	4	4554	288	264	0.35	2.87	0.73	347.3	2.34	350
6	13	6439	279	253	0.16	6.20	1.57	1299	4.99	753
9	5	9737	286	251	0.06	15.7	4.04	2102	13.2	2115
9	7	9423	285	258	0.07	15.3	3.93	2041	12.7	2053
9	11	8481	280	253	0.08	12.3	3.15	1564	12.9	1574

(ENGLI

1	2	3	4	4a	5	6	7	8	9	10
Run Number	Time Slice	Speed (N), rpm	Temperature Total Inlet (T_{t_1}), R	Temperature Total Exit (T_{t_e}), R	Specific Volume at N-1 (V_{sp}), ft^3/lb	Density, lb/ft^3	GH_2 Mass Flow (W_t), lb/sec	Manifold Inlet Pressure (Static), P_{s_1}, psia	Inlet Dynamic Pressure (P_{dyn}), psia	P_{t_1} Total Inlet Pressur (8+9), psia
2	5	14,815	523.7	419.1	39.95	0.025	0.24	70.2	0.54	70.0
4	8	32,308	532.5	473.0	7.58	0.132	1.20	379.9	2.56	382.5
5	4	43,500	517.9	475.0	5.59	0.179	1.61	503.8	3.40	507.2
6	13	61,500	502.8	455.4	2.58	0.387	3.46	1884.4	7.24	1091.6
9	5	93,000	515.6	451.6	1.02	0.978	8.89	3048.5	19.04	3067.5
9	7	90,000	513.9	465.0	1.05	0.956	8.65	2959.8	18.43	2978.2
9	11	81,000	503.3	455.5	1.3	0.769	6.94	2269.1	18.79	2283.0

29. TURBINE TEST DATA

(SI UNITS)

10	11	12	13	14	15	16	17	18	19	20
P_{t_1} Total Inlet Pressure, N/cm^2	P_{t_2} Total Exit Pressure, N/cm^2	Pressure Ratio (T-T)	Isentropic Available Energy (Δh_s), J/kg	Pitch Line Velocity (U), m/s	Theoretical Spouting Velocity/ (U)/C_o, m/s	Velocity Ratio (Rel.) T-T	Compres. (Z)	Turbine HP ($\Delta P, \Delta h, \dot{w}_t$), kW	Turbine HP $\Delta T(T\text{-}T), \dot{w}_t$, kW	Pump HP hp_{fluid}/η_p, kW
48.7	34.5	1.415	0.655	68.9	892	0.077	1.003	13.3	94.4	9.2
263.7	184	1.435	0.693	151	917	0.164	1.011	131	267	108
350	247	1.417	0.667	203	900	0.225	1.015	204	259	162
753	518	1.451	0.673	790	905	0.317	1.032	493	590	421
2115	1340	1.578	0.837	433	1008	0.430	1.095	1489	1472	1417
2053	1302	1.576	0.833	420	1006	0.417	1.092	1455	1501	1371
1574	1036	1.519	0.752	377	955	0.395	1.070	1078	1199	1032

(ENGLISH UNITS)

10	11	12	13	14	15	16	17	18	19	20
P_{t_1} Total Inlet Pressure (8+9), psia	P_{t_2} Total Exit Pressure, psia	Pressure Ratio (T-T)	Isentropic Available Energy (Δh_s), Btu/lb	Pitch Line Velocity (U), ft/sec	Theoretical Spouting Velocity/ (C_o), ft/sec	Velocity Ratio (Rel.) T-T (V/C_o)	Compres. (Z)	Turbine HP ($\Delta P, \Delta h, \dot{w}_t$), hp_t (T)	Turbine HP $\Delta T(T\text{-}T), \dot{w}_t$, $hp_{\Delta t}$ (T)	Pump HP hp_{fluid}/η hp_p (P)
70.0	50.0	1.4148	170.7	226	2927	0.077	1.0031	17.79	126.8	12.4
382.5	266.5	1.4350	180.4	494	3009	0.164	1.0112	175.6	358.9	146
507.2	358.0	1.4167	173.9	665	2954	0.225	1.0148	273.3	346.9	217
1091.6	752.1	1.4514	175.5	940	2968	0.317	1.0321	662	792	565
3067.5	1944.0	1.5779	218.1	1421	3308	0.430	1.0945	1999	1977	1902
2978.2	1889.3	1.5764	216.9	1376	3299	0.417	1.0918	1953	2015	1840
2283.0	1503.3	1.5192	195.8	1238	3134	0.395	1.0702	1447	1609	1385

$$\text{Pump horsepower, } hp_p = \frac{hp_{pf}}{\eta_{pi}}$$

A plot of test hp_t, hp_t, and hp_p vs turbine velocity ratio $[U/C_{o\ (T-T)}]$ data appears in Fig. 156 for the test points appearing in Table 29. The overall agreement is very good. The turbine horsepower calculations would be expected to be somewhat larger than the pump horsepower because of parasitic losses.

A review of the test results indicates the best agreement between hp_{td} and hp_p is at a speed of 9737 rad/s (93,000 rpm) and U/C_o of 0.43. At this operating point, a difference of 77 kW (97 hp) exists between the 1491 kW (1999 hp) turbine-developed horsepower and the 1418 kW (1902 hp) absorbed by the pump; this represents a 4.58% difference when referred to turbine-developed horsepower. This variance is attributed to the following conditions, which influenced the test results:

1. The mixing loss resulting from hydrogen seal leakage entering the turbine gas path. This colder hydrogen flow originates at the pump and reduces the available energy of the gas path turbine working fluid by disrupting channel state conditions and velocities.
2. Turbine mass flow data were calculated with venturi and orifice test parameters which experienced some calibration shifts and instabilities in the higher turbine power test points. A review of test conditions and data indicates that calculated turbine mass flows were higher than experienced during the test. An additional mass flow disruption was caused by seal leakage entering the turbine gas path.
3. The precision of the turbine speed data at the 9737 rad/s (9300 rpm) test point experienced slight operational variations which were traced to instrumentation recording equipment. This type of speed inaccuracy adversely affects the calculated turbine velocity ratio and, subsequently, the reference test efficiency.

The net effect of all these variances upon the calculated value of turbine-developed horsepower, hp_{td}, could account for it being 4.58% greater than pump-required horsepower. A comparison of turbine (hp_t) horsepower, calculated with total temperature drop across the turbine, indicates a 3.79% power difference with pump required horsepower.

In conclusion, a review of the turbine test results indicates the demonstrated overall turbopump efficiency has met the performance objectives of this program.

Mechanical Performance. Testing of the LH_2 turbopump extended over 10 starts, with a total accumulated time of 884 seconds. The longest single test duration was 168 seconds. Operation extended over a rotor speed range of 0 to 9737 rad/s (0 to 93,000 rpm); a maximum pump discharge pressure of 2861 N/cm^2 (4150 psi) was achieved.

The mechanical performance of the turbopump was excellent for an initial test exposure. A satisfactory control over the rotor axial position was maintained

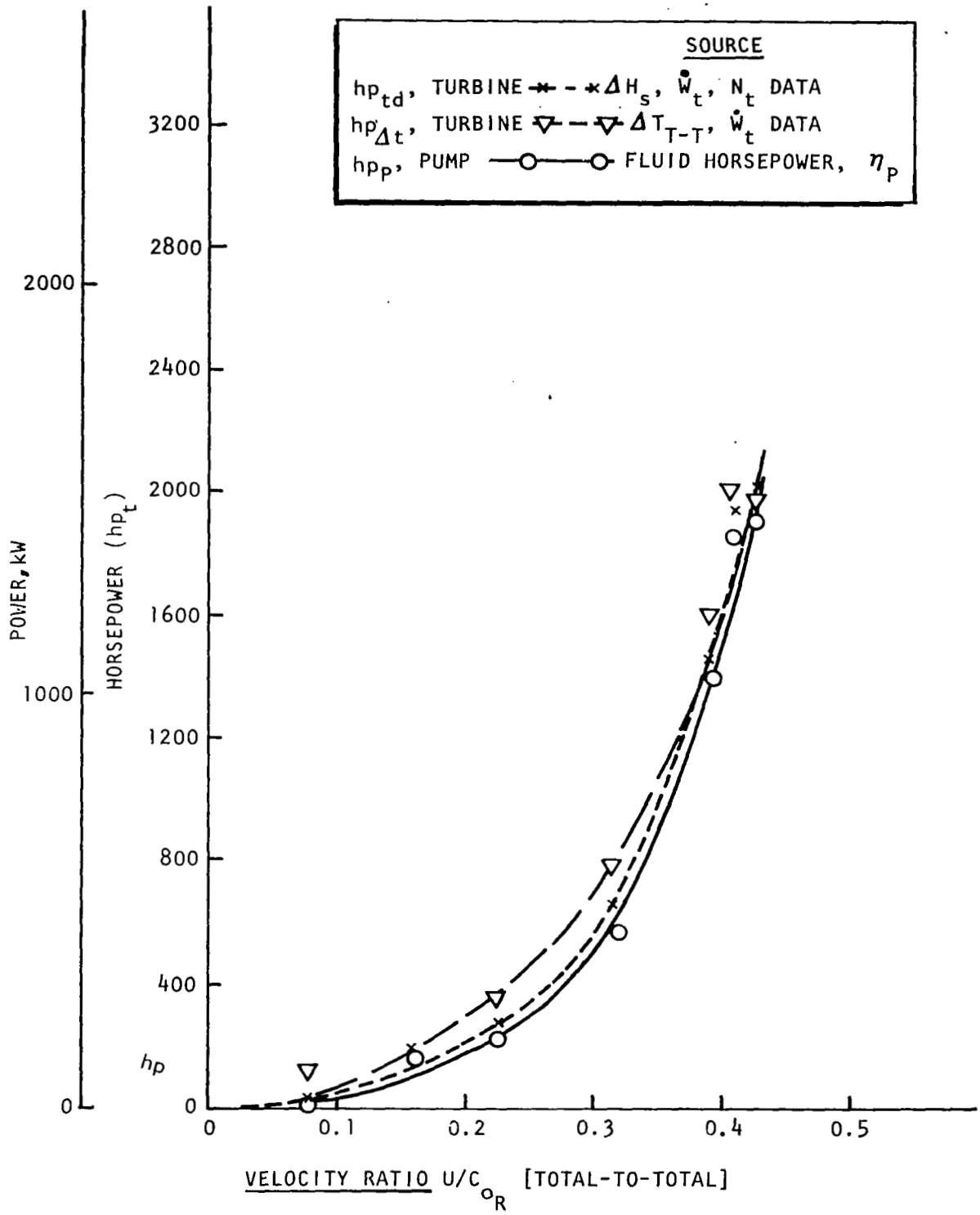

Figure 156. Horsepower Correlation

by the balance piston throughout the test series at all speed levels. It was evident from the rotordynamic indicators such as accelerometers and Bently proximity transducers that the rotor was balanced to a very fine degree. In general, the rotor deflections and synchronous acceleration levels were very low, approximately 0.076 mm (0.003 inch) and 5 g peak to peak, respectively. Only minor increase in these indicators was evident when the rotor passed through the first and second critical speeds. The actual levels of the critical speeds were determined to be at 3874 rad/s (37,000 rpm) and 5371 rad/s (51,300 rpm), close to the predicted value of 3141 rad/s (30,000 rapm) for the first critical and 5444 rad/s (52,000 rpm) for the second critical. There was no evidence of subsynchronous motion at any speed level within the explored range of 0 to 9737 rad/s (0 to 93,000 rpm).

The operation of the turbopump appeared smooth during the test series. Each test was characterized by a smooth quick response start as well as a smooth coastdown at cutoff, indicating a satisfactory transition in the axial control of the shaft position from the bearings to the balance piston.

The turbopump was disassembled after the conclusion of the test series to permit visual inspection of the components. Figure 157 shows the condition of the more significant parts. The pumps components are shown separately in Fig. 158. None of the components disclosed any sign of structural distress, impending failure, or excessive deflection.

Minor discrepancies were noted in two areas of the pump. As shown in Fig. 159, the silver plating from the wear-ring platforms at the third-stage impeller front shroud had partially flaked off, probably as a result of poor bonding between the plating and parent metal. It is expected that more stringent process control at the vendor will eliminate a similar problem in the future.

The other minor discrepancy was a slightly more extensive rubbing between the balance piston low-pressure orifice surfaces than was anticipated. The condition of the rotating and stationary orifice surfaces is illustrated in the enlarged photographs of Fig. 160 and Fig. 161. On future builds, the extent of the rubbing should be reduced by increasing the bearing axial load.

The bearings are shown in Fig. 162 with the bearing cartridges, springs, and spacers. The surface condition of the races and balls was satisfactory. Based on the wear track, it is estimated that the turbine and bearings were subjected to a maximum axial load of 530 pounds.

The posttest condition of the shaft dynamic seal was excellent. There was no indication of overheating, scoring, or grooving, either on the seal rings of the mating surface or the shaft.

The two turbine wheels and the second-stage nozzle are shown in Fig. 163. No sign of axial rubbing was evident on the turbine components. Radially minor rubbing occurred at the sealing land surfaces as expected. The copper plating used on the stationary sealing surfaces took the contact well; there were no signs of erosion, galling, or flaking.

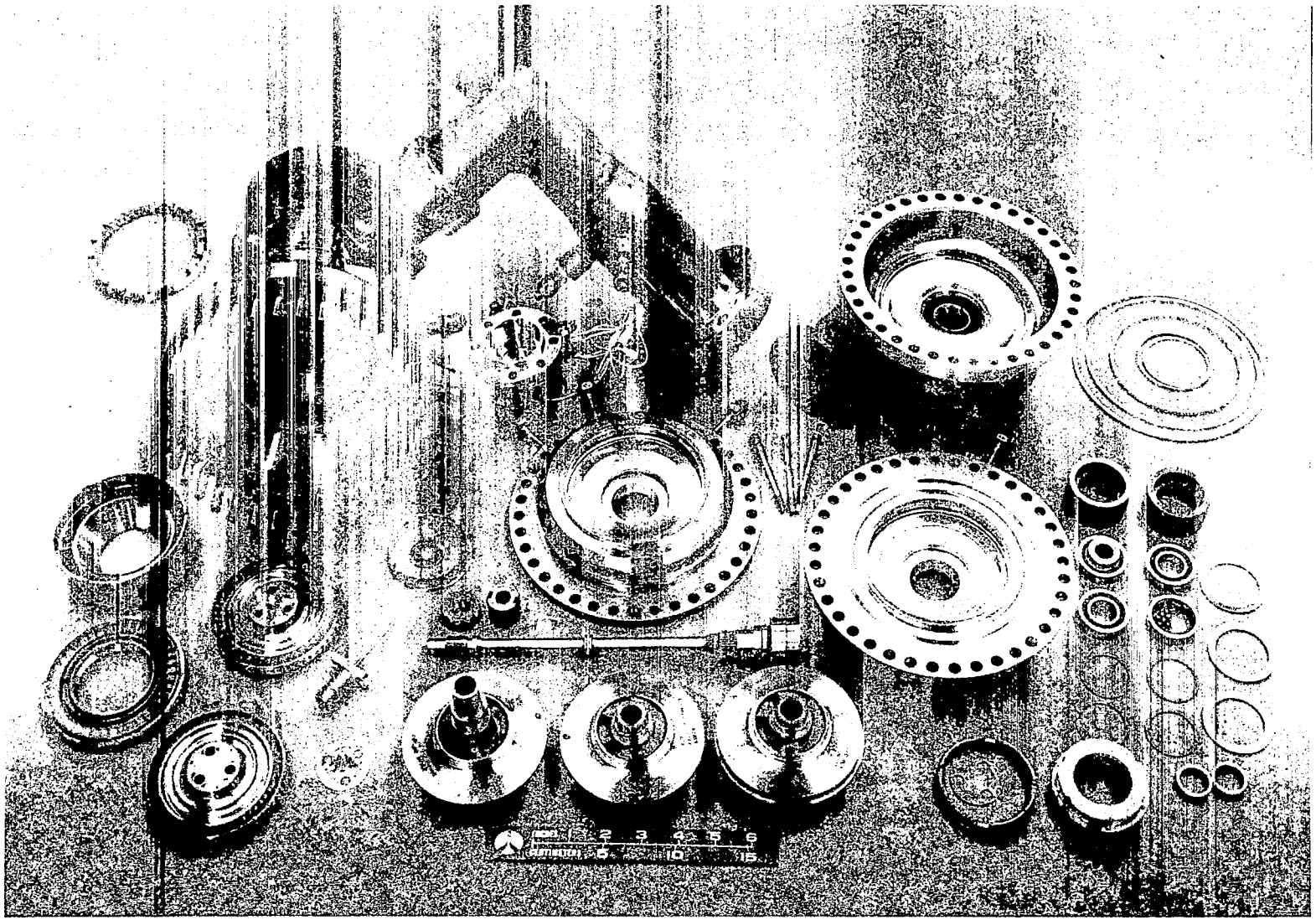

1HS55-6/23/76-C1F*

Figure 157. Mark 48-F Turbopump Hardware After Testing

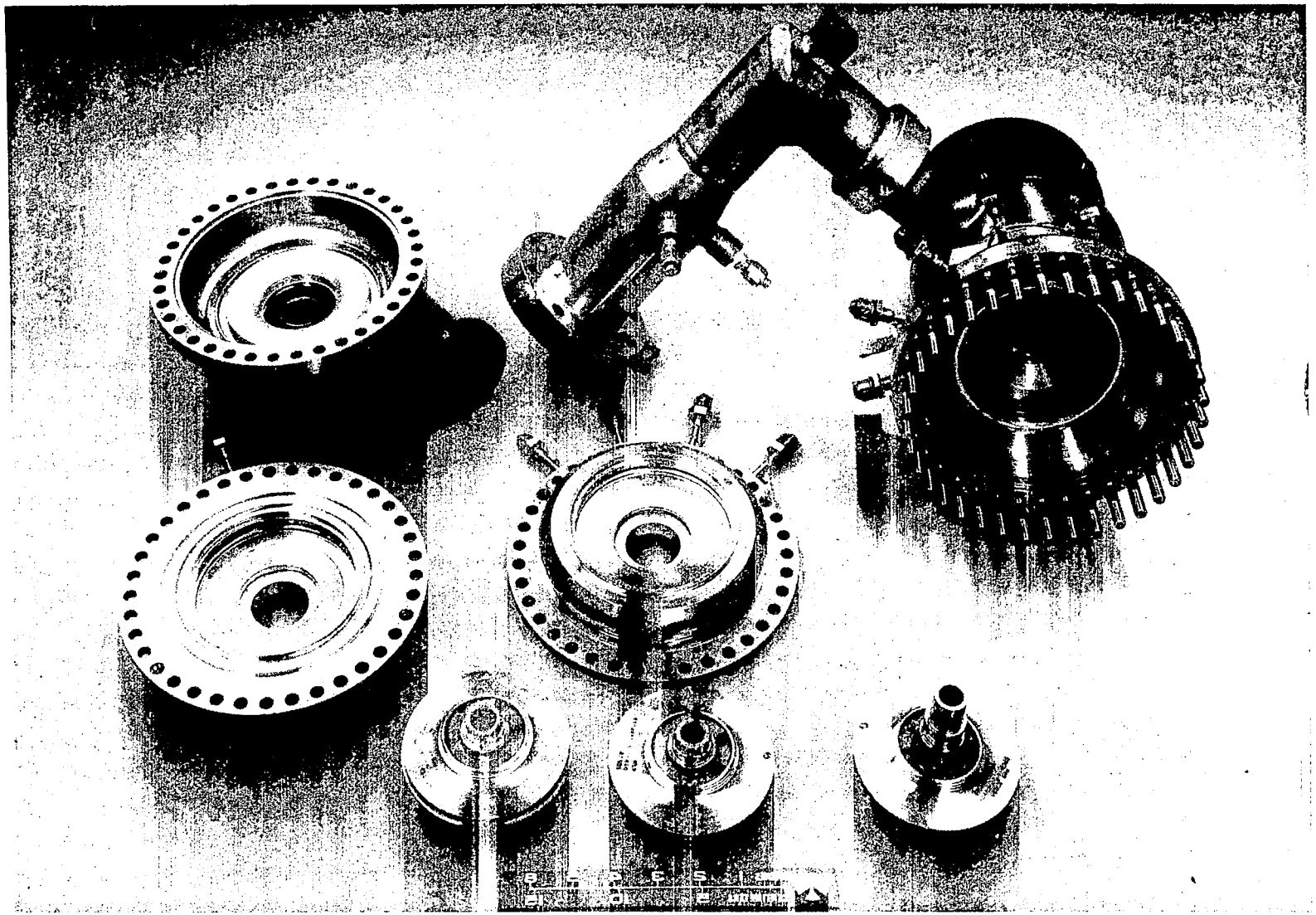

1HS55-6/23/76-C1A*

Figure 158. Mark 48-F Pump Components After Testing

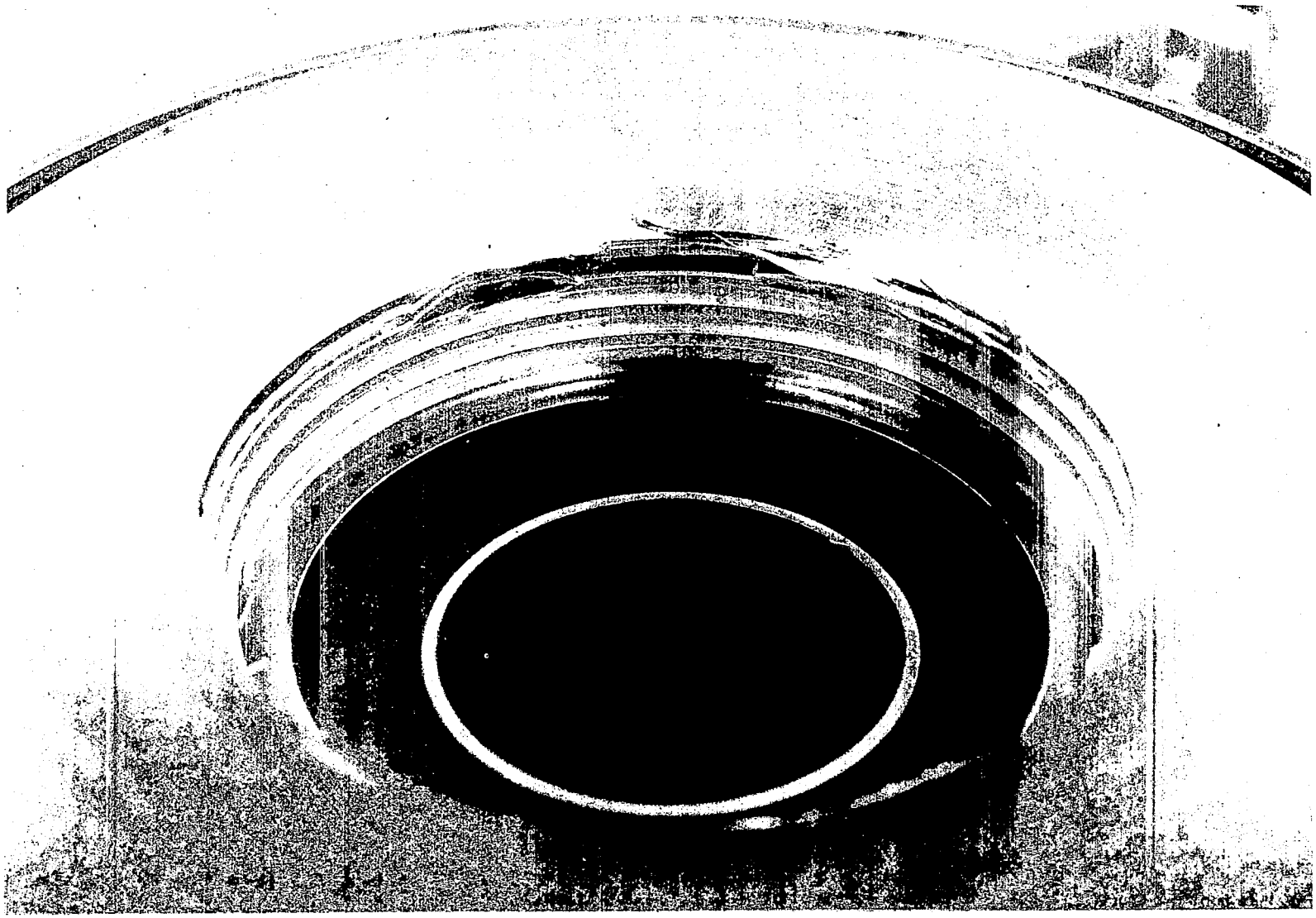

1HS55-6/23/76-C1C*

Figure 159. Mark 48-F Pump Third-Stage Front Wear-Ring Silver Plating Flaking

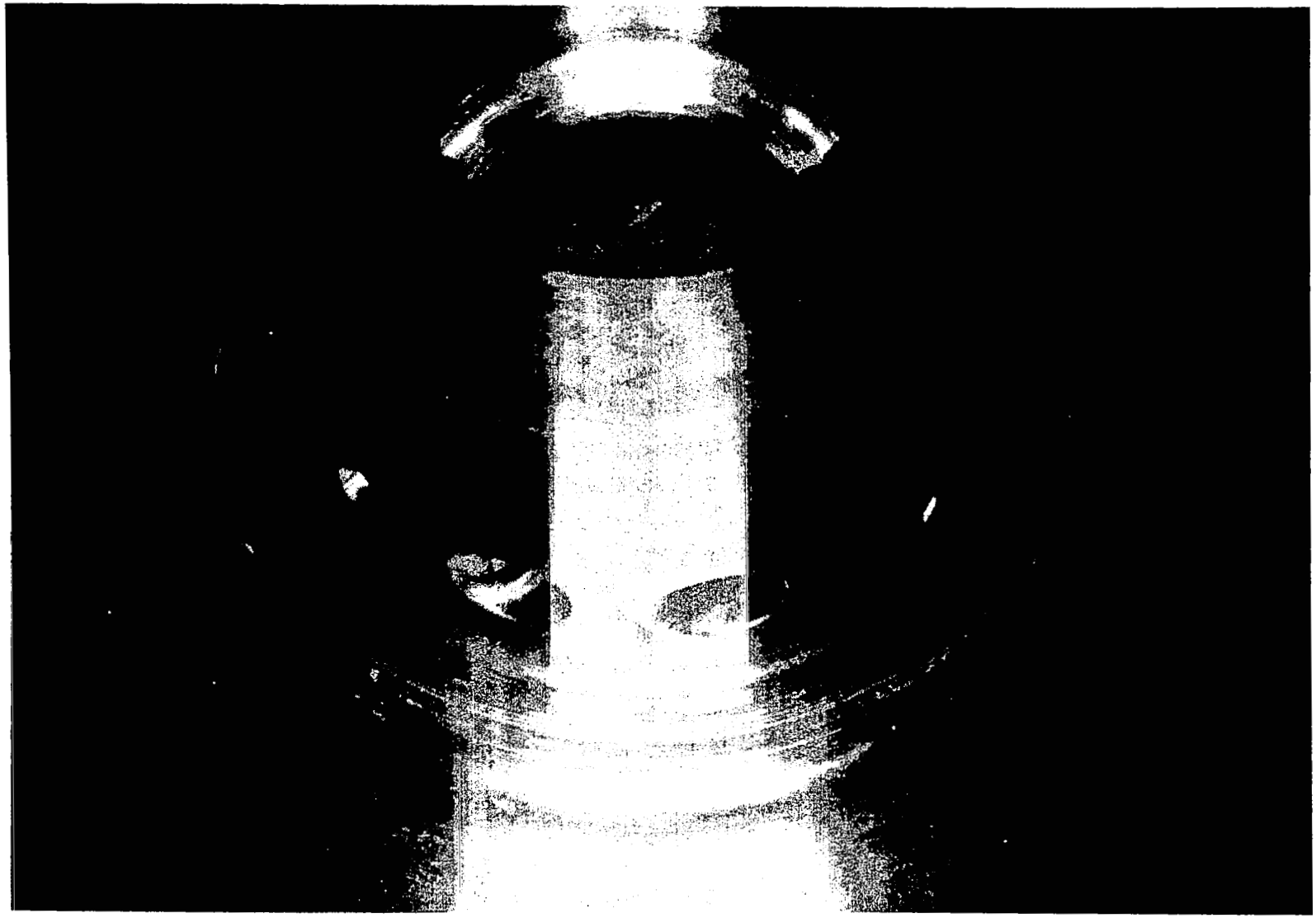

1HS55-6/23/76-C1G*

Figure 160. Mark 48-F Balance Piston Low-Pressure Orifice After Testing

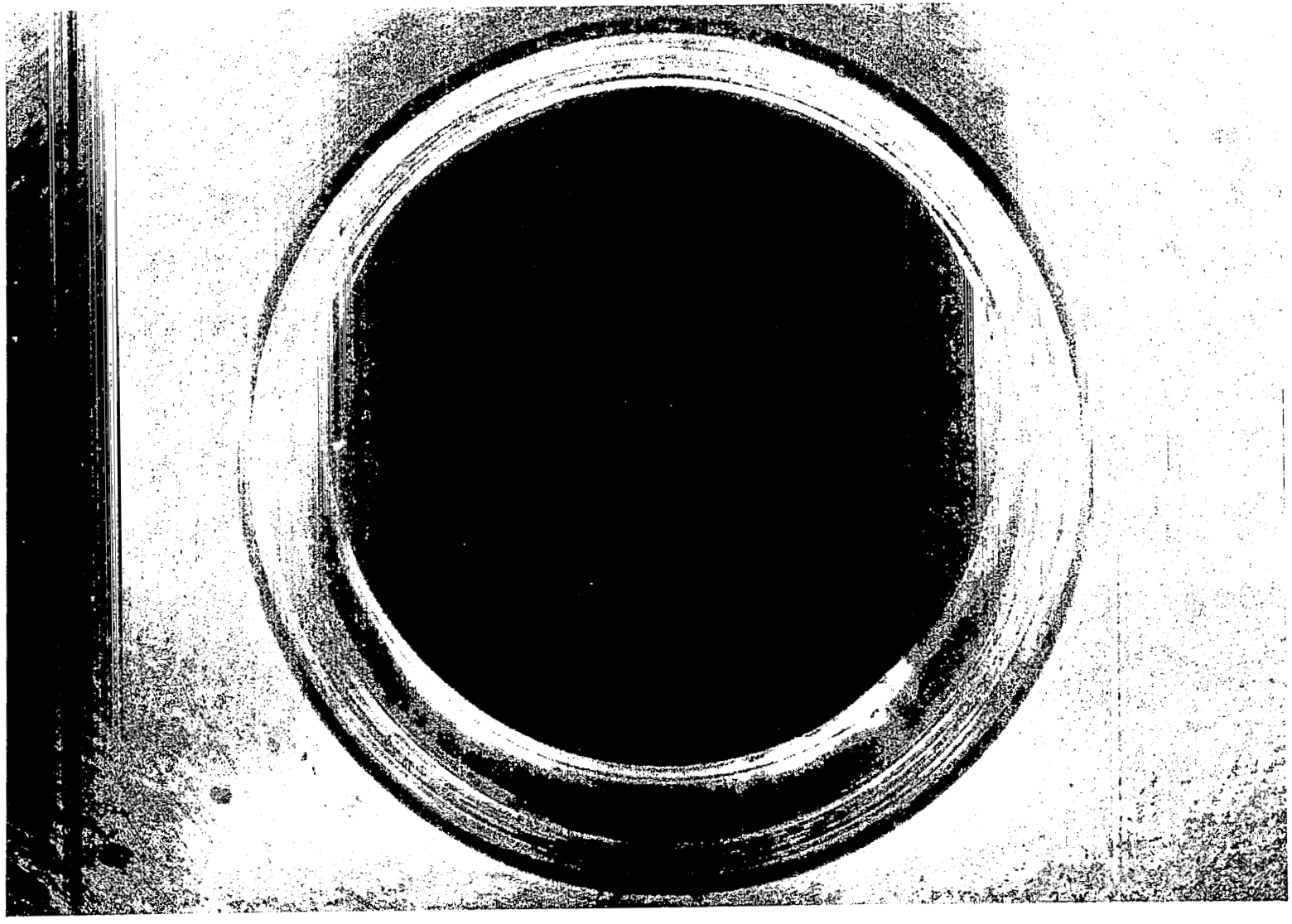

1HS55-6/23/76-C1D*

Figure 161. Mark 48-F Balance Piston Low-Pressure Orifice Rub Ring After Testing

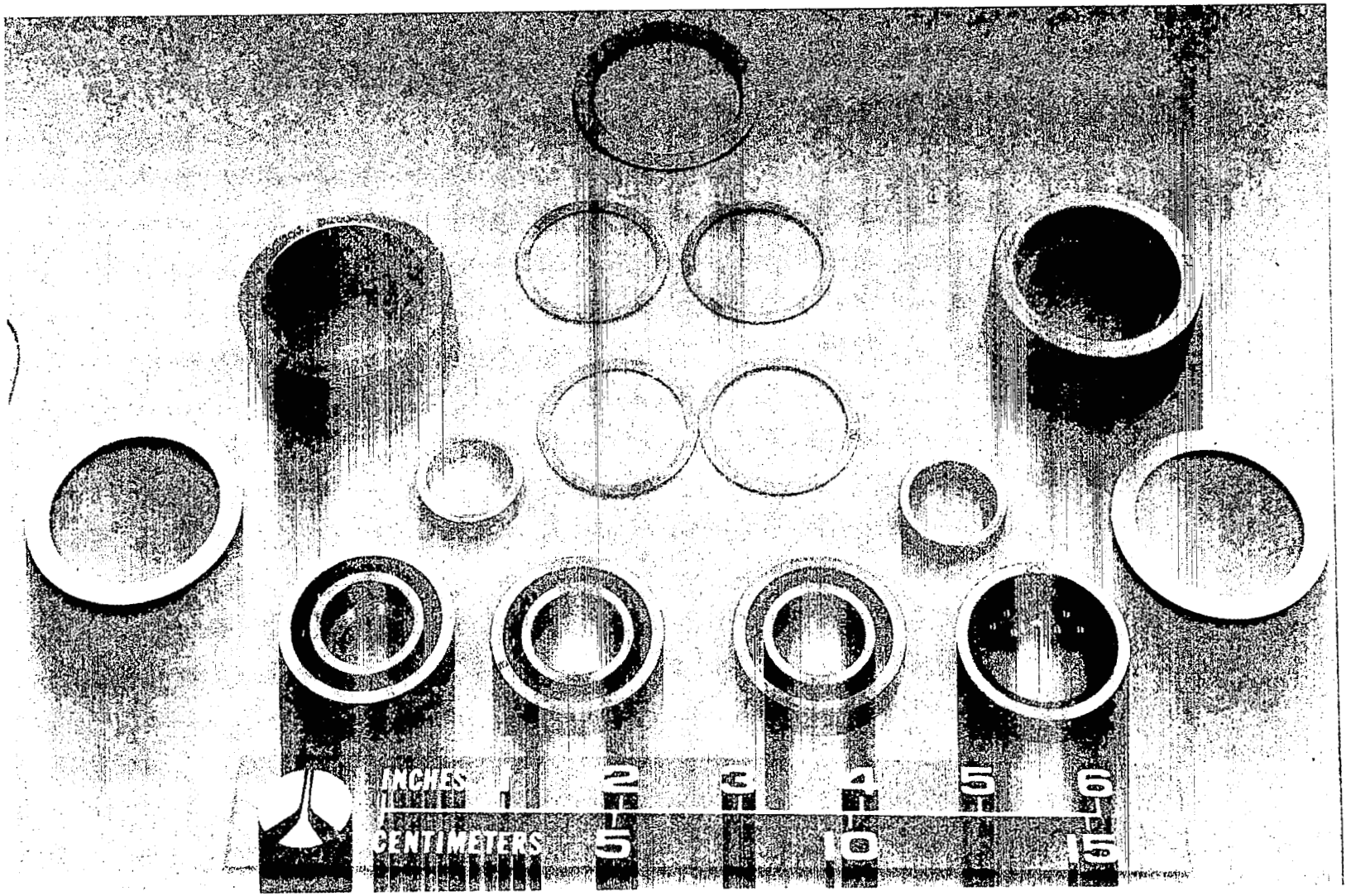

1HS55-6/23/76-C1E*

Figure 162. Mark 48-F Bearings Posttest

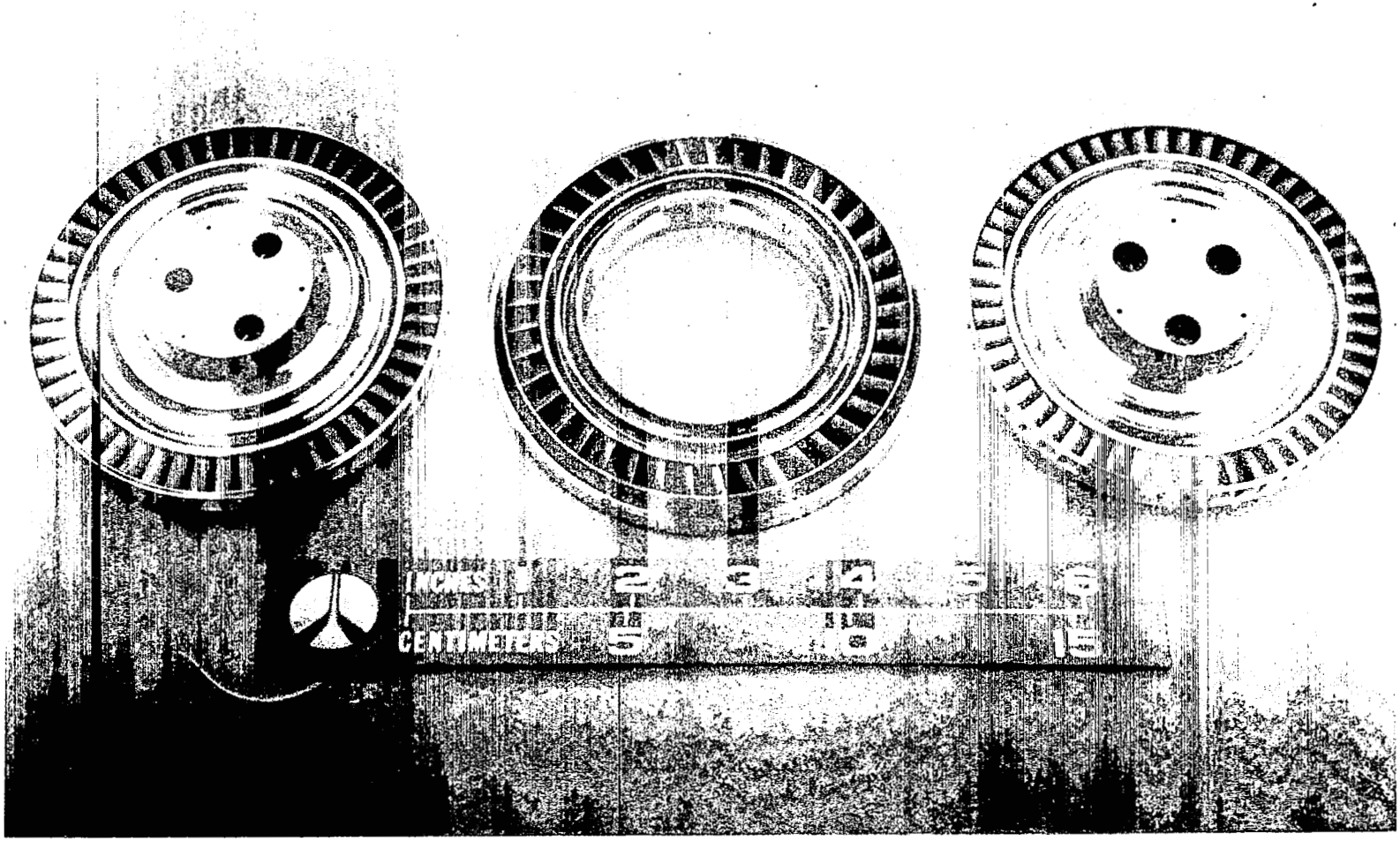

1HS55-6/23/76-C1B*

Figure 163. Mark 48-F Turbine Components Posttest

APPENDIX A

MARK 48-F DESIGN GROUND RULES

APPENDIX A

DESIGN GROUND RULES

General

Components which are subject to a low cycle fatigue mode of failure shall be designed for a minimum of 300 cycles times a safety factor of 4.

Components which are subject to a fracture mode of failure shall be designed for a minimum of 300 cycles times a safety factor of 4.

Components which are subject to a high cycle fatigue mode of failure shall be designed within the allowable stress range diagram (based on the material endurance limit). If stress range material property data are not available, modified Goodman diagrams constructed as shown below shall be utilized.

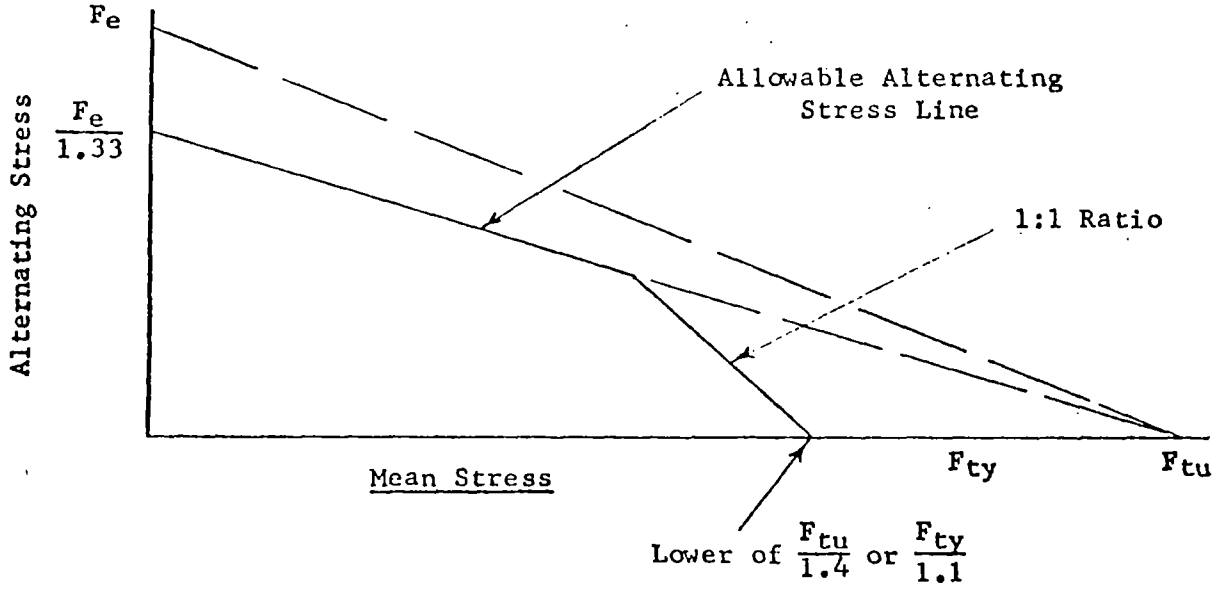

F_e = Material Endurance Limit
F_{ty} = Material Yield Strength (.2% offset)
F_{tu} = Material Ultimate Strength

Effective stress shall be based on the Mises-Hencky constant energy of distortion theory.

Unless otherwise noted under component ground rules specified herein, the following minimum factors of safety shall be utilized:

Factor of Safety (.2% yield) = 1.1 x Limit Load

Factor of Safety (Ultimate) = 1.4 x Limit Load

Limit Load: The maximum predicted load or pressure at the most critical operating condition

Components subject to pressure loading shall be designed to the following minimum proof and burst pressures:

Proof Pressure = 1.2 x Limit Pressure

Burst Pressure = 1.5 x Limit Pressure

Impeller

Inducers and/or impellers utilized in the high pressure pumps shall be designed for operation above incipient cavitation.

Impeller burst speed shall be at least 20% above the maximum operating speed.

Impeller effective stress at 5% above the maximum operating speed shall not exceed the allowable .2% yield stress. (Does not apply to areas in which local yielding is permitted.)

Turbine

Blade root steady-state stress shall not exceed the allowable 1% ten hour creep stress.

Stress state at the blade root as defined by the steady-state stress and an assumed vibratory stress equal to the gas bending stress shall be within the allowable stress range diagram or modified Goodman diagram.

No blade natural frequencies within $\pm$15% of known sources of excitation at steady-state operating speeds.

Disk burst speed shall be at least 20% above the maximum operating speed.

Disk maximum effective stress at 5% above the maximum operating speed shall not exceed the allowable .2% yield stress. (Does not apply to areas in which local yielding is permitted.)

Bearings

Turbopump designs shall utilize ball bearings.

Maximum DN: 2.0×10^6

B_{10} life 100 hours

Material:

Rolling Elements	440C
Races	440C

Seals

Turbopump designs shall utilize conventional type seals.

Face contact seal maximum PV, FV, and P_fV factors:*

	LH_2	H_2+H_2O
PV Factor	50,000	10,000
FV Factor	4,000	800
P_fV Factor	200,000	20,000

*PV = unit load times rubbing velocity (lb/in^2 x ft/sec)
FV = face load per unit length times rubbing velocity (lb/in x ft/sec)
P_fV = fluid pressure differential times rubbing velocity (psig x ft/sec)

Critical Speed

Rotor bending frequency shall be at least 25% above the rotor maximum operating speed.

A minimum margin of 20% shall be maintained between rotor rigid body critical speeds and rotor steady-state operating speeds at full thrust and the pumped-idle thrust condition. Rigid body critical speeds within the throttled-to-full thrust range shall be permitted only if deemed necessary by both the Contractor Program Manager and the NASA Project Engineer.

APPENDIX B

MARK 48-F TURBOPUMP
ASSEMBLY DRAWING
RS009601E

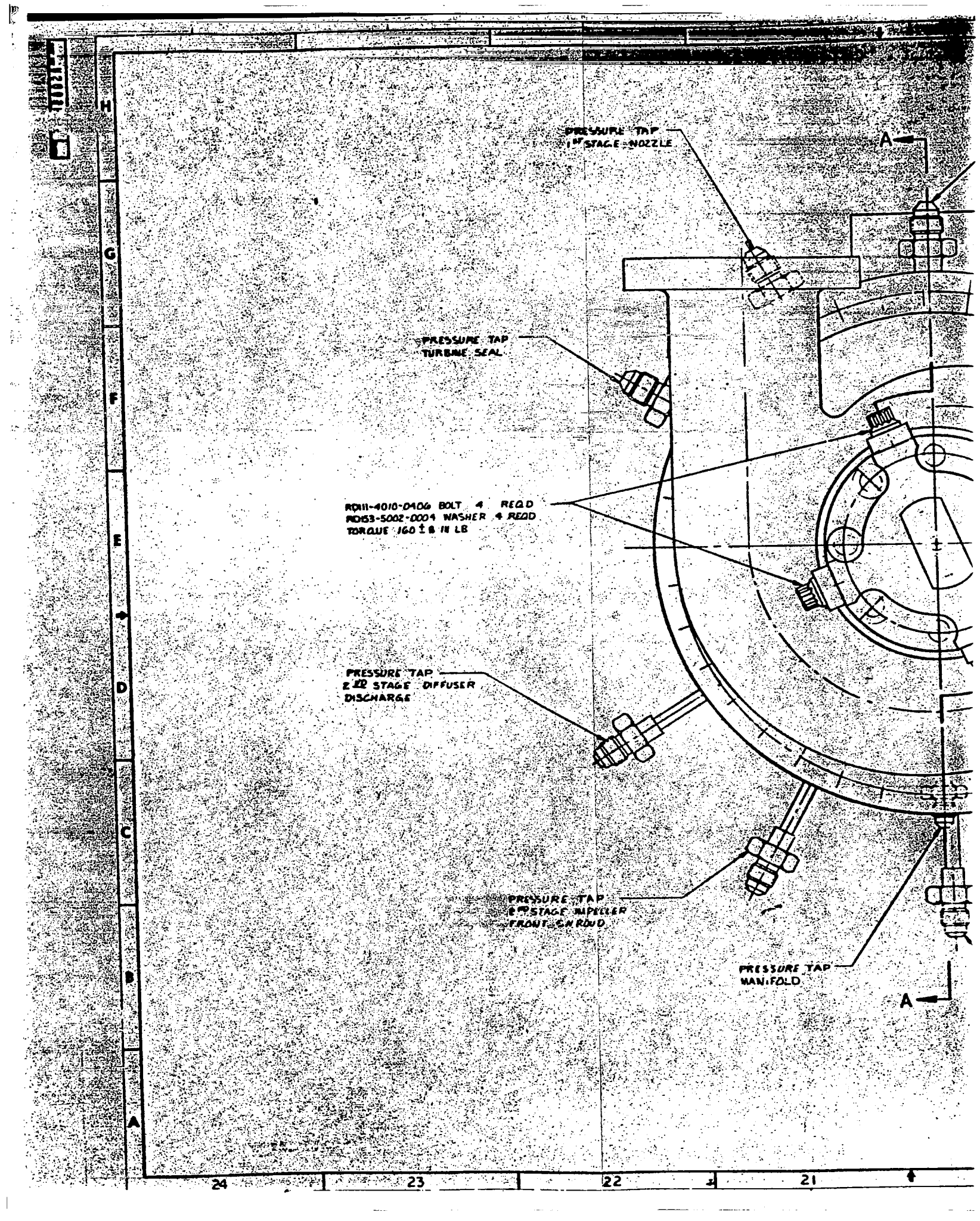
PRESSURE TAP
1ST STAGE NOZZLE
A
PRESSURE TAP
TURBINE SEAL
RD111-4010-0406 BOLT 4 REQD
RD153-5002-0004 WASHER 4 REQD
TORQUE 160 ± 8 IN LB
PRESSURE TAP
2ND STAGE DIFFUSER
DISCHARGE
PRESSURE TAP
2ND STAGE IMPELLER
FRONT SHROUD
PRESSURE TAP
MANIFOLD
A
H
G
F
E
D
C
B
A
24
23
22
21

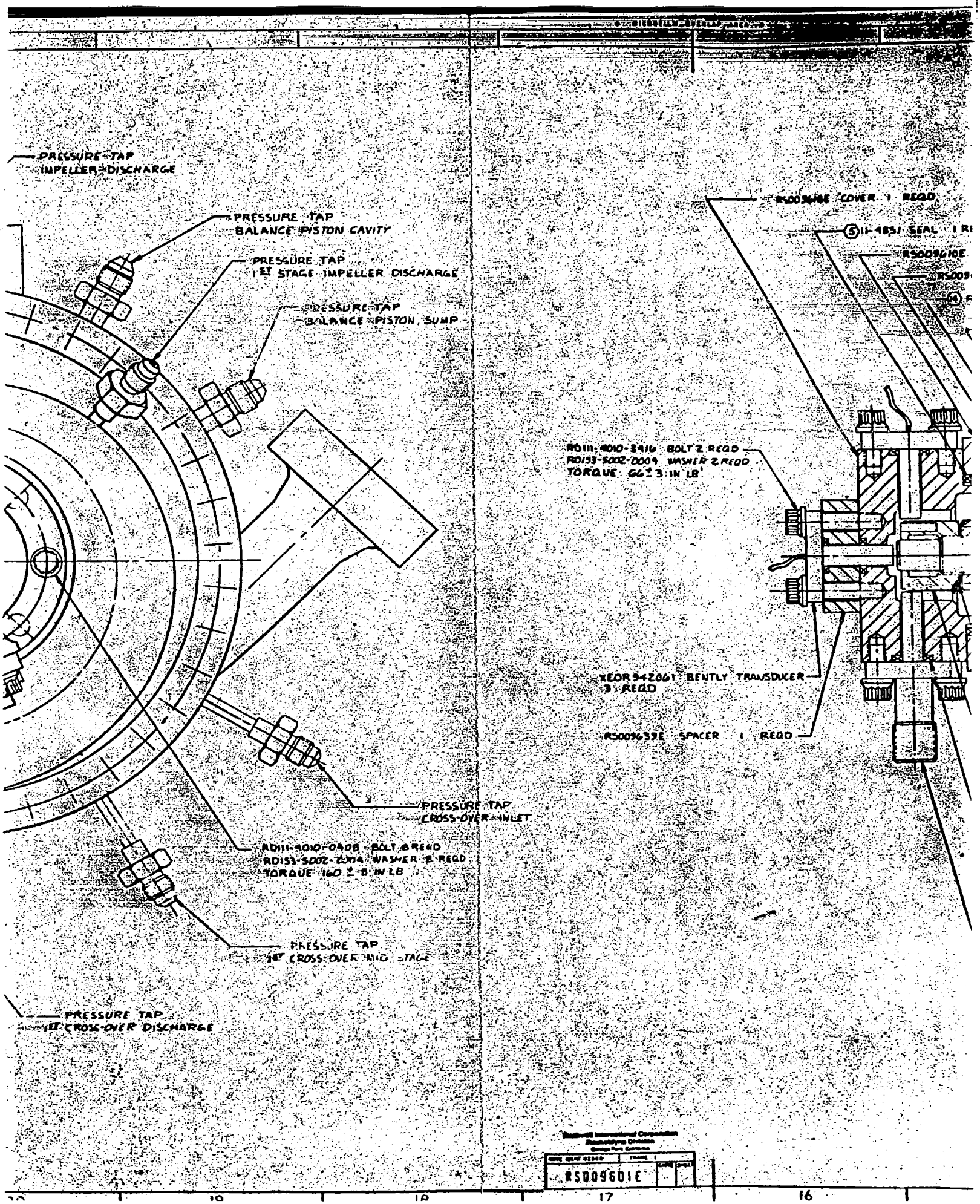
PRESSURE TAP
IMPELLER DISCHARGE
PRESSURE TAP
BALANCE PISTON CAVITY
PRESSURE TAP
1ST STAGE IMPELLER DISCHARGE
PRESSURE TAP
BALANCE PISTON SUMP
PRESSURE TAP
CROSS-OVER INLET
RD111-4010-0408 BOLT 8 REQD
RD133-5002-0014 WASHER 8 REQD
TORQUE 160 ± 8 IN LB
PRESSURE TAP
1ST CROSS-OVER MID-STAGE
PRESSURE TAP
1ST CROSS-OVER DISCHARGE
RS0096BE COVER 1 REQD
RS0096IOE
RD111-4010-3416 BOLT 2 REQD
RD133-5002-0009 WASHER 2 REQD
TORQUE 66 ± 3 IN LB
XEOR942061 BENTLY TRANSDUCER
3 REQD
RS0096J9E SPACER 1 REQD

RS0096D1E

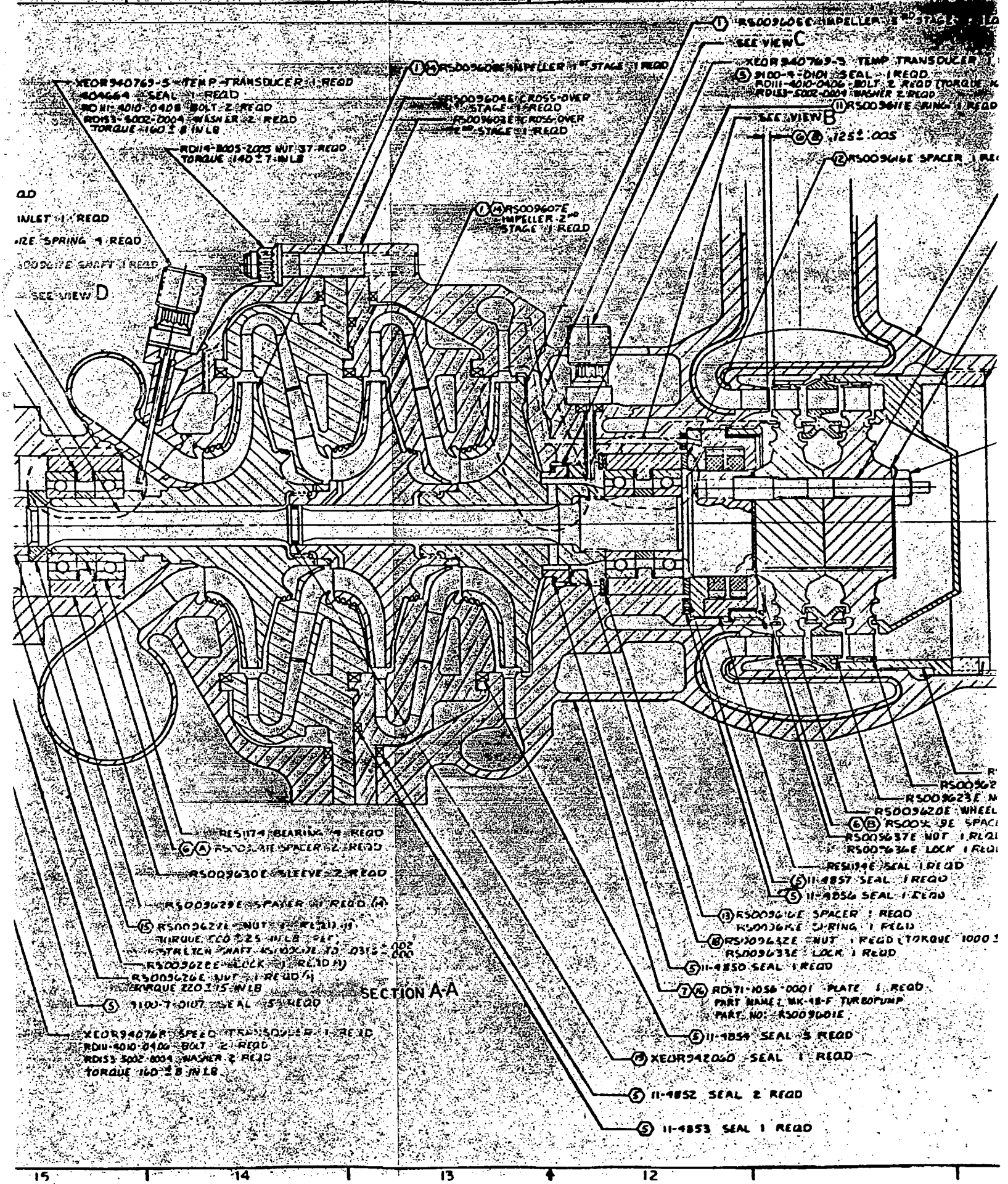
SEE VIEW C
SEE VIEW B
SEE VIEW D
SECTION A-A
XEOR940769-5 TEMP TRANSDUCER 1 REQD
404664 SEAL 1 REQD
RD111-4010-0406 BOLT 2 REQD
RD153-5002-0004 WASHER 2 REQD
TORQUE 160 ± 8 IN LB
RD114-8005-2005 NUT 37 REQD
TORQUE 140 ± 7 IN LB
RS009606E IMPELLER 1ST STAGE 1 REQD
RS009604E CROSS-OVER 1ST STAGE 1 REQD
RS009603E CROSS-OVER 2ND STAGE 1 REQD
RS009607E IMPELLER 2ND STAGE 1 REQD
.125 ± .005
RS009616E SPACER 1 REQD
RES1174 BEARING 4 REQD
RS009631E SPACER 2 REQD
RS009630E SLEEVE 2 REQD
RS009629E SPACER 1 REQD
RS009622E NUT 1 REQD
TORQUE 220 ± 25 IN LB
STRETCH SHAFT .031 ± .002
RS009626E NUT 1 REQD
TORQUE 220 ± 15 IN LB
RS009628E LOCK 1 REQD
9100-7-0107 SEAL 5 REQD
XEOR940768-5 SPEED TRANSDUCER 1 REQD
RD111-4010-0406 BOLT 2 REQD
RD153-5002-0004 WASHER 2 REQD
TORQUE 160 ± 8 IN LB
RS009623E SPACER 1 REQD
RS009620E WHEEL
RS009637E NUT 1 REQD
RS009634E LOCK 1 REQD
RES1134E SEAL 1 REQD
11-4857 SEAL 1 REQD
11-4856 SEAL 1 REQD
RS009616E SPACER 1 REQD
RS009615E O-RING 1 REQD
RS009632E NUT 1 REQD TORQUE 1000
RS009633E LOCK 1 REQD
11-4850 SEAL 1 REQD
RD171-1056-0001 PLATE 1 REQD
PART NAME: MK-48-F TURBOPUMP
PART NO: RS009601E
11-4854 SEAL 3 REQD
XEOR942060 SEAL 1 REQD
11-4852 SEAL 2 REQD
11-4853 SEAL 1 REQD

5 IN LB)

RS009602E HOUSING 1 REQD

RS009635E STUD 3 REQD (14)

RS009638E LOCK 3 REQD (14)

RS009621E NUT 1 REQD
RS009624E LOCK 1 REQD
TORQUE 1100 ± 70 IN LB

MS9357-10 NUT 3 REQD
TORQUE 60 ± 3 IN LB
STRETCH TO .0085 ± .0008

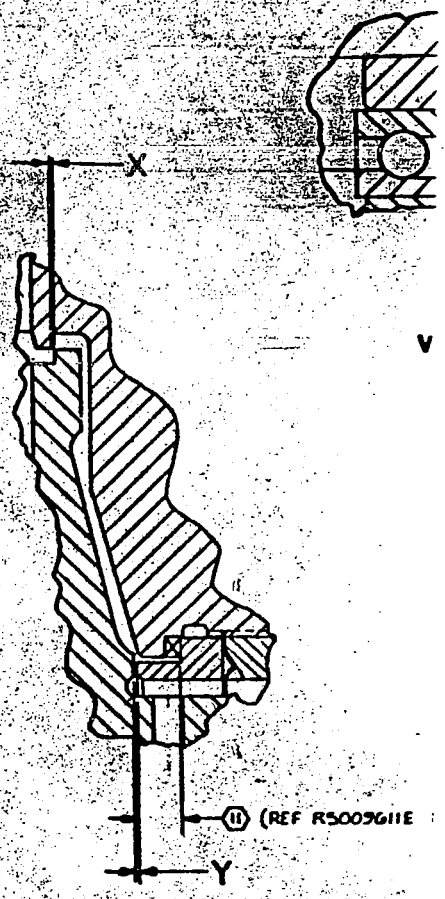

VIEW C

634E COVER 1 REQD
WHEEL 2ND STAGE 1 REQD (14)
E 2ND STAGE 1 REQD
AGE 1 REQD (14)
1 REQD (14)
RQUE 9200 ± 460 (IN LB)

N LB)

RS009601E

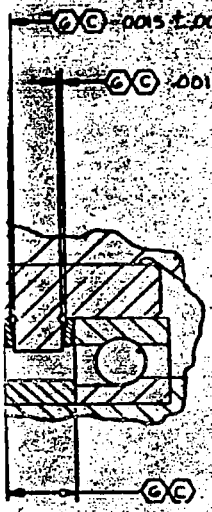

EW D

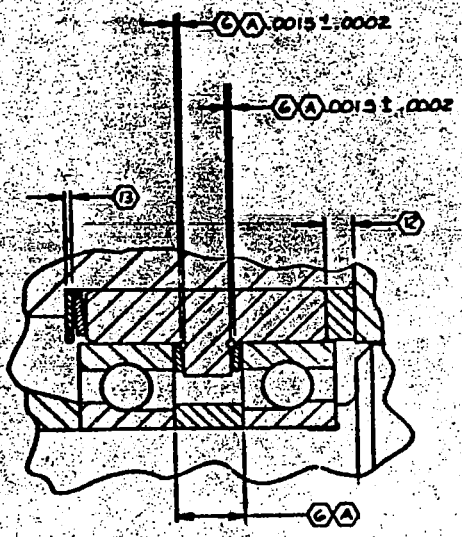

VIEW B

ING)

(M) INSTALL WITH OPEN END TOWARD TURBINE.
(L) LUBRICATE WITH MOLYKOTE TYPE Z POWDER PER RA0112-002 METHOD W ON MATING SURFACE OF RS0096320 & RS0096330.
(K) PRIOR TO ASSEMBLY, CLEAN PER RA0110-004, USE MIL-C-81302 ONLY FOR PARTS CODED (1).
(J) APPLY PER RA0104-010.
(H) (G) SPRAY 65-3 TEFLON-LUBE, RAM CHEMICAL INC., GARDENA, CAL. TO RS0096270 MUTUAL MATING SURFACES.
(F) BALANCE ROTOR ASSEMBLY TO WITHIN .02 GRAM INCHES.
MATCH MARK ALL ROTOR ASSEMBLY COMPONENTS PER RA0104-008 BY ELECTRO CHEM ETCH. CODED PARTS ARE COMPONENTS OF THE ROTOR ASSEMBLY. ALIGN MATCHMARKS.
(E) MACHINE SPACER THICKNESS PER DETAIL DRAWING TO OBTAIN AT LIQUID NITROGEN TEMPERATURE A FORCE OF 800 ± 50 LB ON THE ROTOR WHEN CLEARANCE Y IS .009 INCH.
(D) MACHINE SPACER THICKNESS PER DETAIL DRAWING TO OBTAIN AT LIQUID NITROGEN TEMPERATURE A FORCE OF 800 ± 50 LB ON THE ROTOR WHEN CLEARANCE Y IS ZERO.
(C) MACHINE DIMENSION PER DETAIL DRAWING TO OBTAIN Y = 0. WHEN Y = .0042 ± .0002 AT AMBIENT TEMPERATURE.
(B) GENTLY-NEVADA CORP., MINDEN, NEVADA.
(A) ACCRODYNAMICS, JACKSON, MICH.
8 INSTALL FITTING AND TUBE ASSEMBLIES PER RA0102-008.
(7) IDENTIFY PER RA0104-009.
(6) MACHINE SPACER PER DETAIL DRAWING TO OBTAIN MATCH CODED DIMENSIONS.
(5) HYDRODYNE DIVISION, F.P.I., INC. NORTH HOLLYWOOD, CA.
4. INSTALL PROTECTIVE COVERS OVER ALL EXPOSED FLANGES, TUBE FITTING & PORTS.
3. LEAK CHECK PUMP ASSEMBLY. ALLOWABLE LEAKAGE RATES.

ALL EXTERNAL FLANGES	ZERO
ALL FITTINGS	ZERO
SHAFT SEAL	250 SCIM MAX He GAS

TEST CONDITIONS FOR LEAK TEST:

GG SUPPLY	30 ± 5 PSIG
PUMP SPEED	AS REQ'D
FLUID	AMBIENT

2 INSTALL THREADED FASTENERS PER RA0105-002.
(1) TITANIUM PARTS. CLEAN WITH MIL-C-81302 ONLY.

THIS PRINT REDUCED
RELEASED DOCUMENT

NONE		Rocketdyne Division, Canoga Park, California	
NONE		TURBOPUMP ASSY, FUEL	
		02602	RS009601E

5 4 3 2 1

APPENDIX C

MARK 48-F TEST SEQUENCE

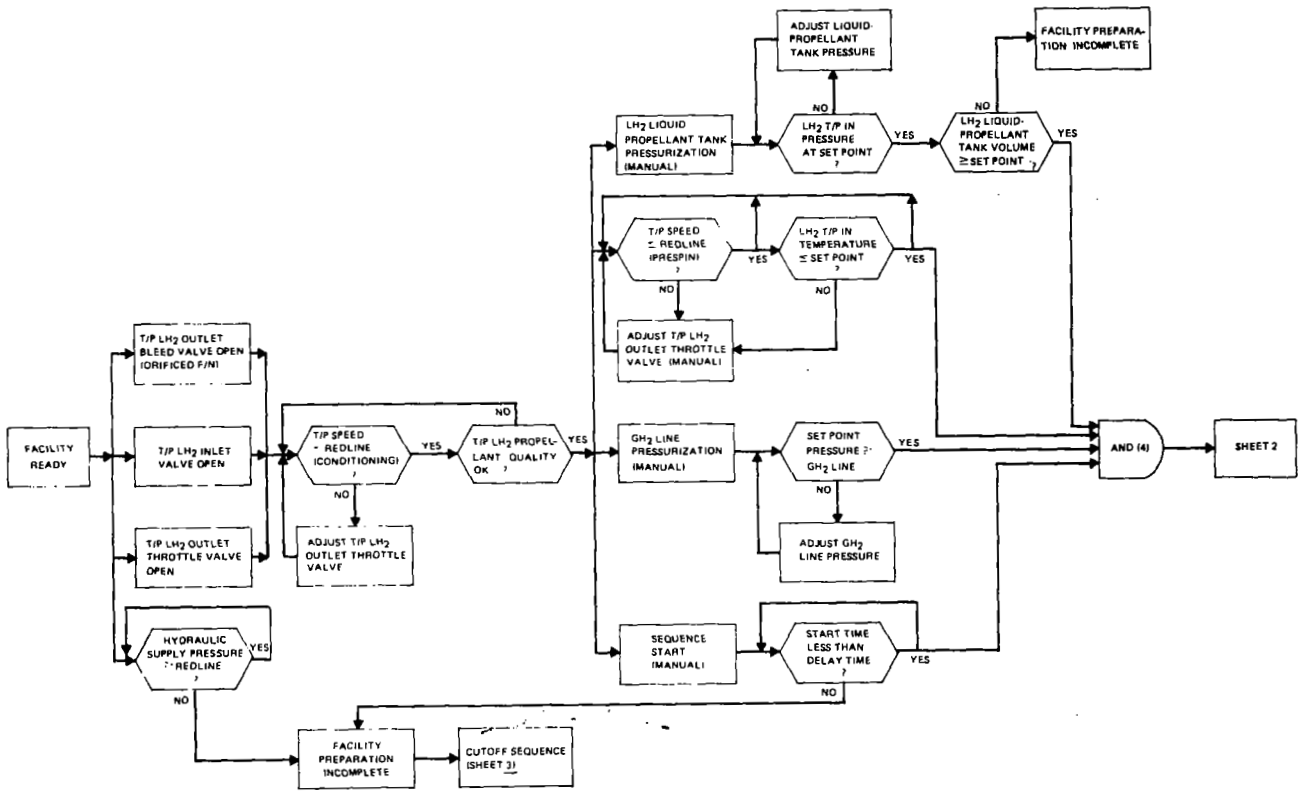

LH_2 Pump Inlet Conditioning and Sequence Start (Sheet 1)

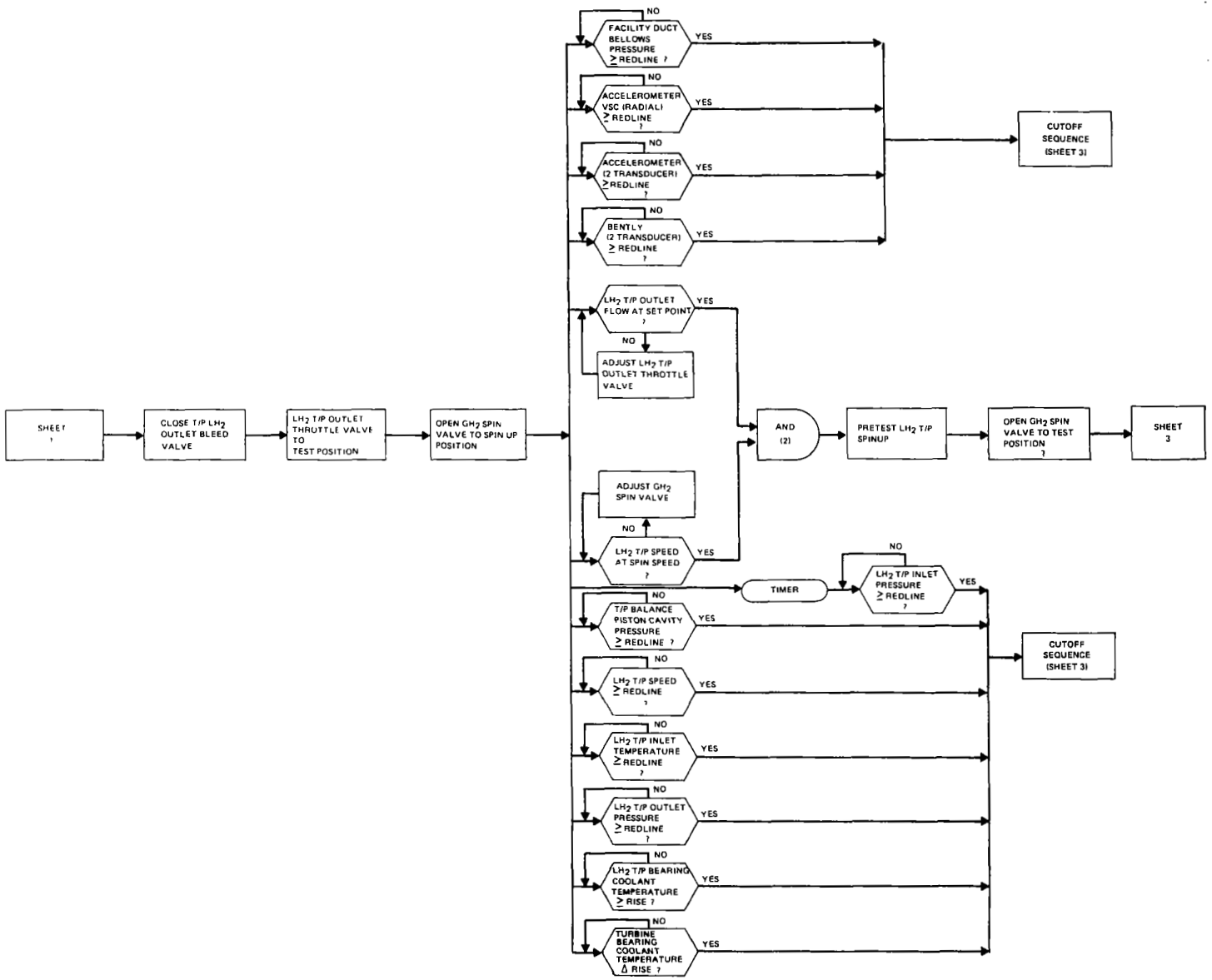

Turbopump Spin-Up and Test Start (Sheet 2)

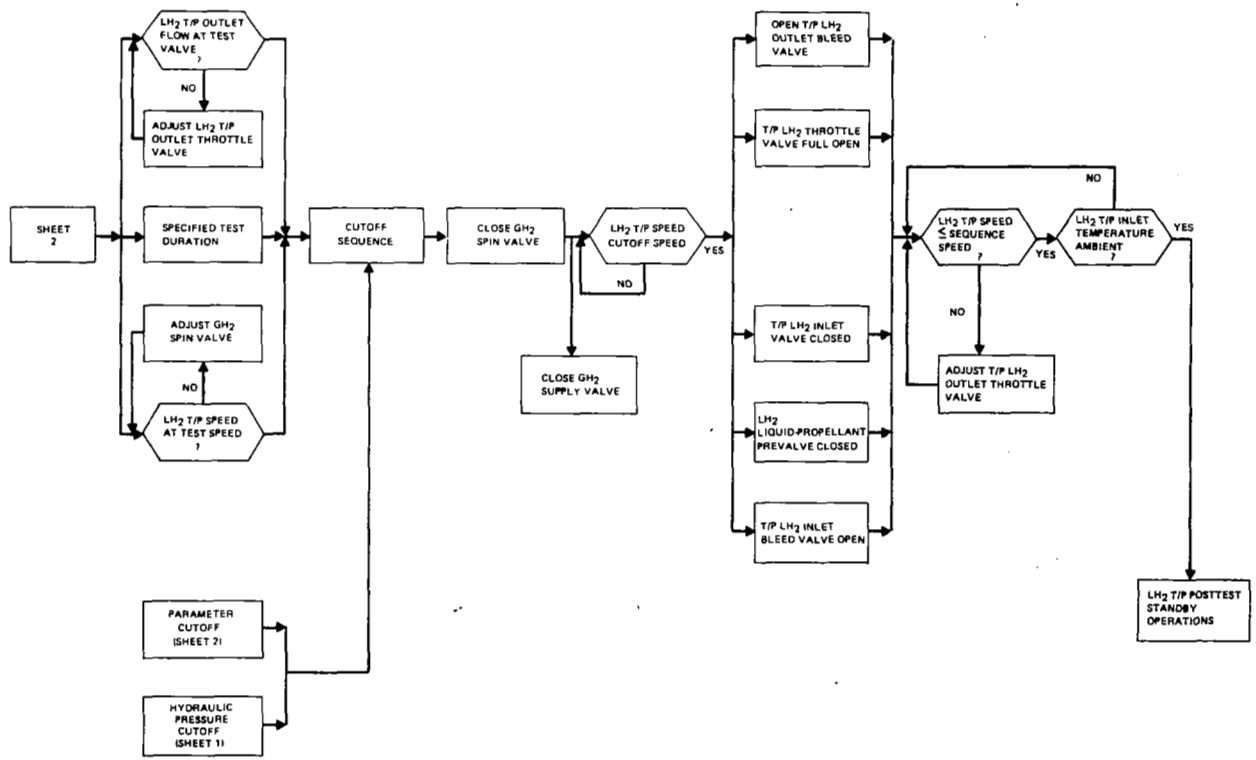

Mainstage and Cutoff (Sheet 3)

APPENDIX D

MARK 48-F TEST DATA

RUN NUMBER 9
TEST DATE 04-15-76
PROCESSING DATE 05-5-76

COMMENTS . . .

TUG PUMP REDUCTION RESEARCH STAND C16
TURB GH2 FLOW IS CALCULATED FROM TURB DISCH ORIFICE DELTA P. * NO DATA

AMBIENT PRESSURE	13.5700
LO2 VENTURI (GG)	
UPSTREAM DIAMETER	0.9570
THROAT DIAMETER	0.3740
THROAT CC	0.9880
GH2 VENTURI (TURB)	
UPSTREAM DIAMETER	2.3000
THROAT DIAMETER	1.3085
THROAT CC	0.9873
LH2 VENTURI (GG)	
UPSTREAM DIAMETER	1.6890
THROAT DIAMETER	0.7090
THROAT CC	0.9760
LH2 VENTURI (PUMP DISCH)	
UPSTREAM DIAMETER	1.6890
THROAT DIAMETER	0.8800
THROAT CC	0.9710

MK48-F
LIQUID HYDROGEN TURBOPUMP ASSEMBLY

RUN NUMBER
TEST DATE

PROCESSING DATE

GASEOUS HYDROGEN TURBINE DRIVE PARAMETERS

TIME SLICE NO	BEGIN TIME (SEC)	END TIME (SEC)	REG U/S PR (PSIA)	VENTURI U/S PR (PSIA)	VENTURI U/S TEMP (DEG R)	VENTURI DELTA PR (PSID)	SPIN VALVE POSN	SPIN VALVE U/S PR (PSIA)	FAC DUCT PRESS (PSIA)	TURB GH2 FLOW LB/SEC
1	22.024	22.540	4269.07	4246.17	511.33	*	0.77	4127.87	68.03	7.336
2	23.014	23.530	4206.67	4181.87	510.78	*	0.70	4054.97	69.54	7.460
3	24.004	24.231	4147.57	4115.87	510.63	*	0.43	3959.67	76.83	8.144
4	25.000	25.839	4030.47	3990.37	509.71	*	-0.19	3800.67	84.50	8.938
5	25.991	26.128	4006.07	3965.67	509.59	*	-0.20	3776.07	83.72	8.891
6	26.981	26.458	3981.77	3942.37	509.54	*	-0.20	3754.17	83.17	8.827
7	28.005	28.552	3843.17	3803.37	508.25	*	-0.33	3616.87	81.39	8.649
8	29.051	29.758	3748.77	3708.67	507.43	*	-0.54	3520.77	80.27	8.532
9	33.057	33.552	3510.67	3472.97	505.03	*	-0.55	3297.87	75.54	8.076
10	37.057	37.953	3275.17	3239.97	502.18	*	-0.55	3074.07	70.46	7.608
11	44.008	44.523	2916.57	2886.27	497.10	*	-0.55	2734.07	62.92	6.940
12	51.019	51.535	2612.47	2585.97	491.70	*	-0.54	2445.87	56.45	6.324

RUN NUMBER 9
TEST DATE
PROCESSING DATE

T U R B I N E P A R A M E T E R S

TIME SLICE NO	SPEED RPM	TURB INLET STAT PR (PSIA)	TURB INLET TOT PR (PSIA)	TURB MANIF PR (PSIA)	TURB 1ST NOZZ D/S PR (PSIA)	TURB SEAL PR (PSIA)	TURB EXH STAT PR (PSIA)	TURB EXH TOT PR (PSIA)	TURB INLET TOT TEMP (DEG R)	TURB EXH TOT TEMP (DEG R)
1	8[illegible]00.	2455.07	2462.97	2473.67	2117.57	2752.97	1650.77	1615.87	521.37	472.26
2	8[illegible]000.	2506.67	2515.07	2527.47	2163.77	2781.07	1684.37	1642.27	520.54	471.75
3	8[illegible]500.	2778.27	2787.07	2802.47	2399.07	3007.47	1860.37	1788.97	518.80	470.07
4	92000.	3038.57	3049.17	3063.77	2623.87	3305.37	2027.97	1955.27	515.61	466.57
5	9[illegible]000.	3021.17	3032.37	3048.47	2609.47	3303.27	2017.47	1943.97	515.55	466.11
6	8[illegible]000.	3001.47	3012.47	3027.17	2592.37	3288.37	2004.57	1929.77	515.49	465.97
7	9[illegible]000.	2954.57	2965.47	2979.77	2534.67	3227.67	1961.57	1889.27	513.87	464.95
8	9[illegible]000.	2892.37	2902.07	2918.87	2498.57	3190.97	1933.87	1862.07	512.97	464.09
9	8[illegible]000.	2741.87	2721.67	2735.17	2342.17	3029.77	1817.27	1759.67	510.49	462.12
10	8[illegible]000.	2627.07	2535.37	2549.27	2180.67	2960.57	1695.57	1654.27	508.07	459.78
11	81000.	2248.47	2255.37	2269.07	1939.27	2600.77	1513.17	1503.27	503.34	455.53
12	77000.	2012.77	2018.47	2031.37	1734.47	2373.57	1357.97	1364.67	498.24	451.55

MK48-F
LIQUID HYDROGEN TURBOPUMP ASSEMBLY

RUN NUMBER 9
TEST DATE

PROCESSING DATE

P U M P T E M P E R A T U R E S

TIME SLICE NO	SPEED RPM	PUMP INLET TEMP 1 (DEG R)	PUMP INLET TEMP 2 (DEG R)	PUMP DISCH TEMP 1 (DEG R)	PUMP DISCH TEMP 2 (DEG R)	FRONT BRG COOL TEMP (DEG R)	REAR BRG COOL TEMP (DEG R)	DISCH VENT L/S TEMP (DEG R)
1	85500.	41.45	40.00	94.18	95.23	106.86	80.46	94.70
2	84000.	41.39	40.00	94.75	95.39	110.73	82.62	95.07
3	83500.	41.35	40.00	99.09	98.87	125.85	83.90	98.98
4	92000.	40.95	39.90	103.28	103.49	184.19	86.78	103.38
5	90000.	40.68	39.76	102.30	102.88	179.88	87.34	102.59
6	89000.	40.58	39.74	101.47	102.08	173.79	87.83	101.78
7	90000.	40.46	39.69	100.01	100.66	157.27	90.13	100.34
8	90000.	40.42	39.69	99.31	100.15	151.67	91.37	99.73
9	85000.	40.21	39.57	95.77	97.15	127.90	93.92	96.46
10	83000.	40.21	39.53	92.32	93.87	118.95	96.70	93.09
11	81000.	40.27	39.53	87.46	89.09	113.80	101.00	88.28
12	77000.	40.32	39.51	82.75	83.71	104.79	102.15	83.23

RUN NUMBER 9
TEST DATE
PROCESSING DATE

PUMP PRESSURES

TIME SLICE NO	SPEED RPM	LH2 TANK PR (PSIA)	PUMP INLET PR #1 (PSIA)	PUMP INLET PR #2 (PSIA)	1ST IMP DISCH PR (PSIA)	1ST XOVER INLET PR (PSIA)	1ST XOVER MID PR (PSIA)	1ST XOVER OUT PR (PSIA)	2ND IMP FR SHD PR (PSIA)
1	85500.	110.04	99.06	102.94	713.28	957.73	1038.39	1039.40	1616.07
2	87000.	109.73	98.36	102.25	708.08	949.54	1000.69	1001.91	1617.77
3	88500.	111.39	99.13	103.29	727.50	984.92	1039.07	1040.37	1710.87
4	92000.	114.23	101.80	106.40	819.02	1113.27	1168.17	1169.77	1898.17
5	93000.	113.93	101.32	105.91	828.71	1125.77	1180.17	1181.57	1907.77
6	93000.	113.68	101.40	105.94	830.92	1128.57	1182.07	1184.17	1905.17
7	93000.	112.33	99.91	104.36	814.51	1105.67	1158.77	1160.47	1866.47
8	93000.	111.45	99.44	103.84	806.35	1092.77	1145.97	1147.47	1847.27
9	88000.	109.82	97.70	101.95	784.90	1058.87	1111.17	1112.27	1773.97
10	85500.	109.07	97.63	101.68	764.97	1029.27	1081.07	1081.77	1696.87
11	81000.	108.73	97.91	101.69	733.26	980.12	1029.97	1029.97	1581.47
12	77000.	109.09	98.80	102.40	714.06	943.47	991.44	991.24	1486.27

MK48-F
LIQUID HYDROGEN TURBOPUMP ASSEMBLY

RUN NUMBER 9
TEST DATE

PROCESSING DATE

P U M P P R E S S U R E S (CONTINUED)

TIME SLICE NO	2ND DIFFUSER DISCH PR (PSIA)	3RD IMP DISCH PR (PSIA)	PUMP DISCH PR (PSIA)	BAL PIST CAVITY PR (PSIA)	BAL PIST SUMP PR (PSIA)	PUMP VENTURI U/S TEMP (DEG R)	PUMP VENTURI U/S PR (PSIA)	PUMP VENTURI DELTA P (PSID)	PUMP DISCH VALVE POSN	PUMP DIS VALVE D/S PR (PSIA)
1	2249.37	3530.37	3550.37	2483.87	1538.27	94.70	3539.47	30.25	-0.56	948.90
2	2256.77	3578.27	3574.97	2498.87	1542.17	95.07	3564.27	30.64	-0.56	957.57
3	2398.77	3793.27	3824.97	2679.97	1643.77	98.98	3813.27	32.37	-0.56	1034.67
4	2642.37	4117.07	4181.27	2943.97	1824.57	103.38	4169.07	33.84	-0.56	1147.47
5	2649.37	4120.97	4182.67	2946.57	1830.37	102.59	4170.77	33.85	-0.56	1146.37
6	2642.47	4107.17	4165.67	2935.97	1825.37	101.78	4154.57	33.94	-0.56	1141.07
7	2594.47	4040.47	4091.27	2877.27	1788.77	100.34	4080.27	33.59	-0.56	1112.57
8	2565.37	3999.37	4047.57	2845.07	1768.97	99.73	4036.47	33.32	-0.56	1097.57
9	2457.77	3840.37	3861.97	2709.67	1691.77	96.46	3852.77	32.19	-0.56	1037.37
10	2345.77	3667.77	3664.17	2570.77	1615.07	93.09	3656.17	31.07	-0.56	973.29
11	2172.47	3389.97	3360.57	2361.77	1496.37	88.28	3354.77	29.36	-0.57	875.92
12	2022.37	2778.77	3092.37	2174.47	1395.47	83.23	3087.87	28.03	-0.57	787.90

RUN NUMBER 9 PROCESSING DATE
TEST DATE

C A L C U L A T E D P U M P P A R A M E T E R S

TIME SLICE NO	TEST SPEED (RPM)	PUMP FLOW GPM	PUMP FLOW (LB/SEC)	HEAD ISEN FT	PRESS RISE (PSI)	FLUID HP (HP)	TURB HP (HP)	EFF ISEN (%)	OVERALL EFF (%)	SPECIFIC SPEED
1	85000.	483.05	4.6203	105579.9	3449.4	886.9	1811.23	57.86	48.97	685.
2	84000.	486.11	4.6502	106254.9	3474.7	898.4	1862.76	57.80	48.23	672.
3	88000.	499.52	4.7814	113382.9	3723.8	985.7	2106.27	57.52	46.80	684.
4	92000.	509.13	4.9040	122935.1	4077.2	1096.1	2299.77	57.37	47.66	675.
5	93000.	508.29	4.9135	122908.2	4079.1	1098.0	2284.14	57.72	48.07	682.
6	88000.	508.35	4.9260	122413.5	4062.0	1096.4	2290.75	58.04	47.86	683.
7	90000.	505.45	4.9033	120368.5	3989.1	1073.1	2221.76	58.31	48.30	669.
8	90000.	503.51	4.8825	119195.5	3945.9	1058.1	2185.45	58.34	48.42	672.
9	85000.	494.46	4.8027	113896.6	3762.1	994.6	2025.70	58.81	49.10	674.
10	85000.	485.45	4.7213	108198.5	3564.5	928.8	1861.72	59.31	49.89	674.
11	81000.	471.73	4.5906	99684.0	3260.8	832.0	1601.87	60.06	51.94	670.
12	77000.	459.77	4.4956	92069.4	2991.8	752.6	1394.74	61.52	53.96	667.

RUN NUMBER 9
TEST DATE
PROCESSING DATE

CALCULATED PUMP PARAMETERS

TIME SLICE NO	TEST SPEED (RPM)	NPSH (FT)	SUCTION SPECIFIC SPEED	1ST STG INL FLOW COEFF	HEAD COEFF	PUMP DELTA T (DEG R)	(Q/N) OVER (Q/N)DES
1	85000.	2494.90	5323.22	0.13122	1.48216	53.97	0.8553
2	84000.	2475.27	5277.54	0.13441	1.54538	54.37	0.8761
3	86000.	2509.72	5578.27	0.13110	1.48562	58.30	0.8545
4	92000.	2631.71	5649.70	0.12854	1.49055	62.96	0.8378
5	93000.	2654.94	5701.10	0.12694	1.45835	62.37	0.8274
6	86000.	2642.61	5260.84	0.13729	1.69855	61.62	0.8949
7	93000.	2659.04	5558.67	0.13044	1.52501	60.26	0.8502
8	90000.	2584.37	5571.62	0.12994	1.51015	59.68	0.8470
9	83000.	2538.48	5471.67	0.13051	1.50936	56.57	0.8507
10	85000.	2553.11	5275.90	0.13188	1.51892	53.22	0.8596
11	81000.	2533.14	4927.06	0.13527	1.55920	48.37	0.8817
12	77000.	2556.78	4591.90	0.13869	1.59360	43.32	0.9040

RUN NUMBER 9
TEST DATE
PROCESSING DATE

TIME SLICE NO	----- SCALED TO TARGET N = 90000. RPM ----- FLOW (GPM)	HEAD (FT)	PRESS RISE (PSI)	HORSE POWER (BHP)	NPSH (FT)	----- SCALED TO N = 95000. RPM ----- FLOW (GPM)	HEAD (FT)	PRESS RISE (PSI)	HORSE POWER (BHP)	NPSH (FT)
1	508.45	116986.01	3822.02	1034.46	2764.43	536.73	130345.52	4258.48	1216.63	3080.12
2	520.84	121976.30	3988.78	1104.97	2841.51	549.77	135905.69	4444.29	1299.55	3166.01
3	507.96	117258.99	3851.05	1036.67	2595.51	536.20	130649.68	4290.83	1219.22	2891.92
4	498.07	117048.24	3901.83	1026.19	2518.53	525.74	131083.38	4347.41	1206.90	2806.14
5	491.83	115106.49	3820.14	995.15	2467.69	519.22	128251.37	4256.39	1170.39	2749.49
6	531.99	134065.66	4448.65	1256.58	2894.15	561.55	149375.63	4956.67	1477.86	3224.65
7	505.45	123568.47	3989.14	1073.10	2599.04	533.53	134114.25	4444.69	1262.07	2895.84
8	503.51	119195.53	3945.92	1058.13	2584.37	531.49	132807.37	4396.55	1244.46	2879.50
9	505.70	119132.55	3935.09	1063.93	2655.18	533.80	132737.19	4384.47	1251.28	2958.39
10	511.00	119087.55	3949.60	1083.30	2806.77	539.39	133578.41	4400.64	1274.06	3127.30
11	524.14	123066.65	4025.64	1141.30	3127.33	553.26	137120.56	4485.36	1342.28	3484.46
12	527.40	125782.18	4087.25	1201.70	3492.99	567.25	140146.19	4554.00	1413.32	3891.88

MK48-F
LIQUID HYDROGEN TURBOPUMP ASSEMBLY

RUN NUMBER 9
TEST DATE

PROCESSING DATE

TURBINE PARAMETERS

TIME SLICE NO	SPEED RPM	INLET TOTAL PR (PSIA)	EXHAUST TOTAL PR (PSIA)	INLET TOTAL TEMP (DEG R)	EXHAUST TOTAL TEMP (DEG R)	FLOW (LB/SEC)	PR RATIO	TORQUE (FT-LB)	BHP (CALIB) (HP)	BHP (DELTA T) (HP)
1	8550.	[illegible]	1615.9	521.37	472.26	7.34	1.5242	111.22	1811.2	1863.2
2	8400.	[illegible]	1642.3	520.54	471.75	7.46	1.5315	116.42	1862.8	1883.5
3	8850.	[illegible]	1769.0	518.80	470.07	8.14	1.5579	124.95	2106.3	2059.0
4	9200.	[illegible]	1955.3	515.61	466.57	8.94	1.5595	131.24	2299.8	2281.3
5	9300.	[illegible]	1944.0	515.55	466.11	8.89	1.5599	128.94	2284.1	2287.5
6	8600.	[illegible]	1929.8	515.49	465.97	8.83	1.5611	139.84	2290.7	2274.4
7	9000.	[illegible]	1889.3	513.87	464.95	8.65	1.5591	129.60	2221.8	2202.0
8	9000.	[illegible]	1862.1	512.97	464.09	8.53	1.5585	127.48	2185.5	2171.0
9	8800.	[illegible]	1759.7	510.49	462.12	8.08	1.5467	120.85	2025.7	2032.9
10	8550.	[illegible]	1654.3	508.07	459.78	7.61	1.5326	114.32	1861.7	1911.2
11	8100.	[illegible]	1503.3	503.34	455.53	6.94	1.5003	103.82	1601.9	1725.6
12	7700.	[illegible]	1364.7	498.24	451.55	6.32	1.4791	95.10	1594.7	1536.0

RUN NUMBER 9
TEST DATE
PROCESSING DATE

T U R B I N E P A R A M E T E R S (CONTINUED)

TIME SLICE NO	SPEED RPM	U/C (T-T)	EFF (T-T) (%)	AVAIL. ENERGY(T-T) (BTU/LB)	GAMMA	CP (BTU/LBM-R)	SPEED PARA-METER	FLOW PARA-METER	TORQUE PARA-METER
1	85000.	0.3965	80.62	216.51	1.4007	3.6556	473.53	2.6709	0.0183
2	84000.	0.3876	80.73	218.64	1.4008	3.6582	465.59	2.6579	0.0188
3	85000.	0.4008	80.54	226.99	1.4015	3.6680	491.36	2.6141	0.0182
4	92000.	0.4167	80.15	226.94	1.4020	3.6793	512.37	2.6143	0.0175
5	93000.	0.4212	80.01	227.01	1.4020	3.6790	517.97	2.6145	0.0172
6	85000.	0.3892	80.72	227.30	1.4019	3.6786	479.01	2.6127	0.0188
7	90000.	0.4085	80.37	225.94	1.4017	3.6794	502.08	2.6143	0.0178
8	90000.	0.4091	80.36	225.34	1.4015	3.6797	502.51	2.6151	0.0178
9	85000.	0.4045	80.47	220.36	1.4009	3.6789	492.54	2.6331	0.0180
10	85000.	0.3982	80.59	214.66	1.4002	3.6775	479.69	2.6564	0.0183
11	82000.	0.3887	80.72	202.13	1.3988	3.6767	456.57	2.7115	0.0187
12	77000.	0.3782	80.79	192.98	1.3973	3.6772	436.24	2.7468	0.0191

APPENDIX E

REFERENCES

REFERENCES

1. Advanced Space Engine Preliminary Report, NASA CR-121236, R-9269

DISTRIBUTION LIST

DISTRIBUTION LIST FOR FINAL REPORT
CONTRACT NAS 3-17794

National Aeronautics & Space Administration
Lewis Research Center
21000 Brookpark Road
Cleveland, Ohio 44135

1	Attn: Contracting Officer, MS 500-313
5	E. A. Bourke, MS 500-205
1	Technical Utilization Office, MS 3-16
1	Technical Report Control Office, MS 5-5
2	AFSC Liaison Office, MS 501-3
2	Library, MS 60-3
1	Office of Reliability & Quality Assurance, MS 500-211
12	R. E. Connelly, MS 500-318

7 National Aeronautics & Space Administration
Headquarters
Washington, D.C. 20546

Attn: Office of Aeronautics & Space Technology
Director, Study, Analysis & Planning/RX
Director, Space Propulsion & Power/RP
F. W. Stephenson/RP

Attn: Office of Space Flight
Director, Advanced Programs/MT
Director, Advanced Studies/MTE

Attn: Office of Industry Affairs & Technology Utilization
Director, Technology Utilization/KT

1 National Aeronautics & Space Administration
Ames Research Center
Moffett Field, California 94035

Attn: Library

1 National Aeronautics & Space Administration
Flight Research Center
P. O. Box 273
Edwards, California 93523

4 National Aeronautics & Space Administration
George C. Marshall Space Flight Center
Huntsville, Alabama 35812

Attn: Library
J. L. Sanders/PD13 J. A. Lombardo/EP21
K. B. Chandler/EP24

1 National Aeronautics & Space Administration
Goddard Space Flight Center
Greenbelt, Maryland 20771

Attn: Library

1 National Aeronautics & Space Administration
John F. Kennedy Space Center
Cocoa Beach, Florida 32931

Attn: Library

2 National Aeronautics & Space Administration
Lyndon B. Johnson Space Center
Houston, Texas 77001

Attn: Library
C. W. Yodzis/EP2

2 National Aeronautics & Space Administration
Langley Research Center
Langley Station
Hampton, Virginia 23365

Attn: Library B. Z. Henry, MS411

10 NASA Scientific & Technical Information Facility
P. O. Box 33
College Park, Maryland 20740

Attn: NASA Representative

1 Office of the Director of Defense
Research & Engineering
Washington, D.C. 20301

Attn: Office of Ass't Director (Chemical Technology)

2 Jet Propulsion Laboratory
4800 Oak Grove Drive
Pasadena, California 91103

Attn: Library D. Dipprey

1 Defense Documentation Center
Cameron Station
Building 5
5010 Duke Street
Alexandria, Virginia 22314

Attn: TISIA

1 Advanced Research Projects Agency
Washington, D.C. 20525

Attn: Library

1 Aeronautical Systems Division
Air Force Systems Command
Wright-Patterson Air Force Base
Dayton, Ohio

Attn: Library

1 Air Force Missile Test Center
Patrick Air Force Base
Florida

Attn: Library

1 Air Force Systems Command
Andrews Air Force Base
Washington, D.C. 20332

Attn: Library

2 Air Force Rocket Propulsion Laboratory
Edwards, California 93523

Attn: Library
R. L. Wiswell, LKDS

1 Air Force Office of Scientific Research
Washington, D.C. 20333

Attn: Library

1 U.S. Air Force
Washington, D.C.

Attn: Library

1 Air Force Aero Propulsion Laboratory
Research & Technology Division
Air Force Systems Command
U.S. Air Force
Wright-Patterson AFB, Ohio 45433

Attn: Library

1 Arnold Engineering Development Center
Air Force Systems Command
Tullahoma, Tennessee

Attn: Library

2 Space & Missile Systems Organization
Worldway Postal Center
P.O. Box 92960
Los Angeles, California 90009

Attn: Library (Technical Data Center)
Lt. Col. J. Graetch

1 Office of Research Analyses (OAR)
Holloman Air Force Base
New Mexico 88330

Attn: Library (RRRD)

1 RTD (RTNP)
Bolling Air Force Base
Washington, D.C. 20332

1 Bureau of Naval Weapons
Department of the Navy
Washington, D.C.

Attn: Library

1 Naval Research Branch Office
1030 E. Green Street
Pasadena, California 91101

Attn: Library

1 Picatinny Arsenal
Dover, New Jersey 07801

Attn: Library

1 U.S. Naval Research Laboratory
Washington, D.C. 20390

Attn: Library

1 U.S. Army Research Office (Durham)
Box CM, Duke Station
Durham, North Carolina 27706

Attn: Library

1 U.S. Army Missile Command
Redstone Scientific Information Center
Redstone Arsenal, Alabama 35808

Attn: Document Section

1 U.S. Naval Missile Center
Point Mugu, California 93041

Attn: Technical Library

1 U.S. Naval Weapons Center
China Lake, California 93557

Attn: Library

1 Aerojet General Corp
9100 E. Flair Dr.
El Monte, California 91734

Attn: Library

3 Aerojet Liquid Rocket Co.
P.O. Box 13222
Sacramento, California 95813

Attn: Library
M.C. Huppert
F. Viteri

3 Aerospace Corporation
2350 E. El Segundo Blvd
Los Angeles, California 90045

Attn: Library
R. L. Doobler
I. Madison

1 Airesearch Mfg. Co. of California
A Div. of the Garrett Corp.
2525 W. 190th St.
Torrence, California 90509

Attn: Library

1 Airesearch Mfg. Co. of Arizona
A Div. of the garrett Corp.
402 South 36th St.
Phoenix, Arizona 85034

Attn: Library

1 Atlantic Research Corp.
5390 Cherokee Ave.
Alexandria, Virginia 22314

Attn: Library

1 Battelle Memorial Institute
505 King Avenue
Columbus, Ohio 43201

Attn: Library

1 Bell Aerospace Company
Box 1
Buffalo, New York 14240

Attn: Library

1 Boeing Company
Space Division
P.O. Box 868
Seattle, Washington 98124

Attn: Library

1 Chemical Propulsion Information Agency
Applied Physics Laboratory
8621 Georgia Avenue
Silver Spring, Maryland 20910

1 Chrysler Corp.
Defense-Space Group
P.O. Box 757
Detroit, Michigan 48231

Attn: Library

1 Curtiss-Wright Corporation
One Rotary Drive
Woodridge, New Jersey 07075

Attn: Library

1 Deposits & Composites Incorporated
318 Victory Drive
Herndon Industrial Park
Herndon, Virginia 22070

Attn: J. C. Withers

1 Fairchild Republic Company
Fairchild Industries
Farmingdale, L.I., N.Y. 11735

Attn: Library

1 General Dynamics/Convair
P.O. Box 1128
San Diego, California 92112

Attn: Library

1 General Electric Company
Valley Forge Space Technology Center
P.O. Box 8555
Philadelphia, Pennsylvania 19101

Attn: Library

1 Grumman Aerospace Corporation
Bethpage, L.I., N.Y. 11714

Attn: Library

1 Hamilton Standard Corporation
Windsor Locks, Connecticut 06096

Attn: Library

1 Hughe's Aircraft Company
Space and Communications Group
P.O. Box 92919
Los Angeles, California 90009

Attn: Library

1 IIT Research Institute
Technology Center
Chicago, Illinois 60616

Attn: Library

1 Walter Kidde & Company
Belleville Division
675 Main St.
Belleville, New Jersey 07109

Attn: Library

1 Lockheed Missiles & Space Company
P.O. Box 504
Sunnyvale, California 94087

Attn: Library

1 Marquardt Corporation
16555 Saticoy Street
Box 2013 South Annex
Van Nuys, California 91409

Attn: Library

1 Martin-Marietta Corporation
P.O. Box 179
Denver, Colorado 80201

Attn: Library

1 McDonnell Douglas Astronautics
5301 Bosa Avenue
Huntington Beach, California 92647

Attn: Library

1 Northrop Corporation
1800 Century Park East
Century City, California 90067

Attn: Library

1 Pratt & Whitney Aircraft Group
United Technologies Corporation
400 Main St.
East Hartford, Connecticut 06108

Attn: Library

1 Pratt & Whitney Aircraft Group
Government Products Division
P.O. Box 2691
West Palm Beach, Florida 33402

Attn: Library

1 Rocketdyne
A Division of Rockwell International
6633 Canoga Avenue
Canoga Park, California 91304

Attn: Library

1 Space Division
A Division of Rockwell International
12214 Lakewood Blvd
Downey, California 90241

Attn: Library

1 Rocket Research Corporation
Willow Road at 116th Street
Redmond, Washington 98052

Attn: Library

1 Sundstrand Aviation Mechanical
2421 Eleventh Street
Rockford, Illinois 61101

Attn: Library

1 Thiokol Corporation
P.O. Box 1000
Newton, Pennsylvania 18940

Attn: Library

1 TRW Systems Group
1 Space Park
Redondo Beach, California 90278

Attn: Library

1 TRW
23555 Euclid Avenue
Cleveland, Ohio 44117

Attn: Library

1 Vought Corporation
P.O. Box 5907
Dallas, Texas 75222

1 J. P. Layton
60 Penn Lyle Road
Princeton Jct., New Jersey 08550

1 R. J. Salkeld
5921 Floris Heights Road
Malibu, California 90265

1 Dept. of Aerospace Engineering
Pennsylvania State University

Attn: B. Lakshminarayana
233 Hammond Bldg.
University Park, Pennsylvania 16802